

Electronic Thesis and Dissertation Repository

11-10-2021 2:00 PM

The Synthesis and Application of Polyglyoxlamides

Quinton EA Sirianni, *The University of Western Ontario*

Supervisor: Gillies, Elizabeth R., *The University of Western Ontario*

A thesis submitted in partial fulfillment of the requirements for the Doctor of Philosophy degree in Chemistry

© Quinton EA Sirianni 2021

Follow this and additional works at: <https://ir.lib.uwo.ca/etd>

 Part of the [Polymer Chemistry Commons](#)

Recommended Citation

Sirianni, Quinton EA, "The Synthesis and Application of Polyglyoxlamides" (2021). *Electronic Thesis and Dissertation Repository*. 8228.

<https://ir.lib.uwo.ca/etd/8228>

This Dissertation/Thesis is brought to you for free and open access by Scholarship@Western. It has been accepted for inclusion in Electronic Thesis and Dissertation Repository by an authorized administrator of Scholarship@Western. For more information, please contact wlsadmin@uwo.ca.

Abstract

Self-immolative polymers (SIPs) are a subset of degradable polymers that can be triggered to fully depolymerize with a single stimulus event. This amplifying behaviour makes them ideal for real-world applications including sensors, recyclable plastics, and drug delivery vehicles. Polyglyoxylates (PGs) are a class of SIPs that can be synthesized in a one-pot reaction and designed to respond to different stimuli including light, heat, reduction, and oxidation. However, with the exception of poly(ethyl glyoxylate) (PEtG), the various glyoxylate monomers must be prepared and purified before polymerization, which can be difficult. Furthermore, PGs typically possess properties such as water-insolubility and low glass transition temperatures that make them unsuited for certain applications. This thesis details the synthesis of a new class of SIPs known as polyglyoxylamides (PGAMs). PGAMs were prepared from precursor PEtGs using post-polymerization amidation reactions with high conversion. The resulting polymers possessed properties differing from the precursor PEtGs, while still remaining capable of self-immolation. Furthermore, the synthetic method to create PGAMs allowed for their properties to be easily tuned. This feature was taken advantage of in subsequent work, where PGAMs were developed with a variety of properties including thermo- and pH-responsiveness. Furthermore, PGAMs were developed that could form nanovesicles that may potentially serve as drug delivery vehicles and non-viral polycationic agents to assist with the transfection of nucleic acids.

Keywords

Self-immolative, polyglyoxylamide, polyglyoxylate, poly(ethyl glyoxylate), degradable, stimuli-responsive, thermo-responsive, pH-responsive, self-assembly, non-viral transfection agent

Summary for Lay Audience

Polymers are large molecules composed of many repeating units. They are essential in the modern world, making up the components of life such as proteins as well as natural and synthetic materials such as wood and commodity plastics. Degradable polymers are those that are capable of being broken down into smaller molecules via naturally occurring processes over a reasonable timespan such as a few years, thereby allowing their degradation products to return to the ecosystem. This behaviour contrasts with non-degradable polymers such as polystyrene, which remain intact in the environment long after their disposal and may require hundreds of years to fully degrade. Degradable polymers are ideal candidates for combating plastic pollution and for certain medical applications such as degradable medical devices. Self-immolative polymers (SIPs) are a subset of degradable polymers that are capable of full degradation after the removal of a stabilizing group via a stimulus such as light or heat. This degradation is controlled and proceeds in a domino-like fashion, making these polymers ideal for real-world applications where an amplifying effect is desired. This thesis documents the development of a novel class of SIPs known as polyglyoxylamides (PGAMs). PGAMs can be prepared via a one-step reaction using another SIP known as poly(ethyl glyoxylate) and a variety of different amines. Depending on the amines used, PGAMs can be tuned to possess interesting properties. The thesis further documents the development of PGAMs with specific properties, such as the ability to alter themselves to changes in temperature or pH. Additionally, the use of PGAMs to form nanoscale assemblies, which may be able to act as responsive drug-delivery vehicles is described. Finally, the application of PGAMs for the delivery of nucleic acids into cells for nucleic acid therapy is presented.

Co-Authorship Statement

This thesis contains contributions from the author as well as a number of collaborators. The nature and extent of each author's contributions are described below.

Chapter 1 provides an overview of the thesis and its objectives. It was written by the author with edits by Prof. Elizabeth Gillies. Some of the text was previously published: Sirianni, Q. E. A.; Gillies, E. R. The Architectural Evolution of Self-Immolative Polymers. *Polymer* **2020**, *202*, 122638.

Chapter 2 provides a review of the relevant literature and background information. It was written by the author with edits by Prof. Gillies. A significant portion of this work was previously published: Sirianni, Q. E. A.; Gillies, E. R. The Architectural Evolution of Self-Immolative Polymers. *Polymer* **2020**, *202*, 122638.

Chapter 3 contains the initial work to synthesize and characterize a library of self-immolative polyglyoxylamides. The poly(ethyl glyoxylate) starting polymers as well as the poly[oligo(ethylene glycol) methyl ether glyoxylamide] graft copolymer were synthesized by Dr. Amir Rabiee Kenaree. All other experimental work, including synthesis of the other polymers and characterization of the final materials was carried out by the author. The published manuscript the chapter is based on was written by the author with edits by Dr. Rabiee Kenaree and Prof. Gillies: Sirianni, Q. E. A.; Rabiee Kenaree, A.; Gillies, E. R. Polyglyoxylamides: Tuning Structure and Properties of Self-Immolative Polymers. *Macromolecules* **2019**, *52*, 262–270.

Chapter 4 contains work concerning the thermo-responsive properties of select self-immolative polyglyoxylamides. Preliminary work investigating if thermo-responsive polyglyoxylamides could be constructed was performed by the author, Mr. Kyle Classen, and Dr. Rabiee Kenaree. Work concerning the investigation of polyglyoxylamides with ethylene glycol and propylene glycol pendent groups was performed by the author and Dr. Rabiee Kenaree. Dr. Rabiee Kenaree synthesized the library of polyglyoxylamides and performed some of the cloud point studies, while cell toxicity studies were performed by Ms. Aneta Borecki. The author resynthesized some polyglyoxylamides and performed

additional experimental work, including polymer characterization, cloud point studies, and depolymerization studies. The published manuscript the chapter is based on was written by the author and Dr. Rabiee Kenaree, with edits by Prof. Gillies: Rabiee Kenaree, A.; Sirianni, Q. E. A.; Classen, K.; Gillies, E. R. *Biomacromolecules* **2020**, *21*, 3817–3825.

Chapter 5 contains work concerning the pursuit of self-immolative polymers capable of selectively depolymerizing in mildly acidic media. In this pursuit, polycationic polyglyoxylamide homopolymers that have pH-sensitive solubility in water were investigated. Additionally, copolymers of the polycationic polyglyoxylamides and poly(ethylene glycol) were investigated for pH-responsive self-assembly. All of the experimental work in this chapter was performed by the author. The final text was written by the author, with edits by Prof. Georgina Such and Prof. Gillies.

Chapter 6 contains work concerning the use of polycationic self-immolative polyglyoxylamides for the complexation and transfection of a plasmid payload. The synthesis of the polyglyoxylamides, their characterization, and the polymer depolymerization studies were performed by the author. Gel electrophoresis and transfection was performed by the author and Mr. Tian Duo Wang. Cell toxicity studies were performed by Ms. Borecki. The chapter was written by the author, with edits by Prof. Gillies.

Chapter 7 provides a summary of the thesis findings and conclusions. Additionally, the future direction of the work is discussed. It was written by the author with edits by Prof. Gillies.

Acknowledgments

There are numerous individuals without whom this thesis would have never been written. First, I thank my supervisor Prof. Elizabeth Gillies for providing her knowledge, experience, and guidance throughout my doctoral studies. From the moment I first inquired about working in your group you have shown enthusiasm towards having me as a student and colleague. You have continuously encouraged me to push the boundaries of what I thought I could achieve. More importantly, you helped me get past my moments of frustration and learn the rewards of perseverance in the lab. I am extremely fortunate to have had you as a mentor and work in such an exciting field.

Many others in the Western Chemistry Department have provided their assistance during my years of study. I thank Aneta Borecki for her invaluable assistance instructing me how to use various instruments, running an inordinate number of samples and assays for me, and teaching me some biology by guiding me through cell culturing and toxicity assays. I thank Dr. Mat Willans in the NMR facility for answering my questions about NMR spectroscopy and helping me fix the instrument when I inevitably triggered a software bug and locked everything up. Thank you to the late Yves Rambour for mending all the glassware that snapped and shattered over the years. I will miss your kind and humble nature and the sense of awe that I always experienced in your workshop. Thank you to Doug Hairsine for his help unseizing a few vacuum pumps, Kristina Jurcic for her help with MALDI mass spectrometry, Reza Khazaei, Karen Nygard, and the staff at the Biotron for their assistance with my imaging needs, and to all the Electronic Shop members for keeping our lab electronics in working condition. Thank you to Warren Lindsay and all the maintenance workers for keeping the lab facility running smoothly. Thank you to all the staff at the ChemBio Stores for always working hard to get research supplies for me as quickly and efficiently as possible.

I want to recognize all the amazing people that I've had the pleasure to work with in the Gillies Group, both past and present. You all have provided me with great experiences, both in and out of the lab, that I will remember for a long time to come. I could not have asked for a better group of individuals to work alongside. Furthermore, I want to thank all

the other research groups, both at Western and abroad, whom I had the opportunity to collaborate with during my degree.

Finally, I want to thank my family for supporting me as I traversed this new chapter of my life. In particular, I want to thank my mother and father for providing the support that I needed, whether it be financial or emotional. I know that these last few years have had their highs and lows, but I appreciate all that you've done and continue to do for me.

Table of Contents

Abstract.....	ii
Summary for Lay Audience.....	iii
Co-Authorship Statement.....	iv
Acknowledgments.....	vi
Table of Contents.....	viii
List of Tables	xv
List of Figures	xvi
List of Schemes.....	xxii
List of Abbreviations	xxiv
Chapter 1.....	1
1 Introduction.....	1
1.1 Overview.....	1
1.2 Research Objectives.....	2
1.3 Thesis Outline	3
1.4 References.....	4
Chapter 2.....	7
2 Literature Review.....	7
2.1 Degradable Polymers	7
2.2 Stimuli-Responsive Polymers.....	9

2.2.1	Thermo-Responsive Polymers	9
2.2.2	pH-Responsive Polymers.....	10
2.3	Stimuli-Responsive Degradable Polymers	11
2.4	Self-Immolative Polymers	12
2.4.1	Chemical Foundations for the Development of Self-immolative Materials	13
2.4.2	Self-Immolative Oligomers (SIOs).....	16
2.4.3	Self-Immolative Dendrimers/Dendrons (SIDs)	19
2.4.4	Self-Immolative Linear Polymers.....	25
2.4.5	Cyclic Self-Immolative Polymers.....	37
2.4.6	Self-Immolative Graft Copolymers and Networks	44
2.4.7	Hyperbranched Self-Immolative Polymers (HSIPs).....	47
2.5	References.....	50
Chapter 3	66
3	The Synthesis of Self-Immolative Polyglyoxylamides via Post-Polymerization Amidation.....	66
3.1	Introduction.....	66
3.2	Results and Discussion	68
3.2.1	Synthetic Approaches to Polyglyoxylamides	68
3.2.2	Synthesis of 4-Monomethoxytrityl End-Capped PEG for Post- Polymerization Modification	69

3.2.3	Synthesis of 4-Monomethoxytrityl End-Capped PGAm-MMTs)	71
3.2.4	Thermal Analysis of PGAm-MMTs	74
3.2.5	Triggered Depolymerization of PGAm-MMTs	75
3.2.6	Synthesis of Trityl End-Capped PGAm-Trits)	79
3.2.7	Triggered Depolymerization of PGAm-Trits	80
3.2.8	Synthesis and Characterization of a Degradable Graft Copolymer Analogue of PEG	81
3.3	Conclusions	83
3.4	Experimental	84
3.4.1	General Experimental Details	84
3.4.2	Synthesis of PEtGs	85
3.4.3	Synthesis of PGAm	87
3.4.4	Depolymerization Studies	91
3.5	References	92
Chapter 4		97
4	Thermo-Responsive Polyglyoxylamides	97
4.1	Introduction	97
4.2	Results and Discussion	99
4.2.1	Polymer Nomenclature	99
4.2.2	Polymer Synthesis	100

4.2.3	Cloud Point Measurements	102
4.2.4	Dynamic Light Scattering (DLS) Measurements	107
4.2.5	Depolymerization.....	108
4.2.6	In Vitro Cytotoxicity Studies	113
4.3	Conclusions.....	115
4.4	Experimental	115
4.4.1	General Experimental Details.....	115
4.4.2	Polymer Synthesis.....	116
4.4.3	NMR Depolymerization Studies.....	120
4.4.4	T_{cp} Measurements	121
4.4.5	DLS Studies	121
4.4.6	Cell Metabolic Activity Assays	122
4.5	Reference	122
Chapter 5.....		127
5	Polyglyoxylamides with a pH-Mediated Solubility and Depolymerization Switch ..	127
5.1	Introduction.....	127
5.2	Results and Discussion	130
5.2.1	Polymer Synthesis.....	130
5.2.2	Homopolymer Depolymerization	133
5.2.3	Block Copolymer Synthesis.....	135

5.2.4	Copolymer Self-Assembly and pH-Responsiveness	137
5.2.5	Copolymer Depolymerization in the Nanoassemblies.....	140
5.3	Conclusions.....	141
5.4	Experimental.....	142
5.4.1	General Experimental Details.....	142
5.4.2	Synthesis of Homopolymers.....	143
5.4.3	Synthesis of Copolymers	145
5.4.4	Depolymerization Studies.....	147
5.4.5	Study of Copolymer Assemblies	148
5.5	References.....	149
Chapter 6	155
6	Depolymerizing Polyplexes for DNA Transfection.....	155
6.1	Introduction.....	155
6.2	Results and Discussion	158
6.2.1	Synthesis of Polyglyoxylamide Polycations.....	158
6.2.2	Depolymerization of the Polyglyoxylamides.....	162
6.2.3	Complexation and Decomplexation of Polyplexes.....	165
6.2.4	Polyplex Characterization.....	167
6.2.5	Cytotoxicity Assays	171
6.2.6	Transfection Assays	173

6.3	Conclusions.....	175
6.4	Experimental.....	176
6.4.1	General Experimental Details.....	176
6.4.2	Synthesis of PEtG.....	177
6.4.3	Synthesis of PGAMs.....	179
6.4.4	Depolymerization of PGAMs.....	181
6.4.5	Complexation of PGAMs with pDNA.....	182
6.4.6	Triggered Decomplexation of the Polyplexes.....	182
6.4.7	DLS of the Polyplexes.....	183
6.4.8	TEM of the Polyplexes.....	183
6.4.9	Cell Cytotoxicity Assays for Polycations.....	183
6.4.10	Cell Cytotoxicity Assays for Polyplexes.....	184
6.4.11	Transfection Assays.....	185
6.5	References.....	185
Chapter 7	190
7	Summary, Conclusions, and Future Directions.....	190
Appendix 1	196
1	Permission to Reuse Copyrighted Material.....	196
Appendix 2	200

2 Supplemental Data for Chapter 3 Including NMR and FT-IR Spectra, Size-Exclusion Chromatograms, TGA and DSC Thermograms, Powder X-Ray Diffractograms, and Depolymerization Studies.....	200
Appendix 3.....	241
3 Supplemental Data for Chapter 4 Including NMR and FT-IR Spectra, Size-Exclusion Chromatograms, Turbidimetry Curves, DLS Studies, Depolymerization Studies, and Depolymerization Kinetic Plots	241
Appendix 4.....	283
4 Supplemental Data for Chapter 5 Including ^1H and ^{13}C NMR Spectra, FT-IR Spectra, Size-Exclusion Chromatograms, Depolymerization Studies, and DLS Studies.....	283
Appendix 5.....	308
5 Supplemental Data for Chapter 6 Including ^1H and ^{13}C NMR Spectra, Size-Exclusion Chromatograms, Depolymerization Studies, Complexation Studies, and Cytotoxicity Assays	308
Curriculum Vitae for Quinton E. A. Sirianni.....	338

List of Tables

Table 3.1. Summary of the physical and thermal properties of the 4-monomethoxytrityl end-capped polymers. For the SEC results, the values in parentheses were determined using MALLS rather than conventional calibration.	74
Table 3.2. Summary of the Physical and Thermal Properties of the Trityl End-Capped Polymers. For the SEC results, the values in parentheses were determined using MALLS rather than conventional calibration.	80
Table 4.1. Molar mass and DP_n data obtained from SEC and T_{cp} values determined by turbidimetry for the polymers. ND = not detected ($T_{cp} > 80$ °C). NM = not measured because no T_{cp} was detected at the higher concentration or in the case of culture media (CM) because only selected polymers were evaluated.	101
Table 4.2. Pseudo-first-order rate constants (k , s^{-1}) for the depolymerization of P(EtMEG)-Trit, P(EtDEG)-Trit, and P(MeMPG)-Trit in D_2O , deuterated PBS, and deuterated pH 3.0 citrate buffer.	112
Table 5.1. 1H NMR spectroscopy and SEC characterization of the polymers.	132
Table 6.1. 1H NMR and SEC characterization of the PEtGs and polycationic PGAMs.	161
Table 6.2. Diameter, PDI, and zeta potential measurements of the polyplexes obtained using DLS (N/P = 50). Values given are the averages and standard deviations of the three measurements obtained of each sample.	168

List of Figures

Figure 2.1. Examples of degradable polymers: a) synthetic polyesters, b) natural polysaccharides.	8
Figure 2.2. Examples of stimuli-responsive degradable polymers: a) polyketal, ³¹ b) polyacetal, ³³ c) disulphide linker between non-degradable PEI chains. ³⁵	12
Figure 2.3. Schematic illustrating the triggering and depolymerization of a SIP.	13
Figure 2.4. Examples of SIOs composed of a) multiple elimination spacers in sequence or b) one or more elimination spacers followed by a cyclization spacer.	17
Figure 2.5. Degradation kinetics of monodisperse SIOs measured by ¹ H NMR spectroscopy in 0.1 M phosphate buffer (D ₂ O):acetone- <i>d</i> ₆ (3:2) at 37°C showing an increase in degradation time with oligomer length: n = 0 (●), n = 1 (■), n = 3 (▲), n = 7 (◆). Adapted with permission from ref. ⁵³ Copyright 2013 American Chemical Society.	18
Figure 2.6. Architectural comparison showing a) a dendron and b) a dendrimer.	19
Figure 2.7. Chemical structures of self-immolative a) benzyl ether, b) cinnamyl carbamate, and c) benzyl carbamate dendrons. R = reporter group.	21
Figure 2.8. General chemical structures of the major classes of linear SIPs: a) PBCs, b) PBCs containing cyclization spacers, c) cyclization-only SIPs, d) PBEs, e) PPAs, f) PGs, g) POSs. EC = end-cap; Init = polymerization initiator; R corresponds to variable pendent groups.	26
Figure 2.9. a) Structure of cPPA and its degradation mechanism in acidic conditions. b) Cyclic alternating copolymer of PA and ethyl glyoxylate. c) Cyclic copolymers of PA and other aldehyde monomers (R denotes the pendent groups from different monomers). d) lariat-shaped PEtG synthesized using BF ₃ ·OEt ₂ . e) Cyclic polydisulfide random copolymers of methyl lipolate.	38

Figure 2.10. a) Structure of a graft copolymer with a polymethacrylate and UV light-triggerable PBC pendent chains. b) Variant of the structure in a) but with pendent acrylate groups that lead to the release of fluorescent molecules upon depolymerization. c) PBE backbone with pendent PEG or PS chains (R group) and a stimuli-responsive end-cap (EC). d) Depolymerizable polycyclopentene with pendent PS chains..... 45

Figure 2.11. a) HSIP with a visible light-responsive trigger (green) and peripheral PEG (orange) and doxorubicin (Dox) (red) moieties. b) HSIP with a H₂O₂-sensitive trigger (purple) and peripheral mitochondrial targeting groups (MTG; gold), PEG (orange), and caged fluorescent reporters (blue). 49

Figure 3.1. a) SIPs are stabilized with an end-cap that can be cleaved off in the presence of a particular stimulus. b) Removal of the end-cap leads to a cascade depolymerization of the polymer chain. c) The depolymerization products include the end-cap and repeat units of the polymer, which may be the original monomers or derivative products depending on the depolymerization mechanism. d) A polyglyoxylamide depolymerizes upon cleavage of the end-cap. Init = polymerization initiator; EC = end-cap..... 67

Figure 3.2. Comparison of the ¹H NMR spectra of PEtG-MMT (top) and PGAm-NEt-MMT (bottom) (CDCl₃, 400 MHz). 72

Figure 3.3. Overlay of the size-exclusion chromatograms of the 4-monomethoxytrityl end-capped polymers. 73

Figure 3.4. a) Depolymerization of PGAm-NEt-MMT in 9:1 acetonitrile:water with acetic acid (0.9 M) as a representative sample of how depolymerization was monitored using ¹H NMR spectroscopy (CD₃CN, 400 MHz). As depolymerization proceeds, there is a decrease in the backbone methine proton peak at ~5.6 ppm and an increase in the methine proton peak of the monomer hydrate at ~5.0 ppm in the NMR spectra. b) Depolymerization behaviours for selected PGAm-MMTs in 9:1 CD₃CN:D₂O with and without acetic acid (0.9 M) as a stimulus. c) Depolymerization behaviours for selected PGAm-Trits in either citrate-buffered D₂O (0.1 M, pH 3.0) or phosphate-buffered D₂O (0.1 M, pH 7.4). 77

Figure 4.1. Thermo-responsive polymers a) PNIPAM and b) POEG(M)A. c) General chemical structure of PGAMs and their depolymerization to glyoxylamide hydrates following end-cap cleavage (Init = polymerization initiator; EC = end-cap)..... 98

Figure 4.2. a) Thermo-responsive behaviour of P(MeMPG)-BOM in water, pH 7.4 PBS, and cell culture media containing FBS, showing dependence on the solvent/media. Minimal hysteresis was observed in the presence of FBS. b) Thermo-responsive behaviour of P(MeMPG)-BOM in pH 3.0 citrate buffer at different points showing minimal change in the T_{cp} . c) Thermo-responsive behaviour of P(MeMPG)-Trit in pH 3.0 citrate buffer at different points showing an increase in the T_{cp} as the polymer depolymerizes..... 106

Figure 4.3. a) Z average diameter and mean count rate of P(EtDEG)-BOM at 43 °C in PBS (1.25 mg/mL) over time. The solution temperature was the T_{cp} of the polymer solution as determined previously by DLS (Figure A3.65). b) The intensity distribution of diameters in the solution at different time points showing the conversion of dissolved polymers and nanoscale assemblies into large micron-sized aggregates over time. 108

Figure 4.4. Depolymerization of P(EtMEG)-Trit, P(EtMEG)-BOM, P(EtDEG)-Trit, P(EtDEG)-BOM, P(MeMPG)-Trit, and P(MeMPG)-BOM in a) D₂O, b) deuterated pH 7.4 PBS, and c) deuterated pH 3.0 (0.1 M) citrate buffer, calculated by ¹H NMR spectroscopy at different time intervals. All depolymerization studies were performed at 20 °C, while spectra for P(EtDEG) and P(MeMPG) polymers were obtained at 25 °C and those for P(EtMEG) polymers were obtained at 5 °C due to their T_{cps} being less than 25 °C. The depolymerization behaviour depended on the medium and polymer structure..... 110

Figure 4.5. Cell metabolic activity (relative to control), as measured by MTT assays, as a function of polymer concentration: a) P(MeMEG)-Trit versus P(EtMEG)-Trit, b) P(MeMEG)-Trit versus P(EtDEG)-Trit, c) P(MeMPG)-Trit versus P(MeMPG)-BOM as measured by MTT assays on C2C12 cells following a 24 h incubation. 114

Figure 5.1. a) Schematic illustrating how pH-mediated dissolution of a PGAm enables its end-cap cleavage and depolymerization, whereas a PEtG with the same end-cap remains insoluble and does not depolymerize. b) Application of the pH-mediated solubility switch enables the disassembly and depolymerization of PEG-PGAm nanoassemblies, while analogous PEG-PEtG assemblies remain intact 129

Figure 5.2. Overlay of ^1H NMR spectra of PEtG-1 and the PGAm homopolymers derived from it (CDCl_3 , 400 MHz)..... 131

Figure 5.3. a) PGAm(DMAE) in deuterated citrate buffer (0.2 M; pH 5.0) monitored by ^1H NMR spectroscopy (400 Hz) over time as a representative example of triggered depolymerization. As depolymerization occurs, the broad backbone methine proton peak decreases and a sharp singlet peak of the monomer hydrate methine peak increases. The overall mechanism is shown above the spectra. b) Depolymerization over time for most of the homopolymers at different pH levels, as measured by ^1H NMR spectroscopy. Depolymerization data for PGAm(DMAE) can be found in Appendix 4. Deuterated phosphate buffer (0.2 M; pH 7.4) or deuterated citrate buffer (0.2 M; pH 5.0, 6.0) was used as the solvent..... 134

Figure 5.4. a) Overlay of the ^1H NMR spectra of PEG-PEtG as well as its constituent blocks, PEtG-2 and mPEG- N_3 , and one of its derivatives, PEG-PEtG(DMAE) (CDCl_3 , 400 MHz). For the block copolymers, 1 = peaks from the mPEG- N_3 block, 2 = peaks from the PEtG-2 block, and 3 = peaks from the PGAm(DMAE) block. b) Overlay of chromatograms of the copolymer PEG-PEtG as well as its constituent blocks, PEtG-2 and mPEG- N_3 136

Figure 5.5. TEM images of a) PEG-PGAm(DPAE) and b) PEG-PEtG after nanoprecipitation and self-assembly at pH 8. Both copolymers assembled into nanoparticles with vesicle morphologies..... 138

Figure 5.6. a) Percent initial count rates and b) Z average diameters of copolymer nanoassemblies at different pH levels. Error bars represent the standard deviation

between three replicate samples. c) Volume distribution from DLS and d) TEM images of PEG-PGAm(DPAE) nanoassemblies at pH 7.5 and 7.0 (at 25 °C)..... 139

Figure 5.7. Depolymerization over time for most of the copolymers at different pH levels, as measured by ¹H NMR spectroscopy. Depolymerization data for PEG-PGAm(DMAE) can be found in Appendix 4. Deuterated phosphate buffer (0.2 M; pH 7.4, 8.0) or deuterated citrate buffer (0.2 M; pH 5.0, 6.0) was used as the solvent..... 141

Figure 6.1. a) Polyplexes formed via the ionic interaction of positively-charged SIPs with the negatively-charged phosphate backbone of DNA. At acidic pH, the SIPs depolymerize, destroying the polyplex and releasing the DNA. b) Depolymerization of a polycationic PGAm into monocations. 158

Figure 6.2. Depolymerization of the PGAm polycations in either citrate buffered D₂O (pH 5.0, 6.0) or phosphate buffered D₂O (pH 7.4). a) Example showing depolymerization of PGAm-DMAE-Trit in citrate buffered D₂O (0.2 M, pH = 5.0) monitored by ¹H NMR spectroscopy (400 MHz). Depolymerization kinetics of b) PGAm-MMTs, c) PGAm-Trits, and d) PGAm-BOMs over time. 163

Figure 6.3. Gel electrophoresis of the polyplexes (N/P = 50) along with a commercial transfection agent (jetPEI; N/P = 5) and free pDNA. a) Polyplexes were prepared in purified water and gel electrophoresis was run after a 15 min incubation time. b) Polyplexes were incubated in a citrate buffer (0.2 M, pH 5.0) for 24 h before gel electrophoresis was performed to allow for PGAm depolymerization. Images are shown in negative contrast..... 167

Figure 6.4. TEM images of pDNA-polycation polyplexes (N/P ratio = 50). The polyplexes were prepared in purified water and dried on a Formvar coated copper grid and then stained with a uranyl acetate solution: a) PGAm-DMAE-Trit, b) PGAm-DMAE-MMT, c) PGAm-DMAE-BOM, d) PGAm-DMAPr-Trit, e) PGAm-DMAPr-MMT, f) PGAm-DMAPr-BOM, g) PGAm-MAE-Trit, h) PGAm-MAE-MMT, i) PGAm-MAE-BOM..... 170

Figure 6.5. MTT assays of HEK 293T cells treated with varying concentrations of the PGAMs for 48 h: a) PGAM-Trits, b) PGAM-MMTs, c) PGAM-BOMs, d) Glyoxylamide hydrate monomers produced during the depolymerization of the PGAMs after end-cap cleavage, e) jetPEI. The results are expressed the percent activity relative to cells not exposed to polymers (culture media alone). Error bars represent the standard deviation of the replicate (n = 6) measurements. 172

Figure 6.6. Transfection of HEK 293T cells with pDNA for FLuc using PGAM and jetPEI polyplexes at different N/P ratios, as measured by luminescence assay (pDNA concentration = 1.5 µg/mL). Cells were incubated for 24 h after being treated with polyplex before the assay was performed. Error bars represent the standard deviation of the replicate (n = 3) measurements. 174

Figure 7.1. Potential future applications of PGAMs based on the work established in this thesis: a) Thermo-responsive PGAMs could be cross-linked to create thermo-responsive hydrogels, which should be capable of expelling a loaded drug when the temperature is raised above the polymer's cloud point; b) pH-responsive PEG-PGAM copolymers may be able to be loaded with both hydrophilic and hydrophobic drugs, given their vesicle morphology. These could then be used for pH-responsive drug-delivery; c) Polycationic PGAMs modified with PEG blocks (to stealth the polymers *in vivo* and prevent serum proteins from adhering) and targeting ligands (to target specific cells for transfection) may serve as improved transfection agents for *in vivo* use. 194

List of Schemes

Scheme 2.1. Mechanisms of a) 1,6-elimination of a 4-aminobenzyl alcohol spacer; b) cyclization of a spacer based on <i>N,N'</i> -dimethylethylenediamine; c) a sequence of elimination and cyclization reactions; and d) an acid-catalyzed equilibrium between a polyaldehyde and the corresponding aldehyde monomer.....	14
Scheme 2.2. a) Structure and proposed degradation mechanism of a poly(benzyl ester). b) Structure of a polythioester that depolymerizes back to bicyclic monomer in basic conditions via cyclization reactions (R^1 corresponds to variable pendent carbamate groups and A^- is a base). c) Structure of a polycarboxypyrrole that depolymerizes into CO_2 and an azafulvene by-product (R^2 corresponds to variable pendent groups).....	35
Scheme 3.1. Synthetic approaches for obtaining PGAMs.	69
Scheme 3.2. Synthesis of PGAMs (MMT = 4-monomethoxytrityl, Trit = trityl).....	70
Scheme 3.3. Hypothesized hydrogen bonding mechanism that assists with the removal of the trityl end-cap. The glyoxylamide repeating unit adjacent to the end-cap is able to form a five-membered ring, accelerating the removal of the end-cap. If water is present, the end-cap is trapped and the polymer begins to depolymerize.	78
Scheme 3.4. Synthesis of PGAM-OEG-Trit.	82
Scheme 4.1. Synthesis of PGAMs having different pendent amide moieties and either Trit or BOM end-caps.	101
Scheme 5.1. Synthesis of pH-responsive PGAM homopolymers and PEG-PGAM copolymers from PEtG.	131
Scheme 6.1. Synthesis of polyglyoxylamide polycations for use as depolymerizable pDNA complexation agents.....	160
Scheme 7.1. Proposed synthetic pathways to yield PGAMs with new self-immolative stimuli responsiveness: a) PGAMs may be produced via the post-polymerization	

amidation of PEtG that has been end-capped with novel ether-linked stimuli-cleavable moieties; b) glyoxylamide monomers of interest could be synthesized and purified before being polymerized in a similar fashion as glyoxylates, with the use of traditional carbonate/carbamate-linked stimuli-cleavable moieties as end-caps. 193

List of Abbreviations

AFM	Atomic force microscopy
ATRP	Atom-transfer radical polymerization
BOC	<i>t</i> -Butyloxycarbonyl
BSA	Bovine serum albumin
CM	Culture media
cPPA	Cyclic polyphthalaldehyde
CuAAC	Copper-Assisted Azide-Alkyne Cycloaddition
<i>D</i>	Dispersity
DBPDA	<i>N,N'</i> -Di- <i>sec</i> -butyl-1,4-phenylenediamine
DBU	1,8-Diazabicyclo[5.4.0]undec-7-ene
DEG	Diethylene glycol
DEP	Diethyl phthalate
DLS	Dynamic light scattering
DMA	<i>N,N</i> -Dimethylacetamide
DMEM	Dulbecco's Modified Eagle Medium
DMF	<i>N,N</i> -Dimethylformamide
DMSO	Dimethyl sulfoxide
DNA	Deoxyribonucleic acid

dn/dc	Refractive index increment
Dox	Doxorubicin
DP_n	Degree of polymerization
DSC	Differential scanning calorimetry
DTT	Dithiothreitol
EC	End-cap
FBS	Fetal bovine serum
FLuc	Firefly luciferase
FT-IR	Fourier-transform infrared
HA	Hyaluronic Acid
HSIP	Hyperbranched self-immolative polymer
Init	Polymerization initiator
LCST	Lower critical solution temperature
MALDI-TOF MS	Matrix-assisted laser absorption ionization time-of-flight mass spectrometry
MALLS	Multi-angle laser light scattering
MEG	Monoethylene glycol
MMT	4-Monomethoxytrityl
M_n	Number-average molecular weight
MPG	Monopropylene glycol

MTG	Mitochondrial targeting group
MTT	3-(4,5-Dimethylthiazol-2-yl)-2,5-diphenyltetrazolium bromide
M_w	Weight-average molecular weight
N/P	Nitrogen/phosphate ratio
NIR	Near infrared
NMAPF ₆	<i>N</i> -Methylacridinium hexafluorophosphate
NMR	Nuclear magnetic resonance
OEG	Oligo(ethylene glycol)
OLED	Organic light emitting diode
PA	Phthalaldehyde
PBC	Poly(benzyl carbamate/carbonate)
PBE	Poly(benzyl ether)
PBS	Phosphate buffered saline
PCL	Polycaprolactone
PDI	Polydispersity Index
PDMAEMA	Poly[2-(dimethylamino)ethyl methacrylate]
pDNA	Plasmid DNA
PEI	Poly(ethylene imine)

PEG	Poly(ethylene glycol)
PEtG	Poly(ethyl glyoxylate)
PG	Polyglyoxylate
PGA	Poly(glycolic acid)
PenGA	Penicillin-G-amidase
PGAm	Polyglyoxylamide
PLA	Poly(lactic acid)
PLL	Poly(L-lysine)
PMA	Polymethacrylate
PMMA	Poly(methyl methacrylate)
PNIPAM	Poly(<i>N</i> -isopropylacrylamide)
POEG(M)A	Poly[oligo(ethylene glycol) (meth)acrylate]
POS	Poly(olefin sulfone)
PPA	Polyphthalaldehyde
PS	Polystyrene
PTFE	Polytetrafluoroethylene
RNA	Ribonucleic acid
ROMP	Ring-opening metathesis polymerization
ROP	Ring-opening polymerization

SDS	Sodium dodecyl sulfate
SEC	Size-exclusion chromatography
SID	Self-immolative dendron/dendrimer
SIO	Self-immolative oligomer
SIP	Self-immolative polymer
TEM	Transmission electron microscopy
TEMPO	(2,2,6,6-Tetramethylpiperidin-1-yl)oxyl
TFA	Trifluoroacetic acid
TGA	Thermogravimetric analysis
THF	Tetrahydrofuran
TPAS	Random terpolymer composed of SO ₂ , 2-methyl-1-pentene, and 4-methyl-4-pentenoic acid
Trit	Trityl
T_c	Ceiling temperature
T_{cp}	Cloud point temperature
T_g	Glass transition temperature
T_m	Melting temperature
T_o	Onset degradation temperature
UV-Vis	Ultraviolet-visible (spectroscopy)

Chapter 1

1 Introduction

1.1 Overview

Polymers are macromolecules made up of many repeating small molecule units known as monomers. They make up many of the materials important in our day to day lives, from biological polymers such as nucleic acids and proteins that sustain life, to natural products like cotton and wood. The development and use of synthetic polymers like polyethylene and polystyrene has changed the world by providing plastic materials now used widely in construction and manufacturing. Unfortunately, many synthetic polymers are non-degradable and persist in the environment after their disposal for hundreds of years. This leads to problems like plastic pollution¹ and makes these polymers unsuitable for situations where degradation is desired, such as in biomedical applications.²⁻⁴ Degradable polymers do exist, such as polyesters and polysaccharides, that can combat the aforementioned issues of non-degradable polymers. These polymers are capable of degrading into smaller molecules via naturally occurring processes over a reasonable timespan such as a few years. Nevertheless, these polymers often degrade slowly and in a non-controlled fashion, which may be undesirable in some situations. The incorporation of stimuli-responsive moieties within polymer backbones, such as acetals and disulfides, can yield stimuli-responsive polymers that possess a more immediate degradation response when a particular stimulus is applied, such as acid or reducing agents.⁵ However, complete degradation to small molecules requires multiple stimuli-mediated events to occur. In some cases where only low concentrations of stimuli or small changes in conditions are accessible, it would be desirable to amplify the response.

Self-immolative polymers (SIPs) are a subset of degradable polymers.⁶⁻⁸ They are capable of complete head-to-tail depolymerization after a single stimulus-mediated bond cleavage, allowing them to amplify the stimulus and degrade in a controlled and timely fashion. Since

*This chapter contains work that has been published previously: Sirianni, Q. E. A.; Gillies, E. R. The Architectural Evolution of Self-Immolative Polymers. *Polymer* **2020**, *202*, 122638. See Co-Authorship Statement for the contributions of each author.

their initial discovery in 2008,⁹ a body of work has been published concerning the development of novel SIP backbones, SIPs with different stimuli-responsive end-groups (end-caps), and the use of these polymers for different potential applications. The field of SIP research is still in its infancy, with every year promising more work and more discoveries from research groups around the world.

1.2 Research Objectives

Our group reported on polyglyoxylates (PGs) as a novel class of SIP in 2014.¹⁰ Since then, we have continued to investigate PGs, in particular poly(ethyl glyoxylate) (PEtG), with different end-caps and its applications including drug-delivery systems,¹¹⁻¹⁴ sensors,¹⁵ and transient plastics.¹⁶⁻¹⁸ Despite the promising work done with PGs, these polymers typically possess physical and thermal properties such as low glass transition temperatures (T_g s) and water-insolubility that make them unsuitable for some applications. Moreover, except for ethyl glyoxylate, the acquisition and purification of other glyoxylate monomers for polymerization is difficult.

The overall goal of this thesis was to overcome the limitations of PGs by exploring analogous macromolecules that possess different physical and thermal properties but retain the self-immolative backbone of PGs. Given the established procedure of producing PEtG in our lab and the ethyl ester pendent groups of this polymer, my research focused on converting these pendent esters to various other moieties via post-polymerization amidation reactions. Such an approach allowed for the production of a library of novel polyglyoxylamides (PGAMs), which could be tuned to possess properties very different from their PEtG precursors, yet still depolymerize due to their self-immolative backbones. Initial experiments led to the discovery of PGAMs that had high T_g s, water-solubility, as well as the production of both polycationic and graft copolymers. Despite all the differences from the precursor polymers, the PGAMs were still capable of self-immolation when an appropriate stimulus was applied.

Once a method to produce PGAMs had been established, subsequent research then explored PGAMs with designed pendent groups, with the objective of installing other stimuli-

responsive properties. Over the course of this thesis, I investigated PGAMs with thermo- and pH-responsive behaviours, and how these additional behaviours could influence self-immolation (and vice-versa).

A final objective of this thesis was to investigate PGAMs for practical applications. An exploration of polycationic PGAMs as non-viral transfection agents for nucleic acids resulted in the transfections of cells *in vitro*, with comparable results to a commercial transfection agent and with lower overall cell toxicity.

1.3 Thesis Outline

This thesis is divided into seven chapters, which either introduce relevant background information, discuss a particular research project pursued to achieve one of the objectives of the thesis, or summarize the overall work. A brief description of each is provided below.

Chapter 1 introduces the overall content of the thesis as well as the research objectives of the work and an outline of the thesis.

Chapter 2 reviews background information pertinent to the thesis' contents. It provides an overview of degradable polymers, stimuli-responsive polymers, their combination to make stimuli-responsive degradable polymers, and finally a history of SIPs and the current state of the art.

Chapter 3 contains the foundational project for this thesis concerning the first synthesis and study of PGAMs from PEtG precursors. The work introduces a library of novel PGAMs synthesized from simple primary and secondary amines. The chapter discusses the characterization of these polymers as well as their depolymerization behaviour. The synthesis of graft copolymers is also demonstrated. This chapter provides a platform from which self-immolative PGAMs can be designed to possess desired properties or for specific applications.

Chapter 4 discusses the investigation of PGAMs with ethylene glycol and propylene glycol pendent groups as the first examples of self-immolative polymers with thermo-responsive behaviour. The library of PGAMs synthesized are investigated for lower critical solution

temperature (LCST) behaviour in aqueous solutions with and without the presence of buffer salts. Depolymerization is also studied, and the relationship between the thermo-responsive and depolymerization behaviours of the polymers is considered. Cytotoxicity studies of select PGAMs are also presented.

Chapter 5 reports on the development of SIPs that can selectively depolymerize in mildly acidic aqueous media. A small library of polycationic PGAM homopolymers with acid-sensitive end-caps and differing pendent tertiary amines are investigated to assess their water-solubility at different pH levels. Depolymerization studies reveal a relationship between depolymerization behaviour and the solubility state of the polymer. Copolymers of the PGAMs are also evaluated for their ability to self-assemble into nanovesicles in neutral/basic pH media with little depolymerization occurring but dissociate and depolymerize upon acidifying the media.

Chapter 6 describes the application of water-soluble polycationic PGAMs as self-immolative non-viral vectors for nucleic acid transfection. A small library of PGAMs with varying pendent amines and acid-responsive end-caps are investigated. These polymers are shown to complex and decomplex with a nucleic acid containing a reporter gene. Characterization of the complexes reveals nanoassemblies with overall positive zeta potentials. These complexes are then evaluated for their transfection potential as well as their cytotoxicity, with comparison of their performance against a non-degradable polycationic transfection agent.

Chapter 7 summarizes the contents of this thesis and what has been learned. Potential future work that may expand upon this thesis and address some of the unresolved questions and issues is also explored.

1.4 References

- (1) Payne, J.; McKeown, P.; Jones, M. D. A Circular Economy Approach to Plastic Waste. *Polym. Degrad. Stab.* **2019**, *165*, 170–181.
- (2) Nair, L. S.; Laurencin, C. T. Biodegradable Polymers as Biomaterials. *Prog. Polym. Sci.* **2007**, *32*, 762–798.

- (3) Bhatia, S. K. Tissue Engineering for Clinical Applications. *Biotechnol. J.* **2010**, *5*, 1309–1323.
- (4) Kamaly, N.; Yameen, B.; Wu, J.; Farokhzad, O. C. Degradable Controlled-Release Polymers and Polymeric Nanoparticles: Mechanisms of Controlling Drug Release. *Chem. Rev.* **2016**, *116*, 2602–2663.
- (5) Guo, X.; Wang, L.; Wei, X.; Zhou, S. Polymer-Based Drug Delivery Systems for Cancer Treatment. *J. Polym. Sci., Part A: Polym. Chem.* **2016**, *54*, 3525–3550.
- (6) Roth, M. E.; Green, O.; Gnam, S.; Shabat, D. Dendritic, Oligomeric, and Polymeric Self-Immolative Molecular Amplification. *Chem. Rev.* **2016**, *116*, 1309–1352.
- (7) Yardley, R. E.; Rabiee Kenaree, A.; Gillies, E. R. Triggering Depolymerization: Progress and Opportunities for Self-Immolative Polymers. *Macromolecules* **2019**, *52*, 6342–6360.
- (8) Sirianni, Q. E. A.; Gillies, E. R. The Architectural Evolution of Self-Immolative Polymers. *Polymer* **2020**, *202*, 122638.
- (9) Sagi, A.; Weinstain, R.; Karton, N.; Shabat, D. Self-Immolative Polymers. *J. Am. Chem. Soc.* **2008**, *130*, 5434–5435.
- (10) Fan, B.; Trant, J. F.; Wong, A. D.; Gillies, E. R. Polyglyoxylates: A Versatile Class of Triggerable Self-Immolative Polymers from Readily Accessible Monomers. *J. Am. Chem. Soc.* **2014**, *136*, 10116–10123.
- (11) Fan, B.; Gillies, E. R. Poly(ethyl glyoxylate)-Poly(ethylene oxide) Nanoparticles: Stimuli-Responsive Drug Release via End-to-End Polyglyoxylate Depolymerization. *Mol. Pharmaceutics* **2017**, *14*, 2548–2559.
- (12) Fan, B.; Trant, J. F.; Hemery, G.; Sandre, O.; Gillies, E. R. Thermo-Responsive Self-Immolative Nanoassemblies: Direct and Indirect Triggering. *Chem. Commun.* **2017**, *53*, 12068–12071.
- (13) Fan, B.; Yardley, R. E.; Trant, J. F.; Borecki, A.; Gillies, E. R. Tuning the Hydrophobic Cores of Self-Immolative Polyglyoxylate Assemblies. *Polym. Chem.* **2018**, *9*, 2601–2610.
- (14) Gambles, M. T.; Fan, B.; Borecki, A.; Gillies, E. R. Hybrid Polyester Self-Immolative Polymer Nanoparticles for Controlled Drug Release. *ACS Omega* **2018**, *3*, 5002–5011.

- (15) Fan, B.; Salazar, R.; Gillies, E. R. Depolymerization of Trityl End-Capped Poly(ethyl glyoxylate): Potential Applications in Smart Packaging. *Macromol. Rapid Commun.* **2018**, *39*, 1800173.
- (16) Fan, B.; Trant, J. F.; Yardley, R. E.; Pickering, A. J.; Lagugné-Labarthet, F.; Gillies, E. R. Photocontrolled Degradation of Stimuli-Responsive Poly(ethyl glyoxylate): Differentiating Features and Traceless Ambient Depolymerization. *Macromolecules* **2016**, *49*, 7196–7203.
- (17) Heuchan, S. M.; MacDonald, J. P.; Bauman, L. A.; Fan, B.; Henry, H. A. L.; Gillies, E. R. Photoinduced Degradation of Polymer Films Using Polyglyoxylate–Polyester Blends and Copolymers. *ACS Omega* **2018**, *3*, 18603–18612.
- (18) Heuchan, S. M.; Fan, B.; Kowalski, J. J.; Gillies, E. R.; Henry, H. A. L. Development of Fertilizer Coatings from Polyglyoxylate-Polyester Blends Responsive to Root-Driven pH Change. *J. Agric. Food. Chem.* **2019**, *67*, 12720–12729.

Chapter 2

2 Literature Review

2.1 Degradable Polymers

Degradable polymers contain labile moieties along their backbones that can be cleaved either hydrolytically or enzymatically, allowing for a passive and often slow depolymerization over time. Both synthetic and naturally occurring degradable polymers exist. For example, synthetic polyesters are some of the most investigated and applied degradable polymers. Polymers such as poly(glycolic acid) (PGA), poly(lactic acid) (PLA), and polycaprolactone (PCL) can be synthesized via the ring-opening polymerization (ROP) of cyclic lactone monomers to yield polymers with controlled and high molar masses (Figure 2.1a).¹⁻³ When exposed to water, the polyester backbones slowly hydrolyze over time into smaller and smaller units until finally returning to monomers. These polyesters have been used for a variety of applications such as tissue engineering scaffolds⁴⁻⁵ and drug-delivery vehicles.⁶⁻⁷ Furthermore, polymers such as PLA are seen as a potential solution to the issue of plastic pollution, since the polymer can be either degraded after use or chemically recycled into either virgin polymer or other useful chemicals.³

*This chapter contains work that has been published previously: Sirianni, Q. E. A.; Gillies, E. R. The Architectural Evolution of Self-Immolative Polymers. *Polymer* **2020**, *202*, 122638. See Co-Authorship Statement for the contributions of each author.

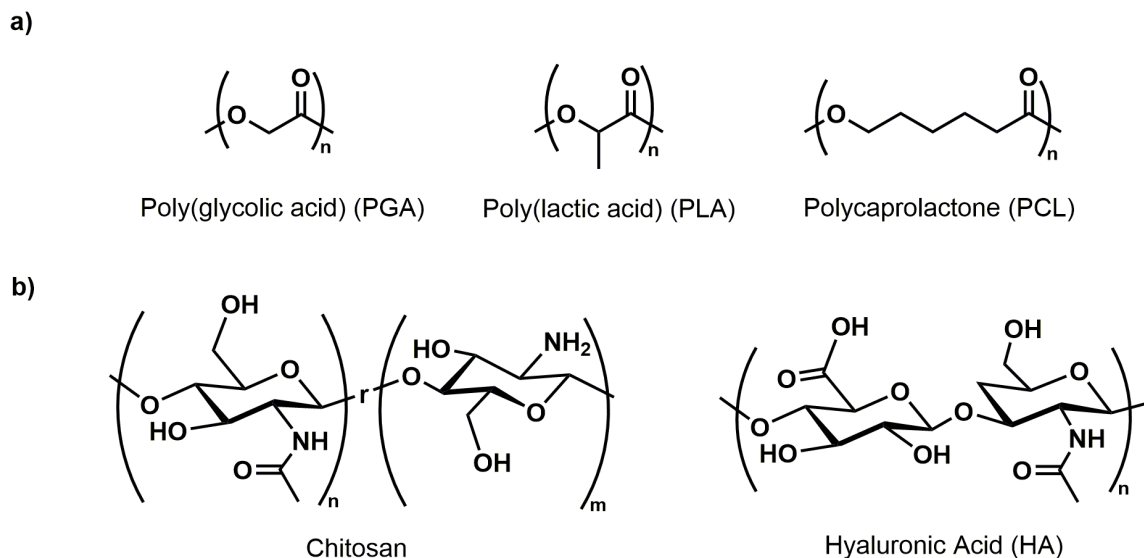


Figure 2.1. Examples of degradable polymers: a) synthetic polyesters, b) natural polysaccharides.

Naturally occurring degradable polymers like polysaccharides have also been extensively explored. For example, chitosan and hyaluronic acid (HA) can be produced from natural sources such as crustacean exoskeletons and animal tissues, respectively (Figure 2.1b).¹⁻² After use, these polymers can be broken down by endogenous enzymes in the body. Both chitosan and HA have been investigated for medical applications including wound dressings⁸⁻⁹ and drug delivery vehicles.¹⁰

While many other degradable polymers exist and have been extensively investigated, a key limitation of these polymers, whether they are of synthetic or natural origin, is their non-responsive nature. Degradation occurs passively based on the amount of water/enzyme that is able to access the labile backbone moieties. These polymers cannot have their degradation turned on in response to an external stimulus, which could limit their application in areas such as drug delivery, where an immediate response to a targeted stimulus may be necessary.

2.2 Stimuli-Responsive Polymers

Stimuli-responsive polymers, also known as “smart” polymers, are macromolecules capable of changing their physical or chemical properties in response to an external stimulus such as light, heat, changes in pH, or reducing conditions.¹¹ While numerous examples exist in the literature, the focus of this section will be placed on those polymers that can respond to changes in temperature (thermo-responsive polymers) and changes in pH (pH-responsive polymers).

2.2.1 Thermo-Responsive Polymers

Thermo-responsive polymers undergo changes in their properties in response to changes in temperature.¹²⁻¹³ These polymers often exhibit a lower critical solution temperature (LCST), where they aggregate and precipitate from solution at or above their cloud point temperature (T_{cp}). Below this temperature, the polymers remain dissolved. LCST behaviour in water can be explained by considering the thermodynamics of mixing during the dissolution of a thermo-responsive polymer chain, which can be represented by:

$$\text{Equation 2.1.} \quad \Delta G = \Delta H - T\Delta S$$

where ΔG is the change in free energy, ΔH is the change of enthalpy for dissolution, T is the absolute temperature in Kelvin, and ΔS is the change in entropy of the system. For dissolution to occur, ΔG must be less than zero. Dissolution in water causes the formation of hydrogen bonds between the polymer chain and water molecules. While this bonding is enthalpically favourable and thus ΔH is less than zero, the ordering of the water molecules around the polymer chain is entropically unfavourable and thus ΔS is greater than zero. Therefore, for a given thermo-responsive polymer, dissolution depends on the current temperature of the solution. If $\Delta G = 0$, Equation 2.1 can be rearranged to determine the T_{cp} :

$$\text{Equation 2.2.} \quad T_{cp} = \frac{\Delta H}{\Delta S}$$

In general, modifying the pendent group composition of thermo-responsive polymers allows for their LCST behaviour to be adjusted.¹² The addition of hydrophilic groups raises

the T_{cp} whereas the addition of hydrophobic groups lowers it. The presence of salts in the solution and polymer concentration can also affect the temperature at which the transition occurs, with higher concentrations of either typically resulting in a lowering of the T_{cp} .

Many different thermo-responsive polymers have been discovered and investigated over the years. One of the oldest and most important thermo-responsive polymers investigated in the literature is poly(*N*-isopropylacrylamide) (PNIPAM), which exhibits a T_{cp} of 32 °C.¹⁴ PNIPAM has been used in medical research to construct drug delivery systems such as vesicles¹⁵ and micelles¹⁶ that can be loaded with drug molecules and stimulated to release the drugs by changing the temperature either below or above the T_{cp} of the system, depending on the design. However, the overall safety of using PNIPAM for medical uses is of concern since it may be potentially toxic and it is not degradable.^{2, 12} Another set of polymers with LCST behaviour that have been extensively explored are poly[oligo(ethylene glycol) (meth)acrylate]s.¹⁷⁻¹⁹ These polymers possess oligo(ethylene glycol) pendent groups that should be non-toxic for biomedical applications,²⁰ and can be easily tuned to possess different T_{cps} by modifying the ratio of the different pendent groups used.¹⁸ However, these polymers also lack a degradable backbone.

2.2.2 pH-Responsive Polymers

pH-Responsive polymers are typically polyionic in nature, possessing ionizable groups that can change charge state depending on the pH of the solution. For example, chitosan has free amine groups on some of its repeat units that can be protonated if the pH of the solution is below the pKa of the amines.¹⁻² This ionization causes the solubility of chitosan to change, which is why this polymer can be dissolved in dilute acidic solutions yet remains insoluble at neutral pH. Other examples of poly(2-dialkylaminoethyl methacrylate)s being used to introduce a pH-mediated solubility switch for drug-delivery vehicles have also been shown.²¹⁻²⁵ These vehicles are loaded with drug and are stable at neutral pH, but dissociate and release their payload upon exposure to mildly acidic conditions, which are often found in the interiors of cells and at diseased sites in the body.

An interesting application of pH-responsive polycations is their use as non-viral transfection agents for the delivery of nucleic acids into cells. Polycations such as

polyethyleneimine (PEI),²⁶ poly(L-lysine),²⁷ and poly(2-dimethylaminoethyl methacrylate)²⁸ have all been used as transfection agents, complexing with nucleic acids and entering target cells via endocytosis before escaping the endosome and releasing the payload. While the endosomal escape mechanism is not fully understood, one prevalent hypothesis states that the polycations are able to act as an internal buffer due to their ionizable pendent groups, absorbing more and more protons that are pumped into the endosome.²⁹ This influx of ions into the endosome then causes an influx of water due to osmosis, and the increased pressure eventually lyses the endosome, releasing its contents into the cytosol.

2.3 Stimuli-Responsive Degradable Polymers

Stimuli-responsive degradable polymers are stimuli-responsive polymers that contain moieties in their backbones or pendent groups capable of cleaving in response to specific stimuli, allowing for a triggered degradation of the polymers. Several different moieties have been used, such as acetal, ketals, hydrazones, oximes, imines, and disulfides to respond to stimuli including acids and reducing agents.³⁰ For example, polyketals and polyacetals³¹⁻³³ are stimuli-responsive polymers capable of depolymerization when exposed to acidic stimulus (Figure 2.2a,b). The acid acts as a catalyst for the hydrolysis of the backbone ketals or acetals, allowing them to revert to ketones or aldehydes respectively, and in doing so introducing a backbone chain scission. Polymers containing disulfide bonds have also been developed to degrade in response to reducing agents like glutathione. Examples include core-shell nanoparticles with a disulfide linker placed between the core and shell to allow for the shell to be shed and thereby increase drug delivery,³⁴ and the inclusion of disulfide bonds in previously non-degradable polymers like PEI to allow for intracellular degradation to reduce cytotoxicity (Figure 2.2c).³⁵

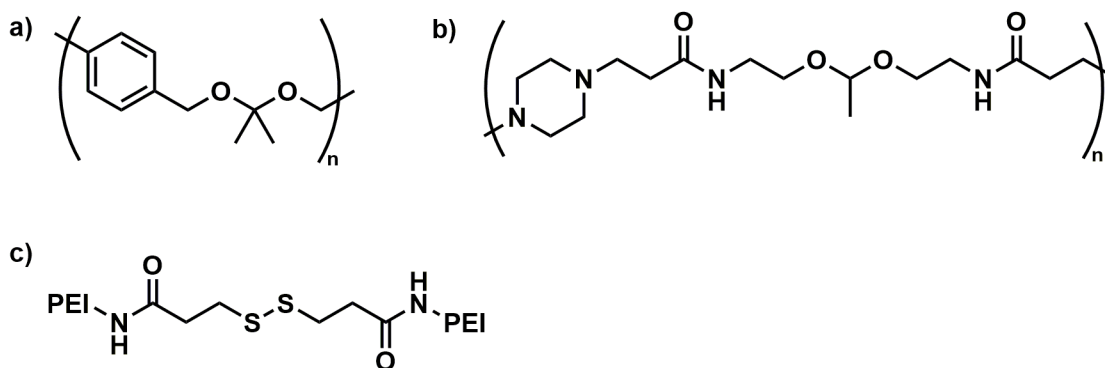


Figure 2.2. Examples of stimuli-responsive degradable polymers: a) polyketal,³¹ b) polyacetal,³³ c) disulphide linker between non-degradable PEI chains.³⁵

In spite of the improvements stimuli-responsive degradable polymers offer over degradable polymers like polyesters and polysaccharides, one potential limitation to these compounds is that they require multiple stimuli mediated bond cleavages in order to fully depolymerize. This may be difficult to achieve in real-world situations where stimuli concentrations and changes in environmental conditions are limited. Stimuli-responsive degradable polymers that can degrade in a controlled fashion after as little as one stimulus mediated bond cleavage would be ideal.

2.4 Self-Immolative Polymers

Self-immolative polymers (SIPs) are a class of degradable polymers characterized by their ability to translate a single bond cleavage event at the polymer terminus or within the backbone into a cascade of reactions that leads to complete depolymerization (Figure 2.3). This mechanism effectively results in an amplification of the stimulus event. Typically, SIPs are either composed of repeating units of self-immolative spacers or backbones with low ceiling temperatures. Our group has characterized the former as “irreversible SIPs” as they depolymerize to small molecules that differ from the monomers from which they were prepared, and can therefore not be repolymerized.³⁶ On the other hand, “reversible” SIPs based on low ceiling temperature backbones depolymerize back to monomers which can be purified and repolymerized under the right conditions. This section will describe how research on SIPs based on self-immolative spacers began by combining multiple spacers

sequentially to form oligomers. Branching versions of these spacers were then combined to develop self-immolative dendrimers. Polymerization of activated self-immolative spacers or low T_c monomers then led to linear and cyclic SIPs with greater synthetic ease. Recent developments have involved hyperbranched and graft copolymer architectures, as well as SIP networks.

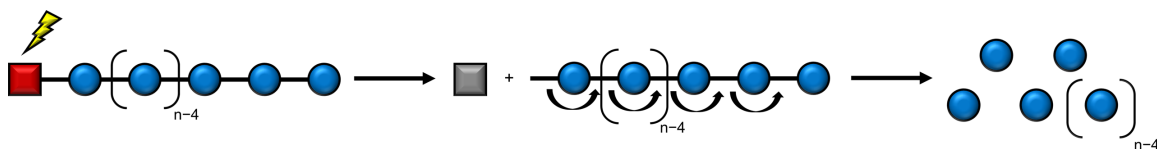


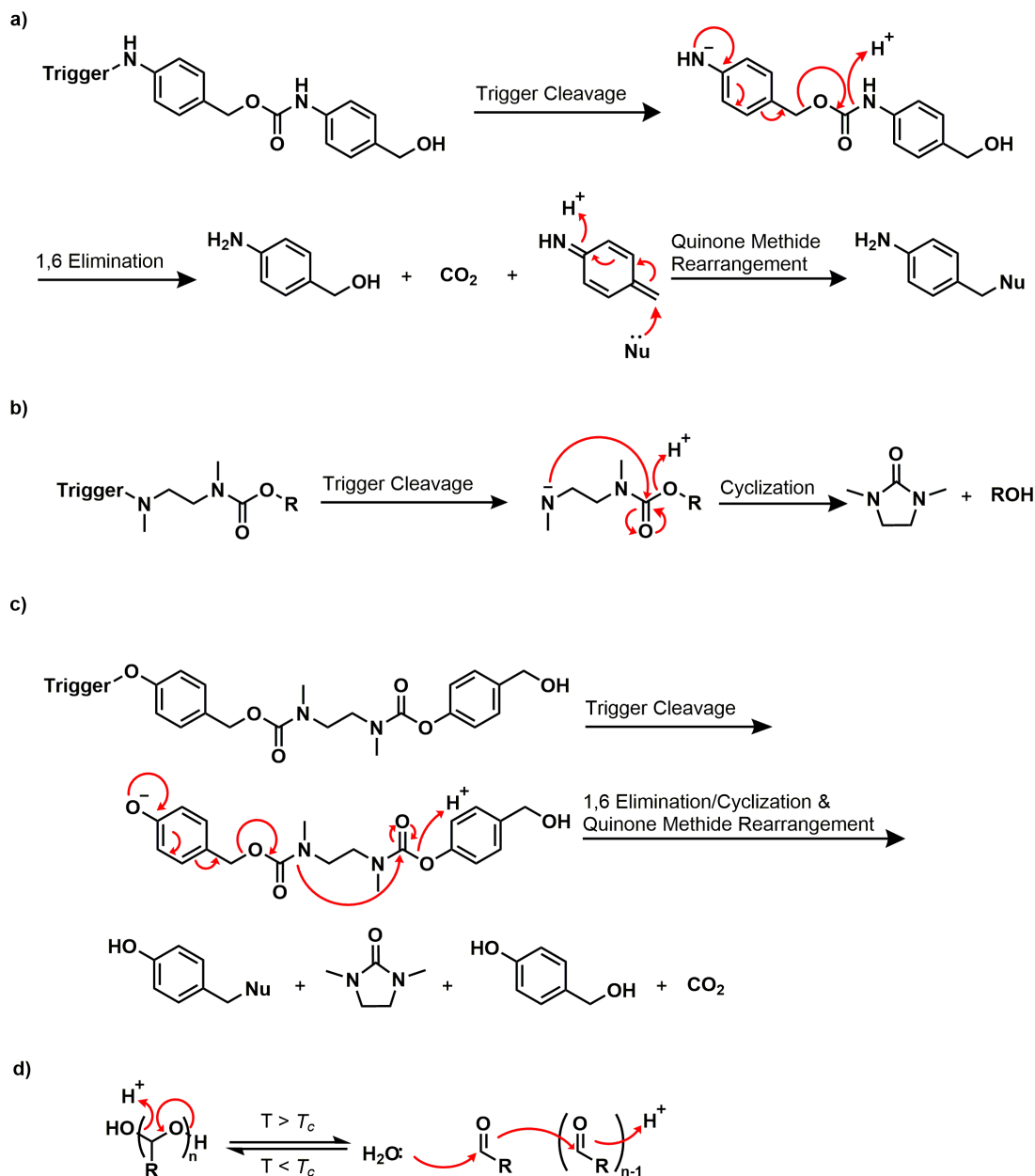
Figure 2.3. Schematic illustrating the triggering and depolymerization of a SIP.

2.4.1 Chemical Foundations for the Development of Self-immolative Materials

2.4.1.1 Self-Immolative Spacers

Originally developed for prodrug chemistry,³⁷ self-immolative spacers are capable of transferring a chemical cleavage event from one end of the spacer to the other. Many of the early spacers employed an electron cascade mechanism. For example, using a 4-aminobenzyl alcohol spacer,³⁸ the initial cleavage event unmasks the electron rich amino group. Electrons from the amino group then participate in a 1,6-elimination to release the 4-aminobenzyl alcohol group and produce an azaquinone methide by-product (Scheme 2.1a). As the hydroxyl of 4-aminobenzyl alcohol is often conjugated via a carbonate or carbamate, its release is then accompanied by the formation of a carbonic or carbamic acid derivative, which decarboxylates to release gaseous CO_2 , providing an additional driving force for the reaction. Spacer variants using other electron rich moieties such as a phenolic group undergo the same mechanism,³⁹ while other variants eliminate using a shorter or longer elimination pathway.⁴⁰⁻⁴¹ Cyclization spacers have also been commonly employed.⁴² Upon cleavage of one terminus, an intramolecular cyclization occurs, producing a cyclic by-product and releasing the moiety at the other terminus. For example, N,N' -dimethylethylenediamine cyclizes on its carbamate derivatives to afford a cyclic urea (Scheme 2.1b). Cyclization spacers can also be used in conjunction with electron cascade

spacers to create a reaction cascade (Scheme 2.1c).⁴³⁻⁴⁴ Self-immolative spacers have been employed in many different architectures as they can be combined through step-wise syntheses or polymerization reactions.



Scheme 2.1. Mechanisms of a) 1,6-elimination of a 4-aminobenzyl alcohol spacer; b) cyclization of a spacer based on *N,N'*-dimethylethylenediamine; c) a sequence of elimination and cyclization reactions; and d) an acid-catalyzed equilibrium between a polyaldehyde and the corresponding aldehyde monomer.

2.4.1.2 Ceiling Temperature

For a given chain polymerization reaction:



where P_x is the growing chain with a degree of polymerization (DP_n) of x and M is a monomer, T_c is defined as the temperature above which high molar mass polymer is not formed.⁴⁵ It is governed by the thermodynamics of the polymerization as described by Equation 2.1. For a reaction to be spontaneous, ΔG must be negative and therefore ΔH must be less than zero and/or ΔS must be greater than zero. Since a polymerization reaction always results in a more ordered system, ΔS is always negative and thus spontaneity of a polymerization depends on ΔH being less than zero. T_c can be mathematically defined as the temperature where $\Delta G = 0$ for the polymerization, and the polymer and monomer are in equilibrium. Therefore, Equation 2.1 can be rearranged to give:

$$\text{Equation 2.4.} \quad T_c = \frac{\Delta H}{\Delta S}$$

Many polymerization reactions have negative ΔH values that are large in magnitude. For example, the polymerization of styrene into polystyrene (PS) relies on the enthalpic change associated with breaking one C=C bond and forming two C-C bonds, which is large and negative. However, the enthalpic change between breaking one C=O bond and forming two C-O bonds in the polymerization of aldehyde monomers to polyacetals is generally only slightly negative, resulting in a low ceiling temperature. Polymers with low T_c can in some cases be polymerized at a low temperature and subsequently stabilized by either cyclization or via the addition of an end-cap, which prevents depolymerization. Depolymerization is triggered by either cleaving the backbone or removing the end-cap. In contrast to self-immolative spacers which have been employed in many different architectures, low T_c polymers have only been employed in polymeric structures as it would be difficult to combine monomers by the step-wise reaction sequences required for the synthesis of well-defined oligomers or dendrimers.

2.4.2 Self-Immolative Oligomers (SIOs)

SIOs are monodisperse, linear sequences of self-immolative spacers with a low DP_n . In 2001, Scheeren and coworkers reported several examples designed to serve as improved spacers in prodrug molecules.⁴⁶ At the time, prodrug spacers were typically single self-immolative moieties that either underwent electron cascades or cyclizations to transfer the cleavage of a stimuli-responsive group called a “specifier” to release the conjugated drug. It was hypothesized that increasing the length of the spacers would reduce steric hindrance effects between the specifier and drug moieties further, allowing for faster enzymatic activation of the specifier. Dimers and trimers of 4-aminobenzyl alcohol elimination spacers linked via carbamates/carbonates, and oligomers consisting of 4-aminobenzyl alcohol elimination spacers connected to a *N,N'*-dimethylethylenediamine cyclization spacer via carbamates were prepared (Figure 2.4). Using enzymatic activation to cleave the specifier, doxorubicin and paclitaxel were indeed released more rapidly using the longer SIOs, with the rate depending on the specific spacer composition and the drug. This chemistry provided the starting point for the development of more complex self-immolative materials.

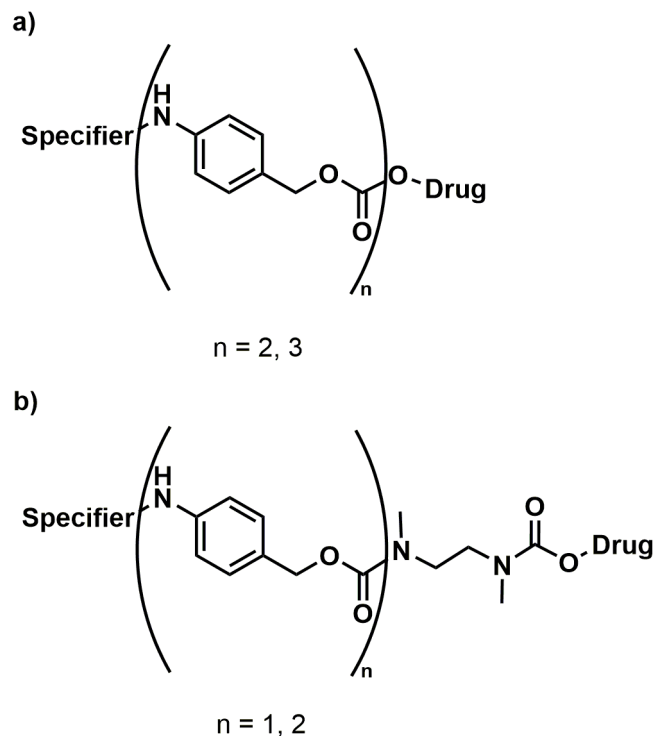


Figure 2.4. Examples of SIOs composed of a) multiple elimination spacers in sequence or b) one or more elimination spacers followed by a cyclization spacer.

The first use of a SIO to amplify a stimulus event was reported several years later by Warnecke and Kratz.⁴⁷ The authors assembled a dimer based on 2,4-bis(hydroxymethyl)aniline. Because each spacer unit possessed two benzylic alcohol derivatives (one *ortho* and one *para* to the amino group), unmasking of the terminal aniline triggered both a 1,6-elimination as well as a 1,4-elimination to occur. The authors attached tryptamine as the pendent group off each unit and at the terminus to serve as a reporter molecule, while the aniline at the other end was masked as a nitro group. Reduction of this nitro group to the aniline triggered a self-immolative cascade that released all of the tryptamine reporters.

Several groups have developed SIOs for different applications. Redy and Shabat reported SIOs for potential theranostic applications.⁴⁸ Phillips and coworkers developed SIOs for point-of-care diagnostic devices.⁴⁹⁻⁵¹ Additionally, Anslyn and coworkers recently reported cyclization-only SIOs that could be chemically sequenced.⁵²

Our group used SIOs to demonstrate the effect of chain length on the depolymerization time.⁵³ Monodisperse SIOs up to octamers were synthesized, based on alternating 4-hydroxybenzyl alcohol and *N,N'*-dimethylethylenediamine spacers linked by carbamates. Deprotection of the *t*-butyloxycarbonyl (BOC) end-cap with trifluoroacetic acid (TFA), followed by increasing the pH to 7, led to depolymerization. The time to 50% degradation was proportional to the length of the oligomers, with longer oligomers taking longer to degrade (Figure 2.5). This observation held true when applied to longer polydisperse SIPs composed of the same self-immolative spacers. Furthermore, the data correlated well with a mixed-mode degradation model that describes the kinetics of linear self-immolation as zero order during the initial degradation but moving to first order as degradation proceeds.

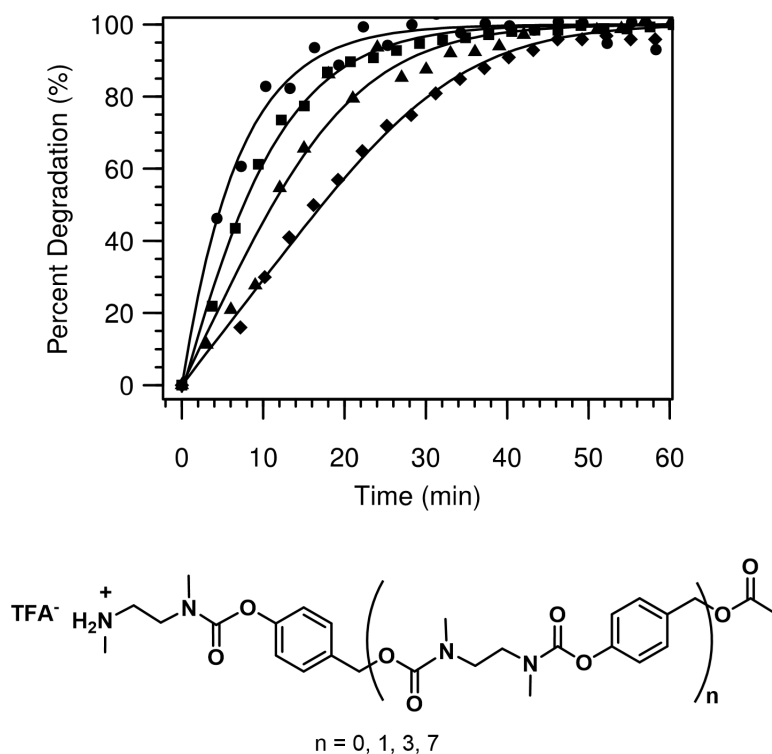


Figure 2.5. Degradation kinetics of monodisperse SIOs measured by ¹H NMR spectroscopy in 0.1 M phosphate buffer (D₂O):acetone-*d*₆ (3:2) at 37°C showing an increase in degradation time with oligomer length: *n* = 0 (●), *n* = 1 (■), *n* = 3 (▲), *n* = 7 (◆). Adapted with permission from ref.⁵³ Copyright 2013 American Chemical Society.

2.4.3 Self-Immolative Dendrimers/Dendrons (SIDs)

Dendrimers and dendrons are monodisperse macromolecules with well-defined branched structures. They are built via stepwise synthesis, with each layer of branching termed a generation. Dendrons refer to examples with a focal point that then branches successively at each generation, resulting in a tree-like architecture. Dendrimers on the other hand are grown from multivalent cores. Each unit of the multivalent core then branches at each generation, creating a globular architecture (Figure 2.6). Dendrimers and dendrons can be synthesized from the focal point or core outwards (divergent synthesis) or from the periphery towards the focal point or core (convergent synthesis). Although they are often referred to as dendrimers, all of the reported examples of SIDs are actually dendrons, as they branch from mono-functional focal points rather than multivalent cores. In 2003, three different groups independently reported the first examples of self-immolative dendrons, each with different backbones.^{40-41, 43}

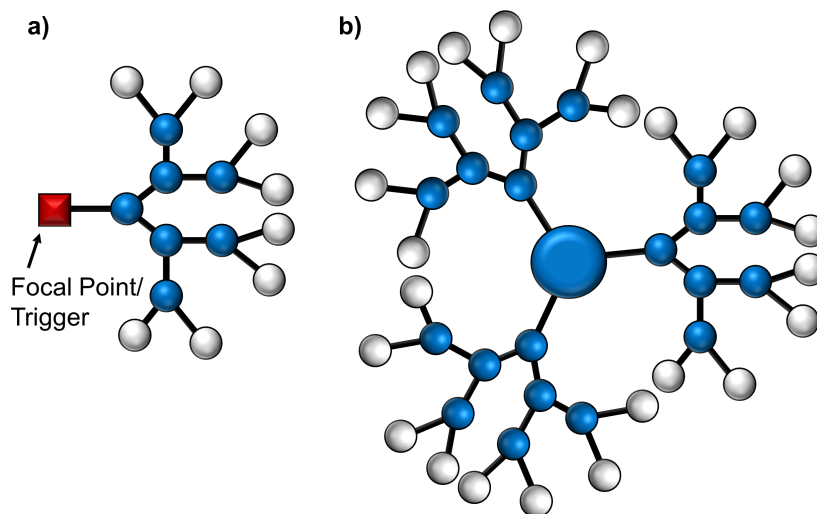


Figure 2.6. Architectural comparison showing a) a dendron and b) a dendrimer.

2.4.3.1 Benzyl Ethers

SIDs based on benzyl ether backbones were first reported by McGrath and coworkers. Originally, the authors reported the convergent synthesis of zeroth- to second-generation dendrons composed of 2-hydroxy-4-(hydroxymethyl)phenol self-immolative spacers with

allyl triggers at the peripheries and a 4-nitrophenol reporter at the focal point.³⁹ Cleavage of the trigger using Pd(PPh₃)₄ and NaBH₄ led to dendron degradation via 1,6-elimination reactions, with the reporter release monitored by ultraviolet-visible (UV-Vis) spectroscopy. Because of the linear degradation pathway, there was a 1:1 relationship between the stimulus event and the reporters. However, later the same year, the group reported dendrons composed of 2,4-bis(hydroxymethyl)phenol repeat units with allyl triggers at the focal points and the 4-nitrophenol reporters at the periphery (Figure 2.7a).⁴⁰ First- and second-generation dendrons were prepared by divergent synthesis and then subjected to allyl deprotection with monitoring of 4-nitrophenol release by UV-Vis spectroscopy. Full degradation via 1,6- and 1,4-elimination pathways was achieved in 15 min for the second generation dendron, with even shorter time required for the first-generation system. Several years later, McGrath and coworkers developed a convergent synthesis for these SIDs.⁵⁴ This synthesis allowed different triggering groups to be installed in the final step. Recently, Kastrati and Bochet developed self-immolative benzyl ether dendrons capable of releasing three species per generation instead of two.⁵⁵

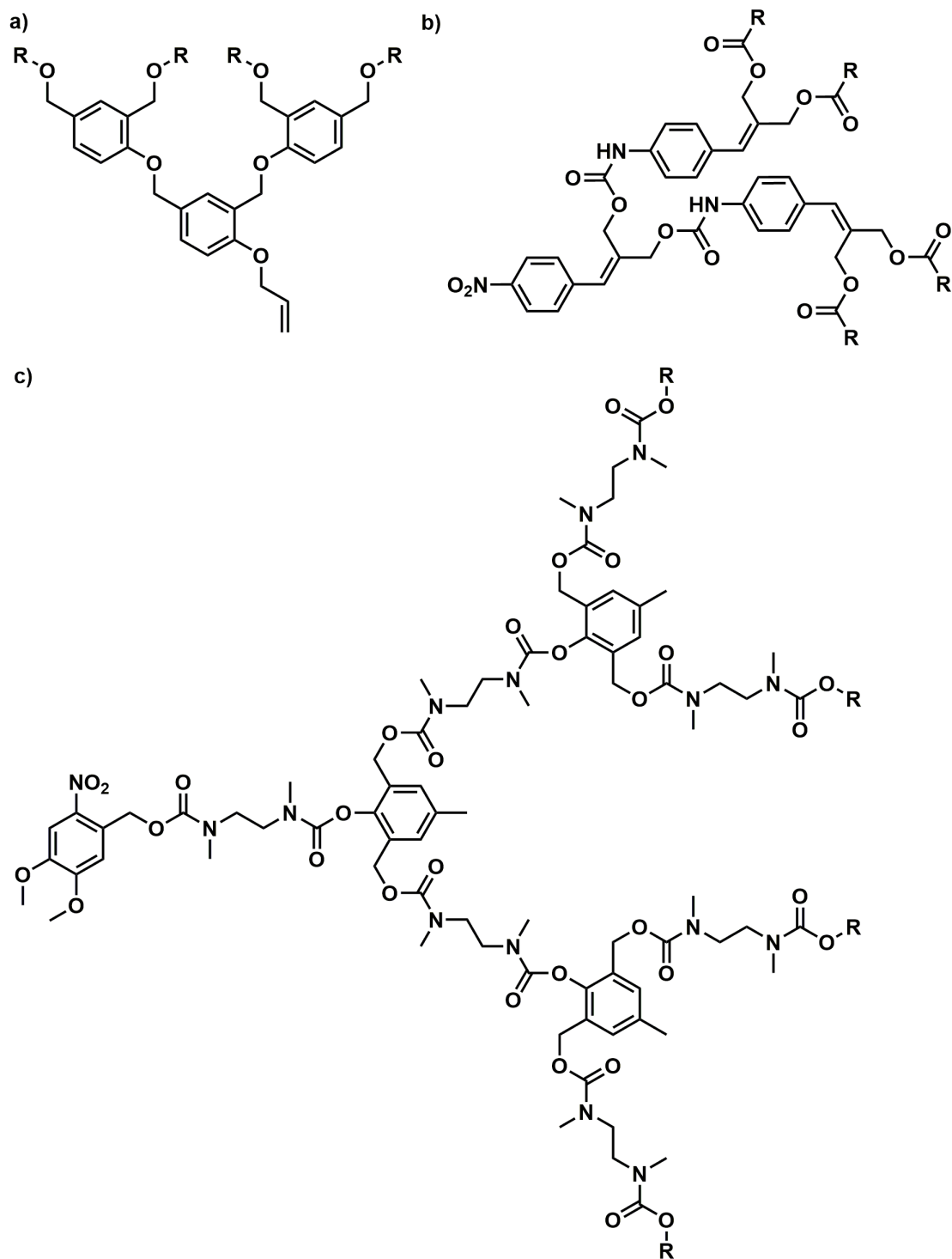


Figure 2.7. Chemical structures of self-immolative a) benzyl ether, b) cinnamyl carbamate, and c) benzyl carbamate dendrons. R = reporter group.

2.4.3.2 Cinnamyl Carbamates/Carbonates

The use of cinnamyl carbamates/carbonates as spacers in SIDs has also been reported, although they have been much less explored than other backbones. de Groot and coworkers divergently synthesized up to second-generation dendrons using 4-aminocinnamyl diol spacers (Figure 2.7b), which allowed for a 1,8-elimination to occur when the nitro group at the focal point of the dendron was reduced to an aniline group.⁴¹ This was the first example involving the incorporation of peripheral drug (paclitaxel) molecules on SIDs, which were released upon focal point triggering. Shabat and coworkers later reported SIDs composed of cinnamyl-based spacers that could be used to amplify a single stimulus event by 6-fold with a single generation.⁵⁶

2.4.3.3 Benzyl Carbamates/Carbonates

Backbones incorporating benzyl carbamate/carbonate spacers have been the most extensively studied in the context of SIDs. These elimination spacers have been used on their own and along with cyclization spacers. Shabat and coworkers reported the first examples of SIDs based on benzyl carbamates.⁴³ *N,N'*-dimethylethylenediamine was used as a cyclization spacer and 2,6-bis(hydroxymethyl)-*p*-cresol was used as an elimination spacer (Figure 2.7c). For self-immolation to occur, a focal point photocleavable trigger connected to the cyclization spacer was cleaved, followed by cyclization and the unmasking of a hydroxy moiety on the elimination spacer. 1,4-Elimination of the two benzyl carbamates followed by a loss of CO₂ then occurred and this sequence of cyclization and elimination reactions propagated to the dendron's periphery where aminomethylpyrene reporters were released. Degradation was monitored by high performance liquid chromatography and the rate-determining step was found to be the cyclization. While first- and second-generation dendrons were successfully synthesized, attempts to prepare the analogous third-generation dendrons were unsuccessful. Changing the peripheral reporters to less sterically bulky 4-nitroaniline groups allowed the third-generation dendrons to be synthesized. This result highlighted one of the challenges with the dendrimer/dendron architecture, which is that many systems cannot be synthesized to high generations, so the ultimate degree of amplification can in some cases be limited based

on the molecules that can be synthesized. Nevertheless, many examples illustrating the potential utility of SIDs based on benzyl carbamate/carbonate spacers have been reported.

Shabat and coworkers followed up their initial report with dendritic prodrugs triggered by the catalytic antibody 38C2.⁵⁷ These first-generation SIDs had either two molecules of doxorubicin, two molecules of camptothecin, or one of each at their peripheries, with the best performance obtained from the heterodimeric dendritic prodrug that released doxorubicin and camptothecin upon self-immolation. The authors later reported trimeric dendritic prodrugs utilizing a slightly altered elimination spacer (2,4,6-tris(hydroxymethyl)phenol) and the same enzymatic trigger.⁵⁸ Almutairi's group also reported a SID capable of releasing L-glutamic acid upon exposure to light by using a two-photon near-infrared (NIR) light responsive trigger group.⁵⁹

Shabat's group further used SIDs to demonstrate the concept of chemical antennas and amplifiers. In the antenna approach, zeroth- to second-generation SIDs were convergently synthesized with the reporter molecule at the focal point and sensors at the periphery.⁶⁰ They used a diethylenetriamine cyclization system with carbamate linkages, with a 4-hydroxybenzyl alcohol elimination spacer also being utilized in the second-generation. This cyclization linker allowed cleavage at any sensor molecule to be propagated to the focal point. Sensors receptive to penicillin-G-amidase (PenGA) and a 4-nitrophenol reporter molecule were used. Shabat's group later extended the system to possess more than one kind of sensor moiety. This development allowed for a molecular "OR" logic gate to be built into a prodrug, where either sensor could cause the dendron to fragment, releasing a drug molecule at the focal point.⁶¹ In contrast to the antenna approach involving the release of a focal point molecule, the amplifier approach involved the release of peripheral molecules.⁶² A PenGA-cleavable moiety was used at the focal point trigger while 4-nitrophenol and 6-aminoquinoline were conjugated to the periphery to serve as absorbance and fluorescence probes, respectively. Self-immolation resulted in the release of both probe molecules simultaneously. Systems incorporating both antenna and amplifier properties were also prepared.⁶³

SIDs have also been constructed from benzyl carbamates/carbonates and no cyclization spacers and it was shown that removal of the cyclization spacers led to more rapid degradation.⁶⁴ A first-generation dendron was divergently synthesized using the elimination spacer 2,4,6-tris(hydroxymethyl)aniline, with PenGA as the focal point trigger and tryptophan as peripheral reporter molecules. The release of tryptophan from this dendron was compared to that from an analogous previously reported dendron containing a cyclization spacer.⁵⁸ The dendron containing the cyclization spacer required about 4 days to fully degrade, whereas the system without the cyclization spacer required only 40 min. The authors then synthesized the analogous two dendrons with the anticancer drug melphalan at their peripheries. Both dendrons exhibited lower toxicity than the free drug when not triggered to degrade. Triggering of the prodrug with the cyclization spacer system increased its toxicity, but the toxicity was still less than that of the free drug. However, the rapid release of drug from the dendron with no cyclization spacers produced a toxicity approximately equal to the free drug. This work therefore demonstrated that the rate of backbone degradation can ultimately affect the properties of dendritic prodrugs. The rapidly degrading dendrons composed of only elimination spacers were also studied as sensors of the explosive triacetone triperoxide.⁶⁵ More recently, Wu and coworkers reported a theranostic SID that released both a drug and two-photon NIR fluorophore reporter molecule to visualize drug release in the body.⁶⁶ The effectiveness of the theranostic was verified in an *in vivo* study where the liposome-encased dendron was injected into tumours in mice, resulting in tumour shrinkage along with a visible fluorescent signal.

To address the challenge of synthesizing high generation dendrons to achieve high degrees of amplification, Shabat and coworkers cleverly introduced dendritic amplification via chain reactions.⁶⁷⁻⁷⁰ Dendrons were constructed to be triggered by molecules that were released from the dendron peripheries upon self-immolative degradation. Thus, one stimulus event would not just trigger the depolymerization of one dendron but potentially all of them. First-generation dendrons were constructed using a 2,4,6-tris(hydroxymethyl)phenol spacer, with an arylboronic acid trigger responsive to H₂O₂ at the focal point.⁶⁷ One peripheral moiety was the reporter molecule (4-nitroaniline) while the other two molecules (choline) could be oxidized by choline oxidase to produce more

H₂O₂. Further work included the use of methanol and alcohol oxidase to improve the stability of the system and consequently signal to noise,⁶⁸ the use of separate probes that released single reporter molecules in response to the H₂O₂ generated from the dendritic chain reaction,⁶⁹ and a dendritic chain reaction system sensitive to thiols rather than H₂O₂.⁷⁰

Overall, the major advantages of SIDs include their well-defined structures afforded by step-wise synthesis as well as their abilities to release multiple peripheral groups in response to a single triggering event at the focal point. Their branched structures also afford antenna capabilities. Limitations in terms of preparing high generation dendrons were addressed to a significant extent by the dendritic chain reaction amplification concept introduced by Shabat. However, dendrimers still involve multi-step synthesis, which would be challenging for many industrial-scale applications. In addition, the relatively low molar masses of dendrons means that their physical properties (e.g., thermal, mechanical) are likely more similar to those of small molecules than polymers, although they have not been studied to any significant extent. These aspects motivated extensive interest in SIPs over the past decade.

2.4.4 Self-Immolative Linear Polymers

Compared to oligomers and dendrimers, SIPs typically have polymeric thermal and mechanical properties, and can be synthesized via one-step polymerization reactions. These potential advantages come at the cost of introducing dispersity (D) in DP_n but often this can be kept low enough to obtain similar properties and performance between batches. Several different polymer architectures have been described to date. Linear SIPs are by far the most common, and several different backbones have been reported (Figure 2.8).

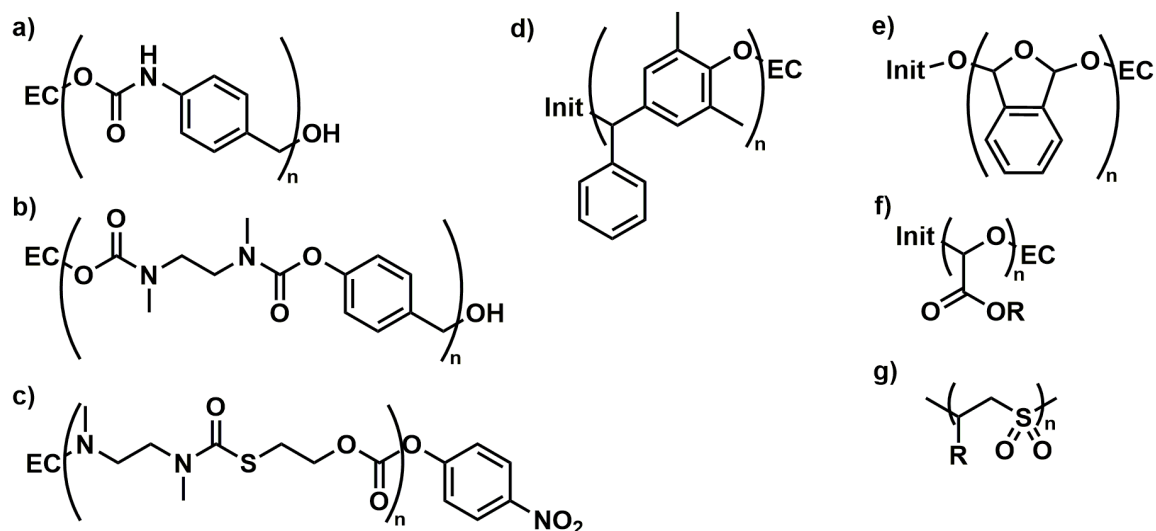


Figure 2.8. General chemical structures of the major classes of linear SIPs: a) PBCs, b) PBCs containing cyclization spacers, c) cyclization-only SIPs, d) PBEs, e) PPAs, f) PGs, g) POSs. EC = end-cap; Init = polymerization initiator; R corresponds to variable pendent groups.

2.4.4.1 Poly(benzyl carbamates/carbonates) (PBCs)

The first example of a linear SIP was reported by Shabat and coworkers in 2008.³⁸ The authors constructed their polymers from 4-aminobenzyl alcohol linked via carbamates (Figure 2.8a). A step-growth polymerization produced the PBCs with DP_n of 15–20 units with a D of about 2. To demonstrate their self-immolative properties and amplification capabilities, *o*-acrylate substituents were introduced on every spacer and an end-cap sensitive to bovine serum albumin (BSA) was installed. The substituents allowed for each spacer to be converted to a fluorophore once released during self-immolation. Incubation of the polymer with BSA in phosphate buffered saline solution produced a visible fluorescence signal over 10 h. Following this initial report, Shabat's group reported polymers constructed from 4-aminobenzyl alcohol spacers with an *o*-substituent that could undergo 1,6-elimination and release 4-nitroaniline reporter molecules during self-immolation.⁷¹ An SIP consisting of approximately 11 units was triggered to degrade in organic media, releasing reporters over 48 h. Ionizable pendent acrylate *o*-substituents were introduced to every second spacer to impart water solubility.

Elimination spacers such as 4-aminobenzyl alcohol produce quinone methide by-products during self-immolation. These by-products are reactive towards nucleophiles such as the solvent or from other sources. This reactivity was harnessed by Shabat and coworkers to create PBCs that were capable of selectively labelling enzymes.⁷² SIPs based on 4-aminobenzyl alcohol spacers have also been employed by Moore and coworkers to generate microcapsules for potential self-healing materials.⁷³ They were also incorporated by Liu and coworkers into block copolymers for the preparation of polymersomes.⁷⁴ Using end-caps responsive to UV light, visible light, or reductive conditions, the polymersomes could be triggered to degrade, releasing their cargo. Furthermore, by encapsulating different enzymes, inhibitors, and/or reagents in different types of polymersomes, systems could be designed with “AND”, “OR”, or “XOR” logic gates. Recently, Thayumanavan and coworkers used PBCs with pendent carboxylic acids to form polymersomes via polyion complexation with poly(diallyldimethylammonium chloride) and horse radish peroxidase was encapsulated into the polymersomes.⁷⁵ Depolymerization triggered by UV light led to breakdown of the complexes, disintegration of the polymersomes, and release of the enzyme, which subsequently catalyzed the formation of a hydrogel. Furthermore, Shabat’s group described poly(benzyl carbonate)s that exhibit chemiluminescence upon self-immolation, with responsiveness to fluoride ions, palladium catalysts, or H₂O₂.⁷⁶

As with oligomers and dendrimers based on benzyl carbamates/carbonates, cyclization linkers could also be incorporated into linear SIPs. The first such SIP containing alternating elimination and cyclization spacers was reported by our group in 2009 (Figure 2.8b).⁴⁴ The PBCs were constructed using 4-hydroxybenzyl alcohol as the elimination spacer and *N,N*-dimethylethylenediamine as the cyclization spacer. A BOC group served as the end-cap and the polymer had a number average molar mass (M_n) of 17 kg/mol. After BOC group cleavage and neutralization, the polymer degraded over 4–5 days. A poly(ethylene glycol) (PEG) end-cap linked to the polymer by an ester linkage could also be incorporated, yielding a block copolymer that self-assembled to form nanoparticles. The assemblies could encapsulate and release Nile red over about 2 weeks as the hydrophobic PBC block depolymerized. Almutairi and coworkers also incorporated UV-sensitive and NIR-sensitive end-caps onto these PBCs and used them to prepare nanoparticles that could be triggered with light to release Nile red.⁷⁷ In addition, our group showed that by replacing

the *N,N'*-dimethylethylenediamine with *N*-methylaminoethanol or 2-mercaptoethanol, the rates of the corresponding cyclization reactions could be increased, accelerating the depolymerization rate.⁷⁸ Thus, the introduction of cyclization spacers allowed the rates of polymer degradation to be tuned.

2.4.4.2 Cyclization-Only Polymers

A few examples of linear SIPs depolymerizing entirely by cyclization reactions have been reported. For example, in 2010 our group reported a polymer constructed from two different cyclization spacers, *N,N'*-dimethylethylenediamine and 2-mercaptoethanol, linked with carbamate and thiocarbamate bonds (Figure 2.8c).⁷⁹ A dimeric monomer composed of the two cyclization spacers was polymerized in a step-growth reaction and end-capped with a disulfide to yield a polymer with an M_n of 1800 g/mol. After cleavage of the end-cap with dithiothreitol (DTT), the polymer depolymerized over 14 days. A fraction of the polymer (approximately 20%) would not degrade even in the presence of DTT, indicating that some cyclic polymers without end-caps were likely formed during the polymerization.

A few years later, Li and coworkers reported another cyclization spacer-based SIP.⁸⁰ Polymerization was achieved in a step-growth reaction via the Passerini reaction of a monomer possessing an aldehyde and a carboxylic acid function group at either end of the molecule with an isocyanide. Post-polymerization hydrogenation of the Passerini reaction products yielded polymers with a poly(4-hydroxybutyrate) backbone. A model polymer ($M_n = 6700$ g/mol) was then investigated for depolymerization at different pH values. At acidic pH, a combination of random chain scission and head-to-tail cyclization reactions resulted in polymer degradation, with the latter dominating. Full degradation at 37 °C was achieved in 144 h when the polymer was dissolved in a $CDCl_3$:DCl mixture. At neutral pH, degradation was much slower as only the head-to-tail cyclization mechanism occurred.

2.4.4.3 Poly(benzyl ether)s (PBEs)

PBEs (Figure 2.8d) are low T_c SIPs based on the linkages used in McGrath's SIDs.³⁹⁻⁴⁰ The ether linkages convey higher stability to these polymers against heat, acid, and base

compared to other more labile backbone linkages such as carbamates and carbonates. Unlike McGrath's SIDs that depolymerized into small molecules that were different from the original monomers, PBEs depolymerized back into their original monomer units, providing a means of recycling the polymers at their end-of-life.⁸¹ Although prior work had been conducted on linear PBEs,⁸² the first triggerable examples were reported by Phillips and coworkers in 2013.⁸³ Quinone methide monomers were polymerized by anionic polymerization from alcohol initiators, then terminated with either acid (to produce an alcohol "end-cap" sensitive to base) or with several different end-caps that could be cleaved with stimuli such as fluoride ions, palladium catalysts, base, or UV light. Polymers with M_n values as high as 484 kg/mol could be synthesized. They depolymerized rapidly over a few hours in a head-to-tail manner upon cleavage of the end-cap.

It has been possible to modify the pendent groups on PBEs. For example, Phillips and coworkers incorporated tri(ethylene glycol) or fluoroalkyl groups to impart different physical and mechanical properties.⁸¹ Ergene and Palermo incorporated alkene pendent groups to click on PEG or cationic moieties via thiol-ene chemistry, thus producing degradable antibacterial polymers.⁸⁴⁻⁸⁵ To improve solid-state depolymerization of PBEs, Phillips and coworkers synthesized and polymerized monomers with masked phenol moieties off of each pendent group.⁸⁶ Unmasking of a phenol by a stimulus event caused a cascading depolymerization of the portion of the polymer downstream from the unmasked monomer. This approach effectively increased the number of triggerable groups on the solid surface, accelerating the depolymerization rate of the solid. Zhang's group expanded on these polymers further by linking a masked 2-mercaptoethanol spacer to the phenol moiety on every pendent chain via a carbonate linkage.⁸⁷ Unmasking of the thiol with a reducing agent resulted in cyclization and subsequent downstream degradation of the PBE.

2.4.4.4 Polyphthalaldehydes (PPAs)

PPAs (Figure 2.8e) are low T_c polyacetals first synthesized and investigated in the late 1960s.⁸⁸⁻⁸⁹ Anionic and cationic synthetic routes can be employed to synthesize PPAs, leading to linear or cyclic polymers respectively. Here we focus on the linear PPAs, while cyclic PPAs will be covered in the section on cyclic SIPs. Through the incorporation of

stimuli-responsive end-caps, which had not been used in the early examples, Phillips and coworkers suggested linear PPAs as a new class of SIPs in 2010.⁹⁰ Phthalaldehyde (PA) was polymerized by a slow chain-addition mechanism using *n*-butyl lithium as an initiator and end-caps responsive to fluoride ions, palladium catalysts, or no stimulus (control) were incorporated. The use of a phosphazene base and alcohol initiators was later demonstrated to afford a more rapid polymerization.⁹¹ Depolymerization was fast, with full degradation in about 5 min at room temperature after triggering. The resulting PPAs were used in the construction of self-powered microscale pumps, where triggering of depolymerization by fluoride ions (model analyte) resulted in the release of a high concentration of soluble monomer above the polymer film.⁹² The high monomer concentration caused the movement of the water towards the film via osmosis, then radially away from the surface of the film, enabling the movement of microscale polymer beads. The pump was further extended to respond to the enzyme β -D-glucuronidase (a specific marker for *E. coli*) by synthesizing a separate self-immolative spacer capable of releasing fluoride ions upon activation by the enzyme. PPAs were also used by Phillips and coworkers to produce core-shell microcapsules.⁹³

Despite their relatively high stability under neutral conditions at room temperature while end-capped, PPAs are prone to degrade when exposed to mechanical force, acid, or elevated temperatures. This phenomenon is a result of their polyacetal backbone, which can undergo a random chain scission producing an unstable hemiacetal terminus that allows depolymerization to occur. While instability may be an issue in some applications, it can be seen as another avenue to trigger depolymerization. For example, Duerig and coworkers developed PPAs as thermally-patternable masks for lithography.⁹⁴⁻⁹⁵ In one instance, a 4 nm thick "soft" mask of PPA was spin-coated onto a stack of "hard" masks previously spin-coated onto a Si wafer.⁹⁶ A pattern was then transferred to the PPA layer via the heated tip of a cantilever. Subsequent reactive ion etching allowed for transfer of the pattern into the hard mask layers and eventually into the Si wafer itself. More recently, thermal lithography with PPAs was used to create nanofluidic rocking motors for nanoparticle separation.⁹⁷ To increase the thermal stability of PPA, Phillips and coworkers synthesized poly(4,5-dichlorophthalaldehyde), based on the hypothesis that electron-withdrawing chloride groups *para* to the benzylic acetals would disfavor oxocarbenium

intermediates, that are involved in nonspecific backbone degradation.⁹⁸⁻⁹⁹ The polymers could be laser sintered to form three-dimensional objects that could be selectively degraded by stimuli such as palladium or fluoride, which cleaved the polymer's end-caps.⁹⁸

2.4.4.5 Polyglyoxylates (PGs)

PGs are another class of low T_c polyacetals (Figure 2.8f). Without stabilization afforded by an end-cap or cyclic structure, PGs depolymerize back into their constituent monomers at room temperature. Similar to PPAs, PGs were also reported decades ago, with early examples involving non-responsive PG salts,¹⁰⁰ poly(methyl glyoxylate)¹⁰¹ and poly(ethyl glyoxylate) (PEtG)¹⁰² as potential biodegradable polymers. One attractive feature of PGs is the fact that glyoxylate monomers produced by depolymerization can undergo further hydrolysis to form glyoxylic acid hydrate and a corresponding alcohol. For monomers such as ethyl glyoxylate, the by-products should be non-toxic and integrate back into the environment through metabolic processes of microorganisms.¹⁰³⁻¹⁰⁴ Through the incorporation of stimuli-responsive end-caps, our group introduced PGs as SIPs in 2014.¹⁰⁵ While ethyl glyoxylate is commercially available, other glyoxylate monomers were prepared from readily available starting materials such as fumarates and maleates. The monomers were homopolymerized and copolymerized with ethyl glyoxylate via a chain-growth mechanism using catalytic triethylamine. Triggering of the UV-sensitive end-caps with light led to rapid depolymerization in solution (~70% after one day). Solid state depolymerization of PEtG films in an aqueous environment proceeded more slowly, over about 17 days. While triethylamine served as a proton transfer agent, we were able to perform anionic polymerization of ethyl glyoxylate using *n*-butyl lithium or lithium alkoxides as initiators.¹⁰⁶ Additionally, Hewitt and Grubbs recently demonstrated that PEtG can be synthesized from either alcohol or thiol initiators using triethylamine as a proton transfer agent.¹⁰⁷

Several other developments have demonstrated the versatility of PGs. The incorporation of different end-caps has allowed depolymerization to be initiated with different stimuli including heat, H₂O₂, and DTT among others, while mechanical force could cleave the backbone of high molar mass PEtG.^{105, 108-109} PEtG has also been incorporated into triblock

copolymers with PEG (PEG-PEtG-PEG), which could be self-assembled to form nanoparticles and vesicles to encapsulate cargo and release it in response to stimuli.¹⁰⁹⁻¹¹¹ Nanoparticles prepared from blends of PLA with PEtG were also prepared by emulsion processes.¹¹² Furthermore, PEtG films have been investigated as a traceless photodegradable coatings for lithography,¹¹³ smart packaging materials for food,¹¹⁴ and as smart coatings for fertilizer pellets when blended with PLA or PCL.¹¹⁵⁻¹¹⁶ While PEtG has a low glass transition temperature (T_g) of about -9 °C and is in a tacky, rubbery state at room temperature, blending with PLA or PCL produced thermal and mechanical properties intermediate between the PEtG and the polyester, depending on the blend ratio.¹¹⁵ Post-polymerization transesterification of PEtG to convert it into other PGs has also been explored by our group in order to obtain a library of PGs with varying properties without having to first synthesize and purify the corresponding monomers.¹¹⁷ Furthermore, transesterification allows for the introduction of functional groups, such as alkynes, that would be otherwise difficult to synthesize as glyoxylate monomers due to the ozonolysis step often involved in their preparation.

More recently, we reported that polyglyoxylamides (PGAMs) could be synthesized via post-polymerization amidation of PEtG.¹¹⁸ PGAMs have very different properties than PGs, with hydrogen bonding leading to higher T_g values (e.g. 85 °C for poly(ethyl glyoxylamide)) and higher water solubility. Ree and coworkers recently demonstrated the potential of PGAMs as clathrate hydrate inhibitors for deep sea oil and gas lines.¹¹⁹ Furthermore, we have used the PGAM platform to synthesize thermo-responsive graft copolymers using amine-terminated oligo(ethylene glycol)s.¹²⁰ These developments and others regarding PGAMs will be discussed at length in the later chapters of this thesis.

2.4.4.6 Poly(olefin sulfone)s (POSs)

POSs are alternating copolymers polymerized from SO_2 and vinyl monomers (Figure 2.8g). Like PPAs and PGs, POSs degrade back into their monomers when triggered. However, unlike the linear polyacetals, POSs are not stabilized with end-caps. Instead, depolymerization proceeds following random backbone scission at one of the weak C–S bonds. Such a backbone cleavage can be induced by either a radical mechanism,¹²¹ making

these polymers sensitive to radical species and radiation that produces radicals, or via an E2 mechanism, making these polymers sensitive to basic conditions.¹²² POSs are polymerized in a chain-growth manner via a radical mechanism, providing high functional group tolerance, contrasting with PPAs and PGs, which are both polymerized via anionic or cationic mechanisms. Initially, POSs were investigated in the 1970s as photoresists for lithography that produced gaseous by-products upon depolymerization.¹²³⁻¹²⁴ Depolymerization could be induced by exposure to UV light or an electron beam. However, they exhibited low thermal stability, which was problematic for lithography applications.¹²⁵ More recently, Moore and coworkers showed that their thermal stability could be tuned by varying the pendent groups.¹²⁶

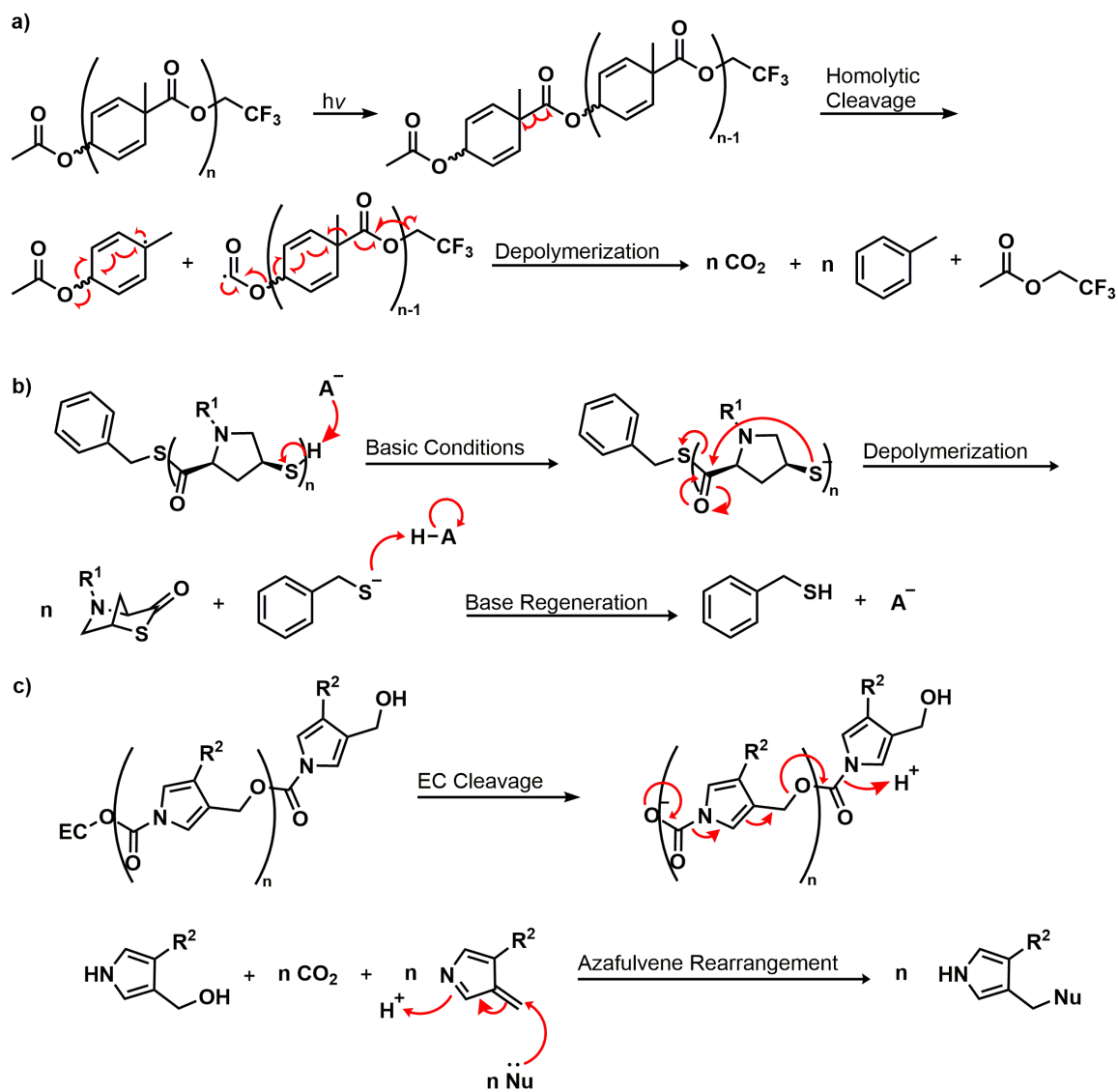
In recent years, POSs have been applied as depolymerizable components in different smart polymer applications. For example, Lobez and Swager used the sensitivity of POSs to radiation in order to construct a sensor device for γ radiation in 2010.¹²⁷ Goodwin and coworkers studied the depolymerization of poly(vinyl acetate sulfone)s by different stimuli including UV light, pH change, reactive oxygen species, and mechanical stimulation and used them to prepare nanoparticles for potential drug delivery applications.¹²⁸⁻¹²⁹ In the case of the mechanical stimulus, the observation that depolymerization continued even after ultrasonication stopped provided evidence for a self-immolative depolymerization mechanism.

2.4.4.7 Other Linear Backbones

While most work on linear SIPs has so far involved the aforementioned backbones, a few new backbones have been recently reported. These backbones are highlighted below.

In 2019, Willson and coworkers reported a poly(benzyl ester) for lithography applications (Scheme 2.2a).¹³⁰ The polymer was synthesized from a benzyl ester monomer with a phenol at one end of the molecule and an activated trifluoroethyl ester at the *para* position of the ring. Step-growth polymerization involved the production of a phenoxide by reaction with *n*-butyl lithium and crown ether, followed by polymerization to produce trifluoroethanol, which was removed from the reaction via an azeotropic distillation with toluene, driving the reaction forward. *Cis* forms of the monomer produced lower molar

mass polymers ($M_n = 7.1$ kg/mol) with oligomeric cyclic by-products. *Trans* monomers, on the other hand, produced a higher M_n of 19 kg/mol. The polymer was susceptible to UV-light induced depolymerization, proposed to occur via a homolytic cleavage between the α carbon and carbonyl carbon on the backbone. The produced radicals could then cascade through the backbone, leading to depolymerization and the production of toluene and CO₂. Studies were performed to validate that the photolysis of the polymer occurred by a Norrish type I like reaction. However, it is not yet validated that depolymerization occurred by a reaction cascade through the polymer backbone as opposed to multiple photolytic cleavages.



Scheme 2.2. a) Structure and proposed degradation mechanism of a poly(benzyl ester). b) Structure of a polythioester that depolymerizes back to bicyclic monomer in basic conditions via cyclization reactions (R^1 corresponds to variable pendent carbamate groups and A^- is a base). c) Structure of a polycarboxypyrrole that depolymerizes into CO_2 and an azafulvene by-product (R^2 corresponds to variable pendent groups).

Lu and coworkers recently reported a self-immolative polythioester backbone (Scheme 2.2b).¹³¹ Cyclic *N*-substituted *cis*-4-thia-*L*-proline thiolactone monomers derived from 4-hydroxyproline were synthesized in a one-pot procedure. The bicyclic nature of the thioester monomers added enough ring strain to drive the polymerization reaction forward

while the structure of the backbone prevented transthioesterification chain transfer reactions due to steric hindrance. The authors prepared three different monomers, each with a different carbamate functional group off the ring nitrogen. Controlled ring-opening polymerizations were conducted with benzyl mercaptan as an initiator and triethylamine or 1,8-diazabicyclo[5.4.0]undec-7-ene (DBU) as the base catalyst. Polymers with M_n values as high as 226 kg/mol were targeted and were synthesized with very low D values of 1.03–1.32. The authors were also able to synthesize block copolymers from different monomers by sequential monomer addition. Depolymerization of the polymers was induced by exposing the polymers to dilute base, with heating increasing the rate of depolymerization. ^1H NMR spectroscopy revealed a regeneration of the cyclic monomers while SEC showed a gradual shift to later elution times. This evidence suggested that the polymers depolymerized via a head-to-tail mechanism rather than by random chain scission. Using the strong base DBU and heating at 50 °C, the authors achieved quantitative monomer regeneration in as little as 2 min. The authors also recently extended their polymerization to β -thiolactone monomers derived from penicillamine.¹³²

Phillips and coworkers recently reported self-immolative polycarboxypyrroles (Fig, 9c).¹³³ These SIPs were inspired by PBCs and share a similar depolymerization mechanism. The authors sought to create polymers with less aromatic repeat units in order to decrease their stability and thus increase their depolymerization rate. Step-growth polymerization of pyrrole monomers functionalized with a phenyl carbamate and an alcohol group was achieved by heating at 60 °C with catalytic amounts of DBU. Alcohol-functionalized end-caps sensitive to H_2O_2 or $\text{Pd}(0)$ were incorporated providing polymers with M_n of ~5 kDa. Following triggering with H_2O_2 or $\text{Pd}(0)$, depolymerization in THF was achieved in ~40 min. To test their hypothesis regarding aromaticity and the depolymerization rate, the authors also synthesized the more aromatic polycarboxyindole. Depolymerization under identical conditions as the analogous polycarboxypyrrole resulted in a 12-fold rate decrease, supporting the hypothesis. Finally, the authors constructed discs of polycarboxylpyrrole and submerged them in acetonitrile solutions. When the appropriate stimulus was present, the discs depolymerized within 9 h, while no solid-state depolymerization occurred in the absence of stimulus.

2.4.5 Cyclic Self-Immolative Polymers

Cyclic SIPs have also been developed and studied. Cyclic polymers can exhibit different properties than their linear analogues such as a more compact structures for the same molecular mass and lower intrinsic viscosity.¹³⁴ However, these aspects have not been the focus of research on cyclic SIPs so far. Instead, most work has focused on their chemistry. Compared to linear SIPs, cyclic SIPs by definition do not possess stabilizing end-caps. Instead, the cycle itself chemically stabilizes the structure as there are no polymer termini from which depolymerization can initiate. As a result, these polymers are usually metastable and any stimulus that breaks the cyclic structure initiates depolymerization.

2.4.5.1 Cyclic Polyphthalaldehydes (cPPAs)

The cyclic structure of cPPAs was suspected for many years but was only definitively confirmed by Moore's group in 2013 (Figure 2.9a).¹³⁵ The authors cationically polymerized PA with Lewis acids such as boron trifluoride etherate ($\text{BF}_3 \cdot \text{OEt}_2$) to yield cPPAs with M_n values as high as 109 kg/mol and D values ranging from 1.6–4.5. In contrast with the anionic polymerization of PA, no end-capping was necessary to isolate stable polymers. Analyses by NMR spectroscopy, matrix-assisted laser absorption ionization time-of-flight mass spectrometry (MALDI-TOF MS), and SEC were consistent with cyclic structures. The authors also demonstrated that the cPPAs could be reopened with the addition of a Lewis acid catalyst, allowing the cycles to be grown or shrunk by adding or removing monomer respectively. This property was exploited in a follow-up study by Moore and coworkers to create random and multiblock copolymers out of different cPPA homopolymers.¹³⁶

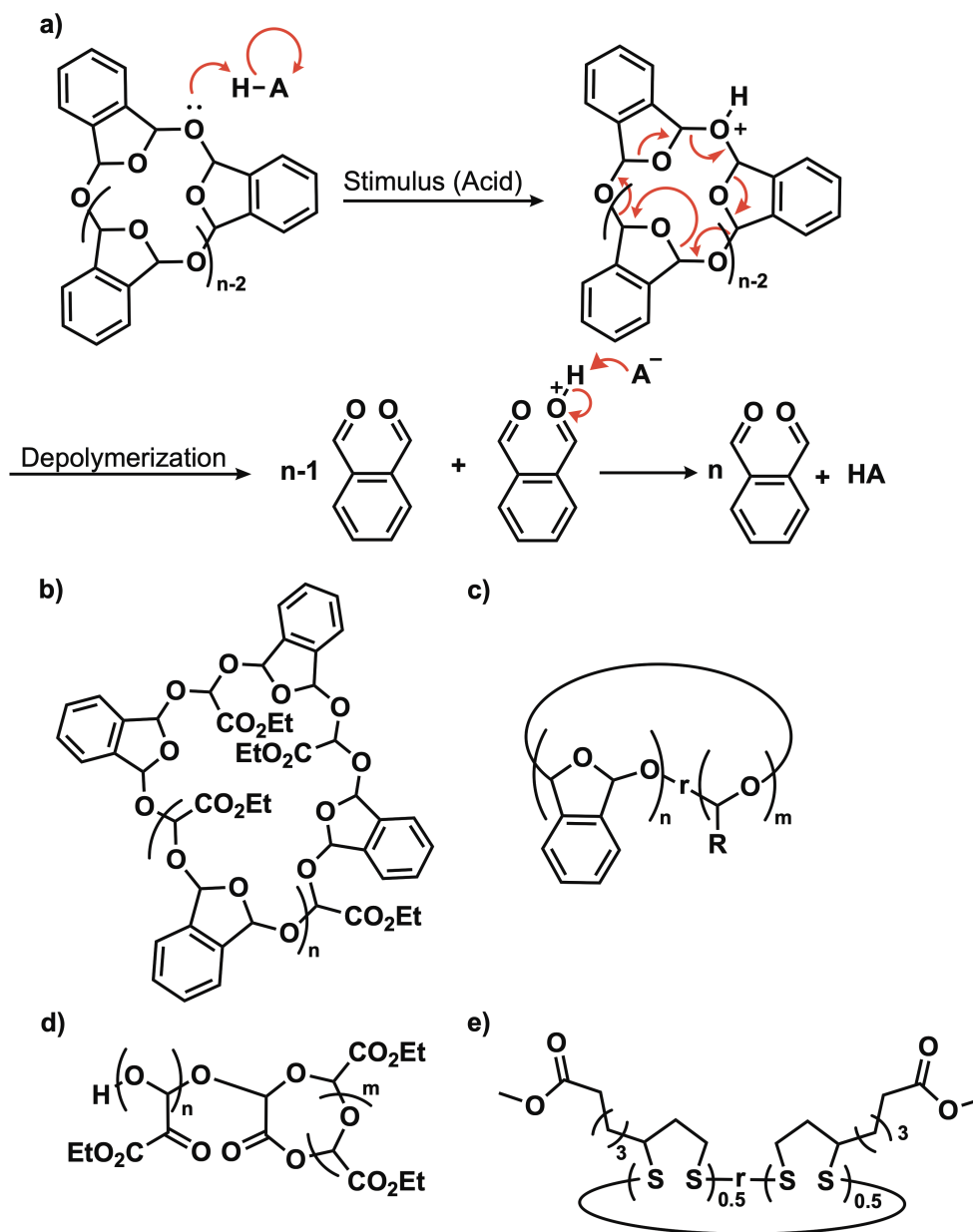


Figure 2.9. a) Structure of cPPA and its degradation mechanism in acidic conditions. b) Cyclic alternating copolymer of PA and ethyl glyoxylate. c) Cyclic copolymers of PA and other aldehyde monomers (R denotes the pendent groups from different monomers). d) lariat-shaped PETG synthesized using $\text{BF}_3 \cdot \text{OEt}_2$. e) Cyclic polydisulfide random copolymers of methyl lipoate.

Moore's group also investigated the cationic copolymerization of PA and ethyl glyoxylate (Figure 2.9b).¹³⁷ Because PETG has a low T_g whereas PPA and cPPA are brittle polymers

with high T_g values (> 180 °C) and relatively limited thermal stability, it was envisioned that a copolymer would possess an intermediate T_g and consequently better properties and processability. A cationic polymerization of the two monomers in a 1:1 ratio with a Lewis acid catalyst yielded the cyclic copolymer as a white sticky solid. NMR spectroscopy and MALDI-TOF MS suggested that the two monomers were incorporated in similar proportions. In addition, the results suggested that alternating copolymers were formed, which was attributed to a combination of steric hindrance between adjacent glyoxylate units as well as the tendency of alternating copolymers to form between electron-rich and electron-poor monomers. As expected, thermal analyses showed that the T_g decreased linearly and the onset degradation temperature (T_o) increased linearly as the percentage of ethyl glyoxylate monomer was increased.

Kohl and coworkers recently investigated the cationic copolymerization of PA with other aldehydes to tune the properties of the resulting polymers (Figure 2.9c). In the initial work, PA was copolymerized with butanal.¹³⁸ Incorporation of butanal resulted in polymers that were more thermally stable and depolymerized faster after triggering with acid compared to cPPA homopolymer. A subsequent study investigated PA copolymerization with various other aldehydes.¹³⁹ Copolymerization of PA with pentanal led to a lack of any end-cap peaks in the NMR spectra, suggesting cyclic structures. cPPA copolymers were also synthesized with a variety of functional groups using aldehyde comonomers with halides, alkynes, alkenes, and tosyl esters. Long blocks of aliphatic aldehydes were not detected, which the authors postulated may be due to a backbiting that may occur with these long blocks and result in the production of non-reactive trioxane compounds. Finally, the post-polymerization modification of the copolymers allowed for further tuning of their properties. The authors were able to install epoxide groups via reaction with the pendent alkenes and were able to replace the tosyl and halide pendent groups with azides. Thiolen chemistry was also used to demonstrate cross-linking of the copolymers into films. The authors note that the tosyl copolymer possessed a T_o of 95 °C, lower than that of the other copolymers ($T_o = 150 \pm 20$ °C). This lowering of thermal stability was postulated to be the result of the thermal cleavage of the tosyl group from the copolymer, which could then form tosylic acid and catalyze the depolymerization.

McNeil and coworkers recently tuned the thermal properties and stability of cPPAs by synthesizing and subjecting PA derivatives with different aromatic substituents such as ethers, thioethers, alkynes and esters *para* to the aldehydes, as well as phthalimide and tetrafluoro derivatives to Lewis acid-catalyzed polymerization conditions.¹⁴⁰ Computations based on density functional theory were used to predict the T_c values of the polymers. As predicted, monomers with electron-donating substituents did not yield polymers due to T_c values below -78 °C, while those with higher T_c values polymerized. Experimentally measured and calculated T_c values were compared. There was general agreement in the trends, but there were substantial quantitative differences due to assumptions made in the calculations. T_o values of the different cPPAs were measured and ranged from 109 °C for the unsubstituted cPPA to 196 °C for the tetrafluoro derivative. Furthermore, T_o could be tuned through copolymerization of different derivatives.

Depolymerization of cPPAs is reliant on a stimulus that can disrupt the cyclic structure, revealing a hemiacetal end-group that can then unzip the polymer into its constituent monomers (Figure 2.9a). cPPAs are susceptible to cleavage by thermal, acidic, and even mechanical stimuli. For example, the Moore and Boydston groups investigated the application of ultrasound as a stimulus and found that the PPA and cPPA backbones could be mechanically broken if the polymer's molar mass was > 30 kg/mol.¹⁴¹ The use of acidic stimuli has been the focus of several novel cPPA applications. Moore and coworkers produced core-shell microcapsules with cPPA walls.¹⁴² Suspension of these capsules in weakly acidic methanol resulted in no degradation over 24 h. However, the addition of a chaotropic salt such as LiCl as a specific ion coactivator resulted in rapid depolymerization of the microcapsules and release of the payload.

White and coworkers incorporated the photoacid (2-(4-methoxystyryl)-4,6-bis(trichloromethyl)-1,3,5-triazine) with cPPA to create a material degradable by UV light.¹⁴³ This material was used as a substrate on which to fabricate microelectronics. Triggered depolymerization led to destruction of the device. The authors later developed microelectronic devices with cPPA where acid microdroplets were contained in separate silicone wax layers.¹⁴⁴ Heating the device melted the wax and released the acid, leading to the rapid depolymerization of the cPPA (~ 2 min). By using different wax layers with

different melting points, a complex microelectronics device was manufactured that only experienced partial degradation and failure at certain temperatures. Rand and coworkers reported the construction of cPPA films containing the photoacid 4-isopropyl-4-methyldiphenyliodoniumtetrakis(pentafluorophenyl)borate and the visible-light sensitizer 5,12-bis(phenylethynyl)tetracene.¹⁴⁵ Visible light excited the sensitizer, which then underwent an electron transfer reaction with the photoacid, resulting in the production of acid within the film. A green organic light-emitting diode (OLED) was fabricated on top of the films with the silver nanowires embedded in the film. Thus, OLED activity was self-destructive as the circuit was broken as the film degraded. On average, self-destruction of the device could be achieved in as little as 20 s. Kohl and coworkers reported the use of a photoacid (an iodonium salt) that was sensitized to visible light using aromatic molecules such as pentacene derivatives.¹⁴⁶ The sensitized photoacid was able to degrade a cPPA in sunlight in as little as 5.5 min.

Kohl and coworkers reported strategies to slow down degradation of triggerable cPPA films both before and after triggering depolymerization. One strategy involved the inclusion of a weak base along with a photoacid in cPPA films.¹⁴⁷ In another strategy, the authors placed photoacid in a thin layer of cPPA and laminated this layer on top of the bulk cPPA.¹⁴⁸ This approach helped prevent unwanted degradation of the bulk cPPA layer from acid generation during storage. Triggering of the cPPA film after the photoacid layer was laminated on resulted in a liquification of the photoacid layer and subsequent diffusion of the acid into the bulk cPPA resulting in depolymerization.

Moore and coworkers developed approaches to increase the thermal stability of cPPAs to improve its processability.¹⁴⁹ At the time, thermal degradation of cPPAs was believed to occur via either radical or a cationic mechanisms. Thus, the authors added the radical trapping agent (2,2,6,6-tetramethylpiperidin-1-yl)oxyl (TEMPO) or the Lewis base *N,N'*-di-*sec*-butyl-1,4-phenylenediamine (DBPDA). Both inhibitors slowed degradation and increased the T_o of the polymers. The authors also carefully removed by precipitation the trace Lewis acid initiators from the cPPA that could be catalyzing their degradation, and this resulted in a significant improvement in the thermal stability of the purified polymer ($T_o = 145$ °C regardless if inhibitors were added or not). Finally, the authors incorporated

diethyl phthalate (DEP) as a plasticizer to lower the T_g of the cPPA below its T_o . A cPPA film with DEP and DBPDA incorporated was pelleted and hot pressed at 100 °C for 15 min twice with the polymer remaining stable throughout the process. The molded cPPA was still degradable at elevated temperatures or after an acid stimulus was added. In subsequent work, Moore's group discovered that the inclusion of the oxidant *p*-chloranil reduced the thermal stability of cPPA, indicating that thermolysis of the polymer may involve an oxidation.¹⁵⁰ Incorporation of antioxidants such as 1,3,5-trimethoxybenzene or TEMPO improved cPPA's thermal stability. With knowledge this new oxidation-based mechanism, the authors used single electron transfer agents to initiate the depolymerization of cPPA. The photooxidant *N*-methylacridinium hexafluorophosphate (NMAPF₆) allowed for complete depolymerization of a cPPA solution within 3–4 min upon irradiation with a 375 nm light. Degradation of solid films was also possible in ambient light conditions over a one-week period. Because of the thermal stability of NMAPF₆, it was possible to thermally process cPPAs with the photooxidant without premature degradation, a feature not possible with cPPAs containing thermally-sensitive photoacids.

Recently, Moore and coworkers also investigated the recyclability of cPPA.¹⁵¹ A cPPA film was heated at 100 °C to induce depolymerization and evaporation of the regenerated monomer. The monomer was collected and subsequently repolymerized with no additional purification. Depolymerization and quantitative recovery of the monomer was possible in less than 1 h if the temperature was raised to 120 °C. The authors noted no mechanical differences between the cPPAs, even after three depolymerization/repolymerization cycles. cPPAs with dyes were also tested and found to be recyclable without dye contamination. Finally, the authors examined cPPA recovery from a carbon fibre composite material. Fibres could be restored from the composites after heating without damage or significant amounts of cPPA matrix residue.

2.4.5.2 Other Cyclic Backbones

Cyclic poly(ethyl glyoxylate) was investigated by Moore and coworkers in 2014.¹⁵² Ethyl glyoxylate was polymerized cationically using a variety of Lewis acid initiators. All of the resulting PEtGs were low molar mass ($M_n = 2\text{--}13$ kg/mol) with a range of D values (1.3–

1.8). ^1H NMR spectroscopy of the PEtGs revealed a lack of end-caps, suggesting cyclic structures. MALDI-TOF MS analysis of PEtGs synthesized using $\text{BF}_3 \cdot \text{OEt}_2$ revealed an unexpected lariat structure corresponding to a pendent ethyl ester backbiting on the terminal acetal (Figure 2.9d). When the initiator was switched to triphenylcarbenium tetrafluoroborate, MALDI-TOF MS revealed a completely macrocyclic structure due to main-chain backbiting. The authors proposed that this change in polymer architecture was partially due to the formation of a gel during the polymerization reaction at high concentrations with $\text{BF}_3 \cdot \text{OEt}_2$, which prevented the polymer chains from equilibrating and forming macrocyclic structures. A low concentration polymerization with $\text{BF}_3 \cdot \text{OEt}_2$, on the other hand, did not solidify and allowed for macrocycles and lariat structures to be formed. When carbocation initiators were used, macrocyclization was favoured. Triple-detection SEC was utilized to compare the intrinsic viscosities of the cyclic PEtGs with linear PEtGs. As expected, the macrocyclic PEtG had the lowest, lariat PEtG had intermediate, and linear PEtG had the highest intrinsic viscosity.

Moore's group also recently reported the synthesis of cyclic polydisulfides via the anionic polymerization of methyl lipoate (Figure 2.9e).¹⁵³ While linear polydisulfides can be obtained via anionic polymerization with initiators such as alkyl thiols,¹⁵⁴⁻¹⁵⁶ it was discovered that the use of aryl thiol initiators with high nucleofugality (such as thiophenol) along with a strong base resulted in mostly cyclic product via main-chain backbiting. Initial polymerizations using thiophenol and various bases as initiators, and quenched with phenyl isocyanate, resulted in cyclic polymers with M_n values from 22–65 kg/mol and relatively low D values (~ 1.4), although a M_n as high as 630 kg/mol was later achieved. The cyclic nature of the polymers was confirmed with ^1H NMR spectroscopy and MS, which both revealed the lack of chain ends on the polymers. SEC analysis also revealed a longer retention time and lower viscosity of the cyclic polymers compared to linear polydisulfides synthesized with a benzyl mercaptan initiator. Due to the relatively low T_c of the polydisulfides ($\sim 27^\circ\text{C}$), their depolymerization was explored by heating at 65°C at a dilute concentration (1 M), with the initiating species acting as a catalyst. Up to 95% of the monomer could be recovered after 1 h. Additionally, ring expansion was achieved by reinitiating the polymerization of cyclic polydisulfides in the presence of monomer. The polymerization of disulfides could be further extended to other lipoate monomers.

2.4.6 Self-Immolative Graft Copolymers and Networks

Graft copolymers, also referred to as bottlebrush copolymers, are copolymers that possess a central polymer backbone with pendent polymer chains. The architecture of the graft polymer confers properties that are different than those of linear polymers. For example, high molar mass graft copolymers have less tendency to entangle, leading to different self-assemblies than their linear analogues.¹⁵⁷ Networks, meanwhile, are constructed by the cross-linking of polymer chains. Cross-linking results in insoluble structures that possess properties such as the ability to swell in particular solvents. So far, there are only a few examples of self-immolative graft copolymers and networks in the literature.

Zhang and coworkers reported graft copolymers composed of self-immolative PBC pendent chains on a non-degradable polymethacrylate (PMA) backbone (Figure 2.10).¹⁵⁸ Short chain PBCs ($DP_n < 10$) were synthesized and end-capped with an alkyne-functionalized photolabile group. Copper-assisted azide-alkyne cycloaddition (CuAAC) chemistry was then used to graft the PBC to poly(3-azido-2-hydroxypropyl methacrylate) backbones ($M_n = 100$ kg/mol or 540 kg/mol). The resulting copolymers formed worm-like structures, which could be visualized with atomic force microscopy (AFM). One of the PBCs was composed of 4-aminobenzyl alcohol spacers with *o*-substituted *t*-butyl esters on each spacer. Hydrolysis of the *t*-butyl esters in acidic media transformed this bottlebrush copolymer from hydrophobic to hydrophilic. UV-light triggered depolymerization of the PBC chains in 36 h for PBC side chains composed of 4-aminobenzyl alcohol spacers (Figure 2.10a). *O*-substituted spacers, meanwhile, degraded in only 1.5 h and produced an increase in fluorescence (Figure 2.10b).

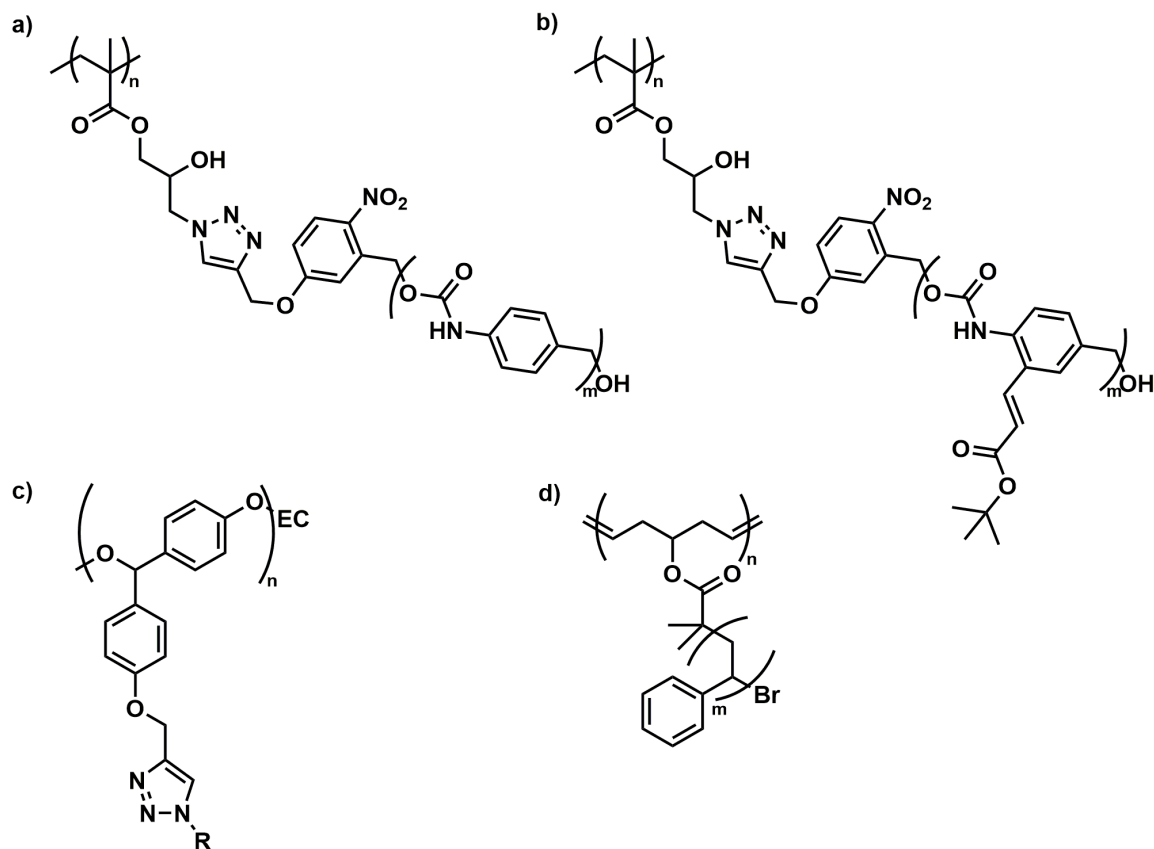


Figure 2.10. a) Structure of a graft copolymer with a polymethacrylate and UV light-triggerable PBC pendent chains. b) Variant of the structure in a) but with pendent acrylate groups that lead to the release of fluorescent molecules upon depolymerization. c) PBE backbone with pendent PEG or PS chains (R group) and a stimuli-responsive end-cap (EC). d) Depolymerizable polycyclopentene with pendent PS chains.

Zhang and coworkers also grafted PS or PEG chains to a PBE backbone via CuAAC (Figure 2.10c).¹⁵⁹ They discovered that the copolymers with PS side chains depolymerized slower than those with the PEG chains. This observation was attributed to the bulky nature of the PS chains, which may hinder the free rotation of the chain-end phenolate unit. This unit must be properly aligned for 1,6-elimination, and consequently depolymerization to occur. In other work, the authors synthesized PBE with thiol pendent groups.⁸⁷ Using a thiol-disulfide exchange reaction, they synthesized a graft copolymer and an organogel from the PBE using a mercapto-terminated PEG or bis-mercapto-terminated PEG respectively.

Moore's group reported the synthesis of both graft copolymers and cross-linked networks by post-polymerization modification of PA/benzaldehyde copolymers.¹⁶⁰ They converted pendent aldehyde groups off of the benzaldehyde units to alcohols, which could then be used to graft PLA to the backbone via a ring-opening polymerization of lactide. Use of a multifunctional isocyanate linker produced self-immolative networks. They later used their PA/benzaldehyde copolymers with 2-ureido-pyrimidinone pendent groups to construct non-covalently bonded self-immolative nanoparticles and networks.¹⁶¹

Recently, Kennemur and coworkers reported depolymerizable graft copolymers based on a polycyclopentene backbone (Figure 2.10d).¹⁶² This polymer possesses a lower T_c than many other cyclic olefin polymers synthesized by ring-opening metathesis polymerization (ROMP) because the ring-strain that drives ROMP is low for cyclopentene. Thus, under the right conditions such as elevated temperatures, the polymerization reaction can be reversed. Cyclopentene monomer with a bromoisobutyryl pendent group was polymerized at low temperature via ROMP using the Grubbs I ruthenium catalyst, and then styrene was grafted from the polymers via an atom-transfer radical polymerization (ATRP) using the bromoisobutyryl pendent groups. They were able to achieve good control over the polymer and side chain lengths, resulting in the targeted molar masses with low backbone D values of 1.18–1.35. Four different graft copolymers were synthesized with variable backbone lengths ($DP_n = 97, 181$) and side chain lengths ($DP_n = 18, 28, 44$). Depolymerization was then investigated by heating the polymers to 70 °C for 24 h in the presence of a ruthenium catalyst (Hoveyda-Grubbs II). Analysis of the depolymerization products by SEC suggested that while the cyclopentene backbone had fully depolymerized, the PS side chains were still intact. Next, the authors tested several different ruthenium-based catalysts (Hoveyda-Grubbs II, Grubbs I, Grubbs II, Grubbs III) against the polymers to observe depolymerization rates. It was discovered that the rates followed the order Grubbs III > Grubbs II > Grubbs I > Hoveyda-Grubbs II, with Grubbs II and III resulting in almost complete depolymerization at room temperature after 30 min. The authors also determined that the depolymerization mechanism involved head-to-tail unzipping of the polymer backbone chain and not a breakdown of the chain through random scission events, as no smaller polymer fragments resulting from random scission were observed by SEC. This result contrasts with non-derivatized polycyclopentene, where random chain scission

events appear to dominate depolymerization. The authors also commented that depolymerization of their bottlebrush polymers could be used to alter macroscopic properties of a material or introduce new functional handles. With regards to the latter, the authors used the cyclopentene functional group created during depolymerization of one of the polymers along with trimethylolpropane tris(3-mercaptopropionate) and a photoinitiator to synthesize three-arm star PS macromolecules as a proof-of-concept.

Lobez and Swager reported the incorporation of POSs into elastomers.¹⁶³ While POSs are typically brittle solids with high T_g values, they incorporated silicone cross-linkers to create elastomeric networks. Different mechanical properties could be obtained by varying the amount of POS to the cross-linker, varying the length of the cross-linker, or by varying the degree of cross-linking. As expected, the more silicone cross-linker that was incorporated, the softer and more elastic the networks. Depolymerization of one of the networks after exposure to piperidine resulted in network failure and dissolution in approximately 5 min.

Sasaki's group reported a self-immolative adhesive composed of cross-linked POSs that could be degraded by raising the pH with a photobase.¹⁶⁴ POS random terpolymers composed of SO₂, 2-methyl-1-pentene, and 4-methyl-4-pentenoic acid were synthesized (TPASs). Cross-linking was explored by mixing different TPASs with a polycarbodiimide cross-linking agent and a photobase compound in chloroform, followed by heating at 100 °C to cure the adhesive mixture. Subsequent irradiation with UV light resulted in depolymerization of the network. The authors then investigated the adhesion of two quartz plates with their POS adhesive mixture. Curing of the mixture at 100 °C for 5 min resulted in a strong thermoset polymer bond between the two plates, comparable in tensile strength to a commercial epoxy adhesive. Subsequent heating at 100 °C for 60 min did not lead to any loss of bond strength whereas UV irradiation followed by heating at 100 °C resulted in the elimination of the bond after 15 min, with a longer degradation time at 80 °C and only a softening of the bond at 60 °C.

2.4.7 Hyperbranched Self-Immolative Polymers (HSIPs)

Hyperbranched polymers are macromolecules that possess features characteristic of both linear polymers and dendrons. Like dendrons, they possess a multi-branched architecture

with a focal point and periphery. However, unlike dendrons, they can be synthesized in a one-step reaction, leading to imperfect structures and some degree of dispersity. Hyperbranched polymers therefore have many of the beneficial architectural effects of dendrons with the synthetic efficiency of linear polymers.

Thus far, Liu and coworkers reported the only examples of HSIPs in 2015 (Figure 2.11).¹⁶⁵ They were synthesized via the step-growth polycondensation of aromatic elimination spacers. Quenching the polymerization reactions with different end-caps installed different stimuli triggers at the focal point of the polymers. Polymers sensitive to visible light, H₂O₂, and reductive compounds were yielded from the use of perylene-3-yl methanol, hydroxymethyl phenylboronic ester, and diethanol disulfide end-caps respectively. Based on NMR spectroscopic analyses, the HSIPs were determined to have 14–19 hydroxyl groups at their peripheries. Post-polymerization modification of these groups afforded polymers with peripheral moieties such as doxorubicin, choline, PEG, and poly[2-(dimethylamino)ethyl methacrylate] (PDMAEMA). The self-immolation rates of the hyperbranched polymers were adjusted by tuning the polymer spacers to eliminate via 1,6 or 1,4 pathways (faster) or by using thiophenol based spacers (slower).

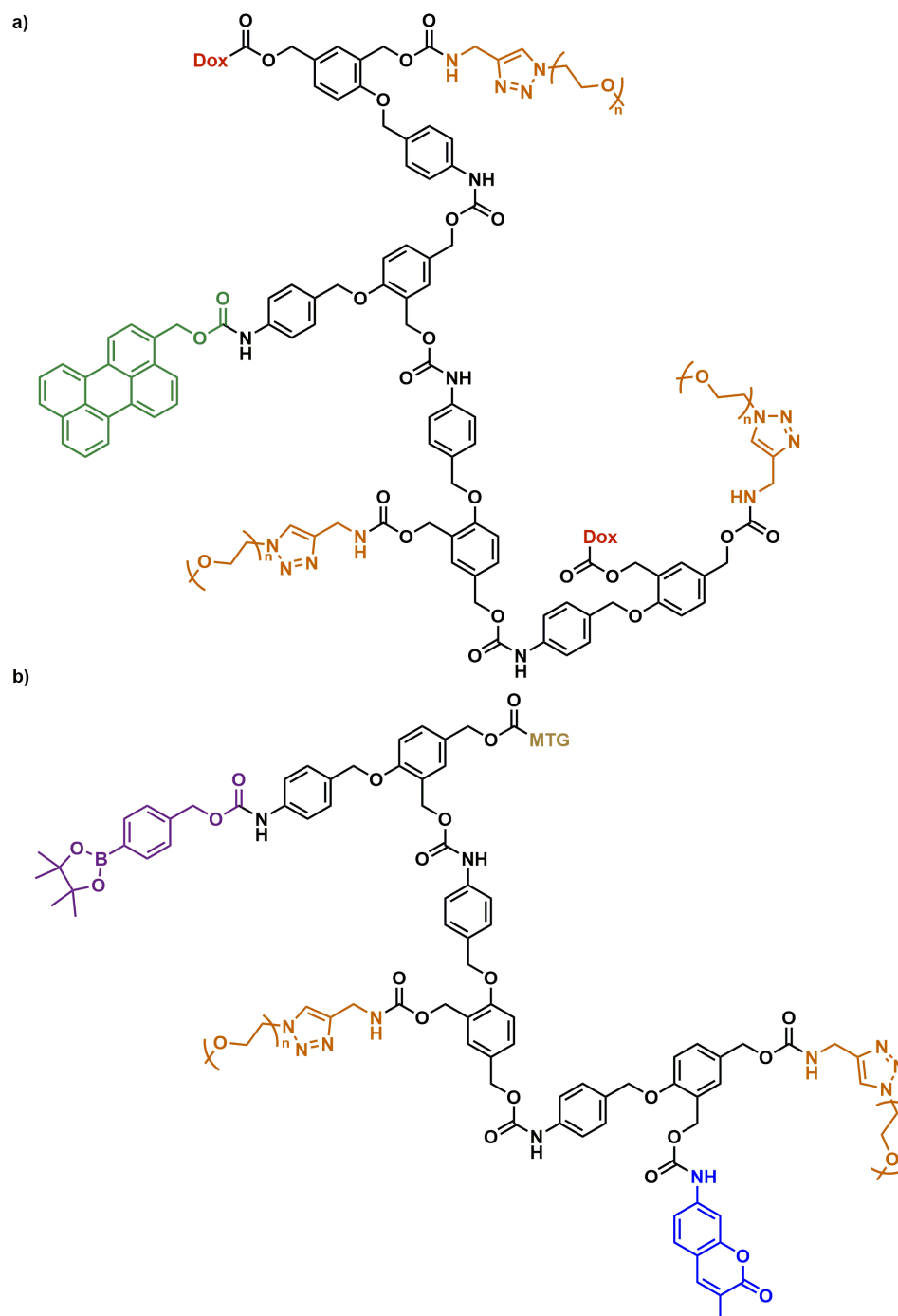


Figure 2.11. a) HSIP with a visible light-responsive trigger (green) and peripheral PEG (orange) and doxorubicin (Dox) (red) moieties. b) HSIP with a H₂O₂-sensitive trigger (purple) and peripheral mitochondrial targeting groups (MTG; gold), PEG (orange), and caged fluorescent reporters (blue).

Various potential applications of the HSIPs were explored. For example, a HSIP sensitive to visible light with some peripheral PEG moieties formed nanoparticles in aqueous solution (Figure 2.11a). Irradiation with blue light for 30 min resulted in nanoparticle degradation over 6 h, with the release of peripheral molecules including doxorubicin. Visible light also induced the *in vitro* release of doxorubicin in cancer cells, highlighting the potential of the HSIP for drug delivery. In another experiment, hyperbranched SIPs with PDMAEMA attached to the periphery and a reduction-sensitive trigger were used as non-viral gene vectors. Deoxyribonucleic acid (DNA)/HSIP complexes were formed and triggering of self-immolation resulted in the dissolution of these complexes. *In vitro* studies revealed DNA transfection of a fluorescent reporter gene. The authors also investigated H₂O₂-sensitive hyperbranched SIPs functionalized with a mitochondrial targeting moiety and a caged fluorescent reporter (Figure 2.11b). *In vitro* studies over 12 h revealed a localization of the fluorescent probe within the mitochondria of the cells, with little localization of probe from hyperbranched SIPs that did not possess the targeting moiety. Finally, the authors built on Shabat's concept of the dendritic chain reaction⁶⁷ to amplify the response of their HSIPs to stimuli. A H₂O₂-sensitive HSIP with peripheral choline moieties was used along with choline oxidase to bind citrate away from citrate-stabilized gold nanoparticles. Removing citrate caused nanoparticle aggregation and turned the mixture from red to blue. An H₂O₂ concentration as little as 1 μM could initiate the chain reaction, destroying the HSIP. Subsequent removal of the freed choline by choline oxidase allowed unbound citrate to stabilize the gold nanoparticle aggregates and turn the mixture back to a red colour. A similar system using a HSIP with caged fluorescent probes and choline on its periphery was also used to detect levels of choline oxidase in solution. This system could be utilized as the basis of an enzyme-linked immunosorbent assay.

2.5 References

- (1) Nair, L. S.; Laurencin, C. T. Biodegradable Polymers as Biomaterials. *Prog. Polym. Sci.* **2007**, *32*, 762–798.
- (2) Kamaly, N.; Yameen, B.; Wu, J.; Farokhzad, O. C. Degradable Controlled-Release Polymers and Polymeric Nanoparticles: Mechanisms of Controlling Drug Release. *Chem. Rev.* **2016**, *116*, 2602–2663.

- (3) Payne, J.; McKeown, P.; Jones, M. D. A Circular Economy Approach to Plastic Waste. *Polym. Degrad. Stab.* **2019**, *165*, 170–181.
- (4) Yang, F.; Murugan, R.; Ramakrishna, S.; Wang, X.; Ma, Y. X.; Wang, S. Fabrication of Nano-Structured Porous PLLA Scaffold Intended for Nerve Tissue Engineering. *Biomaterials* **2004**, *25*, 1891–1900.
- (5) Shigemura, N.; Okumura, M.; Mizuno, S.; Imanishi, Y.; Matsuyama, A.; Shiono, H.; Nakamura, T.; Sawa, Y. Lung Tissue Engineering Technique with Adipose Stromal Cells Improves Surgical Outcome for Pulmonary Emphysema. *Am. J. Respir. Crit. Care. Med.* **2006**, *174*, 1199–1205.
- (6) Xin, H.; Sha, X.; Jiang, X.; Zhang, W.; Chen, L.; Fang, X. Anti-Glioblastoma Efficacy and Safety of Paclitaxel-Loading Angiopep-Conjugated Dual Targeting PEG-PCL Nanoparticles. *Biomaterials* **2012**, *33*, 8167–8176.
- (7) Shi, C.; Guo, X.; Qu, Q.; Tang, Z.; Wang, Y.; Zhou, S. Actively Targeted Delivery of Anticancer Drug to Tumor Cells by Redox-Responsive Star Shaped Micelles. *Biomaterials* **2014**, *35*, 8711–8722.
- (8) Kim, I. Y.; Yoo, M. K.; Seo, J. H.; Park, S. S.; Na, H. S.; Lee, H. C.; Kim, S. K.; Cho, C. S. Evaluation of Semi-Interpenetrating Polymer Networks Composed of Chitosan and Poloxamer for Wound Dressing Application. *Int. J. Pharm.* **2007**, *341*, 35–43.
- (9) Ribeiro, M. P.; Espiga, A.; Silva, D.; Baptista, P.; Henriques, J.; Ferreira, C.; Silva, J. C.; Borges, J. P.; Pires, E.; Chaves, P.; Correia, I. J. Development of a New Chitosan Hydrogel for Wound Dressing. *Wound Repair Regen.* **2009**, *17*, 817–824.
- (10) Fonte, P.; Araujo, F.; Silva, C.; Pereira, C.; Reis, S.; Santos, H. A.; Sarmiento, B. Polymer-Based Nanoparticles for Oral Insulin Delivery: Revisited Approaches. *Biotechnol. Adv.* **2015**, *33*, 1342–1354.
- (11) Wei, M.; Gao, Y.; Li, X.; Serpe, M. J. Stimuli-Responsive Polymers and Their Applications. *Polym. Chem.* **2017**, *8*, 127–143.
- (12) Roy, D.; Brooks, W. L.; Sumerlin, B. S. New Directions in Thermoresponsive Polymers. *Chem. Soc. Rev.* **2013**, *42*, 7214–7243.
- (13) Zhang, Q.; Weber, C.; Schubert, U. S.; Hoogenboom, R. Thermoresponsive Polymers with Lower Critical Solution Temperature: From Fundamental Aspects and Measuring Techniques to Recommended Turbidimetry Conditions. *Mater. Horiz.* **2017**, *4*, 109–116.

- (14) Schild, H. G. Poly(*N*-isopropylacrylamide): Experiment, Theory and Application. *Prog. Polym. Sci.* **1992**, *17*, 163–249.
- (15) Qin, S. H.; Geng, Y.; Discher, D. E.; Yang, S. Temperature-Controlled Assembly and Release from Polymer Vesicles of Poly(ethylene oxide)-*block*-poly(*N*-isopropylacrylamide). *Adv. Mater.* **2006**, *18*, 2905–2909.
- (16) Li, W.; Zhao, H.; Qian, W.; Li, H.; Zhang, L.; Ye, Z.; Zhang, G.; Xia, M.; Li, J.; Gao, J.; Li, B.; Kou, G.; Dai, J.; Wang, H.; Guo, Y. Chemotherapy for Gastric Cancer by Finely Tailoring Anti-Her2 Anchored Dual Targeting Immunomicelles. *Biomaterials* **2012**, *33*, 5349–5362.
- (17) Lutz, J.-F.; Akdemir, Ö.; Hoth, A. Point by Point Comparison of Two Thermosensitive Polymers Exhibiting a Similar LCST: Is the Age of Poly(NIPAM) Over? *J. Am. Chem. Soc.* **2006**, *128*, 13046–13047.
- (18) Lutz, J.-F.; Hoth, A. Preparation of Ideal PEG Analogues with a Tunable Thermosensitivity by Controlled Radical Copolymerization of 2-(2-Methoxyethoxy)ethyl Methacrylate and Oligo(ethylene glycol) Methacrylate. *Macromolecules* **2006**, *39*, 893–896.
- (19) Lutz, J.-F. Thermo-Switchable Materials Prepared Using the OEGMA-Platform. *Adv. Mater.* **2011**, *23*, 2237–2243.
- (20) Badi, N. Non-Linear PEG-Based Thermoresponsive Polymer Systems. *Prog. Polym. Sci.* **2017**, *66*, 54–79.
- (21) Hu, Y.; Litwin, T.; Nagaraja, A. R.; Kwong, B.; Katz, J.; Watson, N.; Irvine, D. J. Cytosolic Delivery of Membrane-Impermeable Molecules in Dendritic Cells using pH-Responsive Core-Shell Nanoparticles. *Nano Lett.* **2007**, *7*, 3056–3064.
- (22) Lomas, H.; Massignani, M.; Abdullah, K. A.; Canton, I.; Lo Presti, C.; MacNeil, S.; Du, J.; Blanz, A.; Madsen, J.; Armes, S. P.; Lewis, A. L.; Battaglia, G. Non-Cytotoxic Polymer Vesicles for Rapid and Efficient Intracellular Delivery. *Faraday Discuss.* **2008**, *139*, 143–159.
- (23) Zhou, K.; Wang, Y.; Huang, X.; Luby-Phelps, K.; Sumer, B. D.; Gao, J. Tunable, Ultrasensitive pH-Responsive Nanoparticles Targeting Specific Endocytic Organelles in Living Cells. *Angew. Chem. Int. Ed.* **2011**, *50*, 6109–6114.

- (24) Wong, A. S. M.; Czuba, E.; Chen, M. Z.; Yuen, D.; Cupic, K. I.; Yang, S.; Hodgetts, R. Y.; Selby, L. I.; Johnston, A. P. R.; Such, G. K. pH-Responsive Transferrin-pHlexi Particles Capable of Targeting Cells in Vitro. *ACS Macro Lett.* **2017**, *6*, 315–320.
- (25) Kongkatigumjorn, N.; Smith, S. A.; Chen, M.; Fang, K.; Yang, S.; Gillies, E. R.; Johnston, A. P. R.; Such, G. K. Controlling Endosomal Escape Using pH-Responsive Nanoparticles with Tunable Disassembly. *ACS Appl. Nano Mater.* **2018**, *1*, 3164–3173.
- (26) Boussif, O.; Lezoualc'h, F.; Zanta, M. A.; Mergny, M. D.; Scherman, D.; Demeneix, B.; Behr, J. P. A Versatile Vector for Gene and Oligonucleotide Transfer into Cells in Culture and *In Vivo*: Polyethylenimine. *Proc. Natl. Acad. Sci. U. S. A.* **1995**, *92*, 7297–7301.
- (27) Wu, G. Y.; Wu, C. H. Receptor-Mediated *In Vitro* Gene Transformation by a Soluble DNA Carrier System. *J. Biol. Chem.* **1987**, *262*, 4429–4432.
- (28) Cherng, J. Y.; van de Wetering, P.; Talsma, H.; Crommelin, D. J.; Hennink, W. E. Effect of Size and Serum Proteins on Transfection Efficiency of Poly((2-dimethylamino)ethyl methacrylate)-Plasmid Nanoparticles. *Pharm. Res.* **1996**, *13*, 1038–1042.
- (29) Bus, T.; Traeger, A.; Schubert, U. S. The Great Escape: How Cationic Polyplexes Overcome the Endosomal Barrier. *J. Mater. Chem. B* **2018**, *6*, 6904–6918.
- (30) Guo, X.; Wang, L.; Wei, X.; Zhou, S. Polymer-Based Drug Delivery Systems for Cancer Treatment. *J. Polym. Sci., Part A: Polym. Chem.* **2016**, *54*, 3525–3550.
- (31) Heffernan, M. J.; Murthy, N. Polyketal Nanoparticles: A New pH-Sensitive Biodegradable Drug Delivery Vehicle. *Bioconjugate Chem.* **2005**, *16*, 1340–1342.
- (32) Rickerby, J.; Prabhakar, R.; Ali, M.; Knowles, J.; Brocchini, S. Water-Soluble Polyacetals Derived from Diphenols. *J. Mater. Chem.* **2005**, *15*, 1849–1856.
- (33) Jain, R.; Standley, S. M.; Fréchet, J. M. J. Synthesis and Degradation of pH-sensitive Linear Poly(amidoamine)s. *Macromolecules* **2007**, *40*, 452–457.
- (34) Wang, J.; Yang, G.; Guo, X.; Tang, Z.; Zhong, Z.; Zhou, S. Redox-Responsive Polyanhydride Micelles for Cancer Therapy. *Biomaterials* **2014**, *35*, 3080–3090.
- (35) Gosselin, M. A.; Guo, W.; Lee, R. J. Efficient Gene Transfer Using Reversibly Cross-Linked Low Molecular Weight Polyethylenimine. *Bioconjugate Chem.* **2001**, *12*, 989–994.

- (36) Yardley, R. E.; Rabiee Kenaree, A.; Gillies, E. R. Triggering Depolymerization: Progress and Opportunities for Self-Immolative Polymers. *Macromolecules* **2019**, *52*, 6342–6360.
- (37) Carl, P. L.; Chakravarty, P. K.; Katzenellenbogen, J. A. A Novel Connector Linkage Applicable in Prodrug Design. *J. Med. Chem.* **1981**, *24*, 479–480.
- (38) Sagi, A.; Weinstain, R.; Karton, N.; Shabat, D. Self-Immolative Polymers. *J. Am. Chem. Soc.* **2008**, *130*, 5434–5435.
- (39) Li, S.; Szalai, M. L.; Kevwitch, R. M.; McGrath, D. V. Dendrimer Disassembly by Benzyl Ether Depolymerization. *J. Am. Chem. Soc.* **2003**, *125*, 10516–10517.
- (40) Szalai, M. L.; Kevwitch, R. M.; McGrath, D. V. Geometric Disassembly of Dendrimers: Dendritic Amplification. *J. Am. Chem. Soc.* **2003**, *125*, 15688–15689.
- (41) de Groot, F. M.; Albrecht, C.; Koekkoek, R.; Beusker, P. H.; Scheeren, H. W. "Cascade-Release Dendrimers" Liberate All End Groups Upon a Single Triggering Event in the Dendritic Core. *Angew. Chem. Int. Ed.* **2003**, *42*, 4490–4494.
- (42) Papot, S.; Tranoy, I.; Tillequin, F.; Florent, J.-C.; Gesson, J.-P. Design of selectively activated anticancer prodrugs: Elimination and cyclization strategies. *Current Medicinal Chemistry: Anti-Cancer Agents* **2002**, *2*, 155–185.
- (43) Amir, R. J.; Pessah, N.; Shamis, M.; Shabat, D. Self-Immolative Dendrimers. *Angew. Chem. Int. Ed.* **2003**, *42*, 4494–4499.
- (44) Dewit, M. A.; Gillies, E. R. A Cascade Biodegradable Polymer Based on Alternating Cyclization and Elimination Reactions. *J. Am. Chem. Soc.* **2009**, *131*, 18327–18334.
- (45) Penczek, S.; Moad, G. Glossary of terms related to kinetics, thermodynamics, and mechanisms of polymerization (IUPAC recommendations 2008). *Pure Appl. Chem.* **2008**, *80*, 2163–2193.
- (46) de Groot, F. M.; Loos, W. J.; Koekkoek, R.; van Berkom, L. W.; Busscher, G. F.; Seelen, A. E.; Albrecht, C.; de Bruijn, P.; Scheeren, H. W. Elongated Multiple Electronic Cascade and Cyclization Spacer Systems in Activatable Anticancer Prodrugs for Enhanced Drug Release. *J. Org. Chem.* **2001**, *66*, 8815–8830.
- (47) Warnecke, A.; Kratz, F. 2,4-Bis(hydroxymethyl)aniline as a Building Block for Oligomers with Self-Eliminating and Multiple Release Properties. *J. Org. Chem.* **2008**, *73*, 1546–1552.

- (48) Redy, O.; Shabat, D. Modular Theranostic Prodrug Based on a FRET-Activated Self-Immolative Linker. *J. Controlled Release* **2012**, *164*, 276–282.
- (49) Lewis, G. G.; Robbins, J. S.; Phillips, S. T. Phase-Switching Depolymerizable Poly(carbamate) Oligomers for Signal Amplification in Quantitative Time-Based Assays. *Macromolecules* **2013**, *46*, 5177–5183.
- (50) Lewis, G. G.; Robbins, J. S.; Phillips, S. T. Point-of-Care Assay Platform for Quantifying Active Enzymes to Femtomolar Levels Using Measurements of Time as the Readout. *Anal. Chem.* **2013**, *85*, 10432–10439.
- (51) Lewis, G. G.; Robbins, J. S.; Phillips, S. T. A Prototype Point-of-Use Assay for Measuring Heavy Metal Contamination in Water Using Time as a Quantitative Readout. *Chem. Commun.* **2014**, *50*, 5352–5354.
- (52) Dahlhauser, S. D.; Escamilla, P. R.; VandeWalle, A. N.; York, J. T.; Rapagnani, R. M.; Shei, J. S.; Glass, S. A.; Coronado, J. N.; Moor, S. R.; Saunders, D. P.; Anslyn, E. V. Sequencing of Sequence-Defined Oligourethanes via Controlled Self-Immolation. *J. Am. Chem. Soc.* **2020**, *142*, 2744–2749.
- (53) McBride, R. A.; Gillies, E. R. Kinetics of Self-Immolative Degradation in a Linear Polymeric System: Demonstrating the Effect of Chain Length. *Macromolecules* **2013**, *46*, 5157–5166.
- (54) Polaske, N. W.; Szalai, M. L.; Shanahan, C. S.; McGrath, D. V. Convergent Synthesis of Geometrically Disassembling Dendrimers Using Cu(I)-Catalyzed C-O Bond Formation. *Org. Lett.* **2010**, *12*, 4944–4947.
- (55) Kastrati, A.; Bochet, C. G. Photochemical Amplifier Based on Self-Immolative Dendritic Spacers. *J. Org. Chem.* **2019**, *84*, 7776–7785.
- (56) Shamis, M.; Shabat, D. Single-Triggered AB₆ Self-Immolative Dendritic Amplifiers. *Chemistry* **2007**, *13*, 4523–4528.
- (57) Shamis, M.; Lode, H. N.; Shabat, D. Bioactivation of Self-Immolative Dendritic Prodrugs by Catalytic Antibody 38C2. *J. Am. Chem. Soc.* **2004**, *126*, 1726–1731.
- (58) Haba, K.; Popkov, M.; Shamis, M.; Lerner, R. A.; Barbas, C. F., 3rd; Shabat, D. Single-Triggered Trimeric Prodrugs. *Angew. Chem. Int. Ed.* **2005**, *44*, 716–720.

- (59) Fomina, N.; McFearin, C. L.; Almutairi, A. Increasing Materials' Response to Two-Photon NIR Light Via Self-Immolative Dendritic Scaffolds. *Chem. Commun.* **2012**, *48*, 9138–9140.
- (60) Amir, R. J.; Shabat, D. Self-Immolative Dendrimer Biodegradability by Multi-Enzymatic Triggering. *Chem. Commun.* **2004**, 1614–1615.
- (61) Amir, R. J.; Popkov, M.; Lerner, R. A.; Barbas, C. F., 3rd; Shabat, D. Prodrug Activation Gated by a Molecular "OR" Logic Trigger. *Angew. Chem. Int. Ed.* **2005**, *44*, 4378–4381.
- (62) Danieli, E.; Shabat, D. Molecular Probe for Enzymatic Activity with Dual Output. *Biorg. Med. Chem.* **2007**, *15*, 7318–7324.
- (63) Amir, R. J.; Danieli, E.; Shabat, D. Receiver-Amplifier, Self-Immolative Dendritic Device. *Chem. Eur. J.* **2007**, *13*, 812–821.
- (64) Sagi, A.; Segal, E.; Satchi-Fainaro, R.; Shabat, D. Remarkable Drug-Release Enhancement with an Elimination-Based AB₃ Self-Immolative Dendritic Amplifier. *Biorg. Med. Chem.* **2007**, *15*, 3720–3727.
- (65) Sella, E.; Shabat, D. Self-Immolative Dendritic Probe for Direct Detection of Triacetone Triperoxide. *Chem. Commun.* **2008**, 5701–5703.
- (66) Wang, Z.; Wu, H.; Liu, P.; Zeng, F.; Wu, S. A Self-Immolative Prodrug Nanosystem Capable of Releasing a Drug and a NIR Reporter for *In Vivo* Imaging and Therapy. *Biomaterials* **2017**, *139*, 139–150.
- (67) Sella, E.; Shabat, D. Dendritic Chain Reaction. *J. Am. Chem. Soc.* **2009**, *131*, 9934–9936.
- (68) Avital-Shmilovici, M.; Shabat, D. Dendritic Chain Reaction: Responsive Release of Hydrogen Peroxide Upon Generation and Enzymatic Oxidation of Methanol. *Biorg. Med. Chem.* **2010**, *18*, 3643–3647.
- (69) Sella, E.; Lubelski, A.; Klafter, J.; Shabat, D. Two-Component Dendritic Chain Reactions: Experiment and Theory. *J. Am. Chem. Soc.* **2010**, *132*, 3945–3952.
- (70) Sella, E.; Weinstain, R.; Erez, R.; Burns, N. Z.; Baran, P. S.; Shabat, D. Sulfhydryl-Based Dendritic Chain Reaction. *Chem. Commun.* **2010**, *46*, 6575–6577.

- (71) Weinstain, R.; Sagi, A.; Karton, N.; Shabat, D. Self-Immolative Comb-Polymers: Multiple-Release of Side-Reporters by a Single Stimulus Event. *Chem. Eur. J.* **2008**, *14*, 6857–6861.
- (72) Weinstain, R.; Baran, P. S.; Shabat, D. Activity-Linked Labeling of Enzymes by Self-Immolative Polymers. *Bioconjugate Chem.* **2009**, *20*, 1783–1791.
- (73) Esser-Kahn, A. P.; Sottos, N. R.; White, S. R.; Moore, J. S. Programmable Microcapsules from Self-Immolative Polymers. *J. Am. Chem. Soc.* **2010**, *132*, 10266–10268.
- (74) Liu, G.; Wang, X.; Hu, J.; Zhang, G.; Liu, S. Self-Immolative Polymersomes for High-Efficiency Triggered Release and Programmed Enzymatic Reactions. *J. Am. Chem. Soc.* **2014**, *136*, 7492–7497.
- (75) Kumar, V.; Harris, J. T.; Ribbe, A.; Franc, M.; Bae, Y.; McNeil, A. J.; Thayumanavan, S. Construction from destruction: Hydrogel formation from triggered depolymerization-based release of an enzymatic catalyst. *ACS Macro Lett.* **2020**, *9*, 377–381.
- (76) Gnaim, S.; Shabat, D. Self-Immolative Chemiluminescence Polymers: Innate Assimilation of Chemiexcitation in a Domino-Like Depolymerization. *J. Am. Chem. Soc.* **2017**, *139*, 10002–10008.
- (77) de Gracia Lux, C.; Joshi-Barr, S.; Nguyen, T.; Mahmoud, E.; Schopf, E.; Fomina, N.; Almutairi, A. Biocompatible Polymeric Nanoparticles Degrade and Release Cargo in Response to Biologically Relevant Levels of Hydrogen Peroxide. *J. Am. Chem. Soc.* **2012**, *134*, 15758–15764.
- (78) Chen, E. K. Y.; McBride, R. A.; Gillies, E. R. Self-Immolative Polymers Containing Rapidly Cyclizing Spacers: Toward Rapid Depolymerization Rates. *Macromolecules* **2012**, *45*, 7364–7374.
- (79) Dewit, M. A.; Beaton, A.; Gillies, E. R. A Reduction Sensitive Cascade Biodegradable Linear Polymer. *J. Polym. Sci., Part A: Polym. Chem.* **2010**, *48*, 3977–3985.
- (80) Zhang, L. J.; Deng, X. X.; Du, F. S.; Li, Z. C. Chemical Synthesis of Functional Poly(4-hydroxybutyrate) with Controlled Degradation via Intramolecular Cyclization. *Macromolecules* **2013**, *46*, 9554–9562.

- (81) Baker, M. S.; Kim, H.; Olah, M. G.; Lewis, G. G.; Phillips, S. T. Depolymerizable Poly(benzyl ether)-Based Materials for Selective Room Temperature Recycling. *Green Chemistry* **2015**, *17*, 4541–4545.
- (82) Uno, T.; Minari, M.; Kubo, M.; Itoh, T. Asymmetric anionic polymerization of 2,6-dimethyl-7-phenyl-1,4-benzoquinone methide. *J. Polym. Sci., Part A: Polym. Chem.* **2004**, *42*, 4548–4555.
- (83) Olah, M. G.; Robbins, J. S.; Baker, M. S.; Phillips, S. T. End-Capped Poly(benzyl ethers): Acid and Base Stable Polymers That Depolymerize Rapidly from Head-to-Tail in Response to Specific Applied Signals. *Macromolecules* **2013**, *46*, 5924–5928.
- (84) Ergene, C.; Palermo, E. F. Cationic Poly(benzyl ether)s as Self-Immolative Antimicrobial Polymers. *Biomacromolecules* **2017**, *18*, 3400–3409.
- (85) Ergene, C.; Palermo, E. F. Self-Immolative Polymers with Potent and Selective Antibacterial Activity by Hydrophilic Side Chain Grafting. *J. Mater. Chem. B* **2018**, *6*, 7217–7229.
- (86) Yeung, K.; Kim, H.; Mohapatra, H.; Phillips, S. T. Surface-Accessible Detection Units in Self-Immolative Polymers Enable Translation of Selective Molecular Detection Events into Amplified Responses in Macroscopic, Solid-State Plastics. *J. Am. Chem. Soc.* **2015**, *137*, 5324–5327.
- (87) Xiao, Y.; Li, Y.; Zhang, B.; Li, H.; Cheng, Z.; Shi, J.; Xiong, J.; Bai, Y.; Zhang, K. Functionalizable, Side Chain-Immolative Poly(benzyl ether)s. *ACS Macro Lett.* **2019**, *8*, 399–402.
- (88) Aso, C.; Tagami, S. Cyclopolymerization of *o*-Phthalaldehyde. *Journal of Polymer Science Part B: Polymer Letters* **1967**, *5*, 217–220.
- (89) Aso, C.; Tagami, S. Polymerization of Aromatic Aldehydes. III. The Cyclopolymerization of Phthalaldehyde and the Structure of the Polymer. *Macromolecules* **1969**, *2*, 414–419.
- (90) Seo, W.; Phillips, S. T. Patterned Plastics That Change Physical Structure in Response to Applied Chemical Signals. *J. Am. Chem. Soc.* **2010**, *132*, 9234–9235.
- (91) DiLauro, A. M.; Robbins, J. S.; Phillips, S. T. Reproducible and Scalable Synthesis of End-Cap-Functionalized Depolymerizable Poly(phthalaldehydes). *Macromolecules* **2013**, *46*, 2963–2968.

- (92) Zhang, H.; Yeung, K.; Robbins, J. S.; Pavlick, R. A.; Wu, M.; Liu, R.; Sen, A.; Phillips, S. T. Self-Powered Microscale Pumps Based on Analyte-Initiated Depolymerization Reactions. *Angew. Chem. Int. Ed.* **2012**, *51*, 2400–2404.
- (93) DiLauro, A. M.; Abbaspourrad, A.; Weitz, D. A.; Phillips, S. T. Stimuli-Responsive Core–Shell Microcapsules with Tunable Rates of Release by Using a Depolymerizable Poly(phthalaldehyde) Membrane. *Macromolecules* **2013**, *46*, 3309–3313.
- (94) Coulembier, O.; Knoll, A.; Pires, D.; Gotsmann, B.; Duerig, U.; Frommer, J.; Miller, R. D.; Dubois, P.; Hedrick, J. L. Probe-Based Nanolithography: Self-Amplified Depolymerization Media for Dry Lithography. *Macromolecules* **2010**, *43*, 572–574.
- (95) Knoll, A. W.; Pires, D.; Coulembier, O.; Dubois, P.; Hedrick, J. L.; Frommer, J.; Duerig, U. Probe-Based 3-D Nanolithography Using Self-Amplified Depolymerization Polymers. *Adv. Mater.* **2010**, *22*, 3361–3365.
- (96) Cheong, L. L.; Paul, P.; Holzner, F.; Despont, M.; Coady, D. J.; Hedrick, J. L.; Allen, R.; Knoll, A. W.; Duerig, U. Thermal Probe Maskless Lithography for 27.5 nm Half-Pitch Si Technology. *Nano Lett.* **2013**, *13*, 4485–4491.
- (97) Skaug, M. J.; Schwemmer, C.; Fringes, S.; Rawlings, C. D.; Knoll, A. W. Nanofluidic Rocking Brownian Motors. *Science* **2018**, *359*, 1505–1508.
- (98) DiLauro, A. M.; Lewis, G. G.; Phillips, S. T. Self-Immolative Poly(4,5-dichlorophthalaldehyde) and its Applications in Multi-Stimuli-Responsive Macroscopic Plastics. *Angew. Chem. Int. Ed.* **2015**, *54*, 6200–6205.
- (99) DiLauro, A. M.; Phillips, S. T. End-Capped Poly(4,5-dichlorophthalaldehyde): A Stable Self-Immolative Poly(aldehyde) for Translating Specific Inputs Into Amplified Outputs, Both in Solution and the Solid State. *Polym. Chem.* **2015**, *6*, 3252–3258.
- (100) Crutchfield, M. M.; Papanu, V. D.; Warren, C. B. Polymeric Acetal Carboxylates. U.S. Patent 4,144,226, March 13, 1979.
- (101) Brachais, C. H.; Huguet, J.; Bunel, C. Synthesis, Characterization and Stabilization of Poly(methyl glyoxylate). *Polymer* **1997**, *38*, 4959–4964.
- (102) Burel, F.; Rossignol, L.; Pontvianne, P.; Hartman, J.; Couesnon, N.; Bunel, C. Synthesis and Characterization of Poly(ethyl glyoxylate) – A New Potentially Biodegradable Polymer. *e-Polymers* **2003**, *3*.

- (103) Belloncle, B.; Burel, F.; Oulyadi, H.; Bunel, C. Study of the *In Vitro* Degradation of Poly(ethyl glyoxylate). *Polym. Degrad. Stab.* **2008**, *93*, 1151–1157.
- (104) Belloncle, B.; Bunel, C.; Menu-Bouaouiche, L.; Lesouhaitier, O.; Burel, F. Study of the Degradation of Poly(ethyl glyoxylate): Biodegradation, Toxicity and Ecotoxicity Assays. *J. Polym. Environ.* **2012**, *20*, 726–731.
- (105) Fan, B.; Trant, J. F.; Wong, A. D.; Gillies, E. R. Polyglyoxylates: A Versatile Class of Triggerable Self-Immolative Polymers from Readily Accessible Monomers. *J. Am. Chem. Soc.* **2014**, *136*, 10116–10123.
- (106) Rabiee Kenaree, A.; Gillies, E. R. Controlled Polymerization of Ethyl Glyoxylate Using Alkylolithium and Alkoxide Initiators. *Macromolecules* **2018**, *51*, 5501–5510.
- (107) Hewitt, D. R. O.; Grubbs, R. B. Amine-Catalyzed Chain Polymerization of Ethyl Glyoxylate from Alcohol and Thiol Initiators. *ACS Macro Lett.* **2021**, *10*, 370–374.
- (108) Fan, B.; Trant, J. F.; Gillies, E. R. End-Capping Strategies for Triggering End-to-End Depolymerization of Polyglyoxylates. *Macromolecules* **2016**, *49*, 9309–9319.
- (109) Fan, B.; Trant, J. F.; Hemery, G.; Sandre, O.; Gillies, E. R. Thermo-Responsive Self-Immolative Nanoassemblies: Direct and Indirect Triggering. *Chem. Commun.* **2017**, *53*, 12068–12071.
- (110) Fan, B.; Gillies, E. R. Poly(ethyl glyoxylate)-Poly(ethylene oxide) Nanoparticles: Stimuli-Responsive Drug Release via End-to-End Polyglyoxylate Depolymerization. *Mol. Pharmaceutics* **2017**, *14*, 2548–2559.
- (111) Fan, B.; Yardley, R. E.; Trant, J. F.; Borecki, A.; Gillies, E. R. Tuning the Hydrophobic Cores of Self-Immolative Polyglyoxylate Assemblies. *Polym. Chem.* **2018**, *9*, 2601–2610.
- (112) Gambles, M. T.; Fan, B.; Borecki, A.; Gillies, E. R. Hybrid Polyester Self-Immolative Polymer Nanoparticles for Controlled Drug Release. *ACS Omega* **2018**, *3*, 5002–5011.
- (113) Fan, B.; Trant, J. F.; Yardley, R. E.; Pickering, A. J.; Lagugn e-Labarthe, F.; Gillies, E. R. Photocontrolled Degradation of Stimuli-Responsive Poly(ethyl glyoxylate): Differentiating Features and Traceless Ambient Depolymerization. *Macromolecules* **2016**, *49*, 7196–7203.

- (114) Fan, B.; Salazar, R.; Gillies, E. R. Depolymerization of Trityl End-Capped Poly(ethyl glyoxylate): Potential Applications in Smart Packaging. *Macromol. Rapid Commun.* **2018**, *39*, 1800173.
- (115) Heuchan, S. M.; MacDonald, J. P.; Bauman, L. A.; Fan, B.; Henry, H. A. L.; Gillies, E. R. Photoinduced Degradation of Polymer Films Using Polyglyoxylate–Polyester Blends and Copolymers. *ACS Omega* **2018**, *3*, 18603–18612.
- (116) Heuchan, S. M.; Fan, B.; Kowalski, J. J.; Gillies, E. R.; Henry, H. A. L. Development of Fertilizer Coatings from Polyglyoxylate-Polyester Blends Responsive to Root-Driven pH Change. *J. Agric. Food. Chem.* **2019**, *67*, 12720–12729.
- (117) Yardley, R. E.; Kenaree, A. R.; Liang, X.; Gillies, E. R. Transesterification of Poly(ethyl glyoxylate): A Route to Structurally Diverse Polyglyoxylates. *Macromolecules* **2020**, *53*, 8600–8609.
- (118) Sirianni, Q. E. A.; Rabiee Kenaree, A.; Gillies, E. R. Polyglyoxylamides: Tuning Structure and Properties of Self-Immolative Polymers. *Macromolecules* **2019**, *52*, 262–270.
- (119) Ree, L. H. S.; Sirianni, Q. E. A.; Gillies, E. R.; Kelland, M. A. Systematic Study of Polyglyoxylamides as Powerful, High-Cloud-Point Kinetic Hydrate Inhibitors. *Energy Fuels* **2019**, *33*, 2067–2075.
- (120) Rabiee Kenaree, A.; Sirianni, Q. E. A.; Classen, K.; Gillies, E. R. Thermoresponsive Self-Immolative Polyglyoxylamides. *Biomacromolecules* **2020**, *21*, 3817–3825.
- (121) Brown, J. R.; O'Donnell, J. H. γ Radiolysis of Poly(butene-1 sulfone) and Poly(hexane-1 sulfone). *Macromolecules* **1972**, *5*, 109–114.
- (122) Sasaki, T.; Le, K. V.; Naka, Y., Poly(olefin sulfone)s. In *Alkenes*; Davarnejad, R.; Sajjadi, B., Eds.; IntechOpen: London, UK, 2018.
- (123) Bowden, M. J.; Thompson, L. F. Poly(styrene sulfone)—A Sensitive Ion-Millable Positive Electron Beam Resist. *J. Electrochem. Soc.* **1974**, *121*, 1620–1623.
- (124) Bowden, M. J.; Chandross, E. A. Poly(vinyl arene sulfones) as Novel Positive Photoresists. *J. Electrochem. Soc.* **1975**, *122*, 1370–1374.
- (125) Jiang, Y.; Fréchet, J. M. J. Design and synthesis of thermally labile polymers for microelectronics. Poly(vinyl *tert*-butyl carbonate-sulfone). *Macromolecules* **1991**, *24*, 3528–3532.

- (126) Lee, O. P.; Lopez Hernandez, H.; Moore, J. S. Tunable Thermal Degradation of Poly(vinyl butyl carbonate sulfone)s via Side-Chain Branching. *ACS Macro Lett.* **2015**, *4*, 665–668.
- (127) Lobe, J. M.; Swager, T. M. Radiation Detection: Resistivity Responses in Functional Poly(olefin sulfone)/Carbon Nanotube Composites. *Angew. Chem. Int. Ed.* **2010**, *49*, 95–98.
- (128) Kumar, K.; Goodwin, A. P. Alternating Sulfone Copolymers Depolymerize in Response to Both Chemical and Mechanical Stimuli. *ACS Macro Lett.* **2015**, *4*, 907–911.
- (129) Kumar, K.; Castaño, E. J.; Weidner, A. R.; Yildirim, A.; Goodwin, A. P. Depolymerizable poly(*O*-vinyl carbamate-*alt*-sulfones) as customizable macromolecular scaffolds for mucosal drug delivery. *ACS Macro Lett.* **2016**, *5*, 636–640.
- (130) Joo, W.; Wang, W.; Mesch, R.; Matsuzawa, K.; Liu, D.; Willson, C. G. Synthesis of Unzipping Polyester and a Study of its Photochemistry. *J. Am. Chem. Soc.* **2019**, *141*, 14736–14741.
- (131) Yuan, J.; Xiong, W.; Zhou, X.; Zhang, Y.; Shi, D.; Li, Z.; Lu, H. 4-Hydroxyproline-Derived Sustainable Polythioesters: Controlled Ring-Opening Polymerization, Complete Recyclability, and Facile Functionalization. *J. Am. Chem. Soc.* **2019**, *141*, 4928–4935.
- (132) Xiong, W.; Chang, W.; Shi, D.; Yang, L.; Tian, Z.; Wang, H.; Zhang, Z.; Zhou, X.; Chen, E.-Q.; Lu, H. Geminal Dimethyl Substitution Enables Controlled Polymerization of Penicillamine-Derived β -Thiolactones and Reversed Depolymerization. *Chem* **2020**, *6*, 1831–1843.
- (133) Kim, H.; Brooks, A. D.; DiLauro, A. M.; Phillips, S. T. Poly(carboxypyrrole)s that Depolymerize from Head to Tail in the Solid State in Response to Specific Applied Signals. *J. Am. Chem. Soc.* **2020**, *142*, 9447–9452.
- (134) Josse, T.; De Winter, J.; Gerbaux, P.; Coulembier, O. Cyclic polymers by ring-closure strategies. *Angew. Chem. Int. Ed.* **2016**, *55*, 13944–13958.
- (135) Kaitz, J. A.; Diesendruck, C. E.; Moore, J. S. End Group Characterization of Poly(phthalaldehyde): Surprising Discovery of a Reversible, Cationic Macrocyclization Mechanism. *J. Am. Chem. Soc.* **2013**, *135*, 12755–12761.

- (136) Kaitz, J. A.; Diesendruck, C. E.; Moore, J. S. Dynamic Covalent Macrocyclic Poly(phthalaldehyde)s: Scrambling Cyclic Homopolymer Mixtures Produces Multi-Block and Random Cyclic Copolymers. *Macromolecules* **2013**, *46*, 8121–8128.
- (137) Kaitz, J. A.; Moore, J. S. Copolymerization of *o*-Phthalaldehyde and Ethyl Glyoxylate: Cyclic Macromolecules with Alternating Sequence and Tunable Thermal Properties. *Macromolecules* **2014**, *47*, 5509–5513.
- (138) Schwartz, J. M.; Gourdin, G.; Phillips, O.; Engler, A.; Lee, J.; Abdulkadir, N. R.; Miller, R. C.; Sutlief, A.; Kohl, P. A. Cationic Polymerization of High-Molecular-Weight Phthalaldehyde-Butanal Copolymer. *J. Appl. Polym. Sci.* **2019**, *136*, 46921.
- (139) Engler, A.; Phillips, O.; Miller, R. C.; Tobin, C.; Kohl, P. A. Cationic Copolymerization of *o*-Phthalaldehyde and Functional Aliphatic Aldehydes. *Macromolecules* **2019**, *52*, 4020–4029.
- (140) Lutz, J. P.; Davydovich, O.; Hannigan, M. D.; Moore, J. S.; Zimmerman, P. M.; McNeil, A. J. Functionalized and Degradable Polyphthalaldehyde Derivatives. *J. Am. Chem. Soc.* **2019**, *141*, 14544–14548.
- (141) Diesendruck, C. E.; Peterson, G. I.; Kulik, H. J.; Kaitz, J. A.; Mar, B. D.; May, P. A.; White, S. R.; Martinez, T. J.; Boydston, A. J.; Moore, J. S. Mechanically Triggered Heterolytic Unzipping of a Low-Ceiling-Temperature Polymer. *Nature Chemistry* **2014**, *6*, 623–628.
- (142) Tang, S.; Tang, L.; Lu, X.; Liu, H.; Moore, J. S. Programmable Payload Release from Transient Polymer Microcapsules Triggered by a Specific Ion Coactivation Effect. *J. Am. Chem. Soc.* **2018**, *140*, 94–97.
- (143) Hernandez, H. L.; Kang, S. K.; Lee, O. P.; Hwang, S. W.; Kaitz, J. A.; Inci, B.; Park, C. W.; Chung, S.; Sottos, N. R.; Moore, J. S.; Rogers, J. A.; White, S. R. Triggered Transience of Metastable Poly(phthalaldehyde) for Transient Electronics. *Adv. Mater.* **2014**, *26*, 7637–7642.
- (144) Park, C. W.; Kang, S. K.; Hernandez, H. L.; Kaitz, J. A.; Wie, D. S.; Shin, J.; Lee, O. P.; Sottos, N. R.; Moore, J. S.; Rogers, J. A.; White, S. R. Thermally Triggered Degradation of Transient Electronic Devices. *Adv. Mater.* **2015**, *27*, 3783–3788.

- (145) Lee, K. M.; Phillips, O.; Engler, A.; Kohl, P. A.; Rand, B. P. Phototriggered Depolymerization of Flexible Poly(phthalaldehyde) Substrates by Integrated Organic Light-Emitting Diodes. *ACS Appl. Mater. Interfaces* **2018**, *10*, 28062–28068.
- (146) Phillips, O.; Engler, A.; Schwartz, J. M.; Jiang, J.; Tobin, C.; Guta, Y. A.; Kohl, P. A. Sunlight Photodepolymerization of Transient Polymers. *J. Appl. Polym. Sci.* **2019**, *136*, 47141.
- (147) Jiang, J.; Phillips, O.; Engler, A.; Vong, M. H.; Kohl, P. A. Time-Delayed Photo-Induced Depolymerization of Poly(phthalaldehyde) Self-Immolative Polymer Via *In Situ* Formation of Weak Conjugate Acid. *Polym. Adv. Technol.* **2019**, *30*, 1656–1662.
- (148) Jiang, J.; Phillips, O.; Engler, A.; Vong, M. H.; Kohl, P. A. Photodegradable Transient Bilayered Poly(phthalaldehyde) with Improved Shelf Life. *Polym. Adv. Technol.* **2019**, *30*, 1198–1204.
- (149) Feinberg, A. M.; Hernandez, H. L.; Plantz, C. L.; Mejia, E. B.; Sottos, N. R.; White, S. R.; Moore, J. S. Cyclic Poly(phthalaldehyde): Thermoforming a Bulk Transient Material. *ACS Macro Lett.* **2018**, *7*, 47–52.
- (150) Feinberg, A. M.; Davydovich, O.; Lloyd, E. M.; Ivanoff, D. G.; Shiang, B.; Sottos, N. R.; Moore, J. S. Triggered Transience of Plastic Materials by a Single Electron Transfer Mechanism. *ACS Central Science* **2020**, *6*, 266–273.
- (151) Lloyd, E. M.; Lopez Hernandez, H.; Feinberg, A. M.; Yourdkhani, M.; Zen, E. K.; Mejia, E. B.; Sottos, N. R.; Moore, J. S.; White, S. R. Fully Recyclable Metastable Polymers and Composites. *Chem. Mater.* **2019**, *31*, 398–406.
- (152) Kaitz, J. A.; Diesendruck, C. E.; Moore, J. S. Divergent Macrocyclization Mechanisms in the Cationic Initiated Polymerization of Ethyl Glyoxylate. *Macromolecules* **2014**, *47*, 3603–3607.
- (153) Liu, Y.; Jia, Y.; Wu, Q.; Moore, J. S. Architecture-Controlled Ring-Opening Polymerization for Dynamic Covalent Poly(disulfide)s. *J. Am. Chem. Soc.* **2019**, *141*, 17075–17080.
- (154) Bang, E.-K.; Gasparini, G.; Molinard, G.; Roux, A.; Sakai, N.; Matile, S. Substrate-initiated synthesis of cell-penetrating poly(disulfide)s. *J. Am. Chem. Soc.* **2013**, *135*, 2088–2091.

- (155) Gasparini, G.; Bang, E.-K.; Molinard, G.; Tulumello, D. V.; Ward, S.; Kelley, S. O.; Roux, A.; Sakai, N.; Matile, S. Cellular uptake of substrate-initiated cell-penetrating poly(disulfide)s. *J. Am. Chem. Soc.* **2014**, *136*, 6069–6074.
- (156) Zhang, X.; Waymouth, R. M. 1,2-Dithiolane-derived dynamic, covalent materials: Cooperative self-assembly and reversible cross-linking. *J. Am. Chem. Soc.* **2017**, *139*, 3822–3833.
- (157) Verduzco, R.; Li, X.; Pesek, S. L.; Stein, G. E. Structure, function, self-assembly, and applications of bottlebrush copolymers. *Chem. Soc. Rev.* **2015**, *44*, 2405–2420.
- (158) Wu, Y.; Zhang, L.; Zhang, M.; Liu, Z.; Zhu, W.; Zhang, K. Bottlebrush Polymers with Self-Immolative Side Chains. *Polym. Chem.* **2018**, *9*, 1799–1806.
- (159) Xiao, Y.; Li, H.; Zhang, B.; Cheng, Z.; Li, Y.; Tan, X.; Zhang, K. Modulating the Depolymerization of Self-Immolative Brush Polymers with Poly(benzyl ether) Backbones. *Macromolecules* **2018**, *51*, 2899–2905.
- (160) Kaitz, J. A.; Moore, J. S. Functional Phthalaldehyde Polymers by Copolymerization with Substituted Benzaldehydes. *Macromolecules* **2013**, *46*, 608–612.
- (161) Kaitz, J. A.; Possanza, C. M.; Song, Y.; Diesendruck, C. E.; Spiering, A. J. H.; Meijer, E. W.; Moore, J. S. Depolymerizable, Adaptive Supramolecular Polymer Nanoparticles and Networks. *Polym. Chem.* **2014**, *5*, 3788–3794.
- (162) Neary, W. J.; Isais, T. A.; Kennemur, J. G. Self-Immolative Bottlebrush Polypentenamers and Their Macromolecular Metamorphosis. *J. Am. Chem. Soc.* **2019**, *141*, 14220–14229.
- (163) Lobez, J. M.; Swager, T. M. Disassembly of Elastomers: Poly(olefin sulfone)–Silicones with Switchable Mechanical Properties. *Macromolecules* **2010**, *43*, 10422–10426.
- (164) Sasaki, T.; Hashimoto, S.; Nogami, N.; Sugiyama, Y.; Mori, M.; Naka, Y.; Le, K. V. Dismantlable Thermosetting Adhesives Composed of a Cross-Linkable Poly(olefin sulfone) with a Photobase Generator. *ACS Appl. Mater. Interfaces* **2016**, *8*, 5580–5585.
- (165) Liu, G.; Zhang, G.; Hu, J.; Wang, X.; Zhu, M.; Liu, S. Hyperbranched Self-Immolative Polymers (hSIPs) for Programmed Payload Delivery and Ultrasensitive Detection. *J. Am. Chem. Soc.* **2015**, *137*, 11645–11655.

Chapter 3

3 The Synthesis of Self-Immolative Polyglyoxylamides via Post-Polymerization Amidation

3.1 Introduction

Stimuli-responsive polymers are a class of materials that can undergo changes in their physical or chemical properties when exposed to specific stimuli. They have been explored for a wide range of applications from smart coatings to drug delivery systems.¹⁻⁴ For example, thermo-responsive polymers such as poly(*N*-isopropylacrylamide) undergo entropically driven aggregation and precipitation above their lower critical solution temperatures.⁵ This property has been exploited for the development of hydrogel valves in microfluidic channels⁶ and for the controlled release of drugs.⁷⁻⁸ In other cases, stimuli led to polymer degradation. For example, polyacetals undergo selective degradation at acidic pH. Various polyacetals have been reported⁹⁻¹¹ and have shown promise for targeted drug delivery *in vivo*.

Self-immolative polymers (SIPs) are a recently developed subset of stimuli-responsive degradable polymers that undergo end-to-end depolymerization in response to stimuli. Most SIPs possess stabilizing end-caps at their termini that can be cleaved off by specific stimuli. Cleavage initiates a cascade of reactions resulting in the conversion of the polymer into small molecules (Figure 3.1a–c).¹² Since their introduction in 2008,¹³ significant developments have been reported including the introduction of backbones such as polycarbamates,¹³⁻¹⁴ poly(benzyl ether)s,¹⁵ and polyacetals¹⁶⁻¹⁷ that depolymerize by different mechanisms such as eliminations,^{13, 15} cyclizations,¹⁸ and combinations of eliminations and cyclizations,^{14, 19} or based on low polymer ceiling temperatures.¹⁶⁻¹⁷ Additionally, various end-caps have been incorporated onto SIPs, enabling their depolymerization to be initiated by different stimuli including light,²⁰⁻²¹ heat,²²⁻²³ changes in redox^{21, 24-25} or pH²⁵⁻²⁶ conditions, and in response to the activity of specific enzymes.^{13,}

*This chapter contains work that has been published previously: Sirianni, Q. E. A.; Rabiee Kenaree, A.; Gillies, E. R. Polyglyoxylamides: Tuning Structure and Properties of Self-Immolative Polymers. *Macromolecules* **2019**, 52, 262–270. See Co-Authorship Statement for the contributions of each author.

²⁷ Furthermore, the utility of SIPs in applications such as transient plastics,^{16, 28} degradable microcapsules,^{26, 29} drug delivery vehicles,^{21, 30-32} microscale pumps,³³ and sensors³⁴⁻³⁸ has been demonstrated.

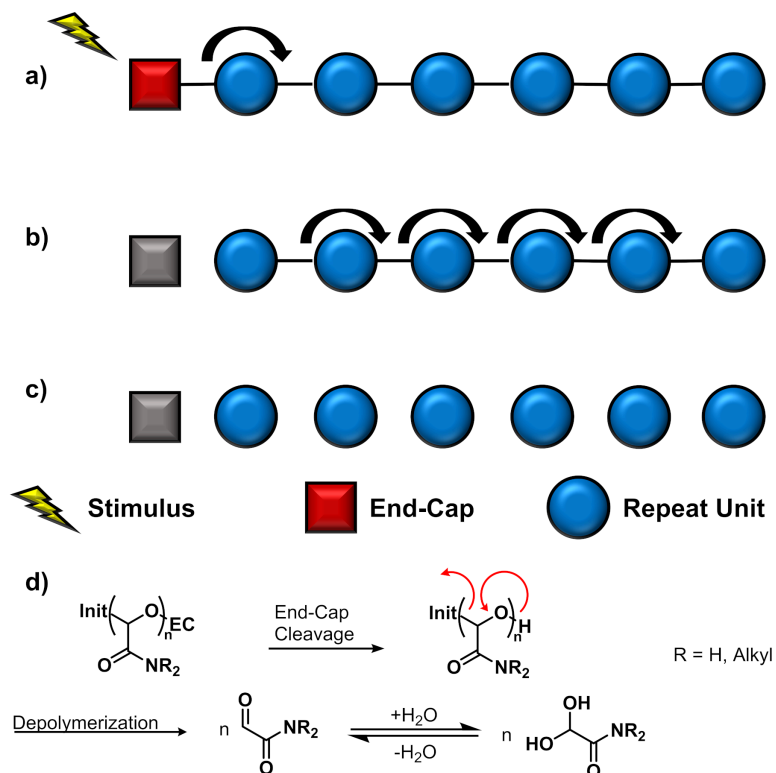


Figure 3.1. a) SIPs are stabilized with an end-cap that can be cleaved off in the presence of a particular stimulus. b) Removal of the end-cap leads to a cascade depolymerization of the polymer chain. c) The depolymerization products include the end-cap and repeat units of the polymer, which may be the original monomers or derivative products depending on the depolymerization mechanism. d) A polyglyoxylamide depolymerizes upon cleavage of the end-cap. Init = polymerization initiator; EC = end-cap.

Our group reported polyglyoxylates as a class of SIPs.¹⁷ Polyglyoxylates have advantages including their preparation from commercially available monomers or monomers that can be synthesized from readily available precursors such as fumaric or maleic acid. In addition, the depolymerization product glyoxylic acid hydrate is an intermediate in the glyoxylic acid cycle and is non-harmful to the environment.³⁹ Based on their properties and depolymerization behaviour, polyglyoxylates are finding applications in areas such as

smart coatings^{38, 40} and drug delivery vehicles.³⁰⁻³² Polyglyoxylates inherently have pendent ester groups at each repeat unit, and the eventual hydrolysis of these esters reveals carboxylic acids that can intramolecularly catalyze backbone acetal hydrolysis, leading to depolymerization. Thus, polyglyoxylates have a limited lifetime even in their non-triggered state, which can be advantage or limitation depending on the application. All of the previously reported polyglyoxylates have been insoluble in water.^{17, 32, 39, 41-42}

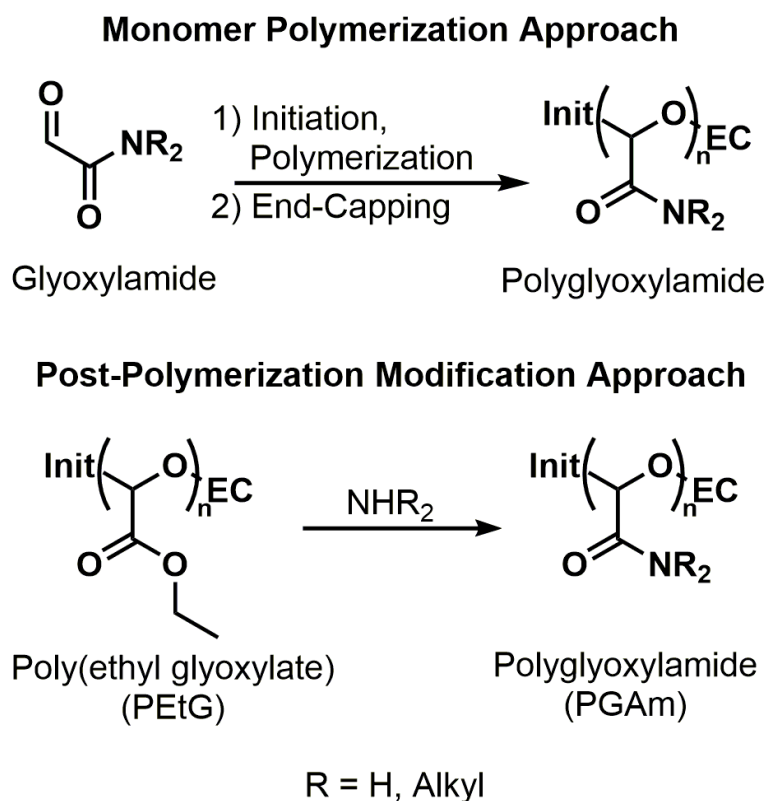
The replacement of the ester pendent groups of polyglyoxylates with amides should slow side chain hydrolysis, stabilizing the polymers in their untriggered state, while at the same time yielding polymers with different physical and thermal properties that are capable of triggered end-to-end depolymerization (Figure 3.1d). Thus, we report here the syntheses of polyglyoxylamides (PGAm), a new class of SIPs. Several different amines were used to prepare PGAm from poly(ethyl glyoxylate) (PEtG) using mild post-polymerization modification conditions to provide an array of new properties and functions while retaining the abilities of the polymers to depolymerize in response to stimuli. For example, relative to 25 °C, the highest glass transition temperature (T_g) reported for a polyglyoxylate,¹⁷ the measured T_g values of the studied PGAm ranged from 39–90 °C. Additionally, several of the new PGAm demonstrated water-solubility. Finally, using amine-terminated oligo(ethylene glycol) (OEG), a PGAm analogue of poly[oligo(ethylene glycol) methacrylate] (POEGMA), a graft copolymer analogue of poly(ethylene glycol) (PEG) that exhibits the favorable stealthy properties of PEG,⁴³ was synthesized.

3.2 Results and Discussion

3.2.1 Synthetic Approaches to Polyglyoxylamides

There are two potential approaches for synthesizing PGAm (Scheme 3.1). The first is the monomer polymerization approach, where glyoxylamide monomers are synthesized and purified before being polymerized. While ensuring amide moieties at each repeat unit, the limitation of this approach is that each unique glyoxylamide would need to be synthesized and purified independently. The second approach to synthesize PGAm is the post-polymerization modification of polyglyoxylates. This approach has several advantages

including the ease of synthesis of the PEtG precursor from commercially available monomer, the one-step amidation reaction of PEtG, and the ability to create a small library of different PGAMs from a single batch of PEtG, allowing all of the PGAMs to have the same degree of polymerization (DP_n) for structure-property comparisons. Post-polymerization modification by amidation has been noted to be an effective method when used to replace ester pendent groups on polymers.⁴⁴ Therefore, to synthesize self-immolative PGAMs for study, post-polymerization modification was pursued.

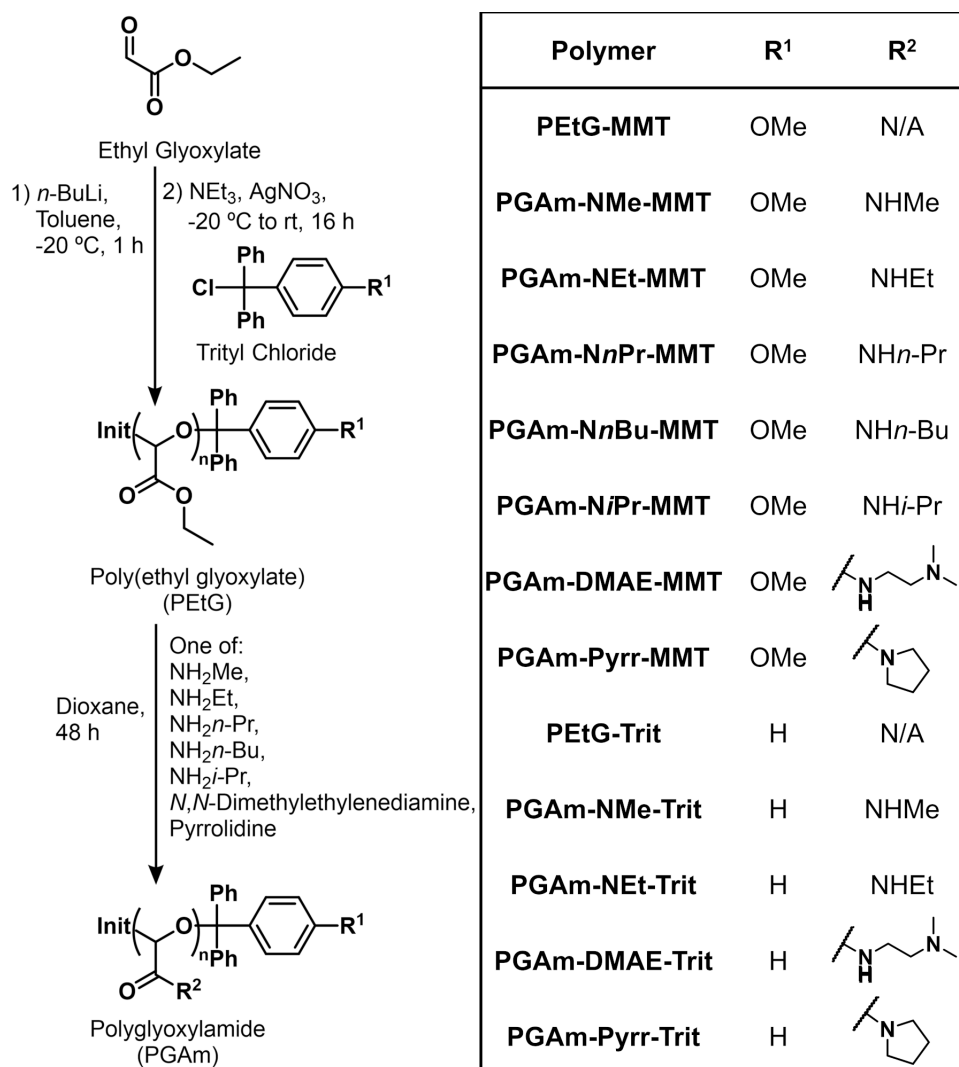


Scheme 3.1. Synthetic approaches for obtaining PGAMs.

3.2.2 Synthesis of 4-Monomethoxytrityl End-Capped PEtG for Post-Polymerization Modification

To synthesize different PGAMs via post-polymerization modification, a PEtG precursor with an appropriate stimuli-responsive end-cap was needed. First, PEtG with a 4-monomethoxytrityl end-cap (**PEtG-MMT**) was targeted (Scheme 3.2). This end-cap was selected because prior work has shown it to serve as an acid-sensitive end-cap for PEtG.²⁵

In addition, unlike many other reported end-caps that are conjugated to the PEtG terminus by a carbonate or carbamate linkage,^{17, 23, 25} the trityl moiety connects to the polymer via an ether linkage. An ether linkage is not susceptible to cleavage in the post-polymerization modification conditions as it does not possess a carbonyl moiety for nucleophilic attack by the amines.



Scheme 3.2. Synthesis of PGAMs (MMT = 4-monomethoxytrityl, Trit = trityl).

PEtG-MMT was synthesized by a modified version of our previously reported method (Scheme 3.2).⁴⁵ *n*-Butyllithium was used to initiate an anionic polymerization of ethyl glyoxylate in toluene at $-20\text{ }^{\circ}\text{C}$. In addition to 4-monomethoxytrityl chloride as an end-cap and triethylamine (NEt_3), AgNO_3 was added as Ag^+ can scavenge Cl^- ions, thereby

enhancing the end-capping yield. Purification resulted in a colourless tacky solid. Analysis by ^1H NMR, ^{13}C NMR, and FT-IR spectroscopic methods confirmed the structure of the polymer by comparison with previous reports (Figure A2.1, Figure A2.15, Figure A2.29).^{17, 25} Size-exclusion chromatography (SEC) in *N,N*-dimethylformamide (DMF) relative to poly(methyl methacrylate) (PMMA) standards suggested that **PEtG-MMT** had a number-average molar mass (M_n) of 51.8 kg/mol and a dispersity (D) of 1.4. Because of the polymer's high molar mass, end-group analysis by ^1H NMR spectroscopy could not be used to determine the DP_n of the **PEtG-MMT** or any of the PGAMs subsequently synthesized from it. However, thermogravimetric analysis (TGA) confirmed that the polymer was effectively end-capped as it was stable to 170 °C, whereas uncapped PEtG was previously demonstrated to degrade at 84 °C during TGA.¹⁷

3.2.3 Synthesis of 4-Monomethoxytrityl End-Capped PGAMs (PGAM-MMTs)

To perform the post-polymerization modification, **PEtG-MMT** was dissolved in dry 1,4-dioxane, then reacted with a 5-fold molar excess of amine for 48 h to afford the corresponding PGAM-MMT (Scheme 3.2). Different primary amines including methylamine, ethylamine, *n*-propylamine, *n*-butylamine, and isopropylamine were used to investigate basic structure-property relationships among simple PGAMs. Pyrrolidine was used as a secondary amine. Other secondary amines such as dimethylamine and diethylamine were also investigated in preliminary work but led to incomplete conversion, suggesting that the ring structure of pyrrolidine is important for its reactivity. *N,N*-Dimethylethylenediamine was selected to introduce pendent pH-sensitive tertiary amine groups to the polymer. The polymers were first isolated by the removal of the volatile amines, ethanol, and solvent from the reaction mixtures under vacuum. The crude polymer residues were subsequently dissolved in minimal CH_2Cl_2 and precipitated in *n*-pentane. Decanting off the liquid and drying the precipitate under vacuum afforded the purified polymers.

The purified polymers were characterized by ^1H NMR, ^{13}C NMR, and FT-IR spectroscopy to confirm that complete conversion to the amides had occurred (Figure A2.2–Figure A2.8,

Figure A2.16–Figure A2.22). Comparison of the ^1H NMR spectrum of **PEtG-MMT** to spectra of the PGAm-MMTs revealed several key differences (Figure 3.2). First, the peak corresponding to the backbone methine protons changed from a sharp multiplet at $\delta \sim 5.6$ ppm in **PEtG-MMT** into a broad singlet in the PGAm-MMTs. In addition, the peaks corresponding to the ester CH_2 and CH_3 protons at δ 4.21 and 1.28 ppm respectively disappeared and new peaks corresponding to the functional groups on the amide appeared. For example, in the spectrum of **PGAm-NEt-MMT**, two new peaks at δ 3.25 and 1.13 ppm corresponding to the amide CH_2 and CH_3 protons respectively were observed. Finally, in all cases except for **PGAm-Pyrr-MMT** (tertiary amide), a broad multiplet appeared within the range of 7.50–9.50 ppm corresponding to the NH protons of the amide pendent groups. In the FT-IR spectra (Figure A2.29) the PGAm-MMTs had a characteristic C=O amide stretch at $\sim 1650\text{ cm}^{-1}$, in contrast with **PEtG-MMT**, which had a characteristic C=O ester stretch at $\sim 1750\text{ cm}^{-1}$. In addition, PGAm-MMTs synthesized from primary amines had peaks at $\sim 3200\text{ cm}^{-1}$ corresponding to the N–H stretch of the amide pendent groups.

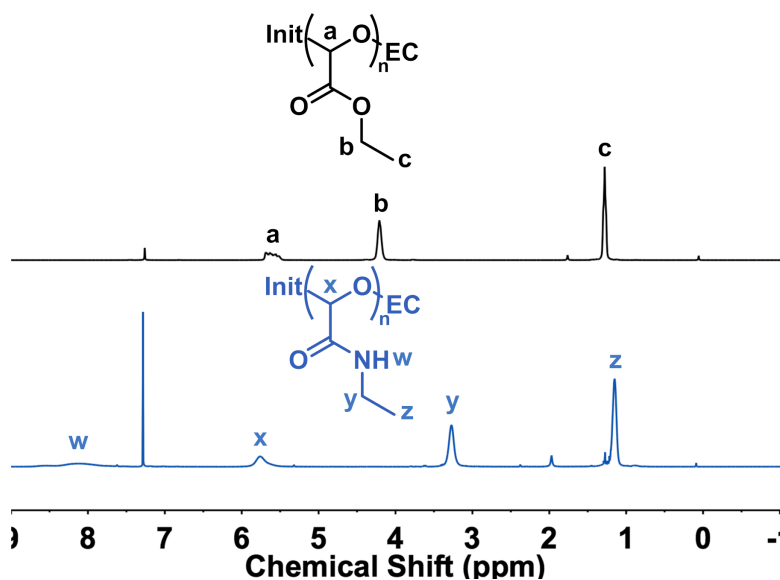


Figure 3.2. Comparison of the ^1H NMR spectra of **PEtG-MMT** (top) and **PGAm-NEt-MMT** (bottom) (CDCl_3 , 400 MHz).

While spectral data confirmed successful conversion of the pendent esters to amides, SEC analysis was used to compare the sizes of the polymers (Figure 3.3). As discussed above, post-polymerization modification of **PEtG-MMT** from the same batch of polymer has the

advantage of creating different polymers with the same DP_n and distribution of chain lengths. Indeed, all of the polymers, including **PEtG-MMT**, had similar D values (Table 3.1). Furthermore, most of the polymers had very similar M_n values of ~ 60 kg/mol. The exception to this was **PGAm-Pyrr-MMT**, which had a measured M_n of 27.4 kg/mol. It is likely that **PGAm-Pyrr-MMT** has a smaller hydrodynamic volume in the DMF eluent than the rest of the polymers, which may relate to its unique tertiary amide structure. To confirm this, multi-angle laser light scattering (MALLS) was used with SEC to obtain the absolute molar masses of **PEtG-MMT** and **PGAm-Pyrr-MMT** (Table 3.1). In contrast to SEC, this MALLS analysis revealed the expected higher M_n for **PGAm-Pyrr-MMT** relative to the precursor polymer **PEtG-MMT**. Overall, spectral and SEC analyses confirmed that the post-polymerization modification of PEtG to form various PGAMs via amidation is an easy and practical synthetic approach that does not cause significant polymer degradation. With regard to solubility, three of the polymers (**PGAm-NMe-MMT**, **PGAm-DMAE-MMT**, and **PGAm-Pyrr-MMT**) were water-soluble at room temperature. This may provide access to different applications than polyglyoxylates, all of which so far have been water-insoluble.^{17, 32, 39, 41-42}

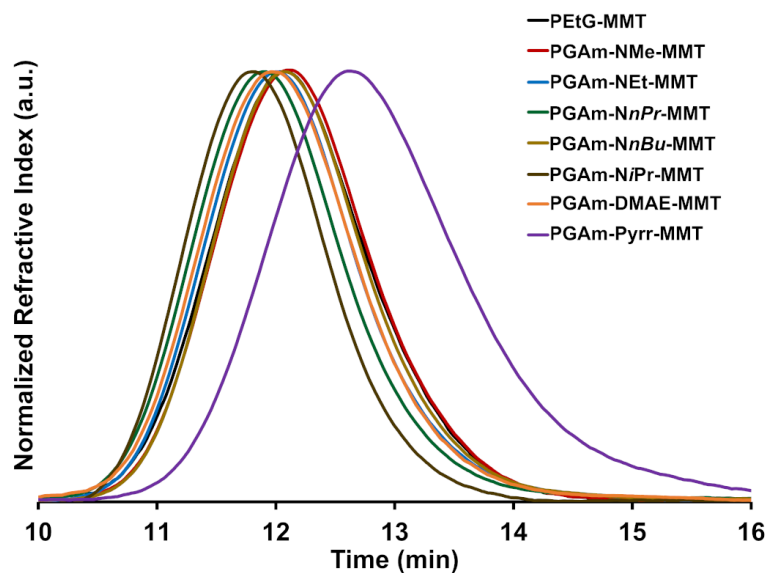


Figure 3.3. Overlay of the size-exclusion chromatograms of the 4-monomethoxytrityl end-capped polymers.

Table 3.1. Summary of the physical and thermal properties of the 4-monomethoxytrityl end-capped polymers. For the SEC results, the values in parentheses were determined using MALLS rather than conventional calibration.

Polymer	M_n (kg/mol)	M_w (kg/mol)	\bar{D}	T_o (°C)	T_g (°C)	Water-Soluble ^b
PEtG-MMT	51.8 (43.2)	73.6 (67.0)	1.4 (1.6)	170	-10	No
PGAm-NMe-MMT	54.1	77.6	1.4	133	90	Yes
PGAm-NEt-MMT	56.7	83.7	1.5	137	85	No
PGAm-N<i>n</i>Pr-MMT	62.4	92.8	1.5	136	68	No
PGAm-N<i>n</i>Bu-MMT	54.2	78.2	1.4	148	58	No
PGAm-NiPr-MMT	73.6	99.2	1.3	130	ND ^a	No
PGAm-DMAE-MMT	60.0	89.2	1.5	141	39	Yes
PGAm-Pyrr-MMT	27.4 (62.6)	47.3 (88.1)	1.7 (1.4)	163	78	Yes

^aNot detected within the range of the measurement (0–100 °C).

^bAt room temperature.

3.2.4 Thermal Analysis of PGAm-MMTs

The thermal properties of the PGAm-MMTs were studied by TGA and differential scanning calorimetry (DSC). Based on TGA, the onset degradation temperatures (T_o s) were at least 130 °C for all of the polymers (Table 3.1, Figure A2.33). In addition, all of the PGAm-MMTs underwent multi-step degradations in contrast to the one-step degradation of **PEtG-MMT**. This may relate to the varying volatilities and degradation pathways for the glyoxylamide depolymerization products in comparison with ethyl glyoxylate, which can readily evaporate above PEtG's T_o . DSC was performed up to 100–115 °C, depending on the polymer, ensuring that the maximum temperature was at least 30 °C less than the T_o . Notably, the T_g values of all of the PGAm-MMTs evaluated were much higher than that of **PEtG-MMT** (Table 3.1, Figure A2.36–Figure A2.43). These higher T_g values likely result from structural features introduced by the amide pendent groups that hinder the movement of the polymer chains. For example, all of the PGAMs with secondary amide pendent groups possess NH moieties that can participate in hydrogen bonding. Hydrogen bonding between polymer chains would hinder segmental motion, thus increasing the T_g . In addition, all of the PGAm pendent amide groups possess a C=N resonance structure. The

C=N bond contributes rigidity to the polymer pendent groups. Finally, polymers with more compact and rigid pendent groups (**PGAm-Pyrr-MMT** and **PGAm-NiPr-MMT**) have decreased segmental motion. **PEtG-NiPr-MMT** in particular possesses all three of the aforementioned factors. This polymer was solid at all temperatures that could be investigated by DSC, suggesting its T_g was greater than 100 °C. In general, the increased T_g values of the PGAm made them glassy solids at room temperature. None of the above PGAm showed evidence of crystallization or melting in the evaluated temperature range, suggesting that they were amorphous like the polyglyoxylates. To exclude the possibility of melting temperatures outside the measured temperature range, powder X-ray diffraction was performed on the polymers. No sharp peaks attributable to the polymers were observed, confirming their amorphous structures (Figure A2.51–Figure A2.57).

3.2.5 Triggered Depolymerization of PGAm-MMTs

To assess if the PGAm retained the stimuli-responsive depolymerization feature of polyglyoxylates, depolymerization experiments were performed. Their depolymerization was studied by ^1H NMR spectroscopy in the absence and presence of 0.9 M acetic acid as a trigger. The percent depolymerization was quantified based on the relative integrations of the peak at $\sim 5.5\text{--}5.6$ ppm corresponding to polymer backbone methine protons and the peak at $\sim 5.0\text{--}5.3$ ppm corresponding to the methine proton of the monomer hydrate depolymerization product (Figure 3.4a, Figure A2.60–Figure A2.71). **PGAm-NEt-MMT**, **PGAm-NnPr-MMT**, **PGAm-NiPr-MMT**, and **PGAm-Pyrr-MMT** were studied in 9:1 $\text{CD}_3\text{CN}:\text{D}_2\text{O}$, a solvent mixture that we have previously used to study the depolymerization of polyglyoxylates, including **PEtG-MMT**.^{17, 25} The other PGAm-MMTs were not soluble in this solvent system. In the presence of acetic acid, **PGAm-Pyrr-MMT** underwent complete depolymerization over a period of 30–35 days, with ~ 10 days required for 50% depolymerization, a behaviour very similar to that reported for **PEtG-MMT** (Figure 3.4b).²⁵ Interestingly, **PGAm-NEt-MMT**, **PGAm-NnPr-MMT**, and **PGAm-NiPr-MMT** all underwent depolymerization much more rapidly, with depolymerization complete in 10–14 days and only ~ 3 days required for 50% depolymerization. The differentiating feature of these PGAm is their ability to hydrogen bond through their amide NH groups. We postulate that intramolecular hydrogen bonding between the oxygen adjacent to the

end-cap and the final amide repeat unit can accelerate the cleavage of the end-cap on the polymer during depolymerization (Scheme 3.3). Such an intramolecular interaction should be favourable since the resulting hydrogen bond creates a five-membered ring. In the absence of acetic acid, all of the PGAMs depolymerized much more slowly, with only ~20% depolymerization observed for **PGAm-NEt-MMT**, **PGAm-N η Pr-MMT**, and **PGAm-N i Pr-MMT** and only 4% for **PGAm-Pyrr-MMT**. Thus, these data support that PGAMs undergo depolymerization in response to stimuli, confirming their self-immolative properties. In addition, the data highlight that structural features influence the depolymerization behaviour.

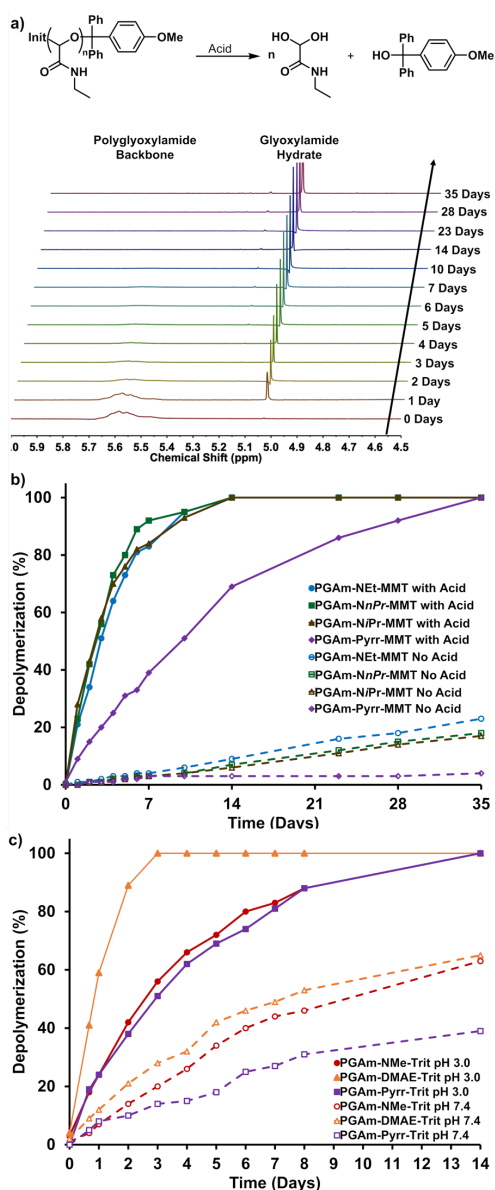
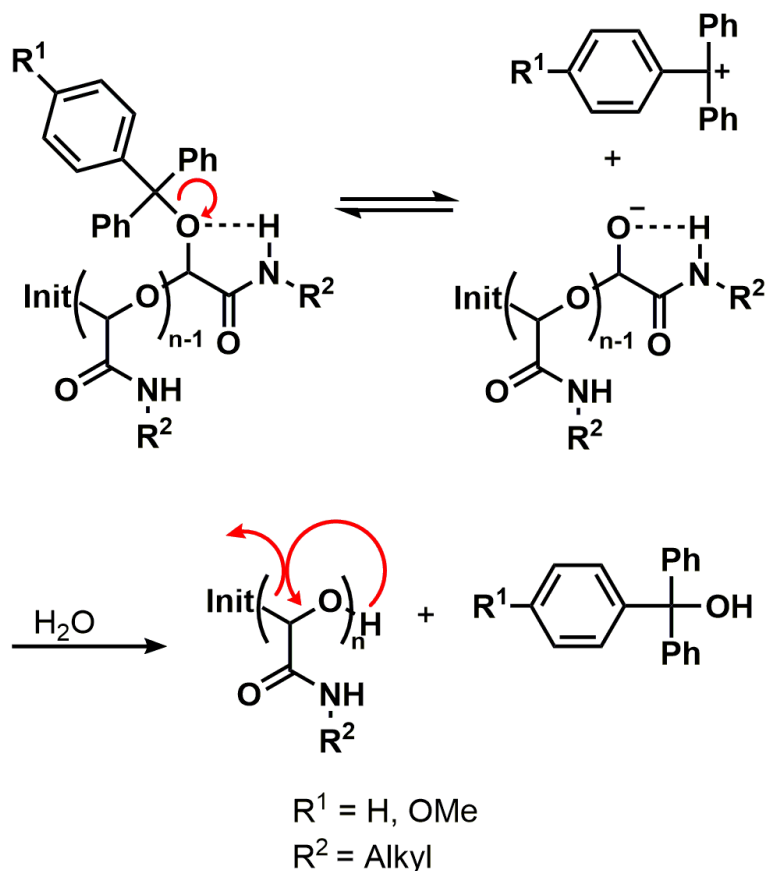


Figure 3.4. a) Depolymerization of **PGAm-NEt-MMT** in 9:1 acetonitrile:water with acetic acid (0.9 M) as a representative sample of how depolymerization was monitored using ^1H NMR spectroscopy (CD_3CN , 400 MHz). As depolymerization proceeds, there is a decrease in the backbone methine proton peak at ~ 5.6 ppm and an increase in the methine proton peak of the monomer hydrate at ~ 5.0 ppm in the NMR spectra. b) Depolymerization behaviours for selected PGAm-MMTs in 9:1 $\text{CD}_3\text{CN}:\text{D}_2\text{O}$ with and without acetic acid (0.9 M) as a stimulus. c) Depolymerization behaviours for selected PGAm-Trits in either citrate-buffered D_2O (0.1 M, pH 3.0) or phosphate-buffered D_2O (0.1 M, pH 7.4).



Scheme 3.3. Hypothesized hydrogen bonding mechanism that assists with the removal of the trityl end-cap. The glyoxylamide repeating unit adjacent to the end-cap is able to form a five-membered ring, accelerating the removal of the end-cap. If water is present, the end-cap is trapped and the polymer begins to depolymerize.

The high hydrophilicity of **PEtG-NMe-MMT** and **PEtG-DMAE-MMT** allowed their depolymerization to be studied in 9:1 $\text{D}_2\text{O}:\text{CD}_3\text{CN}$. Depolymerization was much faster in this solvent system, likely because the more polar, protic solvent accelerates the rate of cleavage of the 4-monomethoxytrityl end-cap, which follows an $\text{S}_{\text{N}}1$ mechanism. Depolymerization in the presence of acetic acid was complete for both polymers in less than 24 h (Figure A2.58). Unfortunately, the polymers were also rapidly degraded in the absence of acid, indicating a lack of end-cap stability in the 9:1 $\text{D}_2\text{O}:\text{CD}_3\text{CN}$ solution. Because we wanted to further investigate the water-soluble PGAMs (Table 3.1), this rapid background degradation in the absence of stimuli was problematic. Thus, more stable end-capped PGAMs were required.

3.2.6 Synthesis of Trityl End-Capped PGAmS (PGAm-Trits)

To address the stability issue, we synthesized a series of new PGAmS with a trityl end-cap instead of a 4-monomethoxytrityl end-cap. Since the simple trityl lacks the methoxy electron donating group, it is less labile than 4-monomethoxytrityl. First, a new polyglyoxylate (**PEtG-Trit**) was synthesized with the trityl end-cap by the method described above (Scheme 3.2). ^1H NMR, ^{13}C NMR, and FT-IR spectroscopy were used to characterize the structure of **PEtG-Trit** (Figure A2.9, Figure A2.23). Both ^1H NMR spectroscopy and SEC suggested an M_n of $\sim 9\text{--}10$ kg/mol, while SEC provided a D of 1.5. The molar mass of **PEtG-Trit** is likely lower than that of the analogous **PEtG-MMT** because trityl chloride reacts more slowly than 4-monomethoxytrityl chloride. Because of this, we suspect that end-capping of the polymer chains occurred at a higher temperature, allowing the chains to partially depolymerize before being end-capped and stabilized. To confirm that the discrepancy between the molar masses of **PEtG-MMT** and **PEtG-Trit** was caused by the end-caps used rather than other factors such as monomer purity, in an additional experiment PEtG was synthesized from the one batch of monomer and capped with each end-cap. The resulting crude polymer mixtures were compared using SEC in tetrahydrofuran (THF) with PMMA standards (Figure A2.32), revealing that PEtG with 4-monomethoxytrityl as the end-cap had a larger M_n (16.5 kg/mol) than PEtG with trityl as the end-cap (6.8 kg/mol).

A subset of the PGAmS (**PGAm-NMe-Trit**, **PGAm-NEt-Trit**, **PGAm-DMAE-Trit**, and **PGAm-Pyrr-Trit**) were synthesized from **PEtG-Trit** by reaction with the corresponding amines as described above (Scheme 3.2). ^1H NMR, ^{13}C NMR, and FT-IR spectroscopy were used to confirm complete conversion of the pendent esters to amides (Figure A2.10–Figure A2.13, Figure A2.24–Figure A2.27). SEC analysis was also performed for each PGAm (Table 3.2). Again, **PGAm-Pyrr-Trit** had a lower M_n than the other PGAmS based on SEC (Figure A2.30). However, because of the lower DP_n of this polymer series, it was possible to perform end-group analysis based on ^1H NMR spectroscopy (Table 3.2). This analysis confirmed that **PEtG-Trit** and all of the PGAm-Trits had very similar DP_n s and that this was not altered in the amidation reaction. Additionally, MALLS was used with SEC to acquire the absolute molar masses of both **PEtG-Trit** and **PGAm-Pyrr-Trit** (Table

3.2). While this analysis gave slightly different values than those acquired from ^1H NMR spectroscopy, it confirmed that **PGAm-Pyrr-Trit** had the expected higher M_n relative to the precursor polymer **PEtG-Trit**. Thus, the lower SEC M_n for **PGAm-Pyrr-Trit** was due to conformational differences with the other polymers. Additionally, the PGAm-Trits were investigated using TGA and DSC (Table 3.2). TGA revealed an increase in the T_o values for trityl end-capped polymers relative to the 4-monomethoxytrityl end-capped polymers (Figure A2.34). The increase in thermal stability of the polymers corresponds to the reduced lability of the trityl end-cap in comparison to its 4-monomethoxytrityl analogue.³⁸ DSC revealed a decrease in the T_g values of the PGAm-Trits relative to their PGAm-MMT analogues (Table 3.2, Figure A2.44–Figure A2.48). As the T_g values of polymers are known to increase with their molar mass,⁴⁶ the decrease in the T_g values is consistent with the lower molar masses of the PGAm-Trits.

Table 3.2. Summary of the Physical and Thermal Properties of the Trityl End-Capped Polymers. For the SEC results, the values in parentheses were determined using MALLS rather than conventional calibration.

Polymer	^1H NMR		SEC			T_o (°C)	T_g (°C)
	DP_n	M_n (kg/mol)	M_n (kg/mol)	M_w (kg/mol)	\mathcal{D}		
PEtG-Trit	90	9.7	8.8 (14.4)	13.5 (18.6)	1.5 (1.3)	206	−3
PGAm-NMe-Trit	83	7.7	8.4	14.6	1.7	172	70
PGAm-NEt-Trit	89	9.5	8.2	14.9	1.8	161	76
PGAm-DMAE-Trit	91	13.6	9.3	14.4	1.6	154	26
PGAm-Pyrr-Trit	96	12.7	4.0 (16.4)	9.8 (21.9)	2.4 (1.3)	169	59

3.2.7 Triggered Depolymerization of PGAm-Trits

The depolymerizations of **PGAm-NMe-Trit**, **PGAm-DMAE-Trit**, and **PGAm-Pyrr-Trit** were studied by ^1H NMR spectroscopy in citrate-buffered D_2O (0.1 M, pH 3.0) and phosphate-buffered D_2O (0.1 M, pH 7.4) over a 14 day period at room temperature (Figure A2.72–Figure A2.77). **PGAm-NEt-Trit** could not be studied under these conditions because it is insoluble in aqueous solutions at room temperature. Interestingly, **PGAm-DMAE-Trit** depolymerized more rapidly than the other polymers, with 50%

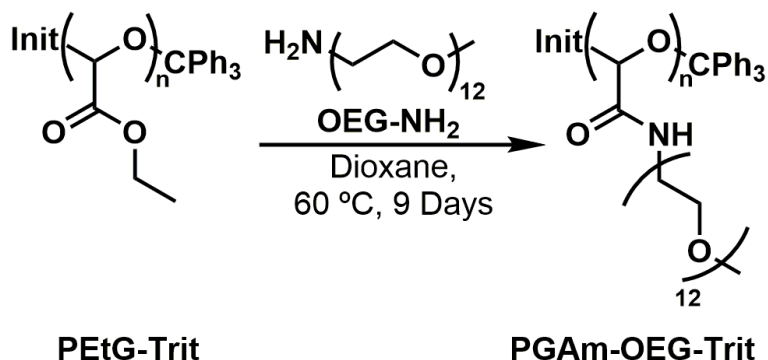
depolymerization in ~24 h at pH 3.0 and complete depolymerization within 3 days (Figure 3.4c). **PGAm-NMe-Trit** and **PGAm-Pyrr-Trit** reached 50% depolymerization in ~3 days and required 10–14 days for complete depolymerization at pH 3.0. At pH 7.4, the studied PGAm-Trits underwent depolymerization at a much slower rate than at pH 3.0, confirming their stimuli-responsive behaviour. They underwent ~30–60% depolymerization over 14 days, which demonstrates a stability improvement over the PGAm-MMTs discussed above. It is anticipated that increased long-term stability could be achieved through the use of different end-caps such as benzyl ether derivatives.

3.2.8 Synthesis and Characterization of a Degradable Graft Copolymer Analogue of PEG

POEGMA is a graft copolymer version of PEG comprising OEG side chains on a methacrylate backbone. It possesses properties similar to those of PEG, including the ability to shield conjugated biomolecules from degradation or clearance.⁴³ However, POEGMA is inherently non-degradable, which may ultimately limit its applications in areas such as drug delivery. As demonstrated above, PGAmS possess an acetal backbone that can undergo depolymerization. If this acetal backbone could be used to replace the methacrylate backbone of POEGMA, the resulting polymer should possess similar properties to POEGMA while at the same time undergo depolymerization when triggered by stimuli. Because the post-polymerization modification of PEtG to different PGAmS with small molecule amines allowed for quantitative conversion, it was anticipated that it should be possible to graft amine-modified OEG chains to the acetal backbone.

To synthesize the graft copolymer, **PEtG-Trit** was dissolved in 1,4-dioxane with methoxypoly(ethylene glycol) amine (**OEG-NH₂**) (Scheme 3.4). We found that the use of 1.0 stoichiometric equivalent of **OEG-NH₂** per pendent ester instead of an excess for this reaction led to easier purification of the final graft copolymer (**PGAm-OEG-Trit**). However, in comparison with the amidation reactions involving small molecules, the use of fewer molar equivalents combined with steric hindrance associated with the relatively large **OEG-NH₂** resulted in slow conversion of the **PEtG-Trit** ester pendent groups to

amides. To drive the reaction, it was heated in a pressure tube at 60 °C for 9 days. The resulting polymer was purified by multiple precipitations in Et₂O.



Scheme 3.4. Synthesis of **PGAm-OEG-Trit**.

PGAm-OEG-Trit was characterized by ¹H NMR, ¹³C NMR, and FT-IR spectroscopy to confirm that conversion was complete (Figure A2.14, Figure A2.28). SEC of the polymer revealed a single peak, confirming residual **OEG-NH₂** was removed during purification (Figure A2.31). The *M_n* of the polymer was 58.5 kg/mol while the *D* was 1.7, very similar to the *M_n* of 54.7 kg/mol expected based on ¹H NMR spectroscopic analysis. Additionally, **PGAm-OEG-Trit** was analyzed via TGA and DSC (Figure A2.35, Figure A2.49). TGA revealed a *T_o* of 339 °C, suggesting much higher thermal stability for this OEG graft copolymer than for the other PGAm-Trits and previously reported polyglyoxylates with various end-caps.^{17, 25} The increase in thermal stability may be due to the high stability and low volatility of the OEG pendent groups as well as their ability to shield the end-cap and the acetal backbone of the main chain from thermal degradation. DSC of the polymer revealed a *T_m* of 23 °C, a property conferred by the OEG side chains. No *T_g* was observed for the polymer over the temperature range from -70 to 200 °C. Like POEGMA, **PGAm-OEG-Trit** is highly water-soluble.

The degradation of **PGAm-OEG-Trit** in citrate-buffered D₂O (0.1 M, pH 3.0) and phosphate-buffered D₂O (0.1 M, pH 7.4) was first examined by ¹H NMR spectroscopy (Figure A2.78, Figure A2.79). **PGAm-OEG-Trit** depolymerized much more slowly than the other PGAm-Trits, with ~60% depolymerization after 7 weeks in the pH 3.0 buffer and only ~10% depolymerization in the pH 7.0 buffer over the same time period (Figure

A2.59). While **PGAm-OEG-Trit** can potentially hydrogen bond to the trityl oxygen as illustrated in Scheme 3.3, it is possible that conformational preferences prevent it from doing so. The structure-dependent depolymerization behaviours of the PGAMs are an interesting aspect that was not noted for polyglyoxylates. To further study the depolymerization, it was also monitored by aqueous SEC for 7 weeks (Figure A2.80, Figure A2.81). At pH 3.0, the chromatograms showed a substantial decrease in the intensity of the polymer peak over this time period. At pH 7.4, only a small decrease in peak intensity was observed over the 7 weeks. These results indicate that the concentration of the polymer in solution was decreasing over time as the polymer depolymerized. The retention time did not increase in either case. This indicates that end-cap cleavage was the rate-limiting step and that depolymerization of **PGAm-OEG-Trit** occurred rapidly after end-cap cleavage.

3.3 Conclusions

We have demonstrated for the first time the synthesis of self-immolative PGAMs. These polymers were synthesized via a simple post-polymerization amidation of PEtG under mild conditions. Complete conversion of the esters to amide groups was demonstrated while avoiding degradation of the polymers. This allowed for the preparation of a library of different PGAMs from a single batch of PEtG for property comparisons. The PGAMs had much higher T_g values than polyglyoxylates, attributed to the rigidity and hydrogen-bonding capabilities of the pendent amide groups. We demonstrated that PGAMs could be triggered to depolymerize, confirming their self-immolative behaviour. Furthermore, some of the PGAMs were water-soluble, opening possibilities for their application in areas such as medicine. Finally, a PGAM analogue of POEGMA was synthesized and characterized, demonstrating that it is possible to easily prepare PGAM graft copolymers from amine-terminated oligomers, affording a new depolymerizable analogue of PEG. Their ease of synthesis and unique properties relative to other self-immolative polymers should make PGAMs a promising new platform for applications.

3.4 Experimental

3.4.1 General Experimental Details

General Materials. Ethyl glyoxylate in toluene solution (50% w/w), *n*-propylamine, *n*-butylamine, *N,N*-dimethylethylenediamine, pyrrolidine, 4-monomethoxytrityl chloride, and citric acid were obtained from Alfa Aesar. Methylamine in THF solution (2.0 M), ethylamine in THF solution (2.0 M), isopropylamine, *n*-butyllithium in hexanes solution (2.5 M), PEG₅₅₀ monomethyl ether, tosyl chloride, trityl chloride, and AgNO₃ were obtained from Sigma Aldrich. NEt₃ and KH₂PO₄ were obtained from Millipore. Ammonium hydroxide solution (~30% w/v in water) and K₂HPO₄ were obtained from Caledon Labs. NaOH and KOH were obtained from Thermo Fisher Scientific. Ethyl glyoxylate was purified over P₂O₅ as previously reported.⁴⁵ OEG-NH₂ was synthesized via the tosylation⁴⁷ then amination⁴⁸ of PEG₅₅₀ monomethyl ether. Toluene was distilled over sodium and benzophenone under nitrogen at atmospheric pressure before use. NEt₃ was distilled over CaH₂ under nitrogen at atmospheric pressure before use. 1,4-Dioxane was obtained from a solvent purification system using alumina columns. All other chemicals were of reagent grade and were used without further purification.

General Methods. ¹H and ¹³C NMR spectra were obtained using either a 400 MHz Bruker AvIII HD instrument or a 400 MHz Varian INOVA instrument. ¹H NMR chemical shifts were calibrated against the residual solvent signal of CHCl₃ (7.26 ppm), CHD₂CN (1.94 ppm), or HOD (4.79 ppm) while ¹³C NMR chemical shifts were calibrated against the solvent signal of CDCl₃ (77.16 ppm) or (CD₃)₂SO (39.52 ppm). FT-IR spectra were obtained using a PerkinElmer FT-IR Spectrum Two instrument with attenuated total reflectance sampling. Size-exclusion chromatograms were obtained using either a THF, DMF, or aqueous chromatograph. The THF chromatograph was equipped with a Viscotek GPC Max VE2001 solvent module, a Viscotek VE3580 RI detector, and two Agilent Polypore (300 × 7.5mm) columns connected in series to a Polypore guard column. Samples were dissolved in THF (glass-distilled grade) at a concentration of ~5 mg/mL, filtered through a 0.2 μm polytetrafluoroethylene (PTFE) syringe filter, and injected using a 100 μL loop. Samples were run at a flow rate of 1 mL/min for 30 min at 30 °C. Molar masses

of the samples were calculated relative to PMMA standards. The DMF chromatograph was equipped with a Waters 515 HPLC pump with a Waters In-Line Degasser AF, two PLgel mixed D 5 μm (300×1.5 mm) columns connected to a corresponding PLgel guard column, a Wyatt miniDawn Treos Light Scattering detector operating at 658 nm, and a Wyatt Optilab Rex RI detector. Samples were dissolved in DMF containing 10 mM LiBr and 1% v/v NEt_3 at a concentration of ~ 5 mg/mL. Each sample was filtered through a 0.2 μm PTFE syringe filter prior to injection using a 50 μL loop. Samples were run at a flow rate of 1 mL/min for 30 min at 85 $^\circ\text{C}$. Molar masses of the samples were calculated relative to PMMA standards when using conventional calibration. The aqueous chromatograph was equipped with a Waters Separations Module 2695, a Refractive Index Detector (Waters 2414) and two PL Aquagel-OH Mixed-M 8 μm (300×7.5 mm) columns (Polymer Laboratories) connected in series with a PL Aquagel-OH 8 μm guard column. The mobile phase consisted of a pH 7.0 buffer solution containing 0.2 M NaNO_3 and 10 mM NaH_2PO_4 , which was eluted at 1 mL/min at room temperature for 40 min/run. Samples were prepared at a concentration of ~ 5 mg/mL, filtered through a 0.2 μm nylon syringe filter, and injected using a 100 μL volume loop. Molar masses of the samples were calculated relative to PEG standards. TGA thermograms were obtained using a TA Q50 instrument with a heating rate of 10 $^\circ\text{C}/\text{min}$ up to a maximum temperature of 1000 $^\circ\text{C}$ under nitrogen. DSC thermograms were obtained using a TA Q2000 instrument with a heating/cooling rate of 10 $^\circ\text{C}/\text{min}$ under nitrogen. The temperature range differed from sample to sample, but the maximum temperature was at least 30 $^\circ\text{C}$ below the T_o of the sample being measured. Powder X-ray diffractograms were obtained using an Inel Powder diffractometer equipped with a $\text{CuK}\alpha$ sealed tube source, an Inel XRG3000 generator, and an Inel CPS 120 detector. The CPS was a curved detector that collected the diffracted X-rays over 120° (2θ). Samples were ground to ensure a uniform particle size was attained before being placed on an aluminum sample holder for analysis.

3.4.2 Synthesis of PEtGs

Synthesis of PEtG-MMT. Purified ethyl glyoxylate (40 mL, 400 mmol, 400 equiv.) was placed into a flame-dried Schlenk flask under nitrogen at atmospheric pressure. To this flask, 100 mL of dry toluene and *n*-butyllithium solution (400 μL , 1.0 mmol, 1.0 equiv.)

were added at room temperature and allowed to mix. The solution was subsequently cooled to $-20\text{ }^{\circ}\text{C}$ and stirred for 1 h. In another flame-dried Schlenk flask under nitrogen at atmospheric pressure, AgNO_3 (1.7 g, 10 mmol, 10 equiv.) and 4-monomethoxytrityl chloride (3.0 g, 9.7 mmol, 9.7 equiv.) were combined with 10 mL of dry toluene. This mixture was stirred with heating at $50\text{ }^{\circ}\text{C}$ for 40 min. The resulting orange mixture was cooled to $-20\text{ }^{\circ}\text{C}$ before being added to the flask containing the polymer. In addition, dry NEt_3 (5.0 mL, 36 mmol, 36 equiv.) was added to the polymerization flask. The reaction mixture was allowed to gradually warm to room temperature over 16 h. After removal of the solvent under vacuum, the crude product was dissolved in 1.25 L of CH_2Cl_2 , mixed with activated charcoal, and filtered. The filtrate was then washed with brine ($2 \times 400\text{ mL}$) and water (200 mL), dried over MgSO_4 , gravity filtered, and concentrated under vacuum. The resulting concentrate was precipitated in 800 mL of methanol to give a pale-yellow precipitate. An additional 600 mL of methanol was added and the mixture was stirred before allowing the precipitate to settle. After decanting off the liquid, the precipitate was dried under vacuum to afford 22 g of a colourless tacky solid. Yield: 53%. ^1H NMR (CDCl_3 , 400 MHz): δ 5.47–5.73 (m, 1H), 4.21 (br s, 2H), 1.28 (br s, 3H). $^{13}\text{C}\{^1\text{H}\}$ NMR (CDCl_3 , 100 MHz): δ 165.3–166.4, 91.0–94.5, 62.2, 14.0. FT-IR: 2990, 1750 cm^{-1} . SEC (DMF, PMMA): $M_n = 51.8\text{ kg/mol}$, $M_w = 73.6\text{ kg/mol}$, $D = 1.4$. SEC (DMF, MALLS): $dn/dc = 0.028\text{ mL/g}$, $M_n = 43.2\text{ kg/mol}$, $M_w = 67.0\text{ kg/mol}$, $D = 1.6$. $T_g = -10\text{ }^{\circ}\text{C}$.

Synthesis of PEtG-Trit. Purified ethyl glyoxylate (20 mL, 200 mmol, 800 equiv.) was placed in a flame-dried Schlenk flask under nitrogen at atmospheric pressure. To this flask, 50 mL of dry toluene and *n*-butyllithium solution (100 μL , 0.25 mmol, 1.0 equiv.) were added at room temperature and allowed to mix for 30 min. The solution was subsequently cooled to $-20\text{ }^{\circ}\text{C}$ and stirred for another 30 min. Dry NEt_3 (3.0 mL, 22 mmol, 88 equiv.) was added to the mixture and it was stirred for an additional 30 min. In another flame-dried Schlenk flask under nitrogen at atmospheric pressure, AgNO_3 (5.5 g, 32 mmol, 130 equiv.) and trityl chloride (5.0 g, 20 mmol, 80 equiv.) were combined with 10 mL of dry toluene. The mixture was stirred while being heated at $70\text{ }^{\circ}\text{C}$ for 90 min. The resulting off-white mixture was cooled to $-20\text{ }^{\circ}\text{C}$ for 30 min before being added to the flask containing the polymer. The reaction mixture was allowed to warm to room temperature over 16 h. After removal of the solvent under vacuum, the crude product was dissolved in 60 mL of CH_2Cl_2

and precipitated into 900 mL of an 8:1 MeOH:H₂O mixture. After decanting off the liquid, the precipitate was dried under vacuum to afford 16 g of an orange tacky solid. Yield: 78%. ¹H NMR (CDCl₃, 400 MHz): δ 7.40–7.48 (m, 12H), 7.08–7.39 (m, 38H), 5.47–5.72 (m, 90H), 4.20 (br s, 186H), 1.28 (br s, 278H). ¹³C{¹H} NMR (CDCl₃, 100 MHz): δ 165.0–166.6, 127.1–129.9, 92.0–94.5, 62.2, 14.0. FT-IR: 2990, 1750 cm⁻¹. SEC (DMF, PMMA): $M_n = 8.8$ kg/mol, $M_w = 13.5$ kg/mol, $D = 1.5$. SEC (DMF, MALLS): dn/dc = 0.031 mL/g, $M_n = 14.4$ kg/mol, $M_w = 18.6$ kg/mol, $D = 1.3$. $T_g = -3$ °C.

Effect of End-Cap on Polymer Molar Mass. In a Schlenk flask, trityl chloride (0.27 g, 0.97 mmol, 9.7 equiv.) and AgNO₃ (0.17 g, 1.0 mmol, 10 equiv.) were combined in dry toluene (3.0 mL) and heated at 70 °C for 2 h before cooling to -20 °C to afford the end-capping mixture. In a separate Schlenk flask, dry toluene (10 mL) and *n*-butyllithium solution (40 μ L, 0.10 mmol, 1.0 equiv.) were combined at room temperature and vigorously stirred for 2 min. The flask was then charged with purified ethyl glyoxylate (4.0 mL, 39 mmol, 390 equiv.) and stirred for another 15 min before cooling the solution to -20 °C and stirring for 60 min. Then, freshly distilled NEt₃ (0.50 mL, 3.6 mmol, 36 equiv.) was added and the resulting solution was stirred for 10 min before the addition of the end-capping mixture. The resulting mixture was stirred at -20 °C for 2 h before it was allowed to gradually reach room temperature over 14 h. An aliquot of the resulting crude mixture was analyzed with SEC without any purifications. SEC (THF, PMMA): $M_n = 6.8$ kg/mol, $M_w = 11.8$ kg/mol, $D = 1.8$.

The above procedure was repeated using the same batch of ethyl glyoxylate and 4-monomethoxytrityl chloride (0.30 g, 0.97 mmol, 9.7 equiv.). An aliquot of the resulting crude mixture was analyzed with SEC without any purifications. SEC (THF, PMMA): $M_n = 16.5$ kg/mol, $M_w = 29.8$ kg/mol, $D = 1.8$.

3.4.3 Synthesis of PGAmS

All PGAmS were synthesized by the same procedure described for the synthesis of PGAm-NMe-MMT (representative PGAm synthesis).

Synthesis of PGAm-NMe-MMT (representative PGAm synthesis). PEtG-MMT (2.1 g) was placed in a round-bottom flask and stoppered with a rubber septum. The flask was evacuated. After charging the flask with nitrogen at atmospheric pressure, 21 mL of dry 1,4-dioxane was injected to give a 100 mg/mL polymer stock solution. From this solution, an aliquot was removed (2.5 mL, 250 mg of polymer, 2.4 mmol of ester, 1.0 equiv.) and placed into a flame-dried Schlenk flask filled with nitrogen at atmospheric pressure. An aliquot of methylamine solution (6.5 mL, 13 mmol, 5.4 equiv.) was then added to the flask. The flask was closed off from the nitrogen line and the reaction mixture was stirred for 48 h. Removal of the solvent, ethanol, and unreacted amine under vacuum gave the crude product. This product was subsequently purified by dissolution in minimal CH₂Cl₂ and precipitation in 100 mL of *n*-pentane. After decanting the liquid, the precipitate was dried under vacuum to afford 210 mg of an off-white powder. Yield: 98%. ¹H NMR (CDCl₃, 400 MHz): δ 7.67–8.64 (m, 1H), 5.73 (br s, 1H), 2.79 (br s, 3H). ¹³C{¹H} NMR (CDCl₃, 100 MHz): δ 166.3–169.0, 94.7–98.9, 26.3. FT-IR: 3290, 3100, 2940, 1660, 1540 cm⁻¹. SEC (DMF, PMMA): *M_n* = 54.1 kg/mol, *M_w* = 77.6 kg/mol, *D* = 1.4. *T_g* = 90 °C.

Synthesis of PGAm-NEt-MMT. From ethylamine solution (6.5 mL, 13 mmol, 5.4 equiv.) and PEtG-MMT (250 mg, 2.4 mmol of esters, 1.0 equiv.), 220 mg of an orange powder was afforded. Yield: 89%. ¹H NMR (CDCl₃, 400 MHz): δ 7.62–8.70 (m, 1H), 5.74 (br s, 1H), 3.25 (br s, 2H), 1.13 (br s, 3H). ¹³C{¹H} NMR (CDCl₃, 100 MHz): δ 165.7–167.7, 95.3–98.1, 34.6, 14.4. FT-IR: 3280, 3080, 2980, 2940, 2880, 1660, 1540 cm⁻¹. SEC (DMF, PMMA): *M_n* = 56.7 kg/mol, *M_w* = 83.7 kg/mol, *D* = 1.5. *T_g* = 85 °C.

Synthesis of PGAm-N*n*Pr-MMT. From *n*-propylamine (1.0 mL, 12 mmol, 5.0 equiv.) and PEtG-MMT (250 mg, 2.4 mmol of esters, 1.0 equiv.), 200 mg of a red powder was afforded. Yield: 71%. ¹H NMR (CDCl₃, 400 MHz): δ 7.55–8.88 (m, 1H), 5.74 (br s, 1H), 3.16 (br s, 2H), 1.52 (br s, 2H) 0.89 (br s, 3H). ¹³C{¹H} NMR (CDCl₃, 100 MHz): δ 166.3–167.8, 95.5–99.1, 41.5, 22.5, 11.5. FT-IR: 3280, 3090, 2960, 2930, 2880, 1660, 1540 cm⁻¹. SEC (DMF, PMMA): *M_n* = 62.4 kg/mol, *M_w* = 92.8 kg/mol, *D* = 1.5. *T_g* = 68 °C.

Synthesis of PGAm-N*n*Bu-MMT. From *n*-butylamine (1.0 mL, 10 mmol, 5.0 equiv.) and PEtG-MMT (200 mg, 2.0 mmol of esters, 1.0 equiv.) in 2.0 mL of dry 1,4-dioxane, 190

mg of a white powder was afforded. Yield: 75%. ^1H NMR (CDCl_3 , 400 MHz): δ 7.60–8.75 (m, 1H), 5.73 (br s, 1H), 3.20 (br s, 2H), 1.49 (br s, 2H), 1.31 (br s, 2H), 0.89 (br s, 3H). $^{13}\text{C}\{^1\text{H}\}$ NMR (CDCl_3 , 100 MHz): δ 166.3–167.8, 95.4–98.7, 39.5, 31.3, 20.2, 13.8. FT-IR: 3270, 3090, 2960, 2930, 2870, 1660, 1540 cm^{-1} . SEC (DMF, PMMA): $M_n = 54.2$ kg/mol, $M_w = 78.2$ kg/mol, $D = 1.4$. $T_g = 58$ °C.

Synthesis of PGAm-NiPr-MMT. From isopropylamine (1.1 mL, 13 mmol, 5.4 equiv.) and **PEtG-MMT** (250 mg, 2.4 mmol of esters, 1.0 equiv.), 220 mg of a white powder was afforded. Yield: 78%. ^1H NMR (CDCl_3 , 400 MHz): δ 7.58–9.05 (m, 1H), 5.69 (br s, 1H), 3.98 (br s, 1H), 1.15 (br s, 6H). $^{13}\text{C}\{^1\text{H}\}$ NMR (CDCl_3 , 100 MHz): δ 164.7–167.5, 95.4–99.7, 41.8, 22.3. FT-IR: 3260, 3070, 2970, 2940, 2880, 1660, 1540 cm^{-1} . SEC (DMF, PMMA): $M_n = 73.6$ kg/mol, $M_w = 99.2$ kg/mol, $D = 1.3$.

Synthesis of PGAm-DMAE-MMT. From *N,N*-dimethylethylenediamine (1.4 mL, 13 mmol, 5.4 equiv.) and **PEtG-MMT** (250 mg, 2.4 mmol of esters, 1.0 equiv.), 240 mg of a colourless tacky solid was afforded. Yield: 68%. ^1H NMR (CDCl_3 , 400 MHz): δ 7.73–8.90 (m, 1H), 5.73 (br s, 1H), 3.32 (br s, 2H), 2.42 (br s, 2H), 2.22 (br s, 6H). $^{13}\text{C}\{^1\text{H}\}$ NMR (CDCl_3 , 100 MHz): δ 166.0–168.1, 95.4–98.0, 58.1, 45.6, 37.6. FT-IR: 3280, 3080, 2940, 2860, 2820, 2770, 1670, 1540 cm^{-1} . SEC (DMF, PMMA): $M_n = 60.0$ kg/mol, $M_w = 89.2$ kg/mol, $D = 1.5$. $T_g = 39$ °C.

Synthesis of PGAm-Pyrr-MMT. From pyrrolidine (1.0 mL, 12 mmol, 5.0 equiv.) and **PEtG-MMT** (250 mg, 2.4 mmol of esters, 1.0 equiv.), 270 mg of a yellow powder was afforded. Yield: 87%. ^1H NMR (CDCl_3 , 400 MHz): δ 5.32–5.98 (m, 1H), 3.66 (br s, 2H), 3.32 (br s, 2H), 1.69–2.03 (m, 5H). $^{13}\text{C}\{^1\text{H}\}$ NMR (CDCl_3 , 100 MHz): δ 162.9–165.7, 91.2–96.2, 45.5–46.7, 26.2, 23.9. FT-IR: 2970, 2880, 1650 cm^{-1} . SEC (DMF, PMMA): $M_n = 27.4$ kg/mol, $M_w = 47.3$ kg/mol, $D = 1.7$. SEC (DMF, MALLS): $\text{dn/dc} = 0.075$ mL/g, $M_n = 62.6$ kg/mol, $M_w = 88.1$ kg/mol, $D = 1.4$. $T_g = 78$ °C.

Synthesis of PGAm-NMe-Trit. From methylamine solution (12 mL, 24 mmol, 4.9 equiv.) and **PEtG-Trit** (500 mg, 4.9 mmol of esters, 1.0 equiv.) in 5.0 mL of dry 1,4-dioxane, 220 mg of a yellow powder was afforded. Yield: 52%. ^1H NMR (CDCl_3 , 400 MHz): δ 7.63–8.68 (m, 78H), 7.40–7.51 (m, 12H), 7.18–7.34 (m, 140H), 5.74 (br s, 83H), 2.78 (br s,

279H). $^{13}\text{C}\{^1\text{H}\}$ NMR ($(\text{CD}_3)_2\text{SO}$, 100 MHz): δ 166.0–167.2, 126.7–129.5, 94.0–97.9, 25.6. FT-IR: 3290, 3100, 2940, 1670, 1540 cm^{-1} . SEC (DMF, PMMA): $M_n = 8.4$ kg/mol, $M_w = 14.6$ kg/mol, $D = 1.7$. $T_g = 70$ °C.

Synthesis of PGAm-NEt-Trit. From ethylamine solution (12 mL, 24 mmol, 4.9 equiv.) and **PEtG-Trit** (500 mg, 4.9 mmol of esters, 1.0 equiv.) in 5.0 mL of dry 1,4-dioxane, 230 mg of a yellow powder was afforded. Yield: 50%. ^1H NMR (CDCl_3 , 400 MHz): δ 7.62–8.71 (m, 87H), 7.41–7.53 (m, 12H), 7.20–7.33 (m, 36H), 5.74 (br s, 89H), 3.25 (br s, 202H), 1.13 (br s, 323H). $^{13}\text{C}\{^1\text{H}\}$ NMR ($(\text{CD}_3)_2\text{SO}$, 100 MHz): δ 165.6–166.5, 126.5–128.7, 93.4–98.8, 33.7, 14.2. FT-IR: 3280, 3080, 2980, 2940, 1660, 1540 cm^{-1} . SEC (DMF, PMMA): $M_n = 8.2$ kg/mol, $M_w = 14.9$ kg/mol, $D = 1.8$. $T_g = 76$ °C.

Synthesis of PGAm-DMAE-Trit. From *N,N*-dimethylethylenediamine (2.7 mL, 25 mmol, 5.1 equiv.) and **PEtG-Trit** (500 mg, 4.9 mmol of esters, 1.0 equiv.) in 5.0 mL of dry 1,4-dioxane, 340 mg of a yellow tacky solid was afforded. Yield: 48%. ^1H NMR (CDCl_3 , 400 MHz): δ 7.76–8.75 (m, 109H), 7.39–7.51 (m, 12H), 7.19–7.36 (m, 166H), 5.71 (br s, 91H), 3.32 (br s, 227H), 2.42 (br s, 223H), 2.21 (br s, 734H). $^{13}\text{C}\{^1\text{H}\}$ NMR ($(\text{CD}_3)_2\text{SO}$, 100 MHz): δ 165.6–167.0, 126.6–128.8, 93.7–98.0, 57.7, 40.2, 37.0. FT-IR: 3280, 3080, 2940, 2860, 2820, 2770, 1670, 1540 cm^{-1} . SEC (DMF, PMMA): $M_n = 9.3$ kg/mol, $M_w = 14.4$ kg/mol, $D = 1.6$. $T_g = 26$ °C.

Synthesis of PGAm-Pyrr-Trit. From pyrrolidine (2.0 mL, 24 mmol, 4.9 equiv.) and **PEtG-Trit** (500 mg, 4.9 mmol of esters, 1.0 equiv.) in 5.0 mL of dry 1,4-dioxane, 410 mg of a yellow powder was afforded. Yield: 66%. ^1H NMR (CDCl_3 , 400 MHz): δ 7.37–7.47 (m, 12H), 7.19–7.33 (m, 146H), 5.36–6.06 (m, 96H), 3.65 (br s, 212H), 3.32 (br s, 241H), 1.65–1.99 (m, 460H). $^{13}\text{C}\{^1\text{H}\}$ NMR ($(\text{CD}_3)_2\text{SO}$, 100 MHz): δ 162.5–164.7, 126.4–129.5, 87.8–97.5, 44.2–47.0, 25.7, 23.4. FT-IR: 2970, 2880, 1650 cm^{-1} . SEC (DMF, PMMA): $M_n = 4.0$ kg/mol, $M_w = 9.8$ kg/mol, $D = 2.4$. SEC (DMF, MALLS): $\text{dn/dc} = 0.066$ mL/g $M_n = 16.4$ kg/mol, $M_w = 21.9$ kg/mol, $D = 1.3$. $T_g = 59$ °C.

Synthesis of PGAm-OEG-Trit. **PEtG-Trit** (210 mg of polymer, 2.1 mmol of ester, 1.0 equiv.) was dissolved in a pressure tube using 10 mL of dry 1,4-dioxane. **OEG-NH₂** (1.2 g, 2.5 mmol, 1.0 equiv.) was subsequently added and the flask was capped. The reaction

mixture was then heated at 60 °C for 9 days. The solution was concentrated, dissolved in 10 mL of CHCl₃, precipitated into 100 mL of Et₂O, and stirred for 20 min before allowing the precipitate to settle. The solvent was then decanted off and the purification procedure was repeated twice over. The precipitate was then dried under vacuum to afford 720 mg of the product. Yield = 57%. ¹H NMR (CDCl₃, 400 MHz): δ 7.62–8.70 (m, 100H), 7.37–7.45 (br s, 12H), 7.13–7.37 (m, 202H) 5.67 (br s, 88H), 3.11–3.93 (m, 4270H). ¹³C{¹H} NMR ((CD₃)₂SO, 100 MHz): δ 71.3, 69.8, 58.0. FT-IR: 3390, 2880, 1650, 1560 cm⁻¹. SEC (DMF, PMMA): *M_n* = 58.5 kg/mol, *M_w* = 97.4 kg/mol, *D* = 1.7. *T_m* = 23 °C.

3.4.4 Depolymerization Studies

Depolymerization of PGAm-MMTs. PGAm-NEt-MMT, PGAm-N*n*Pr-MMT, PGAm-N*i*Pr-MMT, and PGAm-Pyrr-MMT were each dissolved in 1.1 mL of 9:1 CD₃CN:D₂O. PGAm-NMe-MMT and PGAm-DMAE-MMT were each dissolved in 1.1 mL of 9:1 D₂O:CD₃CN. All polymer solutions were 1% w/v in concentration. Each solution was separated into two 550 μL aliquots, which were each placed into an NMR tube. In one of the two aliquots, 30 μL of glacial acetic acid was added to give a 0.9 M concentration of acid. No acid was added to the second aliquot (control). The NMR tubes were promptly sealed and stored at room temperature. Depolymerization was monitored by acquiring ¹H NMR spectra of the samples at specific time points and examining the integration ratios between the peaks corresponding to the polymer backbone methine protons at ~5.5–5.6 ppm and the methine proton of the monomer hydrate (depolymerization product) at ~5.0–5.3 ppm.

Depolymerization of PGAm-Trits. A 0.1 M deuterated citrate buffer was prepared by dissolving 190 mg of citric acid into 10 mL of D₂O and correcting the pH to 3.0 using NaOH. A 0.1 M deuterated phosphate buffer was prepared by dissolving 52 mg of KH₂PO₄ and 110 mg of K₂HPO₄ into 10 mL of D₂O and correcting the pH to 7.4 with KOH. PGAm-NMe-Trit, PGAm-DMAE-Trit, and PGAm-Pyrr-Trit were each dissolved in 600 μL of the pH 3.0 buffer. Additionally, the polymers were each dissolved in 600 μL of the pH 7.4 buffer. All polymer solutions were 1% w/v in concentration. Each solution was placed into an NMR tube and the tubes were promptly sealed and stored at room temperature.

Depolymerization was monitored by acquiring ^1H NMR spectra of the samples at specific time points and examining the integration ratios between the polymer backbone methine protons at ~ 5.5 – 5.6 ppm and the methine proton of monomer hydrate (depolymerization product) at ~ 5.3 – 5.5 ppm.

Depolymerization of PGAm-OEG-Trit. PGAm-OEG-Trit was dissolved at 1% w/v at pH 3.0 and pH 7.4 and depolymerization was monitored by ^1H NMR spectroscopy using the deuterated buffers and techniques described in the section “Depolymerization of PGAm-Trits”. Additionally, PGAm-OEG-Trit was dissolved in 5.0 mL of each buffer to create 0.5% w/v solutions at pH 3.0 and pH 7.4. These solutions were promptly sealed in vials and stored at room temperature. At specified time points, 300 μL of the solution was removed, filtered, and then directly injected for analysis by aqueous SEC. The chromatograms were monitored for changes in the polymer elution time and refractive index intensity over time.

3.5 References

- (1) Cohen Stuart, M. A.; Huck, W. T. S.; Genzer, J.; Müller, M.; Ober, C.; Stamm, M.; Sukhorukov, G. B.; Szleifer, I.; Tsukruk, V. V.; Urban, M.; Winnik, F.; Zauscher, S.; Luzinov, I.; Minko, S. Emerging Applications of Stimuli-Responsive Polymer Materials. *Nat. Mater.* **2010**, *9*, 101–113.
- (2) Mura, S.; Nicolas, J.; Couvreur, P. Stimuli-Responsive Nanocarriers for Drug Delivery. *Nat. Mater.* **2013**, *12*, 991–1003.
- (3) Reineke, T. M. Stimuli-Responsive Polymers for Biological Detection and Delivery. *ACS Macro Lett.* **2016**, *5*, 14–18.
- (4) Wei, M.; Gao, Y.; Li, X.; Serpe, M. J. Stimuli-Responsive Polymers and Their Applications. *Polym. Chem.* **2017**, *8*, 127–143.
- (5) Schild, H. G. Poly(*N*-isopropylacrylamide): Experiment, Theory and Application. *Prog. Polym. Sci.* **1992**, *17*, 163–249.
- (6) Yu, C.; Mutlu, S.; Selvaganapathy, P.; Mastrangelo, C. H.; Svec, F.; Fréchet, J. M. J. Flow Control Valves for Analytical Microfluidic Chips without Mechanical Parts Based on Thermally Responsive Monolithic Polymers. *Anal. Chem.* **2003**, *75*, 1958–1961.

- (7) Qin, S. H.; Geng, Y.; Discher, D. E.; Yang, S. Temperature-Controlled Assembly and Release from Polymer Vesicles of Poly(ethylene oxide)-*block*-poly(*N*-isopropylacrylamide). *Adv. Mater.* **2006**, *18*, 2905–2909.
- (8) Li, W.; Zhao, H.; Qian, W.; Li, H.; Zhang, L.; Ye, Z.; Zhang, G.; Xia, M.; Li, J.; Gao, J.; Li, B.; Kou, G.; Dai, J.; Wang, H.; Guo, Y. Chemotherapy for Gastric Cancer by Finely Tailoring Anti-Her2 Anchored Dual Targeting Immunomicelles. *Biomaterials* **2012**, *33*, 5349–5362.
- (9) Heffernan, M. J.; Murthy, N. Polyketal Nanoparticles: A New pH-Sensitive Biodegradable Drug Delivery Vehicle. *Bioconjugate Chem.* **2005**, *16*, 1340–1342.
- (10) Rickerby, J.; Prabhakar, R.; Ali, M.; Knowles, J.; Brocchini, S. Water-Soluble Polyacetals Derived from Diphenols. *J. Mater. Chem.* **2005**, *15*, 1849–1856.
- (11) Jain, R.; Standley, S. M.; Fréchet, J. M. J. Synthesis and Degradation of pH-sensitive Linear Poly(amidoamine)s. *Macromolecules* **2007**, *40*, 452–457.
- (12) Roth, M. E.; Green, O.; Gnam, S.; Shabat, D. Dendritic, Oligomeric, and Polymeric Self-Immolative Molecular Amplification. *Chem. Rev.* **2016**, *116*, 1309–1352.
- (13) Sagi, A.; Weinstain, R.; Karton, N.; Shabat, D. Self-Immolative Polymers. *J. Am. Chem. Soc.* **2008**, *130*, 5434–5435.
- (14) Dewit, M. A.; Gillies, E. R. A Cascade Biodegradable Polymer Based on Alternating Cyclization and Elimination Reactions. *J. Am. Chem. Soc.* **2009**, *131*, 18327–18334.
- (15) Olah, M. G.; Robbins, J. S.; Baker, M. S.; Phillips, S. T. End-Capped Poly(benzyl ethers): Acid and Base Stable Polymers That Depolymerize Rapidly from Head-to-Tail in Response to Specific Applied Signals. *Macromolecules* **2013**, *46*, 5924–5928.
- (16) Seo, W.; Phillips, S. T. Patterned Plastics That Change Physical Structure in Response to Applied Chemical Signals. *J. Am. Chem. Soc.* **2010**, *132*, 9234–9235.
- (17) Fan, B.; Trant, J. F.; Wong, A. D.; Gillies, E. R. Polyglyoxylates: A Versatile Class of Triggerable Self-Immolative Polymers from Readily Accessible Monomers. *J. Am. Chem. Soc.* **2014**, *136*, 10116–10123.
- (18) Dewit, M. A.; Beaton, A.; Gillies, E. R. A Reduction Sensitive Cascade Biodegradable Linear Polymer. *J. Polym. Sci., Part A: Polym. Chem.* **2010**, *48*, 3977–3985.

- (19) Chen, E. K. Y.; McBride, R. A.; Gillies, E. R. Self-Immolative Polymers Containing Rapidly Cyclizing Spacers: Toward Rapid Depolymerization Rates. *Macromolecules* **2012**, *45*, 7364–7374.
- (20) de Gracia Lux, C.; McFearin, C. L.; Joshi-Barr, S.; Sankaranarayanan, J.; Fomina, N.; Almutairi, A. A Single UV or Near IR Triggering Event Leads to Polymer Degradation into Small Molecules. *ACS Macro Lett.* **2012**, *1*, 922–926.
- (21) Liu, G.; Wang, X.; Hu, J.; Zhang, G.; Liu, S. Self-Immolative Polymersomes for High-Efficiency Triggered Release and Programmed Enzymatic Reactions. *J. Am. Chem. Soc.* **2014**, *136*, 7492–7497.
- (22) Peterson, G. I.; Church, D. C.; Yakelis, N. A.; Boydston, A. J. 1,2-Oxazine Linker as a Thermal Trigger for Self-Immolative Polymers. *Polymer* **2014**, *55*, 5980–5985.
- (23) Fan, B.; Trant, J. F.; Hemery, G.; Sandre, O.; Gillies, E. R. Thermo-Responsive Self-Immolative Nanoassemblies: Direct and Indirect Triggering. *Chem. Commun.* **2017**, *53*, 12068–12071.
- (24) Wong, A. D.; Güngör, T. M.; Gillies, E. R. Multiresponsive Azobenzene End-Cap for Self-Immolative Polymers. *ACS Macro Lett.* **2014**, *3*, 1191–1195.
- (25) Fan, B.; Trant, J. F.; Gillies, E. R. End-Capping Strategies for Triggering End-to-End Depolymerization of Polyglyoxylates. *Macromolecules* **2016**, *49*, 9309–9319.
- (26) Esser-Kahn, A. P.; Sottos, N. R.; White, S. R.; Moore, J. S. Programmable Microcapsules from Self-Immolative Polymers. *J. Am. Chem. Soc.* **2010**, *132*, 10266–10268.
- (27) Weinstain, R.; Baran, P. S.; Shabat, D. Activity-Linked Labeling of Enzymes by Self-Immolative Polymers. *Bioconjugate Chem.* **2009**, *20*, 1783–1791.
- (28) Feinberg, A. M.; Hernandez, H. L.; Plantz, C. L.; Mejia, E. B.; Sottos, N. R.; White, S. R.; Moore, J. S. Cyclic Poly(phthalaldehyde): Thermoforming a Bulk Transient Material. *ACS Macro Lett.* **2018**, *7*, 47–52.
- (29) DiLauro, A. M.; Abbaspourrad, A.; Weitz, D. A.; Phillips, S. T. Stimuli-Responsive Core–Shell Microcapsules with Tunable Rates of Release by Using a Depolymerizable Poly(phthalaldehyde) Membrane. *Macromolecules* **2013**, *46*, 3309–3313.

- (30) Fan, B.; Gillies, E. R. Poly(ethyl glyoxylate)-Poly(ethylene oxide) Nanoparticles: Stimuli-Responsive Drug Release via End-to-End Polyglyoxylate Depolymerization. *Mol. Pharmaceutics* **2017**, *14*, 2548–2559.
- (31) Gambles, M. T.; Fan, B.; Borecki, A.; Gillies, E. R. Hybrid Polyester Self-Immolative Polymer Nanoparticles for Controlled Drug Release. *ACS Omega* **2018**, *3*, 5002–5011.
- (32) Fan, B.; Yardley, R. E.; Trant, J. F.; Borecki, A.; Gillies, E. R. Tuning the Hydrophobic Cores of Self-Immolative Polyglyoxylate Assemblies. *Polym. Chem.* **2018**, *9*, 2601–2610.
- (33) Zhang, H.; Yeung, K.; Robbins, J. S.; Pavlick, R. A.; Wu, M.; Liu, R.; Sen, A.; Phillips, S. T. Self-Powered Microscale Pumps Based on Analyte-Initiated Depolymerization Reactions. *Angew. Chem. Int. Ed.* **2012**, *51*, 2400–2404.
- (34) Weinstain, R.; Sagi, A.; Karton, N.; Shabat, D. Self-Immolative Comb-Polymers: Multiple-Release of Side-Reporters by a Single Stimulus Event. *Chem. Eur. J.* **2008**, *14*, 6857–6861.
- (35) Lewis, G. G.; Robbins, J. S.; Phillips, S. T. Phase-Switching Depolymerizable Poly(carbamate) Oligomers for Signal Amplification in Quantitative Time-Based Assays. *Macromolecules* **2013**, *46*, 5177–5183.
- (36) Lewis, G. G.; Robbins, J. S.; Phillips, S. T. Point-of-Care Assay Platform for Quantifying Active Enzymes to Femtomolar Levels Using Measurements of Time as the Readout. *Anal. Chem.* **2013**, *85*, 10432–10439.
- (37) Lewis, G. G.; Robbins, J. S.; Phillips, S. T. A Prototype Point-of-Use Assay for Measuring Heavy Metal Contamination in Water Using Time as a Quantitative Readout. *Chem. Commun.* **2014**, *50*, 5352–5354.
- (38) Fan, B.; Salazar, R.; Gillies, E. R. Depolymerization of Trityl End-Capped Poly(ethyl glyoxylate): Potential Applications in Smart Packaging. *Macromol. Rapid Commun.* **2018**, *39*, 1800173.
- (39) Belloncle, B.; Bunel, C.; Menu-Bouaouiche, L.; Lesouhaitier, O.; Burel, F. Study of the Degradation of Poly(ethyl glyoxylate): Biodegradation, Toxicity and Ecotoxicity Assays. *J. Polym. Environ.* **2012**, *20*, 726–731.
- (40) Fan, B.; Trant, J. F.; Yardley, R. E.; Pickering, A. J.; Lagugn e-Labarthe, F.; Gillies, E. R. Photocontrolled Degradation of Stimuli-Responsive Poly(ethyl glyoxylate):

Differentiating Features and Traceless Ambient Depolymerization. *Macromolecules* **2016**, *49*, 7196–7203.

(41) Belloncle, B.; Burel, F.; Oulyadi, H.; Bunel, C. Study of the *In Vitro* Degradation of Poly(ethyl glyoxylate). *Polym. Degrad. Stab.* **2008**, *93*, 1151–1157.

(42) Kaitz, J. A.; Diesendruck, C. E.; Moore, J. S. Divergent Macrocyclization Mechanisms in the Cationic Initiated Polymerization of Ethyl Glyoxylate. *Macromolecules* **2014**, *47*, 3603–3607.

(43) Liu, M.; Leroux, J.-C.; Gauthier, M. A. Conformation–Function Relationships for the Comb-Shaped Polymer pOEGMA. *Prog. Polym. Sci.* **2015**, *48*, 111–121.

(44) Gauthier, M. A.; Gibson, M. I.; Klok, H.-A. Synthesis of Functional Polymers by Post-Polymerization Modification. *Angew. Chem. Int. Ed.* **2009**, *48*, 48–58.

(45) Rabiee Kenaree, A.; Gillies, E. R. Controlled Polymerization of Ethyl Glyoxylate Using Alkylolithium and Alkoxide Initiators. *Macromolecules* **2018**, *51*, 5501–5510.

(46) Fox, T. G.; Flory, P. J. Second-Order Transition Temperatures and Related Properties of Polystyrene. I. Influence of Molecular Weight. *J. Appl. Phys.* **1950**, *21*, 581–591.

(47) Harris, J. M.; Struck, E. C.; Case, M. G.; Paley, M. S.; Yalpani, M.; Van Alstine, J. M.; Brooks, D. E. Synthesis and Characterization of Poly(ethylene glycol) Derivatives. *J. Polym. Sci., Part A: Polym. Chem.* **1984**, *22*, 341–352.

(48) Komáromy, D.; Stuart, M. C. A.; Monreal Santiago, G.; Tezcan, M.; Krasnikov, V. V.; Otto, S. Self-Assembly Can Direct Dynamic Covalent Bond Formation Toward Diversity or Specificity. *J. Am. Chem. Soc.* **2017**, *139*, 6234–6241.

Chapter 4

4 Thermo-Responsive Polyglyoxylamides

4.1 Introduction

Thermo-responsive polymers,¹⁻² which exhibit lower critical solution temperature (LCST) behaviour, have attracted significant attention due to their potential for fabricating smart materials including actuators,³ plasmonic sensors,⁴ batteries,⁵ drug delivery vehicles,⁶ and scaffolds for tissue engineering.⁷ For example, poly(*N*-isopropylacrylamide) (PNIPAM) is the most extensively studied thermo-responsive polymer, with a cloud point temperature (T_{cp}) of ~ 32 °C in water (Figure 4.1a).⁸⁻¹⁰ Thermo-responsive poly[oligo(ethylene glycol) (meth)acrylate]s [POEG(M)As, Figure 4.1b] have also been widely explored.¹¹⁻¹³ They are promising candidates for biological applications as their pendent groups are based on oligo(ethylene glycol) and the low toxicity of ethylene glycol-based polymers is well established.¹⁴ POEGMAs exhibit reversible transitions in different environments and their T_{cp} s can be synthetically tuned. For example, for methacrylate-based backbones, increasing the number of ethylene glycol units in the pendent groups from 2 to ~ 10 increased the T_{cp} from 28 to 90 °C.¹²

- *This chapter contains work that has been published previously: Rabiee Kenaree, A.; Sirianni, Q. E. A.; Classen, K.; Gillies, E. R. *Biomacromolecules* **2020**, *21*, 3817–3825. See Co-Authorship Statement for the contributions of each author.

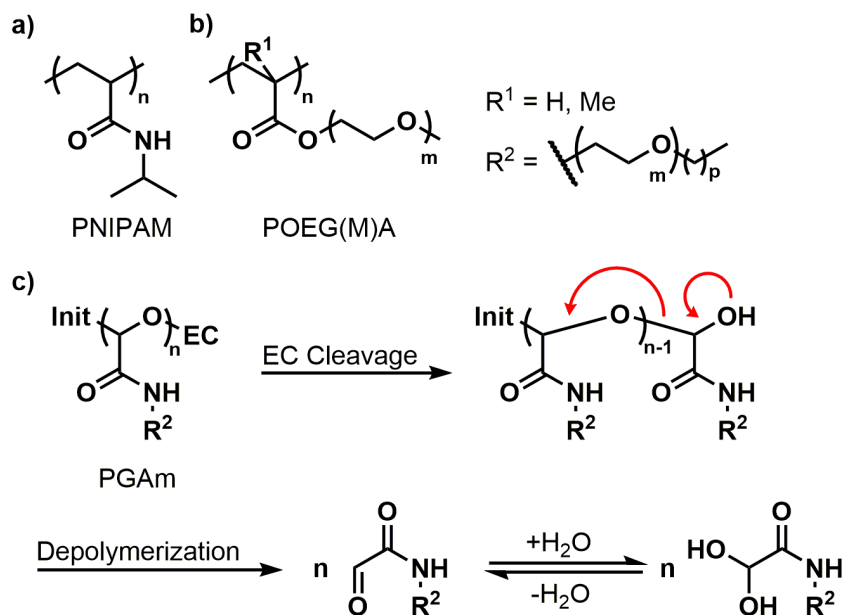


Figure 4.1. Thermo-responsive polymers a) PNIPAM and b) POEG(M)A. c) General chemical structure of PGAm and their depolymerization to glyoxylamide hydrates following end-cap cleavage (Init = polymerization initiator; EC = end-cap).

While PNIPAM and POEGMAs exhibit thermo-responsive behaviour near the physiological temperature of 37 °C, they have fully carbon-carbon backbones, so they are not considered biodegradable *in vivo* and would also be expected to degrade slowly in the environment. To address this challenge, degradable polymers exhibiting LCST behaviour have also been explored. For example, degradable ester linkages were incorporated into the backbones of POEGMAs through copolymerization reactions using 5,6-benzo-2-methylene-1,3-dioxepane, and their degradation into smaller fragments in KOH solution and in the presence of lipases was demonstrated.¹⁵ Reducible disulfide linkages were incorporated into PNIPAM through the polycondensation of telechelic PNIPAM that was prepared by reversible addition-fragmentation chain transfer polymerization.¹⁶ Elastin-like peptides, which undergo temperature-dependent aggregation and enzymatic degradation have also been investigated.¹⁷ Moieties imparting thermo-responsivity have been introduced as pendent groups to degradable backbones such as polyesters¹⁸⁻¹⁹ and chitosan.²⁰ Furthermore, polyacetals with pH-sensitive degradation behaviour and tunable T_{cp} values were synthesized from diols and divinyl ethers based on oligo(ethylene glycol).²¹

However, in all of these examples, the polymers degraded by multiple random backbone cleavage events, resulting in their gradual breakdown into lower molar mass polymers. In addition, very few studies have investigated the effects of degradation on T_{cp} and vice versa.^{16, 18-19}

Self-immolative polymers (SIPs) are a recently developed class of degradable polymers, which undergo end-to-end depolymerization when their end-caps are removed by stimuli such as enzymes, light, changes in pH, or other specific chemical species.²²⁻²³ The most investigated backbones thus far include polycarbamates,²⁴⁻²⁵ poly(benzyl ether)s,²⁶ polyphthalaldehydes,²⁷⁻²⁸ and polyglyoxylates.²⁹ SIPs have been investigated for their potential as sensors,³⁰ drug delivery vehicles,³¹ patterned devices,³² recyclable plastics³³ and composites.³⁴ Despite their unique degradation pathways relative to conventional degradable and stimuli-responsive polymers, to the best of our knowledge, thermo-responsive SIPs have not yet been developed and studied. Described here is the synthesis of a series of self-immolative polyglyoxylamides (PGAMs) with tunable structures and LCST behaviour, the measurement of their T_{cp} s under different conditions, and studies of their depolymerization behaviour. PGAMs depolymerize through the sequential fragmentation of terminal hemiacetals after end-cap cleavage, a reaction that propagates down the entire polymer backbone (Figure 4.1c). We demonstrate that the structure and T_{cp} affect the rate of end-cap cleavage and depolymerization, and that the depolymerization also affects T_{cp} . The polymers are also shown to exhibit low cytotoxicity, demonstrating their potential for further exploration in biomedical applications.

4.2 Results and Discussion

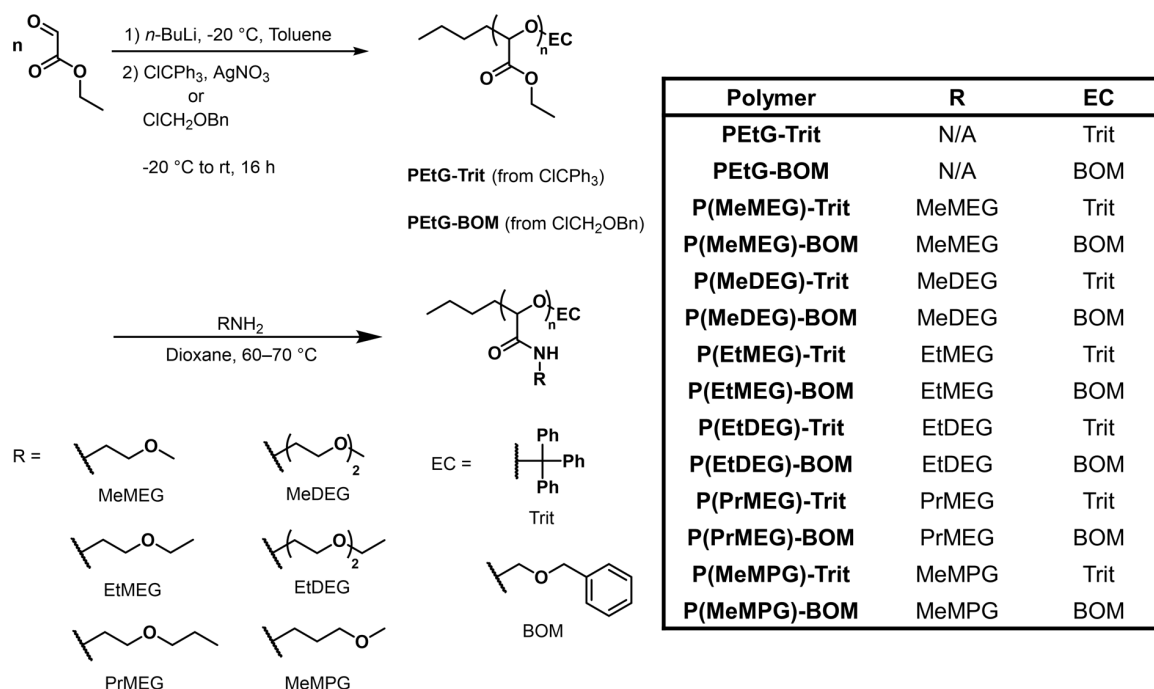
4.2.1 Polymer Nomenclature

The polymers were named as P(Pendent group)-End-cap, where P denotes polymer. Pendent groups are abbreviated as: MeMEG = methoxy monoethylene glycol; MeDEG = methoxy diethylene glycol; EtMEG = ethoxy monoethylene glycol; EtDEG = ethoxy diethylene glycol; PrMEG = propoxy monoethylene glycol; MeMPG = methoxy

monopropylene glycol. End-caps are abbreviated as: Trit = triphenylmethyl; BOM = benzyloxymethyl.

4.2.2 Polymer Synthesis

To synthesize the target thermo-responsive PGAMs, PEtGs with either a pH-sensitive triphenylmethyl (trityl) end-cap (**PEtG-Trit**) or stable benzyloxymethyl (BOM) end-cap (**PEtG-BOM**) were first prepared by *n*-butyl lithium initiated polymerization of ethyl glyoxylate in toluene at $-20\text{ }^{\circ}\text{C}$,³⁵ followed by end-capping with either trityl chloride³⁶ or benzyl chloromethyl ether respectively (Scheme 4.1). The polymers were characterized by ^1H and ^{13}C NMR spectroscopy, FT-IR spectroscopy, and size-exclusion chromatography (SEC) in *N,N*-dimethylformamide (DMF) relative to poly(methyl methacrylate) (PMMA) standards. **PEtG-Trit** had a number average molar mass (M_n) of 8.8 kg/mol, degree of polymerization (DP_n) of ~ 86 , and dispersity (D) of 1.5, while **PEtG-BOM** had an M_n of 8.9 kg/mol, DP_n of ~ 87 , and D of 1.5. Next, to obtain a library of PGAMs with different structures and T_{cp} values, the pendent ester groups on **PEtG-Trit** and **PEtG-BOM** were reacted with different alkoxyalkyl amines (Scheme 4.1). These amidation reactions were performed in 1,4-dioxane solutions of amine and PEtG at $60\text{--}70\text{ }^{\circ}\text{C}$ for 16 h (shorter, less sterically hindered amines) to 72 h (longer, more sterically hindered amines). The resulting PGAMs were isolated in 47–94% yield. NMR spectroscopy showed complete disappearance of the peaks corresponding to the pendent ethyl ester groups (Figure A3.1–Figure A3.26) and FT-IR spectra showed disappearance of the carbonyl absorption bands of the starting ester groups (1750 cm^{-1}) and appearance of peaks at $\sim 1670\text{ cm}^{-1}$ corresponding to the resulting amides (Figure A3.27–Figure A3.39). SEC showed that the DP_n and D values for the PGAMs remained similar to those of the starting polymers, confirming that the amidation reactions did not substantially affect the polymer backbones (Table 4.1, Figure A3.40, Figure A3.41).



Scheme 4.1. Synthesis of PGAMs having different pendent amide moieties and either Trit or BOM end-caps.

Table 4.1. Molar mass and DP_n data obtained from SEC and T_{cp} values determined by turbidimetry for the polymers. ND = not detected ($T_{cp} > 80$ °C). NM = not measured because no T_{cp} was detected at the higher concentration or in the case of culture media (CM) because only selected polymers were evaluated.

	P(MeMEG)-Trit	P(MeMEG)-BOM	P(MeDEG)-Trit	P(MeDEG)-BOM	P(EtMEG)-Trit	P(EtMEG)-BOM	P(EtDEG)-Trit	P(EtDEG)-BOM	P(MeMPG)-Trit	P(MeMPG)-BOM
M_n (kg/mol)	12.0	14.6	18.0	14.7	12.6	14.0	16.0	17.4	12.4	13.7
M_w (kg/mol)	20.0	23.1	30.0	27.0	23.5	20.8	31.0	26.4	21.7	19.6
D	1.8	1.6	1.7	1.8	1.9	1.5	1.9	1.5	1.8	1.4
DP_n	92	111	103	84	87	96	85	92	85	94

T_{cp} , water, 10.0 mg/mL (°C)	66	ND	ND	ND	14	38	45	49	33	45
T_{cp} , water, 5.0 mg/mL (°C)	ND	ND	NM	NM	17	41	48	52	36	46
T_{cp} , water, 2.5 mg/mL (°C)	NM	ND	NM	NM	20	ND	ND	58	39	47
T_{cp} , water, 1.25 mg/mL (°C)	NM	ND	NM	NM	24	ND	ND	ND	43	48
T_{cp} , PBS, 10.0 mg/mL (°C)	52	ND	65	ND	12	26	39	41	28	42
T_{cp} , PBS, 5.0 mg/mL (°C)	64	NM	ND	NM	16	25	41	41	32	43
T_{cp} , PBS, 2.5 mg/mL (°C)	ND	NM	NM	NM	19	28	42	42	36	44
T_{cp} , PBS, 1.25 mg/mL (°C)	NM	NM	NM	NM	22	31	44	44	40	44
T_{cp} , CM, 10.0 mg/mL (°C)	NM	NM	NM	NM	NM	23	NM	40	NM	40

4.2.3 Cloud Point Measurements

The T_{cp} values for the polymers were first measured in water and in PBS, to examine the effects of biologically relevant salt concentrations. The polymer solutions were prepared at 10.0 mg/mL concentration, filtered at 4 °C, then their transmittance at 600 nm as a function of temperature was measured at a heating rate of 1 °C/min. The temperature corresponding to 50% transmittance was taken as the T_{cp} . Three runs performed on one polymer under the same conditions indicated a standard deviation of less than 1 °C on the T_{cp} values (Figure A3.62).

Previously, POEGMA with diethylene glycol (DEG) pendent groups had a T_{cp} of ~28 °C at 3.0 mg/mL in water.¹² In contrast, **P(MeDEG)-Trit** had a T_{cp} of greater than 80 °C in water and 65 °C in PBS at 10.0 mg/mL (Table 4.1). The higher T_{cp} of the PGAm likely arises from its higher hydrophilicity, as the backbone acetal oxygens and pendent amides can participate in hydrogen bonding with water. The lower T_{cp} in PBS than in water is common for thermo-responsive polymers and has been attributed to the salting-out effect.³⁷ **P(MeDEG)-BOM** did not have a T_{cp} below 80 °C in either water or PBS, indicating that

the trityl end-cap played a role in the overall hydrophobicity of **P(MeDEG)-Trit**, lowering its T_{cp} .

To lower the T_{cp} values into a more biologically relevant range, PGAMs with monoethylene glycol (MEG) pendent groups were investigated next. In PBS at 10.0 mg/mL, **P(MeMEG)-Trit** had a T_{cp} of 52 °C, compared 65 °C for **P(MeDEG)-Trit**, showing the effect of shortening the pendent oligo(ethylene glycol) chain. Lowering the concentration of **P(MeMEG)-Trit** in PBS to 5.0 mg/mL resulted in an increase in T_{cp} to 64 °C. Decreasing the polymer concentration has been found previously to increase the T_{cp} of some thermo-responsive polymers, which may be due in part to the slower aggregation of polymer chains in more dilute solutions.³⁸ In addition, **P(MeMEG)-Trit** had a T_{cp} of 66 °C in water. However, **P(MeMEG)-BOM** did not have a detectable T_{cp} in either water or PBS.

To further lower the hydrophilicity of the pendent groups and consequently T_{cp} , **P(EtMEG)-Trit**, **P(EtMEG)-BOM**, **P(PrMEG)-Trit**, and **P(PrMEG)-BOM** with longer ethyl and propyl hydrophobic tails, were examined. **P(PrMEG)-Trit** and **P(PrMEG)-BOM** were so hydrophobic that they did not dissolve in water at 4 °C. In contrast, **P(EtMEG)-Trit** had T_{cps} of 12 and 14 °C in PBS and water respectively at 10.0 mg/mL. These values increased to 22 and 24 °C respectively as the polymer concentration was decreased to 1.25 mg/mL. **P(EtMEG)-BOM** demonstrated similar behaviour but with higher T_{cps} of 26–31 °C in PBS due to the end-cap effect. The fact that **P(EtMEG)** has a T_{cp} below the physiological temperature of 37 °C across a range of concentrations and with different end-caps is particularly interesting for biomedical applications. For example, thermo-responsive polymers can be used to produce injectable formulations that exist as soluble polymers at low temperature (e.g., in the fridge), but spontaneously gel through aggregation *in vivo*.³⁹

Further tuning of T_{cp} was achieved through the use of DEG in combination with an ethyl tail in **P(EtDEG)-Trit** and **P(EtDEG)-BOM**. The presence of an additional ethylene glycol unit in the pendent groups made the DEG analogues more hydrophilic, leading to T_{cps} of 39 and 41 °C in PBS and 45 and 49 °C in water at 10.0 mg/mL for **P(EtDEG)-Trit** and **P(EtDEG)-BOM** respectively, about 30 °C higher than their corresponding MEG

analogues **P(EtMEG)-Trit** and **P(EtMEG)-BOM**. Interestingly, these DEG polymers showed little sensitivity to the identity of the end-cap or to concentration in PBS, with **P(EtDEG)-Trit** and **P(EtDEG)-BOM** both having T_{cp} s of 44 °C at 1.25 mg/mL. This property is particularly useful as it suggests that different end-caps can be used to enable triggering of depolymerization by different stimuli. In addition, the polymers should retain their thermo-responsiveness upon dilution. Furthermore, the presence of a T_{cp} just above physiological temperature should make these polymers useful for applications such as thermally-triggered drug release, which could be induced either through direct heating or magnetic hyperthermia.⁶

Monopropylene glycol (MPG) pendent groups with methyl tails were also investigated. The corresponding polymers, **P(MeMPG)-Trit** and **P(MeMPG)-BOM**, had T_{cp} values of 28 and 42 °C respectively in PBS and 33 and 45 °C in water respectively at 10.0 mg/mL. The variation in the T_{cp} values across the different media was relatively minimal but a substantial end-cap effect was observed for these polymers. In terms of concentration dependence, **P(MeMPG)-Trit** exhibited concentration dependent T_{cp} values, which increased to 40 °C in PBS and 43 °C in water at 1.25 mg/mL. However, the T_{cp} values of **P(MeMPG)-BOM** were relatively insensitive to concentration, increasing from 42 to 44 °C in PBS and from 45 to 48 °C in water as the concentration was decreased from 10.0 to 1.25 mg/mL. Though more pronounced for the MPG derivatives, the BOM end-capped PGAMs tended to exhibit less concentration dependence than the trityl end-capped PGAMs overall. As the trityl group can be considered as a highly hydrophobic moiety, concentration dependent intermolecular interactions may be important in the early phases of aggregation for the trityl series. It should also be noted that the methoxy-MPG pendent group is a structural isomer of the ethoxy-MEG pendent group. This structural change resulted in ~18 °C increase of the T_{cp} values for **P(MeMPG)-Trit** compared to **P(EtMEG)-Trit** across different concentrations and conditions. This result can likely be attributed to the higher dipole moment and polarity of the methoxy-MPG substituents, which is in agreement with the higher boiling point of methoxypropylamine (117 °C) compared to ethoxyethylamine (105 °C).

Finally, the thermo-responsive behaviour of **P(EtMEG)-BOM**, **P(EtDEG)-BOM**, and **P(MeMPG)-BOM** in Dulbecco's Modified Eagle's Medium containing 10% fetal bovine serum (FBS) was investigated, to understand how the polymers would behave in cell culture media containing proteins. These polymers were selected as they exhibited T_{cp} s close to room and physiological temperatures. For each polymer, the T_{cp} was within 1–3 °C of that measured in PBS, showing a minimal effect of culture media components such as proteins (from FBS), inorganic salts, amino acids, glucose, and vitamins. In addition, each polymer exhibited a reversible transition with negligible (~ 1 °C) hysteresis (Figure 4.2a, Figure A3.63, Figure A3.64). These properties are favourable, as they indicate that the polymers should exhibit relatively predictable thermo-responsive behaviour. In contrast, T_{cp} of PNIPAM copolymers were previously found to be highly sensitive to the presence of serum proteins.⁴⁰

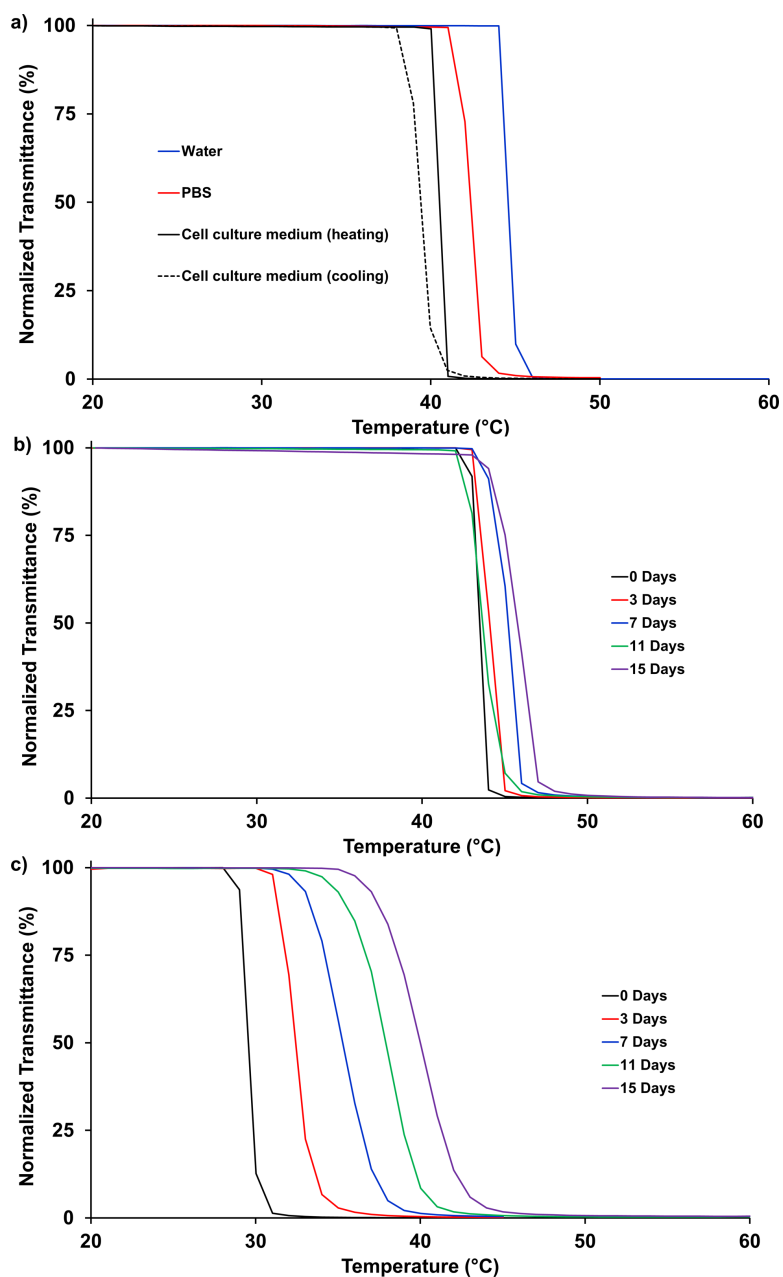


Figure 4.2. a) Thermo-responsive behaviour of P(MeMPG)-BOM in water, pH 7.4 PBS, and cell culture media containing FBS, showing dependence on the solvent/media. Minimal hysteresis was observed in the presence of FBS. b) Thermo-responsive behaviour of P(MeMPG)-BOM in pH 3.0 citrate buffer at different points showing minimal change in the T_{cp} . c) Thermo-responsive behaviour of P(MeMPG)-Trit in pH 3.0 citrate buffer at different points showing an increase in the T_{cp} as the polymer depolymerizes.

4.2.4 Dynamic Light Scattering (DLS) Measurements

To further understand the aggregation behaviour of the polymers below, at, and above their cloud points, six of the synthesized polymers with cloud points closest to room and physiological temperature [**P(EtMEG)-Trit**, **P(EtMEG)-BOM**, **P(EtDEG)-Trit**, **P(EtDEG)-BOM**, **P(MeMPG)-Trit**, **P(MeMPG)-BOM**] were investigated using DLS. First, solutions of these polymers in PBS (1.25 mg/mL) were monitored for changes in the Z average diameters and mean scattering count rates as the temperature was increased from below to above the T_{cp} . Below the T_{cp} , the solutions comprised mainly molecularly dissolved polymers, as indicated by diameters well below 100 nm (Figure A3.65). However, some polymers including **P(EtDEG)-Trit** and **P(EtDEG)-BOM** exhibited some tendency to aggregate, forming nanoscale assemblies, likely due to their amphiphilic structures. It is possible that this tendency to aggregate explains the lower concentration and end-cap dependence of these polymers compared to the other derivatives. At temperatures very similar to the T_{cp} values measured in the turbidimetry experiments for each polymer, there was a rapid increase in diameter to micro-sized aggregates and corresponding increase in the count rate. When the solutions were incubated over time at the T_{cp} , again initially dissolved polymers and nanoscale assemblies were observed (Figure 4.3, Figure A3.66). Over 200–800 s these transformed first to larger nano-sized aggregates, and then to micron-sized aggregates.

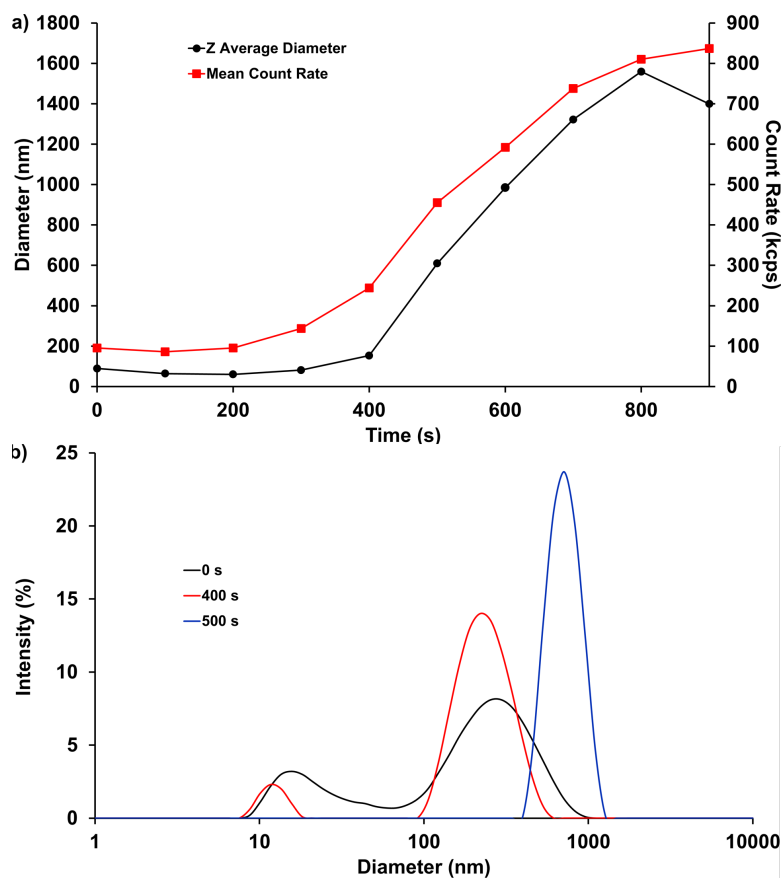


Figure 4.3. a) Z average diameter and mean count rate of **P(EtDEG)-BOM** at 43 °C in PBS (1.25 mg/mL) over time. The solution temperature was the T_{cp} of the polymer solution as determined previously by DLS (Figure A3.65). b) The intensity distribution of diameters in the solution at different time points showing the conversion of dissolved polymers and nanoscale assemblies into large micron-sized aggregates over time.

4.2.5 Depolymerization

Depolymerization of the PGAMs was examined to understand how their thermo-responsive properties would impact their depolymerization behaviour and how their depolymerization would affect their T_{cp} values. Again, we chose **P(EtMEG)-Trit**, **P(EtDEG)-Trit**, and **P(MeMPG)-Trit** and their non-stimuli-responsive analogues **P(EtMEG)-BOM**, **P(EtDEG)-BOM**, and **P(MeMPG)-BOM** as they had T_{cp} values closest to room and physiological temperatures. 10.0 mg/mL solutions of the polymers in D₂O, deuterated PBS (pH 7.4), and deuterated citrate buffer (pH 3.0) were placed in NMR tubes, which were

then sealed and stored at 20 °C. pH 7.4 was selected to mimic neutral physiological conditions. pH 3.0 was selected to achieve sufficient responsiveness of the trityl end-cap, while mimicking physiological environments such as the stomach. Their depolymerization behaviour was monitored *via* ^1H NMR spectroscopy at different time intervals by integrating the peaks associated with the methine (CH) proton of the hydrate depolymerization product (Figure 4.1c) at ~ 5.1 ppm and the methine proton of the PGAm backbone at ~ 5.5 ppm. As **P(EtMEG)-Trit** and **P(EtMEG)-BOM** were insoluble in the aqueous media at room temperature ($T_{cp} < 20$ °C) their spectra were obtained at 5 °C to ensure dissolution of both the polymer and depolymerization products for accurate quantification of the depolymerization. The spectra for the other systems were obtained at the standard instrument operating temperature of 25 °C.

In D_2O (Figure 4.4a), **P(EtDEG)-Trit** and **P(MeMPG)-Trit** depolymerized the most rapidly, with $\sim 15\%$ depolymerization after 13 days. This depolymerization occurs as a result of gradual cleavage of the trityl end-cap, even under neutral conditions.³⁶ On the other hand, **P(EtMEG)-Trit** depolymerized more slowly, with only 7% depolymerization over the same time period. Under the depolymerization conditions (10.0 mg/mL, 20 °C), **P(EtMEG)-Trit** would be in an aggregated state which may slow depolymerization, as we and other groups have found the depolymerization of self-immolative polymers to be slower in the solid state compared to solution.^{29, 41-42} All of the control polymers **P(EtMEG)-BOM**, **P(EtDEG)-BOM**, and **P(MeMPG)-BOM** exhibited less than 1% depolymerization in D_2O over 13 days, showing that the backbone is inherently stable under these conditions, and that depolymerization of the trityl end-capped polymers can indeed be attributed to end-cap cleavage followed by end-to-end depolymerization rather than random backbone cleavage. Very similar results were obtained in pH 7.4 PBS (Figure 4.4b), except that, like **P(EtMEG)-Trit** (above its T_{cp}), **P(EtDEG)-Trit** was also slower than **P(MeMPG)-Trit** despite being below its T_{cp} (39 °C). This result may arise from the tendency of **P(EtDEG)-Trit** to self-assemble, even below its T_{cp} (Figure A3.65), which would make the trityl end-cap less accessible for hydrolytic cleavage.

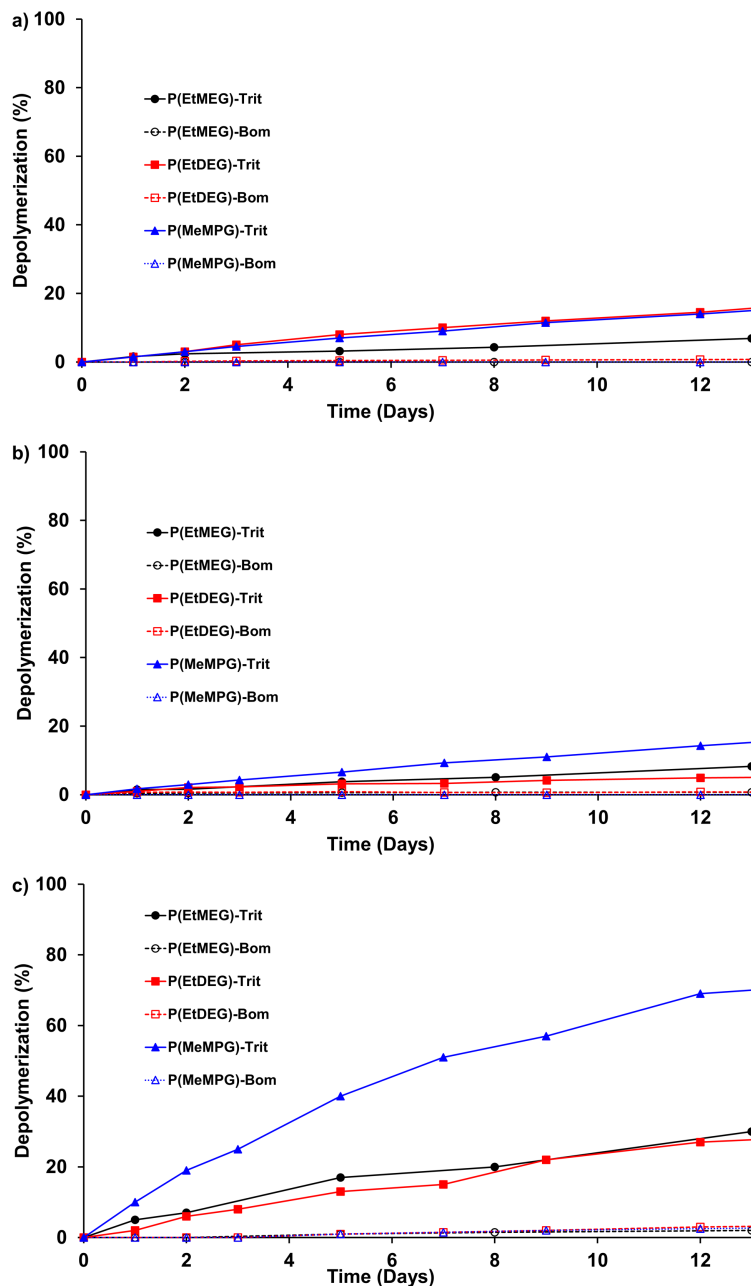


Figure 4.4. Depolymerization of P(EtMEG)-Trit, P(EtMEG)-BOM, P(EtDEG)-Trit, P(EtDEG)-BOM, P(MeMPG)-Trit, and P(MeMPG)-BOM in a) D₂O, b) deuterated pH 7.4 PBS, and c) deuterated pH 3.0 (0.1 M) citrate buffer, calculated by ¹H NMR spectroscopy at different time intervals. All depolymerization studies were performed at 20 °C, while spectra for P(EtDEG) and P(MeMPG) polymers were obtained at 25 °C and those for P(EtMEG) polymers were obtained at 5 °C due to their T_{cps} being less than 25 °C. The depolymerization behaviour depended on the medium and polymer structure.

In pH 3.0 citrate buffer, the depolymerization was faster for all of the trityl end-capped polymers compared to the other conditions (Figure 4.4c). This result can be attributed to the sensitivity of the trityl end-cap to the acid stimulus. Consistent with the other conditions, **P(MeMPG)-Trit** depolymerized most rapidly, with about 70% depolymerization over 13 days. **P(EtMEG)-Trit** and **P(EtDEG)-Trit** depolymerized similarly, with about 30% depolymerization over 13 days. These behaviours can be rationalized in the same manner as for the pH 7.4 results. While these rates of depolymerization are relatively slow due to the limited pH-sensitivity of the trityl group, the rate of trityl end-cap cleavage can be increased by the introduction of electron-donating substituents on the phenyl rings. All of the BOM end-capped polymers exhibited negligible depolymerization over 13 days, showing that the backbone is very stable, even at pH 3.0. Overall, the end-cap, pendent group structure, and T_{cp} of the polymer influence the depolymerization behaviour.

We previously found that the rate of PGAm depolymerization was limited by the rate of end-cap cleavage.³⁶ Depolymerization was fast following end-cap cleavage and partially depolymerized polymers were not observed by SEC. The current depolymerization kinetics data for the trityl end-capped polymers fit well with a pseudo-first-order kinetics model. This analysis suggests that end-cap cleavage is indeed the rate limiting step for these polymers as well, since for self-immolative polymers that undergo slow depolymerization after end-cap cleavage, the kinetics are instead pseudo-zero-order in the early phases of depolymerization.⁴³ Comparison of the pseudo-first-order rate constants (k) confirmed the qualitative trends and indicated that depolymerization was four to seven-fold faster at pH 3.0 than at pH 7.4 and two to seven-fold faster than in D₂O (Table 4.2).

Table 4.2. Pseudo-first-order rate constants (k , s^{-1}) for the depolymerization of **P(EtMEG)-Trit**, **P(EtDEG)-Trit**, and **P(MeMPG)-Trit** in D_2O , deuterated PBS, and deuterated pH 3.0 citrate buffer.

	P(EtMEG)-Trit	P(EtDEG)-Trit	P(MeMPG)-Trit
D₂O	5.6×10^{-8}	1.5×10^{-7}	1.4×10^{-7}
PBS	7.3×10^{-8}	3.9×10^{-8}	1.4×10^{-7}
pH 3.0 Citrate Buffer	3.1×10^{-7}	2.8×10^{-7}	1.0×10^{-6}

The effect of depolymerization on T_{cp} was also studied by performing turbidimetry measurements for **P(EtMEG)-Trit**, **P(EtMEG)-BOM**, **P(EtDEG)-Trit**, **P(EtDEG)-BOM**, **P(MeMPG)-Trit**, and **P(MeMPG)-BOM** over time in pH 3.0 citrate buffer (10.0 mg/mL). In each case, the BOM end-capped polymers exhibited less than 3 °C change in T_{cp} over 15 days (Figure 4.2b, Figure A3.86, Figure A3.88). In contrast, substantial changes in T_{cp} of 9–13 °C were observed for the trityl end-capped PGAMs (Figure 4.2c, Figure A3.87, Figure A3.89). For example, **P(MeMPG)-Trit** exhibited an increase in T_{cp} from 30 to 40 °C over 15 days. This finding, combined with the observed rate-limiting end-cap cleavage and concentration dependence of T_{cp} for **P(MeMPG)-Trit** (i.e., increase in T_{cp} from 28–40 °C as the concentration was decreased from 10.0 to 1.25 mg/mL in PBS), indicates that the increase in T_{cp} over time can likely be attributed to a decrease in polymer concentration as depolymerization occurred. This interpretation differs from that of previous studies involving the random backbone cleavage of polyesters and PNIPAM containing disulfide linkages, where a decrease in T_{cp} was attributed primarily to decreasing polymer chain length as random backbone cleavages occurred.^{16, 18-19} It also suggests that the T_{cp} can therefore be modulated according to the rate of end-cap cleavage, which is a key difference between self-immolative polymers and conventional backbone-degradable polymers.

4.2.6 In Vitro Cytotoxicity Studies

3-(4,5-Dimethylthiazol-2-yl)-2,5-diphenyltetrazolium bromide (MTT) assays were performed to provide an indication of the cytotoxicities of the polymers. C2C12 mouse myoblast cells were used as they are a common cell line for *in vitro* work. The polymers were incubated with the cells for 24 h prior to performing the assay. Six different polymers were evaluated to determine the effects of the pendent groups and the end-caps on cytotoxicity. Comparing **P(MeMEG)-Trit** and **P(EtMEG)-Trit**, both polymers exhibited high cell metabolic activity (> 75%) at concentrations up to 0.25 mg/mL (Figure 4.5a). However, the more hydrophobic polymer **P(EtMEG)-Trit** with the ethyl tail was less toxic at higher concentrations than the analogue with the methyl tail. **P(EtMEG)-Trit** was initially dissolved and diluted in the cell culture media at 4 °C, due to its low T_{cp} . However, it would be expected to aggregate during cell culture at 37 °C, so may interact less with cells and be taken up to a different extent than the soluble analogue. **P(MeDEG)-Trit** and **P(EtDEG)-Trit** followed the same trend as the MEG analogues, with the more hydrophobic polymer with the ethyl tails being less toxic, likely because its T_{cp} is very close to the incubation temperature of 37 °C (Figure 4.5b). The effect of the end-cap was also examined by comparing **P(MeMPG)-Trit** and **P(MeMPG)-BOM** (Figure 4.5c). No significant end-cap effects were observed. Overall, the polymers exhibited low cytotoxicity, suggesting their potential for biomedical applications.

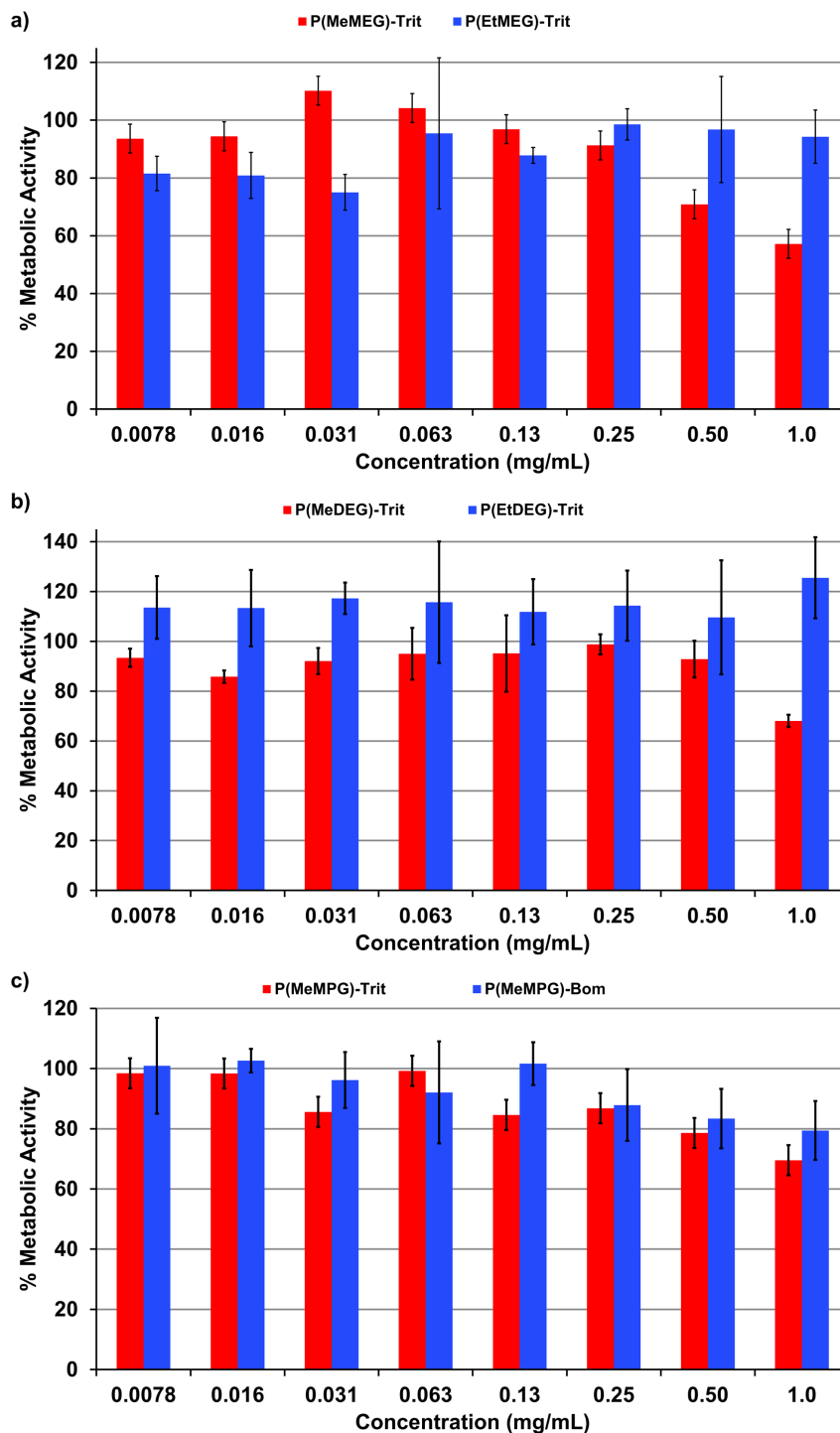


Figure 4.5. Cell metabolic activity (relative to control), as measured by MTT assays, as a function of polymer concentration: a) **P(MeMEG)-Trit** versus **P(EtMEG)-Trit**, b) **P(MeMEG)-Trit** versus **P(EtDEG)-Trit**, c) **P(MeMPG)-Trit** versus **P(MeMPG)-BOM** as measured by MTT assays on C2C12 cells following a 24 h incubation.

4.3 Conclusions

Thermo-responsive PGAMs were readily synthesized through the amidation of PEtGs and their LCST behaviour was tuned through the introduction of different pendent alkoxyalkyl amines. PGAMs with T_{cp} values just below room temperature and just above physiological temperature were obtained, demonstrating the promise for these polymers in applications such as injectable hydrogels and drug delivery vehicles, where aggregation above T_{cp} could be used to induce gelation or drug release. The influence of the end-cap and polymer concentration on T_{cp} depended on the particular structure of the pendent group. The trityl end-capped polymers depolymerized more rapidly than the BOM end-capped polymers, showing that depolymerization occurred selectively through an end-cap cleavage and end-to-end depolymerization process under all of the evaluated conditions. It was found that both the structure and T_{cp} of the polymers influenced their depolymerization behaviours and that depolymerization led to an increase in T_{cp} . Furthermore, the polymers exhibiting the most interesting T_{cp} values, near physiological and room temperature, exhibited low cytotoxicity, demonstrating their promise for biomedical and other applications. While the polymers in the current work underwent relatively slow end-cap cleavage and consequently slow depolymerization, the advantage of SIPs is that the end-cap can be readily substituted to afford responsiveness to different stimuli and to tune the rate of depolymerization, without changing the polymer backbone.

4.4 Experimental

4.4.1 General Experimental Details

General materials. All reactions and manipulations were carried out under a nitrogen atmosphere using standard Schlenk techniques unless otherwise stated. All reagents were used as received unless otherwise stated. Ethyl glyoxylate solution (~50% in toluene) was obtained from Alfa Aesar and purified according to a previously published procedure.³⁵ Triphenylmethyl end-capped poly(ethyl glyoxylate) (**PEtG-Trit**) was synthesized as previously reported.³⁶ Citric acid was obtained from Alfa Aesar. NaOH was obtained from Fisher Scientific. Phosphate buffered saline (PBS, pH 7.4) was prepared from sachets of

premixed salts (SKU No. P38135, Sigma-Aldrich) according to the manufacturer's instructions. Ultrapure water was obtained from a Barnstead EASYpure II system. Chloromethyl benzyl ether (technical, ~60%), LiBr, *n*-butyl lithium solution (2.5 M in hexanes), 2-methoxyethylamine (99%), 3-methoxypropylamine (99%), 2-(2-ethoxyethoxy)ethanamine ($\geq 95\%$), and 2-(2-methoxyethoxy)ethanamine ($\geq 95\%$), and all cell culture reagents were obtained from Sigma-Aldrich. 2-Ethoxyethylamine (95–98%) and 2-propoxyethylamine (95–98%) were purchased from Aurora Fine Chemicals LLC. 1,4-Dioxane, acetone, methanol, and chromatography-grade DMF were obtained from Caledon Laboratories. NEt_3 was purchased from Fisher Scientific and distilled over CaH_2 . Toluene was purchased from Caledon Laboratories and distilled over Na/benzophenone.

General procedures. For NMR spectroscopy, D_2O and CDCl_3 were purchased from Sigma-Aldrich and used as received. ^1H and ^{13}C NMR spectra were recorded using a 400 MHz Bruker AvIII HD 400 instrument and referenced to residual CHCl_3 (7.26 ppm), HOD (4.79 ppm) or CDCl_3 (77.2 ppm). FT-IR spectra were recorded using a PerkinElmer Spectrum Two FT-IR spectrometer with an attenuated total reflectance (ATR) attachment and a single reflection diamond. SEC was performed on an instrument equipped with a Waters 515 HPLC pump with a Waters In-Line Degasser AF, two PLgel mixed D 5 μm (300×1.5 mm) columns connected to a corresponding PLgel guard column, and a Wyatt Optilab Rex RI detector. Polymer solutions (at a concentration of ~5 mg/mL) in DMF containing LiBr (10 mM) and NEt_3 (1% v/v) were filtered (using 0.2 μm polytetrafluoroethylene syringe filters) before they were injected (using a 50 μL loop) and run at a flow rate of 1 mL/min for 30 min at 85 °C in the same solvent as an eluent. Molar masses were determined by comparison to PMMA standards purchased from Viscotek. DLS measurements were obtained using a Malvern Zetasizer Nano ZS instrument equipped with a 633 nm laser and at a scattering angle of 173°.

4.4.2 Polymer Synthesis

PEtG-Trit used in this chapter was previously synthesized and characterized in Chapter 3. See 3.4.2 for experimental details. All PGAMs were synthesized by the same procedure

described for the synthesis of P(MeMEG)-Trit (representative PGAm synthesis). End group analysis could not be performed for the PGAm due to significant peak broadening.

Synthesis of PEtG-BOM. In a Schlenk flask, freshly distilled toluene (20 mL) and an *n*-butyl lithium solution (200 μ L of 2.5 M in hexanes, 0.50 mmol, 1.0 equiv) were combined at room temperature and vigorously stirred for 3 min. The flask was then instantly charged with freshly distilled ethyl glyoxylate (5.0 mL, 50 mmol, 100 equiv.) and stirred for another 10 min before cooling the solution to -20 $^{\circ}$ C and stirring at that temperature for 20 min. Then, freshly distilled NEt₃ (0.30 mL, 2.2 mmol, 4.4 equiv.) was added and the resulting solution was stirred for 10 min before the addition of chloromethyl benzyl ether (0.30 mL of 60%, \sim 1.3 mmol, \sim 2.6 equiv.). The resulting mixture was stirred for another 3 h, at -20 $^{\circ}$ C, then it was allowed to gradually reach 20 $^{\circ}$ C, over 16 h. Concentration of the polymerization mixture under vacuum at 45 $^{\circ}$ C gave crude residue. The residue was dissolved in CH₂Cl₂ (10 mL) and slowly added to a vigorously stirring methanol/water mixture (4/1; 250 mL). The flask was then sealed and transferred into a -20 $^{\circ}$ C freezer where it was kept for 16 h before decanting the solvent and drying under vacuum the resulting purified residue. Yield = 3.9 g, 76%. ¹H NMR (CDCl₃, 400 MHz): δ 7.31 (br s, 5 H), 5.46–5.76 (m, 110 H), 4.86–5.04 (m, 2 H), 4.21 (br s, 224 H), 1.28 (br s, 346 H), 0.87 (br s, 3 H). ¹³C {¹H} NMR (CDCl₃, 100 MHz): δ 165.0–166.9, 128.5, 128.0, 90.8–94.4, 62.2, 14.0. FT-IR: 2990, 1750 cm⁻¹. SEC (DMF, PMMA): M_n = 8.9 kg/mol, M_w = 13.3 kg/mol, D = 1.5.

Synthesis of P(MeMEG)-Trit (representative PGAm synthesis). In air, a pressure tube (25 mL) was charged with PEtG-Trit (270 mg of polymer, 2.6 mmol of ester, 1.0 equiv.), 2-methoxyethanamine (900 mg, 12 mmol, 4.6 equiv.), and 1,4-dioxane (3.0 mL) before it was sealed and heated for 40 h at 70 $^{\circ}$ C. The crude mixture was dialyzed against acetone (1.0 L) using a 6–8 kg/mol molecular weight cut-off membrane (Spectra/Por, regenerated cellulose) for 40 h (solvent was changed once after 16 h). The PGAm solution was then concentrated and the resulting residues were dried under vacuum for 16 h. Yield = 200 mg, 58%. ¹H NMR (CDCl₃, 400 MHz): δ 7.59–8.70 (m, 1 H), 5.74 (br s, 1 H), 3.05–3.71 (m, 7 H). ¹³C {¹H} NMR (CDCl₃, 100 MHz): δ 166.5–167.9, 129.0, 128.0, 127.7, 96.7, 58.7,

39.4. FT-IR: 3290, 3080, 2990, 2930, 2890, 2830, 1670, 1540 cm^{-1} . SEC (DMF, PMMA): $M_n = 12.0$ kg/mol, $M_w = 20.0$ kg/mol, $D = 1.8$.

Synthesis of P(MeMEG)-BOM. From **PEtG-BOM** (140 mg of polymer, 1.4 mmol of ester, 1.0 equiv.), 1,4-dioxane (3.0 mL), 2-methoxyethanamine (600 mg, 8.0 mmol, 5.7 equiv.), 40 h at 70 °C. Yield = 160 mg, 89%. ^1H NMR (CDCl_3 , 400 MHz): δ 7.56–8.71 (m, 1 H), 5.74 (br s, 1 H), 3.09–3.72 (m, 7 H). $^{13}\text{C}\{^1\text{H}\}$ NMR (CDCl_3 , 100 MHz): δ 166.3–168.2, 128.4, 128.0, 127.8, 96.5, 70.6, 58.6, 39.3. FT-IR: 3280, 3090, 2960, 2930, 2890, 2830, 1670, 1540 cm^{-1} . SEC (DMF, PMMA): $M_n = 14.6$ kg/mol, $M_w = 23.1$ kg/mol, $D = 1.6$.

Synthesis of P(MeDEG)-Trit. From **PEtG-Trit** (230 mg of polymer, 2.3 mmol of ester, 1.0 equiv.), 1,4-dioxane (3.0 mL), 2-(2-methoxyethoxy)ethanamine (1.1 g, 9.2 mmol, 4.0 equiv.), 40 h at 70 °C. Yield = 230 mg, 58%. ^1H NMR (CDCl_3 , 400 MHz): δ 7.56–8.94 (m, 1 H), 5.71 (br s, 1 H), 3.04–3.98 (m, 11 H). $^{13}\text{C}\{^1\text{H}\}$ NMR (CDCl_3 , 100 MHz): δ 167.4, 96.6, 72.0, 70.3, 69.3, 59.0, 39.4. FT-IR: 3300, 3080, 2970, 2930, 2880, 2820, 1670, 1540 cm^{-1} . SEC: $M_n = 18.0$ kg/mol, $M_w = 30.0$ kg/mol, $D = 1.7$.

Synthesis of P(MeDEG)-BOM. From **PEtG-BOM** (210 mg of polymer, 2.1 mmol of ester, 1.0 equiv.), 1,4-dioxane (3.0 mL), 2-(2-methoxyethoxy)ethanamine (1.0 g, 8.4 mmol, 4.0 equiv.), 40 h at 70 °C. Yield = 220 mg, 61%. ^1H NMR (CDCl_3 , 400 MHz): δ 7.51–8.81 (m, 1 H), 5.71 (br s, 1 H), 3.16–3.75 (m, 11 H). $^{13}\text{C}\{^1\text{H}\}$ NMR (CDCl_3 , 100 MHz): δ 167.3, 96.4, 71.9, 70.2, 69.2, 59.0, 39.4. FT-IR: 3280, 3080, 2920, 2880, 2820, 1670, 1540 cm^{-1} . SEC (DMF, PMMA): $M_n = 14.7$ kg/mol, $M_w = 27.0$ kg/mol, $D = 1.8$.

Synthesis of P(EtMEG)-Trit. From **PEtG-Trit** (310 mg of polymer, 3.0 mmol of ester, 1.0 equiv.), 1,4-dioxane (10 mL), 2-ethoxyethylamine (810 mg, 9.1 mmol, 3.0 equiv.), 16 h at 60 °C. Yield = 220 mg, 50%. ^1H NMR (CDCl_3 , 400 MHz): δ 7.77–8.71 (m, 1 H), 5.75 (br s, 1 H), 3.23–3.65 (m, 6 H), 1.15 (br s, 3 H). $^{13}\text{C}\{^1\text{H}\}$ NMR (CDCl_3 , 100 MHz): δ 166.4–168.1, 129.0, 128.1, 127.7, 96.6, 68.5, 66.4, 39.5, 15.2. FT-IR: 3280, 3080, 2980, 2930, 2870, 1670, 1540 cm^{-1} . SEC (DMF, PMMA): $M_n = 12.6$ kg/mol, $M_w = 23.5$ kg/mol, $D = 1.9$.

Synthesis of P(EtMEG)-BOM. From **PEtG-BOM** (260 mg of polymer, 2.5 mmol of ester, 1.0 equiv.), 1,4-dioxane (10 mL), 2-ethoxyethylamine (1.0 g, 11 mmol, 4.4 equiv.), 16 h at 60 °C. Yield = 280 mg, 76%. ^1H NMR (CDCl_3 , 400 MHz): δ 7.61–9.11 (m, 1 H), 5.74 (br s, 1 H), 3.23–3.61 (m, 6 H), 0.87 (br s, 3 H). $^{13}\text{C}\{^1\text{H}\}$ NMR (CDCl_3 , 100 MHz): 166.4–167.7, 96.5, 68.3, 66.3, 39.4, 15.1. FT-IR: 3280, 3090, 2980, 2890, 2870, 1670, 1540 cm^{-1} . SEC (DMF, PMMA): M_n = 14.0 kg/mol, M_w = 20.8 kg/mol, D = 1.5.

Synthesis of P(EtDEG)-Trit. From **PEtG-Trit** (350 mg of polymer, 3.4 mmol of ester, 1.0 equiv.), 1,4-dioxane (10 mL), 2-(2-ethoxyethoxy)ethanamine (1.2 g, 9.0 mmol, 2.6 equiv.), 72 h at 60 °C. Yield = 340 mg, 52%. ^1H NMR (CDCl_3 , 400 MHz): δ 7.52–8.75 (m, 1 H), 5.70 (br s, 1 H), 3.23–3.66 (m, 10 H), 1.17 (t, J = 7 Hz, 3 H). $^{13}\text{C}\{^1\text{H}\}$ NMR (CDCl_3 , 100 MHz): δ 166.4–168.3, 129.0, 128.0, 127.7, 96.5, 70.4, 69.8, 69.3, 66.7, 39.4, 15.3. FT-IR: 3270, 3080, 2970, 2900, 2870, 1670, 1540 cm^{-1} . SEC (DMF, PMMA): M_n = 16.0 kg/mol, M_w = 31.0 kg/mol, D = 1.9.

Synthesis of P(EtDEG)-BOM. From **PEtG-BOM** (200 mg of polymer, 2.0 mmol of ester, 1.0 equiv.), 1,4-dioxane (10 mL), 2-(2-ethoxyethoxy)ethanamine (940 mg, 7.1 mmol, 3.6 equiv.), 72 h at 60 °C. Yield = 310 mg, 84%. ^1H NMR (CDCl_3 , 400 MHz): δ 7.62–8.97 (m, 1 H), 5.71 (br s, 1 H), 3.21–3.76 (m, 10 H), 1.18 (t, J = 7 Hz, 3 H). $^{13}\text{C}\{^1\text{H}\}$ NMR (CDCl_3 , 100 MHz): δ 166.3–167.9, 96.5, 70.4, 69.8, 69.2, 66.6, 39.4, 15.2. FT-IR: 3270, 3070, 2970, 2900, 2870, 1670, 1540 cm^{-1} . SEC (DMF, PMMA): M_n = 17.4 kg/mol, M_w = 26.4 kg/mol, D = 1.5.

Synthesis of P(PrMEG)-Trit. From **PEtG-Trit** (200 mg of polymer, 2.0 mmol of ester, 1.0 equiv.), 1,4-dioxane (3.0 mL), 2-propoxyethylamine (800 mg, 7.8 mmol, 3.9 equiv.), 40 h at 70 °C. Yield = 190 mg, 61%. ^1H NMR (CDCl_3 , 400 MHz): δ 7.61–9.09 (m, 1 H), 5.73 (br s, 1 H), 3.01–3.82 (m, 6 H), 1.55 (br s, 2 H), 0.89 (br s, 3 H). $^{13}\text{C}\{^1\text{H}\}$ NMR (CDCl_3 , 100 MHz): δ 165.8–168.6, 129.1, 128.2, 96.6, 72.8, 68.7, 39.5, 22.9, 10.6. FT-IR: 3290, 3090, 2960, 2940, 2880, 2810, 1670, 1540 cm^{-1} . SEC (DMF, PMMA): M_n = 13.9 kg/mol, M_w = 23.1 kg/mol, D = 1.7.

Synthesis of P(PrMEG)-BOM. From **PEtG-BOM** (160 mg of polymer, 1.6 mmol of ester, 1.0 equiv.), 1,4-dioxane (3.0 mL), 2-propoxyethylamine (700 mg, 6.8 mmol, 4.3

equiv.), 40 h at 70 °C. Yield = 190 mg, 76%. ^1H NMR (CDCl_3 , 400 MHz): δ 7.57–8.90 (m, 1 H), 5.76 (br s, 1 H), 3.03–3.85 (m, 6 H), 1.55 (br s, 2 H), 0.88 (br s, 3 H). $^{13}\text{C}\{^1\text{H}\}$ NMR (CDCl_3 , 100 MHz): δ 165.9–168.8, 128.5, 128.1, 127.8, 96.5, 72.8, 68.6, 39.4, 22.8, 10.5. FT-IR: 3260, 3080, 2940, 2940, 2880, 1670, 1540 cm^{-1} . SEC (DMF, PMMA): M_n = 14.6 kg/mol, M_w = 23.8 kg/mol, D = 1.6.

Synthesis of P(MeMPG)-Trit. From **PEtG-Trit** (300 mg of polymer, 2.9 mmol of ester, 1.0 equiv.), 1,4-dioxane (10 mL), 3-methoxypropylamine (1.2 g, 13 mmol, 4.5 equiv.), 16 h at 60 °C. Yield = 200 mg, 47%. ^1H NMR (CDCl_3 , 400 MHz): δ 7.73–8.99 (m, 1 H), 5.72 (br s, 1 H), 3.00–3.63 (m, 7 H), 1.78 (br s, 3 H). $^{13}\text{C}\{^1\text{H}\}$ NMR (CDCl_3 , 100 MHz): δ 166.1–168.3, 128.9, 128.1, 127.7, 96.6, 70.3, 58.6, 37.0, 29.1. FT-IR: 3270, 3080, 2930, 2880, 2830, 1660, 1540 cm^{-1} . SEC (DMF, PMMA): M_n = 12.4 kg/mol, M_w = 21.7 kg/mol, D = 1.8.

Synthesis of P(MeMPG)-BOM. From **PEtG-BOM** (250 mg of polymer, 2.4 mmol of ester, 1.0 equiv.), 1,4-dioxane (10 mL), 3-methoxypropylamine (1.1 g, 12 mmol, 5.0 equiv.), 16 h at 60 °C. Yield = 210 mg, 59%. ^1H NMR (CDCl_3 , 400 MHz): δ 7.70–8.88 (m, 1 H), 5.73 (br s, 1 H), 3.04–3.61 (m, 7 H), 1.77 (br s, 2 H). $^{13}\text{C}\{^1\text{H}\}$ NMR (CDCl_3 , 100 MHz): δ 165.9–168.5, 128.5, 128.1, 96.8, 70.4, 58.6, 37.1, 29.1. FT-IR: 3280, 3090, 2930, 2880, 2830, 1660, 1540 cm^{-1} . SEC (DMF, PMMA): M_n = 13.7 kg/mol, M_w = 19.6 kg/mol, D = 1.4.

4.4.3 NMR Depolymerization Studies

Polymer samples (10.0 mg/mL) were dissolved in D_2O or buffers made from D_2O (deuterated PBS or 0.1 M pH 3.0 citrate buffered D_2O) and incubated at room temperature (20 °C) for 13 days. ^1H NMR spectra were obtained periodically at either 25 °C [**P(EtDEG)-Trit**, **P(MeMPG)-Trit**, **P(EtDEG)-BOM**, **P(MeMPG)-BOM**] or 5 °C [**P(EtMEG)-Trit**, **P(EtMEG)-BOM**]. The depolymerization percent values were calculated by comparison of the intensity of the backbone methine peak (CH) of polymers (broad peak at ~5.5 ppm) and that of the CH peak of the resulting hydrate depolymerization product (sharp peak at ~5.1 ppm).

4.4.4 T_{cp} Measurements

The measurements were obtained using a Varian UV-Vis Cary 300 instrument equipped with a temperature controller unit. Polymer solutions (10.0 mg/mL) were prepared by dissolving the polymers in water, buffer, or Dulbecco's Modified Eagle's Medium (DMEM) with 10% FBS (at 4 °C), then filtering through 0.2 μ m Nylon syringe filters. Then, they were placed inside low-volume quartz cuvettes and their absorbance values, at 600 nm, were recorded after every 1 °C temperature change while they were being gradually heated (1 °C/min) to maximum temperatures and subsequently cooled (1 °C/min) to the initial temperature (see Figure A3.42–Figure A3.64 and Figure A3.86–Figure A3.89 for the specific temperature ranges used). The T_{cp} was taken as the temperature at which 50% of the initial transmittance was observed. For polymers where T_{cp} was observed, the solution was diluted 2-fold to 5.00 mg/mL and the T_{cp} measurement was repeated. The dilution and measurement steps were repeated down to 1.25 mg/mL. Three runs were performed on **P(MeMPG)-BOM** at 10.0 mg/mL to determine the reproducibility of the T_{cp} measurements.

4.4.5 DLS Studies

The position and attenuation of the DLS light source were fixed between measurements to allow for direct comparisons of the measured count rates. Polymer solutions (1.25 mg/mL) were prepared by dissolving the polymers in PBS (at 4 °C), then filtering through 0.2 μ m Nylon syringe filters and placing them inside low volume polystyrene cuvettes. For monitoring over temperature ranges, measurements were taken every 1 °C, with a 2 min equilibration time at each temperature before the measurement was taken. For monitoring over time, the instrument was set to the T_{cp} of the polymer that was previously determined by DLS monitoring of the polymer solution over temperature. The polymer solution was kept below its T_{cp} and was quickly inserted into the instrument and measured in 100 s intervals, with no additional delays between measurements.

4.4.6 Cell Metabolic Activity Assays

C2C12 mouse myoblast cells were thawed and cultured as previously described.⁴⁴ The culture media consisted of DMEM (500 mL) supplemented with 10 mL of penicillin-streptomycin (1000 units/mL), 5 mL of L-glutamine (200 mM) and 50 mL of FBS. The cells were then seeded in a Nunclon 96-well U bottom transparent polystyrol plate to obtain approximately 10,000 cells/well in 100 μ L of media and were allowed to adhere to the plate in a 5% CO₂ incubator at 37 °C for 24 h. The growth media was then aspirated from the cells and replaced with either solutions of sodium dodecyl sulfate (SDS) in the cell culture media at concentrations of 0.20, 0.15, 0.10, or 0.050 mg/mL, which were used as positive controls, serial 2-fold dilutions of polymer in culture media ranging from 1.0 mg/mL to 7.8 μ g/mL, or fresh media as a negative control. The cells were then incubated at 37 °C (5% CO₂) for 24 h. The media was again aspirated and replaced with 110 μ L of fresh media containing 0.5 mg/mL MTT. After 4 h of incubation (37 °C, 5% CO₂), the MTT solution was carefully aspirated and the purple crystals were dissolved by the addition of 50 μ L of spectroscopic grade dimethyl sulfoxide (DMSO). After shaking (1 s, 2 mm amp, 654 rpm), the absorbance of the wells at 540 nm was read using an M1000-Pro plate reader (Tecan). The absorbance of wells prepared in the same way but without cells was subtracted as a background and the metabolic activity was calculated relative to the negative control. No metabolic activity was detected for cells exposed to the highest concentrations of SDS, confirming the sensitivity of the assay.

4.5 Reference

- (1) Roy, D.; Brooks, W. L.; Sumerlin, B. S. New Directions in Thermoresponsive Polymers. *Chem. Soc. Rev.* **2013**, *42*, 7214–7243.
- (2) Zhang, Q.; Weber, C.; Schubert, U. S.; Hoogenboom, R. Thermoresponsive Polymers with Lower Critical Solution Temperature: From Fundamental Aspects and Measuring Techniques to Recommended Turbidimetry Conditions. *Mater. Horiz.* **2017**, *4*, 109–116.
- (3) Chin, S. M.; Synatschke, C. V.; Liu, S.; Nap, R. J.; Sather, N. A.; Wang, Q.; Álvarez, Z.; Edelbrock, A. N.; Fyrner, T.; Palmer, L. C.; Szleifer, I.; Olvera de la Cruz, M.; Stupp,

- S. I. Covalent-Supramolecular Hybrid Polymers as Muscle-Inspired Anisotropic Actuators. *Nat. Commun.* **2018**, *9*, 2395.
- (4) Zheng, Y.; Soeriyadi, A. H.; Rosa, L.; Ng, S. H.; Bach, U.; Justin Gooding, J. Reversible Gating of Smart Plasmonic Molecular Traps using Thermoresponsive Polymers for Single-Molecule Detection. *Nat. Commun.* **2015**, *6*, 8797.
- (5) Chen, Z.; Hsu, P.-C.; Lopez, J.; Li, Y.; To, J. W. F.; Liu, N.; Wang, C.; Andrews, Sean C.; Liu, J.; Cui, Y.; Bao, Z. Fast and Reversible Thermoresponsive Polymer Switching Materials for Safer Batteries. *Nat. Energy* **2016**, *1*, 15009.
- (6) Bordat, A.; Boissenot, T.; Nicolas, J.; Tsapis, N. Thermoresponsive Polymer Nanocarriers for Biomedical Applications. *Adv. Drug Delivery Rev.* **2019**, *138*, 167–192.
- (7) Zhang, R.; Mjoseng, H. K.; Hoeve, M. A.; Bauer, N. G.; Pells, S.; Besseling, R.; Velugotla, S.; Tourniaire, G.; Kishen, R. E.; Tsenkina, Y.; Armit, C.; Duffy, C. R.; Helfen, M.; Edenhofer, F.; de Sousa, P. A.; Bradley, M. A Thermoresponsive and Chemically Defined Hydrogel for Long-Term Culture of Human Embryonic Stem Cells. *Nat. Commun.* **2013**, *4*, 1335.
- (8) Schild, H. G. Poly(*N*-isopropylacrylamide): Experiment, Theory and Application. *Prog. Polym. Sci.* **1992**, *17*, 163–249.
- (9) Nagase, K.; Yamato, M.; Kanazawa, H.; Okano, T. Poly(*N*-isopropylacrylamide)-Based Thermoresponsive Surfaces Provide New Types of Biomedical Applications. *Biomaterials* **2018**, *153*, 27–48.
- (10) Rey, M.; Fernandez-Rodriguez, M. A.; Karg, M.; Isa, L.; Vogel, N. Poly-*N*-Isopropylacrylamide Nanogels and Microgels at Fluid Interfaces. *Acc. Chem. Res.* **2020**, *53*, 414–424.
- (11) Lutz, J.-F.; Akdemir, Ö.; Hoth, A. Point by Point Comparison of Two Thermosensitive Polymers Exhibiting a Similar LCST: Is the Age of Poly(NIPAM) Over? *J. Am. Chem. Soc.* **2006**, *128*, 13046–13047.
- (12) Lutz, J.-F.; Hoth, A. Preparation of Ideal PEG Analogues with a Tunable Thermosensitivity by Controlled Radical Copolymerization of 2-(2-Methoxyethoxy)ethyl Methacrylate and Oligo(ethylene glycol) Methacrylate. *Macromolecules* **2006**, *39*, 893–896.

- (13) Lutz, J.-F. Thermo-Switchable Materials Prepared Using the OEGMA-Platform. *Adv. Mater.* **2011**, *23*, 2237–2243.
- (14) Badi, N. Non-Linear PEG-Based Thermoresponsive Polymer Systems. *Prog. Polym. Sci.* **2017**, *66*, 54–79.
- (15) Lutz, J.-F.; Andrieu, J.; Üzgün, S.; Rudolph, C.; Agarwal, S. Biocompatible, Thermoresponsive, and Biodegradable: Simple Preparation of “All-in-One” Biorelevant Polymers. *Macromolecules* **2007**, *40*, 8540–8543.
- (16) Phillips, D. J.; Gibson, M. I. Degradable Thermoresponsive Polymers Which Display Redox-Responsive LCST Behaviour. *Chem. Commun.* **2012**, *48*, 1054–1056.
- (17) Rodríguez-Cabello, J. C.; Arias, F. J.; Rodrigo, M. A.; Girotti, A. Elastin-Like Polypeptides in Drug Delivery. *Adv. Drug Delivery Rev.* **2016**, *97*, 85–100.
- (18) Swanson, J. P.; Monteleone, L. R.; Haso, F.; Costanzo, P. J.; Liu, T.; Joy, A. A Library of Thermoresponsive, Coacervate-Forming Biodegradable Polyesters. *Macromolecules* **2015**, *48*, 3834–3842.
- (19) Swanson, J. P.; Martinez, M. R.; Cruz, M. A.; Mankoci, S. G.; Costanzo, P. J.; Joy, A. A Coacervate-Forming Biodegradable Polyester with Elevated LCST Based on Bis-(2-methoxyethyl)amine. *Polym. Chem.* **2016**, *7*, 4693–4702.
- (20) Wang, F.; Xia, G.; Lang, X.; Wang, X.; Bao, Z.; Shah, Z.; Cheng, X.; Kong, M.; Feng, C.; Liu, Y.; Chen, X. Influence of the Graft Density of Hydrophobic Groups on Thermo-Responsive Nanoparticles for Anti-Cancer Drugs Delivery. *Colloids Surf., B* **2016**, *148*, 147–156.
- (21) Samanta, S.; Bogdanowicz, D. R.; Lu, H. H.; Koberstein, J. T. Polyacetals: Water-Soluble, pH-Degradable Polymers with Extraordinary Temperature Response. *Macromolecules* **2016**, *49*, 1858–1864.
- (22) Roth, M. E.; Green, O.; Gnaim, S.; Shabat, D. Dendritic, Oligomeric, and Polymeric Self-Immolative Molecular Amplification. *Chem. Rev.* **2016**, *116*, 1309–1352.
- (23) Yardley, R. E.; Rabiee Kenaree, A.; Gillies, E. R. Triggering Depolymerization: Progress and Opportunities for Self-Immolative Polymers. *Macromolecules* **2019**, *52*, 6342–6360.
- (24) Sagi, A.; Weinstain, R.; Karton, N.; Shabat, D. Self-Immolative Polymers. *J. Am. Chem. Soc.* **2008**, *130*, 5434–5435.

- (25) Dewit, M. A.; Gillies, E. R. A Cascade Biodegradable Polymer Based on Alternating Cyclization and Elimination Reactions. *J. Am. Chem. Soc.* **2009**, *131*, 18327–18334.
- (26) Olah, M. G.; Robbins, J. S.; Baker, M. S.; Phillips, S. T. End-Capped Poly(benzyl ethers): Acid and Base Stable Polymers That Depolymerize Rapidly from Head-to-Tail in Response to Specific Applied Signals. *Macromolecules* **2013**, *46*, 5924–5928.
- (27) Seo, W.; Phillips, S. T. Patterned Plastics That Change Physical Structure in Response to Applied Chemical Signals. *J. Am. Chem. Soc.* **2010**, *132*, 9234–9235.
- (28) Kaitz, J. A.; Diesendruck, C. E.; Moore, J. S. End Group Characterization of Poly(phthalaldehyde): Surprising Discovery of a Reversible, Cationic Macrocyclization Mechanism. *J. Am. Chem. Soc.* **2013**, *135*, 12755–12761.
- (29) Fan, B.; Trant, J. F.; Wong, A. D.; Gillies, E. R. Polyglyoxylates: A Versatile Class of Triggerable Self-Immolative Polymers from Readily Accessible Monomers. *J. Am. Chem. Soc.* **2014**, *136*, 10116–10123.
- (30) Lewis, G. G.; Robbins, J. S.; Phillips, S. T. Phase-Switching Depolymerizable Poly(carbamate) Oligomers for Signal Amplification in Quantitative Time-Based Assays. *Macromolecules* **2013**, *46*, 5177–5183.
- (31) Fan, B.; Gillies, E. R. Poly(ethyl glyoxylate)-Poly(ethylene oxide) Nanoparticles: Stimuli-Responsive Drug Release via End-to-End Polyglyoxylate Depolymerization. *Mol. Pharmaceutics* **2017**, *14*, 2548–2559.
- (32) Knoll, A. W.; Pires, D.; Coulembier, O.; Dubois, P.; Hedrick, J. L.; Frommer, J.; Duerig, U. Probe-Based 3-D Nanolithography Using Self-Amplified Depolymerization Polymers. *Adv. Mater.* **2010**, *22*, 3361–3365.
- (33) Baker, M. S.; Kim, H.; Olah, M. G.; Lewis, G. G.; Phillips, S. T. Depolymerizable Poly(benzyl ether)-Based Materials for Selective Room Temperature Recycling. *Green Chemistry* **2015**, *17*, 4541–4545.
- (34) Lloyd, E. M.; Lopez Hernandez, H.; Feinberg, A. M.; Yourdkhani, M.; Zen, E. K.; Mejia, E. B.; Sottos, N. R.; Moore, J. S.; White, S. R. Fully Recyclable Metastable Polymers and Composites. *Chem. Mater.* **2019**, *31*, 398–406.
- (35) Rabiee Kenaree, A.; Gillies, E. R. Controlled Polymerization of Ethyl Glyoxylate Using Alkylolithium and Alkoxide Initiators. *Macromolecules* **2018**, *51*, 5501–5510.

- (36) Sirianni, Q. E. A.; Rabiee Kenaree, A.; Gillies, E. R. Polyglyoxylamides: Tuning Structure and Properties of Self-Immolative Polymers. *Macromolecules* **2019**, *52*, 262–270.
- (37) Zhang, Y.; Furyk, S.; Bergbreiter, D. E.; Cremer, P. S. Specific Ion Effects on the Water Solubility of Macromolecules: PNIPAM and the Hofmeister Series. *J. Am. Chem. Soc.* **2005**, *127*, 14505–14510.
- (38) Bebis, K.; Jones, M. W.; Haddleton, D. M.; Gibson, M. I. Thermoresponsive Behaviour of Poly[(oligo(ethyleneglycol methacrylate)]s and Their Protein Conjugates: Importance of Concentration and Solvent System. *Polym. Chem.* **2011**, *2*, 975–982.
- (39) Liow, S. S.; Dou, Q.; Kai, D.; Karim, A. A.; Zhang, K.; Xu, F.; Loh, X. J. Thermogels: In Situ Gelling Biomaterial. *ACS Biomater. Sci. Eng.* **2016**, *2*, 295–316.
- (40) Hiruta, Y.; Nagumo, Y.; Suzuki, Y.; Funatsu, T.; Ishikawa, Y.; Kanazawa, H. The Effects of Anionic Electrolytes and Human Serum Albumin on the LCST of poly(*N*-isopropylacrylamide)-Based Temperature-Responsive Copolymers. *Colloids Surf., B* **2015**, *132*, 299–304.
- (41) Yeung, K.; Kim, H.; Mohapatra, H.; Phillips, S. T. Surface-Accessible Detection Units in Self-Immolative Polymers Enable Translation of Selective Molecular Detection Events into Amplified Responses in Macroscopic, Solid-State Plastics. *J. Am. Chem. Soc.* **2015**, *137*, 5324–5327.
- (42) Fan, B.; Trant, J. F.; Yardley, R. E.; Pickering, A. J.; Lagugné-Labarthet, F.; Gillies, E. R. Photocontrolled Degradation of Stimuli-Responsive Poly(ethyl glyoxylate): Differentiating Features and Traceless Ambient Depolymerization. *Macromolecules* **2016**, *49*, 7196–7203.
- (43) McBride, R. A.; Gillies, E. R. Kinetics of Self-Immolative Degradation in a Linear Polymeric System: Demonstrating the Effect of Chain Length. *Macromolecules* **2013**, *46*, 5157–5166.
- (44) McMahan, D. K.; Anderson, P. A.; Nassar, R.; Bunting, J. B.; Saba, Z.; Oakeley, A. E.; Malouf, N. N. C2C12 Cells: Biophysical, Biochemical, and Immunocytochemical Properties. *Am. J. Physiol.* **1994**, *266*, C1795–C1802.

Chapter 5

5 Polyglyoxylamides with a pH-Mediated Solubility and Depolymerization Switch

5.1 Introduction

Self-immolative polymers (SIPs) are a class of degradable polymers that undergo end-to-end depolymerization to small molecules after the cleavage of their backbone or stabilizing end-cap by a stimulus.¹⁻³ Unlike traditional degradable or stimuli-responsive polymers, only a single bond cleavage is needed to initiate complete SIP degradation. This property makes SIPs attractive for applications such as sensing,⁴⁻⁵ patterning,⁶⁻¹⁰ degradable/recyclable plastics,¹¹⁻¹⁴ and drug delivery,¹⁵⁻²⁹ where an amplified or highly sensitive response to stimuli is desired. Several SIP backbones have been developed, including poly(benzyl carbamates),³⁰⁻³¹ poly(benzyl ethers),³² poly(acetals),³³⁻³⁵ poly(olefin sulfones),³⁶⁻³⁷ and more recently poly(benzyl esters),³⁸ polythioesters,³⁹⁻⁴⁰ polycarboxypyrroles,⁴¹ polycyclopentenes,⁴² and polydisulfides.⁴³ By introducing different end-caps, many of these backbones can be readily tuned to respond to different stimuli.

Polyglyoxylate (PG) SIPs have been of particular interest to our group.^{24, 35, 44-45} The monomer ethyl glyoxylate can be readily obtained from commercial sources for the preparation of poly(ethyl glyoxylate) (PEtG) through proton transfer-mediated^{35, 46} or anionic polymerization.⁴⁷ PEtG has been synthesized to incorporate different end-caps that are responsive to light,³⁵ heat,²² thiols,⁴⁴ and hydrogen peroxide.⁴⁴ Furthermore, the pendent ethyl ester groups on PEtG can be replaced with other alcohols to give other PGs⁴⁵ or with amines to give polyglyoxylamides (PGAMs), allowing their properties to be readily tuned.⁴⁸⁻⁵⁰ However, the development of PGs that depolymerize rapidly and selectively in response to mildly acidic aqueous conditions (e.g., pH 5–6) has been a significant ongoing challenge. This challenge arises partly from the fact that pH-responsive end-caps such as trityl (Trit) and 4-monomethoxytrityl (MMT) exhibit only modest dependence on pH between pH 5 and pH 7.4. In addition, hemiacetal fragmentation, the key step in the

backbone depolymerization mechanism exhibits a rate minimum at pH 5,^{9, 21} thereby partially offsetting the enhanced rate of end-cap cleavage at mildly acidic pH. Therefore, we have not achieved rapidly-triggered depolymerization of PGs at mildly acidic pH compared to pH 7.4. In fact, due to the above-mentioned challenge with polyaldehydes in general, and the fact that commonly investigated polycarbamate SIPs also often undergo slower depolymerization at mildly acidic pH due to amine protonation, to the best of our knowledge, there have been no reported examples of SIPs that on their own can be triggered to depolymerize selectively in mildly acidic aqueous conditions (i.e., pH 5–6) over a reasonable time period (i.e., a few days or less). Such polymers are of significant interest for applications such as drug delivery, agriculture, or recycling.

In previous work, we and others have observed that SIPs depolymerize much more rapidly in their solubilized state compared to when they are aggregated or insoluble.^{9, 50-52} This behaviour is attributed to the increased accessibility of the end-cap for cleavage by the stimulus when the polymer is soluble. Therefore, we postulated that a pH-mediated solubility switch could potentially be established to enable the selective triggering of PGAm at mildly acidic pH. Such and coworkers as well as other groups have shown that the solubility and aggregation behaviour of poly(2-dialkylaminoethyl methacrylate)s can be tuned by adjusting the alkyl groups on pendent amines.⁵³⁻⁵⁷ Our groups recently combined these poly(2-dialkylaminoethyl methacrylate)s with a PGAm to induce particle disassembly and facilitate depolymerization of the PGAm.⁵⁸ We describe here the synthesis and study of alkoxytrityl end-capped PGAm with different pendent amino groups that enable selective solubilization at mildly acidic pH. This solubilization enables end-cap cleavage and depolymerization. We show that only when solubility switching occurs can a significant difference in the depolymerization behaviour between pH levels be achieved (Figure 5.1a). We also demonstrate the use of this approach to achieve pH-mediated disassembly and depolymerization of poly(ethylene glycol) (PEG)-PGAm block copolymer vesicles at mildly acidic pH (Figure 5.1b).

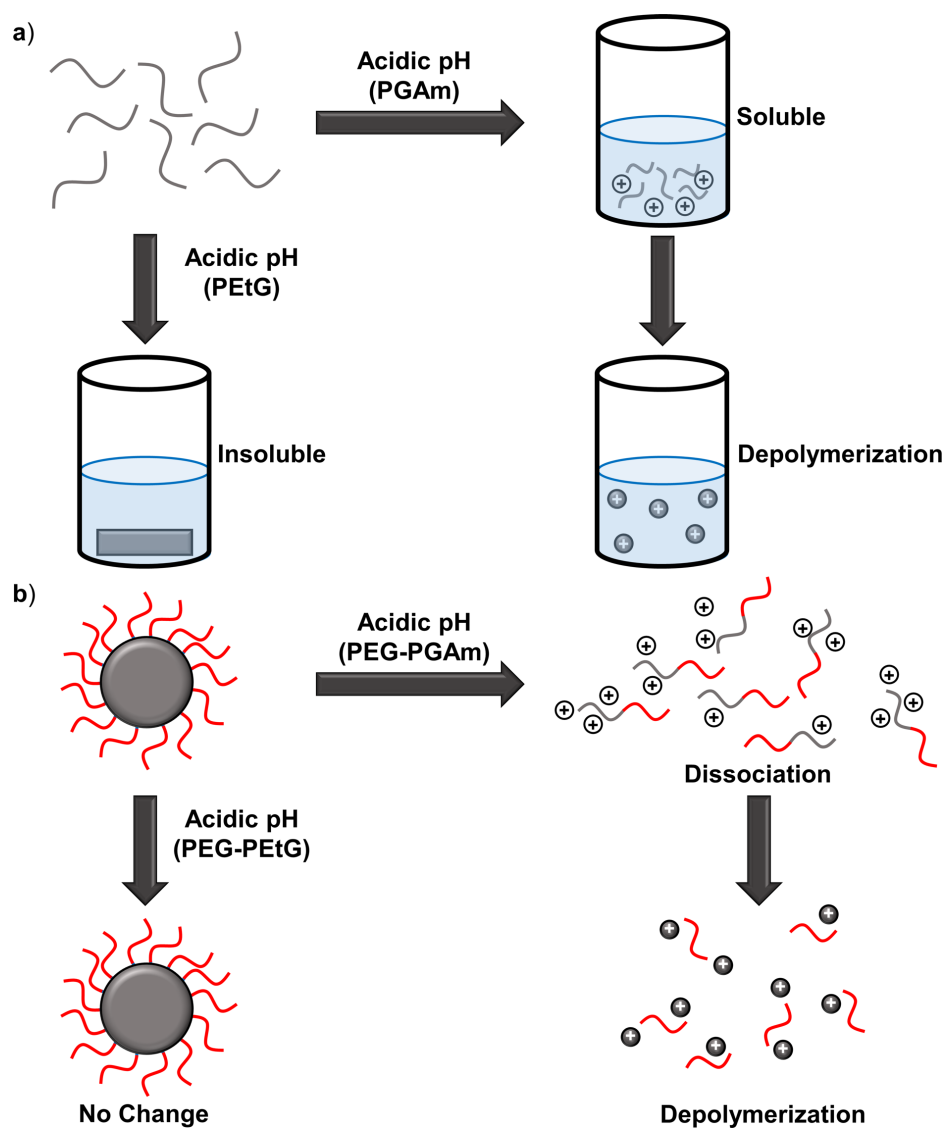
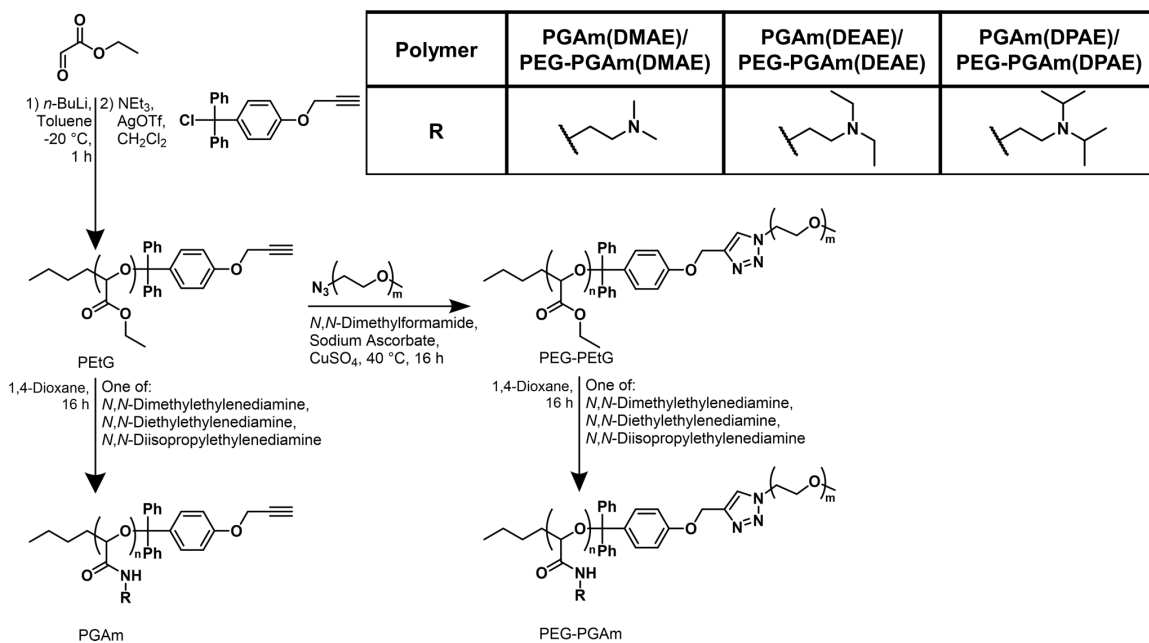


Figure 5.1. a) Schematic illustrating how pH-mediated dissolution of a PGAm enables its end-cap cleavage and depolymerization, whereas a PEtG with the same end-cap remains insoluble and does not depolymerize. b) Application of the pH-mediated solubility switch enables the disassembly and depolymerization of PEG-PGAm nanoassemblies, while analogous PEG-PEtG assemblies remain intact

5.2 Results and Discussion

5.2.1 Polymer Synthesis

PEtG was synthesized via *n*-butyl lithium initiated polymerization of purified ethyl glyoxylate (Scheme 5.1).⁴⁷ The PEtG was end-capped with 4-propargyloxytrityl chloride,⁵ as the alkyne moiety would allow for later conjugation of PEG to produce block copolymers. A number average molar mass (M_n) of 22 kg/mol was targeted as this chain length allows for well-controlled polymerization and easy isolation of the resulting polymer by precipitation in cold methanol. The resulting polymer (**PEtG-1**) was characterized by ¹H NMR, ¹³C NMR, and FT-IR spectroscopic methods, confirming its identity as well as the presence of the alkyne moiety at the terminus (Figure 5.2, Figure A4.1, Figure A4.10). Size exclusion chromatography (SEC) in *N,N*-dimethylformamide (DMF) revealed that the polymer had a number average molar mass (M_n) of 17.8 kg/mol and a dispersity (D) of 1.7 relative to poly(methyl methacrylate) (PMMA) standards (Table 5.1). The M_n reported by SEC is a bit lower than the targeted molecular weight, but end group analysis of the ¹H NMR spectrum indicated an M_n of 20.2 kg/mol, very close to the targeted value.



Scheme 5.1. Synthesis of pH-responsive PGAm homopolymers and PEG-PGAm copolymers from PEtG.

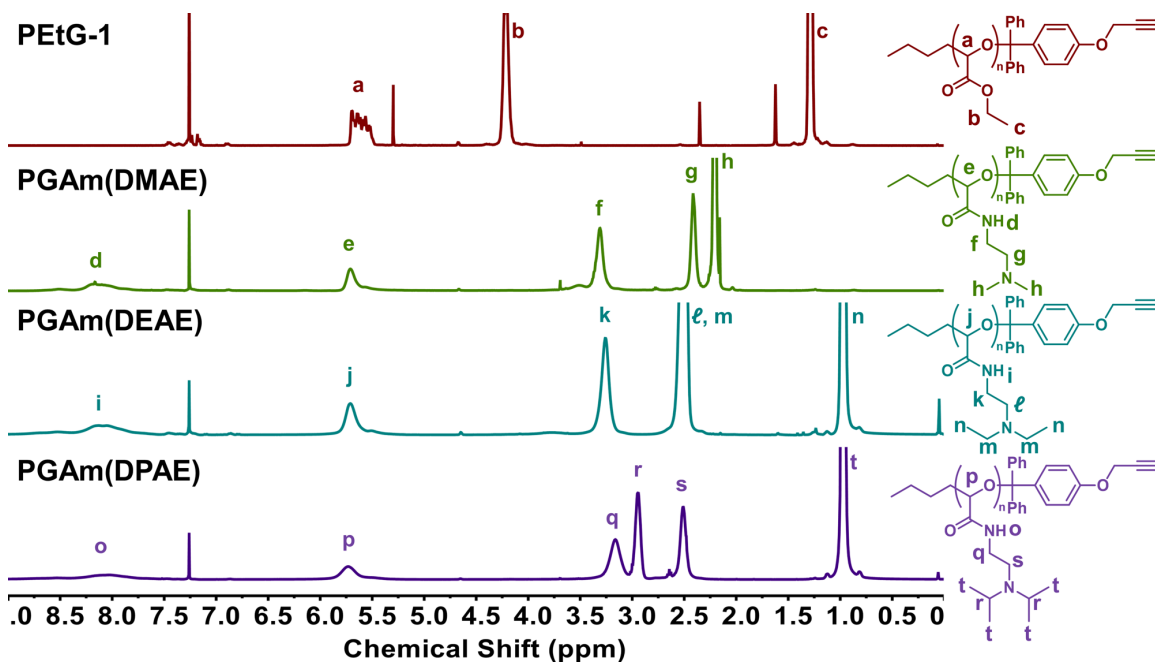


Figure 5.2. Overlay of ¹H NMR spectra of PEtG-1 and the PGAm homopolymers derived from it (CDCl₃, 400 MHz).

Table 5.1. ^1H NMR spectroscopy and SEC characterization of the polymers.

Polymer	^1H NMR		SEC		
	DP_n^b	M_n (kg/mol)	M_n (kg/mol)	M_w (kg/mol)	\mathcal{D}
PEtG-1	198	20.2	17.8	28.6	1.7
PGAm(DMAE)	206	29.7	30.5	37.5	1.6
PGAm(DEAE)	177	30.5	11.3	23.2	2.1
PGAm(DPAE)^a	203	40.7	--	--	--
PEtG-2	100	10.2	10.9	16.8	1.5
PEG-PEtG	103	12.5	14.4	19.8	1.4
PEG-PGAm(DMAE)	100	16.4	20.6	29.1	1.4
PEG-PGAm(DEAE)	104	19.9	18.7	25.0	1.3
PEG-PGAm(DPAE)	104	22.8	16.2	21.1	1.3

^aDid not dissolve sufficiently in DMF and thus could not be run on the SEC column.

^b DP_n of the entire polymer for homopolymers or of the PEtG/PGAm block for block copolymers.

Next, **PEtG-1** was converted to different PGAmS. To obtain pH-responsive PGAmS, three different diamines were chosen that would produce PGAmS with amino pendent groups of variable hydrophobicity and thus different solubilities. Specifically, *N,N*-dimethylethylenediamine was used to produce the relatively hydrophilic **PGAm(DMAE)**, which has good solubility in water even at neutral pH. To obtain PGAmS with lower solubility at neutral pH, the more hydrophobic *N,N*-diethylethylenediamine and *N,N*-diisopropylethylenediamine were investigated to yield **PGAm(DEAE)** and **PGAm(DPAE)** respectively. ^1H NMR, ^{13}C NMR, and FT-IR spectroscopy were used to characterize the new polymers (Figure 5.2, Figure A4.2–Figure A4.4, Figure A4.11–Figure A4.13). SEC results showed a decrease in retention time between the original **PEtG-1** and **PGAm(DMAE)** as expected due to the latter's increased molar mass (Table 5.1, Figure A4.20). **PGAm(DEAE)** produced a broad SEC peak corresponding to an M_n of only 11.3 kg/mol and a \mathcal{D} of 2.1. This result was likely caused by the poor solubility of the polymer in DMF, which resulted in the removal of the higher molar mass chains through filtration prior to analysis. **PGAm(DPAE)** was too insoluble in DMF to be analyzed. Attempts at analyzing these polymers by SEC in tetrahydrofuran (THF) or acidic aqueous buffer were

also unsuccessful due to column adsorption. However, end group analysis by ^1H NMR spectroscopy confirmed DP_n values for the PGAMs that were very similar to those of the PEtG precursor, indicating post-polymerization amidation did not cause any substantial depolymerization (Table 5.1).

5.2.2 Homopolymer Depolymerization

Depolymerization of the homopolymers at different pH levels was investigated to evaluate the effects of the pendent groups on the depolymerization behaviours. **PGAm(DMAE)**, **PGAm(DEAE)**, **PGAm(DPAE)**, and the **PEtG-1** precursor were each placed into NMR tubes as solids and then deuterated buffer solutions at either pH 5.0, 6.0, or 7.4 were added. For polymers that didn't fully dissolve (**PGAm(DEAE)** and **PGAm(DPAE)** at pH 6.0 and 7.4, **PEtG-1** under all conditions), *N,N*-dimethylacetamide (DMA) was added as an internal standard against which to quantify the extent of depolymerization. The tubes were sealed and probed via ^1H NMR spectroscopy over the course of a week (Figure 5.3a, Figure A4.24–Figure A4.35).

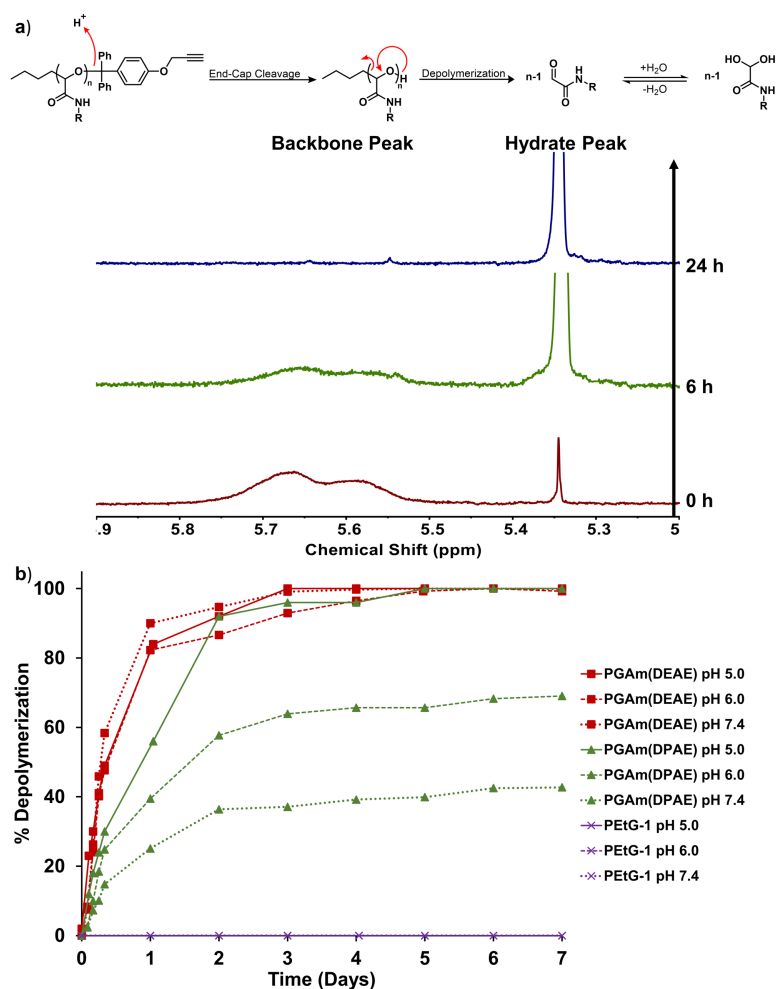


Figure 5.3. a) **PGAm(DMAE)** in deuterated citrate buffer (0.2 M; pH 5.0) monitored by ^1H NMR spectroscopy (400 Hz) over time as a representative example of triggered depolymerization. As depolymerization occurs, the broad backbone methine proton peak decreases and a sharp singlet peak of the monomer hydrate methine peak increases. The overall mechanism is shown above the spectra. b) Depolymerization over time for most of the homopolymers at different pH levels, as measured by ^1H NMR spectroscopy. Depolymerization data for **PGAm(DMAE)** can be found in Appendix 4. Deuterated phosphate buffer (0.2 M; pH 7.4) or deuterated citrate buffer (0.2 M; pH 5.0, 6.0) was used as the solvent.

The depolymerization behaviours of the homopolymers were found to depend on both the pendent groups and the pH. **PGAm(DMAE)** underwent complete depolymerization in a day at pH 5.0, and over two days at pH 6.0 and 7.4, showing that in the absence of a

solubility switch, the depolymerization behaviour was not very dependent on pH (Figure A4.22). **PGAm(DEAE)** depolymerization was slightly slower due to this polymer's increased hydrophobicity, requiring 3 days for full depolymerization at pH 5.0 (Figure 5.3). Despite **PGAm(DEAE)** being somewhat insoluble at pH 6.0 and 7.4, this polymer did not exhibit greatly reduced depolymerization at these pH levels and the insoluble polymer in the NMR tubes dissolved as depolymerization proceeded. In contrast, **PGAm(DPAE)** underwent > 90% depolymerization over two days at pH 5.0, where the polymer was fully soluble, and progressively slower depolymerization as the pH increased to 6.0 and 7.4. **PEtG-1**, which was completely insoluble at all pH levels tested and does not contain a pH-mediated solubility switch, underwent no significant depolymerization under any of the tested conditions. These results demonstrate that pH-dependent solubilization can be used to achieve pH-dependent depolymerization of the PGAm between pH 7.4 and pH 5.0.

5.2.3 Block Copolymer Synthesis

Next, PEG-PGAm block copolymers were prepared with the aim of creating pH-responsive nanoassemblies. Initially, **PEtG-1** was used to synthesize a PEG-PEtG block copolymer via copper-assisted azide-alkyne cycloaddition (CuAAC) click chemistry with an azide-modified PEG methyl ether (**mPEG-N₃**; $M_n = 2$ kg/mol), followed by the conversion of this copolymer to the PEG-PGAm block copolymers using the same three amines used for the PGAm homopolymers. However, preliminary work with the copolymers revealed poor self-assembly behaviour with extensive aggregation. Thus, we synthesized a shorter PEtG molecule (**PEtG-2**), reasoning that a shorter hydrophobic block would result in less aggregation. **PEtG-2** was synthesized as described above (Scheme 5.1) with a target average molar mass of 10 kg/mol and characterized by ¹H NMR, ¹³C NMR, and FT-IR spectroscopic methods (Figure A4.5, Figure A4.14, Figure A4.19). SEC results revealed a M_n of 10.9 kg/mol and a D of 1.5. This polymer was then reacted with **mPEG-N₃** using CuAAC to produce **PEG-PEtG** and the product was characterized by ¹H NMR, ¹³C NMR, and FT-IR spectroscopic methods (Figure A4.6, Figure A4.15, Figure A4.19). Success of the coupling and polymer purity was confirmed by comparing the integration values of the backbone methine proton peaks of **PEtG-2** and **PEG-PEtG** at ~5.6 ppm after using the PEG resonance peak at ~3.6 ppm as a reference peak in the latter (Figure 5.4a). Since the

backbone peak integration values in both spectra were similar, the results indicated that the PEG was bound in a 1:1 ratio with the PEtG in the block copolymer. Furthermore, SEC results showed that negligible free **mPEG-N₃** was present in the final product, indicating that the PEG block was covalently conjugated (Figure 5.4b), and no azide peak was present when examined by FT-IR spectroscopy (Figure A4.19), again indicating a lack of free **mPEG-N₃**.

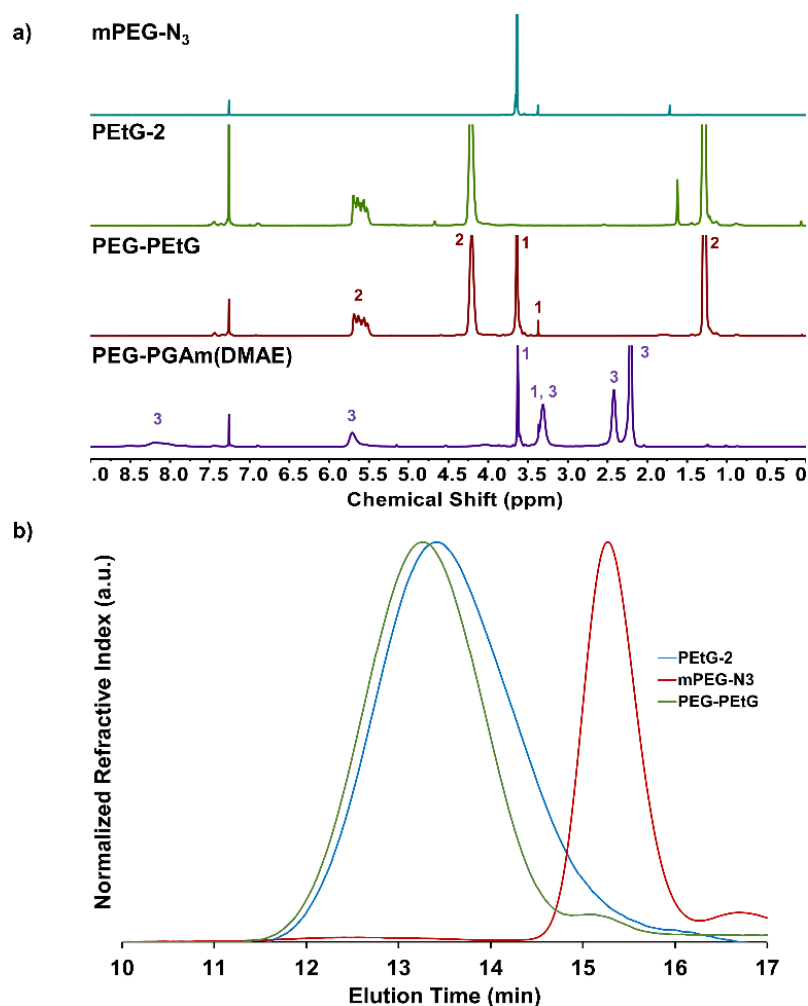


Figure 5.4. a) Overlay of the ¹H NMR spectra of **PEG-PEtG** as well as its constituent blocks, **PEtG-2** and **mPEG-N₃**, and one of its derivatives, **PEG-PEtG(DMAE)** (CDCl₃, 400 MHz). For the block copolymers, 1 = peaks from the **mPEG-N₃** block, 2 = peaks from the **PEtG-2** block, and 3 = peaks from the **PGAm(DMAE)** block. b) Overlay of chromatograms of the copolymer **PEG-PEtG** as well as its constituent blocks, **PEtG-2** and **mPEG-N₃**.

PEG-PEtG was then amidated to yield the block copolymers **PEG-PGAm(DMAE)**, **PEG-PGAm(DEAE)**, and **PEG-PGAm(DPAE)**. ^1H NMR, ^{13}C NMR, and FT-IR spectroscopy were used to confirm the identity and purity of the compounds (Figure A4.7–Figure A4.9, Figure A4.16–Figure A4.18). SEC analyses of all the block copolymers resulted in similar retention times (Figure A4.21). While the M_n values of **PEG-PEtG** and **PEG-PGAm(DMAE)** were near what was expected, the M_n values of **PEG-PGAm(DEAE)** and **PEG-PGAm(DPAE)** were lower than expected (Table 5.1). Although these copolymers dissolved better in DMF than their homopolymer analogues, they may have still had a reduced hydrodynamic volume due to the collapsed state of the partially insoluble PGAm blocks, yielding longer elution times and lower than expected molar masses. Nevertheless, ^1H NMR spectroscopic analysis shows that the DP_n of all of the PEG-PGAm block copolymers was similar to that of **PEG-PEtG**, indicating that no substantial depolymerization occurred during the amidation reactions (Table 5.1).

5.2.4 Copolymer Self-Assembly and pH-Responsiveness

Self-assembly of the block copolymers was investigated next. By dissolving the block copolymers in THF and precipitating them into rapidly stirring phosphate buffer (0.2 M, pH 8.0), assemblies for **PEG-PGAm(DPAE)** and **PEG-PEtG** could be obtained. The other copolymers were too hydrophilic at this pH and did not self-assemble. After evaporating the organic solvent, the assemblies were evaluated using dynamic light scattering (DLS). **PEG-PGAm(DPAE)** assemblies had a Z-average diameter of 72 ± 1 nm while **PEG-PEtG** assemblies had a Z-average diameter of 70 ± 1 nm. Both assemblies had polydispersity indices of ~ 0.2 . Transmission electron microscopy (TEM) images revealed that both **PEG-PGAm(DPAE)** and **PEG-PEtG** adopted vesicle morphologies (Figure 5.5). The sizes of the vesicles were in reasonable agreement with the DLS results.

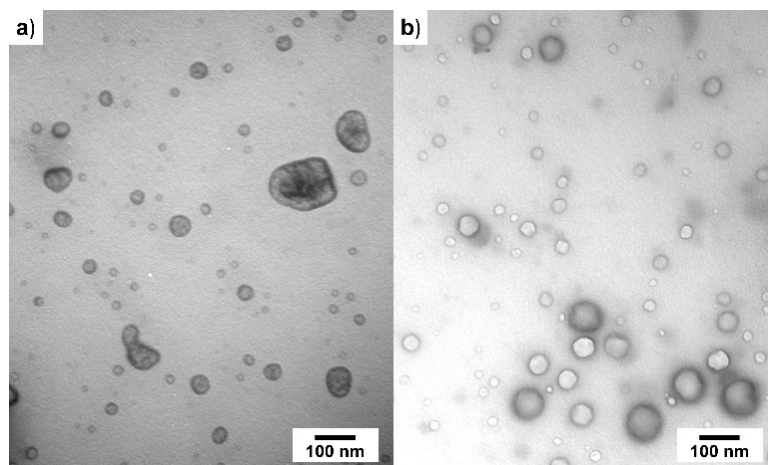


Figure 5.5. TEM images of a) **PEG-PGAm(DPAE)** and b) **PEG-PEtG** after nanoprecipitation and self-assembly at pH 8. Both copolymers assembled into nanoparticles with vesicle morphologies.

Next, the copolymers were investigated for pH-responsive assembly/disassembly using DLS. **PEG-PGAm(DPAE)** and **PEG-PEtG** were self-assembled via precipitation in phosphate buffer (0.2 M, pH 8.0) as described previously. After preparation, count rate and Z-average diameter of each sample was monitored as the pH was lowered step-wise by the addition of acid (Figure 5.6a, b). As expected, **PEG-PGAm(DPAE)** exhibited a substantial drop in count rate as the pH was reduced, falling to ~10% of the initial value at pH 7 and even lower at pH 6. This drop reflects the dissociation of the majority of the nanoassemblies due to the protonation of their cores and subsequent solubilization. Nevertheless, it was still possible to measure diameter distributions at the lower pH values. An increase in Z average diameter, visible also in the volume distribution (Figure 5.6c) was initially observed as the pH was reduced to 7, which may be due to swelling of the remaining nanoassemblies due to repulsion of the positively-charged PGAm blocks. Based on the volume distribution, a further reduction in pH to 6 resulted in primarily species of about 10 nm in diameter (Figure 5.6c), although larger assemblies were observed in the intensity distribution, which influenced the Z-average diameter (Figure A4.48). In contrast, **PEG-PEtG** nanoassemblies did not undergo any substantial change in either count rate or Z-average diameter as the pH was lowered due to their lack of pH-responsiveness (Figure 5.6a,b, Figure A4.49, Figure A4.50). Conducting these experiments at 37 °C gave similar

results to the studies conducted at room temperature, although **PEG-PGAm(DPAE)** nanoassemblies did not exhibit as great of an increase in Z average diameter.

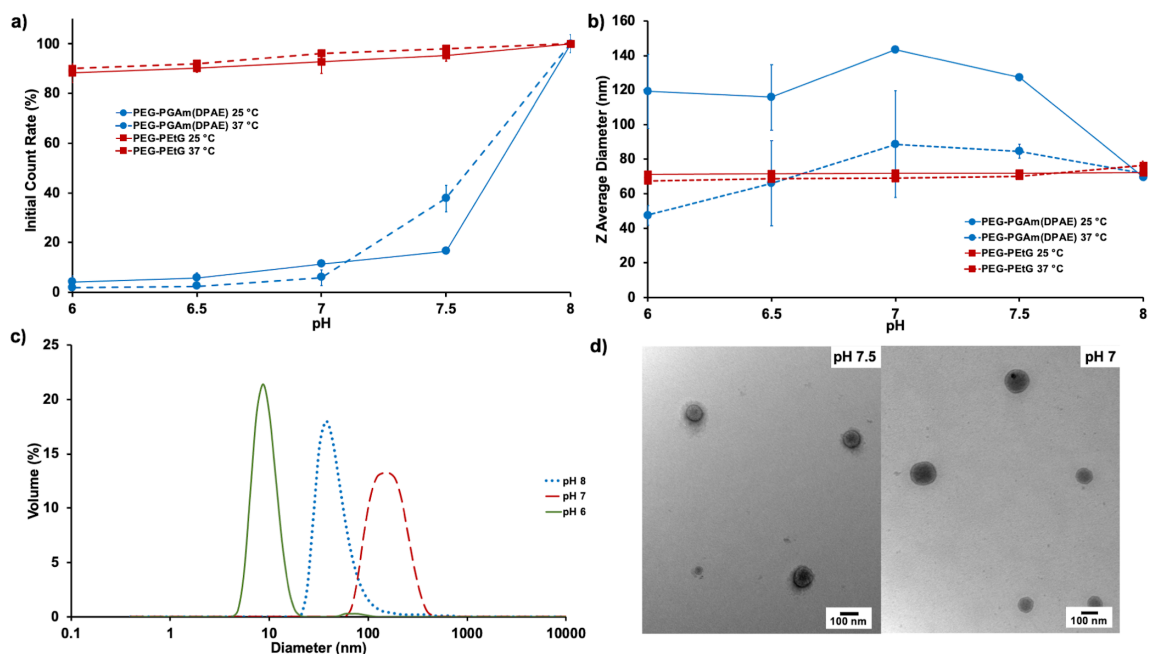


Figure 5.6. a) Percent initial count rates and b) Z average diameters of copolymer nanoassemblies at different pH levels. Error bars represent the standard deviation between three replicate samples. c) Volume distribution from DLS and d) TEM images of **PEG-PGAm(DPAE)** nanoassemblies at pH 7.5 and 7.0 (at 25 °C).

To further understand the behaviour of the pH-responsive nanoassemblies, we also examined TEM images of the **PEG-PGAm(DPAE)** assemblies deposited on the grids at different pH levels. Vesicle morphologies were observed at both pH 8 (Figure 5.5a) and at pH 7.5 (Figure 5.6d). However, at pH 7 the assemblies transitioned from vesicles to nanoparticles with solid cores (i.e., compound micelles). This transition can presumably be attributed to destabilization of the vesicle membrane due to charge repulsion upon protonation of the pendent amines of the **PGAm(DPAE)** block.

5.2.5 Copolymer Depolymerization in the Nanoassemblies

Finally, the block copolymers and their nanoassemblies were studied by ^1H NMR spectroscopy to understand their depolymerization behaviour at different pH levels. Each copolymer was dissolved in deuterated THF and injected into rapidly stirring D_2O containing DMA as an internal standard. After 30 min, the suspensions were adjusted to pH 5.0, 6.0, 7.4, or 8.0 using buffers and sealed in NMR tubes. Spectra were then obtained at various time points over a week (Figure A4.36–Figure A4.47).

In general, the depolymerization of **PEG-PGAm(DMAE)** and **PEG-PGAm(DEAE)** proceeded similar to their corresponding homopolymers, with over 90% depolymerization observed after 3 days, regardless of the pH (Figure 5.7, Figure A4.23). These results align well with the DLS studies of these copolymers, which revealed that the copolymers were fully soluble and not self-assembled at pH 5–7.4. Conversely, **PEG-PEtG** exhibited no detectable depolymerization over the week at any pH due to the hydrophobicity and insolubility of the PEtG, regardless of pH. **PEG-PGAm(DPAE)**, on the other hand, exhibited pH-dependent depolymerization behaviour. At pH 5–6, about 80% depolymerization occurred over 7 days, whereas at pH 7.4 only about 40% depolymerization occurred over the same time period. The more rapid depolymerization at pH 5–6 can be rationalized by the fact that the PGAm blocks are soluble at these pH levels, so the copolymers are not self-assembled, and the trityl end-cap is readily accessible to water for cleavage. At pH 7.4, **PEG-PGAm(DPAE)** was self-assembled, but the PGAm block was evidently partially accessible to water, allowing the trityl end-cap to be gradually cleaved and for the system to gradually dissolve as depolymerization proceeded. In contrast, at pH 8.0, no significant depolymerization was observed, reflecting lack of access of water to the PGAm block in the copolymer's self-assembled state. Thus, although all polymers had the same backbone and end-cap, pH-dependent depolymerization behaviour was only achieved using the **PEG-PGAm(DPAE)**, which exhibits pH-dependent solubility between pH 5 and 8.

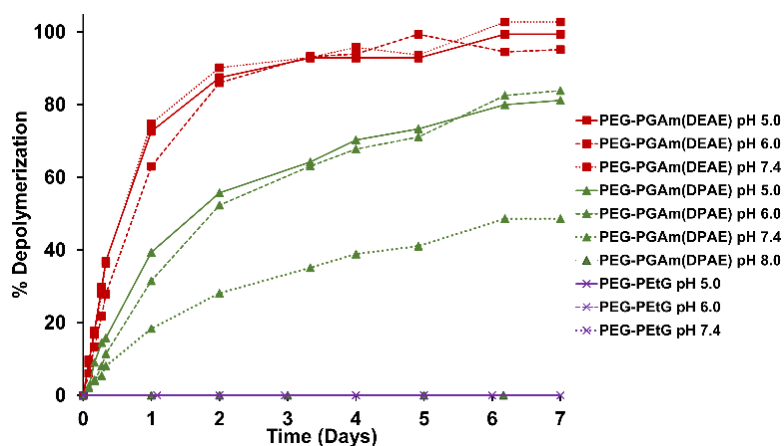


Figure 5.7. Depolymerization over time for most of the copolymers at different pH levels, as measured by ^1H NMR spectroscopy. Depolymerization data for **PEG-PGAm(DMAE)** can be found in Appendix 4. Deuterated phosphate buffer (0.2 M; pH 7.4, 8.0) or deuterated citrate buffer (0.2 M; pH 5.0, 6.0) was used as the solvent.

5.3 Conclusions

SIPs capable of depolymerizing in response to mildly acidic stimuli were successfully developed using PGAMs with ionizable pendent amines. While the presence of an acid-responsive trityl end-cap was not sufficient to provide pH-dependent depolymerization in the range of pH 5–8 using either fully soluble **PGAm(DMAE)** or fully insoluble **PEtG**, by tuning the hydrophobicity of the pendent amines, it was possible to achieve pH-dependent depolymerization using a solubility switch with **PGAm(DPAE)**. These PGAMs were easily prepared from a PEtG precursor, and it was also possible to incorporate them into block copolymers with PEG, thereby providing pH-dependent amphiphilic block copolymer SIPs. **PEG-PGAm(DPAE)** block copolymers self-assembled into vesicles at pH 8, and then underwent a transition to solid core nanoparticles as the pH was reduced, while simultaneously undergoing increasingly rapid depolymerization as the pH was reduced from 8 to 5. In contrast, PEG copolymers incorporating more hydrophilic **PGAm(DMAE)** or **PGAm(DEAE)** blocks did not self-assemble over this pH range and underwent rapid depolymerization regardless of pH. **PEG-PEtG** nanoassemblies did not depolymerize at any detectable level over this pH range. Overall, this new approach using SIPs in combination with a solubility switch opens up potential new avenues for the

encapsulation and controlled release of species under mild conditions such as those encountered *in vivo* or in the environment. Furthermore, we envision that the pH where depolymerization is “turned on” can be further tuned for different applications based on the structure of the pendent amines and through the use of varying ratios of different pendent groups.

5.4 Experimental

5.4.1 General Experimental Details

General Materials. mPEG-N₃ was synthesized as previously reported.⁵⁹ 4-Propargyloxytrityl chloride was prepared as previously reported.⁵ Ethyl glyoxylate in toluene solution (50% w/w), *N,N*-dimethylethylenediamine, *N,N*-diisopropylethylenediamine, AgOTf, CuSO₄, and citric acid were obtained from Alfa Aesar. *n*-Butyl lithium in hexanes solution (2.5 M), Methoxy poly(ethylene glycol)₂₀₀₀, sodium L-ascorbate, *N,N*-diethylethylenediamine, and HCl were obtained from Sigma Aldrich. *N,N*-Dimethylacetamide (DMA) was obtained from TCI. NEt₃ and KH₂PO₄ were obtained from Millipore. NaOH and KOH were obtained from Thermo Fisher Scientific. K₂HPO₄ was obtained from Caledon Laboratories. Spectra/Por 6 regenerated cellulose (RC) dialysis membrane was obtained from Spectrum Laboratories. 400 mesh Formvar-coated nickel grids were obtained from Electron Microscopy Sciences. Ethyl glyoxylate was purified over P₂O₅ as previously reported.⁴⁷ Toluene was distilled over sodium/benzophenone under a nitrogen atmosphere before use. NEt₃ and CH₂Cl₂ were distilled over CaH₂ under a nitrogen atmosphere before use. Purified water was obtained from a Barnstead EASYpure II system. All other chemicals were of reagent grade and were used without further purification.

General Methods. ¹H and ¹³C NMR spectra were obtained using one of the following instruments: 400 MHz Bruker AvIII HD, 400 MHz Varian INOVA, or 600 MHz Varian INOVA. ¹H NMR chemical shifts were calibrated against the residual solvent signal of CHCl₃ (7.26 ppm) or HOD (4.79 ppm) while ¹³C NMR chemical shifts were calibrated against the solvent signal of CDCl₃ (77.16 ppm). FT-IR spectra were obtained using a

PerkinElmer FT-IR Spectrum Two instrument with attenuated total reflectance (ATR) sampling. Size-exclusion chromatograms were obtained using a DMF chromatograph equipped with a Waters 515 HPLC pump with a Waters In-Line Degasser AF, two PLgel mixed D 5 μm (300×1.5 mm) columns connected to a corresponding PLgel guard column, and a Wyatt Optilab Rex RI detector. Samples were dissolved in DMF containing 10 mM LiBr and 1% v/v NEt_3 at a concentration of ~ 5 mg/mL. Each sample was filtered through a 0.2 μm polytetrafluoroethylene syringe filter prior to injection using a 50 μL loop. Samples were run at a flow rate of 1 mL/min for 30 min at 85 $^\circ\text{C}$. Molar masses of the samples were calculated relative to PMMA standards. DLS measurements were performed using a Malvern Zetasizer Nano S instrument equipped with a 633 nm laser at a scattering angle of 173 $^\circ$. TEM images were obtained using a Phillips Electron Optics CM10 transmission electron microscope operating at 80 kV.

5.4.2 Synthesis of Homopolymers

*All PEtG homopolymers were synthesized by the same procedure described for the synthesis of **PEtG-1** (representative PEtG synthesis). All PGAm homopolymers were synthesized by the same procedure described for the synthesis of **PGAm(DMAE)** (representative PGAm synthesis).*

Synthesis of PEtG-1 (representative PEtG synthesis). AgOTf (0.44 g, 1.7 mmol, 2.8 equiv) and 4-propargyloxytrityl chloride (0.57 g, 1.7, 2.8 equiv) were added to a flask, which was subsequently evacuated and purged with nitrogen. A 10 mL aliquot of dry CH_2Cl_2 was then added and the flask was stirred at room temperature for 1 h to yield the end-capping mixture. Separately, 60 mL of dry toluene were added to a flame-dried Schlenk flask under a nitrogen atmosphere along with *n*-butyl lithium (0.24 mL, 0.60 mmol, 1.0 equiv) Purified ethyl glyoxylate (13 mL, 130 mmol, 220 equiv) was subsequently added to the flask and the system was stirred and cooled at -20 $^\circ\text{C}$. After 30 min, dry NEt_3 (0.50 mL, 3.6 mmol, 6.0 equiv) was added to the polymerization flask and the mixture was allowed to stir for another 30 min. The end-capping mixture was then cooled to -20 $^\circ\text{C}$ before being transferred with a wide mouth pipette to the polymerization flask. The polymerization flask was stoppered and stirred at -20 $^\circ\text{C}$ for 4.5 h before being

allowed to warm up to room temperature over 16 h. Concentration of the crude polymerization mixture under vacuum followed by filtration and precipitation in 550 mL of MeOH:H₂O (10:1) afforded 8.1 g of pure polymer residue as a clear pale orange tacky solid. Yield = 60%. ¹H NMR (CDCl₃, 400 MHz): δ 7.32–7.50 (m, 10H), 7.12–7.32 (m, 45H), 6.85–6.93 (m, 3H), 5.46–5.74 (m, 198H), 4.67 (br s, 3H), 4.21 (br s, 413H), 2.54 (br s, 2H), 1.29 (br s, 617H), 0.88 (br s, 3H). ¹³C{¹H} NMR (CDCl₃, 100 MHz): δ 165.1–166.5, 127.2–129.3, 90.7–94.3, 62.2, 14.0. FT-IR (ATR): 2990, 1750 cm⁻¹. SEC (DMF, PMMA): M_n = 16 kg/mol, M_w = 29 kg/mol, D = 1.7.

Synthesis of PEtG-2. Purified ethyl glyoxylate (15 mL, 150 mmol, 100 equiv), *n*-butyl lithium (0.61 mL, 1.5 mmol, 1.0 equiv), NEt₃ (0.84 mL, 6.0 mmol, 4.0 equiv), AgOTf (0.85 g, 3.3 mmol, 2.2 equiv), 4-propargyloxytrityl chloride (1.1 g, 3.3 mmol, 2.2 equiv). After addition of the end-cap mixture, the reaction was stirred for 4 h before being allowed to warm up over 16 h. Purification was achieved by concentration of the reaction mixture followed by filtration and precipitation into 750 mL of MeOH:H₂O (4:1). The resulting precipitate was dissolved in CH₂Cl₂ and mixed with activated carbon before being further filtered through Celite to afford 5.9 g of a yellow-orange tacky solid. Yield = 38%. ¹H NMR (CDCl₃, 400 MHz): δ 7.33–7.49 (m, 8H), 7.17–7.33 (m, 21H), 6.86–6.93 (m, 2H), 5.40–5.82 (m, 100H), 4.67 (br s, 2H), 4.22 (br s, 197H), 2.55 (br s, 1H), 1.29 (br s, 296H), 0.88 (br s, 3H). ¹³C{¹H} NMR (CDCl₃, 100 MHz): δ 165.2–166.5, 18.7, 128.0, 127.5, 90.6–94.4, 62.2, 14.0. FT-IR (ATR): 2960, 1750 cm⁻¹. SEC (DMF, PMMA): M_n = 11 kg/mol, M_w = 17 kg/mol, D = 1.5.

Synthesis of PGAm(DMAE) (representative PGAm synthesis). PEtG-1 (0.30 g of polymer, 2.9 mmol of ester, 1.0 equiv) was dissolved in 6.0 mL of 1,4-dioxane in a vial. *N,N*-Dimethylethylenediamine (0.96 mL, 8.8 mmol, 3.0 equiv) was added to the solution and the vial was sealed and stirred for 17.5 h at room temperature. The crude mixture was concentrated and precipitated in 50 mL of *n*-pentane to afford 0.38 g of a clear, colourless, brittle solid. Yield = 90%. ¹H NMR (CDCl₃, 400 MHz): δ 7.71–8.83 (m, 171H), 7.31–7.52 (m, 4H), 7.17–7.31 (m, 28H), 6.88 (br s, 2H), 5.71 (br s, 206H), 4.67 (br s, 2H), 3.31 (br s, 449H), 2.42 (br s, 462H), 2.21 (br s, 1354H). ¹³C{¹H} NMR (CDCl₃, 100 MHz): δ 167.2,

94.4–98.6, 58.1, 45.6, 37.6. FT-IR (ATR): 3270, 3080, 2940, 2860, 2820, 2770, 1670, 1540 cm^{-1} . SEC (DMF, PMMA): $M_n = 23$ kg/mol, $M_w = 38$ kg/mol, $D = 1.7$.

Synthesis of PGAm(DEAE). *N,N*-Diethylethylenediamine (1.2 mL, 8.5 mmol, 2.9 equiv) was used and the crude mixture was dialyzed in a 10 kg/mol molecular weight cut off (MWCO) regenerated cellulose membrane against acetone to afford 0.34 g of a clear, colourless, tacky solid. Yield = 67%. ^1H NMR (CDCl_3 , 400 MHz): δ 7.56–8.90 (m, 178H), 7.30–7.56 (m, 9H), 7.16–7.30 (m, 14H), 6.86 (br s, 3H), 5.71 (br s, 177H), 4.65 (br s, 2H), 3.26 (br s, 350H), 2.50 (br s, 1037H), 0.97 (br s, 1027H). $^{13}\text{C}\{^1\text{H}\}$ NMR (CDCl_3 , 100 MHz): δ 167.1, 99.1, 94.7, 51.6, 47.3, 37.7, 12.1. FT-IR (ATR): 3270, 3080, 2970, 2930, 2880, 2810, 1670, 1540 cm^{-1} . SEC (DMF, PMMA): $M_n = 11$ kg/mol, $M_w = 23$ kg/mol, $D = 2.1$.

Synthesis of PGAm(DPAE). *N,N*-Diisopropylethylenediamine (1.5 mL, 8.6 mmol, 3.0 equiv) was used and the crude mixture was precipitated in 50 mL of MeOH to afford 0.35 g of a clear, colourless, brittle solid. Yield = 59%. ^1H NMR (CDCl_3 , 400 MHz): δ 7.52–9.07 (m, 214H), 7.33–7.52 (m, 8H), 7.15–7.33 (m, 17H), 6.87 (s, 2H), 5.73 (s, 203H), 4.65 (s, 2H), 3.16 (s, 388H), 2.94 (s, 416H), 2.51 (s, 432H), 0.97 (s, 2447H). $^{13}\text{C}\{^1\text{H}\}$ NMR (CDCl_3 , 100 MHz): δ 167.0, 93.9–100.2, 48.8, 44.0, 40.8, 21.0. FT-IR (ATR): 3280, 3080, 2960, 2870, 2820, 1670, 1540 cm^{-1} .

5.4.3 Synthesis of Copolymers

All PGAm copolymers were synthesized by the same procedure described for the synthesis of PEG-PGAm(DMAE) (representative PGAm block copolymer synthesis).

Synthesis of PEG-PEtG. PEtG-2 (1.5 g, 0.15 mmol, 1.0 equiv), mPEG-N₃ (1.2 g, 0.60 mmol, 4.0 equiv), CuSO₄ (0.018 g, 0.11 mmol, 0.73 equiv), and sodium L-ascorbate (0.023 g, 0.12 mmol, 0.80 equiv) were dissolved in 15 mL of glass-distilled DMF. After purging the solution for 1 h by bubbling through nitrogen gas, the reaction mixture was heated to 40 °C and stirred under nitrogen for 20 h. The crude reaction mixture was dialyzed in a 10 kg/mol MWCO regenerated cellulose membrane against water for 16 h until the mixture turned turbid. The mixture was then centrifuged, and the supernatant was discarded. The

pellet that remained was resuspended in 30 mL of water, centrifuged again, and the supernatant was discarded to wash out unreacted **mPEG-N₃**. This wash procedure was repeated three-fold before the pellet was resuspended, flash frozen, and lyophilized to afford 1.3 g of a white spongy solid. Yield = 72%. ¹H NMR (CDCl₃, 400 MHz): δ 7.40–7.48 (m, 4H), 7.18–7.38 (m, 14H), 6.87–6.98 (m, 2H), 5.40–5.76 (m, 103H), 4.60 (br s, 2H), 4.22 (br s, 210H), 3.64 (br s, 178H), 3.37 (s, 3H), 1.28 (br s, 327H), 0.87 (br s, 3H). ¹³C{¹H} NMR (CDCl₃, 100 MHz): δ 164.9–166.7, 90.3–94.3, 70.7, 62.2, 14.0. FT-IR (ATR): 2980, 2940, 2880, 1750 cm⁻¹. SEC (DMF, PMMA): M_n = 14 kg/mol, M_w = 20 kg/mol, D = 1.4.

Synthesis of PEG-PGAm(DMAE) (representative PGAm block copolymer synthesis).

PEG-PEtG (0.35 g, 2.8 mmol of ester, 1.0 equiv) was dissolved in 8.0 mL of 1,4-dioxane. To this mixture, *N,N*-dimethylethylenediamine (0.97 mL, 8.9 mmol, 3.2 equiv) was added and the reaction flask was sealed and stirred for 20 h. The crude mixture was subsequently dialyzed in a 10 kg/mol molecular weight cut off RC membrane against acetone for 16 h to afford 0.31 g of an off-white brittle solid. Yield = 66%. ¹H NMR (CDCl₃, 400 MHz): δ 7.70–8.77 (m, 83H), 7.34–7.50 (m, 4H), 7.19–7.34 (m, 13H), 6.86–6.94 (m, 1H), 5.71 (br s, 100H), 4.53 (br s, 2H), 3.63 (br s, 178H), 3.31 (br s, 210H), 2.42 (br s, 238H), 2.21 (br s, 641H). ¹³C{¹H} NMR (CDCl₃, 100 MHz): δ 167.2, 94.1–98.3, 70.7, 58.1, 45.6, 37.6. FT-IR (ATR): 3280, 3080, 2940, 2860, 2820, 2770, 1670, 1540 cm⁻¹. SEC (DMF, PMMA): M_n = 20.6 kg/mol, M_w = 29.1 kg/mol, D = 1.4.

Synthesis of PEG-PGAm(DEAE). *N,N*-Diethylethylenediamine (1.3 mL, 9.3 mmol, 3.3 equiv) was used to afford 0.31 g of an off-yellow tacky solid. Yield = 56%. ¹H NMR (CDCl₃, 400 MHz): δ 7.78–8.77 (m, 133H), 7.36–7.50 (m, 10H), 7.18–7.36 (m, 56H), 6.86–6.93 (m, 4H), 5.74 (br s, 104H), 4.54 (br s 4H), 3.64 (br s, 178H), 3.29 (br s, 232H), 2.55 (br s, 750H), 1.01 (br s, 712H). ¹³C{¹H} NMR (CDCl₃, 100 MHz): δ 167.1, 94.2–99.5, 70.7, 51.6, 47.3, 37.7, 12.1. FT-IR (ATR): 3280, 3080, 2970, 2930, 2870, 2810, 1670 cm⁻¹. SEC (DMF, PMMA): M_n = 19 kg/mol, M_w = 25 kg/mol, D = 1.3.

Synthesis of PEG-PGAm(DPAE). *N,N*-Diisopropylethylenediamine (1.6 mL, 9.2 mmol, 3.3 equiv) was used and the crude mixture was dialyzed against a 1:1 ethyl acetate:acetone

solution to afford 0.40 g of a yellow brittle solid. Yield = 62%. ^1H NMR (CDCl_3 , 400 MHz): δ 7.72–8.78 (m, 110H), 7.40–7.49 (m, 6H), 7.16–7.40 (m, 24H), 6.89 (br s, 2H), 5.72 (br s, 104H), 4.54 (br s, 2H), 3.64 (br s, 178H), 3.37 (s, 5H), 3.17 (br s, 239H), 2.96 (br s, 251H), 2.52 (br s, 243H), 0.98 (br s, 1530H). $^{13}\text{C}\{^1\text{H}\}$ NMR (CDCl_3 , 100 MHz): δ 166.9, 94.4–100.1, 70.7, 48.9, 44.0, 40.6, 21.0. FT-IR (ATR): 3280, 3080, 2960, 2870, 2820, 1670, 1540 cm^{-1} . SEC (DMF, PMMA): $M_n = 16$ kg/mol, $M_w = 21$ kg/mol, $D = 1.3$.

5.4.4 Depolymerization Studies

Depolymerization of PGAm Homopolymers. Each PGAm homopolymer was measured and placed in an NMR tube, followed by the addition of either deuterated citrate buffer (0.2 M; pH 5.0, 6.0) or deuterated phosphate buffer (0.2 M; pH 7.0) to give 10 mg/mL solutions. For the homopolymers that were insoluble (**PGAm(DEAE)** and **PGAm(DPAE)** at pH 6.0 and 7.4, **PEtG-1** in all conditions), an additional drop of DMA was added to serve as an internal standard. The tubes were sealed and ^1H NMR spectra were acquired at specific time points, with constant agitation of the insoluble samples in between measurements to ensure exposure of the solid samples to their buffer solutions. Percent depolymerization for soluble samples was determined by comparing the integrations of the broad backbone methine proton peak at ~ 5.6 ppm and the monomer hydrate methine proton peak at ~ 5.3 ppm. For the insoluble samples, depolymerization was monitored by setting the integration of the DMA internal standard's acetyl peak (~ 2.1 ppm) to a constant value and reading the integration value of the monomer hydrate methine proton peak at ~ 5.3 ppm. After the monitoring period of the study had elapsed, 1 M HCl was added to the samples to accelerate depolymerization to completion if required. The percent depolymerization of these samples was then calculated by using Equation 5.1:

$$\text{Equation 5.1.} \quad \frac{i_{\text{current}}}{i_{\text{final}}} \times 100\%$$

Where i_{current} is the current integration of the monomer hydrate methine proton peak relative to the internal standard at a particular time point and i_{final} is the final integration of the monomer hydrate methine proton peak relative to the internal standard once the polymer is fully depolymerized.

Depolymerization of Copolymers. Each block copolymer was dissolved in deuterated THF (20 mg/mL). A 100 μL aliquot of each solution was then injected into 400 μL of rapidly stirring D_2O containing a drop of DMA. After stirring for 30 min, each mix was placed in an NMR tube and 100 μL of either 1 M deuterated citrate buffer (pH 5.0, 6.0) or 1 M deuterated phosphate buffer (pH 7.4, 8.0) was added before sealing the tubes and acquiring ^1H NMR spectra at specific time points. Depolymerization was monitored by setting the integration of the DMA internal standard's acetyl peak (~ 2.1 ppm) to a constant value and reading the integration value of the monomer hydrate methine proton peak at ~ 5.3 ppm. After the monitoring period of the study had elapsed, 1 M HCl was added to the samples to accelerate depolymerization to completion if required. The percent depolymerization of these samples was then calculated using Equation 5.1.

5.4.5 Study of Copolymer Assemblies

Block Copolymer Self-Assembly. Each block copolymer was dissolved in THF (10 mg/mL) and then injected into a rapidly stirring phosphate buffer (0.2 M; pH 8.0) in a 1:10 ratio. The resulting mixtures were stirred for at least 16 h to evaporate off the THF, and then filtered through a 0.45 μm Nylon syringe filter. The Z average diameter and count rate of each mixture were then obtained with DLS. Additionally, samples of the suspensions were dropped onto TEM grids and allowed to sit for ~ 5 min before wicking away the excess liquid. The grids were then allowed to fully dry before imaging with the microscope.

Study of Assembly pH Response. Assemblies of the block copolymers were prepared as described above in the section "Block Copolymer Self-Assembly." Each assembly batch was divided equally into 6 cuvettes (3 replicates each for the pH response experiments at either 25 or 37 $^\circ\text{C}$). Z average diameter and count rate of the samples were then monitored via DLS, with pH being lowered between measurement using 0.2 μm Nylon syringe filtered 1 M HCl. Additionally, samples of 25 $^\circ\text{C}$ **PEG-PGAm(DPAE)** assemblies at various pH levels were used to prepare TEM grids in order to visualize the transition of these pH-responsive assemblies. The TEM grids were prepared as previously described in the section "Block Copolymer Self-Assembly."

5.5 References

- (1) Roth, M. E.; Green, O.; Gnaim, S.; Shabat, D. Dendritic, Oligomeric, and Polymeric Self-Immolative Molecular Amplification. *Chem. Rev.* **2016**, *116*, 1309–1352.
- (2) Yardley, R. E.; Rabiee Kenaree, A.; Gillies, E. R. Triggering Depolymerization: Progress and Opportunities for Self-Immolative Polymers. *Macromolecules* **2019**, *52*, 6342–6360.
- (3) Sirianni, Q. E. A.; Gillies, E. R. The Architectural Evolution of Self-Immolative Polymers. *Polymer* **2020**, *202*, 122638.
- (4) Lobeze, J. M.; Swager, T. M. Radiation Detection: Resistivity Responses in Functional Poly(olefin sulfone)/Carbon Nanotube Composites. *Angew. Chem. Int. Ed.* **2010**, *49*, 95–98.
- (5) Fan, B.; Salazar, R.; Gillies, E. R. Depolymerization of Trityl End-Capped Poly(ethyl glyoxylate): Potential Applications in Smart Packaging. *Macromol. Rapid Commun.* **2018**, *39*, 1800173.
- (6) Coulembier, O.; Knoll, A.; Pires, D.; Gotsmann, B.; Duerig, U.; Frommer, J.; Miller, R. D.; Dubois, P.; Hedrick, J. L. Probe-Based Nanolithography: Self-Amplified Depolymerization Media for Dry Lithography. *Macromolecules* **2010**, *43*, 572–574.
- (7) Knoll, A. W.; Pires, D.; Coulembier, O.; Dubois, P.; Hedrick, J. L.; Frommer, J.; Duerig, U. Probe-Based 3-D Nanolithography Using Self-Amplified Depolymerization Polymers. *Adv. Mater.* **2010**, *22*, 3361–3365.
- (8) Cheong, L. L.; Paul, P.; Holzner, F.; Despont, M.; Coady, D. J.; Hedrick, J. L.; Allen, R.; Knoll, A. W.; Duerig, U. Thermal Probe Maskless Lithography for 27.5 nm Half-Pitch Si Technology. *Nano Lett.* **2013**, *13*, 4485–4491.
- (9) Fan, B.; Trant, J. F.; Yardley, R. E.; Pickering, A. J.; Lagugné-Labarthet, F.; Gillies, E. R. Photocontrolled Degradation of Stimuli-Responsive Poly(ethyl glyoxylate): Differentiating Features and Traceless Ambient Depolymerization. *Macromolecules* **2016**, *49*, 7196–7203.
- (10) Skaug, M. J.; Schwemmer, C.; Fringes, S.; Rawlings, C. D.; Knoll, A. W. Nanofluidic Rocking Brownian Motors. *Science* **2018**, *359*, 1505–1508.
- (11) Hernandez, H. L.; Kang, S. K.; Lee, O. P.; Hwang, S. W.; Kaitz, J. A.; Inci, B.; Park, C. W.; Chung, S.; Sottos, N. R.; Moore, J. S.; Rogers, J. A.; White, S. R. Triggered

Transience of Metastable Poly(phthalaldehyde) for Transient Electronics. *Adv. Mater.* **2014**, *26*, 7637–7642.

(12) Park, C. W.; Kang, S. K.; Hernandez, H. L.; Kaitz, J. A.; Wie, D. S.; Shin, J.; Lee, O. P.; Sottos, N. R.; Moore, J. S.; Rogers, J. A.; White, S. R. Thermally Triggered Degradation of Transient Electronic Devices. *Adv. Mater.* **2015**, *27*, 3783–3788.

(13) Heuchan, S. M.; MacDonald, J. P.; Bauman, L. A.; Fan, B.; Henry, H. A. L.; Gillies, E. R. Photoinduced Degradation of Polymer Films Using Polyglyoxylate–Polyester Blends and Copolymers. *ACS Omega* **2018**, *3*, 18603–18612.

(14) Heuchan, S. M.; Fan, B.; Kowalski, J. J.; Gillies, E. R.; Henry, H. A. L. Development of Fertilizer Coatings from Polyglyoxylate–Polyester Blends Responsive to Root-Driven pH Change. *J. Agric. Food. Chem.* **2019**, *67*, 12720–12729.

(15) Esser-Kahn, A. P.; Sottos, N. R.; White, S. R.; Moore, J. S. Programmable Microcapsules from Self-Immolative Polymers. *J. Am. Chem. Soc.* **2010**, *132*, 10266–10268.

(16) DiLauro, A. M.; Abbaspourrad, A.; Weitz, D. A.; Phillips, S. T. Stimuli-Responsive Core–Shell Microcapsules with Tunable Rates of Release by Using a Depolymerizable Poly(phthalaldehyde) Membrane. *Macromolecules* **2013**, *46*, 3309–3313.

(17) Kaitz, J. A.; Possanza, C. M.; Song, Y.; Diesendruck, C. E.; Spiering, A. J. H.; Meijer, E. W.; Moore, J. S. Depolymerizable, Adaptive Supramolecular Polymer Nanoparticles and Networks. *Polym. Chem.* **2014**, *5*, 3788–3794.

(18) Liu, G.; Zhang, G.; Hu, J.; Wang, X.; Zhu, M.; Liu, S. Hyperbranched Self-Immolative Polymers (hSIPs) for Programmed Payload Delivery and Ultrasensitive Detection. *J. Am. Chem. Soc.* **2015**, *137*, 11645–11655.

(19) Kumar, K.; Castaño, E. J.; Weidner, A. R.; Yildirim, A.; Goodwin, A. P. Depolymerizable poly(*O*-vinyl carbamate-*alt*-sulfones) as customizable macromolecular scaffolds for mucosal drug delivery. *ACS Macro Lett.* **2016**, *5*, 636–640.

(20) Tang, S.; Yourdkhani, M.; Possanza Casey, C. M.; Sottos, N. R.; White, S. R.; Moore, J. S. Low-Ceiling-Temperature Polymer Microcapsules with Hydrophobic Payloads via Rapid Emulsion-Solvent Evaporation. *ACS Appl. Mater. Interfaces* **2017**, *9*, 20115–20123.

- (21) Fan, B.; Gillies, E. R. Poly(ethyl glyoxylate)-Poly(ethylene oxide) Nanoparticles: Stimuli-Responsive Drug Release via End-to-End Polyglyoxylate Depolymerization. *Mol. Pharmaceutics* **2017**, *14*, 2548–2559.
- (22) Fan, B.; Trant, J. F.; Hemery, G.; Sandre, O.; Gillies, E. R. Thermo-Responsive Self-Immolative Nanoassemblies: Direct and Indirect Triggering. *Chem. Commun.* **2017**, *53*, 12068–12071.
- (23) Tang, S.; Tang, L.; Lu, X.; Liu, H.; Moore, J. S. Programmable Payload Release from Transient Polymer Microcapsules Triggered by a Specific Ion Coactivation Effect. *J. Am. Chem. Soc.* **2018**, *140*, 94–97.
- (24) Fan, B.; Yardley, R. E.; Trant, J. F.; Borecki, A.; Gillies, E. R. Tuning the Hydrophobic Cores of Self-Immolative Polyglyoxylate Assemblies. *Polym. Chem.* **2018**, *9*, 2601–2610.
- (25) Gambles, M. T.; Fan, B.; Borecki, A.; Gillies, E. R. Hybrid Polyester Self-Immolative Polymer Nanoparticles for Controlled Drug Release. *ACS Omega* **2018**, *3*, 5002–5011.
- (26) Lutz, J. P.; Davydovich, O.; Hannigan, M. D.; Moore, J. S.; Zimmerman, P. M.; McNeil, A. J. Functionalized and Degradable Polyphthalaldehyde Derivatives. *J. Am. Chem. Soc.* **2019**, *141*, 14544–14548.
- (27) Eriksson, V.; Andersson Trojer, M.; Vavra, S.; Hulander, M.; Nordstierna, L. Formulation of Polyphthalaldehyde Microcapsules for Immediate UV-Light Triggered Release. *J. Colloid Interface Sci.* **2020**, *579*, 645–653.
- (28) Gisbert-Garzarán, M.; Berkmann, J. C.; Giasafaki, D.; Lozano, D.; Spyrou, K.; Manzano, M.; Steriotis, T.; Duda, G. N.; Schmidt-Bleek, K.; Charalambopoulou, G.; Vallet-Regí, M. Engineered pH-Responsive Mesoporous Carbon Nanoparticles for Drug Delivery. *ACS Appl. Mater. Interfaces* **2020**, *12*, 14946–14957.
- (29) Fukumoto, S.; Kawade, M.; Kimura, K.; Akiyama, Y.; Kikuchi, A. Preparation of Spherical Nucleic Acid Nanoparticles Containing Self-Immolative Poly(carbamate) Core. *Anal. Sci.* **2021**, *37*, 781–784.
- (30) Sagi, A.; Weinstain, R.; Karton, N.; Shabat, D. Self-Immolative Polymers. *J. Am. Chem. Soc.* **2008**, *130*, 5434–5435.
- (31) Dewit, M. A.; Gillies, E. R. A Cascade Biodegradable Polymer Based on Alternating Cyclization and Elimination Reactions. *J. Am. Chem. Soc.* **2009**, *131*, 18327–18334.

- (32) Olah, M. G.; Robbins, J. S.; Baker, M. S.; Phillips, S. T. End-Capped Poly(benzyl ethers): Acid and Base Stable Polymers That Depolymerize Rapidly from Head-to-Tail in Response to Specific Applied Signals. *Macromolecules* **2013**, *46*, 5924–5928.
- (33) Seo, W.; Phillips, S. T. Patterned Plastics That Change Physical Structure in Response to Applied Chemical Signals. *J. Am. Chem. Soc.* **2010**, *132*, 9234–9235.
- (34) Kaitz, J. A.; Diesendruck, C. E.; Moore, J. S. End Group Characterization of Poly(phthalaldehyde): Surprising Discovery of a Reversible, Cationic Macrocyclization Mechanism. *J. Am. Chem. Soc.* **2013**, *135*, 12755–12761.
- (35) Fan, B.; Trant, J. F.; Wong, A. D.; Gillies, E. R. Polyglyoxylates: A Versatile Class of Triggerable Self-Immolative Polymers from Readily Accessible Monomers. *J. Am. Chem. Soc.* **2014**, *136*, 10116–10123.
- (36) Bowden, M. J.; Thompson, L. F. Poly(styrene sulfone)—A Sensitive Ion-Millable Positive Electron Beam Resist. *J. Electrochem. Soc.* **1974**, *121*, 1620–1623.
- (37) Bowden, M. J.; Chandross, E. A. Poly(vinyl arene sulfones) as Novel Positive Photoresists. *J. Electrochem. Soc.* **1975**, *122*, 1370–1374.
- (38) Joo, W.; Wang, W.; Mesch, R.; Matsuzawa, K.; Liu, D.; Willson, C. G. Synthesis of Unzipping Polyester and a Study of its Photochemistry. *J. Am. Chem. Soc.* **2019**, *141*, 14736–14741.
- (39) Yuan, J.; Xiong, W.; Zhou, X.; Zhang, Y.; Shi, D.; Li, Z.; Lu, H. 4-Hydroxyproline-Derived Sustainable Polythioesters: Controlled Ring-Opening Polymerization, Complete Recyclability, and Facile Functionalization. *J. Am. Chem. Soc.* **2019**, *141*, 4928–4935.
- (40) Xiong, W.; Chang, W.; Shi, D.; Yang, L.; Tian, Z.; Wang, H.; Zhang, Z.; Zhou, X.; Chen, E.-Q.; Lu, H. Geminal Dimethyl Substitution Enables Controlled Polymerization of Penicillamine-Derived β -Thiolactones and Reversed Depolymerization. *Chem* **2020**, *6*, 1831–1843.
- (41) Kim, H.; Brooks, A. D.; DiLauro, A. M.; Phillips, S. T. Poly(carboxypyrrole)s that Depolymerize from Head to Tail in the Solid State in Response to Specific Applied Signals. *J. Am. Chem. Soc.* **2020**, *142*, 9447–9452.
- (42) Neary, W. J.; Isais, T. A.; Kennemur, J. G. Self-Immolative Bottlebrush Polypentenamers and Their Macromolecular Metamorphosis. *J. Am. Chem. Soc.* **2019**, *141*, 14220–14229.

- (43) Liu, Y.; Jia, Y.; Wu, Q.; Moore, J. S. Architecture-Controlled Ring-Opening Polymerization for Dynamic Covalent Poly(disulfide)s. *J. Am. Chem. Soc.* **2019**, *141*, 17075–17080.
- (44) Fan, B.; Trant, J. F.; Gillies, E. R. End-Capping Strategies for Triggering End-to-End Depolymerization of Polyglyoxylates. *Macromolecules* **2016**, *49*, 9309–9319.
- (45) Yardley, R. E.; Kenaree, A. R.; Liang, X.; Gillies, E. R. Transesterification of Poly(ethyl glyoxylate): A Route to Structurally Diverse Polyglyoxylates. *Macromolecules* **2020**, *53*, 8600–8609.
- (46) Hewitt, D. R. O.; Grubbs, R. B. Amine-Catalyzed Chain Polymerization of Ethyl Glyoxylate from Alcohol and Thiol Initiators. *ACS Macro Lett.* **2021**, *10*, 370–374.
- (47) Rabiee Kenaree, A.; Gillies, E. R. Controlled Polymerization of Ethyl Glyoxylate Using Alkylolithium and Alkoxide Initiators. *Macromolecules* **2018**, *51*, 5501–5510.
- (48) Sirianni, Q. E. A.; Rabiee Kenaree, A.; Gillies, E. R. Polyglyoxylamides: Tuning Structure and Properties of Self-Immolative Polymers. *Macromolecules* **2019**, *52*, 262–270.
- (49) Ree, L. H. S.; Sirianni, Q. E. A.; Gillies, E. R.; Kelland, M. A. Systematic Study of Polyglyoxylamides as Powerful, High-Cloud-Point Kinetic Hydrate Inhibitors. *Energy Fuels* **2019**, *33*, 2067–2075.
- (50) Rabiee Kenaree, A.; Sirianni, Q. E. A.; Classen, K.; Gillies, E. R. Thermoresponsive Self-Immolative Polyglyoxylamides. *Biomacromolecules* **2020**, *21*, 3817–3825.
- (51) DiLauro, A. M.; Zhang, H.; Baker, M. S.; Wong, F.; Sen, A.; Phillips, S. T. Accessibility of Responsive End-Caps in Films Composed of Stimuli-Responsive, Depolymerizable Poly(phthalaldehydes). *Macromolecules* **2013**, *46*, 7257–7265.
- (52) Yeung, K.; Kim, H.; Mohapatra, H.; Phillips, S. T. Surface-Accessible Detection Units in Self-Immolative Polymers Enable Translation of Selective Molecular Detection Events into Amplified Responses in Macroscopic, Solid-State Plastics. *J. Am. Chem. Soc.* **2015**, *137*, 5324–5327.
- (53) Hu, Y.; Litwin, T.; Nagaraja, A. R.; Kwong, B.; Katz, J.; Watson, N.; Irvine, D. J. Cytosolic Delivery of Membrane-Impermeable Molecules in Dendritic Cells using pH-Responsive Core-Shell Nanoparticles. *Nano Lett.* **2007**, *7*, 3056–3064.

- (54) Lomas, H.; Massignani, M.; Abdullah, K. A.; Canton, I.; Lo Presti, C.; MacNeil, S.; Du, J.; Blanz, A.; Madsen, J.; Armes, S. P.; Lewis, A. L.; Battaglia, G. Non-Cytotoxic Polymer Vesicles for Rapid and Efficient Intracellular Delivery. *Faraday Discuss.* **2008**, *139*, 143–159.
- (55) Zhou, K.; Wang, Y.; Huang, X.; Luby-Phelps, K.; Sumer, B. D.; Gao, J. Tunable, Ultrasensitive pH-Responsive Nanoparticles Targeting Specific Endocytic Organelles in Living Cells. *Angew. Chem. Int. Ed.* **2011**, *50*, 6109–6114.
- (56) Wong, A. S. M.; Czuba, E.; Chen, M. Z.; Yuen, D.; Cupic, K. I.; Yang, S.; Hodgetts, R. Y.; Selby, L. I.; Johnston, A. P. R.; Such, G. K. pH-Responsive Transferrin-pHlexi Particles Capable of Targeting Cells in Vitro. *ACS Macro Lett.* **2017**, *6*, 315–320.
- (57) Kongkatigumjorn, N.; Smith, S. A.; Chen, M.; Fang, K.; Yang, S.; Gillies, E. R.; Johnston, A. P. R.; Such, G. K. Controlling Endosomal Escape Using pH-Responsive Nanoparticles with Tunable Disassembly. *ACS Appl. Nano Mater.* **2018**, *1*, 3164–3173.
- (58) Zhang, C.; Kermaniyan, S.; Smith, S. A.; Gillies, E. R.; Such, G. K. Acid-Responsive Poly(glyoxylate) Self-Immolative Star Polymers. *Biomacromolecules* **2021**, *22*, 3892–3900.
- (59) Nguyen, P. K.; Snyder, C. G.; Shields, J. D.; Smith, A. W.; Elbert, D. L. Clickable Poly(ethylene glycol)-Microsphere-Based Cell Scaffolds. *Macromol. Chem. Phys.* **2013**, *214*, 948–956.

Chapter 6

6 Depolymerizing Polyplexes for DNA Transfection

6.1 Introduction

Nucleic acid therapy is an area of intense research interest with the potential to treat numerous diseases. The delivery of ribonucleic acid (RNA) and deoxyribonucleic acid (DNA) into target cells may prove invaluable in treating inherited genetic disorders such as cystic fibrosis,¹ inoculating against pathogens,² and stimulating the immune system to fight cancer.³ However, one of the prevailing challenges hindering nucleic acid therapy is the efficient delivery of the nucleic acids into the appropriate domains of the target cells. The use of naked nucleic acids results in low transfection efficiency due to their intrinsic properties such as their large size, hydrophilicity, and negative charge, which makes it difficult for them to traverse the cell membrane.⁴ Furthermore, if the naked nucleic acids are injected *in vivo*, they are rapidly degraded by endogenous nucleases.

Both viral and non-viral vectors have been employed to assist with nucleic acid transfection.⁴⁻⁵ While viral vectors tend to have a higher transfection efficiency than non-viral ones, there are safety concerns. Non-viral vectors such as lipids and polymers, on the other hand, are non-immunogenic, can be loaded with more genetic material, and can be more easily scaled up in production.⁵⁻⁶ Polymeric vectors are typically polycations that can interact with the anionic phosphate backbones of nucleic acids, allowing for the formation of compact nucleic acid-polymer complexes (polyplexes). These polyplexes with an overall positive charge can then bind to the anionic surfaces of cells, allowing for their uptake via endocytosis. Once inside the endosome, the polycation must disrupt the endosomal membrane allowing for escape into the cytoplasm. The exact mechanism for this disruption is not known, although different hypotheses exist.⁶ The “proton sponge” hypothesis postulates that the polycations of the polyplex buffer against the influx of protons being pumped into the endosome to lower the pH, causing more protons and counterions to flow into the compartment. The subsequent influx of water leads to an

osmotic pressure buildup and eventual lysis of the endosome. An alternative hypothesis reasons that the polyplex or free polycations interact with the negatively-charged surface of the endosomal membrane, leading to localized membrane destabilization, allowing the polyplex to escape without completely lysing the endosome. In any case, for the final step of transfection, the polycation must decomplex and release the genetic material, which will either remain in the cytoplasm (RNA) or transfer into the nucleus (DNA) to alter cellular gene expression.

Several well-known polycations have been investigated as transfection agents, including poly(L-lysine) (PLL),⁷ poly[2-(dimethylaminoethyl) methacrylate] (PDMAEMA),⁸ and polyethyleneimine (PEI).⁹ Unfortunately, many polycations do not have high transfection efficiencies. Moreover, polycations that do transfect well, such as high molecular weight PEI (~25 kg/mol), tend to be cytotoxic. Lowering the molecular weight of PEI reduces cytotoxicity at the cost of reduced transfection efficiency.¹⁰⁻¹¹ The use of degradable polycations is one potential strategy to improve transfection efficiencies while simultaneously decreasing cytotoxicity caused by residual polymer.¹² Polycations that incorporate moieties in their backbones sensitive to the reducing or acidic conditions present in the cytoplasm and endosome, respectively, have been reported with improvements to both transfection efficiency and cytotoxicity when compared to non-degradable polycations.¹³⁻¹⁷ However, these degradable polycations require multiple stimuli-mediated cleavage events to achieve complete degradation.

Self-immolative polymers (SIPs) are macromolecules capable of a continuous head-to-tail depolymerization following exposure to a particular stimulus.¹⁸⁻¹⁹ This capability makes SIPs attractive for situations where low concentrations of stimuli are available and amplification of the triggering event would be desired. Various different classes of SIPs such as poly(benzyl carbamate)s,²⁰⁻²¹ poly(benzyl ether)s,²² and polyacetals²³⁻²⁴ have been reported within the last two decades. Thus far, SIPs have been harnessed for applications including sensors,²⁵ drug delivery vehicles,²⁶⁻²⁹ lithography,³⁰⁻³³ and transient plastics^{23, 34-35} and composites.³⁶ To the best of our knowledge, the only example of an SIP being investigated for nucleic acid delivery involved the attachment of multiple PDMAEMA chains to the periphery of a hyperbranched SIP with a reduction-sensitive trigger group.²⁶

While the results of this study demonstrated the potential of these polymers for transfection, the polycationic PDMAEMA blocks did not degrade. In addition, concerns regarding potential toxicity were raised due to the production of quinone methides during the depolymerization of the hyperbranched SIP.

We describe here the exploration of polycationic SIPs that depolymerize completely into monocations for DNA delivery (Figure 6.1). Polyglyoxylamides (PGAMs) were selected as the SIP backbone as they can be readily prepared with different pendent amino groups via the post-polymerization amidation of poly(ethyl glyoxylate) (PEtG).³⁷ We compare nine different PGAMs from three different pendent amino groups and three end-caps in terms of their depolymerization behaviour, plasmid DNA (pDNA) complexation and release, as well as their toxicities and transfection capabilities relative to that of a commercially available linear PEI-based polycation transfection agent (jetPEI; Polyplus-transfection SA). Overall, the work demonstrates the promise for PGAMs to provide similar transfection efficiency to jetPEI with lower toxicity.

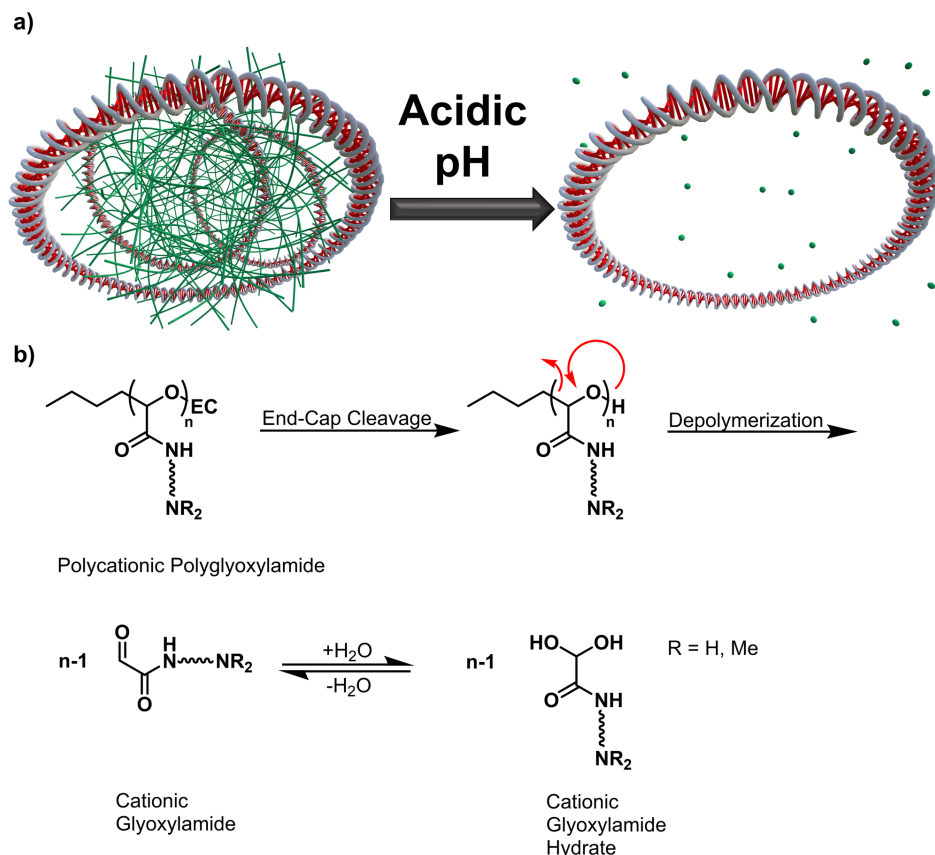


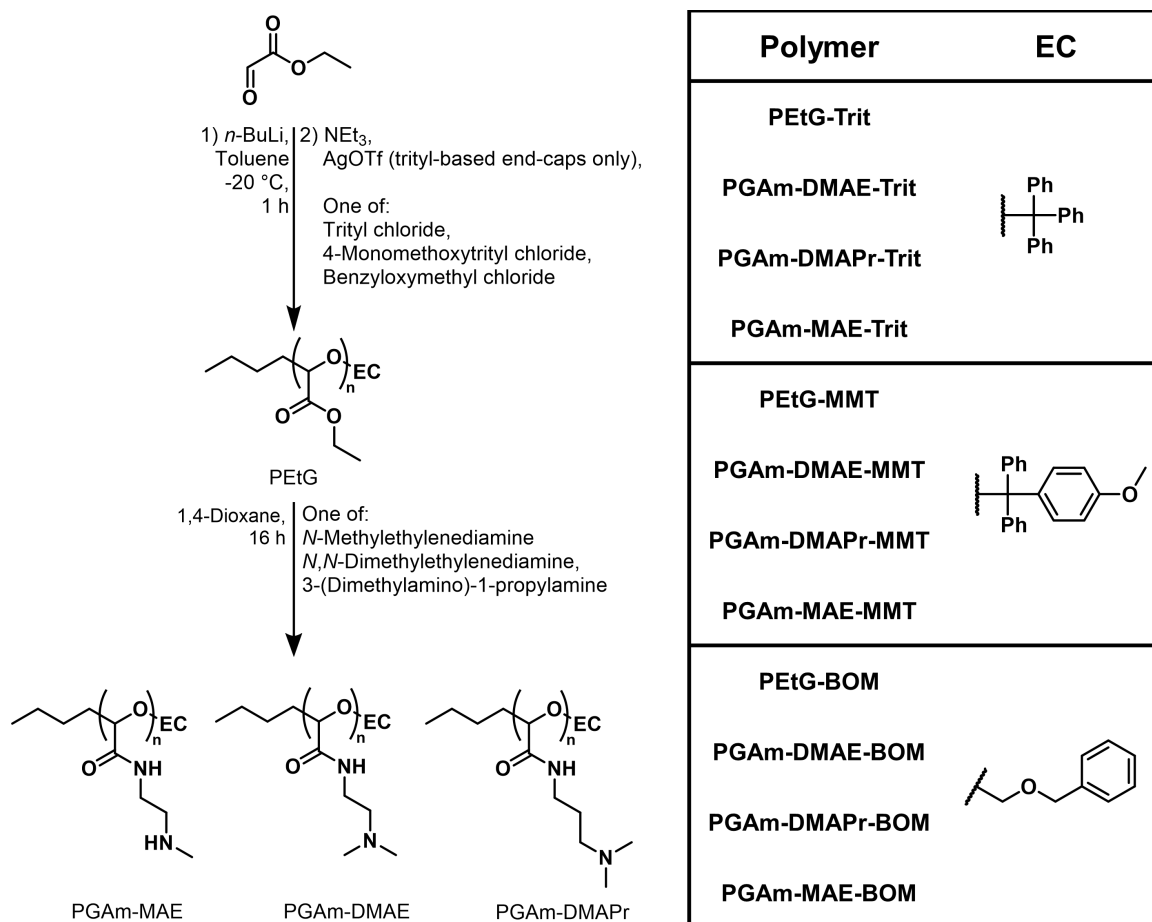
Figure 6.1. a) Polyplexes formed via the ionic interaction of positively-charged SIPs with the negatively-charged phosphate backbone of DNA. At acidic pH, the SIPs depolymerize, destroying the polyplex and releasing the DNA. b) Depolymerization of a polycationic PGAm into monocations.

6.2 Results and Discussion

6.2.1 Synthesis of Polyglyoxylamide Polycations

First, three different precursor PEtGs were synthesized via the anionic initiation of purified ethyl glyoxylate using *n*-butyl lithium, as previously reported (Scheme 6.1).³⁸ A common molecular weight of 25 kg/mol was targeted for all of the PEtGs. Because polyplexes are known to be taken up via endocytosis and exposed to acidic conditions,^{4, 6} polymers that can be triggered to depolymerize due a drop in pH are ideal. Thus, end-capping was performed with trityl chloride (**PEtG-Trit**) or 4-monomethoxytrityl chloride (**PEtG-MMT**). AgOTf was mixed with these end-caps before their addition to the polymerization

mixtures to scavenge chloride ions from the end-caps and produce trityl cations to react with the polymer termini, allowing for more efficient end-capping at the low polymerization temperatures. Additionally, benzyloxymethyl chloride was used for one of the PEtGs to create a control polymer (**PEtG-BOM**) that would be stable at neutral and acidic conditions. ^1H NMR, ^{13}C NMR, and FT-IR spectroscopy were used to confirm the successful synthesis of the PEtGs (Figure A5.1–Figure A5.3 and Figure A5.13–Figure A5.15). Size-exclusion chromatography (SEC) in *N,N*-dimethylformamide (DMF) relative poly(methyl methacrylate) (PMMA) standards revealed dispersities (D_s) of 1.4–1.8 (Table 6.1 and Figure A5.25–Figure A5.27). The number average molar mass (M_n) of **PEtG-Trit** was 21.4 kg/mol, slightly below the targeted 25 kg/mol, while the **PEtG-MMT** had a M_n of 18.8 kg/mol. The M_n values obtained from analysis of the same polymers using ^1H NMR spectroscopy were closer to the targeted 25 kg/mol, indicating an underestimation of the molecular weight when using SEC. **PEtG-BOM**'s M_n was lower than targeted (16.5 kg/mol) despite numerous polymerization attempts. We attribute the lack of molecular weight control not to the polymerization reaction but rather to the poor end-capping efficiency of benzyloxymethyl chloride at the polymerization temperature of $-20\text{ }^\circ\text{C}$. It is likely that the end-capping reaction mostly occurred during the warming of the polymerization mixture to room temperature, which would have allowed for some depolymerization of the uncapped polymer chains to occur before end-capping.



Scheme 6.1. Synthesis of polyglyoxylamide polycations for use as depolymerizable pDNA complexation agents.

Table 6.1. ¹H NMR and SEC characterization of the PEtGs and polycationic PGAMs.

Polymer	¹ H NMR		SEC		
	<i>DP_n</i>	<i>M_n</i> (kg/mol)	<i>M_n</i> (kg/mol)	<i>M_w</i> (kg/mol)	<i>Đ</i>
PEtG-Trit	241	24.6	21.4	36.4	1.7
PEtG-MMT	210	21.4	18.8	33.0	1.8
PEtG-BOM	156	15.9	16.5	22.7	1.4
PGAm-DMAE-Trit	211	30.4	26.7	45.7	1.7
PGAm-DMAPr-Trit	216	34.2	28.4	46.6	1.6
PGAm-MAE-Trit^a	217	28.2	--	--	--
PGAm-DMAE-MMT	198	28.5	24.4	44.9	1.8
PGAm-DMAPr-MMT	218	34.5	26.4	42.9	1.6
PGAm-MAE-MMT^a	193	25.1	--	--	--
PGAm-DMAE-BOM	162	23.4	24.5	42.2	1.7
PGAm-DMAPr-BOM	156	24.7	24.0	34.2	1.4
PGAm-MAE-BOM^a	139	18.1	--	--	--

^aThe PGAm-MAEs did not elute from the SEC column and thus could not be measured using this technique.

Next, the polycationic PGAMs were prepared by modifying the PEtGs with different diamines in 1,4-dioxane at room temperature for 16 h (Scheme 6.1). Use of *N,N*-dimethylethylenediamine afforded **PGAm-DMAE-Trit**, **PGAm-DMAE-MMT**, and **PGAm-DMAE-BOM**. To investigate the effects of the alkyl spacer length in the pendent group, 3-(dimethylamino)-1-propylamine was used to synthesize **PGAm-DMAPr-Trit**, **PGAm-DMAPr-MMT**, and **PGAm-DMAPr-BOM**. Given that well known polycation transfection agents in the literature, such as PEI, possess primary and/or secondary amines in their structures, we also sought to produce PGAMs with these functional groups. The use of *N*-methylethylenediamine allowed for the synthesis of **PGAm-MAE-Trit**, **PGAm-MAE-MMT**, and **PGAm-MAE-BOM**. The synthesis of PGAMs with primary amino pendent groups proved challenging, as primary diamines such as ethylenediamine simply cross-linked the precursor polymers when post-polymerization amidation was attempted. The use of a large diamine excess and the use of protecting groups were explored, but we were unable to obtain PGAMs with pendent primary amine moieties in any significant yield or purity. Nevertheless, the library of PGAMs successfully synthesized possessed variety

in both end-caps and polycationic pendent groups. ^1H and ^{13}C NMR as well as FT-IR spectroscopy confirmed the identity and purity of the PGAMs (Figure A5.4–Figure A5.12 and Figure A5.16–Figure A5.24) while SEC confirmed that the PGAM-DMAEs and PGAM-DMAPrs did not depolymerize during the post-polymerization amidation of the precursor PEtGs (Figure A5.25–Figure A5.27). Size-exclusion chromatograms for the PGAM-MAEs could not be obtained as these polymers adsorbed to the column both in DMF as well as aqueous conditions. Nevertheless, their degrees of polymerization (DP_n) values obtained from ^1H NMR spectroscopy are similar to those of their PEtG precursors as well as those of the other PGAMs made from the same precursors (Table 6.1).

6.2.2 Depolymerization of the Polyglyoxalamides

The PGAMs were next evaluated for their self-immolative depolymerization capabilities. Each PGAM was dissolved in a deuterated buffer solution at either pH 5.0, 6.0, or 7.4 and placed in an NMR tube that was promptly sealed. Monitoring the solutions using ^1H NMR spectroscopy revealed the extent of depolymerization over time by comparing the integration of the polymer backbone methine proton peak (~ 5.6 ppm) against that of the monomer hydrate methine proton peak (~ 5.3 ppm) (Figure 6.2a and Figure A5.28–Figure A5.54). For the PGAM-MAE samples, an additional depolymerization peak identified as the monomer hemiaminal methine proton peak caused by intramolecular cyclization (~ 4.5 ppm) of the secondary amine pendent group was also integrated and accounted for.

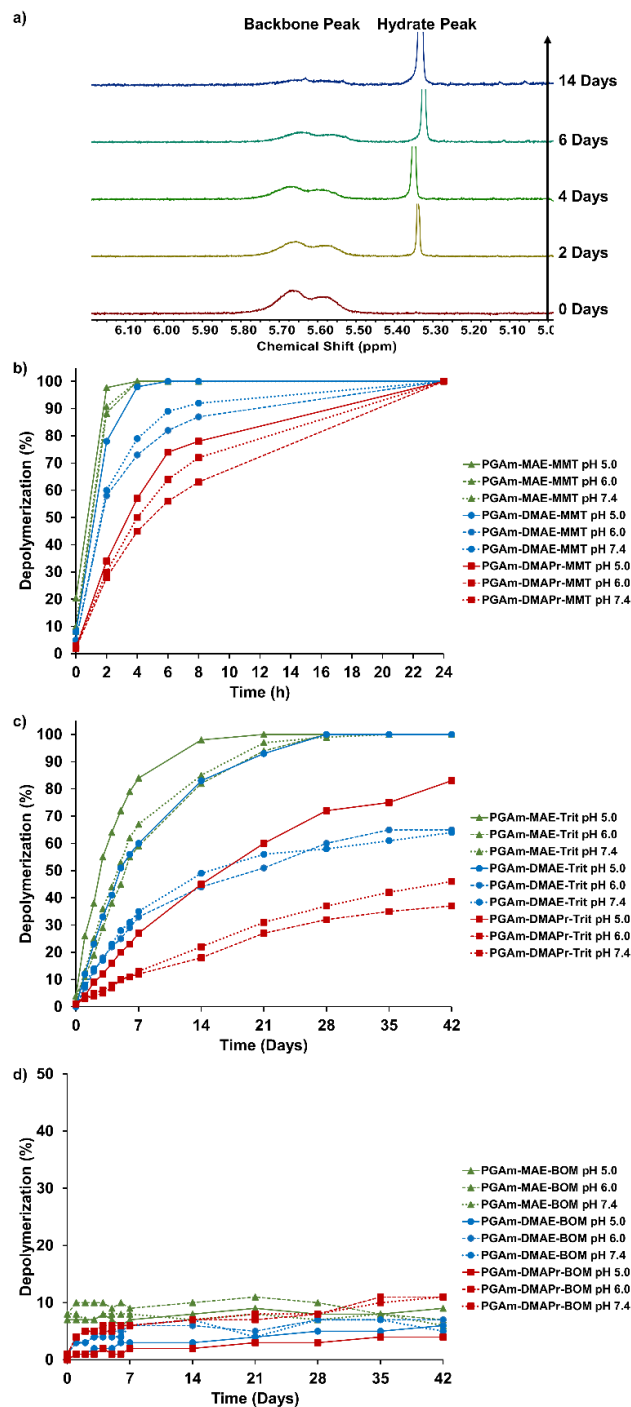


Figure 6.2. Depolymerization of the PGAm polycations in either citrate buffered D_2O (pH 5.0, 6.0) or phosphate buffered D_2O (pH 7.4). a) Example showing depolymerization of PGAm-DMAE-Trit in citrate buffered D_2O (0.2 M, pH = 5.0) monitored by ^1H NMR spectroscopy (400 MHz). Depolymerization kinetics of b) PGAm-MMTs, c) PGAm-Trits, and d) PGAm-BOMs over time.

The depolymerization behaviours were influenced by the end-cap and pendent groups of each polymer as well as the pH. As expected, the MMT end-capped polymers depolymerized the fastest, with full depolymerization of all of the samples within 24 h (Figure 6.2b). Among the different pendent groups, **PGAm-MAE-MMT** depolymerized the fastest (full depolymerization of all samples by 4 h), followed by **PGAm-DMAE-MMT** and then **PGAm-DMAPr-MMT**. This trend correlates well with the hydrophilicity of the polymer pendent groups, with **PGAm-MAE-MMT** having the greatest hydrophilicity due to the fact that its secondary amine pendent groups can act as both hydrogen donors and acceptors. Conversely, **PGAm-DMAPr-MMT** had the slowest depolymerization, likely due to its pendent groups' tertiary amine group and longer alkyl chain spacer, making it the most hydrophobic of the three polymers. **PGAm-DMAE-MMT**'s depolymerization was intermediate between those of the other two. The reason for this observed behaviour is unclear. We initially hypothesized that the polymers may be self-assembling in solution due to the differences in solubility between the hydrophilic polymer chains and hydrophobic end-caps. Such assembly would place the end-caps in the core, where their cleavage may be slowed due to lack of water access. The dependence of depolymerization on the solubility state of an SIP and accessibility of its end-caps has been reported by our group and others in the past.^{33, 39-41} However, an investigation of the trityl end-capped polymers in buffer solutions using dynamic light scattering (DLS) revealed no assembly or aggregation at any of the tested pH levels. Accelerated depolymerization was evident for all of the polymer samples at pH 5.0, with both **PGAm-MAE-MMT** and **PGAm-DMAE-MMT** reaching over 90% depolymerization by 4 h and **PGAm-DMAPr-MMT** reaching over 50% depolymerization by the same time point. All PGAmS at pH 6.0 and 7.4 underwent slower depolymerization than at pH 5.0. Interestingly, pH 7.4 resulted in faster depolymerization than pH 6.0. This result can likely be attributed to the fact that hemiacetal depolymerization is known to exhibit a rate minimum at mildly acidic pH.⁴²⁻⁴³ Because the depolymerization mechanism involves the sequential breakdown of hemiacetals, depolymerization is slowed overall under slightly acidic conditions. This phenomenon has also been reported previously for PEtG, which possesses the same polyacetal backbone as PGAmS.^{27, 33}

The trityl end-capped polymers followed the same trends as the MMT end-capped polymers, albeit with slower depolymerization (Figure 6.2c). Again, **PGAm-MAE-Trit** achieved complete depolymerization most rapidly at pH 5.0, although it required ~14 days. Samples of this polymer at pH 6.0 and 7.4 needed twice as long for full depolymerization to occur. Over the timespan of the experiment (42 days), only **PGAm-DMAE-Trit** in pH 5.0 buffer fully depolymerized among the tertiary amine pendent group polymers. **PGAm-DMAPr-Trit** reached a maximum depolymerization of ~80% by 42 days at pH 5.0.

In addition to the stimuli-responsive PGAmS, the BOM end-capped polymers were also assessed for depolymerization over 42 days using the same conditions (Figure 6.2d). None of the samples showed depolymerization greater than ~10% over this time period. A small amount of early depolymerization was evident, which was likely not due to cleavage of the BOM end-caps, but rather the presence of some unend-capped polymer chains that underwent depolymerization once dissolved. Unend-capped polyacetals such as PEtG are metastable and have been isolated previously.²⁴ Overall, these experiments demonstrate the selected depolymerization of the trityl and MMT end-capped PGAmS, with tunable depolymerization behaviours dependent on the end-caps, pendent groups, and pH. Additionally, BOM end-capped PGAmS were shown to undergo negligible depolymerization, thus providing control polymers for further experiments where the effects of depolymerization were evaluated.

6.2.3 Complexation and Decomplexation of Polyplexes

For the evaluation of the polycations as transfection vectors, pDNA containing the reporter gene firefly luciferase (FLuc) was selected. Gel electrophoresis was used to assess the abilities of the PGAmS to complex the pDNA. Different ratios of PGAm and DNA stock solutions were used to adjust the nitrogen/phosphorus (N/P) ratio, and the polyplexes were compared to a DNA ladder, pDNA only (N/P ratio = 0), and a pDNA-jetPEI polyplex prepared at the N/P ratio of 5 (as recommended by the manufacturer) (Figure A5.55). Among the different polycations tested, PGAm-MAEs most efficiently complexed the pDNA, requiring an N/P ratio of ~5. The secondary amine pendent groups of the PGAm-MAEs are less sterically hindered than those of the other PGAmS, allowing them to bind

to the phosphate groups on the DNA easier. The PGAm-DMAE polycations required N/P ratios of ~ 10 , whereas PGAm-DMAPr required ~ 25 , presumably as a result of their increasing steric hindrance.

Decomplexation in response to an acidic stimulus was also evaluated using gel electrophoresis. Polyplexes of pDNA with PGAmS at an N/P ratio of 50 were evaluated. pDNA with jetPEI (N/P = 5) and free pDNA were also examined. The samples were either subjected to gel electrophoresis 15 min after their preparation or incubated in a buffer solution at pH 5.0 for 24 h to allow for potential decomplexation to occur prior to gel electrophoresis. Without incubation at pH 5, the DNA remained complexed in all of the polyplexes tested (Figure 6.3a). On the other hand, incubation under acidic conditions resulted in the release of some pDNA from most of the polyplexes prepared from PGAmS with trityl and MMT end-caps (Figure 6.3b). pDNA was not released from most of the BOM end-capped controls. However, **PGAm-MAE-Trit** did not appear to release any pDNA even at pH 5. While some depolymerization almost certainly occurred with this sample, we postulate that the interactions between the pDNA and this polymer were strong enough that the polyplexes remained stable despite the loss of some polymer chains. This strong interaction between PGAm-MAEs and pDNA was noted previously during the initial complexation experiments. **PGAm-MAE-BOM** similarly showed no pDNA release since it did not depolymerize significantly over 24 h. In contrast, **PGAm-MAE-MMT** did depolymerize enough over 24 h that the polyplexes became unstable and pDNA was ultimately released. Another unexpected result was the release of some pDNA from the **PGAm-DMAPr-BOM** sample after its incubation. This release may be due to the weaker interactions of this polymer's pendent amines with the pDNA (more hydrophobic and sterically hindered than the other two pendent groups). Nevertheless, some complexation was still clearly evident as complexed pDNA was still present in the well.

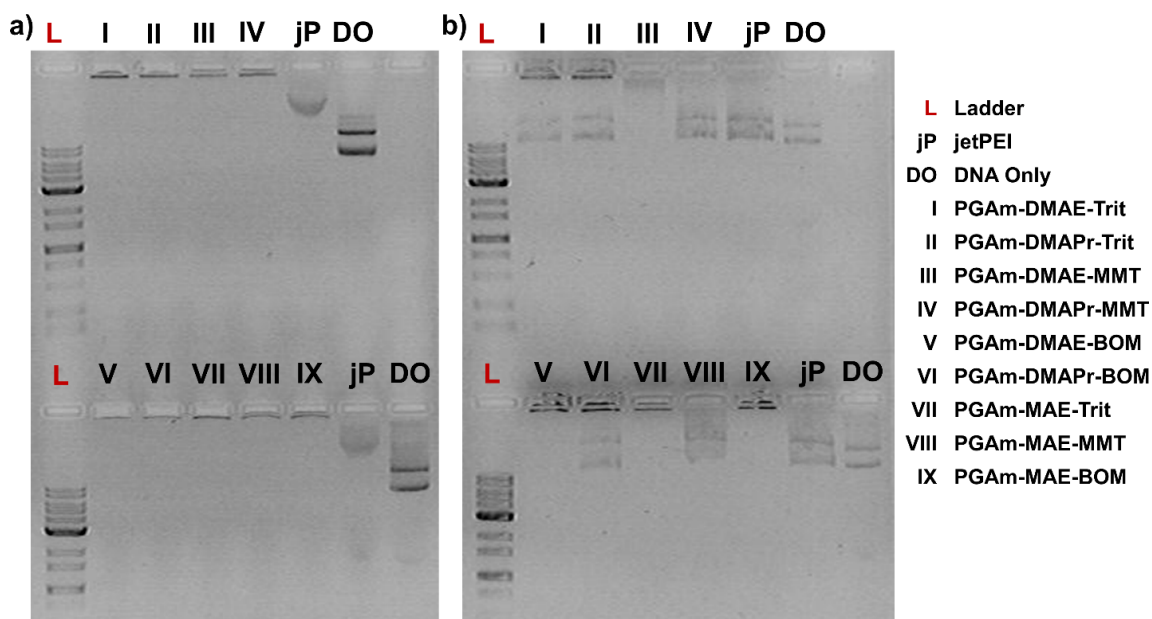


Figure 6.3. Gel electrophoresis of the polyplexes ($N/P = 50$) along with a commercial transfection agent (jetPEI; $N/P = 5$) and free pDNA. a) Polyplexes were prepared in purified water and gel electrophoresis was run after a 15 min incubation time. b) Polyplexes were incubated in a citrate buffer (0.2 M, pH 5.0) for 24 h before gel electrophoresis was performed to allow for PGAm depolymerization. Images are shown in negative contrast.

6.2.4 Polyplex Characterization

To further investigate the polyplexes formed between the PGAm and pDNA, DLS and transmission electron microscopy (TEM) were employed to examine the polyplexes at an N/P ratio of 50. For DLS, the polyplexes were prepared in purified water and allowed to incubate for 15 minutes before being examined. The polyplexes were then diluted with a 20 mM saline solution for zeta potential measurements. In general, the polyplexes had Z-average diameter sizes below 100 nm and low polydispersity indices (PDIs) of ~ 0.2 (Table 6.2). The PGAm-MAEs showed very similar results regardless of the end-cap employed, with the smallest Z average diameters among all of the samples (40–49 nm). When the zeta potentials of these polyplexes were measured, values of 34–40 mV were obtained, reflecting the overall positive charge and stability of the polyplexes. The PGAm-DMAPrs had similar Z-average diameters with the exception of **PGAm-DMAPr-MMT**, which had a diameter of 97 nm. This discrepancy between the end-caps is most likely due to the fast

depolymerization behaviour of the MMT polymer, which in turn should result in less stable and larger polyplexes. All of the PGAm-DMAPrs had positive zeta potentials ranging from 20–25 mV, which agrees well with their larger diameters and end-cap dependence when compared to the more stable PGAm-MAE polyplexes. The PGAm-DMAEs polyplexes exhibited the greatest variation between the different PGAm end-caps employed. While **PGAm-DMAE-Trit** polyplexes had a diameter of 79 nm, the other PGAm-DMAE polymers produced large micron sized aggregates when mixed with the pDNA in purified water. Dilution in saline solution did not improve the measurements, however, filtration through a syringe filter removed most of the aggregates, allowing for the measurement of polyplexes under 100 nm in diameter. PDIs for **PGAm-DMAE-MMT** and **PGAm-DMAE-BOM** were quite high after filtration, likely due to the dilute solutions possessing a lower count rate. Zeta potential measurements of the PGAm-DMAEs revealed low positive values ranging from 10–18 mV, explaining the partial instability of some of the suspensions and the observation of aggregates.

Table 6.2. Diameter, PDI, and zeta potential measurements of the polyplexes obtained using DLS (N/P = 50). Values given are the averages and standard deviations of the three measurements obtained of each sample.

Polymer	Z Average Diameter (nm)	PDI	Zeta Potential (mV)
PGAm-MAE-Trit	49 ± 0.2	0.20 ± 0.004	34 ± 1
PGAm-MAE-MMT	40 ± 0.1	0.14 ± 0.01	40 ± 2
PGAm-MAE-BOM	41 ± 1	0.20 ± 0.01	39 ± 1
PGAm-DMAE-Trit	79 ± 1	0.06 ± 0.02	18 ± 1
PGAm-DMAE-MMT^a	59 ± 2	0.54 ± 0.02	10 ± 1
PGAm-DMAE-BOM^a	97 ± 11	0.60 ± 0.10	16 ± 1
PGAm-DMAPr-Trit	43 ± 1	0.21 ± 0.02	20 ± 1
PGAm-DMAPr-MMT	97 ± 3	0.04 ± 0.02	23 ± 1
PGAm-DMAPr-BOM	50 ± 0.2	0.15 ± 0.01	25 ± 1

^aFiltered through a 0.45 µm Nylon syringe filter before size and zeta potentials were read in 10 mM saline solution.

TEM images of the polyplexes at an N/P ratio of 50 were obtained by preparing the polyplexes in purified water and drop casting them onto copper grids to dry, followed by

the application of a uranyl acetate stain to provide contrast. The PGAm-DMAE polyplexes generally appeared as spherical particles smaller than 100 nm, that did not stain with uranyl acetate, indicative of fully complexed pDNA (Figure 6.4a–c). However, **PGAm-DMAE-MMT** polyplexes differed from the other end-caps in that multiple dark spheres were also present along with the larger particles. Given that this polymer may have depolymerized to a greater degree than the other PGAm-DMAEs by the time it was imaged, it is likely that these dark spheres are composed of partially complexed pDNA that was not sufficiently shielded from the uranyl acetate stain. The PGAm-DMAPr polyplexes were larger and more irregular shaped (Figure 6.4d–f). These morphologies may result from a reduced capacity of the PGAm-DMAPrs to condense pDNA compared to the other PGAm studied. The PGAm-MAEs, on the other hand, produced the smallest polyplexes with a spherical morphology (Figure 6.4g–i), likely indicative of their strong capacity to condense pDNA, as noted previously in section 6.2.3. Interestingly, some dark spheres were present in the TEM images of the PGAm-MAEs, especially with **PGAm-MAE-Trit**. This may again be attributed to partial polymer depolymerization between polyplex preparation and imaging. In general, the TEM images agreed well with the DLS size data discussed above. Nevertheless, by TEM we did not observe aggregates for **PGAm-DMAE-MMT** and **PGAm-DMAE-BOM** as indicated by the DLS studies (Figure 6.4b, c). DLS is highly sensitive to large aggregates.

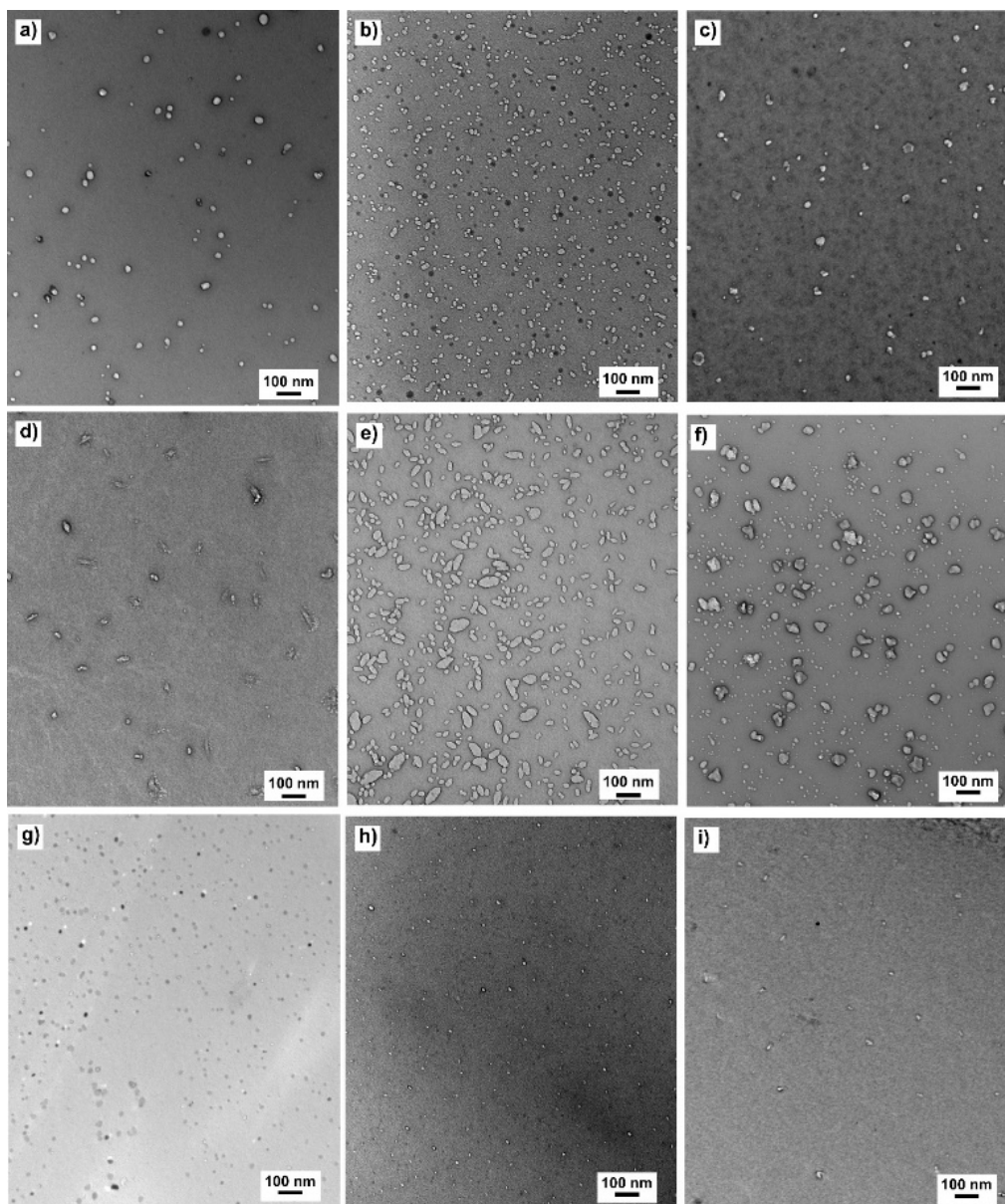


Figure 6.4. TEM images of pDNA-polycation polyplexes (N/P ratio = 50). The polyplexes were prepared in purified water and dried on a Formvar coated copper grid and then stained with a uranyl acetate solution: a) PGAm-DMAE-Trit, b) PGAm-DMAE-MMT, c) PGAm-DMAE-BOM, d) PGAm-DMAPr-Trit, e) PGAm-DMAPr-MMT, f) PGAm-DMAPr-BOM, g) PGAm-MAE-Trit, h) PGAm-MAE-MMT, i) PGAm-MAE-BOM.

6.2.5 Cytotoxicity Assays

One hypothesis underlying the choice of SIPs for nucleic acid delivery was that these depolymerizable polycationic PGAMs would be less cytotoxic than commonly used polycations such as PEI, which is not considered degradable. To test this hypothesis, we incubated (48 h) the PGAMs with HEK 293T cells, a commonly used cell line in DNA transfection studies, and evaluated their effects on metabolic activity using 3-(4,5-dimethylthiazol-2-yl)-2,5-diphenyltetrazolium bromide (MTT) assays. We also tested the three different depolymerization products *N,N*-dimethylaminoethyl glyoxylamide hydrate (**DMAE**), *N,N*-dimethylaminopropyl glyoxylamide hydrate (**DMAPr**), and *N*-methylaminoethyl glyoxylamide hydrate (**MAE**), as well as jetPEI.

All of the tested molecules exhibited concentration-dependent toxicity (Figure 6.5). As expected, jetPEI was highly toxic, with only 60% metabolic activity at 0.25 $\mu\text{g/mL}$ and less than 5% activity at 4.0 $\mu\text{g/mL}$, which is 4-fold lower than the minimum concentration tested for the PGAMs. This toxicity can be attributed to the high charge density of PEI as well as its non-degradable nature.^{4, 12} Of the PGAMs, the most toxic were the PGAM-MAEs. While these polymers showed low cytotoxicity at the lowest concentration tested (16 $\mu\text{g/mL}$), they led to less than 60% metabolic activity at 31 $\mu\text{g/mL}$, regardless of the end-cap, and with no toxicity decrease in the monomeric (depolymerized) form. However, they were still much less toxic than jetPEI. The PGAM-DMAEs and PGAM-DMAPrs, with tertiary amine pendent groups, were even less toxic and exhibited further reduced toxicities in their monomeric forms. Notably, **PGAM-DMAE-MMT** and **PGAM-DMAPr-MMT** exhibited similar effects on cellular metabolic activity to their monomeric forms, which can be attributed to the rapid depolymerization of these polymers. Unexpectedly, the control polymers **PGAM-DMAE-BOM** and **PGAM-DMAPr-BOM** exhibited less cytotoxicity than their trityl analogues, despite not being degradable. A possible explanation for this result may be the somewhat lower molecular weights of these polymers, which has been shown with other polycations like PEI and PLL to decrease toxicity overall.¹¹

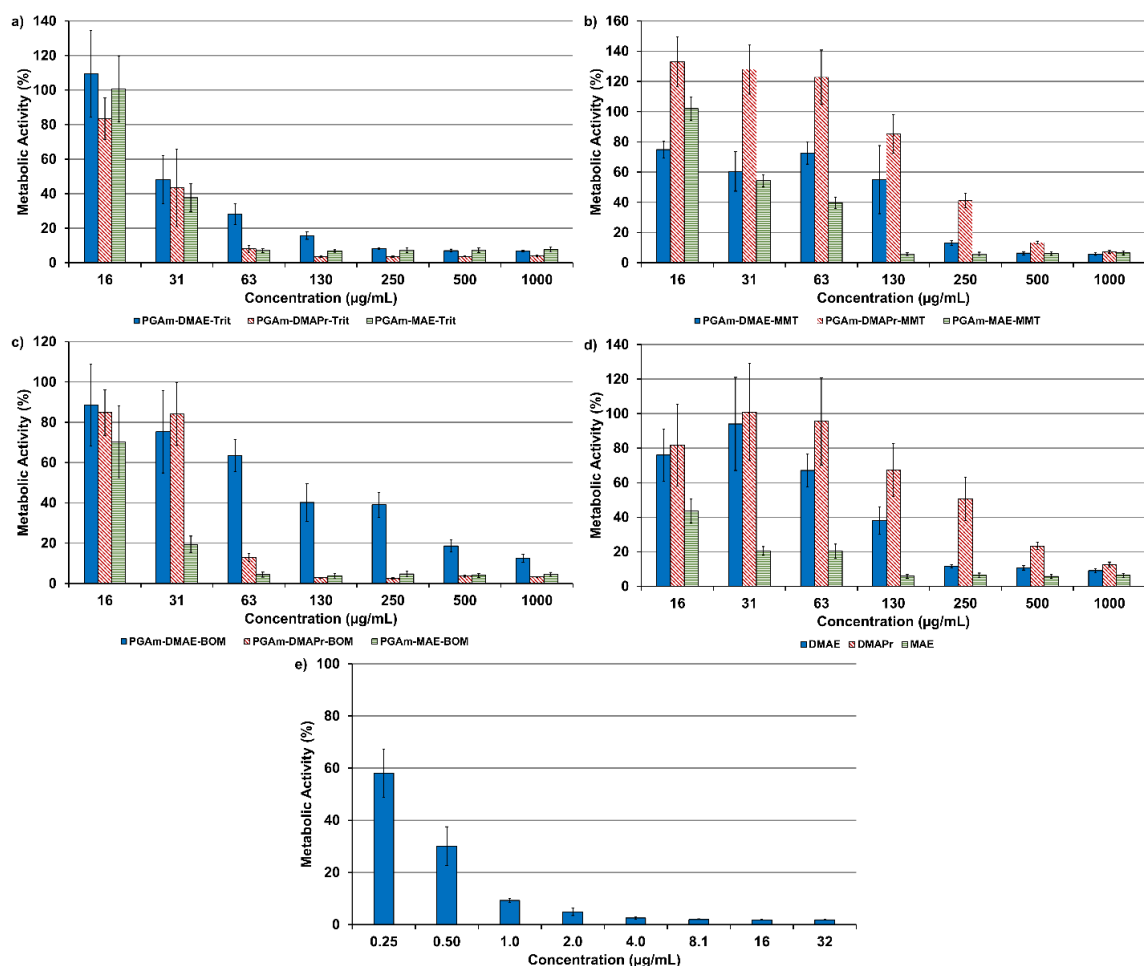


Figure 6.5. MTT assays of HEK 293T cells treated with varying concentrations of the PGAm-Trits, PGAm-MMTs, PGAm-BOMs, Glyoxylamide hydrate monomers produced during the depolymerization of the PGAm-Trits after end-cap cleavage, jetPEI. The results are expressed the percent activity relative to cells not exposed to polymers (culture media alone). Error bars represent the standard deviation of the replicate (n = 6) measurements.

At low polycation concentrations, we unexpectedly found that many of the tested materials resulted in metabolic activities higher than 100% compared to control cells that were not exposed to polymers. This phenomenon has been noted in the literature before and was discussed by Monnery *et al.* during their investigation of polycation toxicity in relation to molecular weight.¹¹ The authors proposed that since polycations damage cell membranes without outright killing the cells at low concentrations, the affected cells would have higher

metabolic activities as they attempt to repair themselves. Thus, MTT assay results would be higher for the damaged cells than they would be for the untreated cells.

Additionally, because transfection is performed using polyplexes rather than just polycations alone, we also investigated using MTT assays HEK 293T cells that had been treated with pDNA-polycation polyplexes at different N/P ratios. The pDNA concentration was fixed at 1.5 $\mu\text{g/mL}$, as would be used in the subsequent transfection experiments. Overall, the PGAm polyplexes exhibited low cytotoxicities, particularly compared to polyplexes prepared with jetPEI (Figure A5.56). Similar levels of metabolic activity were obtained compared to those of the PGAm polycations alone when considering the concentration of PGAm in the polyplexes. MMT end-capped PGAm polyplexes had the lowest cytotoxicities as a result of their breakdown to monomers during the experiment. Of the three different PGAm pendent groups examined, PGAm-DMAE polyplexes retained the highest metabolic activities at the highest N/P ratios.

6.2.6 Transfection Assays

To evaluate the effectiveness of the new PGAmS as FLuc pDNA transfection agents, luminescence assays were performed on HEK 293T cells using polyplexes with different N/P ratios and the results were compared to those obtained with jetPEI. After incubation of the polyplexes with the cells for 24 h, D-luciferin was added to visualize the transfection efficiency (Figure 6.6). Among the samples tested, jetPEI resulted in the highest transfection efficiency at the manufacturer's recommended N/P ratio of 5, with slightly lower efficiencies at $N/P > 5$. Of the PGAmS tested, **PGAm-DMAE-Trit**, **PGAm-MAE-Trit**, **PGAm-DMAE-BOM**, and **PGAm-MAE-BOM** all demonstrated some level of transfection, with all except **PGAm-DMAE-BOM** producing transfection comparable to jetPEI at higher N/P ratios. The need for higher N/P ratios for the PGAmS to obtain similar transfection efficiencies as jetPEI may be due to the reduced charge density of the PGAmS, resulting in a need for more polymer to obtain stable polyplexes. The MMT end-capped PGAmS as well as the PGAm-DMAPrs did not show any appreciable transfection. The results with the MMT end-cap can be explained by the rapid depolymerization of these

polyplexes before transfection could occur. The poor efficiency of the PGAm-DMAPrs can likely be explained by their weak binding to the DNA, as described above.

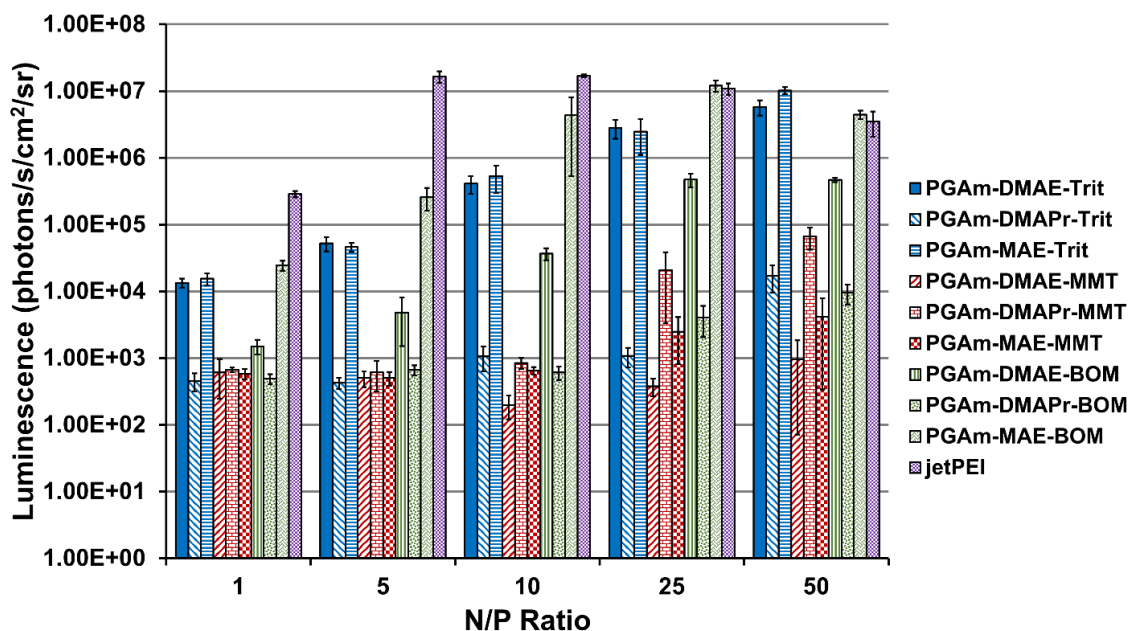


Figure 6.6. Transfection of HEK 293T cells with pDNA for FLuc using PGAm and jetPEI polyplexes at different N/P ratios, as measured by luminescence assay (pDNA concentration = 1.5 $\mu\text{g/mL}$). Cells were incubated for 24 h after being treated with polyplex before the assay was performed. Error bars represent the standard deviation of the replicate ($n = 3$) measurements.

In addition to toxicity considerations, an additional initial motivation for exploring polycationic PGAm as potential transfection agents was that depolymerization of the PGAm would facilitate release the pDNA in the cell, leading to greater cell transfection efficiencies. For **PGAm-DMAE-Trit**, which consistently exhibited an order of magnitude higher luminescence than **PGAm-DMAE-BOM** at any given N/P ratio, release of pDNA may have indeed been assisted by depolymerization. Given the depolymerization kinetics of **PGAm-DMAE-Trit**, polyplexes constructed with this polymer would have ample time to enter the cell before any significant depolymerization would occur. Subsequent trafficking to acidic endosomes would then enhance the rate of depolymerization. However, a comparison of **PGAm-MAE-Trit** and **PGAm-MAE-BOM** surprisingly did

not show the same trend, with the latter outperforming the former at all N/P ratios except for 50. Since **PGAm-MAE-Trit** does not depolymerize much faster than **PGAm-DMAE-Trit**, it is unlikely premature depolymerization of the polycation and destruction of the polyplexes could explain this result. Rather, it may be that the secondary amine pendent groups of these polymers excel at both polyplex formation and endosomal escape, with pDNA release occurring in some other fashion. In this way, both of these PGAm-MAE polymers may undergo a similar transfection mechanism to PEI.

6.3 Conclusions

A library of self-immolative polycationic PGAmS with varying pendent amino groups and end-caps were synthesized from precursor PEtGs. The PGAmS were all readily soluble in water and varied in their depolymerization kinetics, depending on both their pendent groups and end-caps. All of the polymers were found to complex with pDNA, with the less sterically hindered pendent groups leading to complete pDNA complexation at lower N/P ratios. With an acidic stimulus applied, stimuli-responsive polyplexes were able to release their pDNA payloads as the polycations depolymerized. Cytotoxicity assays confirmed that all of the PGAmS synthesized were substantially less toxic than jetPEI, a commercial transfection agent. Furthermore, PGAmS with pendent groups possessing tertiary amines exhibited decreased toxicity when depolymerized to their monomer units, highlighting their potential to possess a high density of cationic charge necessary for polyplex formation yet depolymerize into less toxic by-products once transfection has occurred. Finally, transfection assays revealed that some of the PGAmS had transfection efficiencies similar to jetPEI. Of the PGAmS investigated, **PGAm-DMAE-Trit** was the most promising as it possesses the best balance of transfection efficiency and toxicity. Overall, this work demonstrates the use of PGAmS as the first examples of fully self-immolative polycationic transfection agents. Given their promise, future work should focus on further exploring their mechanisms of nucleic acid release and their behaviour *in vivo*.

6.4 Experimental

6.4.1 General Experimental Details

General Materials. Ethyl glyoxylate in toluene solution (50% w/w), *N,N*-dimethylethylenediamine, *N*-methylethylenediamine, 4-monomethoxytrityl chloride, AgOTf, and citric acid were obtained from Alfa Aesar. *n*-Butyl lithium in toluene solution (1.4 M), benzyl chloromethyl ether, 3-(dimethylamino)-1-propylamine, trityl chloride, and Tris acetate EDTA buffer solution were obtained from Sigma Aldrich. NEt₃ and KH₂PO₄ were obtained from Millipore. NaOH and KOH were obtained from Thermo Fisher Scientific. jetPEI solution was obtained from Polyplus-transfection SA. Agarose gel solution (1% w/v), RedSafe electrophoresis stain, and a 1 kb DNA ladder were obtained from FroggBio. Gel electrophoresis loading dye was obtained from New England Biolabs. Uranyl acetate and 400 mesh Formvar-coated copper grids were obtained from Electron Microscopy Sciences. Dulbecco's Modified Eagle's Medium with 10% v/v fetal bovine serum and antibiotic-antimycotic was obtained from VWR. MTT was obtained from Gibco. D-luciferin was obtained from Thermo Fischer. Ethyl glyoxylate was purified over P₂O₅ as previously reported.³⁸ Toluene was distilled over sodium and benzophenone under a nitrogen atmosphere before use. NEt₃ was distilled over CaH₂ under a nitrogen atmosphere before use. Purified water was obtained from VWR or from a Barnstead EASYpure II system. pDNA used for the complexation and transfection experiments was composed of a human elongation factor 1 alpha promotor driven plasmid expressing tdTomato and FLuc separated by a self-cleaving 2A peptide. The pDNA was produced by transfecting ZYCY10P3S2T *E. coli* and viable kanamycin-resistant colonies were selected and cultured at 37 °C in lysogeny broth overnight. The bacteria were then pelleted and isolated using an endotoxin-free Maxi kit (Qiagen) according to the manufacturer's instructions. All other chemicals were of reagent grade and were used without further purification.

General Methods. ¹H and ¹³C NMR spectra were obtained using a 400 MHz Bruker AvIII HD instrument, a 400 MHz Varian INOVA instrument, or a 600 MHz Varian INOVA instrument. ¹H NMR chemical shifts were calibrated against the residual solvent signal of

CHCl_3 (7.26 ppm) or HOD (4.79 ppm) while ^{13}C NMR chemical shifts were calibrated against the solvent signal of CDCl_3 (77.16 ppm). FT-IR spectra were obtained using a PerkinElmer FT-IR Spectrum Two instrument with attenuated total reflectance (ATR) sampling. Size-exclusion chromatograms were obtained using a DMF chromatograph equipped with a Waters 515 HPLC pump with a Waters In-Line Degasser AF, two PLgel mixed D 5 μm (300×1.5 mm) columns connected to a corresponding PLgel guard column, and a Wyatt Optilab Rex RI detector. Samples were dissolved in DMF containing 10 mM LiBr and 1% v/v NEt_3 at a concentration of ~ 5 mg/mL. Each sample was filtered through a 0.2 μm polytetrafluoroethylene syringe filter prior to injection using a 50 μL loop. Samples were run at a flow rate of 1 mL/min for 30 min at 85 $^\circ\text{C}$. Molar masses of the samples were calculated relative to PMMA standards. Gel electrophoresis was performed using agarose gel in a Tris acetate EDTA running buffer at an applied voltage of 100 V for 1 h. Gels were subsequently imaged using a Gel Doc (Biorad). DMEM was used as the media for all HEK 293T cell culture experiments. Dynamic light scattering measurements were obtained using a Malvern Zetasizer Nano ZS instrument equipped with a 633 nm laser and at a scattering angle of 173 $^\circ$. Transmission electron microscopy images were obtained using a Phillips Electron Optics CM10 transmission electron microscope operating at 80 kV. Visible light absorbance of cell culture wells was recorded using a Tecan Infinite M1000 Pro plate reader. Luminescence readings of the transfected cells were obtained using a PerkinElmer IVIS Lumina XRMS scanner. Cell plates were continually imaged until a peak signal was achieved. Average radiance per well was quantified by placing regions of interest over each well using Living Image 4.5.2 software.

6.4.2 Synthesis of PEtG

*All PEtGs were synthesized using the same procedure as **PEtG-Trit** (representative PEtG synthesis).*

Synthesis of PEtG-Trit (representative PEtG synthesis). AgOTf (1.0 g, 3.9 mmol, 9.5 equiv) and trityl chloride (1.1 g, 3.9 mmol, 9.5 equiv) were added to a flask, which was subsequently evacuated and purged with nitrogen. A 10 mL aliquot of dry toluene was then added, and the flask was stirred and heated at 70 $^\circ\text{C}$ for 1 h to yield the end-capping

mixture. Separately, 40 mL of dry toluene was added to a flame-dried Schlenk flask under a nitrogen atmosphere along with *n*-butyl lithium (0.29 mL, 0.41 mmol, 1.0 equiv) Purified ethyl glyoxylate (10 mL, 100 mmol, 240 equiv) was subsequently added to the flask and the system was stirred and cooled at $-20\text{ }^{\circ}\text{C}$. After 30 min, dry NEt_3 (1.1 mL, 7.9 mmol, 19 equiv) was added to the polymerization flask and the mixture was allowed to stir for another 30 min. The end-capping mixture was then cooled to $-20\text{ }^{\circ}\text{C}$ before being transferred with a wide mouth pipette to the polymerization flask. The polymerization flask was stoppered and stirred at $-20\text{ }^{\circ}\text{C}$ for 4 h before being allowed to warm up to room temperature over 16 h. Concentration of the crude polymerization mixture under vacuum followed by filtration and precipitation in 440 mL of $\text{MeOH}:\text{H}_2\text{O}$ (10:1) afforded 6.9 g of pure polymer residue as a clear off-yellow tacky solid, which was collected by decanting off the supernatant and concentrating under vacuum. Yield = 67%. ^1H NMR (CDCl_3 , 400 MHz): δ 7.42–7.49 (m, 7H), 7.09–7.33 (m, 54H), 5.46–5.74 (m, 241H), 4.21 (br s, 485H), 1.27 (br s, 696H), 0.88 (br s, 3H). $^{13}\text{C}\{^1\text{H}\}$ NMR (CDCl_3 , 100 MHz): δ 166.1–166.5, 127.2–129.8, 90.4–94.3, 62.2, 14.0. FT-IR (ATR): 2990, 1750 cm^{-1} . SEC (DMF, PMMA): $M_n = 21.4\text{ kg/mol}$, $M_w = 36.4\text{ kg/mol}$, $D = 1.7$.

Synthesis of PEtG-MMT. 4-monomethoxytrityl chloride (1.2 g, 3.9 mmol, 9.5 equiv) was used to afford 6.0 g of a clear off-yellow tacky solid. Yield = 58%. ^1H NMR (CDCl_3 , 400 MHz): δ 7.38–7.51 (m, 6H), 7.08–7.38 (m, 45H), 6.78–6.87 (m, 3H), 5.42–5.78 (m, 210H), 4.22 (br s, 416H), 3.74–3.81 (m, 7H), 1.29 (br s, 623H), 0.88 (br s, 3H). $^{13}\text{C}\{^1\text{H}\}$ NMR (CDCl_3 , 100 MHz): δ 165.2–166.5, 127.2–129.6, 90.6–94.4, 62.2, 14.0. FT-IR (ATR): 2990, 1750 cm^{-1} . SEC (DMF, PMMA): $M_n = 18.8\text{ kg/mol}$, $M_w = 33.0\text{ kg/mol}$, $D = 1.8$.

Synthesis of PEtG-BOM. Dry NEt_3 (2.2 mL, 16 mmol, 39 equiv) and 60% benzyl chloromethyl ether (1.9 mL, 8.2 mmol, 20 equiv) were used at the 30 min and 1 h mark of the reaction respectively. After addition of the benzyl chloromethyl ether, the reaction flask was stirred for 1 h at $-20\text{ }^{\circ}\text{C}$ before it was transferred to a $-20\text{ }^{\circ}\text{C}$ freezer for 4 days, stirring occasionally. Purification afforded 5.9 g of a clear, colourless, tacky solid. Yield = 57%. ^1H NMR (CDCl_3 , 400 MHz): δ 7.30–7.35 (m, 6H), 5.43–5.77 (m, 156H), 4.22 (br s, 307H), 1.29 (br s, 465H), 0.84–0.93 (m, 3H). $^{13}\text{C}\{^1\text{H}\}$ NMR (CDCl_3 , 100 MHz): δ 165.2–166.7,

127.8–129.3, 90.7–94.2, 62.2, 14.0. FT-IR (ATR): 2990, 1750 cm^{-1} . SEC (DMF, PMMA): $M_n = 16.5$ kg/mol, $M_w = 22.7$ kg/mol, $D = 1.4$.

6.4.3 Synthesis of PGAmS

All PGAmS were synthesized using the same procedure as PGAm-DMAE-Trit (representative PGAm synthesis).

Synthesis of PGAm-DMAE-Trit (representative PGAm synthesis). PEtG-Trit (0.30 g of polymer, 2.9 mmol of ester, 1.0 equiv) was dissolved in 6.0 mL of 1,4-dioxane in a vial. *N,N*-Dimethylethylenediamine (0.96 mL, 8.8 mmol, 3.0 equiv) was added to the solution and the vial was sealed and stirred for 16 h at room temperature. The crude mixture was concentrated and precipitated in 50 mL of *n*-pentane. After decanting, the purified polymer residue was dried to afford 0.40 g of a clear, colourless, brittle solid. Yield = 94%. ^1H NMR (CDCl_3 , 400 MHz): δ 7.63–8.92 (m, 230H), 7.45–7.51 (m, 6H), 5.72 (br s, 211H), 3.32 (br s, 451H), 2.43 (br s, 403H), 2.22 (br s, 1160H). $^{13}\text{C}\{^1\text{H}\}$ NMR (CDCl_3 , 100 MHz): δ 166.0–168.2, 94.6–98.5, 58.0, 45.5, 37.5. FT-IR (ATR): 3274, 3085, 2944, 2860, 2820, 2768, 1666, 1539 cm^{-1} . SEC (DMF, PMMA): $M_n = 26.7$ kg/mol, $M_w = 45.7$ kg/mol, $D = 1.7$.

Synthesis of PGAm-DMAPr-Trit. 3-(dimethylamino)-1-propylamine (1.1 mL, 8.7 mmol, 3.0 equiv) was used to afford 0.38 g of a clear, colourless, tacky solid. Yield = 82%. ^1H NMR (CDCl_3 , 400 MHz): δ 8.12–9.05 (m, 210H), 7.43–7.51 (m, 6H), 5.71 (br s, 216H), 3.25 (br s, 408H), 2.30 (br s, 403H), 2.17 (br s, 1215H), 1.66 (br s, 413H). $^{13}\text{C}\{^1\text{H}\}$ NMR (CDCl_3 , 100 MHz): δ 166.0–168.0, 94.8–98.5, 57.3, 45.4, 38.2, 26.8. FT-IR (ATR): 3270, 3080, 2940, 2860, 2820, 2760, 1670, 1540 cm^{-1} . SEC (DMF, PMMA): $M_n = 28.4$ kg/mol, $M_w = 46.6$ kg/mol, $D = 1.6$.

Synthesis of PGAm-MAE-Trit. 0.36 g of PEtG-Trit (3.5 mmol of ester, 1.0 equiv) and *N*-methylethylenediamine (0.92 mL, 11 mmol, 3.1 equiv) were used to afford 0.44 g of a white brittle solid. Yield = 96%. ^1H NMR (CDCl_3 , 400 MHz): δ 7.99–9.10 (m, 184H), 7.40–7.50 (m, 6H), 5.70 (br s, 217H), 3.34 (br s, 448H), 2.71 (br s, 472H), 2.37 (br s, 681H). $^{13}\text{C}\{^1\text{H}\}$ NMR (CDCl_3 , 100 MHz): δ 167.3, 96.5, 50.5, 39.2, 36.0. FT-IR (ATR): 3290, 3070, 2930, 2890, 2850, 2800, 1660, 1540 cm^{-1} .

Synthesis of PGAm-DMAE-MMT. PEtG-MMT (0.30 g of polymer, 2.9 mmol of ester, 1.0 equiv) was used to afford 0.36 g of a clear, colourless, brittle solid. Yield = 85%. ^1H NMR (CDCl_3 , 400 MHz): δ 7.77–8.92 (m, 198H), 7.40–7.52 (m, 9H), 7.20–7.40 (m, 70H), 6.78–6.85 (m, 4H), 5.73 (br s, 196H), 3.78 (br s, 6H), 3.32 (br s, 335H), 2.43 (br s, 323H), 2.22 (br s, 959H). $^{13}\text{C}\{^1\text{H}\}$ NMR (CDCl_3 , 100 MHz): δ 166.0–168.3, 94.6–98.7, 58.1, 45.6, 37.6. FT-IR (ATR): 3270, 3080, 2940, 2860, 2820, 2770, 1670, 1540 cm^{-1} . SEC (DMF, PMMA): $M_n = 24.4$ kg/mol, $M_w = 44.9$ kg/mol, $D = 1.8$.

Synthesis of PGAm-DMAPr-MMT. PEtG-MMT (0.30 g of polymer, 2.9 mmol of ester, 1.0 equiv) and 3-(dimethylamino)-1-propylamine (1.1 mL, 8.7 mmol, 3.0 equiv) were used to afford 0.37 g of a clear, colourless, tacky solid. Yield = 80%. ^1H NMR (CDCl_3 , 400 MHz): δ 8.15–9.01 (m, 229 H), 7.42–7.53 (m, 8H), 7.15–7.42 (m, 74H), 6.76–6.86 (m, 4H), 5.72 (br s, 218 H), 3.77 (br s, 6H), 3.25 (br s, 428 H), 2.30 (br s, 434H), 2.18 (br s, 1301H), 1.66 (br s, 439H). $^{13}\text{C}\{^1\text{H}\}$ NMR (CDCl_3 , 100 MHz): δ 167.1, 96.6, 57.4, 45.5, 38.3, 26.7. FT-IR (ATR): 3270, 3090, 2940, 2860, 2820, 2760, 1670, 1540 cm^{-1} . SEC (DMF, PMMA): $M_n = 26.4$ kg/mol, $M_w = 42.9$ kg/mol, $D = 1.6$.

Synthesis of PGAm-MAE-MMT. PEtG-MMT (0.30 g of polymer, 2.9 mmol of ester, 1.0 equiv) and *N*-methylethylenediamine (0.77 mL, 8.8 mmol, 3.0 equiv) were used to afford 0.35 g of a white, brittle solid. Yield = 92%. ^1H NMR (CDCl_3 , 400 MHz): δ 7.97–9.22 (m, 196H), 7.38–7.51 (m, 8H), 7.71–7.38 (m, 62H), 6.78–6.86 (m, 4H), 5.71 (br s, 193H), 3.78 (br s, 6H), 3.36 (br s, 402H), 2.72 (br s, 629H), 2.38 (br s, 613H). $^{13}\text{C}\{^1\text{H}\}$ NMR (CDCl_3 , 100 MHz): δ 167.3, 96.6, 50.4, 39.1, 36.0. FT-IR (ATR): 3290, 3080, 2940, 2850, 2800, 1660, 1540 cm^{-1} .

Synthesis of PGAm-DMAE-BOM. PEtG-BOM (0.30 g of polymer, 2.9 mmol of ester, 1.0 equiv) was used to afford 0.23 g of a clear, pale-yellow, brittle solid. Yield = 54%. ^1H NMR (CDCl_3 , 400 MHz): δ 7.74–8.82 (m, 173H), 7.30–7.34 (m, 5H), 5.72 (s, 162H), 3.32 (s, 305H), 2.43 (s, 302H), 2.22 (s, 878H). $^{13}\text{C}\{^1\text{H}\}$ NMR (CDCl_3 , 100 MHz): δ 167.3, 95.0–97.9, 58.1, 45.5, 37.5. FT-IR (ATR): 3280, 3090, 2950, 2360, 2820, 2770, 1670, 1540 cm^{-1} . SEC (DMF, PMMA): $M_n = 24.5$ kg/mol, $M_w = 42.2$ kg/mol, $D = 1.7$.

Synthesis of PGAm-DMAPr-BOM. PEtG-BOM (0.30 g of polymer, 2.9 mmol of ester, 1.0 equiv) and 3-(dimethylamino)-1-propylamine (1.1 mL, 8.7 mmol, 3.0 equiv) were used to afford 0.15 g of a clear, colourless, tacky solid. Yield = 32%. ^1H NMR (CDCl_3 , 400 MHz): δ 8.19–9.00 (m, 150H), 7.30–7.34 (m, 5H), 5.72 (s, 156H), 3.25 (s, 265H), 2.29 (s, 397H), 2.71 (s, 821H), 1.66 (s, 287H). $^{13}\text{C}\{^1\text{H}\}$ NMR (CDCl_3 , 100 MHz): δ 167.2, 96.5, 57.5, 45.5, 38.2, 27.0. FT-IR (ATR): 3270, 3090, 2940, 2860, 2820, 2770, 1670, 1540 cm^{-1} . SEC (DMF, PMMA): $M_n = 24.0$ kg/mol, $M_w = 34.2$ kg/mol, $D = 1.4$.

Synthesis of PGAm-MAE-BOM. PEtG-BOM (0.30 g of polymer, 2.9 mmol of ester, 1.0 equiv) and *N*-methylethylenediamine (0.77 mL, 8.8 mmol, 3.0 equiv) were used and the crude was precipitated in Et_2O to afford 0.25 g of an off-white, brittle solid. Yield = 65%. ^1H NMR (CDCl_3 , 400 MHz): δ 8.08–9.17 (m, 140H), 7.30–7.34 (m, 5H), 5.71 (br s, 139H), 3.37 (br s, 293H), 2.73 (br s, 519 H), 2.39 (br s, 370H). $^{13}\text{C}\{^1\text{H}\}$ NMR (CDCl_3 , 100 MHz): δ 167.1, 96.4, 50.5, 39.1, 36.0. FT-IR (ATR): 3290, 3090, 2940, 2850, 2800, 1660, 1540 cm^{-1} .

6.4.4 Depolymerization of PGAMs

Deuterated pH 5.0 and 6.0 buffers were prepared by dissolving citric acid into D_2O followed by correction to the desired pH with NaOH. Deuterated pH 7.4 buffer was prepared by dissolving KH_2PO_4 into D_2O followed by correction to the desired pH with KOH. All buffers were made at a 0.2 M concentration. To examine the depolymerization of the PGAMs, each PGAM was dissolved into each buffer solution at 10 mg/mL and placed into an NMR tube. The tubes were promptly sealed, and the solutions were monitored over time via ^1H NMR spectroscopy. Percent depolymerization at any one time point was determined by comparing the integration value of the polymer backbone methine proton peak at ~ 5.6 ppm with that of the monomer hydrate methine proton peak at ~ 5.3 ppm. For PGAm-MAE samples, an additional peak (corresponding to the monomer hemiaminal methine proton peak) was observed at ~ 4.5 ppm and its integration value was combined with that of the monomer hydrate.

6.4.5 Complexation of PGAMs with pDNA

Each of the PGAMs was dissolved in purified water to prepare 1.0 mg/mL solutions immediately prior to being used. An appropriate aliquot of each solution was mixed with 300 ng of pDNA and purified water was added to the mixture to make up a total volume of 20 μ L. Aliquots of the PGAM solutions were determined using Equation 6.1 and selecting for N/P ratios of 1, 5, 10, 25, and 50:

$$\text{Equation 6.1.} \quad v = \frac{rm(3 \text{ nmol}/\mu\text{g})}{c}$$

where v = volume of aliquot, r = N/P ratio, m = mass of pDNA (in μ g), and c = molarity of cationic nitrogen in the polymer solution (in mM; for PGAM-DMAE samples, c = 6.9 mM; for PGAM-DMAPr samples, c = 6.3 mM; and for PGAM-MAE samples, c = 7.7 mM). The polyplex mixtures were incubated for 15 min before each being placed in a well and gel electrophoresis was run. Examination of the gels afterwards revealed pDNA travel through the gels, with delayed travel of the pDNA compared to the lane with pDNA only (N/P ratio = 0) indicative of the presence of polyplexes.

6.4.6 Triggered Decomplexation of the Polyplexes

Each of the PGAMs was dissolved in purified water to prepare 1.0 mg/mL solutions immediately prior to being used. Aliquots of polymer solution needed to prepare 50 N/P ratio polyplex mixtures were calculated using Equation 6.1 and mixed with 300 ng of pDNA. For each polyplex tested, two different polyplex mixtures were prepared. One mixture was diluted with purified water to a total volume of 20 μ L before being loaded into a gel and run through electrophoresis. The other mixture was diluted with concentrated citrate buffer to a total volume of 20 μ L and a final buffer concentration of 0.2 M. The buffered polyplexes were stored at room temperature for 1 day before being loaded into a gel and run through electrophoresis. Examination of the gels after electrophoresis revealed pDNA travel through the gel, with delayed travel of the pDNA compared to the lane with pDNA only (N/P ratio = 0) indicative of the presence of polyplexes.

6.4.7 DLS of the Polyplexes

Each of the PGAMs was dissolved in purified water to prepare 10 mg/mL solutions immediately prior to use. Appropriate aliquots of each PGAM solution for a N/P ratio of 50 (determined using Equation 6.1) were added to 10 μg of pDNA along with purified water to give a final volume of 500 μL . The samples were then examined for size before being further diluted with 500 μL of 20 mM saline solution and examined for zeta potential. For samples **PGAM-DMAE-MMT** and **PGAM-DMAE-BOM**, the final dilute saline solutions each were filtered through a 0.45 μm Nylon syringe filter in order to remove aggregates before their sizes and zeta potentials were determined.

6.4.8 TEM of the Polyplexes

Each of the PGAMs was dissolved in purified water to prepare 10 mg/mL solutions immediately prior to use. Appropriate aliquots of each PGAM solution for a N/P ratio of 50 (determined using Equation 6.1) were added to 1.8 μg of pDNA and diluted to 9.0 μL using purified water. After incubation for 15 min, a drop of each polyplex suspension (0.20 $\mu\text{g}/\text{mL}$ of pDNA) was placed on a Formvar-coated copper TEM grid and allowed to sit for 5 min before wicking away the excess liquid. The grids were allowed to dry before being stained with a 1% w/v uranyl acetate solution. After excess stain was removed and the grids allowed to dry, each grid was loaded into the microscope and imaged.

6.4.9 Cell Cytotoxicity Assays for Polycations

HEK 293T cells were cultured in media and subsequently seeded in 96 well plates at a concentration of $\sim 10,000$ cells/well before being incubated at 37 $^{\circ}\text{C}$ under a 5% CO_2 atmosphere for 24 h. Following incubation, the media was aspirated and replaced with either the sodium dodecyl sulfate (SDS) in the cell media at concentrations of 200, 150, 100, or 50 $\mu\text{g}/\text{mL}$ (positive controls), just media (negative control), or the sample (PGAMs and monomers, jetPEI) in media (150 μL). Monomers were prepared from the PGAM-MMTs by dissolving them at 10 mg/mL in purified water and letting them sit at room temperature for at least 24 h before use to allow for complete depolymerization. For each PGAM sample, 10 mg was dissolved in 1.0 mL of purified water immediately prior to being

used and subsequently diluted to 10 mL with cell media. Each solution was further serially diluted 2-fold to obtain the following concentrations: 1000, 500, 250, 130, 63, 31, and 16 $\mu\text{g}/\text{mL}$. For the jetPEI sample, jetPEI solution provided by the manufacturer was diluted 10-fold with cell media to give a concentration of 32 $\mu\text{g}/\text{mL}$. This solution was further serially diluted 2-fold to obtain the following concentrations: 32, 16, 8.1, 4.0, 2.0, 1.0, 0.50, and 0.25 $\mu\text{g}/\text{mL}$. The cells were incubated for 48 h before the media was aspirated out and replaced with 110 μL of media containing 0.5 mg/mL of MTT reagent. After another 4 h of incubation, the media was aspirated out and replaced with 50 μL of dimethyl sulfoxide (DMSO). The plates were placed in a plate reader and each well's absorbance at 540 nm was read. Six replicates of each sample condition were measured. The mean absorbance of wells containing only DMSO was subtracted from the other readings as a background correction. Cell metabolic activity was calculated for each sample by comparing its mean absorbance with that of the negative control. No activity was observed for cells exposed to the highest concentrations of SDS, confirming the sensitivity of the assay.

6.4.10 Cell Cytotoxicity Assays for Polyplexes

Each of the PGAMs was dissolved in purified water to prepare 1.0 mg/mL solutions immediately prior to analysis. Additionally, jetPEI solution ($c = 7.5$ mM of cationic nitrogen) was used for comparison. An appropriate aliquot of each solution was mixed with 250 ng of pDNA and a 150 mM solution of NaCl was added to the mixture to make up a total volume of 20 μL (aliquots of the PGAM and jetPEI solutions were determined by using Equation 6.1 and selecting for N/P ratios of 0, 5, 10, 25, and 50). Each complex mixture was allowed to sit for 15 min after dilution to the final volume. HEK 293T cells were seeded and incubated in 96 well plates as described previously. After incubating the cells for 24 h and exchanging the used media with fresh media (150 μL), the complexes were added to the wells directly and the cells were incubated for an additional 48 h before the MTT assay was performed (see section 6.4.9 for additional details on the cell culturing and assay procedures).

6.4.11 Transfection Assays

PGAMs and jetPEI were prepared with pDNA as polyplexes as described in section 6.4.10. HEK 293T cells were prepared as described in section 6.4.9. After incubating the cells for 24 h and exchanging the used media with fresh media (150 μ L), the polyplex mixtures were added to the wells directly and the cells were incubated for an additional 24 h. D-luciferin was then added to the wells (final concentration 150 μ g/mL) and luminescence readings were taken to determine transfection efficiency. Due to the time sensitive nature of the luminescence assay, samples were only examined in triplicate.

6.5 References

- (1) Yan, Z.; McCray, P. B., Jr.; Engelhardt, J. F. Advances in Gene Therapy for Cystic Fibrosis Lung Disease. *Hum. Mol. Genet.* **2019**, *28*, R88–R94.
- (2) Hobernik, D.; Bros, M. DNA Vaccines—How Far From Clinical Use? *Int. J. Mol. Sci.* **2018**, *19*, 3605.
- (3) Song, X.; Liu, C.; Wang, N.; Huang, H.; He, S.; Gong, C.; Wei, Y. Delivery of CRISPR/Cas Systems for Cancer Gene Therapy and Immunotherapy. *Adv. Drug Delivery Rev.* **2020**, *168*, 158–180.
- (4) Pitard, B.; Habrant, D., Supramolecular Gene Transfection Agents. In *Comprehensive Supramolecular Chemistry II*; Atwood, J. L., Ed. Elsevier: Amsterdam, NL, 2017; pp 365–389.
- (5) Agarwal, S.; Zhang, Y.; Maji, S.; Greiner, A. PDMAEMA Based Gene Delivery Materials. *Mater. Today* **2012**, *15*, 388–393.
- (6) Bus, T.; Traeger, A.; Schubert, U. S. The Great Escape: How Cationic Polyplexes Overcome the Endosomal Barrier. *J. Mater. Chem. B* **2018**, *6*, 6904–6918.
- (7) Wu, G. Y.; Wu, C. H. Receptor-Mediated *In Vitro* Gene Transformation by a Soluble DNA Carrier System. *J. Biol. Chem.* **1987**, *262*, 4429–4432.
- (8) Cherng, J. Y.; van de Wetering, P.; Talsma, H.; Crommelin, D. J.; Hennink, W. E. Effect of Size and Serum Proteins on Transfection Efficiency of Poly((2-dimethylamino)ethyl methacrylate)-Plasmid Nanoparticles. *Pharm. Res.* **1996**, *13*, 1038–1042.

- (9) Boussif, O.; Lezoualc'h, F.; Zanta, M. A.; Mergny, M. D.; Scherman, D.; Demeneix, B.; Behr, J. P. A Versatile Vector for Gene and Oligonucleotide Transfer into Cells in Culture and *In Vivo*: Polyethylenimine. *Proc. Natl. Acad. Sci. U. S. A.* **1995**, *92*, 7297–7301.
- (10) Falco, A.; Encinas, P.; Carbajosa, S.; Cuesta, A.; Chaves-Pozo, E.; Tafalla, C.; Estepa, A.; Coll, J. M. Transfection Improvements of Fish Cell lines by Using Deacylated Polyethylenimine of Selected Molecular Weights. *Fish Shellfish Immunol.* **2009**, *26*, 559–566.
- (11) Monnery, B. D.; Wright, M.; Cavill, R.; Hoogenboom, R.; Shaunak, S.; Steinke, J. H. G.; Thanou, M. Cytotoxicity of Polycations: Relationship of Molecular Weight and the Hydrolytic Theory of the Mechanism of Toxicity. *Int. J. Pharm.* **2017**, *521*, 249–258.
- (12) Jere, D.; Jiang, H. L.; Arote, R.; Kim, Y. K.; Choi, Y. J.; Cho, M. H.; Akaike, T.; Cho, C. S. Degradable Polyethylenimines as DNA and Small Interfering RNA Carriers. *Expert Opin. Drug Delivery* **2009**, *6*, 827–834.
- (13) Gosselin, M. A.; Guo, W.; Lee, R. J. Efficient Gene Transfer Using Reversibly Cross-Linked Low Molecular Weight Polyethylenimine. *Bioconjugate Chem.* **2001**, *12*, 989–994.
- (14) Forrest, M. L.; Koerber, J. T.; Pack, D. W. A Degradable Polyethylenimine Derivative with Low Toxicity for Highly Efficient Gene Delivery. *Bioconjugate Chem.* **2003**, *14*, 934–940.
- (15) Knorr, V.; Russ, V.; Allmendinger, L.; Ogris, M.; Wagner, E. Acetal Linked Oligoethylenimines for Use as pH-Sensitive Gene Carriers. *Bioconjugate Chem.* **2008**, *19*, 1625–1634.
- (16) Arote, R. B.; Hwang, S. K.; Yoo, M. K.; Jere, D.; Jiang, H. L.; Kim, Y. K.; Choi, Y. J.; Nah, J. W.; Cho, M. H.; Cho, C. S. Biodegradable Poly(ester amine) Based on Glycerol Dimethacrylate and Polyethylenimine as a Gene Carrier. *J. Gene Med.* **2008**, *10*, 1223–1235.
- (17) Agarwal, S.; Ren, L.; Kissel, T.; Bege, N. Synthetic Route and Characterization of Main Chain Ester-Containing Hydrolytically Degradable Poly(*N,N*-dimethylaminoethyl methacrylate)-Based Polycations. *Macromol. Chem. Phys.* **2010**, *211*, 905–915.

- (18) Yardley, R. E.; Rabiee Kenaree, A.; Gillies, E. R. Triggering Depolymerization: Progress and Opportunities for Self-Immolative Polymers. *Macromolecules* **2019**, *52*, 6342–6360.
- (19) Sirianni, Q. E. A.; Gillies, E. R. The Architectural Evolution of Self-Immolative Polymers. *Polymer* **2020**, *202*, 122638.
- (20) Sagi, A.; Weinstain, R.; Karton, N.; Shabat, D. Self-Immolative Polymers. *J. Am. Chem. Soc.* **2008**, *130*, 5434–5435.
- (21) Dewit, M. A.; Gillies, E. R. A Cascade Biodegradable Polymer Based on Alternating Cyclization and Elimination Reactions. *J. Am. Chem. Soc.* **2009**, *131*, 18327–18334.
- (22) Olah, M. G.; Robbins, J. S.; Baker, M. S.; Phillips, S. T. End-Capped Poly(benzyl ethers): Acid and Base Stable Polymers That Depolymerize Rapidly from Head-to-Tail in Response to Specific Applied Signals. *Macromolecules* **2013**, *46*, 5924–5928.
- (23) Seo, W.; Phillips, S. T. Patterned Plastics That Change Physical Structure in Response to Applied Chemical Signals. *J. Am. Chem. Soc.* **2010**, *132*, 9234–9235.
- (24) Fan, B.; Trant, J. F.; Wong, A. D.; Gillies, E. R. Polyglyoxylates: A Versatile Class of Triggerable Self-Immolative Polymers from Readily Accessible Monomers. *J. Am. Chem. Soc.* **2014**, *136*, 10116–10123.
- (25) Fan, B.; Salazar, R.; Gillies, E. R. Depolymerization of Trityl End-Capped Poly(ethyl glyoxylate): Potential Applications in Smart Packaging. *Macromol. Rapid Commun.* **2018**, *39*, 1800173.
- (26) Liu, G.; Zhang, G.; Hu, J.; Wang, X.; Zhu, M.; Liu, S. Hyperbranched Self-Immolative Polymers (hSIPs) for Programmed Payload Delivery and Ultrasensitive Detection. *J. Am. Chem. Soc.* **2015**, *137*, 11645–11655.
- (27) Fan, B.; Gillies, E. R. Poly(ethyl glyoxylate)-Poly(ethylene oxide) Nanoparticles: Stimuli-Responsive Drug Release via End-to-End Polyglyoxylate Depolymerization. *Mol. Pharmaceutics* **2017**, *14*, 2548–2559.
- (28) Gambles, M. T.; Fan, B.; Borecki, A.; Gillies, E. R. Hybrid Polyester Self-Immolative Polymer Nanoparticles for Controlled Drug Release. *ACS Omega* **2018**, *3*, 5002–5011.
- (29) Gisbert-Garzarán, M.; Berkmann, J. C.; Giasafaki, D.; Lozano, D.; Spyrou, K.; Manzano, M.; Steriotis, T.; Duda, G. N.; Schmidt-Bleek, K.; Charalambopoulou, G.;

Vallet-Regí, M. Engineered pH-Responsive Mesoporous Carbon Nanoparticles for Drug Delivery. *ACS Appl. Mater. Interfaces* **2020**, *12*, 14946–14957.

(30) Coulembier, O.; Knoll, A.; Pires, D.; Gotsmann, B.; Duerig, U.; Frommer, J.; Miller, R. D.; Dubois, P.; Hedrick, J. L. Probe-Based Nanolithography: Self-Amplified Depolymerization Media for Dry Lithography. *Macromolecules* **2010**, *43*, 572–574.

(31) Knoll, A. W.; Pires, D.; Coulembier, O.; Dubois, P.; Hedrick, J. L.; Frommer, J.; Duerig, U. Probe-Based 3-D Nanolithography Using Self-Amplified Depolymerization Polymers. *Adv. Mater.* **2010**, *22*, 3361–3365.

(32) Cheong, L. L.; Paul, P.; Holzner, F.; Despont, M.; Coady, D. J.; Hedrick, J. L.; Allen, R.; Knoll, A. W.; Duerig, U. Thermal Probe Maskless Lithography for 27.5 nm Half-Pitch Si Technology. *Nano Lett.* **2013**, *13*, 4485–4491.

(33) Fan, B.; Trant, J. F.; Yardley, R. E.; Pickering, A. J.; Lagurné-Labarthe, F.; Gillies, E. R. Photocontrolled Degradation of Stimuli-Responsive Poly(ethyl glyoxylate): Differentiating Features and Traceless Ambient Depolymerization. *Macromolecules* **2016**, *49*, 7196–7203.

(34) DiLauro, A. M.; Lewis, G. G.; Phillips, S. T. Self-Immolative Poly(4,5-dichlorophthalaldehyde) and its Applications in Multi-Stimuli-Responsive Macroscopic Plastics. *Angew. Chem. Int. Ed.* **2015**, *54*, 6200–6205.

(35) Heuchan, S. M.; MacDonald, J. P.; Bauman, L. A.; Fan, B.; Henry, H. A. L.; Gillies, E. R. Photoinduced Degradation of Polymer Films Using Polyglyoxylate–Polyester Blends and Copolymers. *ACS Omega* **2018**, *3*, 18603–18612.

(36) Lloyd, E. M.; Lopez Hernandez, H.; Feinberg, A. M.; Yourdkhani, M.; Zen, E. K.; Mejia, E. B.; Sottos, N. R.; Moore, J. S.; White, S. R. Fully Recyclable Metastable Polymers and Composites. *Chem. Mater.* **2019**, *31*, 398–406.

(37) Sirianni, Q. E. A.; Rabiee Kenaree, A.; Gillies, E. R. Polyglyoxylamides: Tuning Structure and Properties of Self-Immolative Polymers. *Macromolecules* **2019**, *52*, 262–270.

(38) Rabiee Kenaree, A.; Gillies, E. R. Controlled Polymerization of Ethyl Glyoxylate Using Alkylolithium and Alkoxide Initiators. *Macromolecules* **2018**, *51*, 5501–5510.

- (39) DiLauro, A. M.; Zhang, H.; Baker, M. S.; Wong, F.; Sen, A.; Phillips, S. T. Accessibility of Responsive End-Caps in Films Composed of Stimuli-Responsive, Depolymerizable Poly(phthalaldehydes). *Macromolecules* **2013**, *46*, 7257–7265.
- (40) Yeung, K.; Kim, H.; Mohapatra, H.; Phillips, S. T. Surface-Accessible Detection Units in Self-Immolative Polymers Enable Translation of Selective Molecular Detection Events into Amplified Responses in Macroscopic, Solid-State Plastics. *J. Am. Chem. Soc.* **2015**, *137*, 5324–5327.
- (41) Rabiee Kenaree, A.; Sirianni, Q. E. A.; Classen, K.; Gillies, E. R. Thermoresponsive Self-Immolative Polyglyoxylamides. *Biomacromolecules* **2020**, *21*, 3817–3825.
- (42) Funderburk, L. H.; Aldwin, L.; Jencks, W. P. Mechanisms of General Acid and Base Catalysis of the Reactions of Water and Alcohols with Formaldehyde. *J. Am. Chem. Soc.* **1978**, *100*, 5444–5459.
- (43) Przystas, T. J.; Fife, T. H. The Mechanism of Hemiacetal Decomposition. Substituent Effects in Breakdown of Substituted Benzaldehyde Ethyl Hemiacetals. *J. Am. Chem. Soc.* **1981**, *103*, 4884–4890.

Chapter 7

7 Summary, Conclusions, and Future Directions

This thesis encompassed work on the development and application of a new class of self-immolative polymers (SIPs) known as polyglyoxylamides (PGAMs). In the initial work (Chapter 3), the synthesis of PGAMs from self-immolative poly(ethyl glyoxylates) PEGs with acid-sensitive trityl or 4-monomethoxytrityl (MMT) end-caps was investigated for the first time. The PGAMs were synthesized from these precursor PEGs using different simple primary and secondary amines via one-pot post-polymerization amidation reactions. The resulting PGAMs were characterized and had substantially different properties than the precursor polymers, including higher T_g (as high as 90 °C versus the precursor's T_g of -10 °C) and water-solubility. Despite these changes, the PGAMs all underwent triggered depolymerization using an acid stimulus in much the same way as the precursor polymers, albeit at an accelerated rate. Furthermore, graft copolymers were constructed using an amine-terminated oligo(ethylene glycol) by using higher temperatures and longer reaction times during the post-polymerization modification. This initial work allowed for the facile synthesis of novel SIPs with tunable properties and thereby provided a platform to investigate and further develop SIPs for targeted applications.

With the synthesis of PGAMs established, the next project investigated creating SIPs that also possessed thermo-responsive behaviour for possible biomedical applications (Chapter 4). Inspired by analogous polymethacrylates, a library of PGAMs was constructed using PEGs with either acid-sensitive or stable end-caps and amine terminated ethylene or propylene glycol-based pendent groups. The resulting library of polymers had lower critical solution temperature (LCST) behaviour when measured via turbidimetry and dynamic light scattering (DLS). Some of the PGAMs synthesized possessed cloud point temperatures (T_{cps}) near or below body temperature. Furthermore, it was discovered that depolymerization caused a gradual loss of LCST behaviour as the concentration of polymer in solution decreased, and that aggregation slowed depolymerization. Finally, *in vitro*

cytotoxicity assays of the most interesting PGAMs revealed negligible toxicity, providing evidence that these polymers may be suitable for future biomedical applications.

In addition to thermal stimuli, pH-responsive SIPs were also explored via the use of polycationic PGAMs (Chapter 5). The introduction of tertiary amines with different levels of hydrophobicity as pendent groups allowed for the formation of PGAM homopolymers that switched solubility at different pH levels. This capability coupled with the acid sensitive end-caps of the PGAMs allowed for control of the depolymerization behaviour using pH, as insoluble polymers self-immolate very slowly. The control afforded by these polymers allowed for the synthesis of SIPs that could depolymerize in mildly acidic aqueous conditions quickly yet remain stable at higher pH levels, a property not reported for other SIP systems. Furthermore, copolymers of these PGAMs with poly(ethylene glycol) (PEG) formed nanoscale vesicles at higher pH levels which could dissociate and degrade once the pH was reduced. This contrasted with an analogous PEG-PEtG system, which remained assembled despite the pH changes. This work demonstrates not only an example of an SIP capable of selectively depolymerizing in a mildly acidic environment, but also pH-sensitive nanovesicles that may be of used as drug delivery vehicles.

Finally, polycationic PGAMs were applied as non-viral fully self-immolative transfection agents for nucleic acids (Chapter 6). A small library of SIPs with varying amine pendent groups and acid-responsive or stable end-caps were synthesized and found to complex a plasmid to varying degrees. The acid-responsive complexes could be decomplexed by triggering self-immolation, which was hypothesized to assist with transfection by providing a mechanism for nucleic acid release once in the cell. Characterization of the complexes revealed nanoparticle assemblies with positive zeta potentials, while cell assays revealed lower cytotoxicity when compared to a non-degradable polycationic transfection agent jetPEI, with large toxicity improvements due to depolymerization. Moreover, transfection assays showed similar transfection efficiencies between some of the PGAMs and the commercial transfection agent, with some evidence that depolymerization increased this efficiency with at least one set of polymers tested.

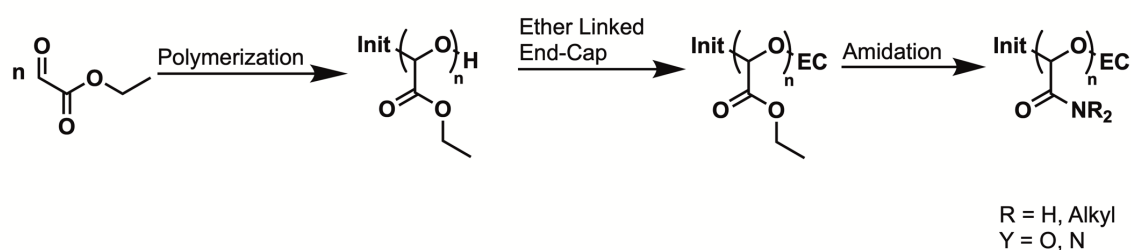
The body of work presented in this thesis demonstrates that PGAMs are a viable and versatile class of SIPs that can be tuned easily from precursor PEGs. Nevertheless, there are several avenues of future work that could be pursued to expand upon and improve these polymers.

First, while a great variety of different PGAMs can be synthesized from PEG just by selecting different amines using post-polymerization modification, there remains some limitations in using this process. Post-polymerization modification does not always allow for 100% conversion of the precursor PEG to the desired PGAMs. We often found during our preliminary investigations that many of the more sterically hindered or secondary amines failed to react fully or in a reasonable time frame. This limitation is especially evident for the PGAM-OEG graft copolymer (Chapter 3) and the thermo-responsive PGAMs (Chapter 4), which both required additional reaction time and heating to accomplish full conversion due to the use of sterically hindered amines. Another issue that may occur is partially converted PEG crashing out of solution, thereby halting the reaction. While this was not an issue for any of the work presented in this thesis, it has been observed with other PGAMs where solubility changes drastically due to the pendent groups being introduced. Moreover, the use of post-polymerization modification also limits the end-caps that can be used. Since amines are nucleophiles, they can cleave end-caps linked to the PEGs via carbonates, which are often used since end-capping of the PEGs with chloroformates is simple to perform at the low temperatures necessary for polymerization. All the polymers used in this work were either trityl or benzyloxymethyl ethers, which were some of the only groups we could install with high success at cold temperatures, whereas with carbonate end-caps our lab could previously induce responsiveness to a broader range of stimuli including UV light, thiols, and reducing agents among other stimuli.

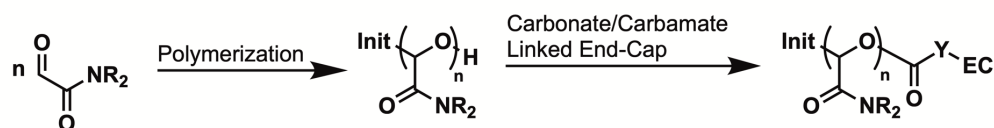
The issues presented by post-polymerization modification may be best addressed using two different approaches. On the one hand, it would be beneficial to continue to optimize the end-capping of PEG with ethers (Scheme 7.1a). We found for the trityl end-caps that Ag^+ ions could help remove the halides of the trityl reagents, allowing for more efficient end-capping to occur. Perhaps these or other catalysts could be used, or polymerization

conditions could be modified, to encourage other end-caps to react. Alternatively, post-polymerization modification could be used as a quick method to synthesize PGAMs that may have interesting properties. Once preliminary work has established PGAMs of interest, effort could then be expended to synthesize and purify the monomers of these PGAMs. These monomers could then be polymerized using the more traditional and effective chloroformate/isocyanate end-caps (Scheme 7.1b). Furthermore, the preparation of homo and copolymers with exact compositions could be controlled by simply adjusting the stoichiometry of the monomers used.

a)



b)



Scheme 7.1. Proposed synthetic pathways to yield PGAMs with new self-immolative stimuli responsiveness: a) PGAMs may be produced via the post-polymerization amidation of PEtG that has been end-capped with novel ether-linked stimuli-cleavable moieties; b) glyoxylamide monomers of interest could be synthesized and purified before being polymerized in a similar fashion as glyoxylates, with the use of traditional carbonate/carbamate-linked stimuli-cleavable moieties as end-caps.

Second, several of the thermo-responsive PGAMs investigated in this thesis (Chapter 4) possessed T_{cps} close to body temperature. Given the low toxicity of these polymers, it would be worthwhile to select the most promising polymers and incorporate them into a drug delivery system, such as a hydrogel (Figure 7.1a). Work in the Gillies Group is currently underway to investigate this possibility, using PGAM copolymers composed of

the thermo-responsive pendent groups along with other pendent groups to allow for cross-linking and tuning of the gel's thermal behaviour.

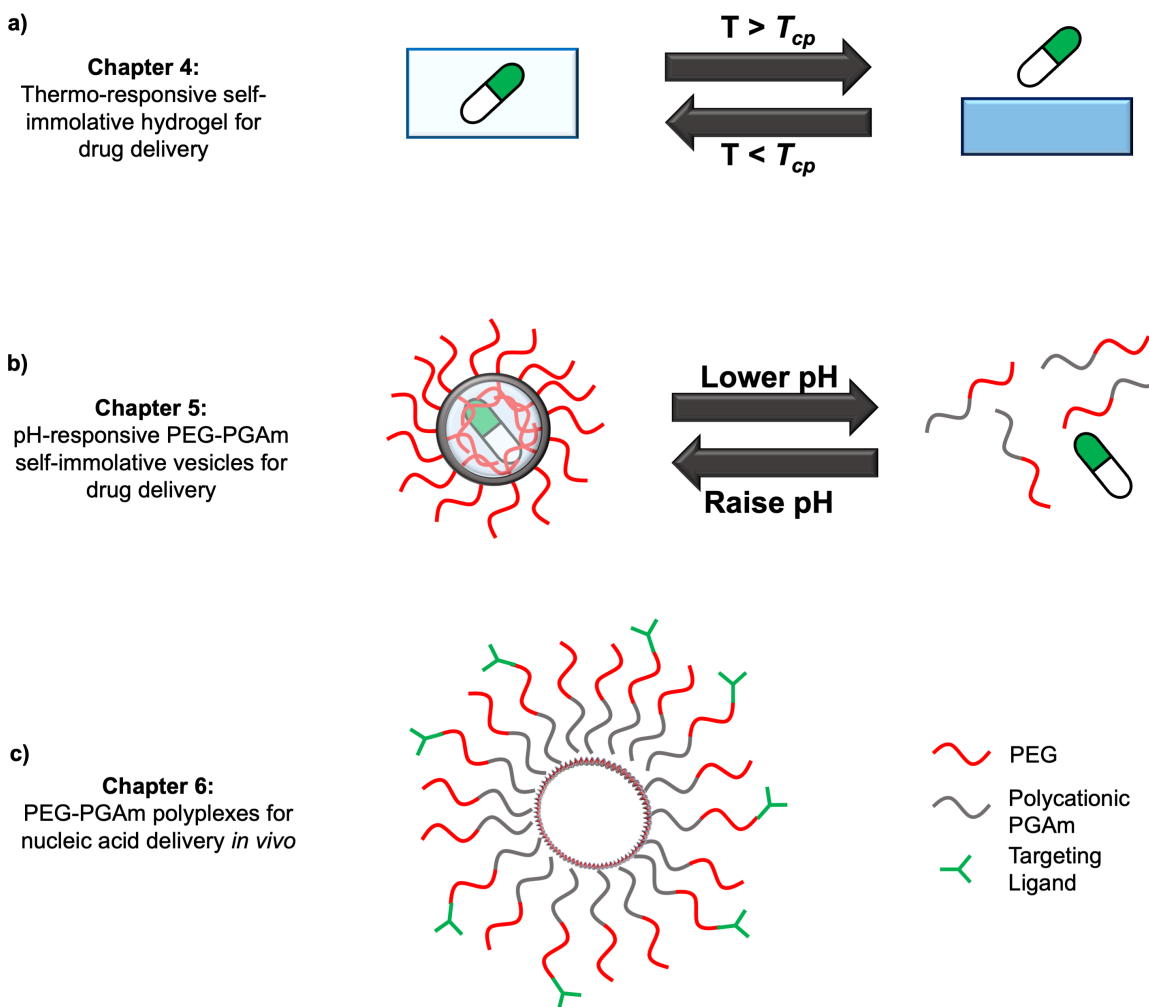


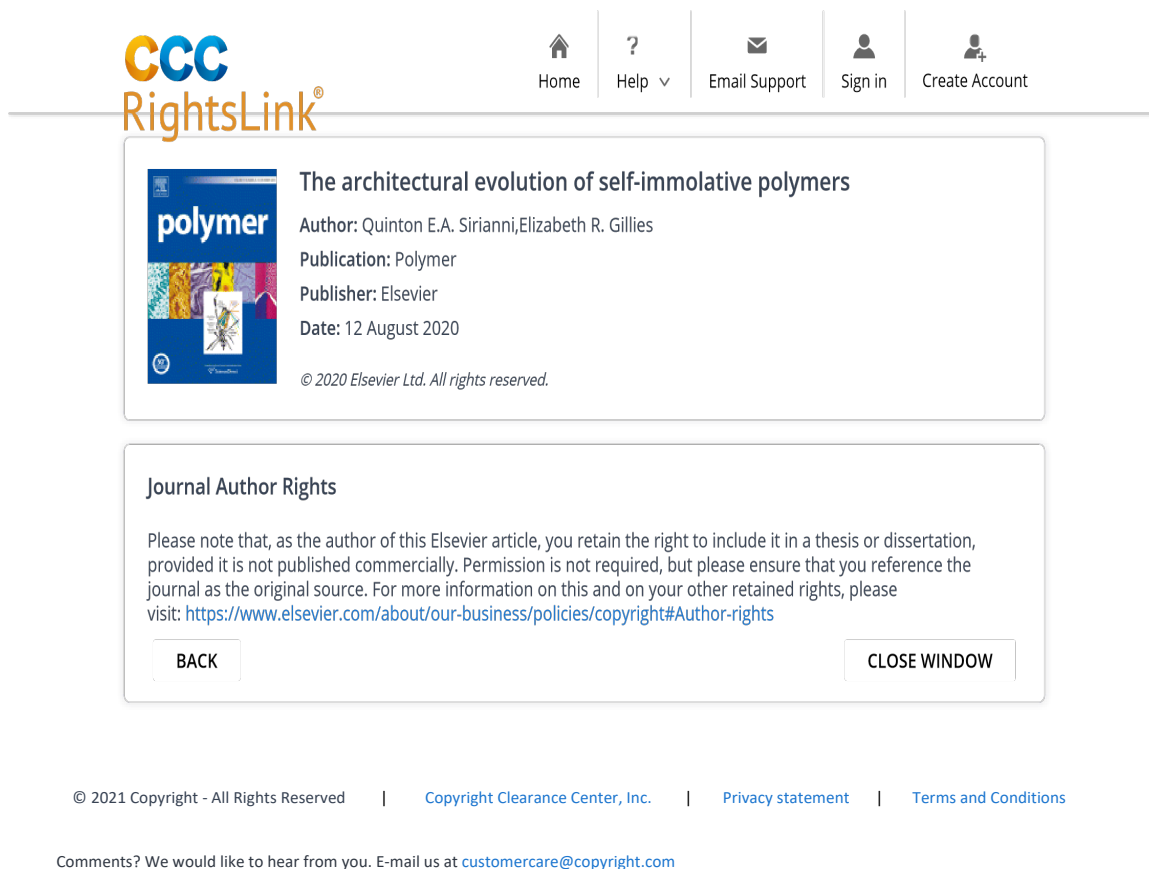
Figure 7.1. Potential future applications of PGAMs based on the work established in this thesis: a) Thermo-responsive PGAMs could be cross-linked to create thermo-responsive hydrogels, which should be capable of expelling a loaded drug when the temperature is raised above the polymer's cloud point; b) pH-responsive PEG-PGAm copolymers may be able to be loaded with both hydrophilic and hydrophobic drugs, given their vesicle morphology. These could then be used for pH-responsive drug-delivery; c) Polycationic PGAMs modified with PEG blocks (to stealth the polymers *in vivo* and prevent serum proteins from adhering) and targeting ligands (to target specific cells for transfection) may serve as improved transfection agents for *in vivo* use.

Third, the development of pH-sensitive PEG-PGAm nanovesicles was an unexpected result of the work concerning pH-responsive PGAmS (Chapter 5). Given the potential biomedical uses of a self-immolative acid-sensitive drug delivery vehicle, future work should explore developing other PEG-PGAm copolymers with variation on what pH level causes dissociation and depolymerization. The assemblies should be assessed for cytotoxicity, loaded with a model drug, and release studies should be performed (Figure 7.1b). If the results are promising *in vitro*, *in vivo* work may be warranted.

Last, the pursuit of self-immolative transfection agents resulted in some promising results *in vitro*, including the lowering of cytotoxicity due to depolymerization and good transfection efficiency when compared to a non-degradable polycationic transfection agent (Chapter 6). Given the time constraints, this work could be expanded upon in several ways in the future, including developing and testing other PGAmS with different end-caps and pendent groups, assessing other cell lines for cytotoxicity and transfection efficiency, and developing PEG-PGAm copolymers that can effectively complex nucleic acids for possible *in vivo* applications (Figure 7.1c).

Appendix 1

1 Permission to Reuse Copyrighted Material



The screenshot displays the CCC RightsLink interface. At the top left is the logo for CCC RightsLink®. To the right is a navigation menu with icons and labels: Home, Help (with a dropdown arrow), Email Support, Sign in, and Create Account. Below the navigation is a white box containing article information. On the left is a thumbnail of a journal cover for 'polymer'. To the right of the thumbnail, the article title is 'The architectural evolution of self-immolative polymers'. Below the title, the author is listed as 'Quinton E.A. Sirianni, Elizabeth R. Gillies'. Further down, the publication is 'Polymer', the publisher is 'Elsevier', and the date is '12 August 2020'. At the bottom of this box is the copyright notice: '© 2020 Elsevier Ltd. All rights reserved.' Below this is another white box titled 'Journal Author Rights'. It contains a paragraph of text explaining that authors retain the right to include their work in a thesis or dissertation, provided it is not published commercially. It also includes a link to 'https://www.elsevier.com/about/our-business/policies/copyright#Author-rights'. At the bottom of this box are two buttons: 'BACK' and 'CLOSE WINDOW'. At the very bottom of the page, there is a footer with copyright information: '© 2021 Copyright - All Rights Reserved | Copyright Clearance Center, Inc. | Privacy statement | Terms and Conditions'. Below the footer is a line of text: 'Comments? We would like to hear from you. E-mail us at customercare@copyright.com'.

Figure A1.1. Permission to reuse copyrighted article: Sirianni, Q. E. A.; Gillies, E. R. The Architectural Evolution of Self-Immolative Polymers. *Polymer* **2020**, *202*, 122638.

Kinetics of Self-Immulative Degradation in a Linear Polymeric System: Demonstrating the Effect of Chain Length

Author: Ryan A. McBride, Elizabeth R. Gillies



Publication: *Macromolecules*

Publisher: American Chemical Society

Date: Jul 1, 2013

Copyright © 2013, American Chemical Society

PERMISSION/LICENSE IS GRANTED FOR YOUR ORDER AT NO CHARGE

This type of permission/license, instead of the standard Terms and Conditions, is sent to you because no fee is being charged for your order. Please note the following:

- Permission is granted for your request in both print and electronic formats, and translations.
- If figures and/or tables were requested, they may be adapted or used in part.
- Please print this page for your records and send a copy of it to your publisher/graduate school.
- Appropriate credit for the requested material should be given as follows: "Reprinted (adapted) with permission from {COMPLETE REFERENCE CITATION}. Copyright {YEAR} American Chemical Society." Insert appropriate information in place of the capitalized words.
- One-time permission is granted only for the use specified in your RightsLink request. No additional uses are granted (such as derivative works or other editions). For any uses, please submit a new request.

If credit is given to another source for the material you requested from RightsLink, permission must be obtained from that source.

[BACK](#)

[CLOSE WINDOW](#)

Figure A1.2. Permission to reuse figure from copyrighted article: McBride, R. A.; Gillies, E. R. Kinetics of Self-Immulative Degradation in a Linear Polymeric System: Demonstrating the Effect of Chain Length. *Macromolecules* **2013**, *46*, 5157–5166.

Polyglyoxylamides: Tuning Structure and Properties of Self-Immolative Polymers



Author: Quinton E. A. Sirianni, Amir Rabiee Kenaree, Elizabeth R. Gillies

Publication: *Macromolecules*

Publisher: American Chemical Society

Date: Jan 1, 2019

Copyright © 2019, American Chemical Society

PERMISSION/LICENSE IS GRANTED FOR YOUR ORDER AT NO CHARGE

This type of permission/license, instead of the standard Terms and Conditions, is sent to you because no fee is being charged for your order. Please note the following:

- Permission is granted for your request in both print and electronic formats, and translations.
- If figures and/or tables were requested, they may be adapted or used in part.
- Please print this page for your records and send a copy of it to your publisher/graduate school.
- Appropriate credit for the requested material should be given as follows: "Reprinted (adapted) with permission from {COMPLETE REFERENCE CITATION}. Copyright {YEAR} American Chemical Society." Insert appropriate information in place of the capitalized words.
- One-time permission is granted only for the use specified in your RightsLink request. No additional uses are granted (such as derivative works or other editions). For any uses, please submit a new request.

If credit is given to another source for the material you requested from RightsLink, permission must be obtained from that source.

[BACK](#)

[CLOSE WINDOW](#)

Figure A1.3. Permission to reuse copyrighted article: Sirianni, Q. E. A.; Rabiee Kenaree, A.; Gillies, E. R. Polyglyoxylamides: Tuning Structure and Properties of Self-Immolative Polymers. *Macromolecules* **2019**, *52*, 262–270.

Thermoresponsive Self-Immolative Polyglyoxylamides



Author: Amir Rabiee Kenaree, Quinton E. A. Sirianni, Kyle Classen, et al

Publication: Biomacromolecules

Publisher: American Chemical Society

Date: Sep 1, 2020

Copyright © 2020, American Chemical Society

PERMISSION/LICENSE IS GRANTED FOR YOUR ORDER AT NO CHARGE

This type of permission/license, instead of the standard Terms and Conditions, is sent to you because no fee is being charged for your order. Please note the following:

- Permission is granted for your request in both print and electronic formats, and translations.
- If figures and/or tables were requested, they may be adapted or used in part.
- Please print this page for your records and send a copy of it to your publisher/graduate school.
- Appropriate credit for the requested material should be given as follows: "Reprinted (adapted) with permission from {COMPLETE REFERENCE CITATION}. Copyright {YEAR} American Chemical Society." Insert appropriate information in place of the capitalized words.
- One-time permission is granted only for the use specified in your RightsLink request. No additional uses are granted (such as derivative works or other editions). For any uses, please submit a new request.

If credit is given to another source for the material you requested from RightsLink, permission must be obtained from that source.

[BACK](#)

[CLOSE WINDOW](#)

Figure A1.4. Permission to reuse copyrighted article: Rabiee Kenaree, A.; Sirianni, Q. E. A.; Classen, K.; Gillies, E. R. Thermoresponsive Self-Immolative Polyglyoxylamides. *Biomacromolecules* **2020**, *21*, 3817–3825.

Appendix 2

2 Supplemental Data for Chapter 3 Including NMR and FT-IR Spectra, Size-Exclusion Chromatograms, TGA and DSC Thermograms, Powder X-Ray Diffractograms, and Depolymerization Studies

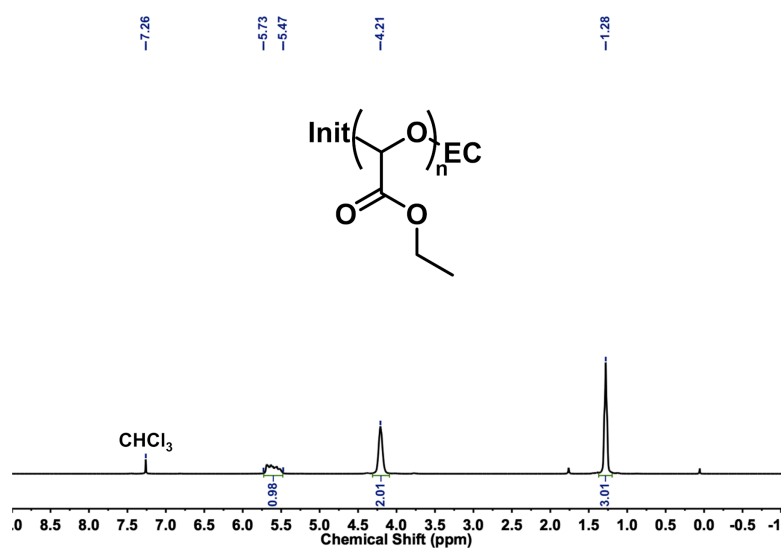


Figure A2.1. ¹H NMR spectrum of PEtG-MMT (CDCl₃, 400 MHz). The end-groups could not be accurately integrated due to the high molar mass of the polymer.

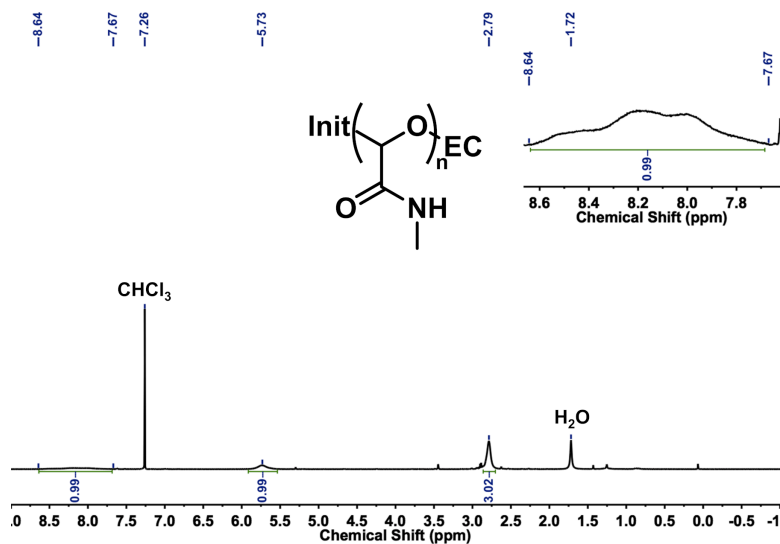


Figure A2.2. ^1H NMR spectrum of **PGAm-NMe-MMT** (CDCl_3 , 400 MHz). The end-groups could not be accurately integrated due to the high molar mass of the polymer

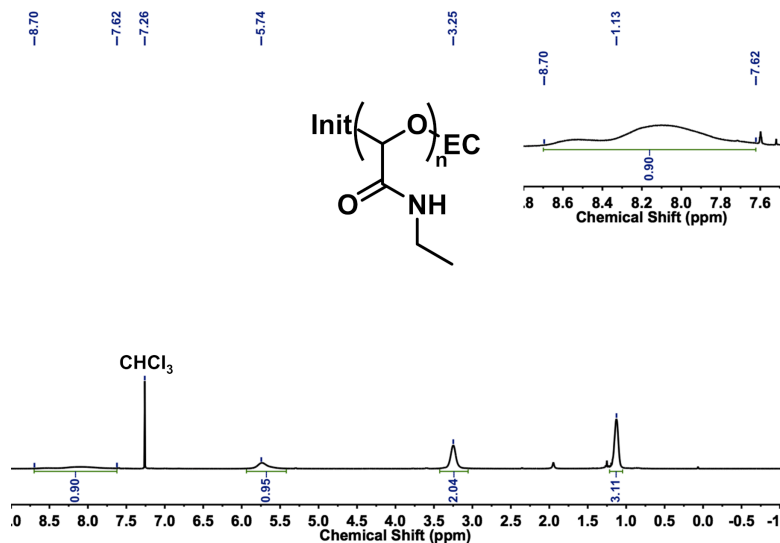


Figure A2.3. ^1H NMR spectrum of **PGAm-NEt-MMT** (CDCl_3 , 400 MHz). The end-groups could not be accurately integrated due to the high molar mass of the polymer.

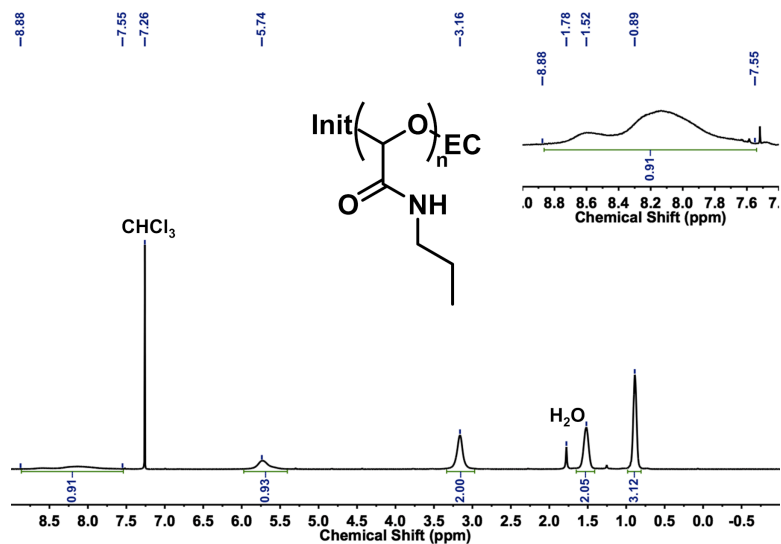


Figure A2.4. ^1H NMR spectrum of PGAm-NnPr-MMT (CDCl_3 , 400 MHz). The end-groups could not be accurately integrated due to the high molar mass of the polymer.

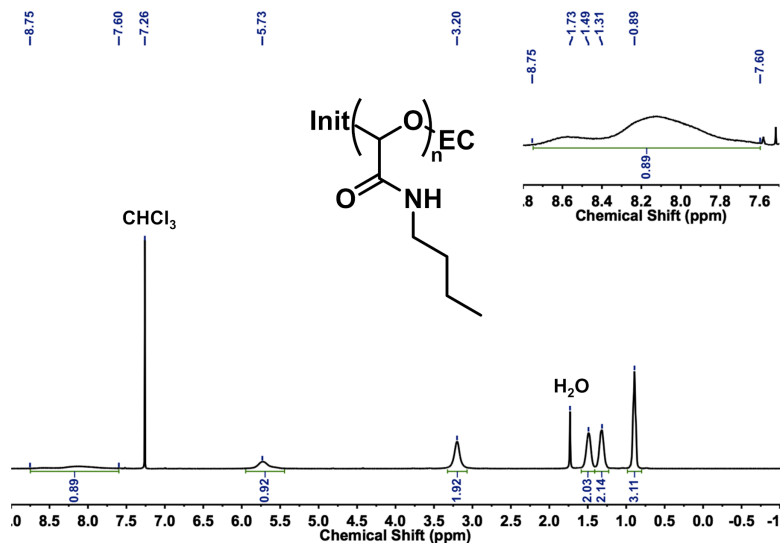


Figure A2.5. ^1H NMR spectrum of PGAm-NnBu-MMT (CDCl_3 , 400 MHz). The end-groups could not be accurately integrated due to the high molar mass of the polymer.

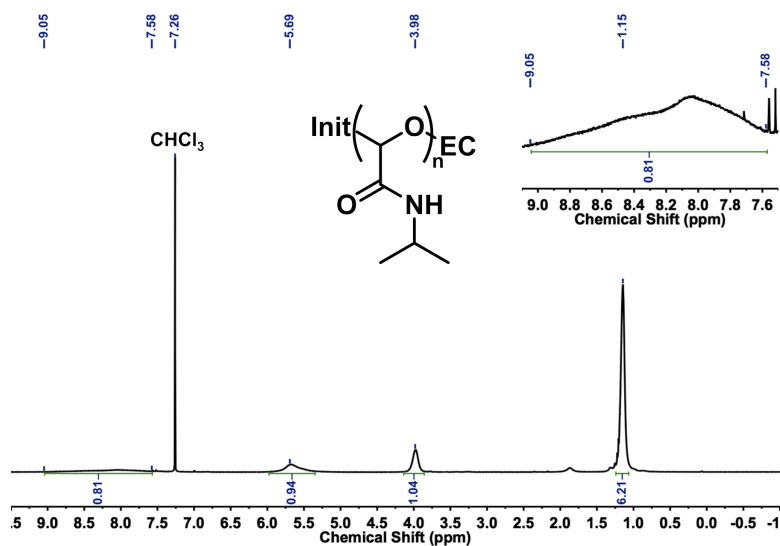


Figure A2.6. ^1H NMR spectrum of **PGAm-NiPr-MMT** (CDCl_3 , 400 MHz). The end-groups could not be accurately integrated due to the high molar mass of the polymer.

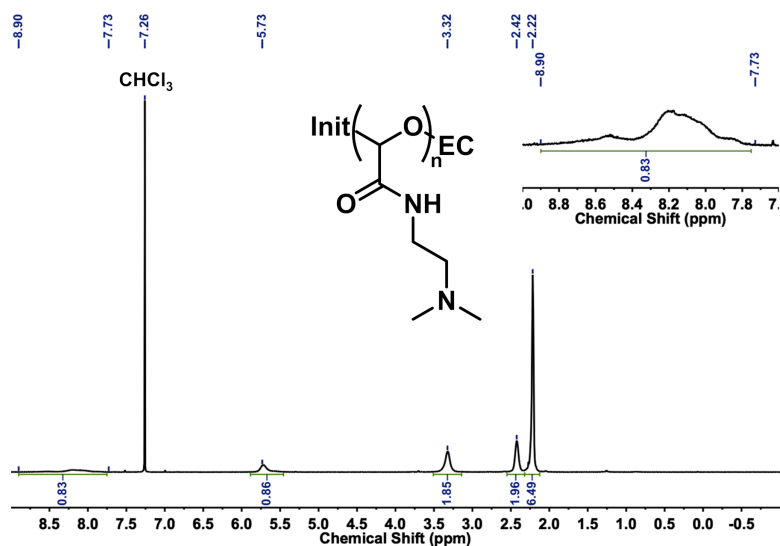


Figure A2.7. ^1H NMR spectrum of **PGAm-DMAE-MMT** (CDCl_3 , 400 MHz). The end-groups could not be accurately integrated due to the high molar mass of the polymer.

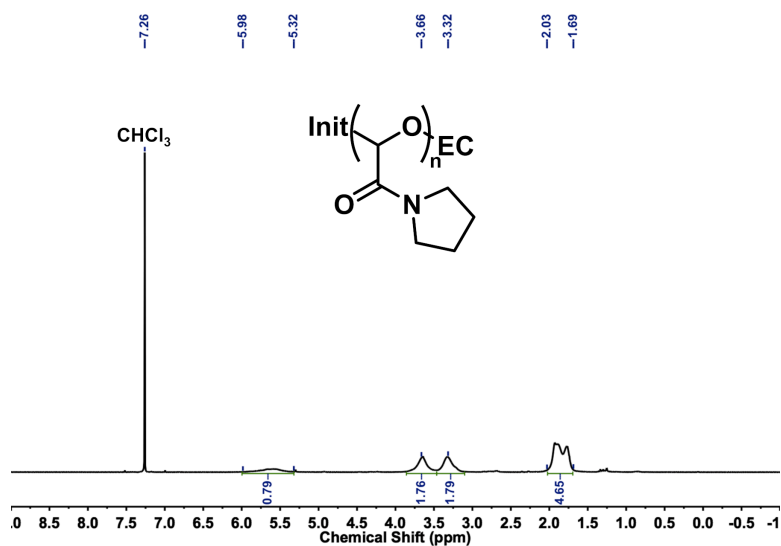


Figure A2.8. ^1H NMR spectrum of **PGAm-Pyrr-MMT** (CDCl_3 , 400 MHz). The end-groups could not be accurately integrated due to the high molar mass of the polymer.

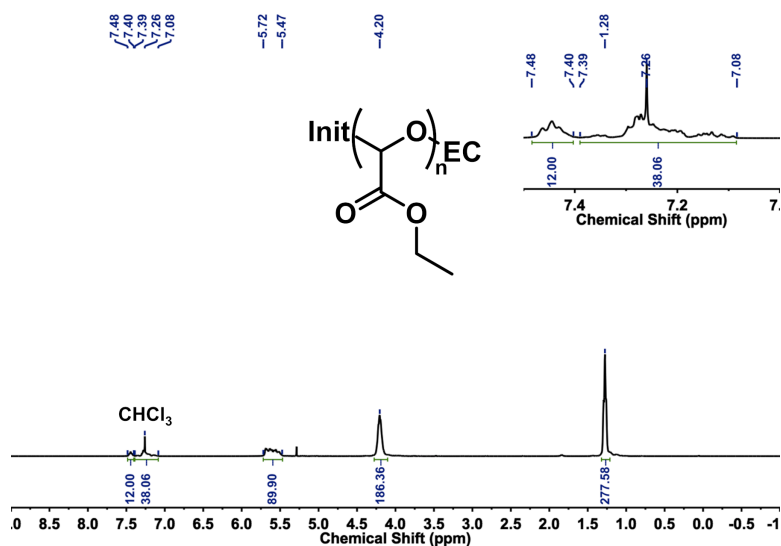


Figure A2.9. ^1H NMR spectrum of **PEtG-Trit** (CDCl_3 , 400 MHz). Because the molar mass of **PEtG-Trit** was low, end-group analysis could be performed. Good agreement was found between the ^1H NMR end-group analysis and the SEC results only when it was assumed that two trityl end-caps were present per polymer chain (Table 3.2). Thus, despite our attempts to initiate the polymerization with *n*-butyl lithium, it appears that **PEtG-Trit** mainly polymerized bi-directionally from ethyl glyoxylate hydrate initiator.

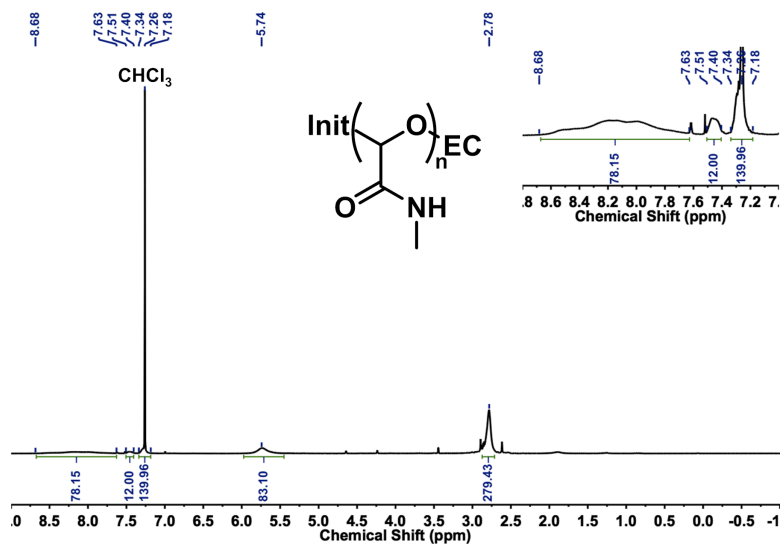


Figure A2.10. ^1H NMR spectrum of PGAm-NMe-Trit (CDCl_3 , 400 MHz).

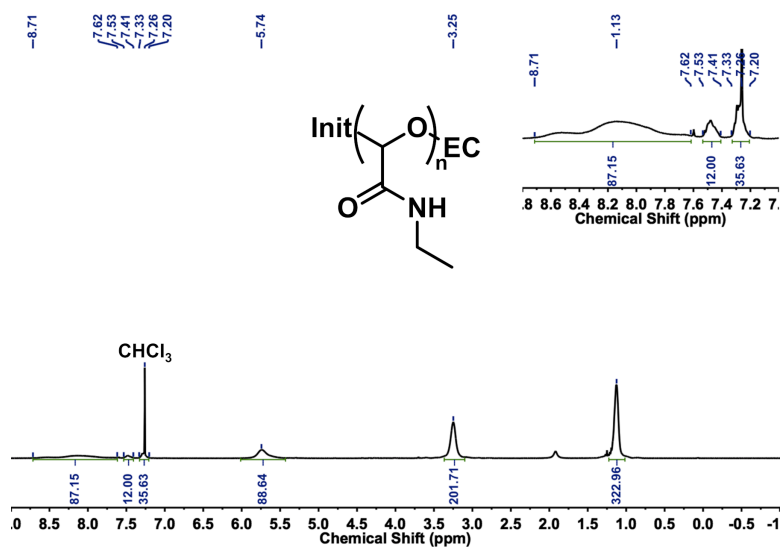


Figure A2.11. ^1H NMR spectrum of PGAm-NEt-Trit (CDCl_3 , 400 MHz).

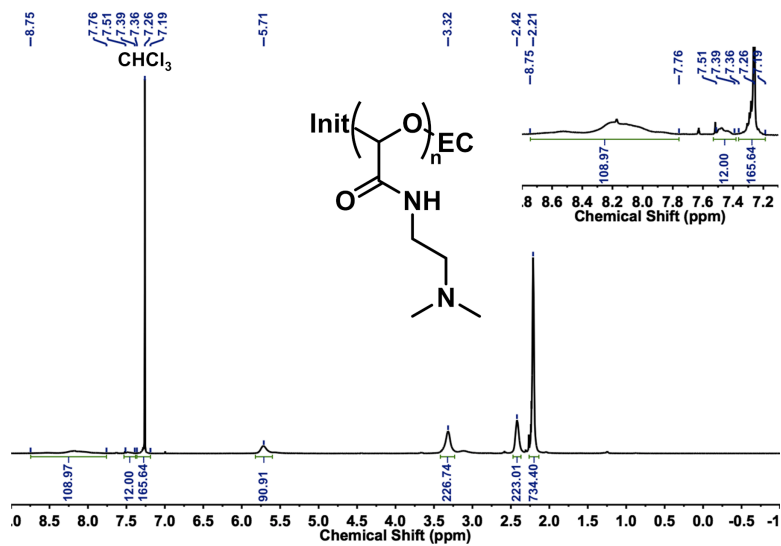


Figure A2.12. ^1H NMR spectrum of PGAm-DMAE-Trit (CDCl_3 , 400 MHz).

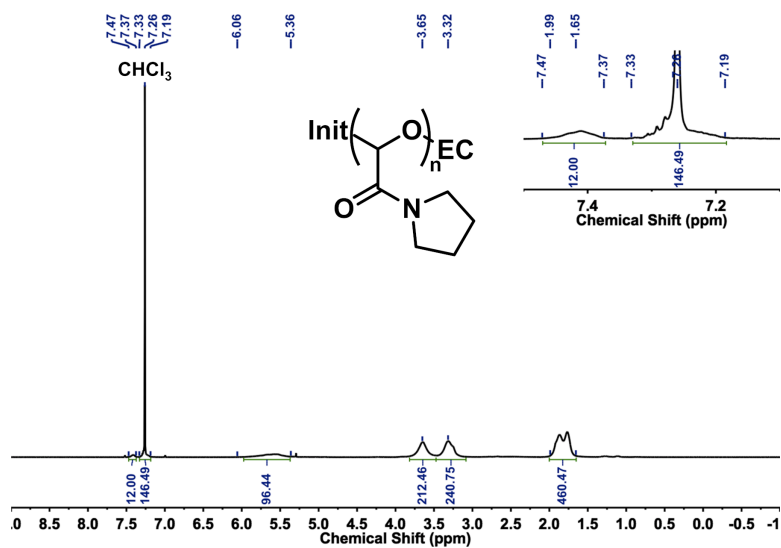


Figure A2.13. ^1H NMR spectrum of PGAm-Pyrr-Trit (CDCl_3 , 400 MHz).

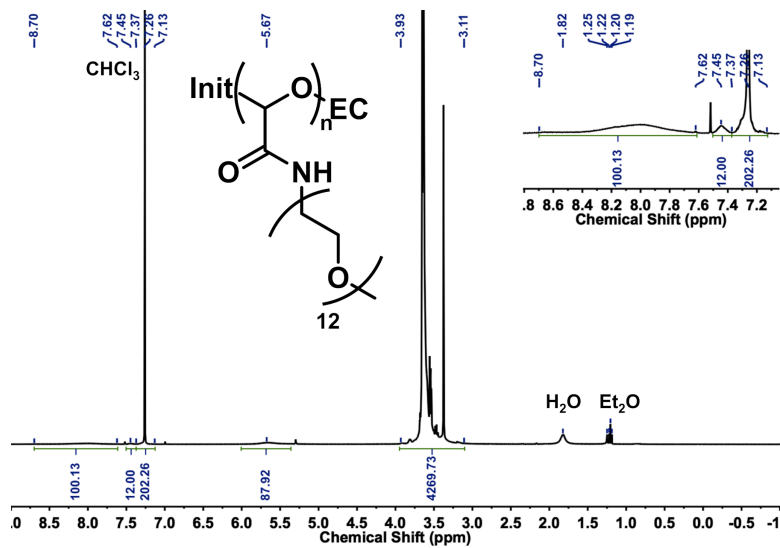


Figure A2.14. ^1H NMR spectrum of PGAm-OEG-Trit (CDCl₃, 400 MHz).

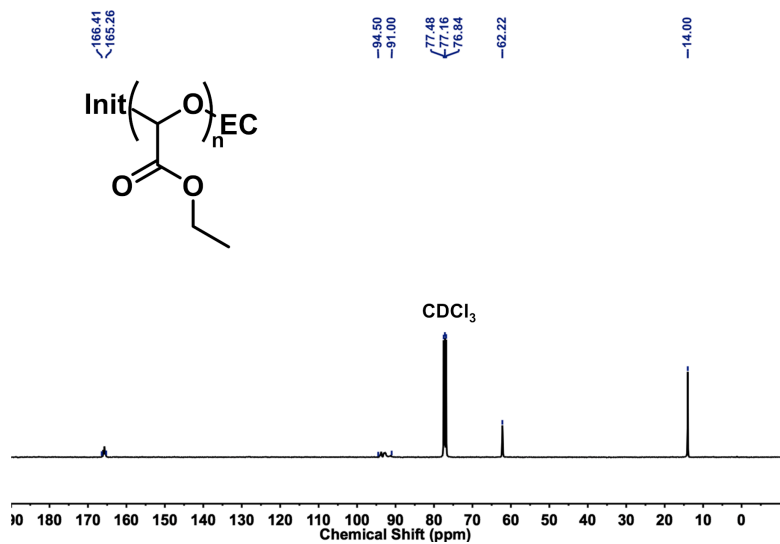


Figure A2.15. $^{13}\text{C}\{^1\text{H}\}$ NMR spectrum of PEtG-MMT (CDCl₃, 100 MHz). The end-groups are not visible due to the high molar mass of the polymer.

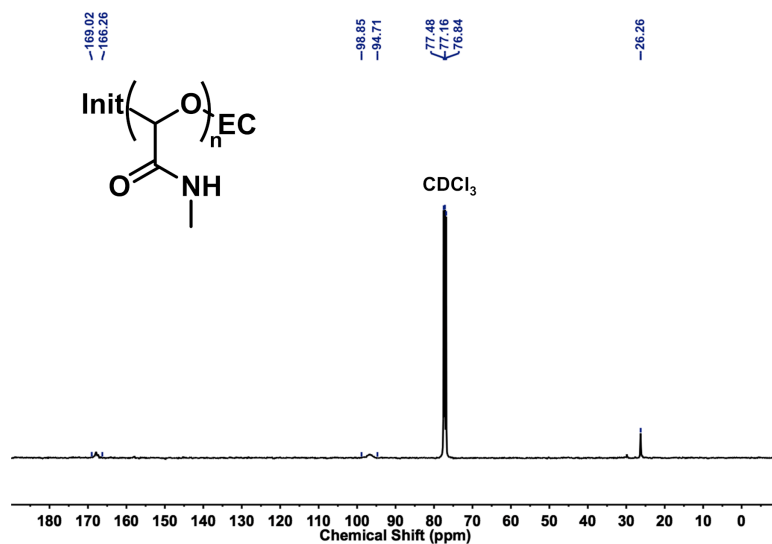


Figure A2.16. $^{13}\text{C}\{^1\text{H}\}$ NMR spectrum of PGAm-NMe-MMT (CDCl₃, 100 MHz). The end-groups are not visible due to the high molar mass of the polymer.

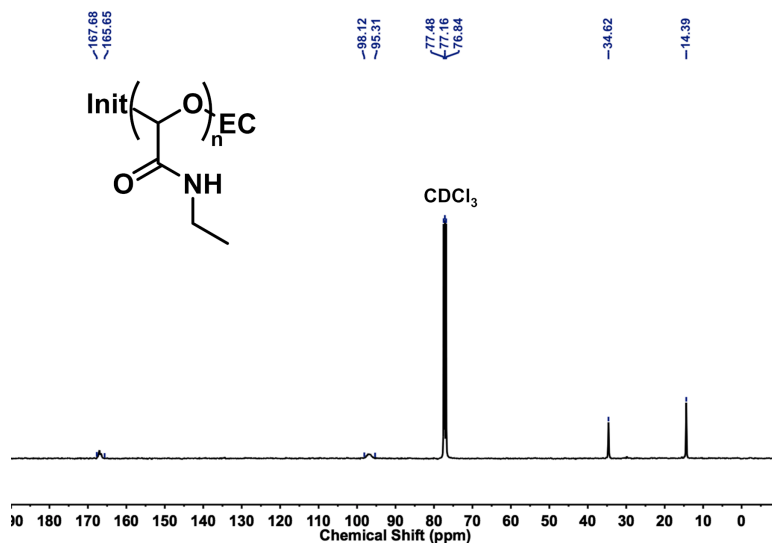


Figure A2.17. $^{13}\text{C}\{^1\text{H}\}$ NMR spectrum of PGAm-NEt-MMT (CDCl₃, 100 MHz). The end-groups are not visible due to the high molar mass of the polymer.

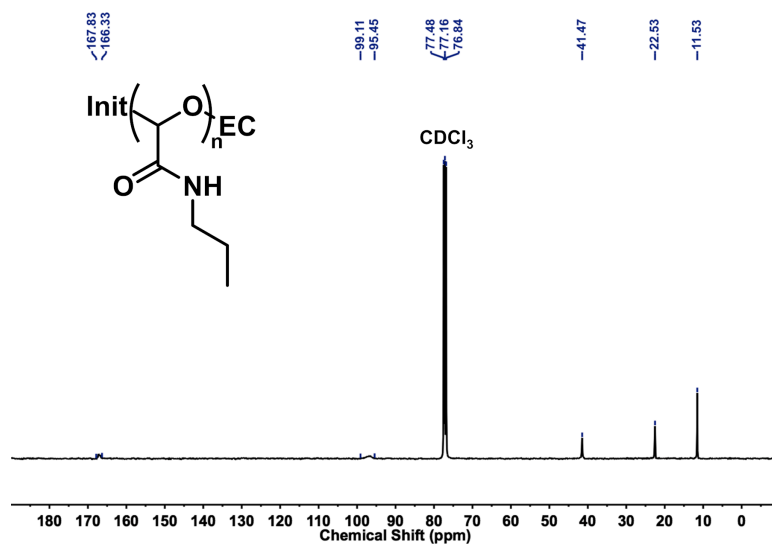


Figure A2.18. $^{13}\text{C}\{^1\text{H}\}$ NMR spectrum of **PGAm-NnPr-MMT** (CDCl₃, 100 MHz). The end-groups are not visible due to the high molar mass of the polymer.

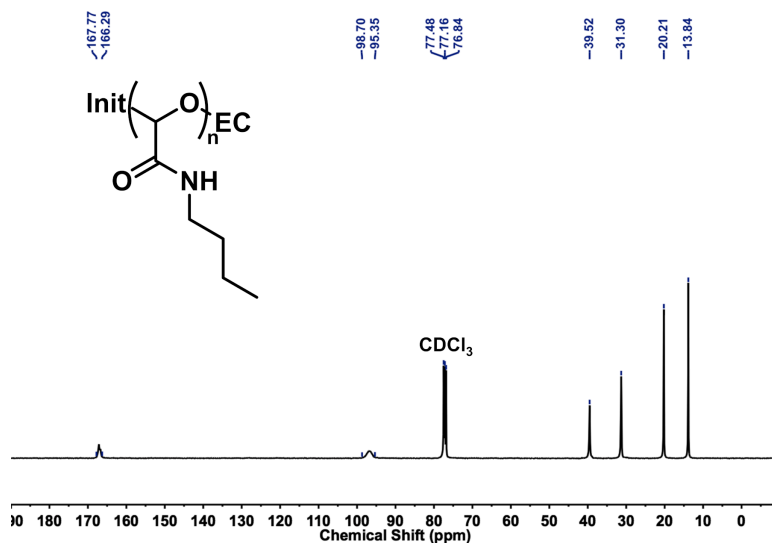


Figure A2.19. $^{13}\text{C}\{^1\text{H}\}$ NMR spectrum of **PGAm-NnBu-MMT** (CDCl₃, 100 MHz). The end-groups are not visible due to the high molar mass of the polymer.

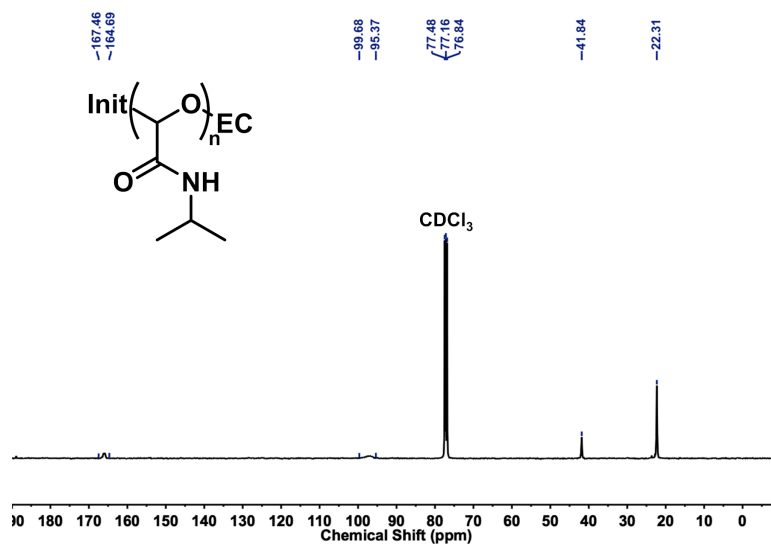


Figure A2.20. $^{13}\text{C}\{^1\text{H}\}$ NMR spectrum of **PGAm-NiPr-MMT** (CDCl_3 , 100 MHz). The end-groups are not visible due to the high molar mass of the polymer.

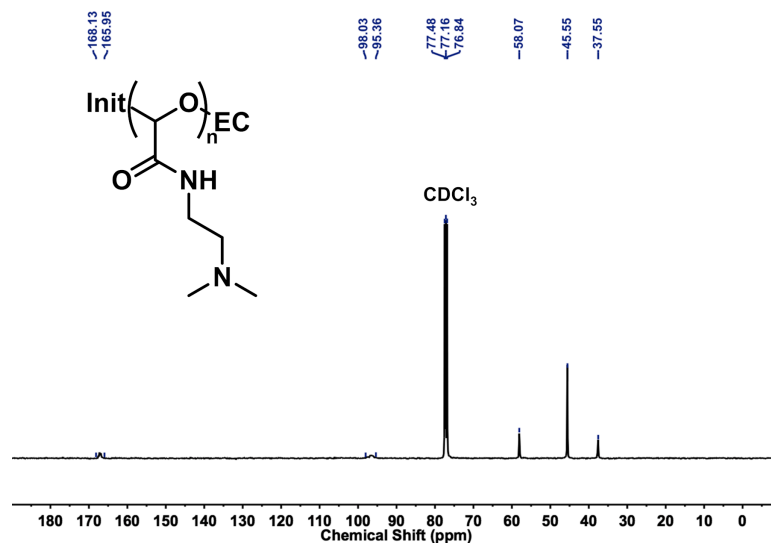


Figure A2.21. $^{13}\text{C}\{^1\text{H}\}$ NMR spectrum of **PGAm-DMAE-MMT** (CDCl_3 , 100 MHz). The end-groups are not visible due to the high molar mass of the polymer.

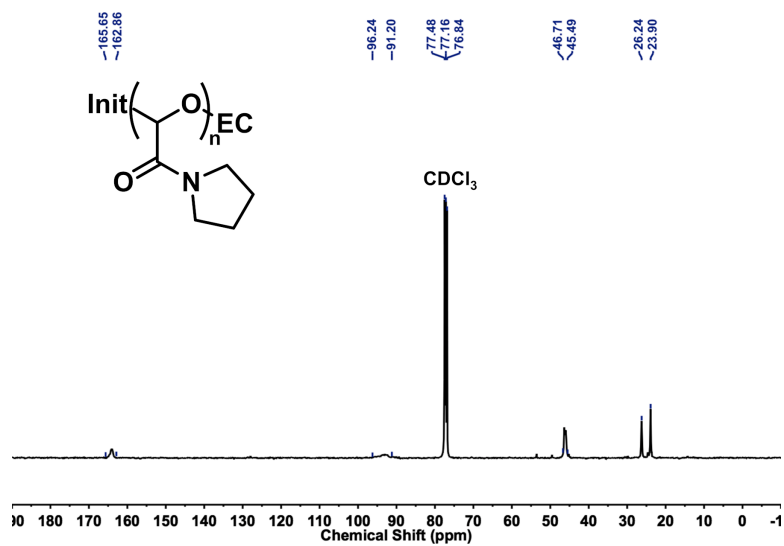


Figure A2.22. $^{13}\text{C}\{^1\text{H}\}$ NMR spectrum of **PGAm-Pyrr-MMT** (CDCl_3 , 100 MHz). The end-groups are not visible due to the high molar mass of the polymer.

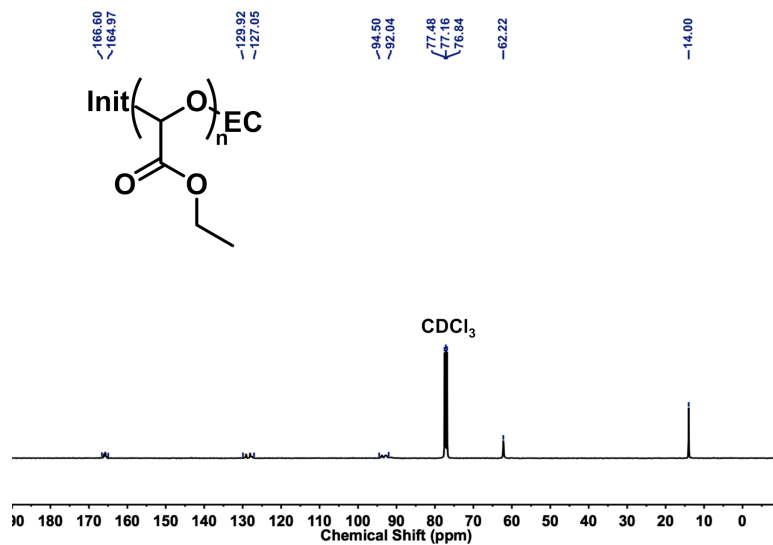


Figure A2.23. $^{13}\text{C}\{^1\text{H}\}$ NMR spectrum of **PETG-Trit** (CDCl_3 , 100 MHz).

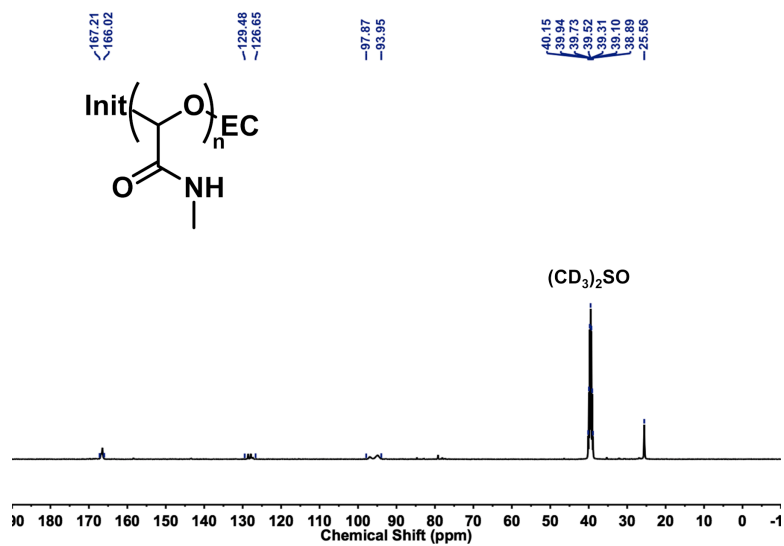


Figure A2.24. $^{13}C\{^1H\}$ NMR spectrum of **PGAm-NMe-Trit** ($(CD_3)_2SO$, 100 MHz).

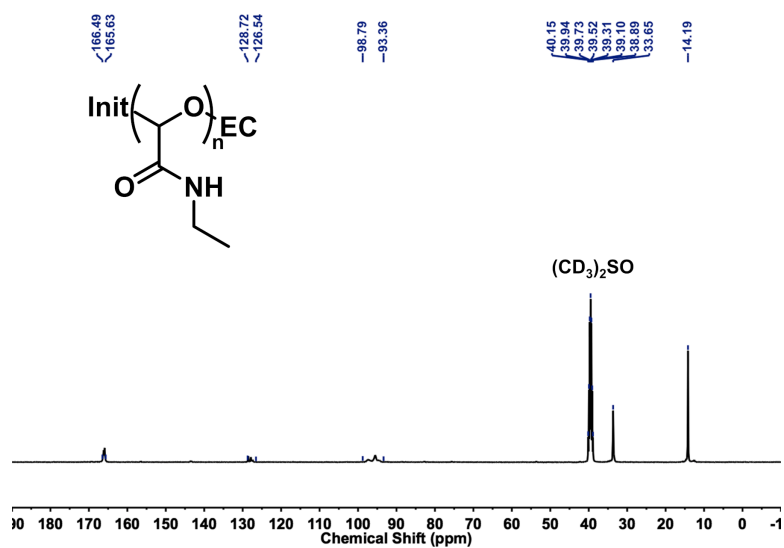


Figure A2.25. $^{13}C\{^1H\}$ NMR spectrum of **PGAm-NEt-Trit** ($(CD_3)_2SO$, 100 MHz).

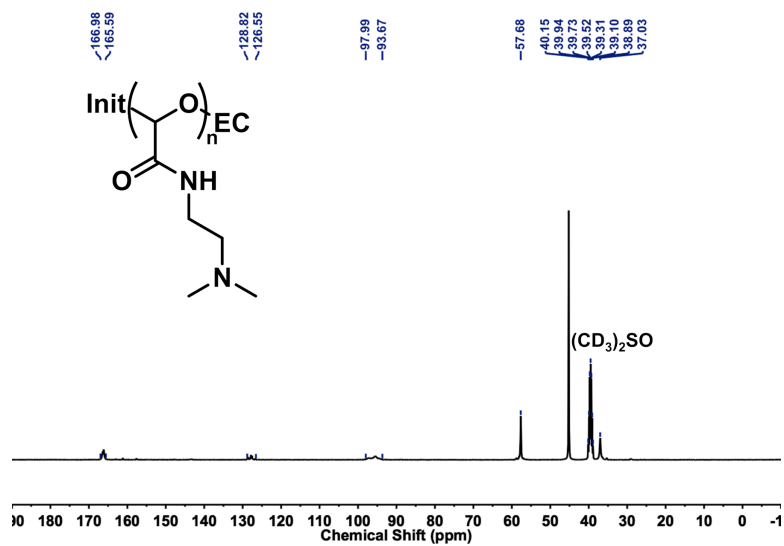


Figure A2.26. $^{13}\text{C}\{^1\text{H}\}$ NMR spectrum of PGAm-DMAE-Trit ($(\text{CD}_3)_2\text{SO}$, 100 MHz).

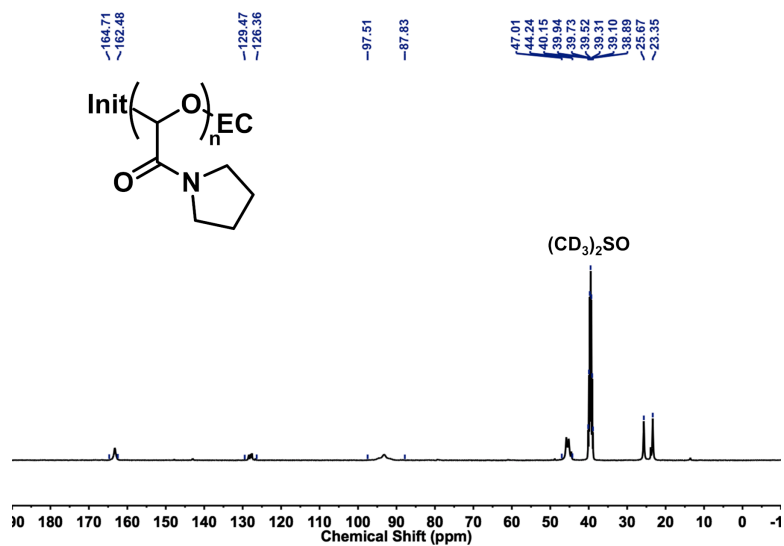


Figure A2.27. $^{13}\text{C}\{^1\text{H}\}$ NMR spectrum of PGAm-Pyrr-Trit ($(\text{CD}_3)_2\text{SO}$, 100 MHz).

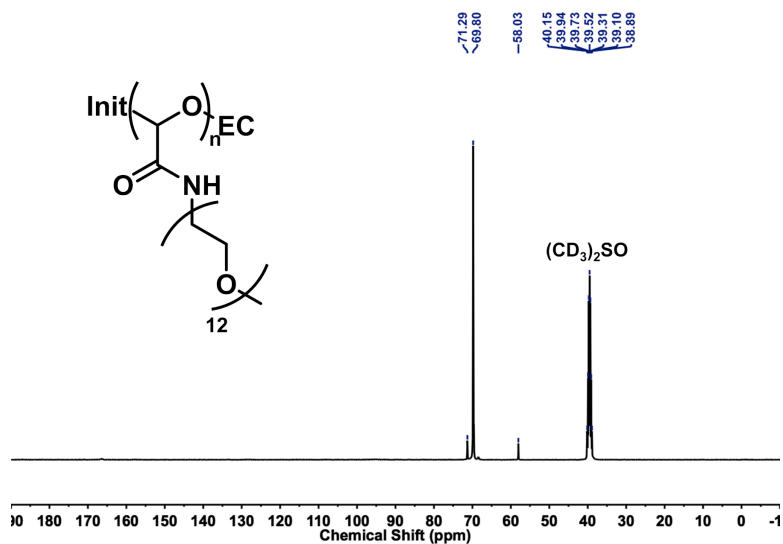


Figure A2.28. $^{13}\text{C}\{^1\text{H}\}$ NMR spectrum of **PGAm-OEG-Trit** ($(\text{CD}_3)_2\text{SO}$, 100 MHz). The backbone, carbonyl, and end-group carbons are not visible in this spectrum, however, ^1H NMR and SEC results (Figure A2.14, Figure A2.31) confirm the identity of this polymer.

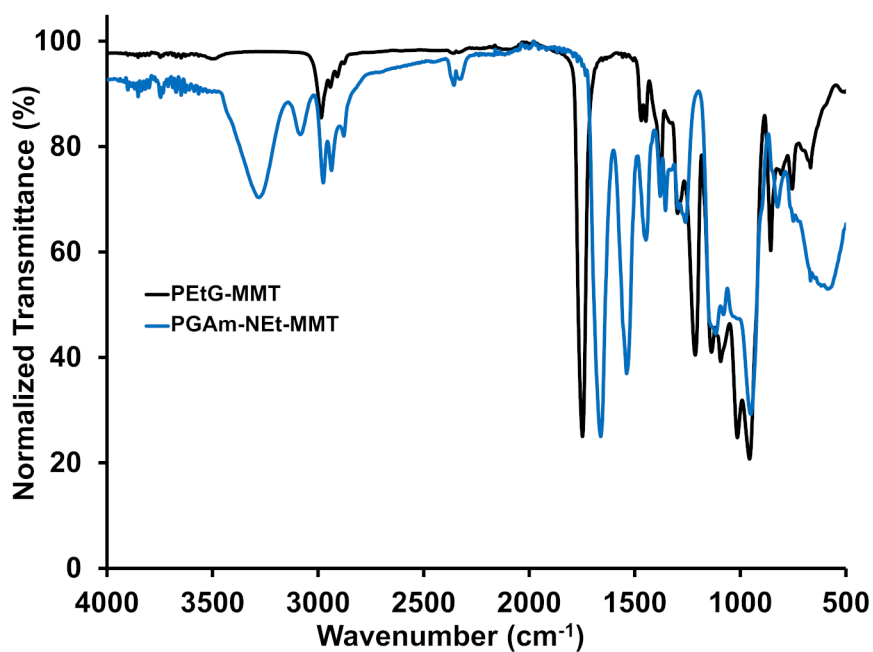


Figure A2.29. Overlay of the FT-IR spectra of **PEtG-MMT** and **PGAm-NEt-MMT**.

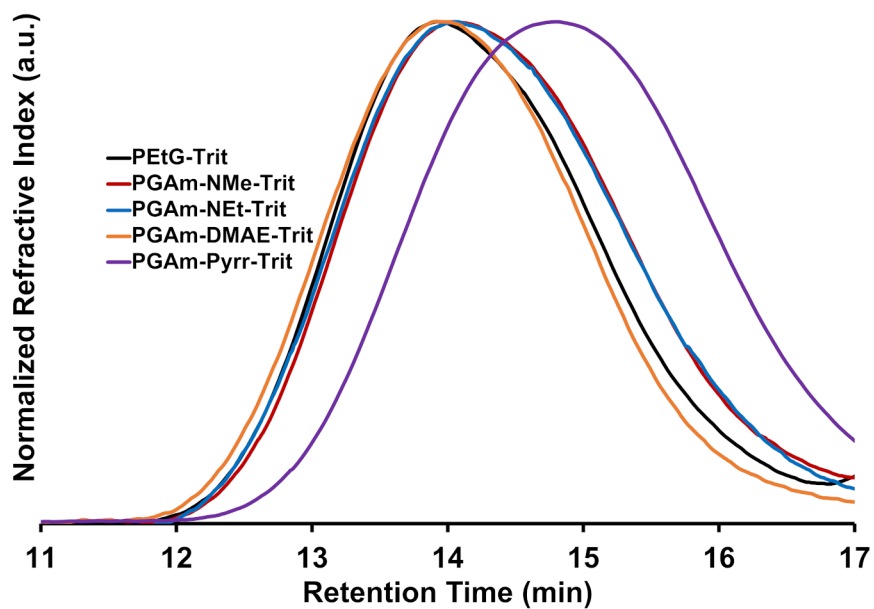


Figure A2.30. Overlay of size-exclusion chromatograms of the trityl end-capped PGAMs.

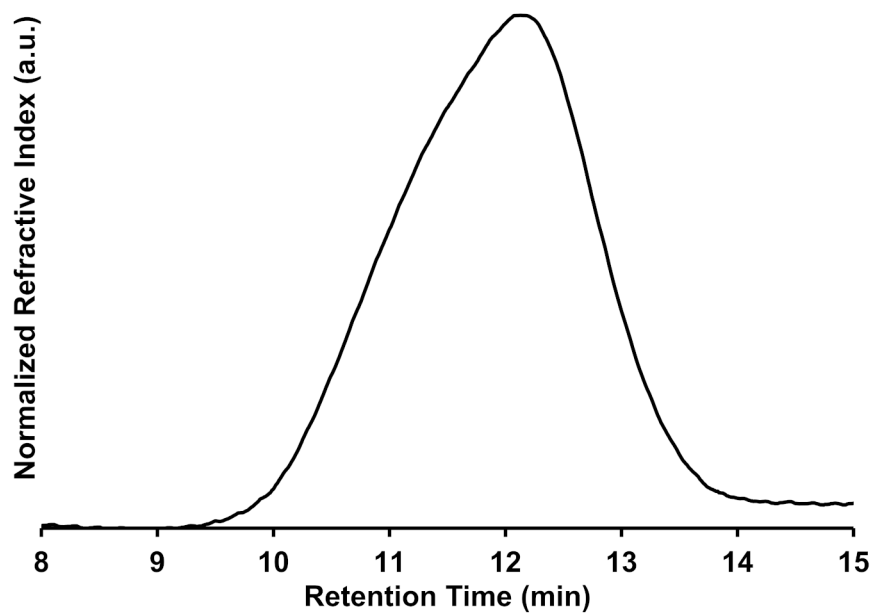


Figure A2.31. Size-exclusion chromatogram of PGAm-OEG-Trit.

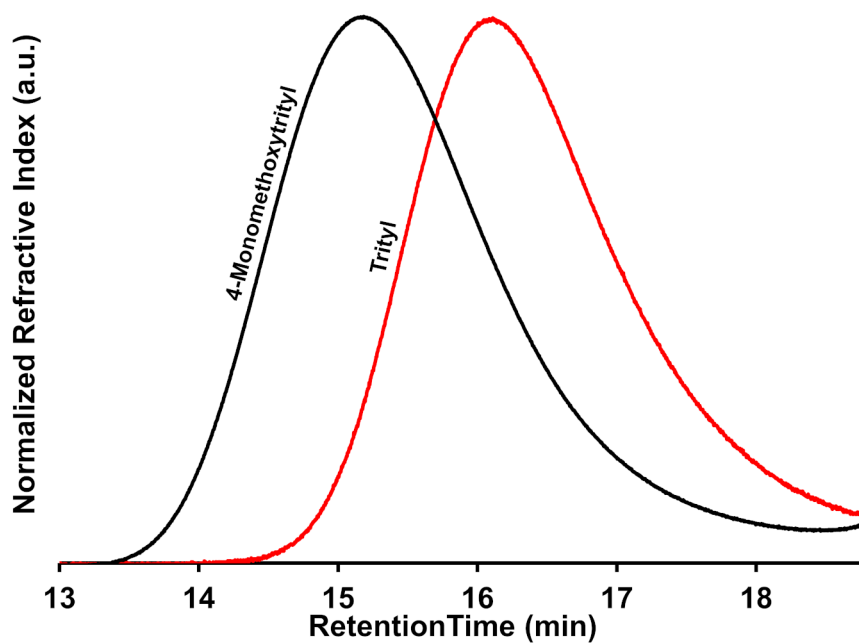


Figure A2.32. Overlay of size-exclusion chromatograms of crude PEtG synthesized from the same batch of monomer with different end-caps.

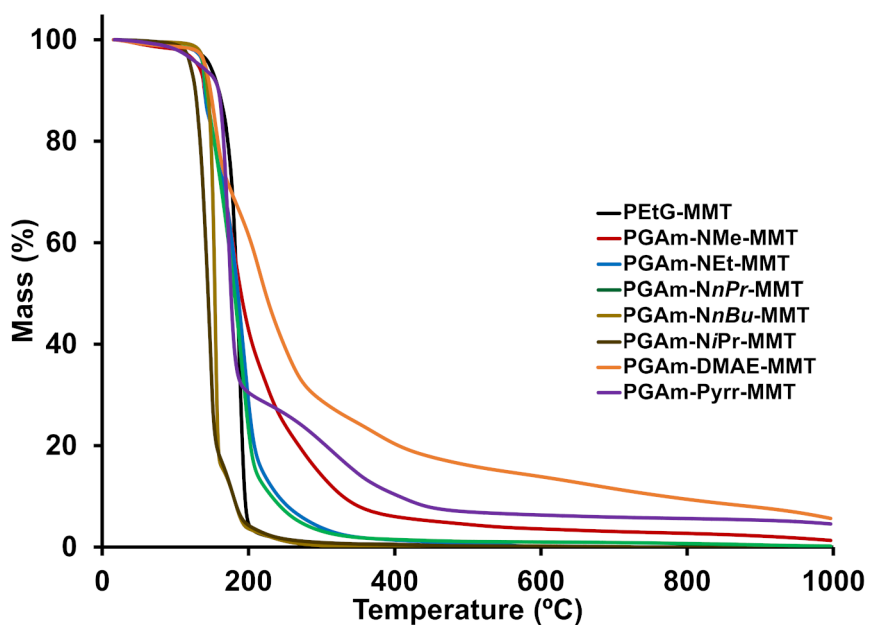


Figure A2.33. Overlay of the TGA thermograms of the 4-monomethoxytrityl end-capped polymers.

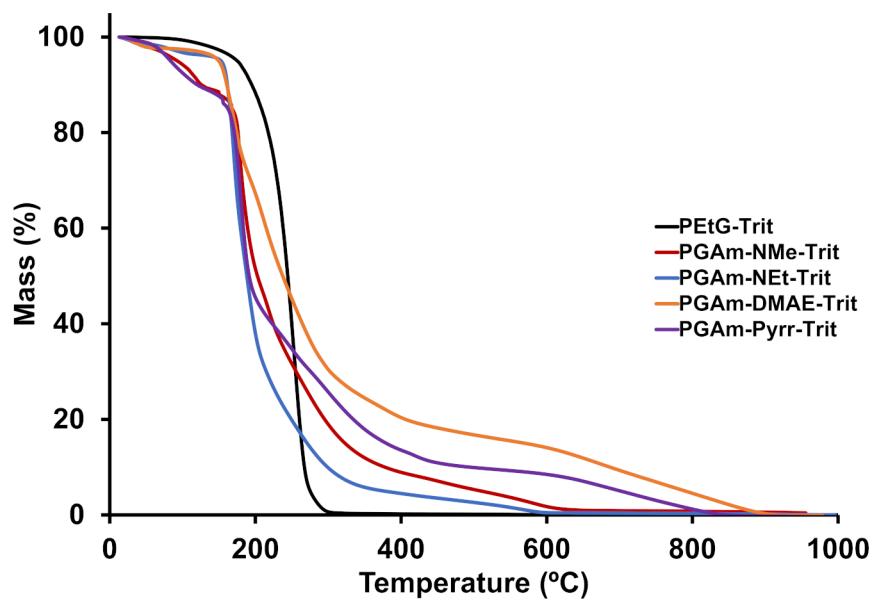


Figure A2.34. Overlay of the TGA thermograms of the trityl end-capped polymers. Note that the mass loss at ~ 100 °C for **PGAm-NMe-Trit** and **PGAm-Pyrr-Trit** is likely water as these polymers are quite hygroscopic.

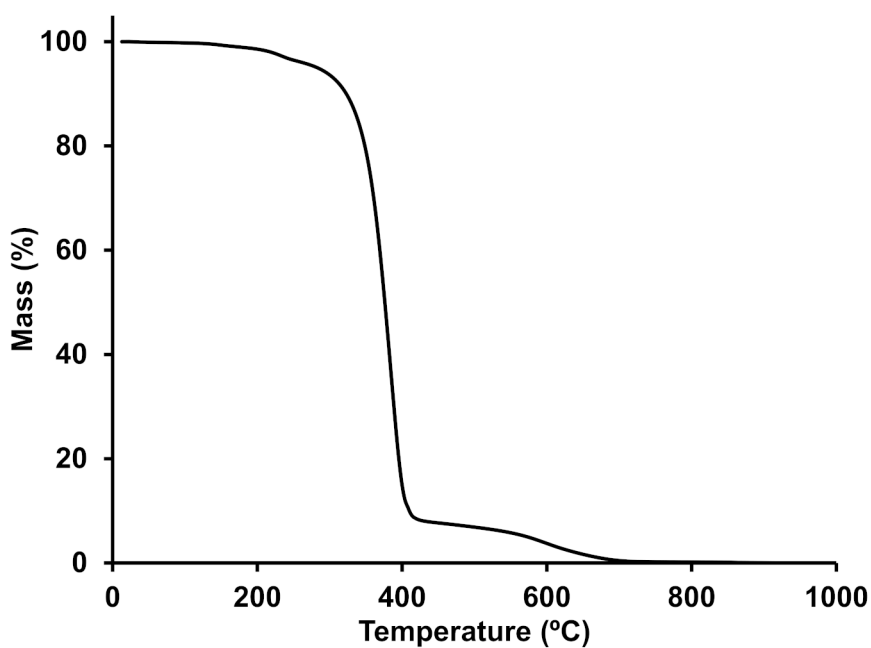


Figure A2.35. TGA thermogram of **PGAm-OEG-Trit**.

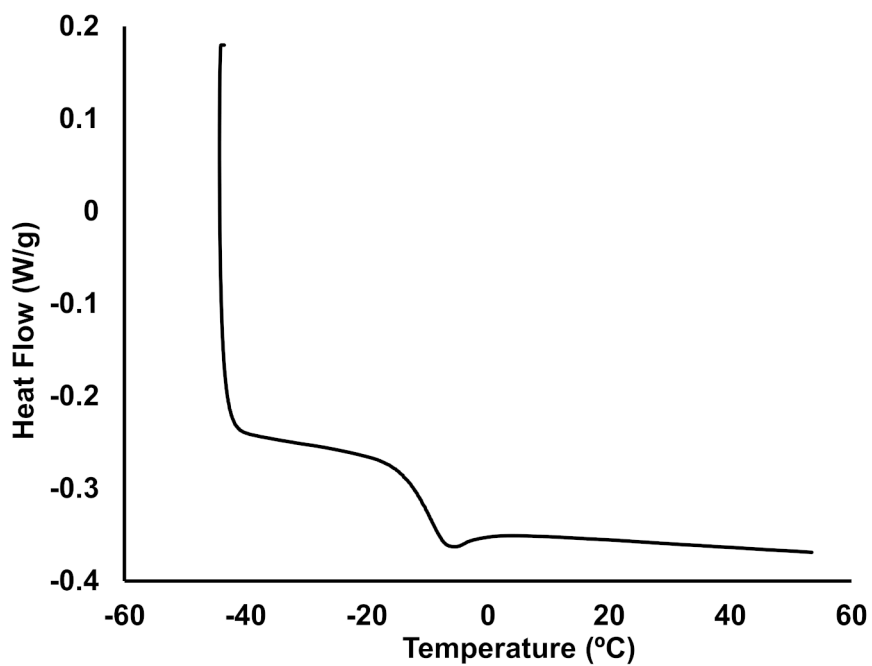


Figure A2.36. DSC thermogram of PEtG-MMT.

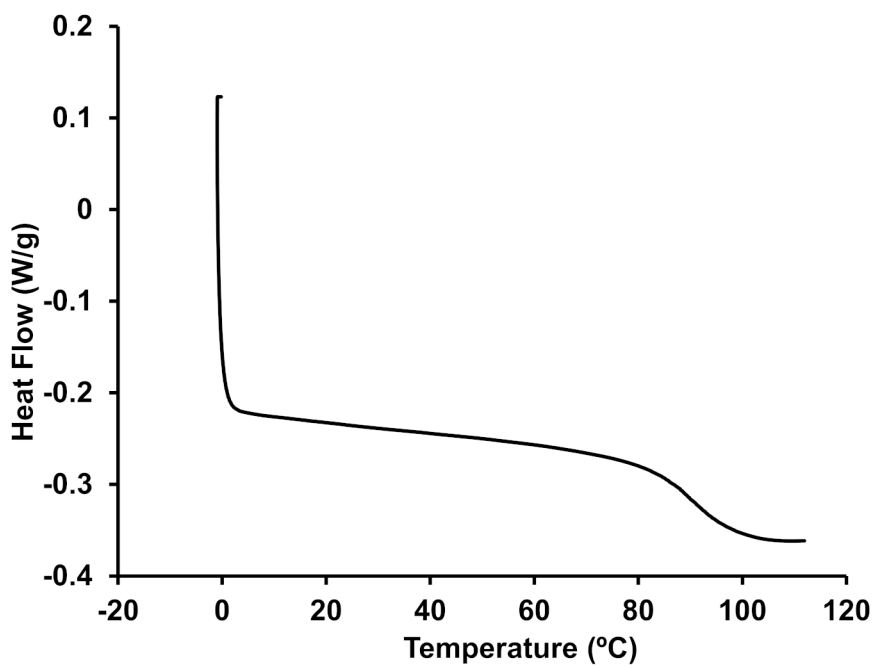


Figure A2.37. DSC thermogram of PGAm-NMe-MMT.

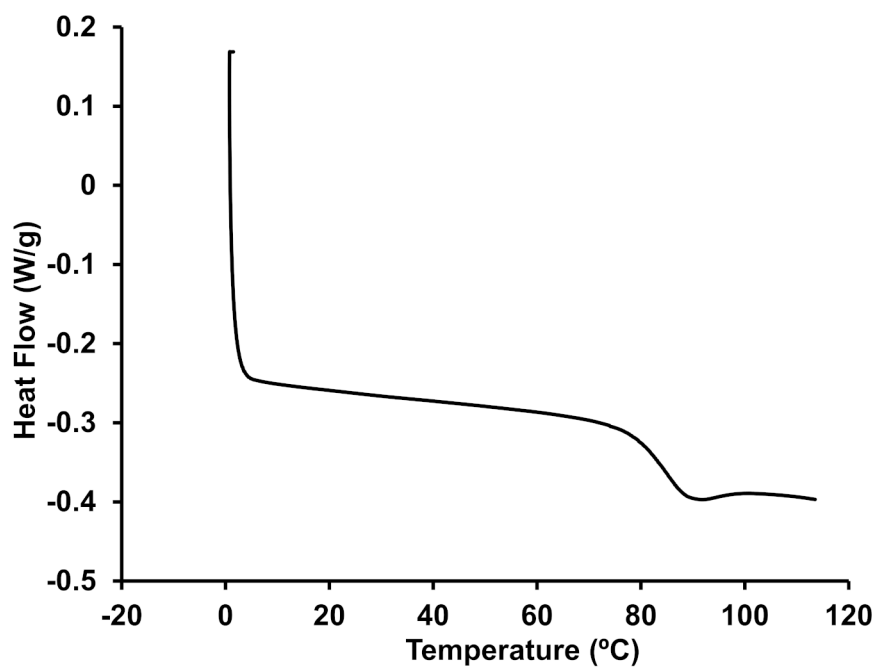


Figure A2.38. DSC thermogram of PGAm-NEt-MMT.

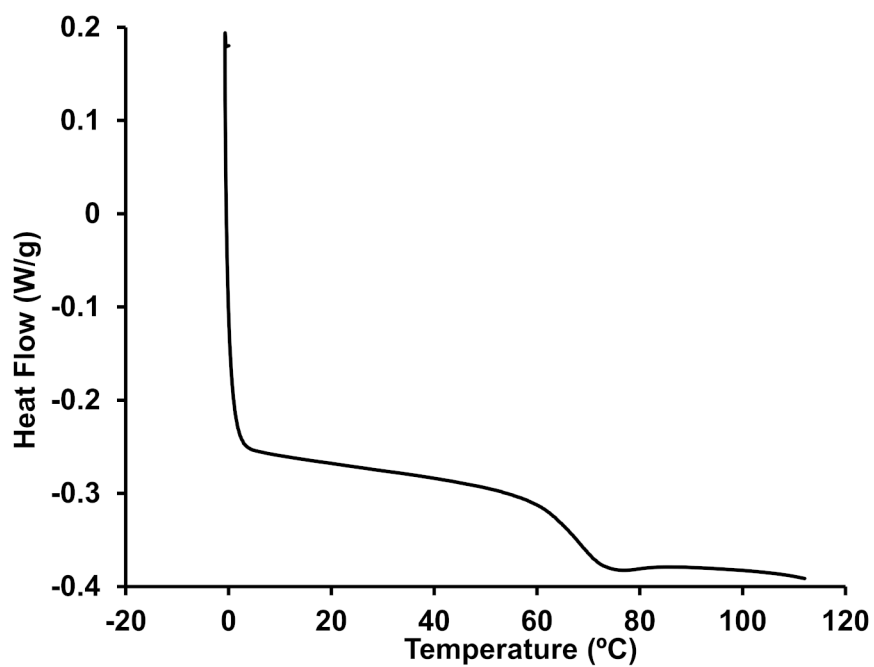


Figure A2.39. DSC thermogram of PGAm-NnPr-MMT.

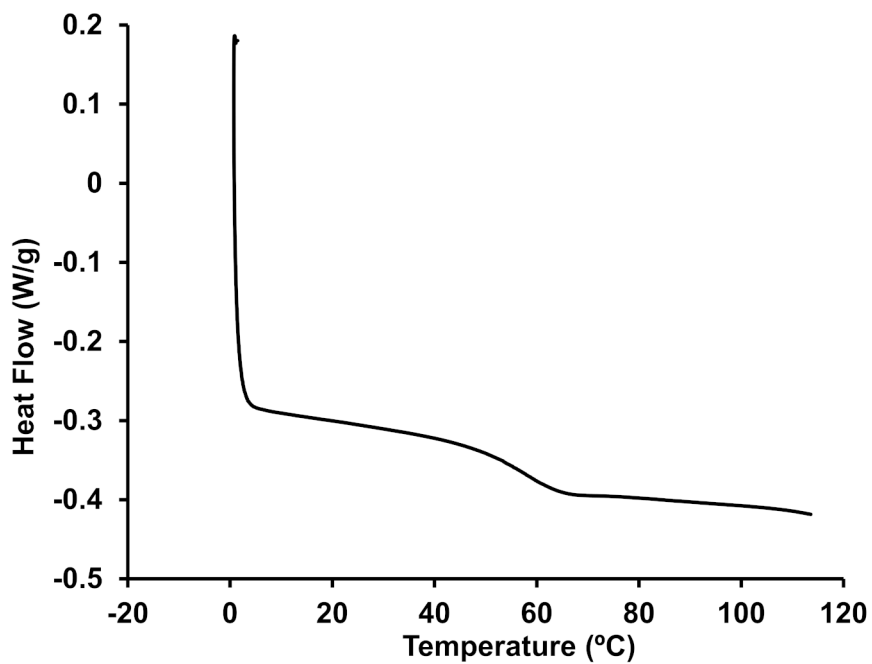


Figure A2.40. DSC thermogram of PGAm-NnBu-MMT.

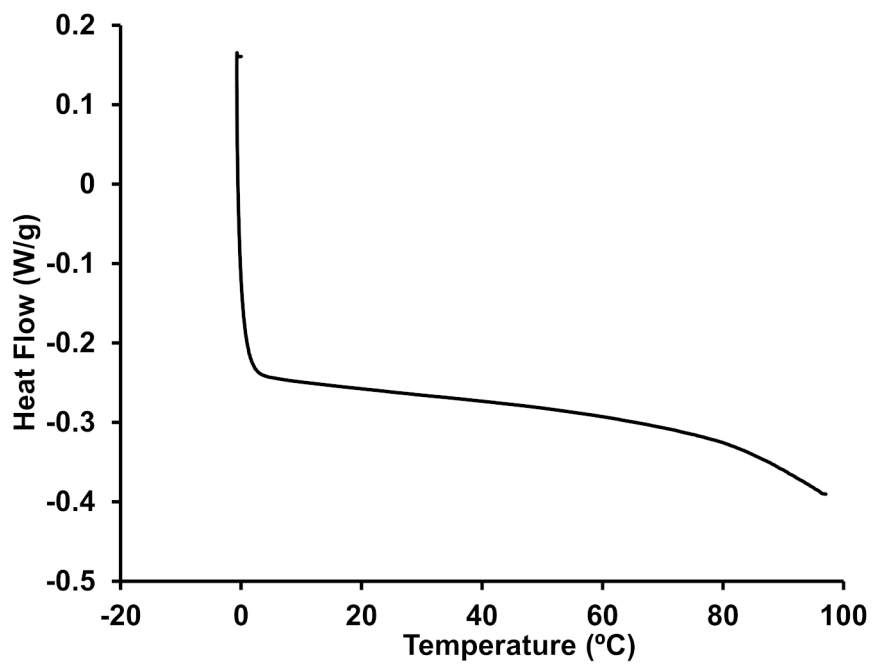


Figure A2.41. DSC thermogram of PGAm-NiPr-MMT.

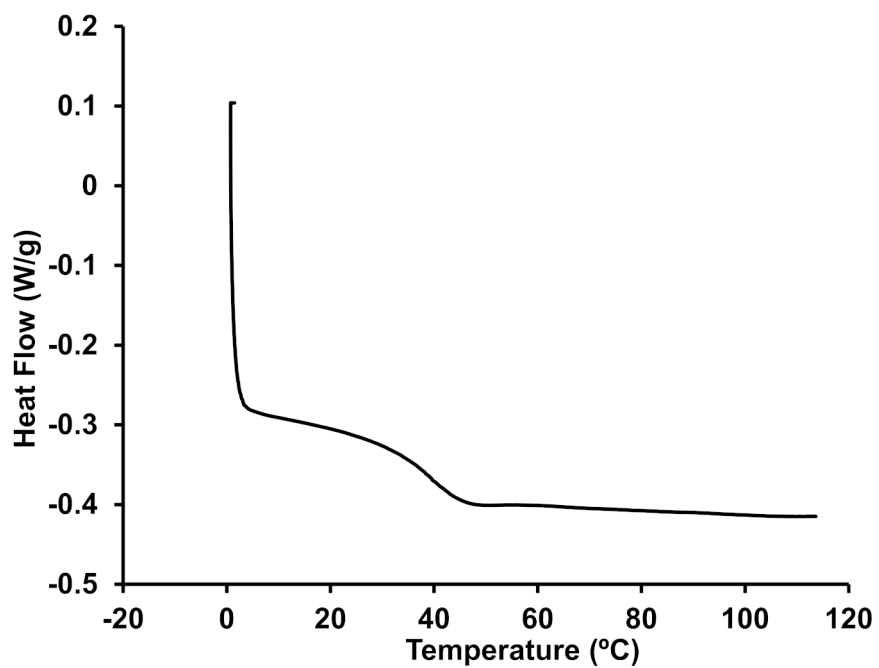


Figure A2.42. DSC thermogram of PGAm-DMAE-MMT.

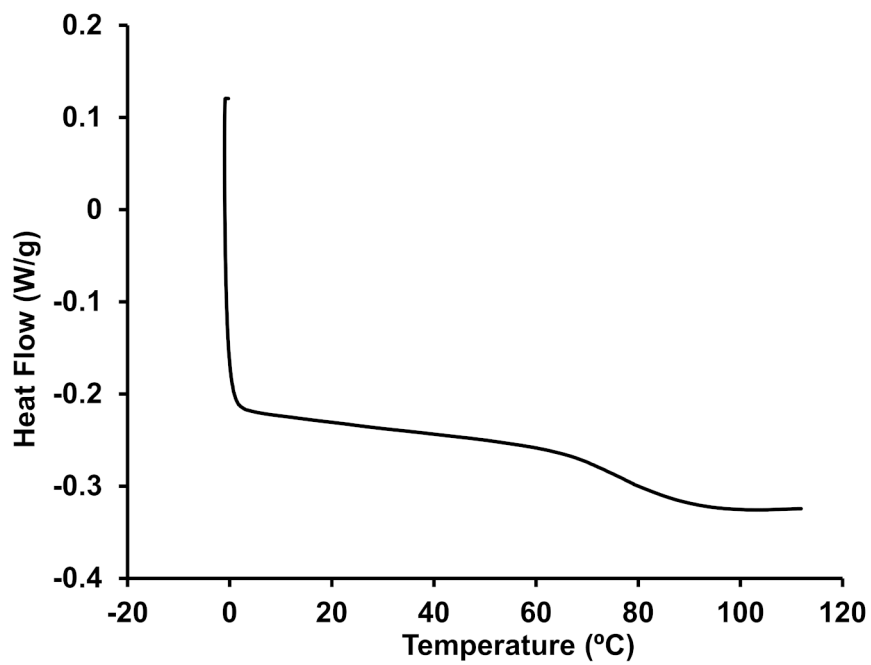


Figure A2.43. DSC thermogram of PGAm-Pyrr-MMT.

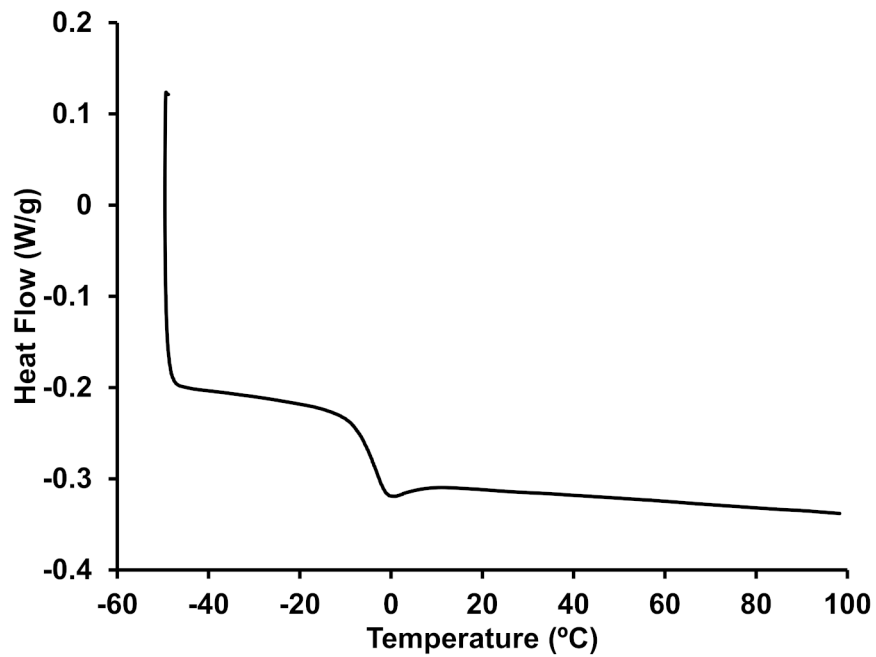


Figure A2.44. DSC thermogram of PEtG-Trit.

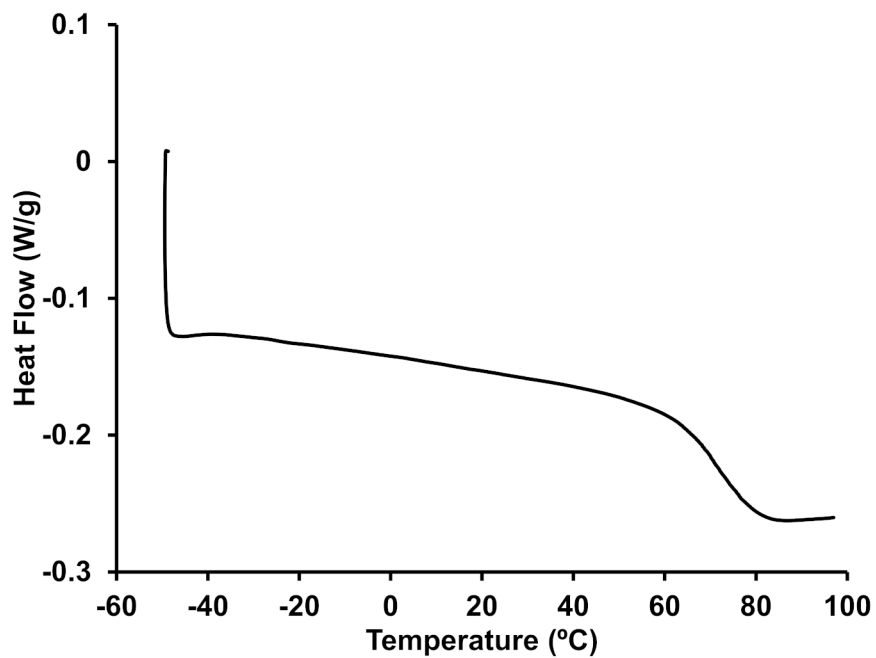


Figure A2.45. DSC thermogram of PGAm-NMe-Trit.

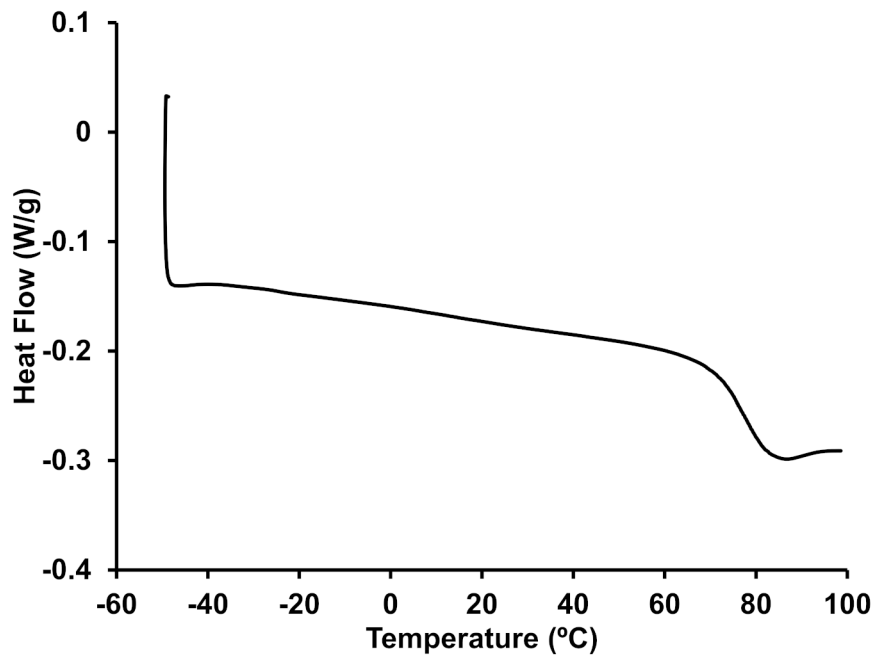


Figure A2.46. DSC thermogram of PGAm-NEt-Trit.

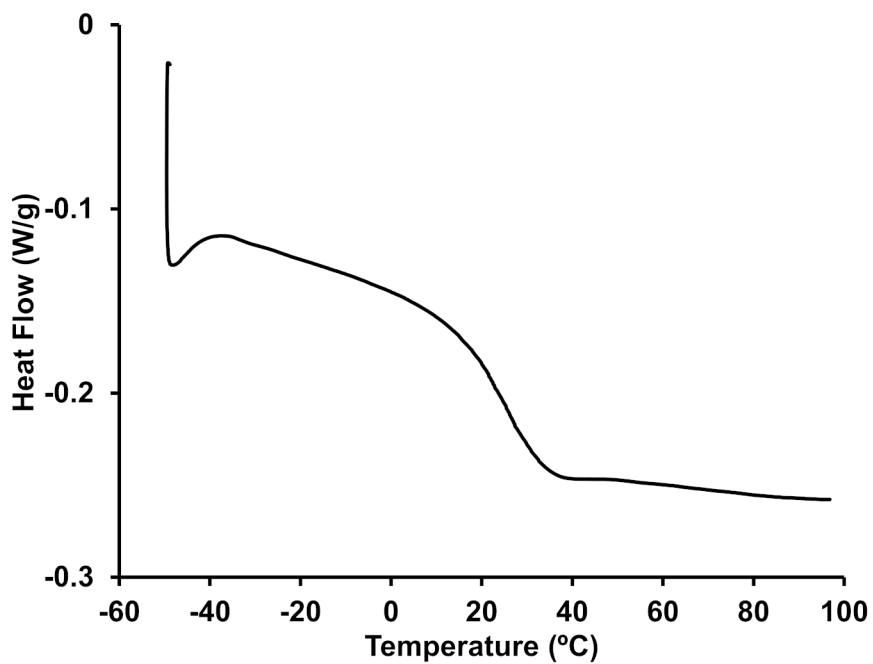


Figure A2.47. DSC thermogram of PGAm-DMAE-Trit.

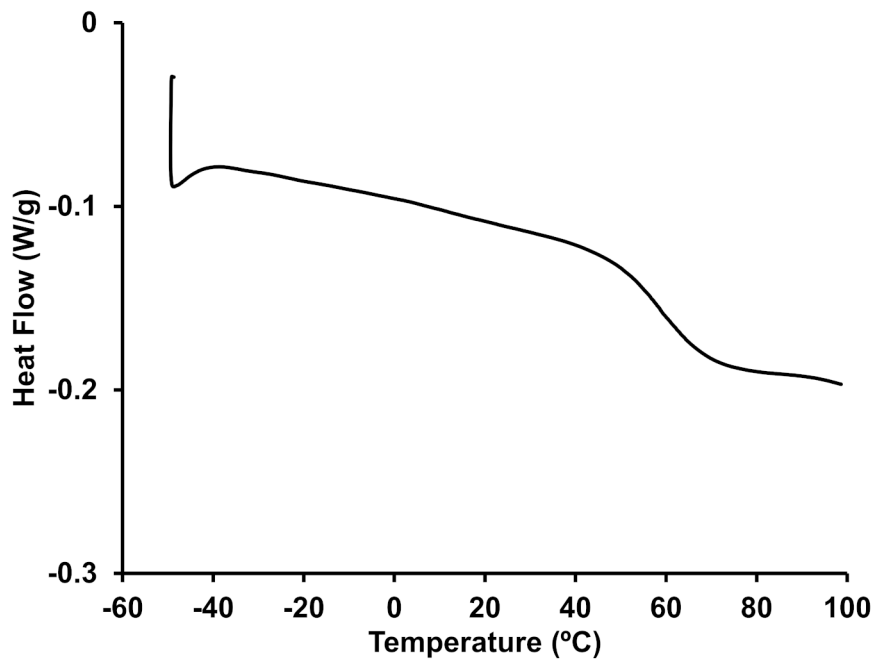


Figure A2.48. DSC thermogram of PGAm-Pyrr-Trit.

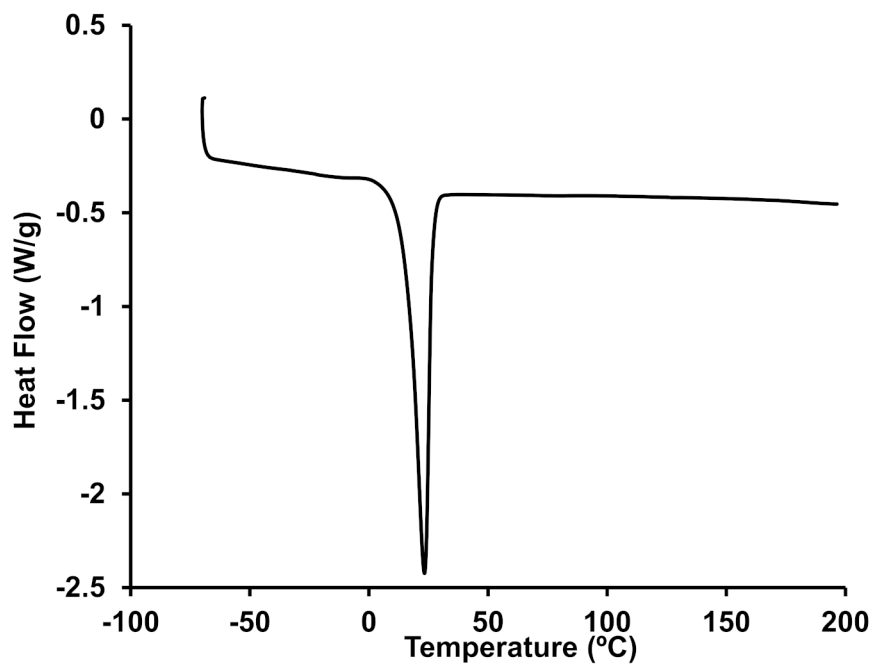


Figure A2.49. DSC thermogram of PGAm-OEG-Trit.

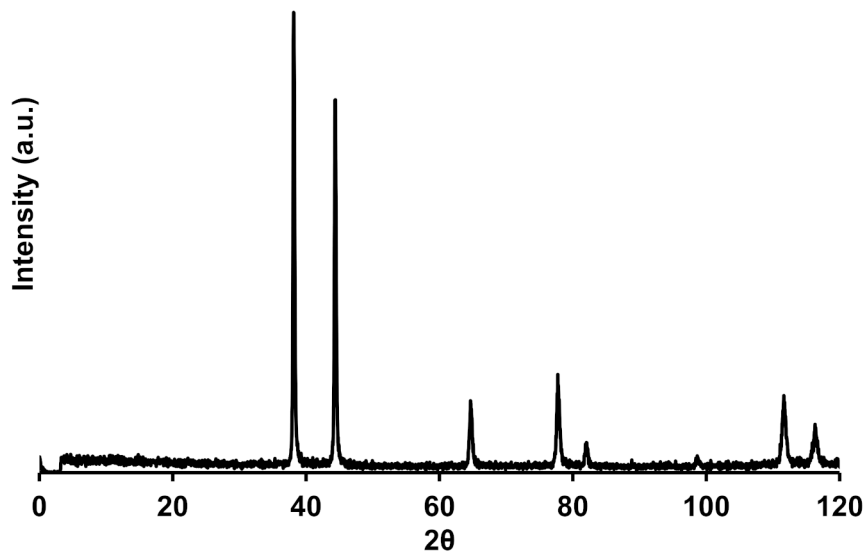


Figure A2.50. Powder X-ray diffractogram of the background (Al sample holder).

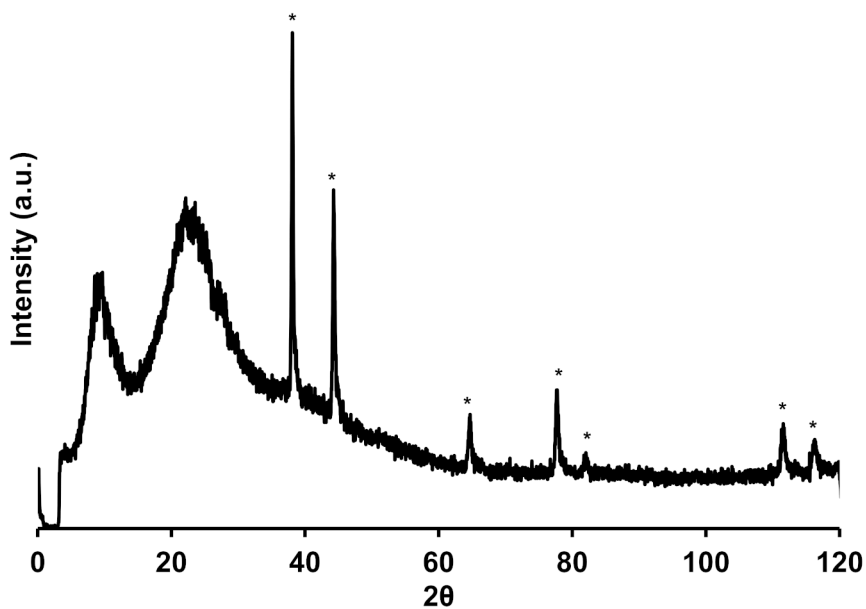


Figure A2.51. Powder X-ray diffractogram of **PGAm-NMe-MMT**. The background peaks from the Al sample holder (Figure A2.50) are identified with asterisks.

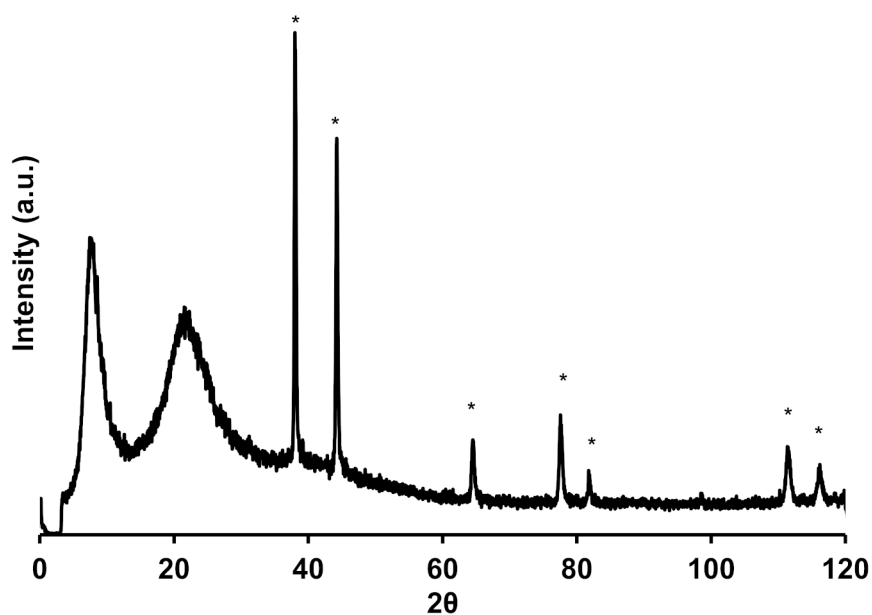


Figure A2.52. Powder X-ray diffractogram of **PGAm-NEt-MMT**. The background peaks from the Al sample holder (Figure A2.50) are identified with asterisks.

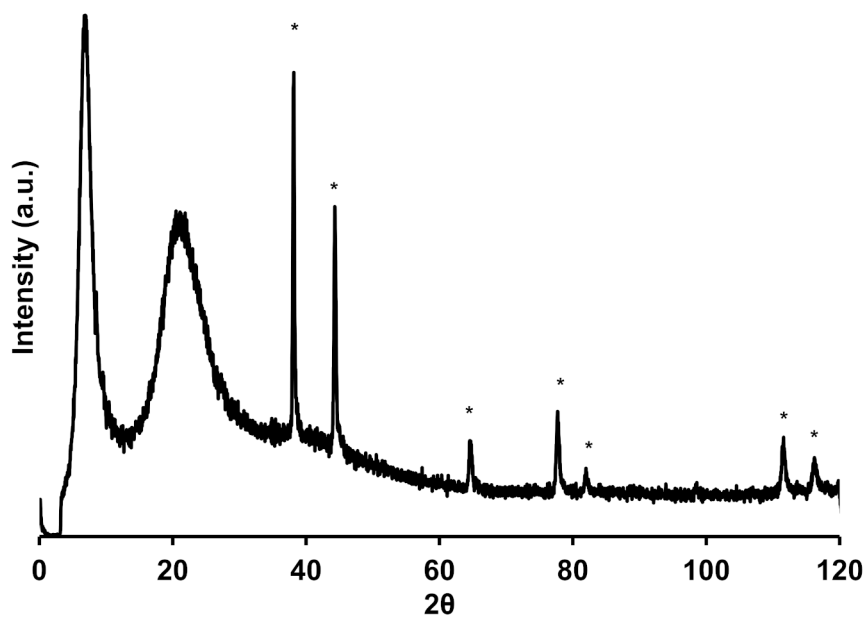


Figure A2.53. Powder X-ray diffractogram of **PGAm-NnPr-MMT**. The background peaks from the Al sample holder (Figure A2.50) are identified with asterisks.

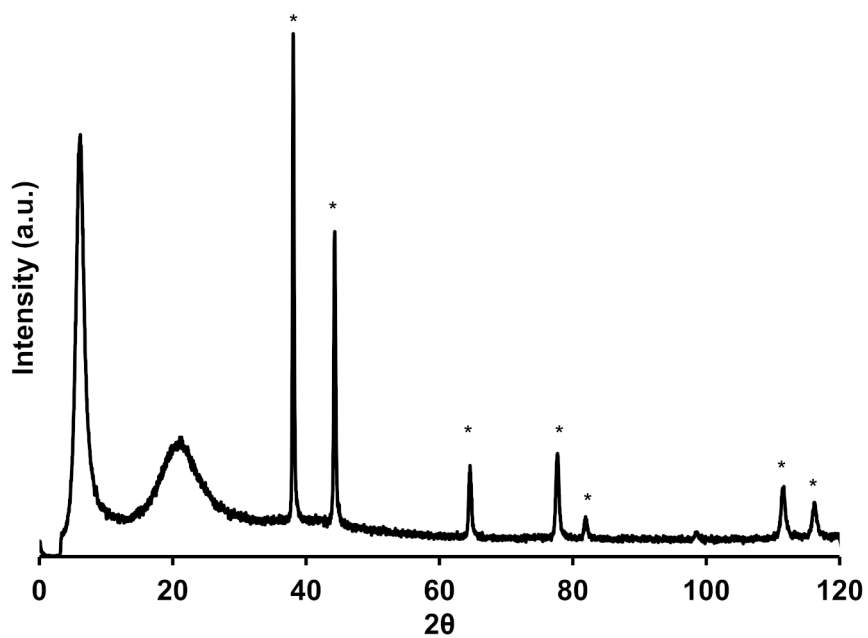


Figure A2.54. Powder X-ray diffractogram of PGAm-NnBu-MMT. The background peaks from the Al sample holder (Figure A2.50) are identified with asterisks.

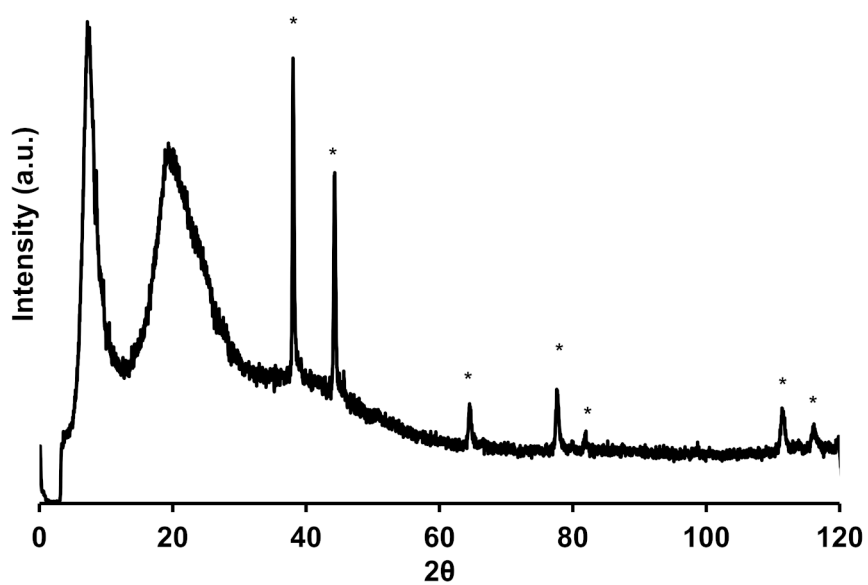


Figure A2.55. Powder X-ray diffractogram of PGAm-NiPr-MMT. The background peaks from the Al sample holder (Figure A2.50) are identified with asterisks.

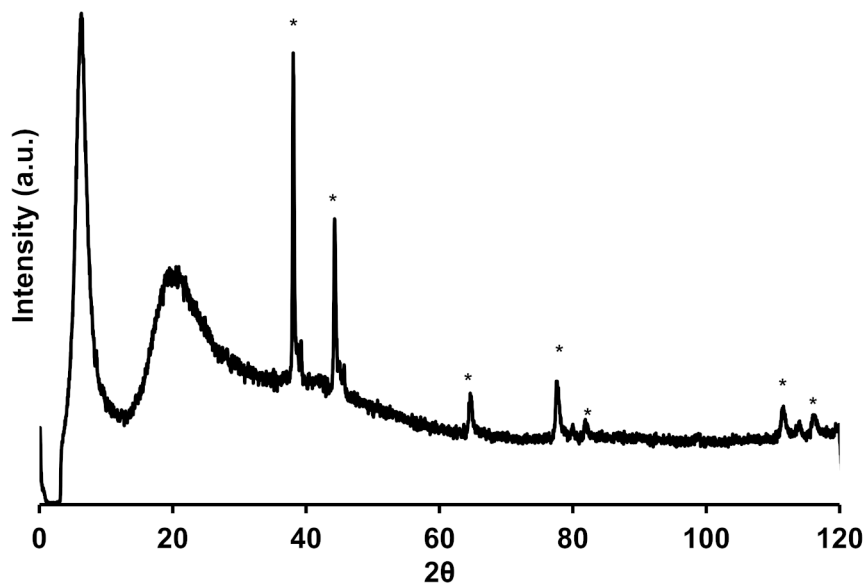


Figure A2.56. Powder X-ray diffractogram of **PGAm-DMAE-MMT**. The background peaks from the Al sample holder (Figure A2.50) are identified with asterisks.

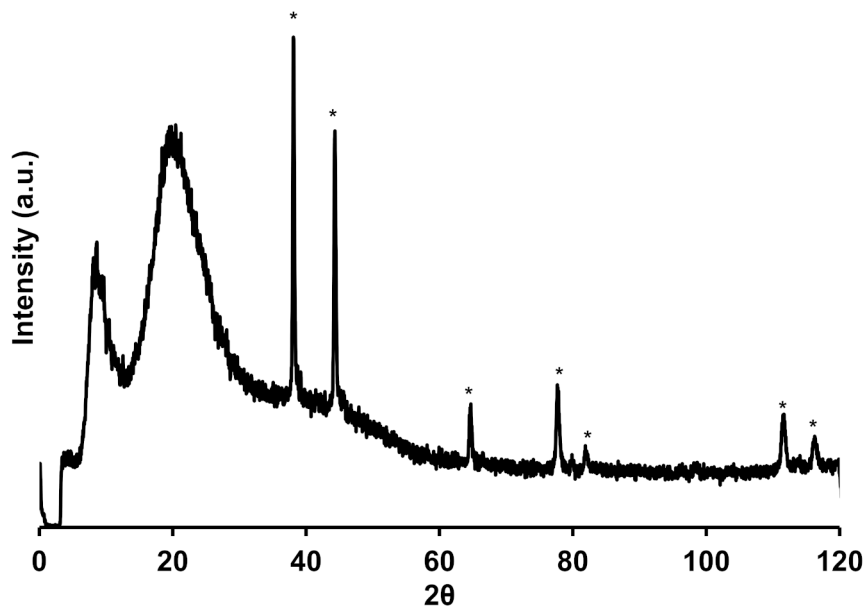


Figure A2.57. Powder X-ray diffractogram of **PGAm-Pyrr-MMT**. The background peaks from the Al sample holder (Figure A2.50) are identified with asterisks.

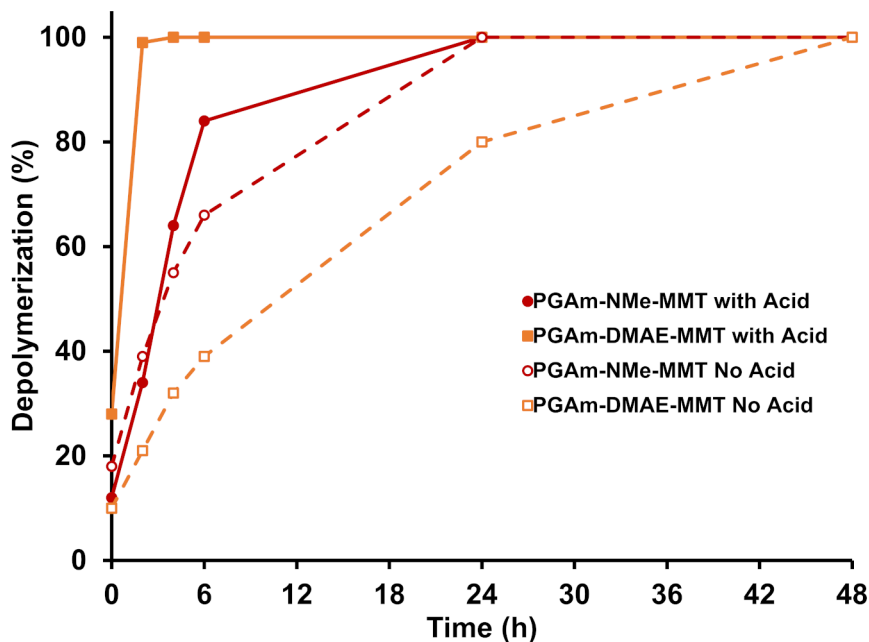


Figure A2.58. Depolymerization of **PGAm-NMe-MMT** and **PGAm-DMAE-MMT** in 9:1 deuterated water:acetonitrile with and without glacial acetic acid (0.9 M) as the stimulus.

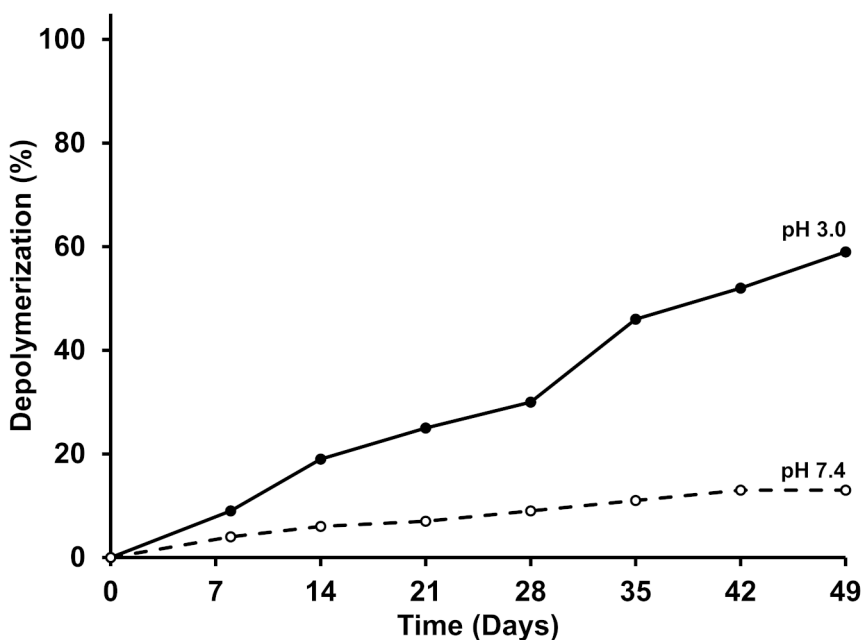


Figure A2.59. Depolymerization of **PGAm-OEG-Trit** in either citrate-buffered D_2O (0.1 M, pH 3.0) or phosphate-buffered D_2O (0.1 M, pH 7.4).

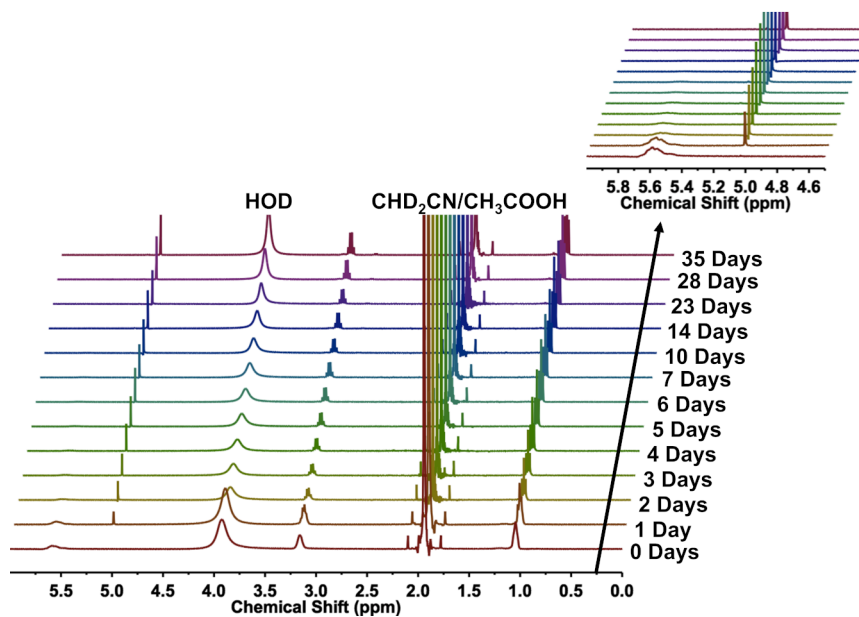


Figure A2.60. Depolymerization of PGAm-NET-MMT in 9:1 deuterated acetonitrile:water with acetic acid (0.9 M) monitored by ^1H NMR (400 MHz).

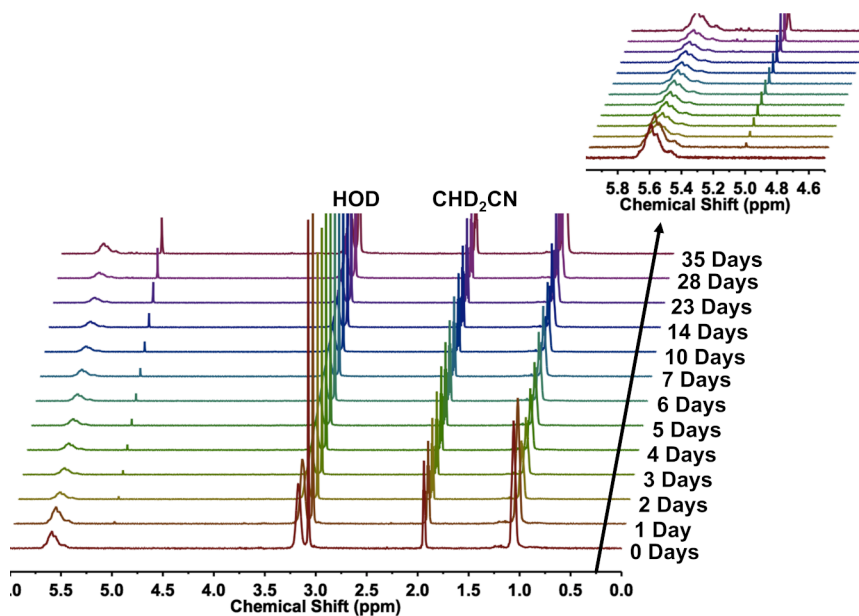


Figure A2.61. Depolymerization of PGAm-NET-MMT in 9:1 deuterated acetonitrile:water with acetic acid (0.9 M) monitored by ^1H NMR (400 MHz).

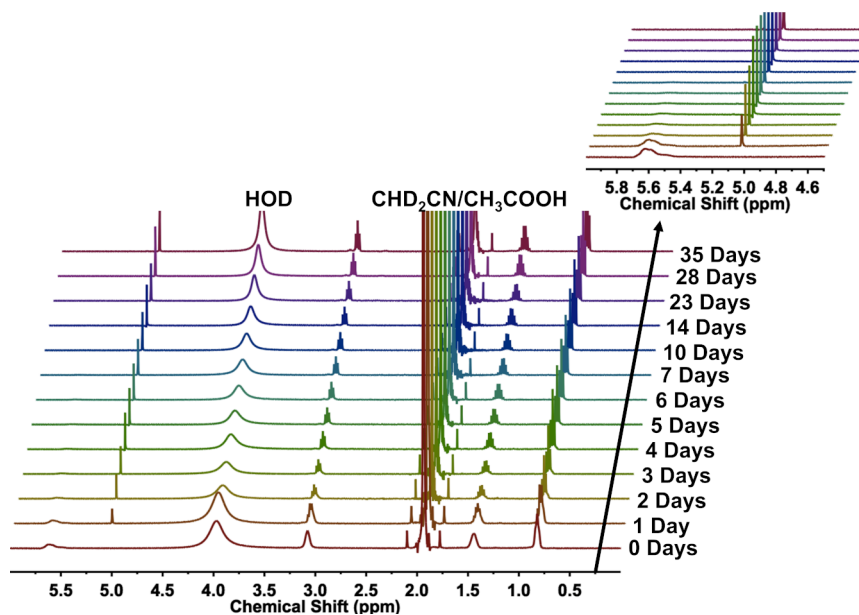


Figure A2.62. Depolymerization of PGAm-NnPr-MMT in 9:1 deuterated acetonitrile:water with acetic acid (0.9 M) monitored by ^1H NMR (400 MHz).

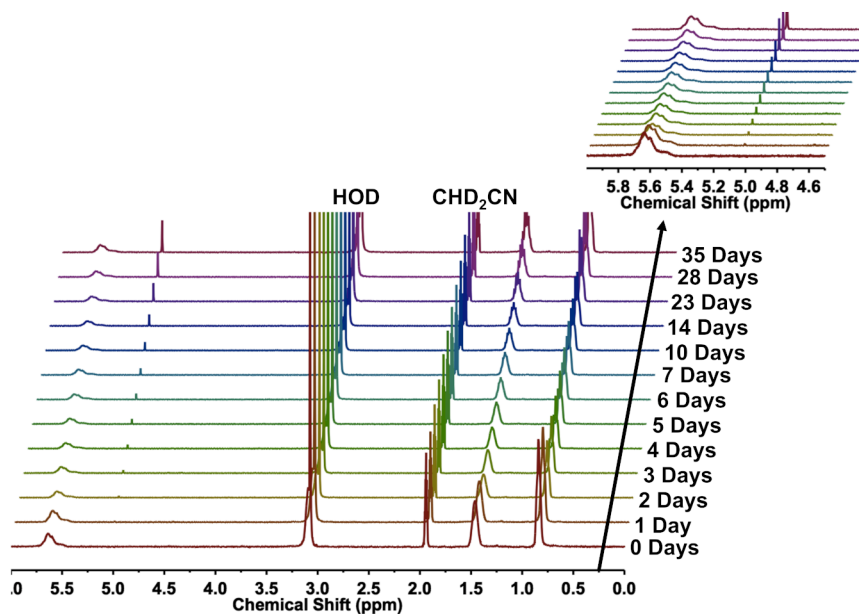


Figure A2.63. Depolymerization of PGAm-NnPr-MMT in 9:1 deuterated acetonitrile:water monitored by ^1H NMR (400 MHz).

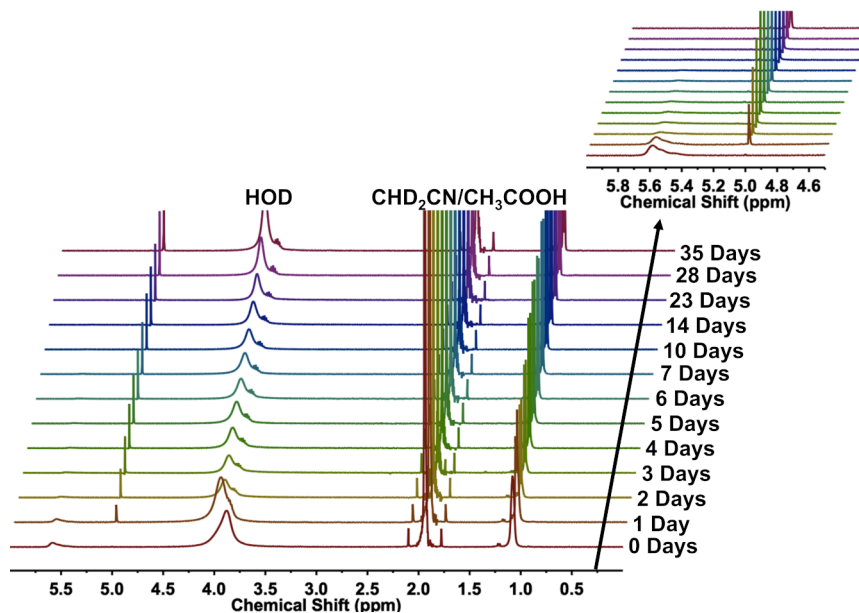


Figure A2.64. Depolymerization of **PGAm-NiPr-MMT** in 9:1 deuterated acetonitrile:water with acetic acid (0.9 M) monitored by ^1H NMR (400 MHz).

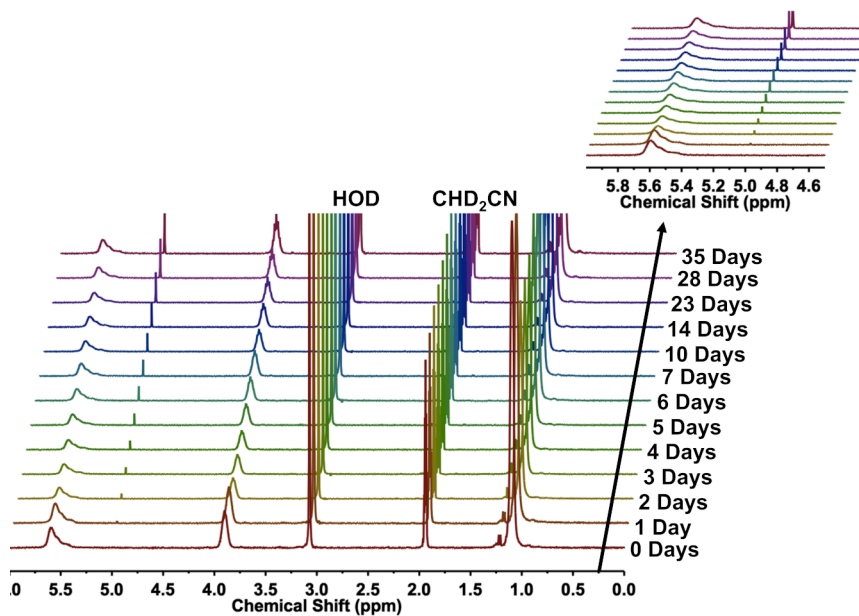


Figure A2.65. Depolymerization of **PGAm-NiPr-MMT** in 9:1 deuterated acetonitrile:water monitored by ^1H NMR (400 MHz).

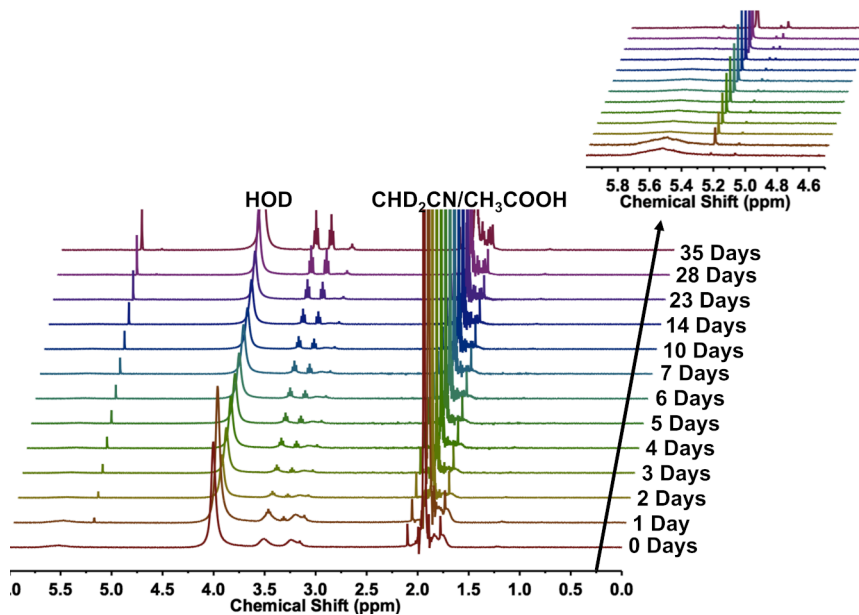


Figure A2.66. Depolymerization of **PGAm-Pyrr-MMT** in 9:1 deuterated acetonitrile:water with acetic acid (0.9 M) monitored by ^1H NMR (400 MHz).

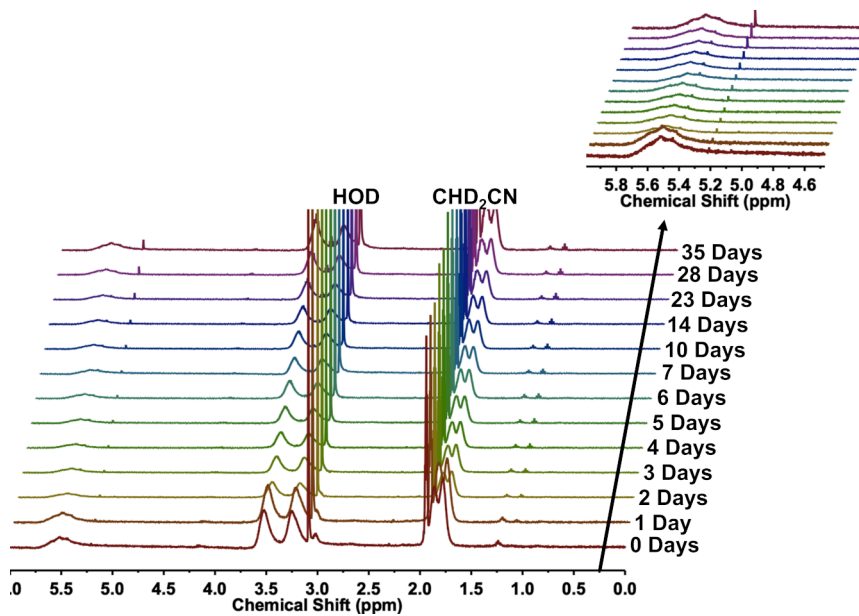


Figure A2.67. Depolymerization of **PGAm-Pyrr-MMT** in 9:1 deuterated acetonitrile:water monitored by ^1H NMR (400 MHz).

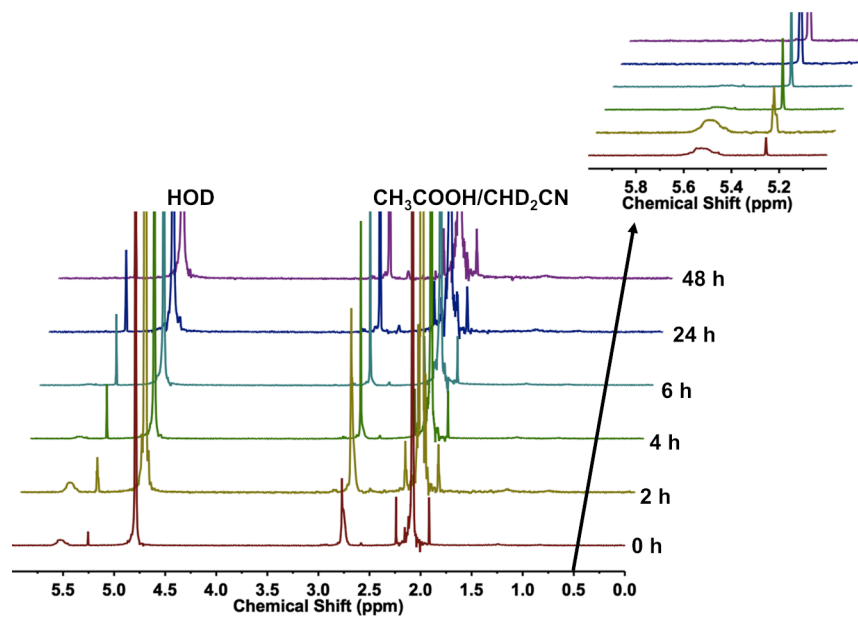


Figure A2.68. Depolymerization of PGAm-NMe-MMT in 9:1 deuterated water:acetonitrile with acetic acid (0.9 M) monitored by ^1H NMR (400 MHz).

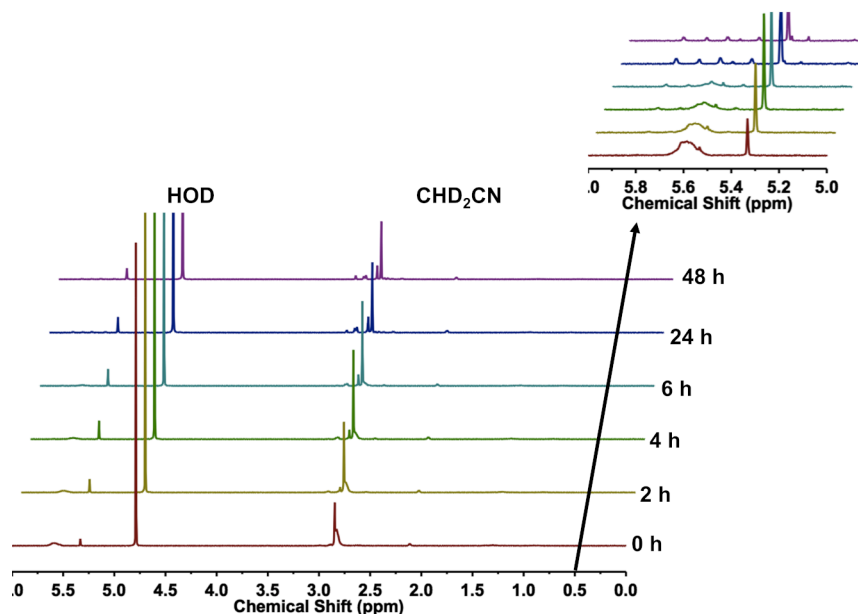


Figure A2.69. Depolymerization of PGAm-NMe-MMT in 9:1 deuterated water:acetonitrile monitored by ^1H NMR (400 MHz).

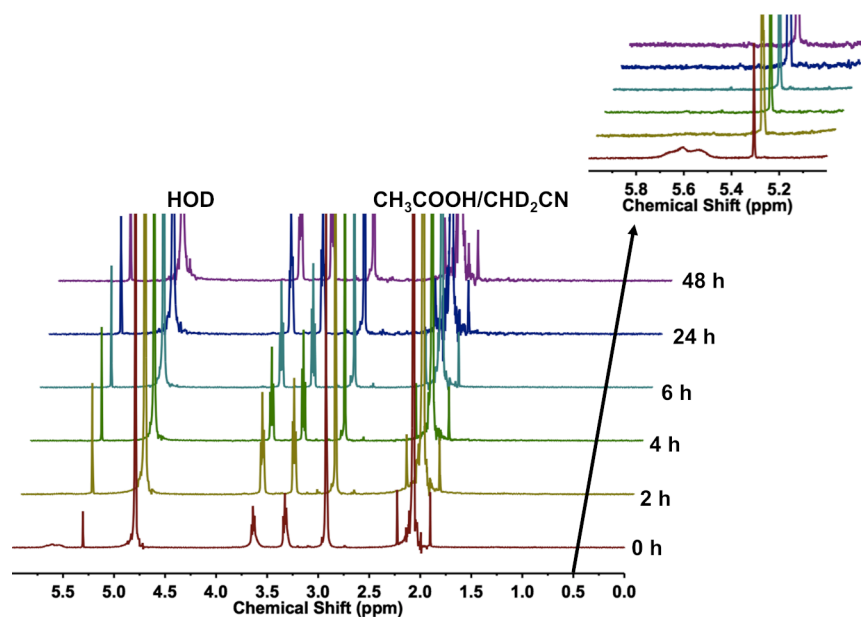


Figure A2.70. Depolymerization of PGAm-DMAE-MMT in 9:1 deuterated water:acetonitrile with acetic acid (0.9 M) monitored by ^1H NMR (400 MHz).

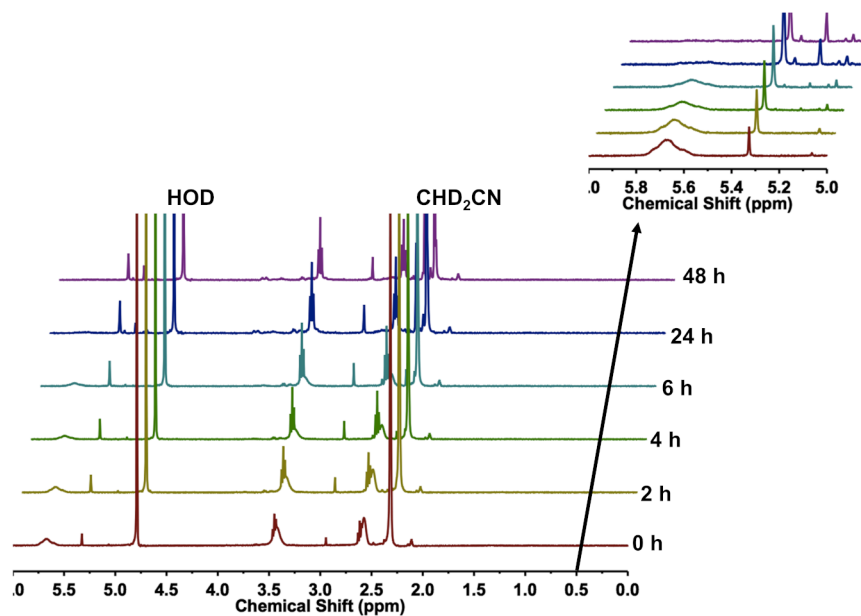


Figure A2.71. Depolymerization of PGAm-DMAE-MMT in 9:1 deuterated water:acetonitrile monitored by ^1H NMR (400 MHz).

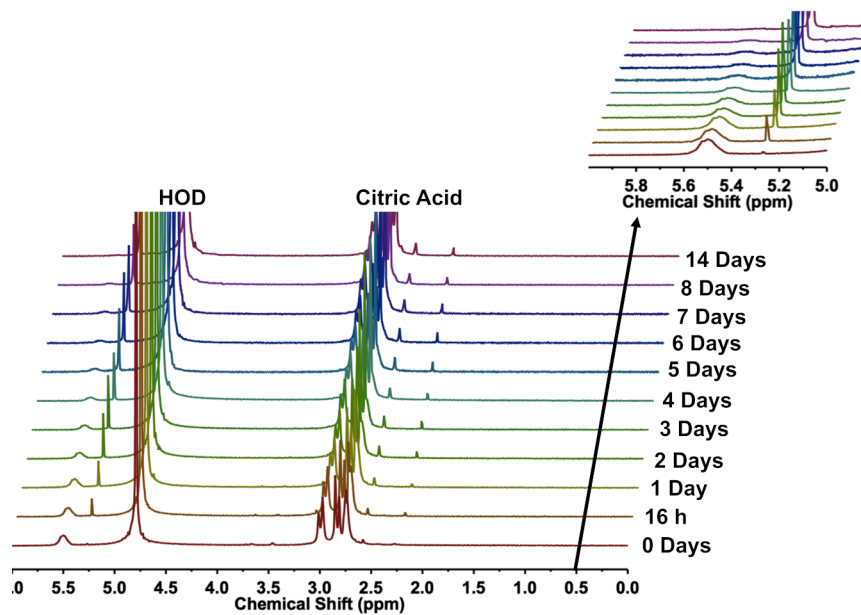


Figure A2.72. Depolymerization of **PGAm-NMe-Trit** in citrate-buffered D_2O (0.1 M, pH 3.0) monitored by 1H NMR (400 MHz).

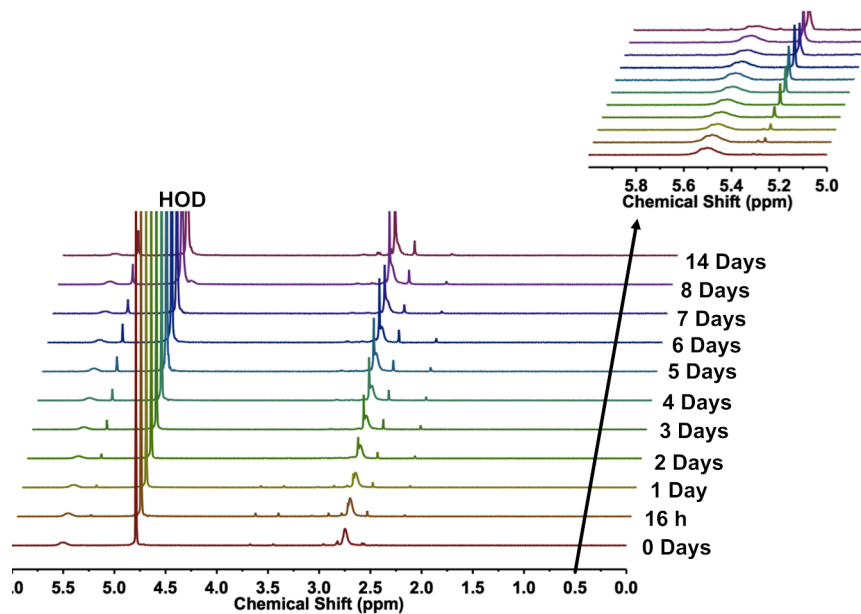


Figure A2.73. Depolymerization of **PGAm-NMe-Trit** in phosphate-buffered D_2O (0.1 M, pH 7.4) monitored by 1H NMR (400 MHz).

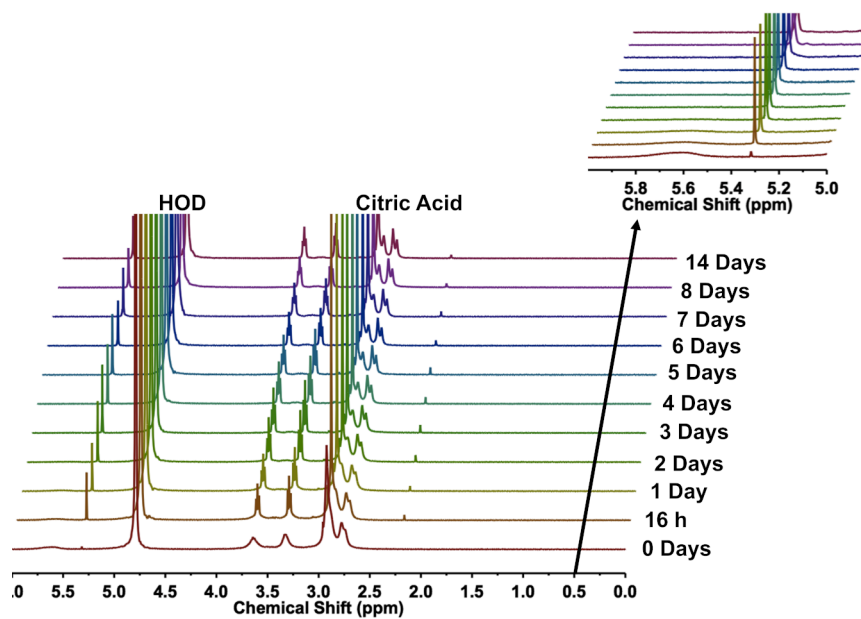


Figure A2.74. Depolymerization of **PGAm-DMAE-Trit** in citrate-buffered D_2O (0.1 M, pH 3.0) monitored by ^1H NMR (400 MHz).

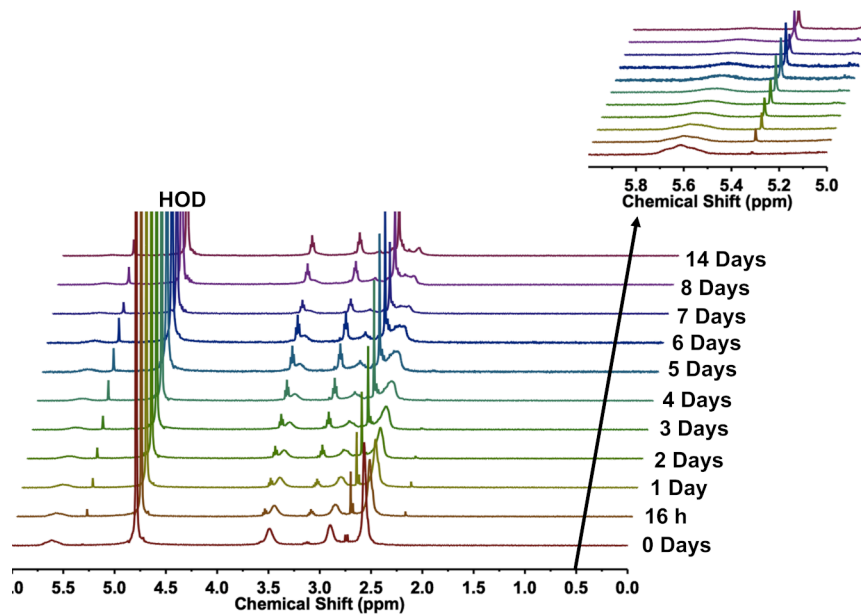


Figure A2.75. Depolymerization of **PGAm-DMAE-Trit** in phosphate-buffered D_2O (0.1 M, pH 7.4) monitored by ^1H NMR (400 MHz).

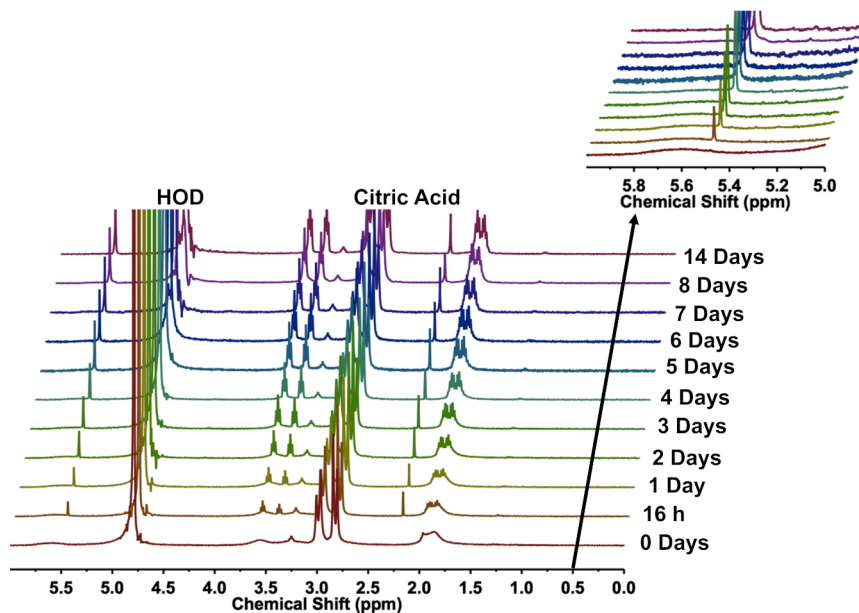


Figure A2.76. Depolymerization of PGAm-Pyrr-Trit in citrate-buffered D_2O (0.1 M, pH 3.0) monitored by ^1H NMR (400 MHz).

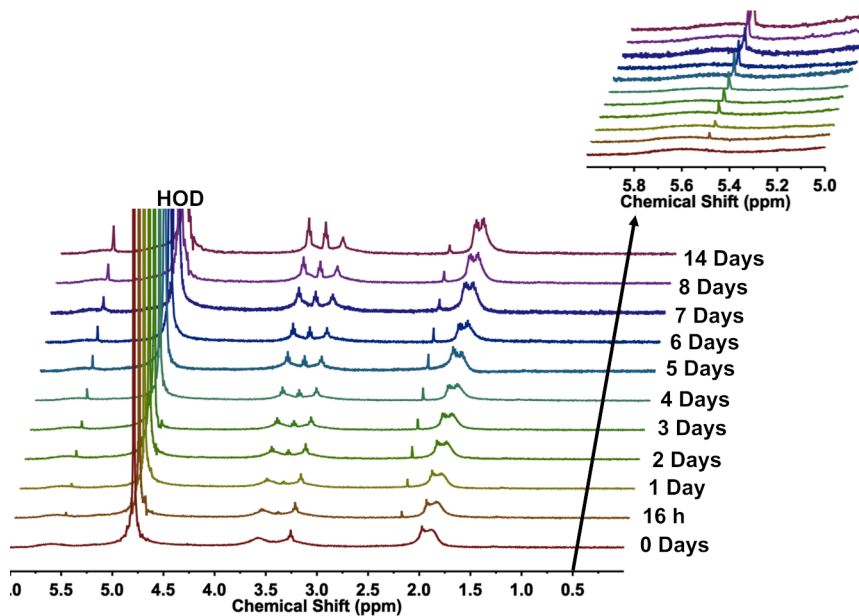


Figure A2.77. Depolymerization of PGAm-Pyrr-Trit in phosphate-buffered D_2O (0.1 M, pH 7.4) monitored by ^1H NMR (400 MHz).

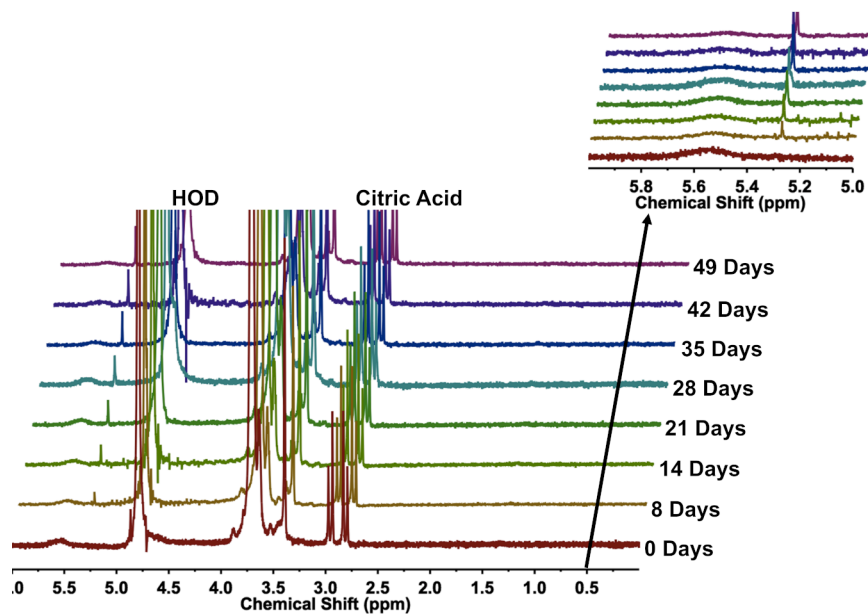


Figure A2.78. Depolymerization of PGAm-OEG-Trit in citrate-buffered D_2O (0.1 M, pH 3.0) monitored by ^1H NMR (400 MHz).

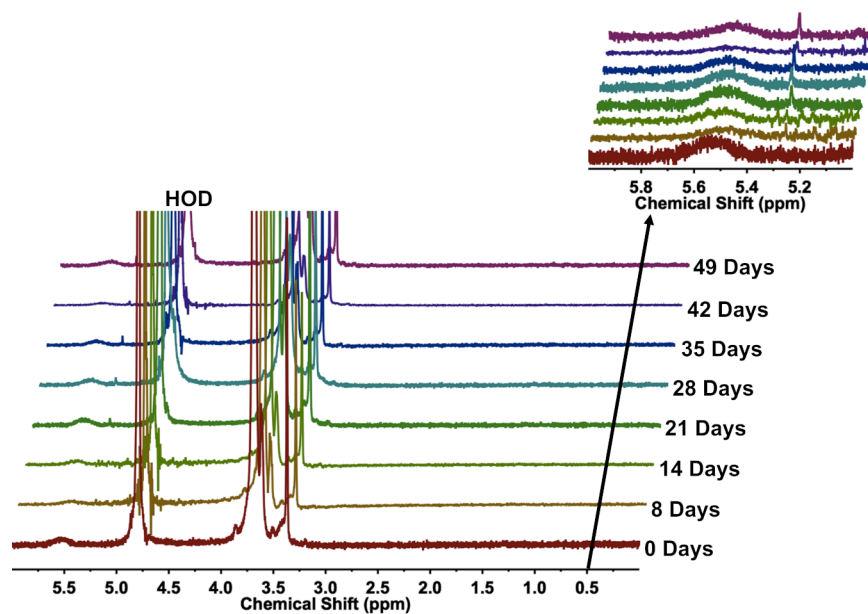


Figure A2.79. Depolymerization of PGAm-OEG-Trit in phosphate-buffered D_2O (0.1 M, pH 7.4) monitored by ^1H NMR (400 MHz).

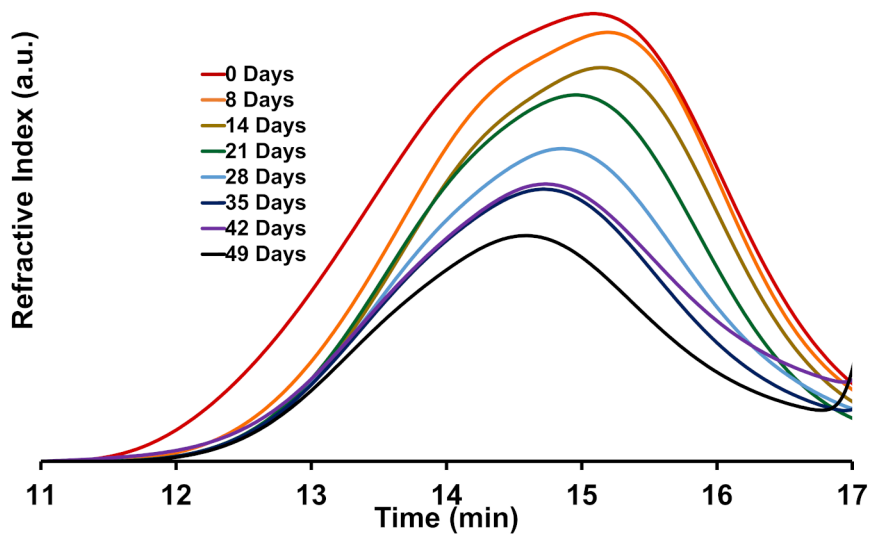


Figure A2.80. Depolymerization of PGAm-OEG-Trit in citrate-buffered D₂O (0.1 M, pH 3.0) monitored by SEC.

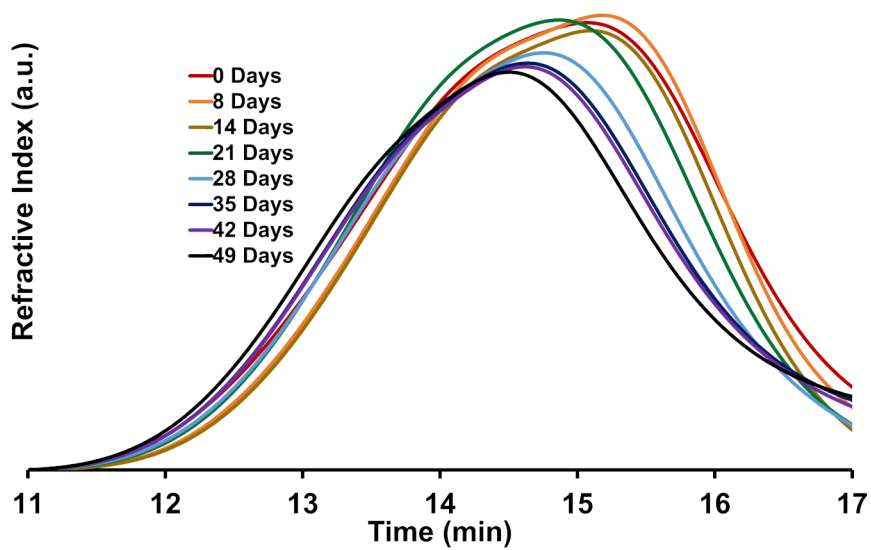


Figure A2.81. Depolymerization of PGAm-OEG-Trit in phosphate-buffered D₂O (0.1 M, pH 7.4) monitored by SEC.

Appendix 3

3 Supplemental Data for Chapter 4 Including NMR and FT-IR Spectra, Size-Exclusion Chromatograms, Turbidimetry Curves, DLS Studies, Depolymerization Studies, and Depolymerization Kinetic Plots

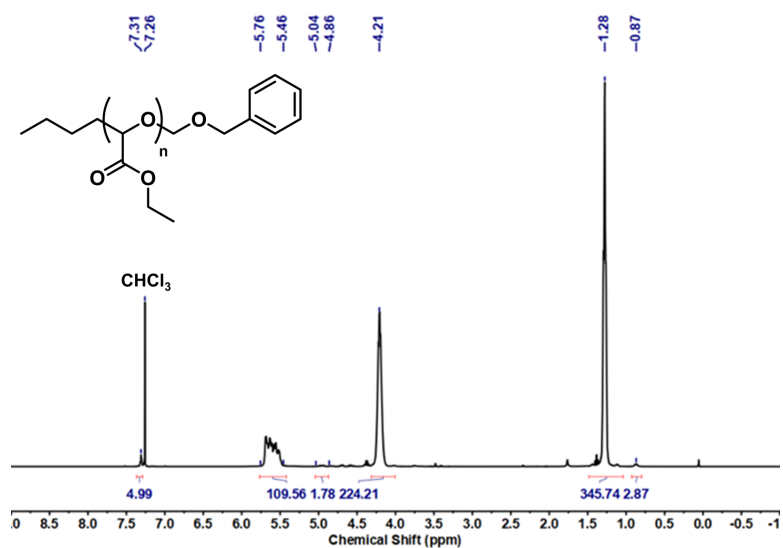


Figure A3.1. ¹H NMR spectrum of PEtG-BOM (CDCl₃, 400 MHz).

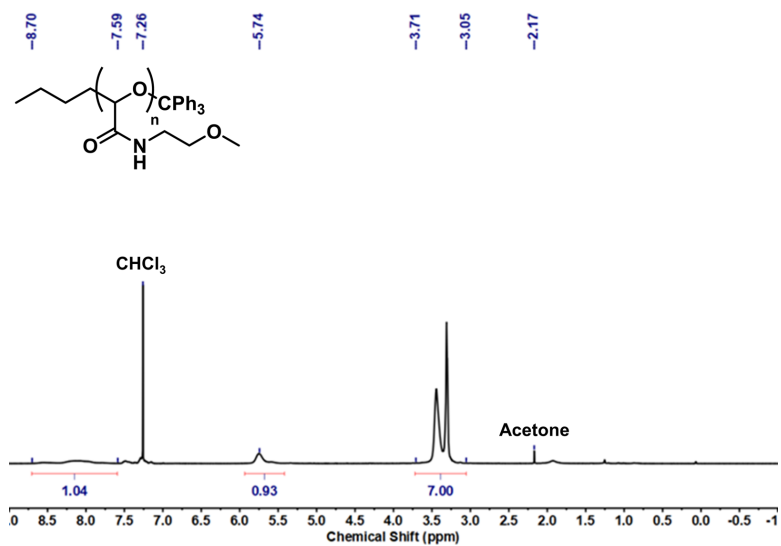


Figure A3.2. ¹H NMR spectrum of P(MeMEG)-Trit (CDCl₃, 400 MHz).

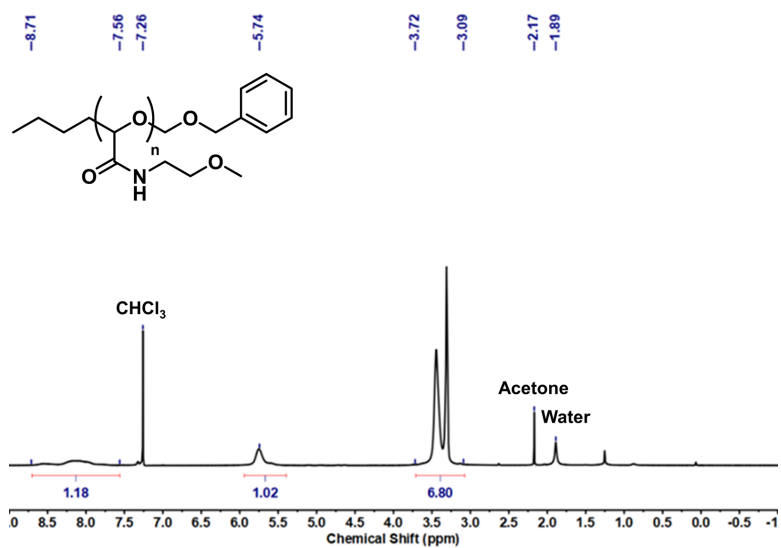


Figure A3.3. ¹H NMR spectrum of P(MeMEG)-BOM (CDCl₃, 400 MHz).

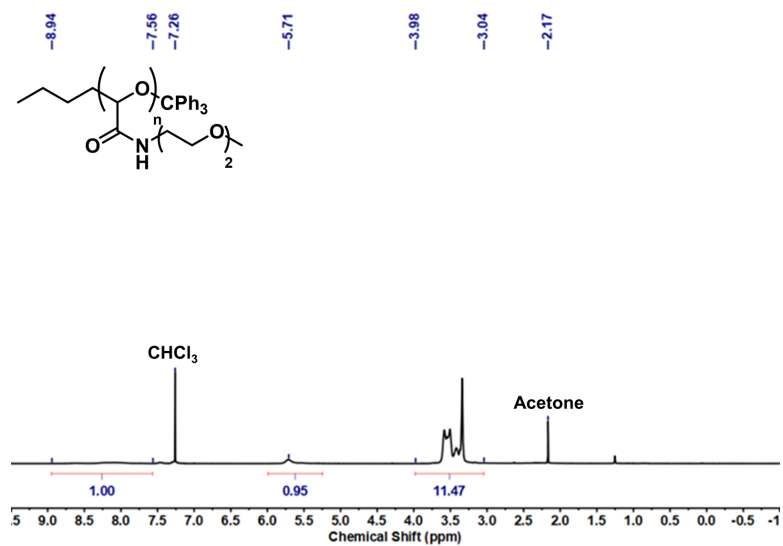


Figure A3.4. ^1H NMR spectrum of **P(MeDEG)-Trit** (CDCl_3 , 400 MHz).

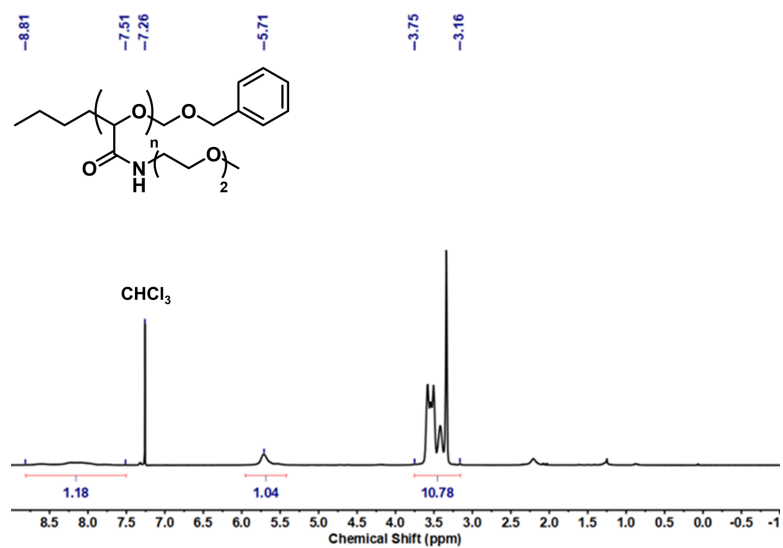


Figure A3.5. ^1H NMR spectrum of **P(MeDEG)-BOM** (CDCl_3 , 400 MHz).

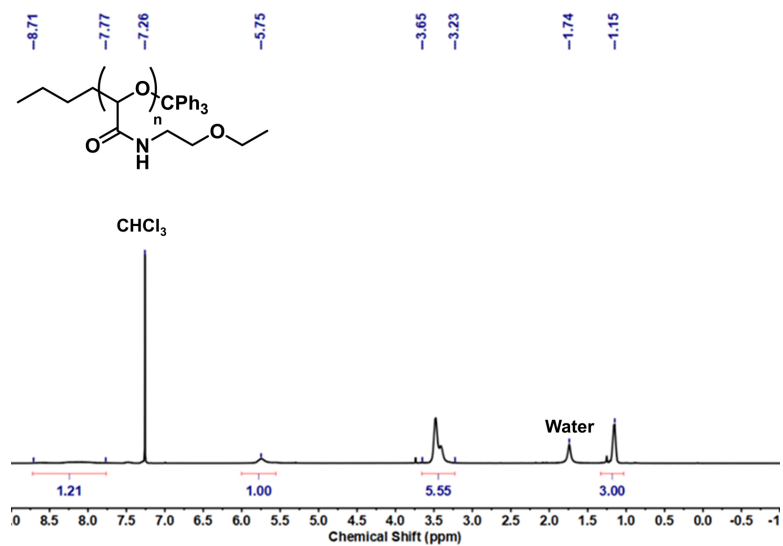


Figure A3.6. ^1H NMR spectrum of P(EtMEG)-Trit (CDCl₃, 400 MHz).

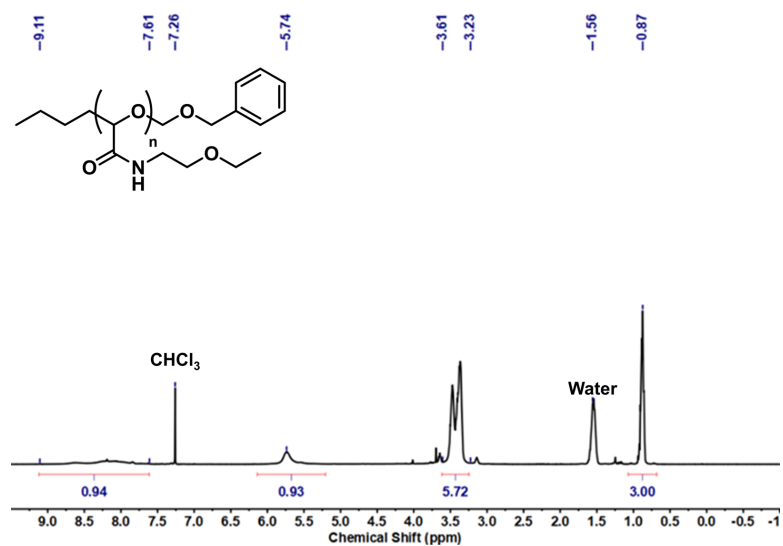


Figure A3.7. ^1H NMR spectrum of P(EtMEG)-BOM (CDCl₃, 400 MHz).

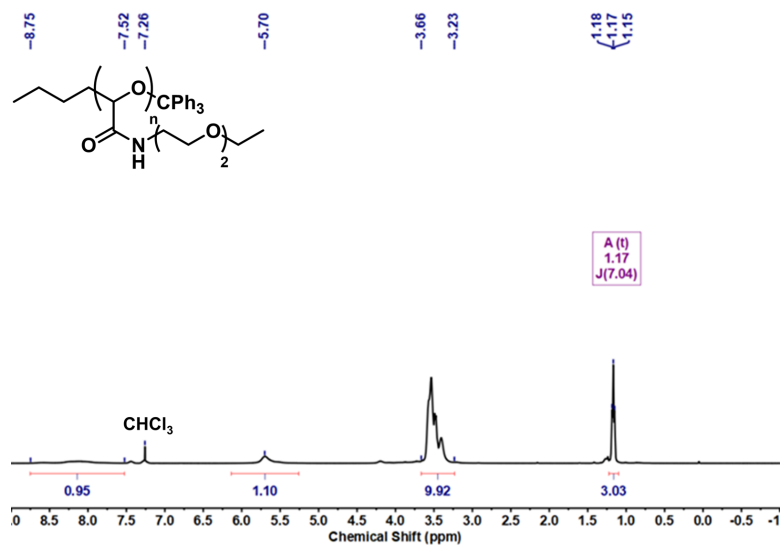


Figure A3.8. ¹H NMR spectrum of P(EtDEG)-Trit (CDCl₃, 400 MHz).

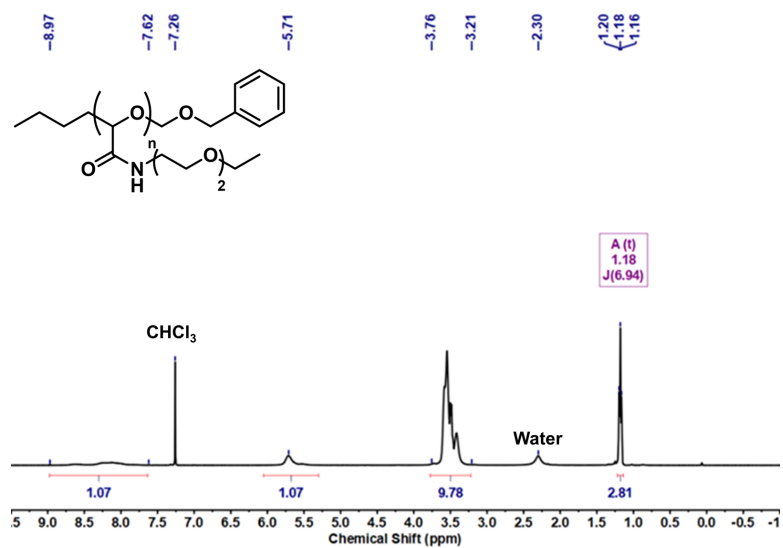


Figure A3.9. ¹H NMR spectrum of P(EtDEG)-BOM (CDCl₃, 400 MHz).

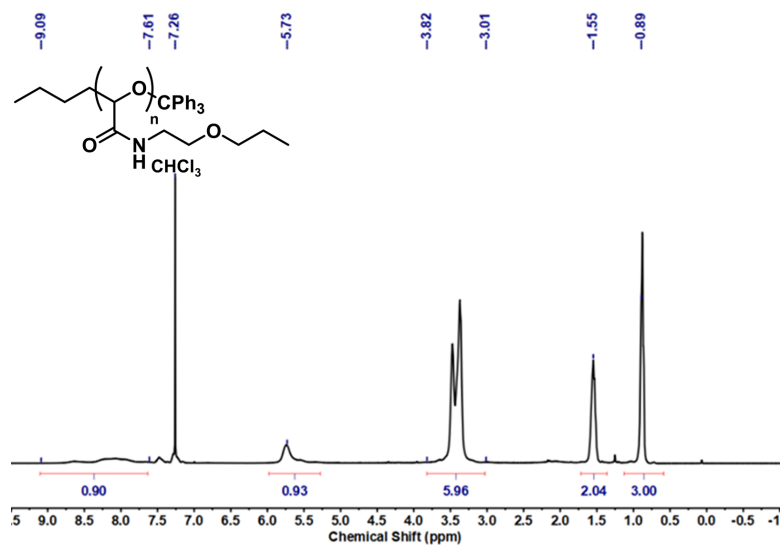


Figure A3.10. ¹H NMR spectrum of P(PrMEG)-Trit (CDCl₃, 400 MHz).

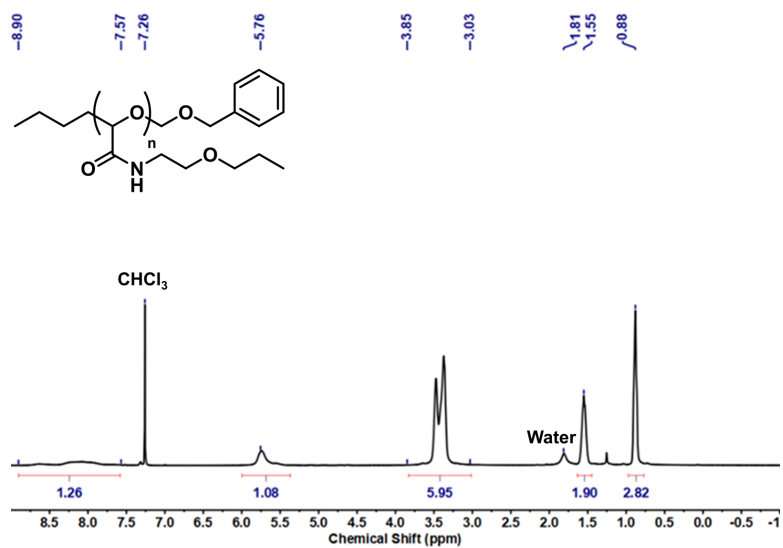


Figure A3.11. ¹H NMR spectrum of P(PrMEG)-BOM (CDCl₃, 400 MHz).

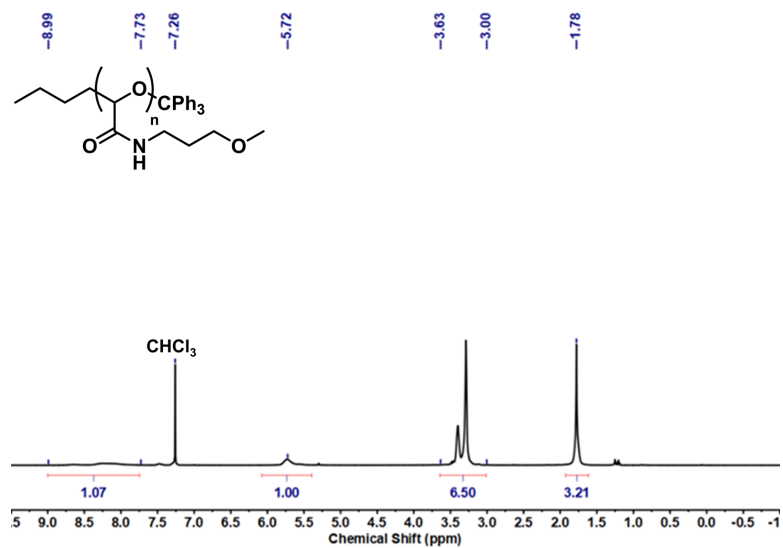


Figure A3.12. ^1H NMR spectrum of **P(MeMPG)-Trit** (CDCl_3 , 400 MHz). The residual water peak overlapped with a **P(MeMPG)-Trit** peak appearing at 1.78 ppm.

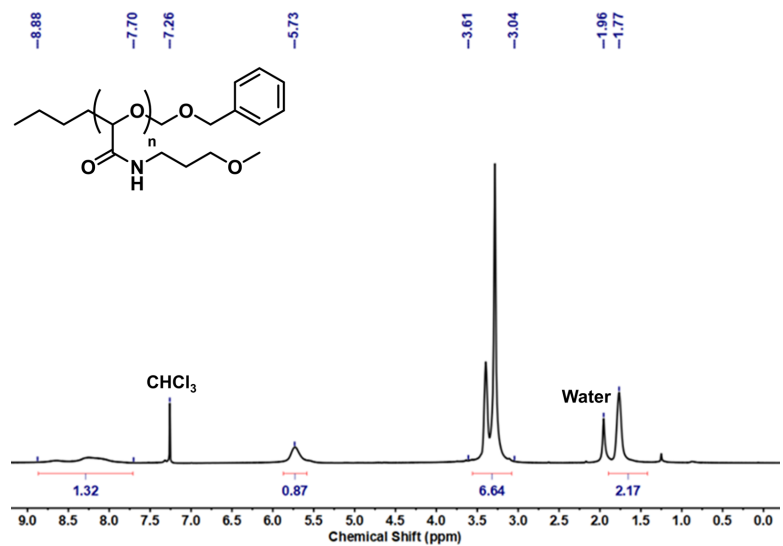


Figure A3.13. ^1H NMR spectrum of **P(MeMPG)-BOM** (CDCl_3 , 400 MHz).

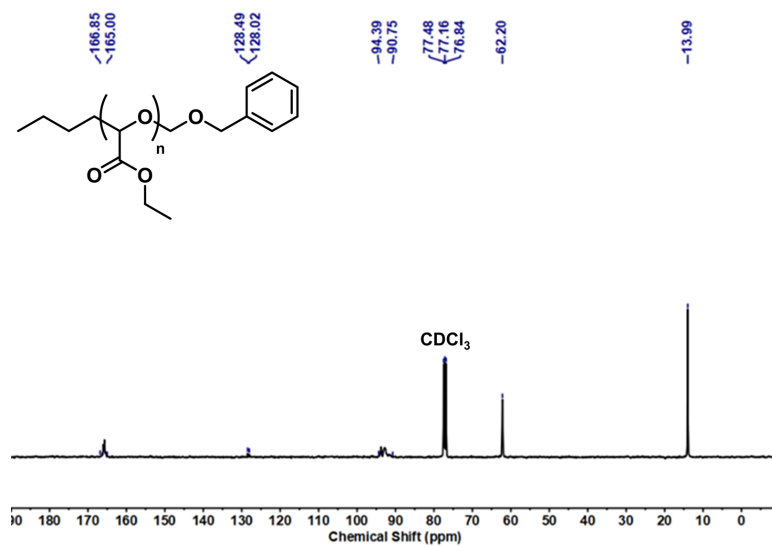


Figure A3.14. $^{13}\text{C}\{^1\text{H}\}$ NMR spectrum of PETG-BOM (CDCl₃, 100 MHz).

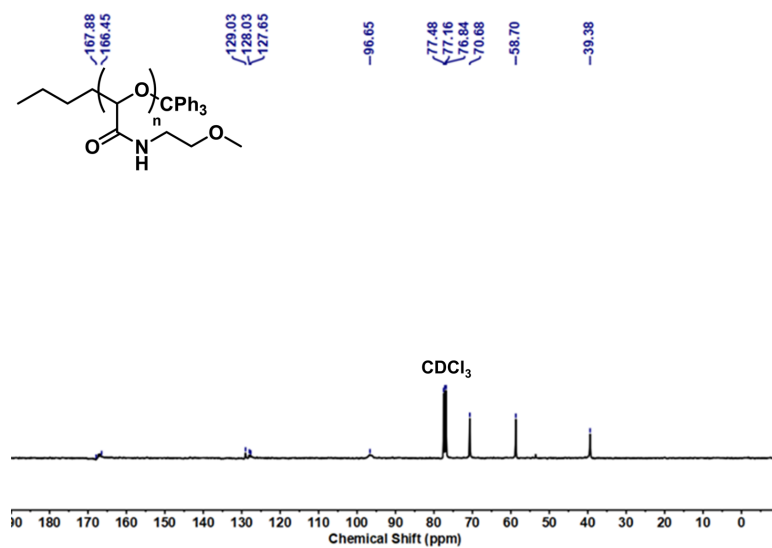


Figure A3.15. $^{13}\text{C}\{^1\text{H}\}$ NMR spectrum of P(MeMEG)-Trit (CDCl₃, 100 MHz).

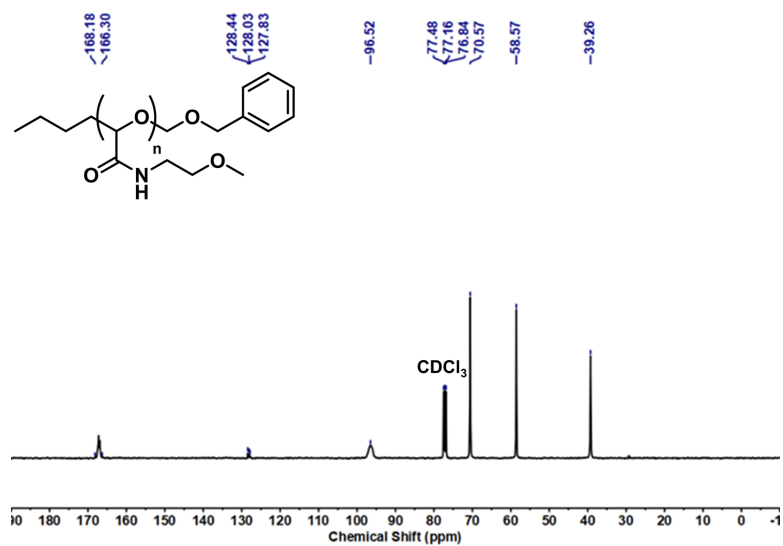


Figure A3.16. $^{13}\text{C}\{^1\text{H}\}$ NMR spectrum of P(MeMEG)-BOM (CDCl₃, 100 MHz).

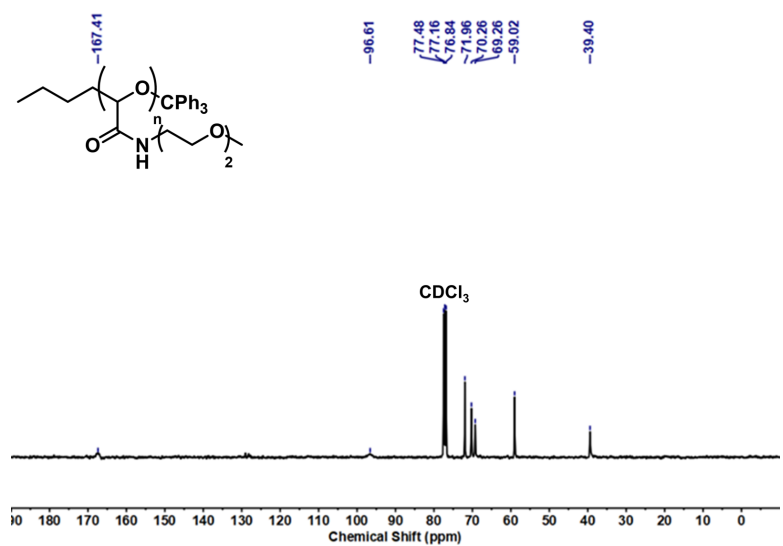


Figure A3.17. $^{13}\text{C}\{^1\text{H}\}$ NMR spectrum of P(MeDEG)-Trit (CDCl₃, 100 MHz).

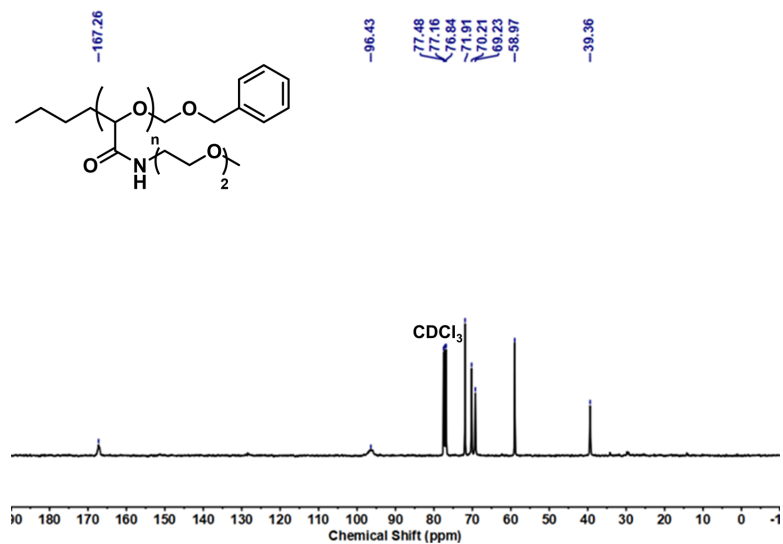


Figure A3.18. $^{13}\text{C}\{^1\text{H}\}$ NMR spectrum of P(MeDEG)-BOM (CDCl₃, 100 MHz).

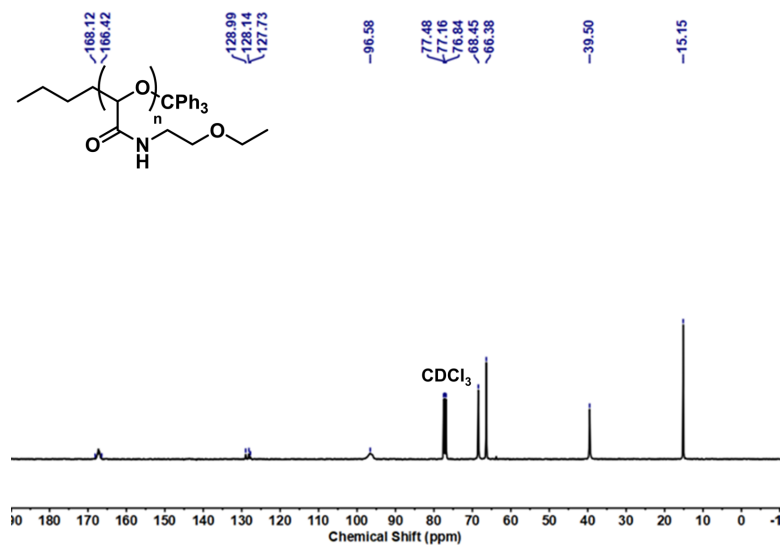


Figure A3.19. $^{13}\text{C}\{^1\text{H}\}$ NMR spectrum of P(EtMEG)-Trit (CDCl₃, 100 MHz).

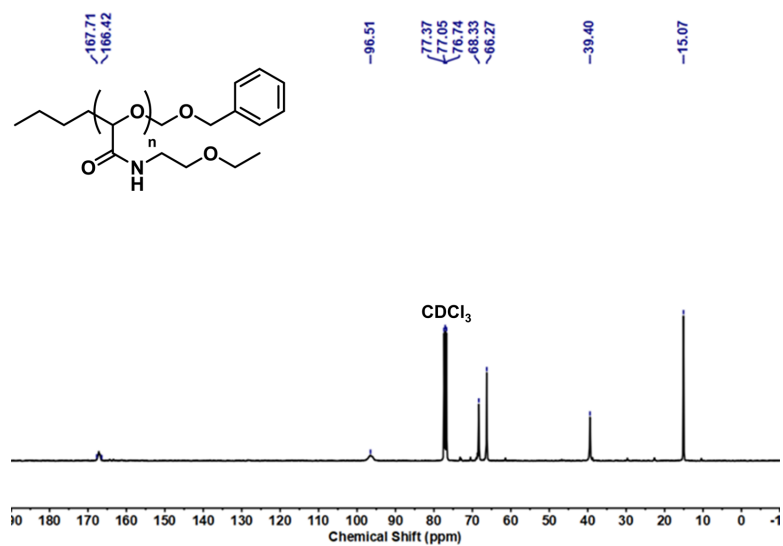


Figure A3.20. $^{13}\text{C}\{^1\text{H}\}$ NMR spectrum of P(EtMEG)-BOM (CDCl₃, 100 MHz).

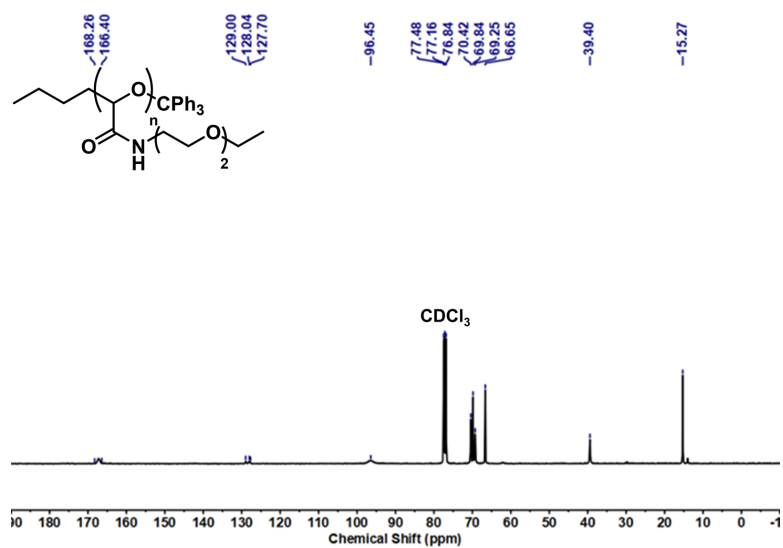


Figure A3.21. $^{13}\text{C}\{^1\text{H}\}$ NMR spectrum of P(EtDEG)-Trit (CDCl₃, 100 MHz).

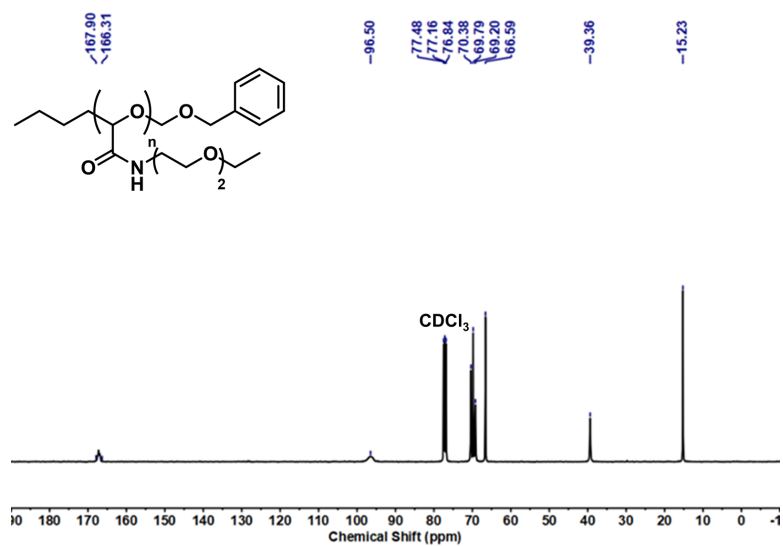


Figure A3.22. $^{13}\text{C}\{^1\text{H}\}$ NMR spectrum of P(EtDEG)-BOM (CDCl_3 , 100 MHz).

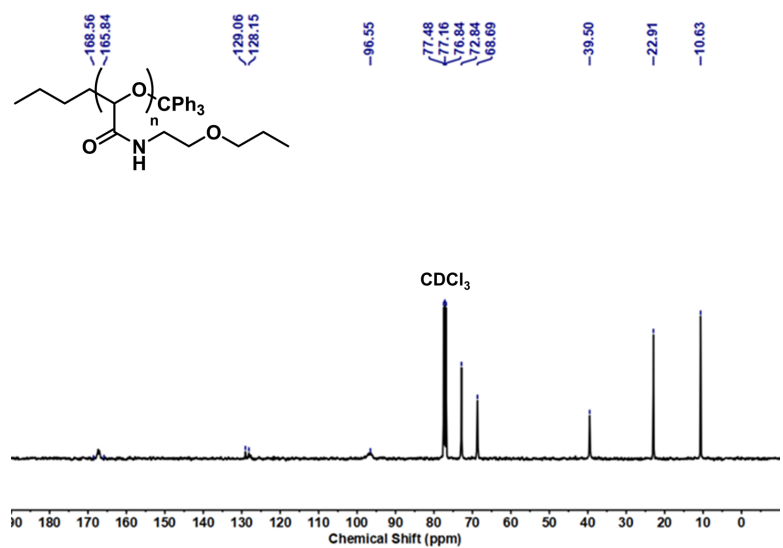


Figure A3.23. $^{13}\text{C}\{^1\text{H}\}$ NMR spectrum of P(PrMEG)-Trit (CDCl_3 , 100 MHz).

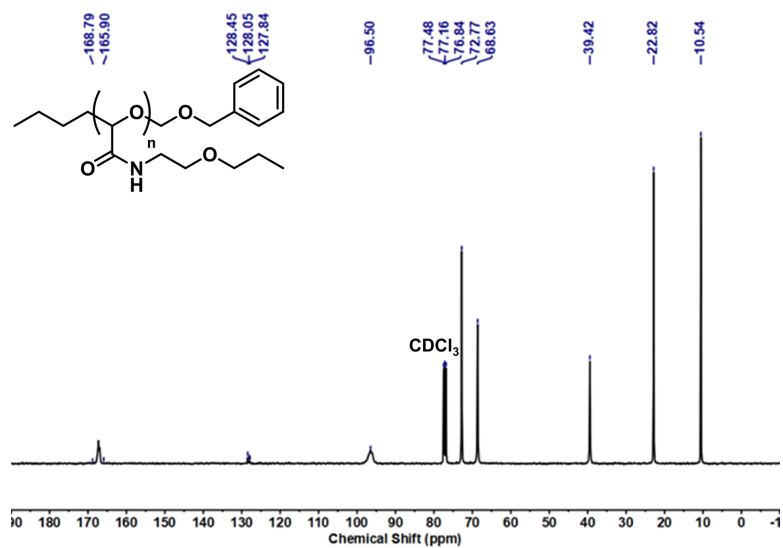


Figure A3.24. $^{13}\text{C}\{^1\text{H}\}$ NMR spectrum of P(PrMEG)-BOM (CDCl₃, 100 MHz).

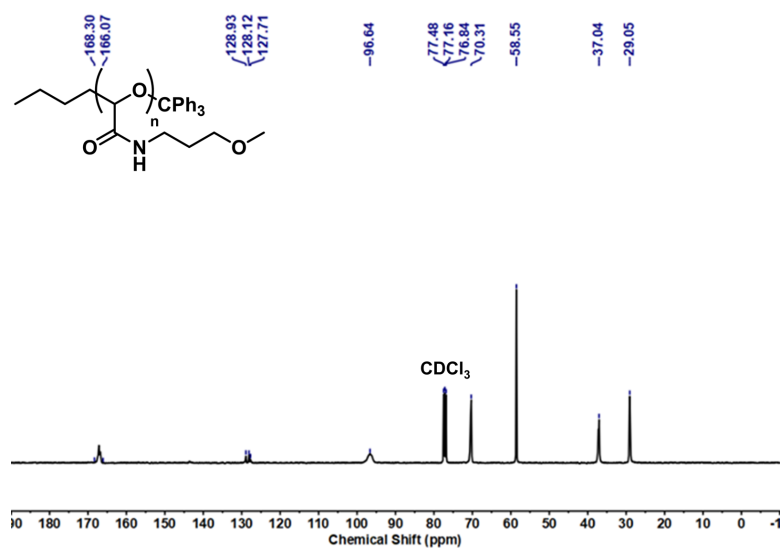


Figure A3.25. $^{13}\text{C}\{^1\text{H}\}$ NMR spectrum of P(MeMPG)-Trit (CDCl₃, 100 MHz).

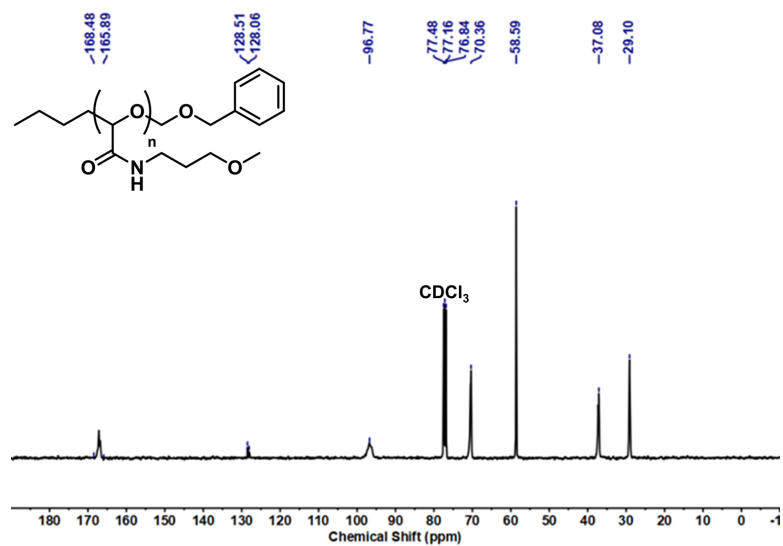


Figure A3.26. $^{13}\text{C}\{^1\text{H}\}$ NMR spectrum of P(MeMPG)-BOM (CDCl_3 , 100 MHz).

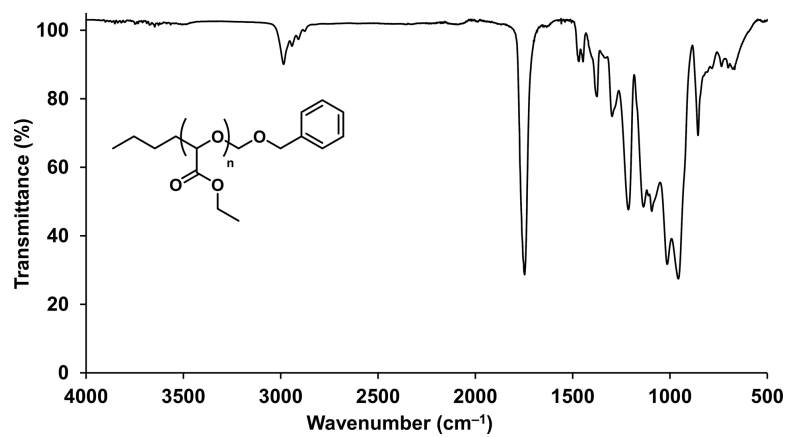


Figure A3.27. FT-IR spectrum of PEtG-BOM.

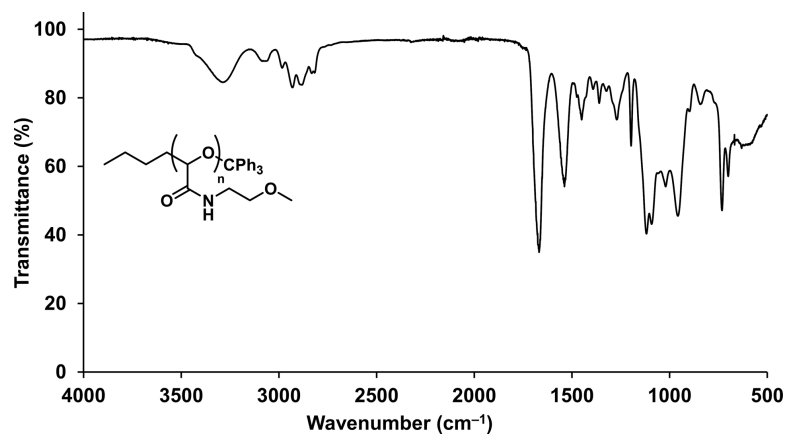


Figure A3.28. FT-IR spectrum of P(MeMEG)-Trit.

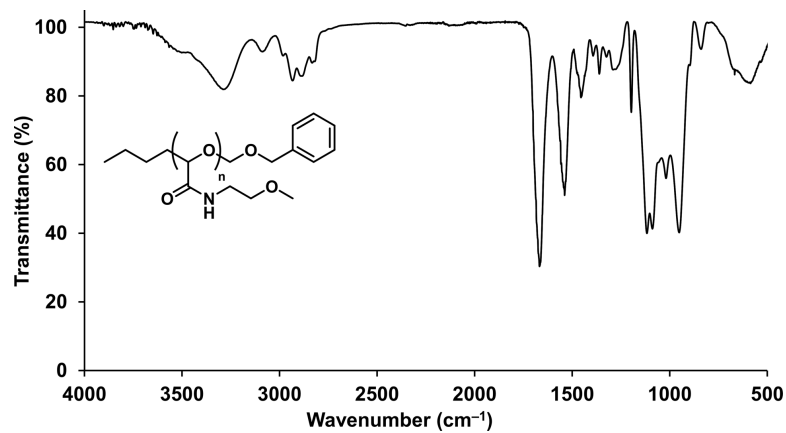


Figure A3.29. FT-IR spectrum of P(MeMEG)-BOM.

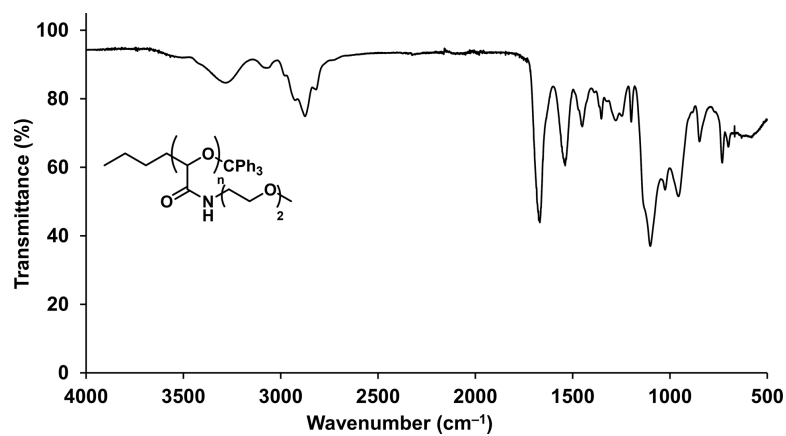


Figure A3.30. FT-IR spectrum of P(MeDEG)-Trit.

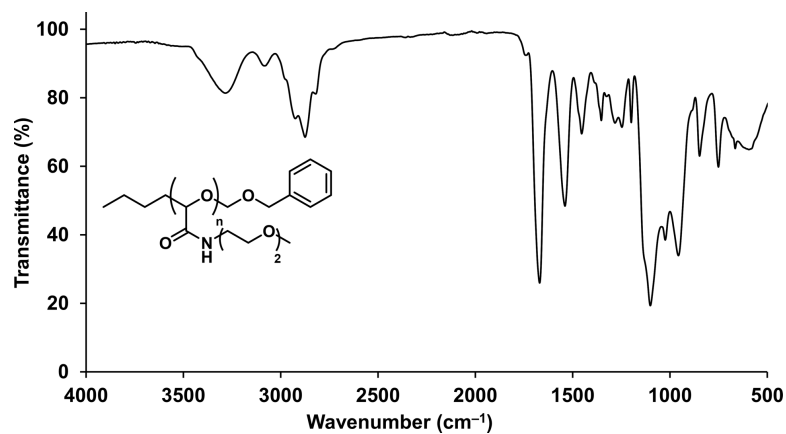


Figure A3.31. FT-IR spectrum of P(MeDEG)-BOM.

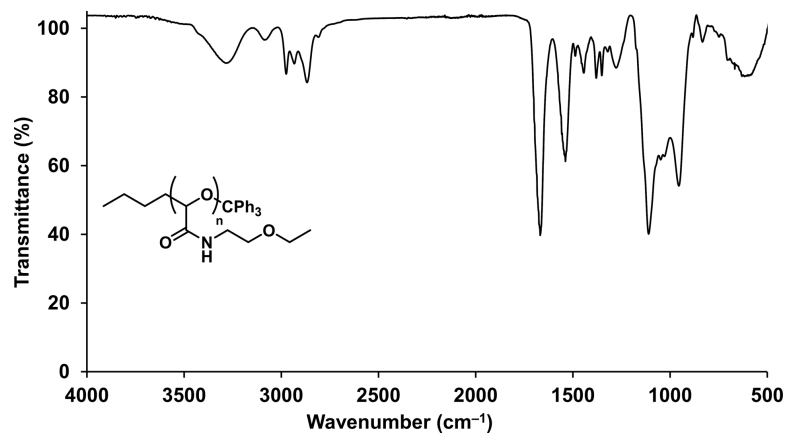


Figure A3.32. FT-IR spectrum of P(EtMEG)-Trit.

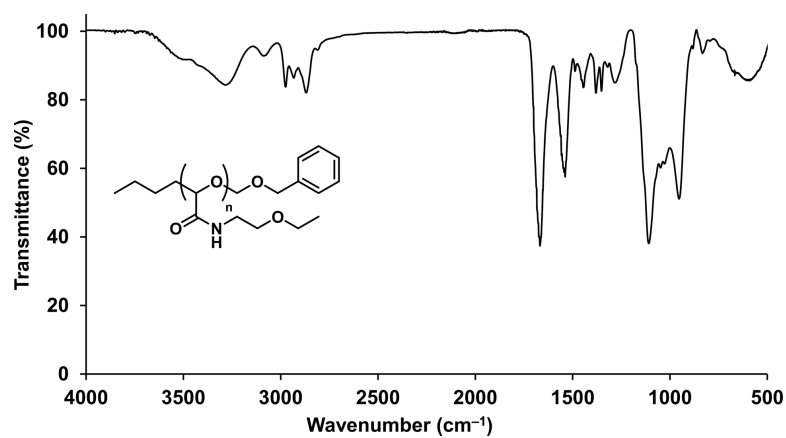


Figure A3.33. FT-IR spectrum of P(EtMEG)-BOM.

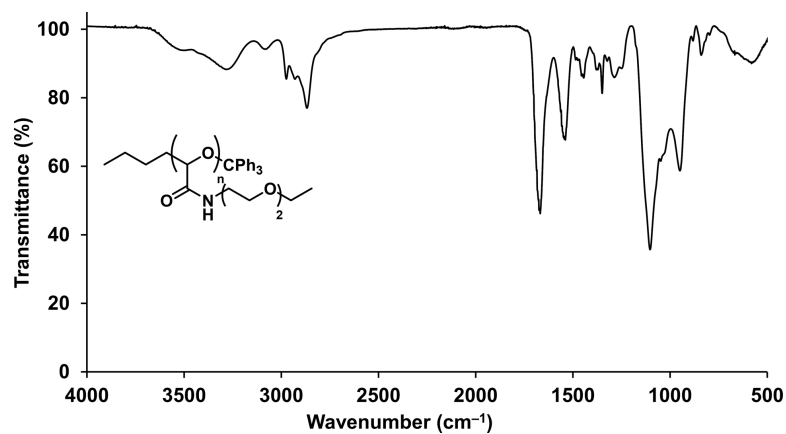


Figure A3.34. FT-IR spectrum of P(EtDEG)-Trit.

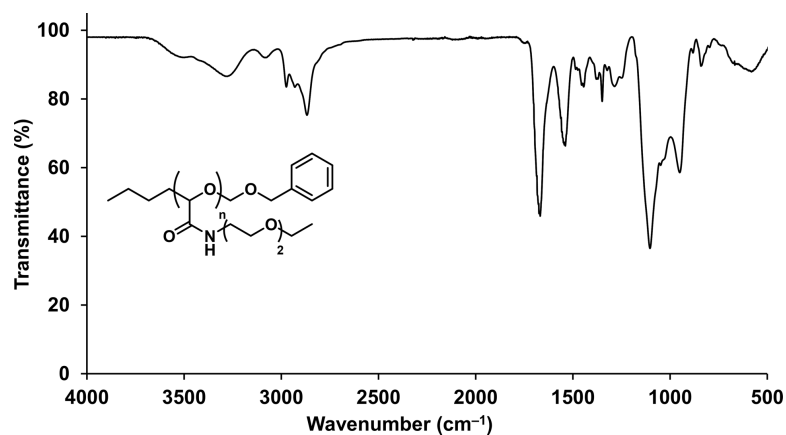


Figure A3.35. FT-IR spectrum of P(EtDEG)-BOM.

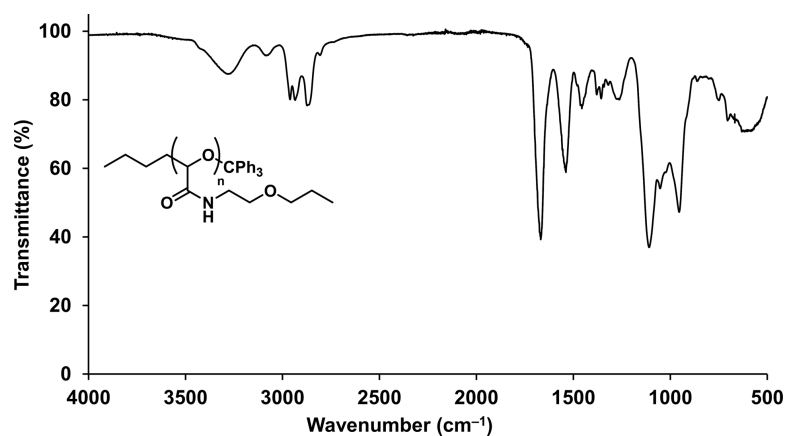


Figure A3.36. FT-IR spectrum of P(PrMEG)-Trit.

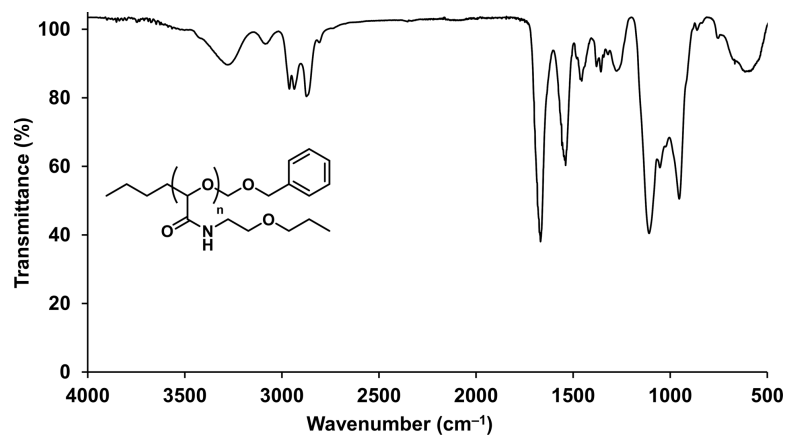


Figure A3.37. FT-IR spectrum of P(PrMEG)-BOM.

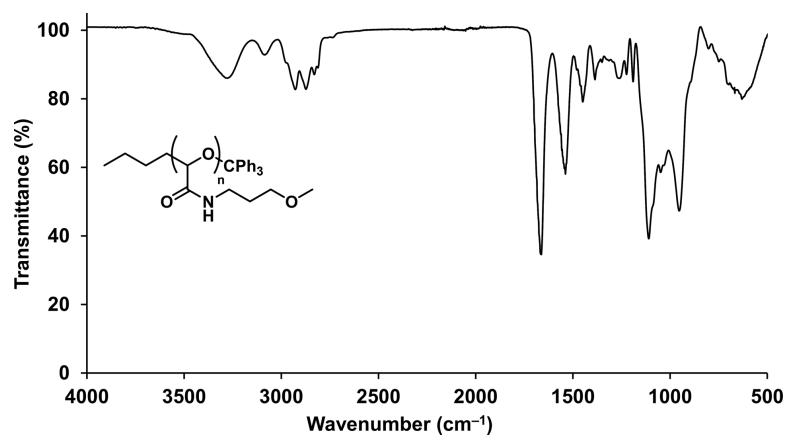


Figure A3.38. FT-IR spectrum of P(MeMPG)-Trit.

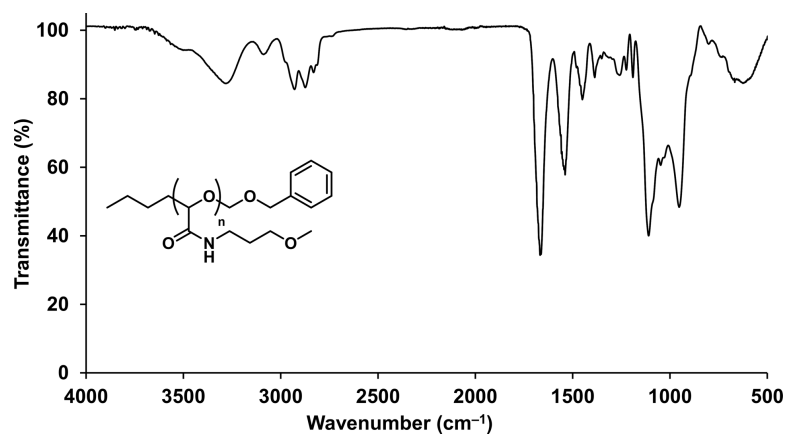


Figure A3.39. FT-IR spectrum of P(MeMPG)-BOM.

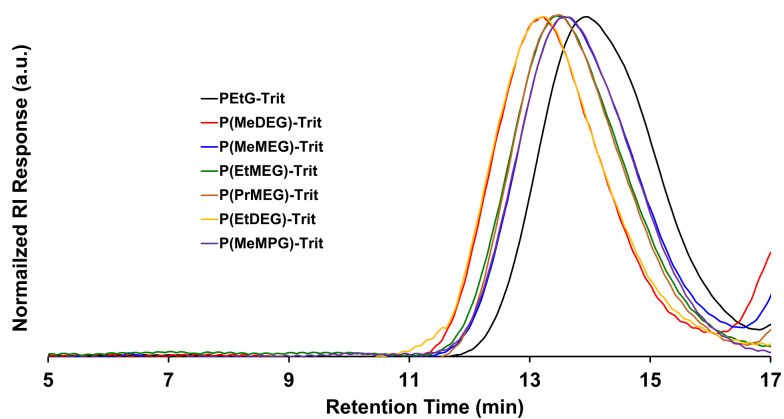


Figure A3.40. SEC traces (refractive index detection) for **PEtG-Trit** and the PGAMs derived from this polymer.

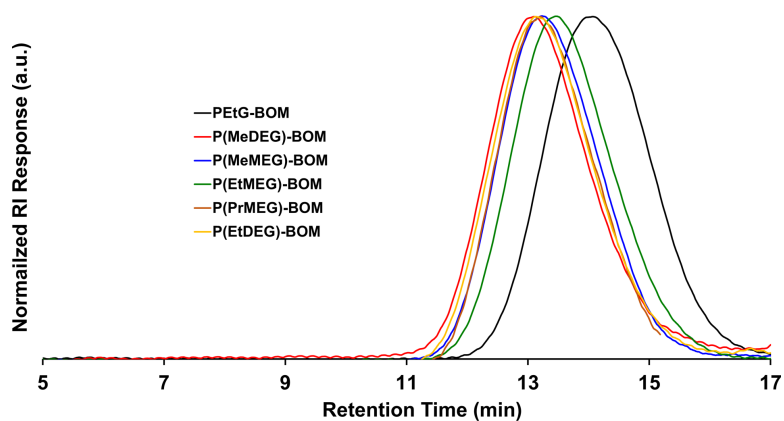


Figure A3.41. SEC traces (refractive index detection) for **PEtG-BOM** and the PGAMs derived from this polymer.

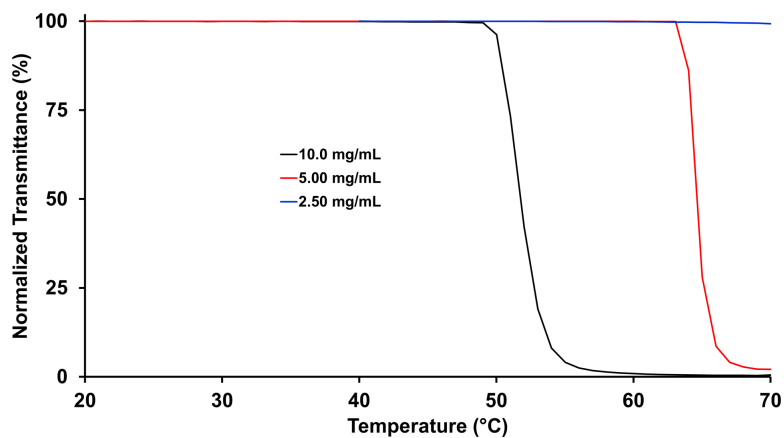


Figure A3.42. Turbidimetry curves obtained for solutions of **P(MeMEG)-Trit** in PBS.

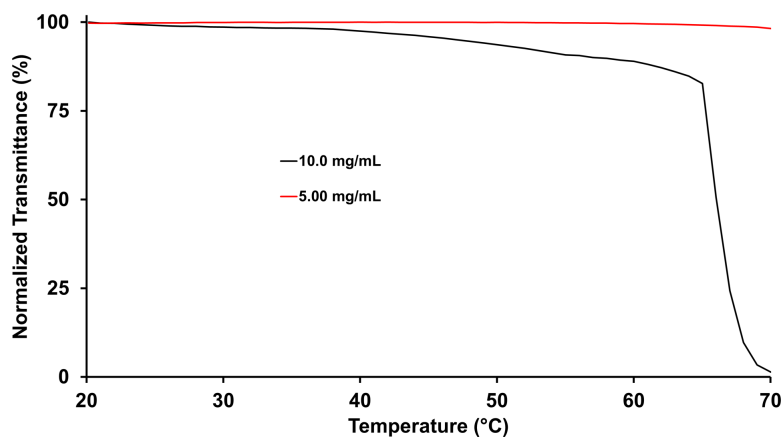


Figure A3.43. Turbidimetry curves obtained for solutions of P(MeMEG)-Trit in water.

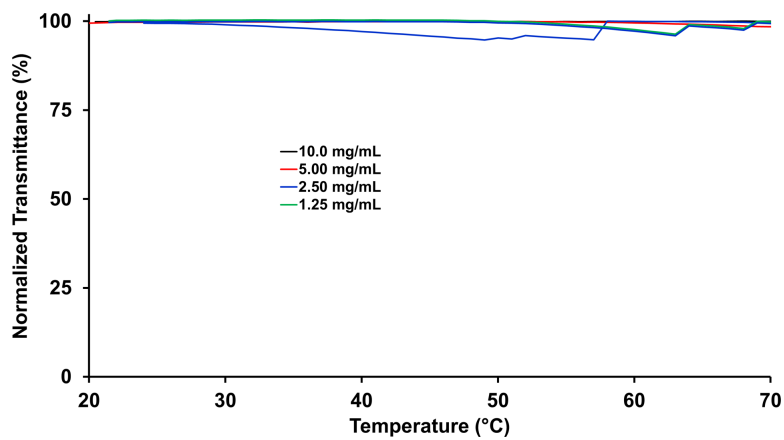


Figure A3.44. Turbidimetry curve obtained for solutions of P(MeMEG)-BOM in PBS.

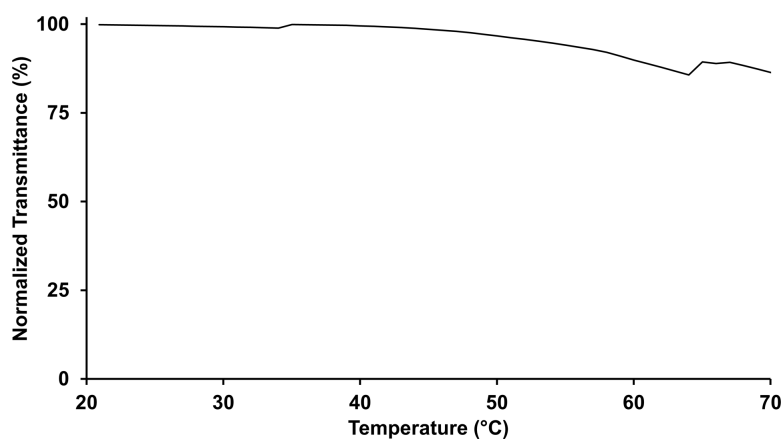


Figure A3.45. Turbidimetry curve obtained for a 10.0 mg/mL solution of P(MeMEG)-BOM in water.

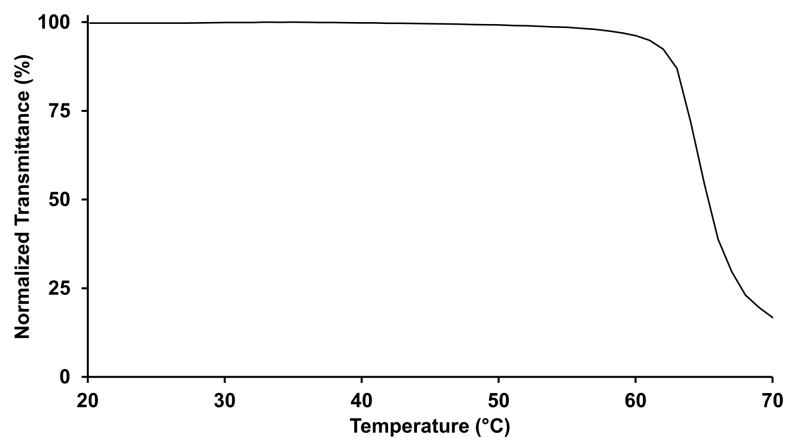


Figure A3.46. Turbidimetry curve obtained for a 10.0 mg/mL solution of P(MeDEG)-Trit in PBS.

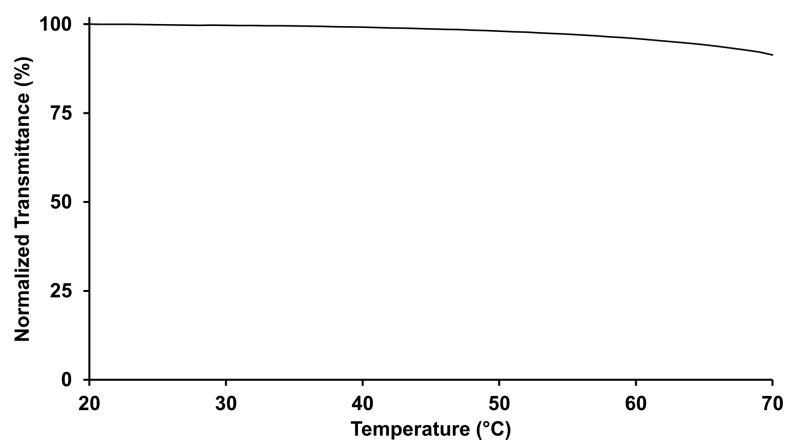


Figure A3.47. Turbidimetry curve obtained for a 10.0 mg/mL solution of P(MeDEG)-Trit in water.

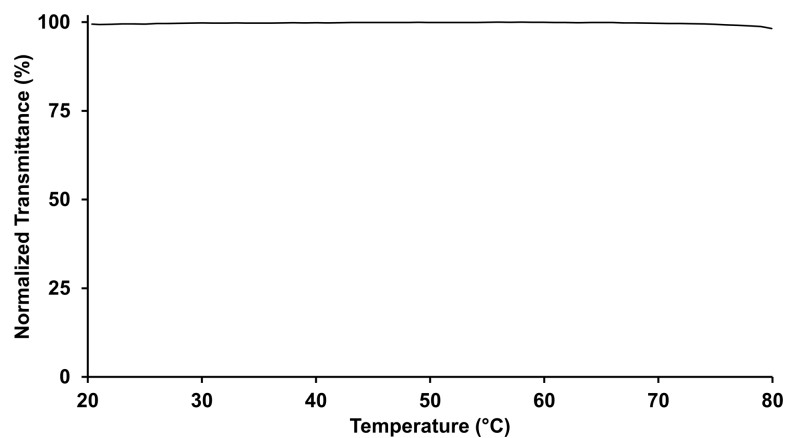


Figure A3.48. Turbidimetry curve obtained for a 10.0 mg/mL solution of **P(MeDEG)-BOM** in PBS.

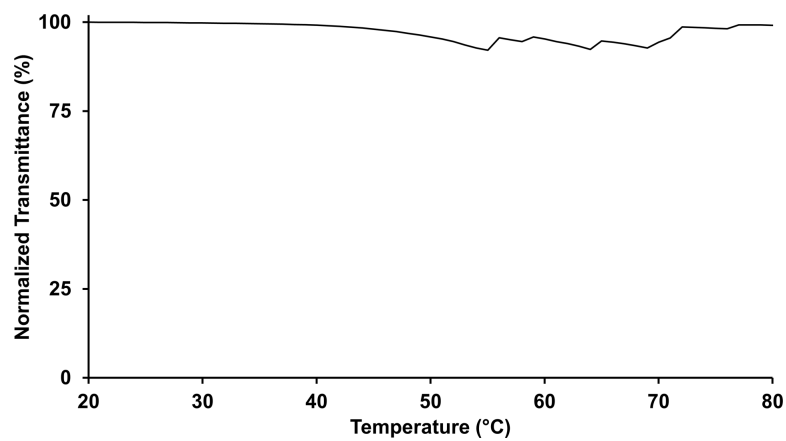


Figure A3.49. Turbidimetry curve obtained for a 10.0 mg/mL solution of **P(MeDEG)-BOM** in water.

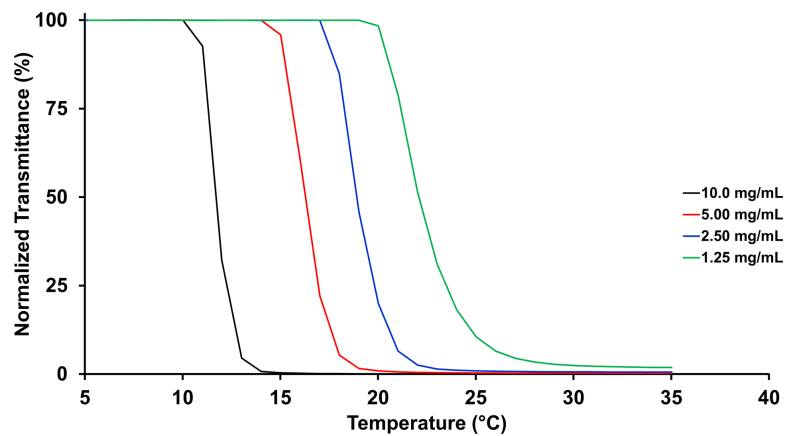


Figure A3.50. Turbidimetry curves obtained for solutions of P(EtMEG)-Trit in PBS.

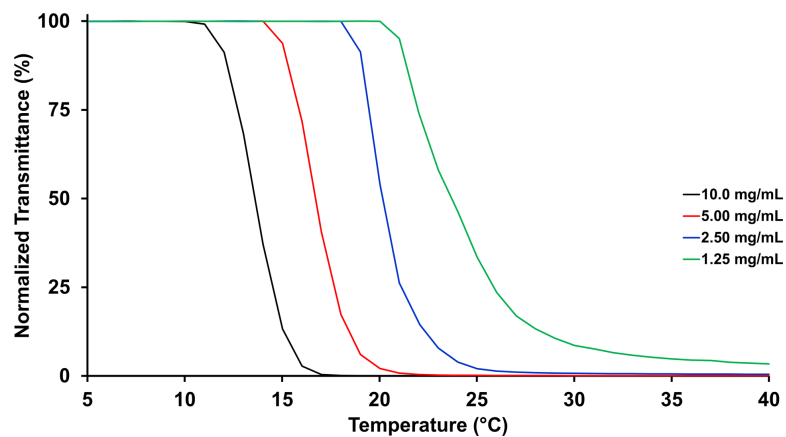


Figure A3.51. Turbidimetry curves obtained for solutions of P(EtMEG)-Trit in water.

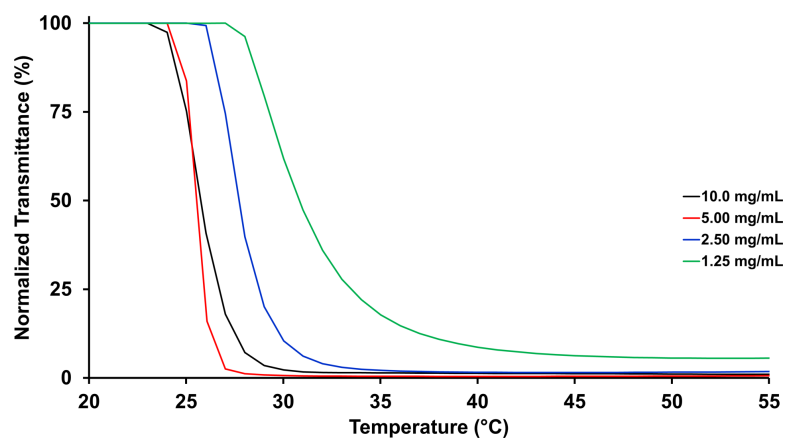


Figure A3.52. Turbidimetry curves obtained for solutions of P(EtMEG)-BOM in PBS.

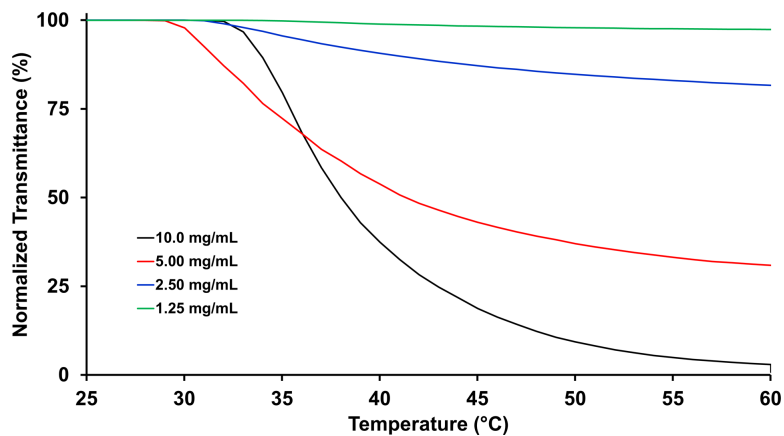


Figure A3.53. Turbidimetry curves obtained for solutions of **P(EtMEG)-BOM** in water.

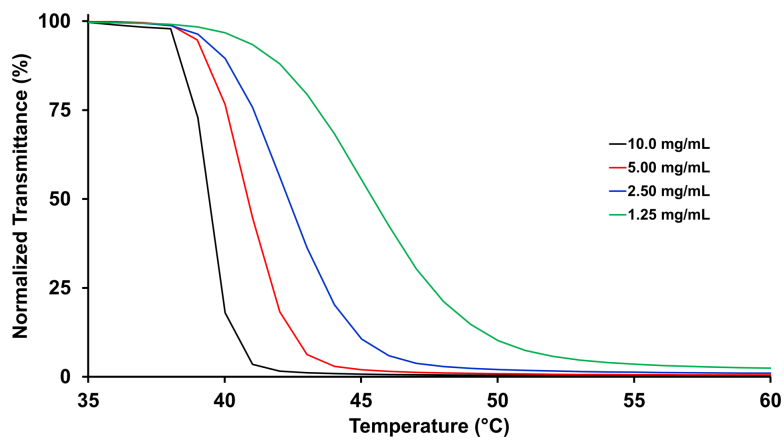


Figure A3.54. Turbidimetry curves obtained for solutions of **P(EtDEG)-Trit** in PBS.

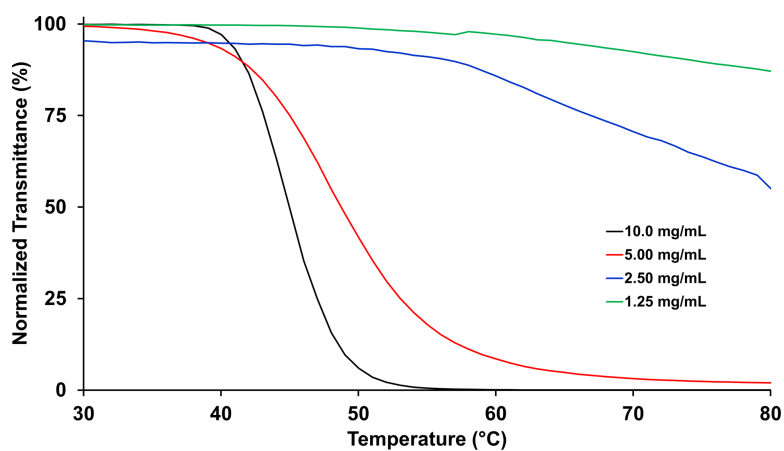


Figure A3.55. Turbidimetry curves obtained for solutions of **P(EtDEG)-Trit** in water.

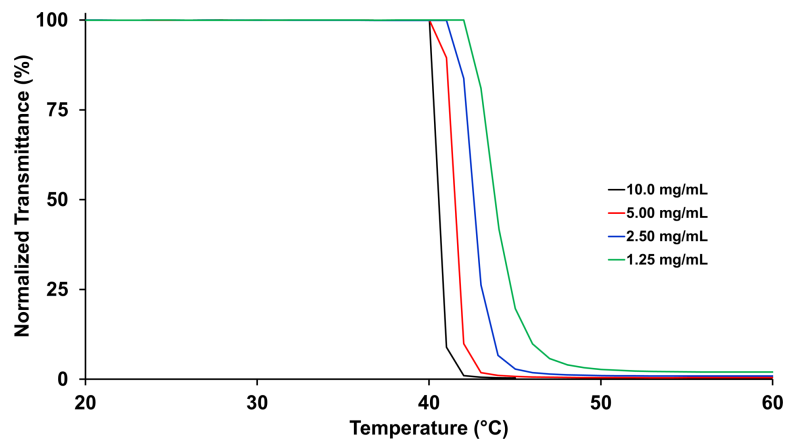


Figure A3.56. Turbidimetry curve obtained for solutions of **P(EtDEG)-BOM** in PBS.

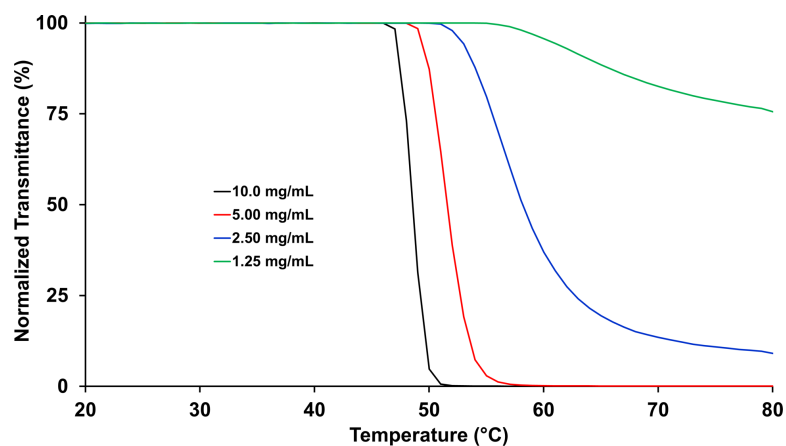


Figure A3.57. Turbidimetry curve obtained for solutions of **P(EtDEG)-BOM** in water.

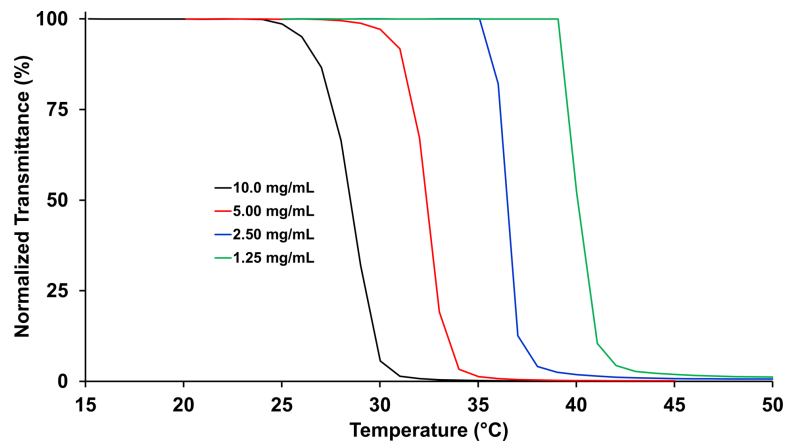


Figure A3.58. Turbidimetry curves obtained for solutions of **P(MeMPG)-Trit** in PBS.

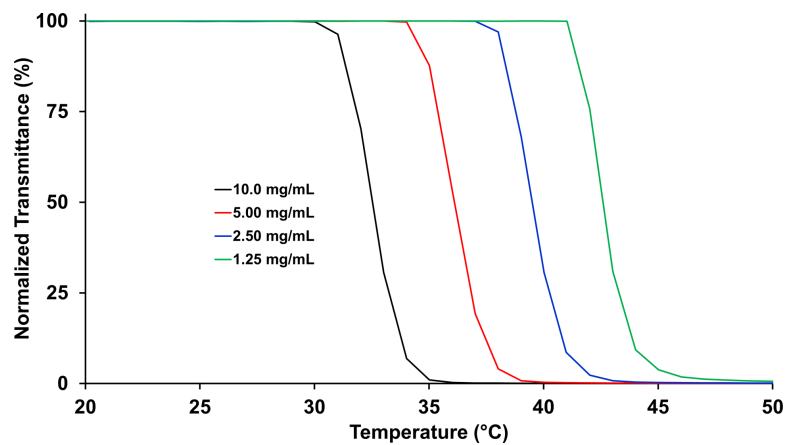


Figure A3.59. Turbidimetry curves obtained for solutions of P(MeMPG)-Trit in water.

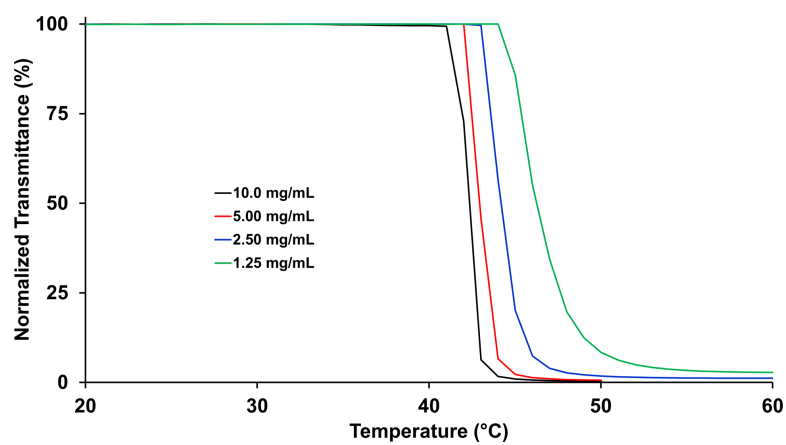


Figure A3.60. Turbidimetry curves obtained for solutions of P(MeMPG)-BOM in PBS.

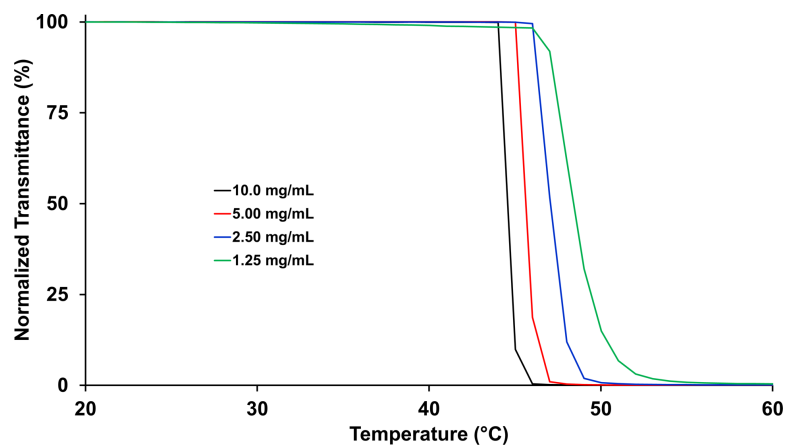


Figure A3.61. Turbidimetry curves obtained for solutions of **P(MeMPG)-BOM** in water.

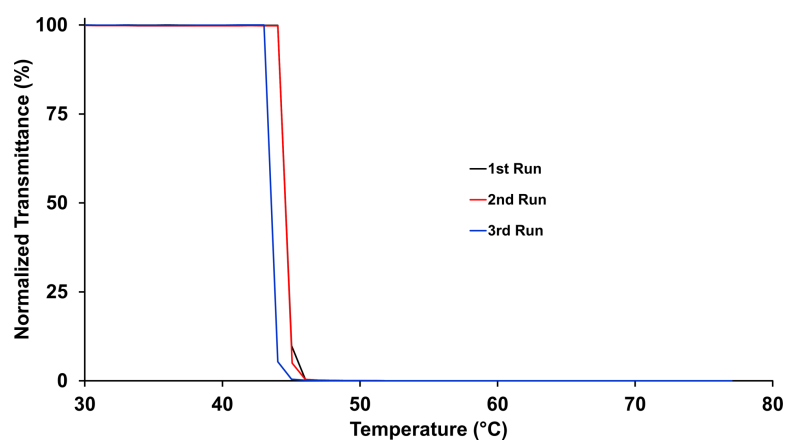


Figure A3.62. Three turbidimetry curves obtained for a 10.0 mg/mL **P(MeMPG)-BOM** solution in water showing a standard deviation of less than 1 °C in T_{cp} .

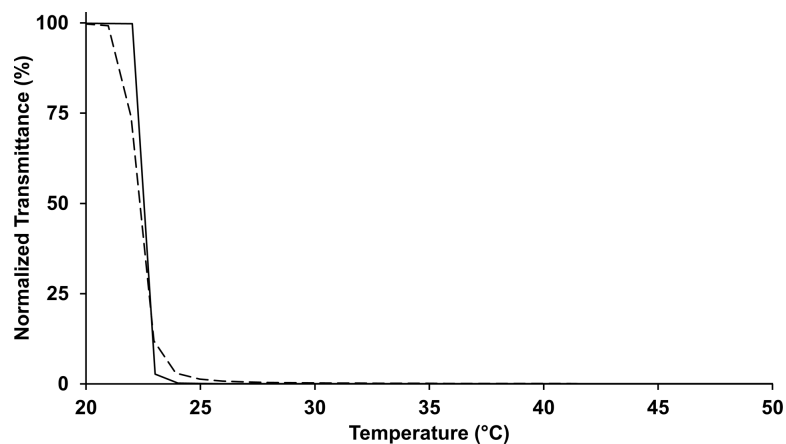


Figure A3.63. Turbidimetry curves obtained for a 10.0 mg/mL solution of **P(EtMEG)-BOM** in cell culture media. The solid and broken lines depict the heating and cooling cycles, respectively.

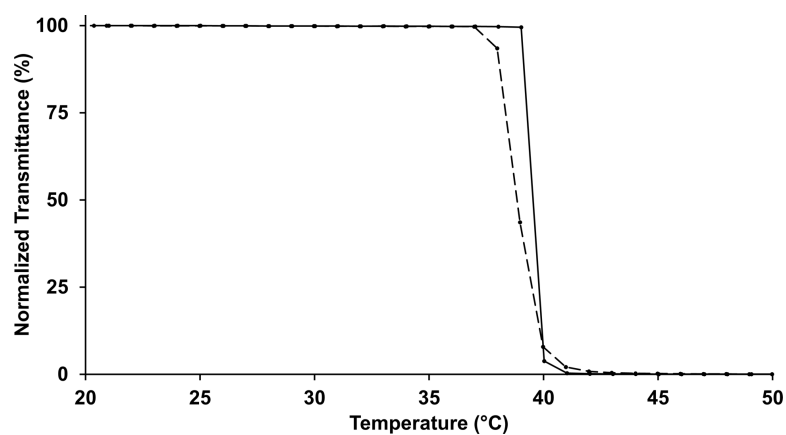


Figure A3.64. Turbidimetry curves obtained for a 10.0 mg/mL solution of **P(EtDEG)-BOM** in cell culture media. The solid and broken lines depict the heating and cooling cycles, respectively.

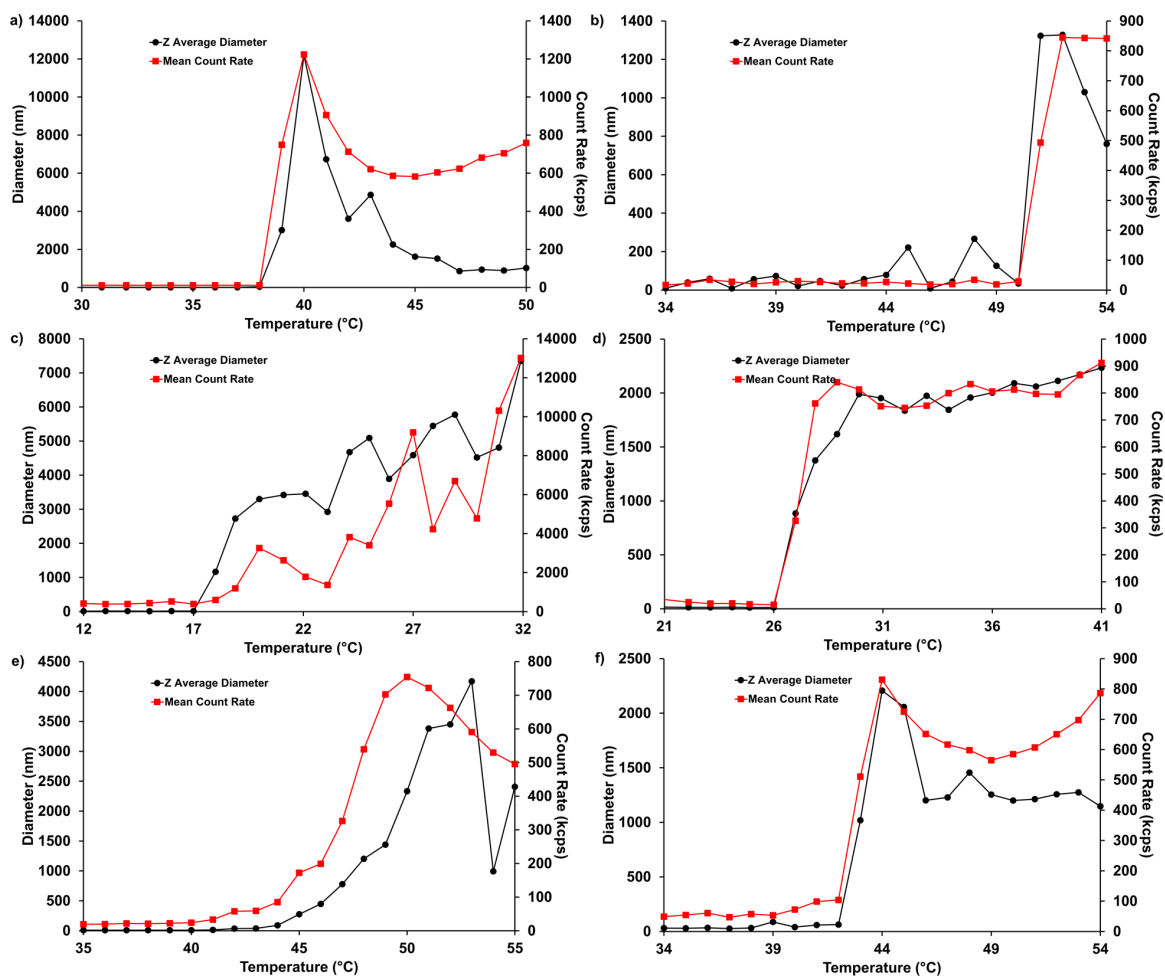


Figure A3.65. Z average diameter and mean count rate over temperature of a) P(MeMPG)-Trit, b) P(MeMPG)-BOM, c) P(EtMEG)-Trit, d) P(EtMEG)-BOM, e) P(EtDEG)-Trit, and f) P(EtDEG)-BOM in PBS (1.25 mg/mL) monitored by DLS. In general, large increases in diameter and count rate were observed at the T_{cp} . Subsequent decreases at higher temperature can likely be attributed to sedimentation.

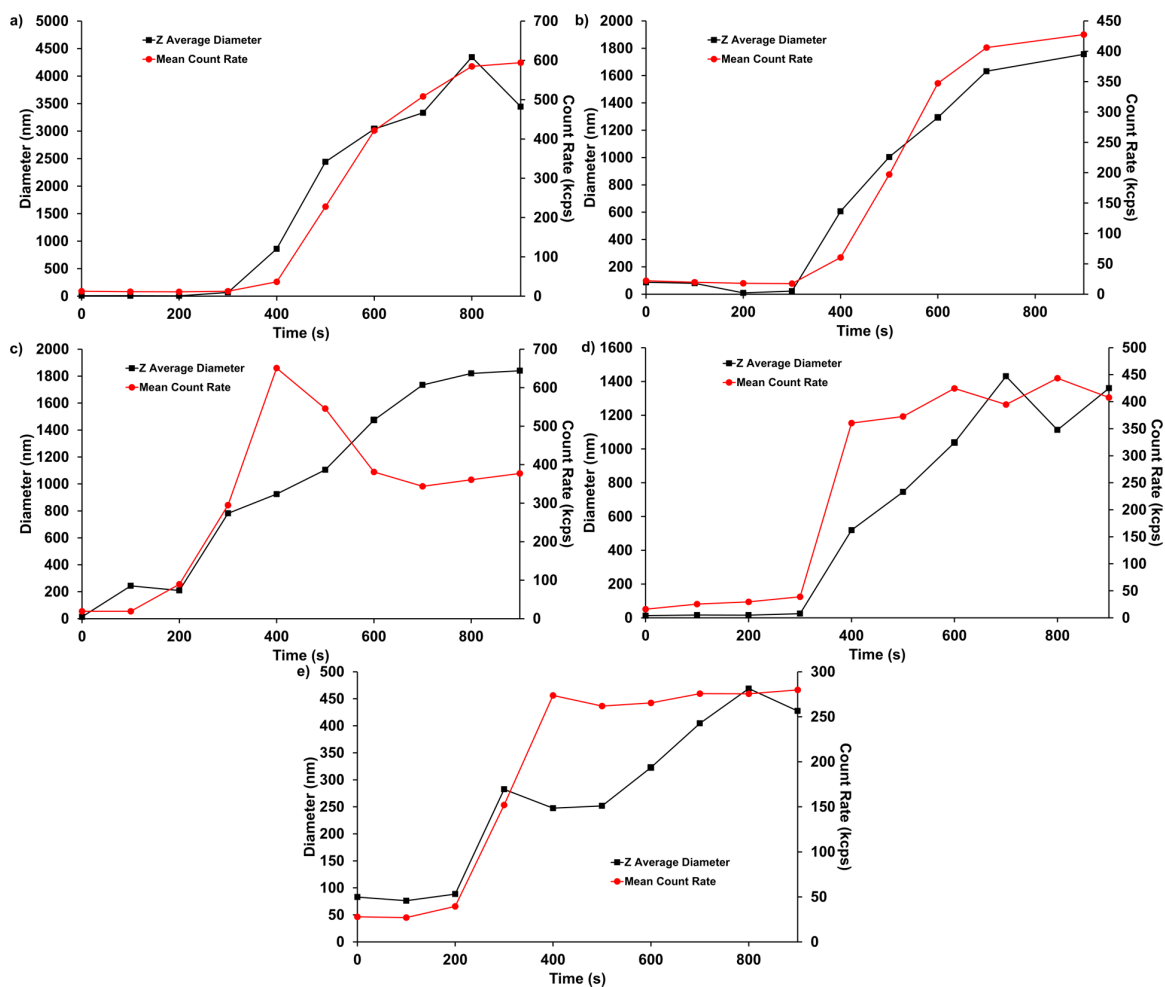


Figure A3.66. Z average diameter and mean count rate over time of a) P(MeMPG)-Trit at 40 °C, b) P(MeMPG)-BOM at 50 °C, c) P(EtMEG)-Trit at 18 °C, d) P(EtMEG)-BOM at 27 °C, and e) P(EtDEG)-Trit, at 46 °C in PBS (1.25 mg/mL) monitored by DLS. The measurements for each polymer were conducted at that polymer's T_{cp} as determined previously by DLS (Figure A3.65).

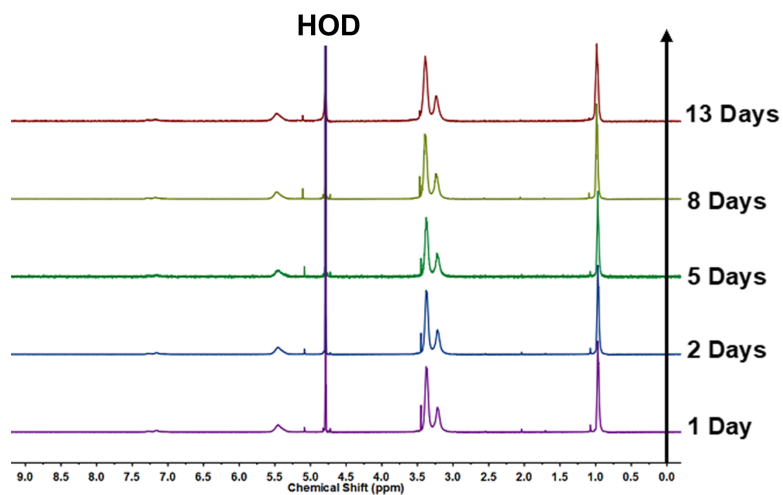


Figure A3.67. Depolymerization behaviour of **P(EtMEG)-Trit** in D₂O monitored by ¹H NMR spectroscopy (400 MHz, 5 °C).

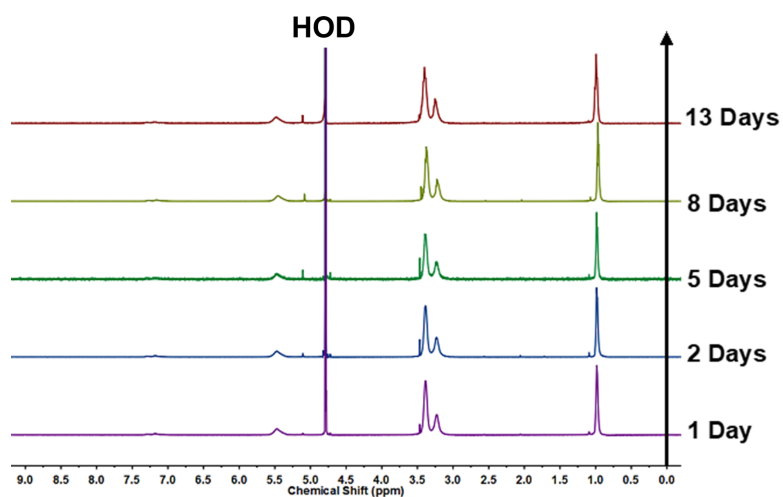


Figure A3.68. Depolymerization behaviour of **P(EtMEG)-Trit** in deuterated PBS (pH 7.4) monitored by ¹H NMR spectroscopy (400 MHz, 5 °C).

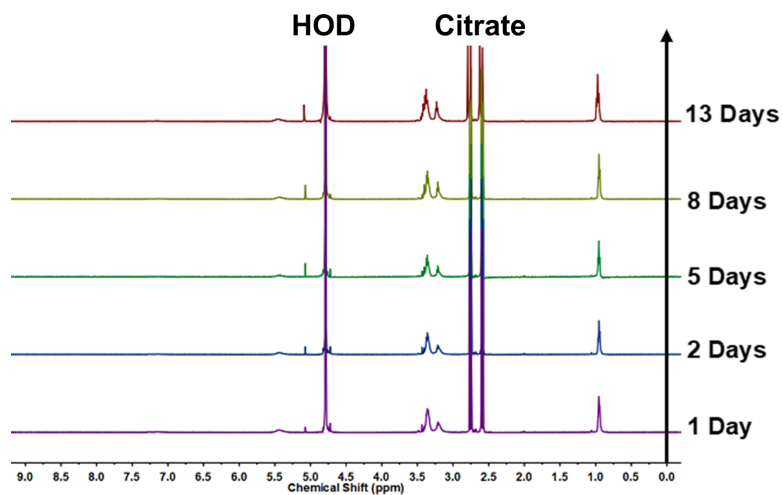


Figure A3.69. Depolymerization behaviour of **P(EtMEG)-Trit** in deuterated citrate buffer (pH 3.0) monitored by ^1H NMR spectroscopy (400 MHz, 5 °C).

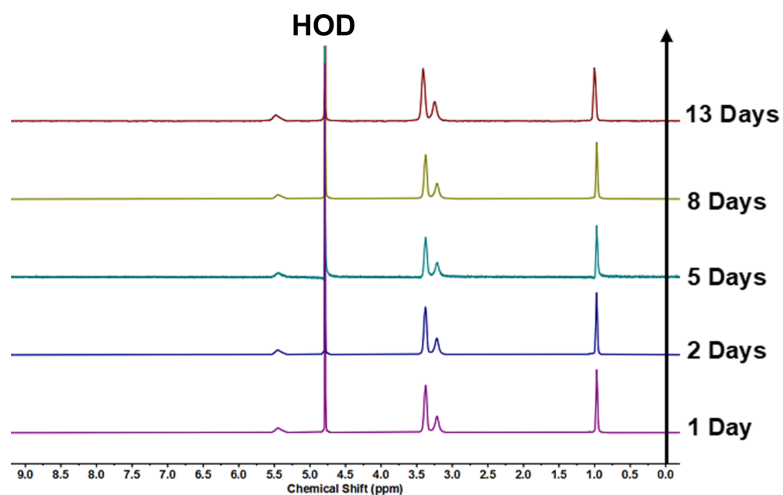


Figure A3.70. Depolymerization behaviour of **P(EtMEG)-BOM** in D_2O monitored by ^1H NMR spectroscopy (400 MHz, 5 °C).

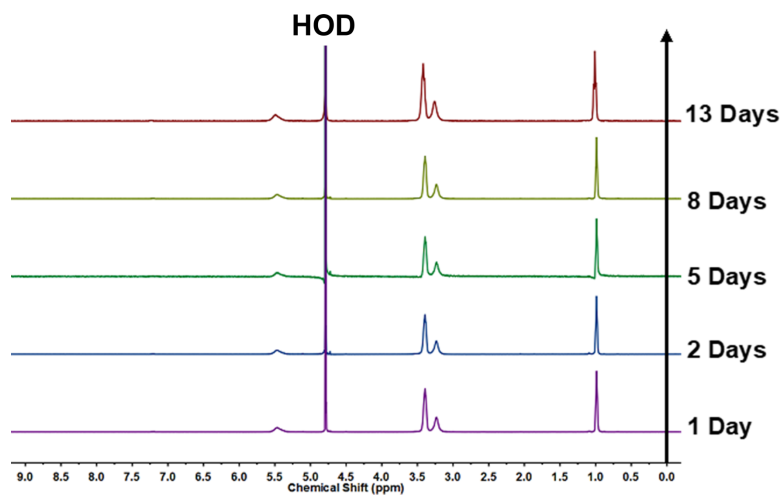


Figure A3.71. Depolymerization behaviour of **P(EtMEG)-BOM** in deuterated PBS (pH 7.4) monitored by ^1H NMR spectroscopy (400 MHz, 5 °C).

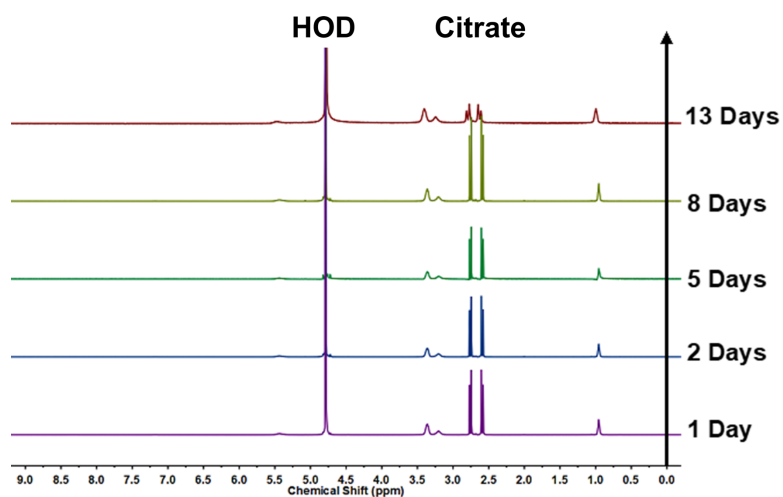


Figure A3.72. Depolymerization behaviour of **P(EtMEG)-BOM** in deuterated citrate buffer (pH 3.0) monitored by ^1H NMR spectroscopy (400 MHz, 5 °C).

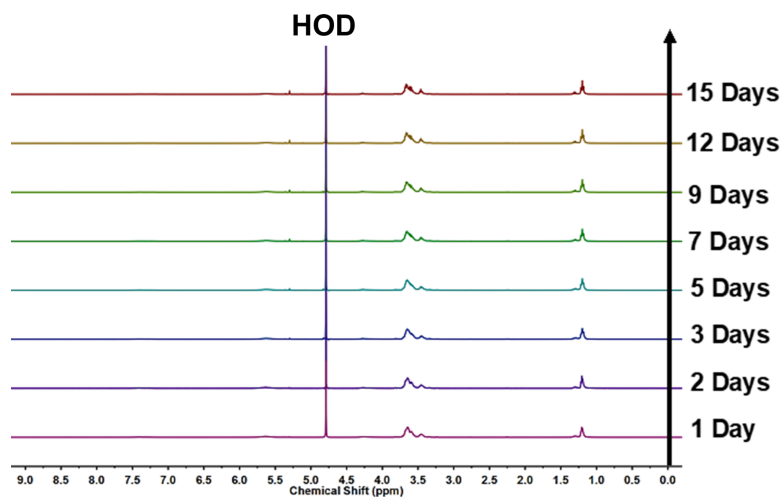


Figure A3.73. Depolymerization behaviour of **P(EtDEG)-Trit** in deuterated D_2O monitored by ^1H NMR spectroscopy (400 MHz, 25 °C).

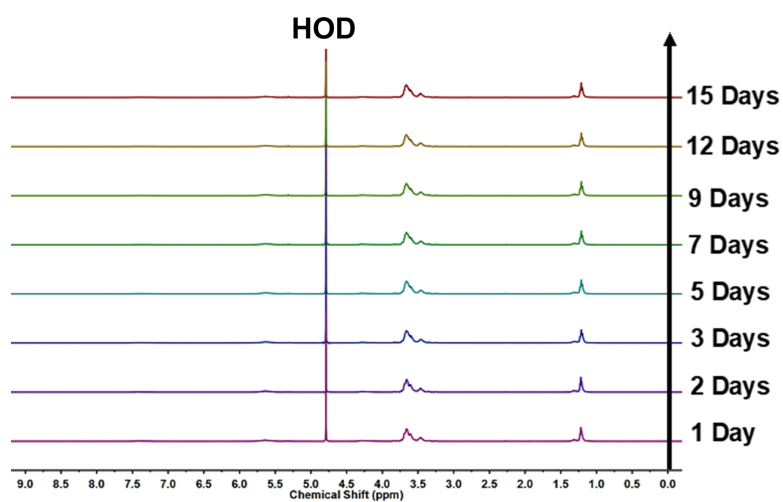


Figure A3.74. Depolymerization behaviour of **P(EtDEG)-Trit** in deuterated PBS (pH 7.4) monitored by ^1H NMR spectroscopy (400 MHz, 25 °C).

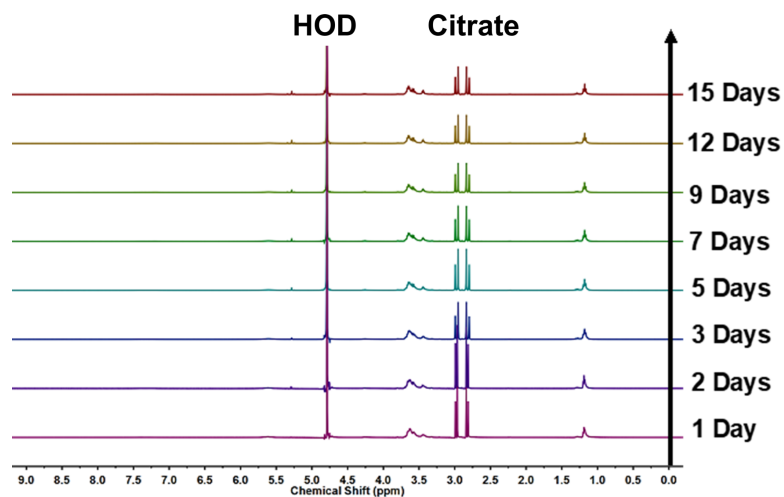


Figure A3.75. Depolymerization behaviour of P(EtDEG)-Trit in deuterated citrate buffer (pH 3.0) monitored by ^1H NMR spectroscopy (400 MHz, 25 °C).

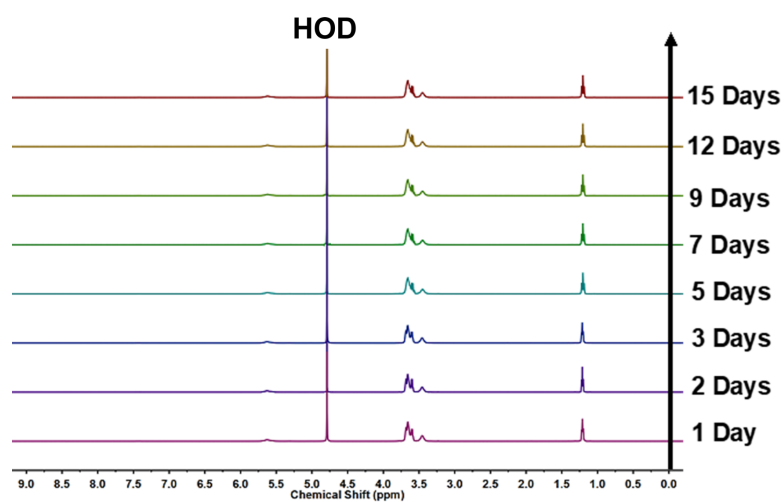


Figure A3.76. Depolymerization behaviour of P(EtDEG)-BOM in deuterated D_2O monitored by ^1H NMR spectroscopy (400 MHz, 25 °C).

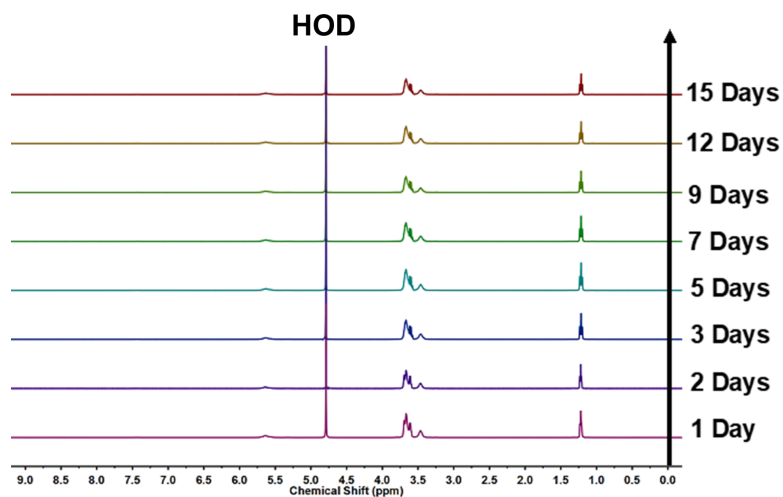


Figure A3.77. Depolymerization behaviour of P(EtDEG)-BOM in deuterated PBS (pH 7.4) monitored by ^1H NMR spectroscopy (400 MHz, 25 °C).

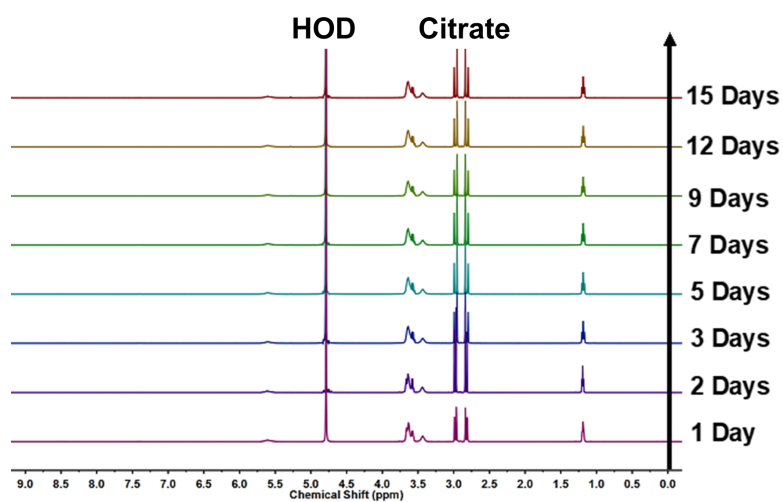


Figure A3.78. Depolymerization behaviour of P(EtDEG)-BOM in deuterated citrate buffer (pH 3.0) monitored by ^1H NMR spectroscopy (400 MHz, 25 °C).

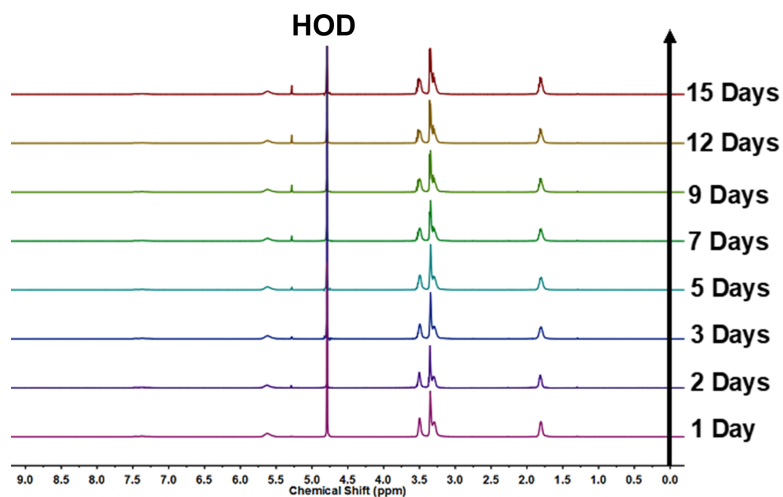


Figure A3.79. Depolymerization behaviour of P(MeMPG)-Trit in D_2O monitored by ^1H NMR spectroscopy (400 MHz, 25 °C).

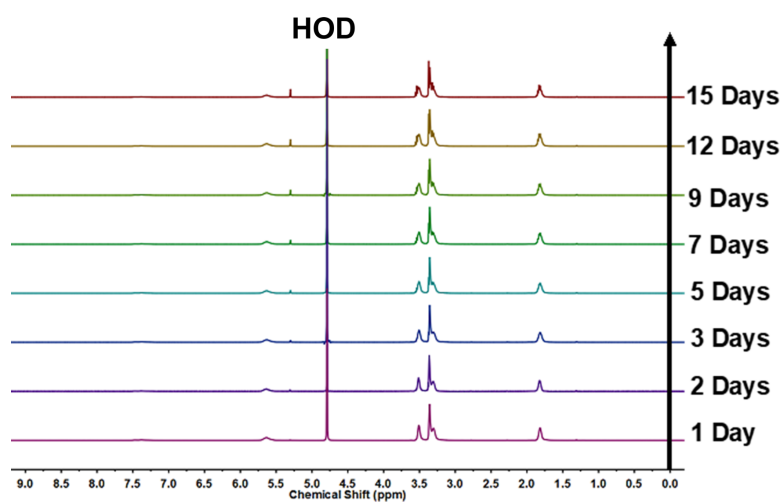


Figure A3.80. Depolymerization behaviour of P(MeMPG)-Trit in deuterated PBS (pH 7.4) monitored by ^1H NMR spectroscopy (400 MHz, 25 °C).

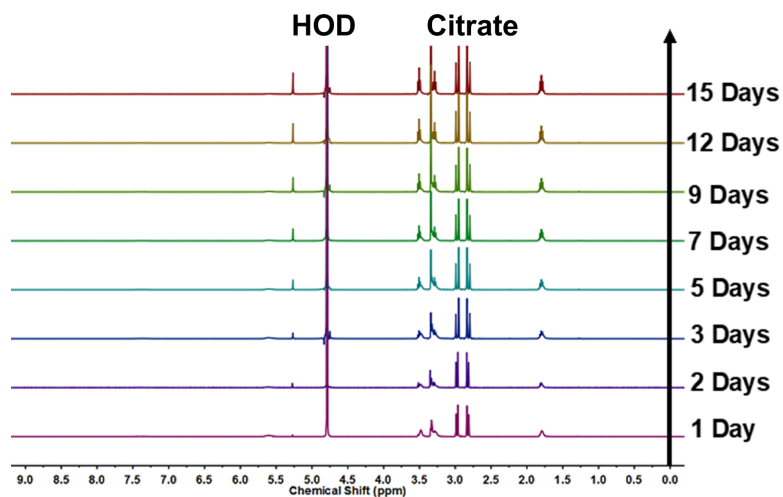


Figure A3.81. Depolymerization behaviour of P(MeMPG)-Trit in deuterated citrate buffer (pH 3.0) monitored by ^1H NMR spectroscopy (400 MHz, 25 °C).

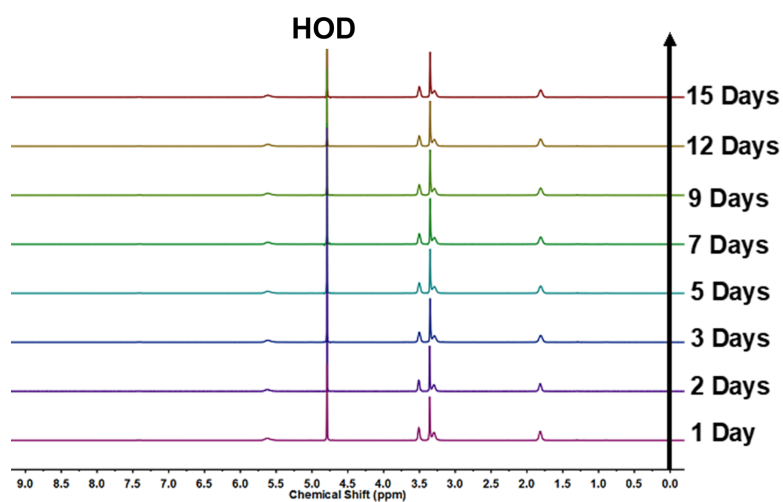


Figure A3.82. Depolymerization behaviour of P(MeMPG)-BOM in D_2O monitored by ^1H NMR spectroscopy (400 MHz, 25 °C).

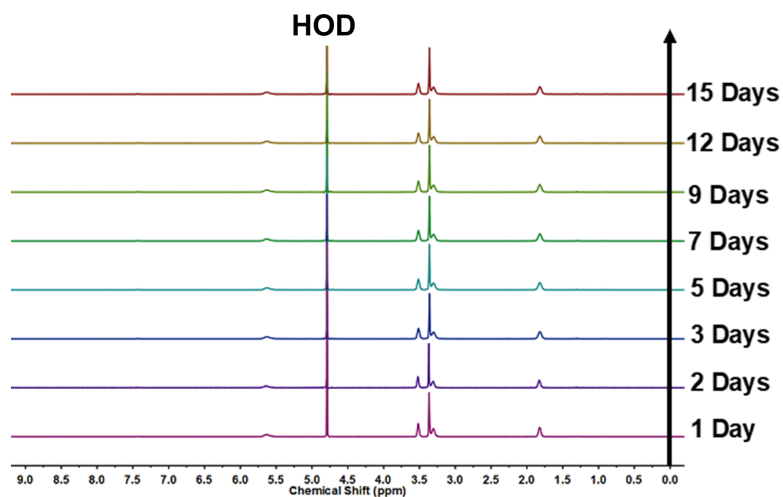


Figure A3.83. Depolymerization behaviour of **P(MeMPG)-BOM** in deuterated PBS (pH 7.4) monitored by ^1H NMR spectroscopy (400 MHz, 25 °C).

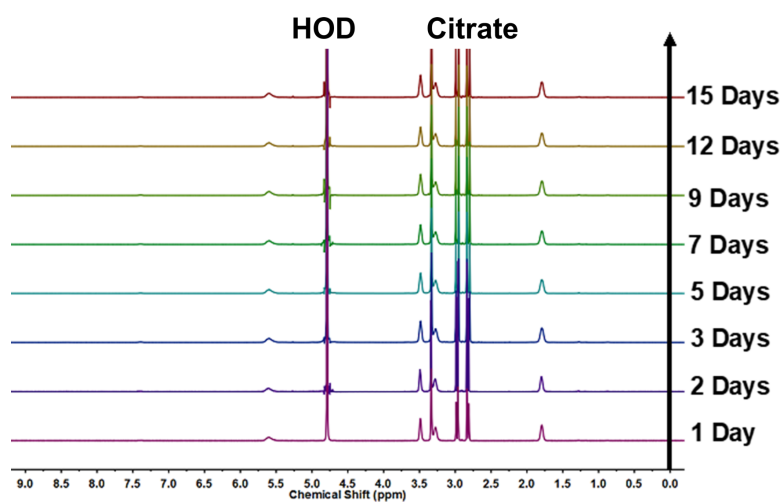


Figure A3.84. Depolymerization behaviour of **P(MeMPG)-BOM** in deuterated citrate buffer (pH 3.0) monitored by ^1H NMR spectroscopy (400 MHz, 25 °C).

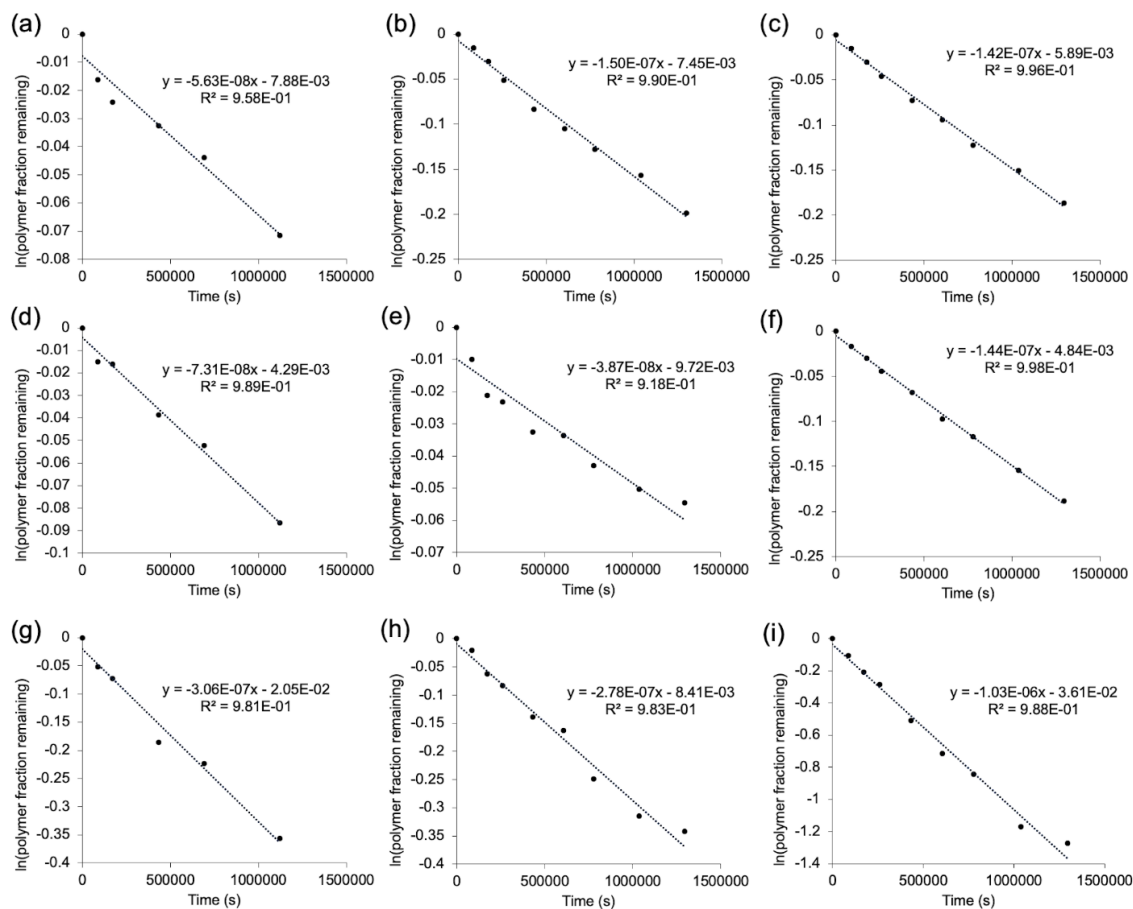


Figure A3.85. Pseudo-first-order kinetics plots for **P(EtMEG)-Trit** (a, d, g), **P(EtDEG)-Trit** (b, e, h), and **P(MeMPG)-Trit** (c, f, i) in D₂O (a–c), deuterated PBS (d–f), and deuterated citrate buffer, pH 3.0 (g–i).

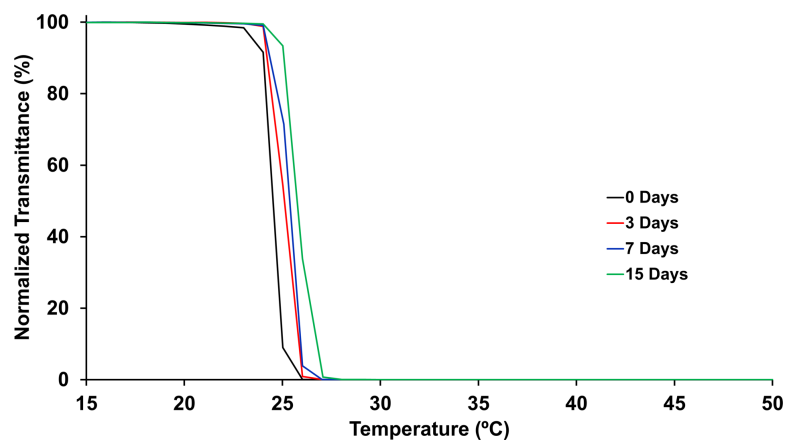


Figure A3.86. Thermo-responsive behaviour of **P(EtMEG)-BOM** in pH 3.0 citrate buffer at different points showing minimal change in the T_{cp} .

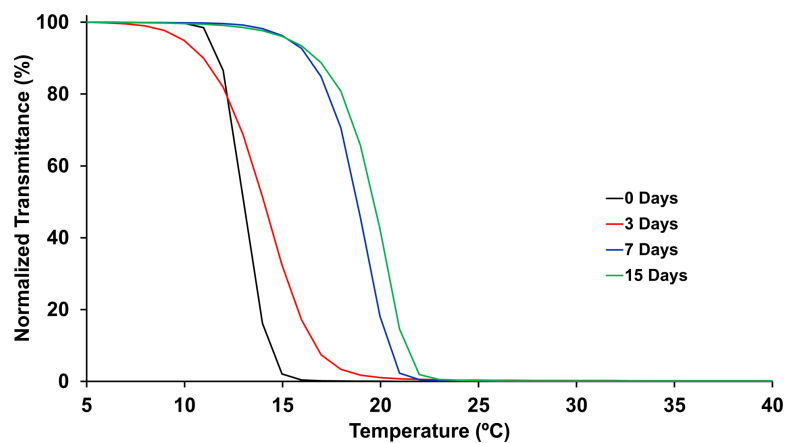


Figure A3.87. Thermo-responsive behaviour of **P(EtMEG)-Trit** in pH 3.0 citrate buffer (10.0 mg/mL) at different points showing an increase in the T_{cp} as the polymer depolymerizes.

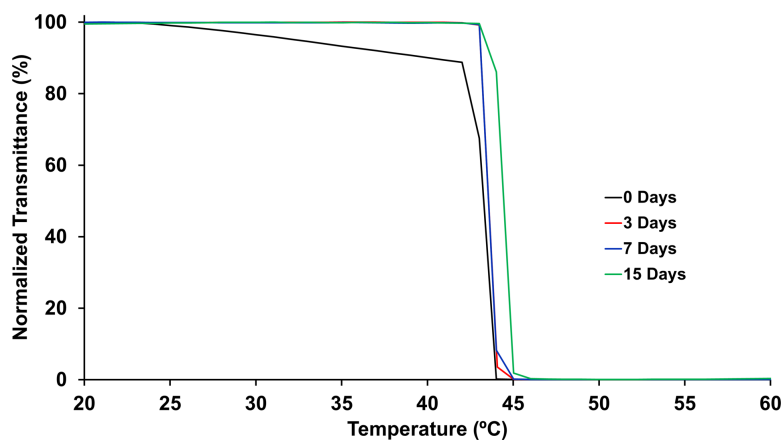


Figure A3.88. Thermo-responsive behaviour of **P(EtDEG)-BOM** in pH 3.0 citrate buffer (10.0 mg/mL) at different points showing minimal change in the T_{cp} .

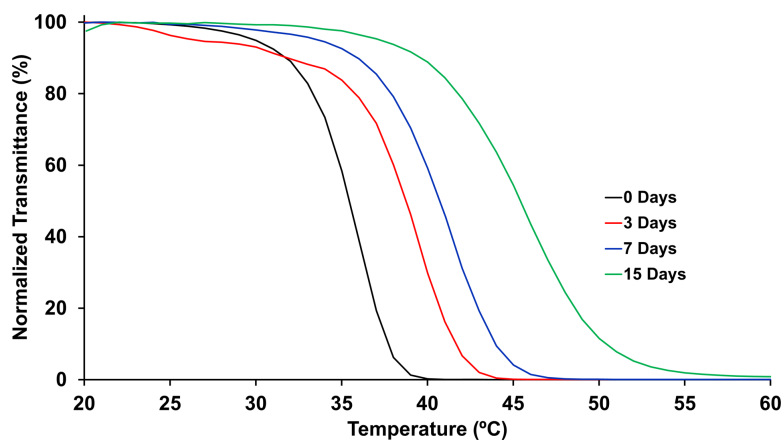
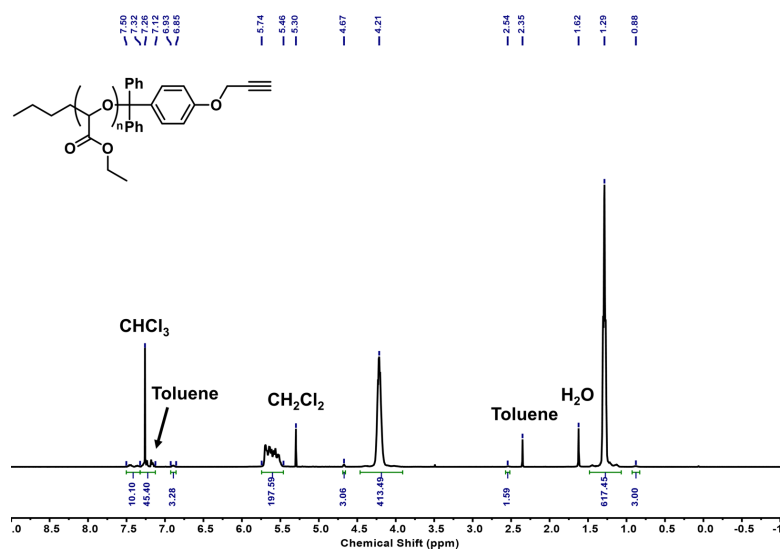
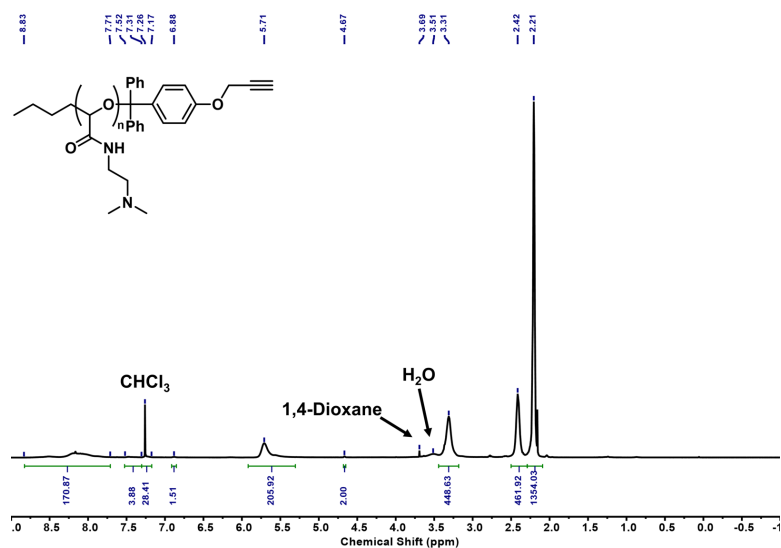


Figure A3.89. Thermo-responsive behaviour of **P(EtDEG)-Trit** in pH 3.0 citrate buffer (10.0 mg/mL) at different points showing an increase in the T_{cp} as the polymer depolymerizes.

Appendix 4

4 Supplemental Data for Chapter 5 Including ^1H and ^{13}C NMR Spectra, FT-IR Spectra, Size-Exclusion Chromatograms, Depolymerization Studies, and DLS StudiesFigure A4.1. ^1H NMR spectrum of PEtG-1 (CDCl₃, 400 MHz).Figure A4.2. ^1H NMR spectrum of PGAm(DMAE) (CDCl₃, 400 MHz).

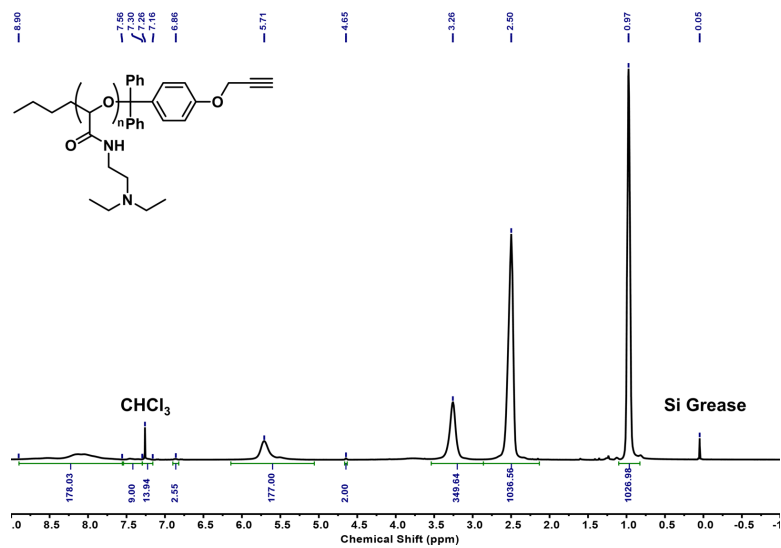


Figure A4.3. ^1H NMR spectrum of PGAm(DEAE) (CDCl_3 , 400 MHz).

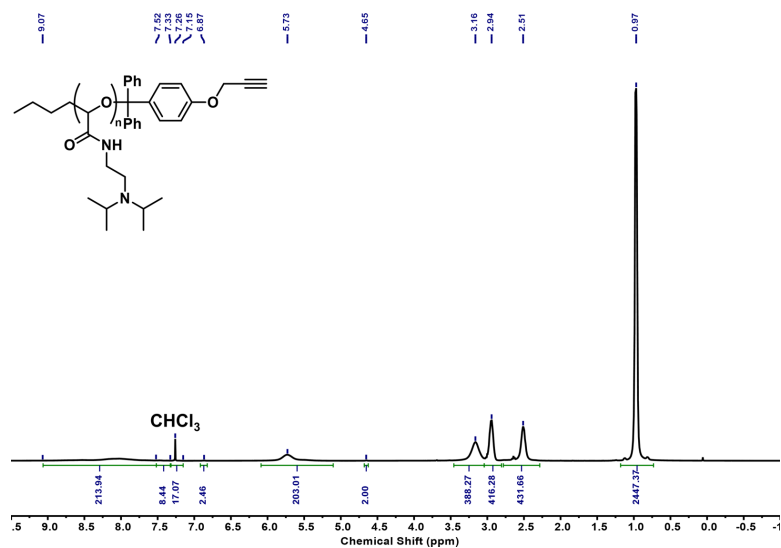


Figure A4.4. ^1H NMR spectrum of PGAm(DPAE) (CDCl_3 , 400 MHz).

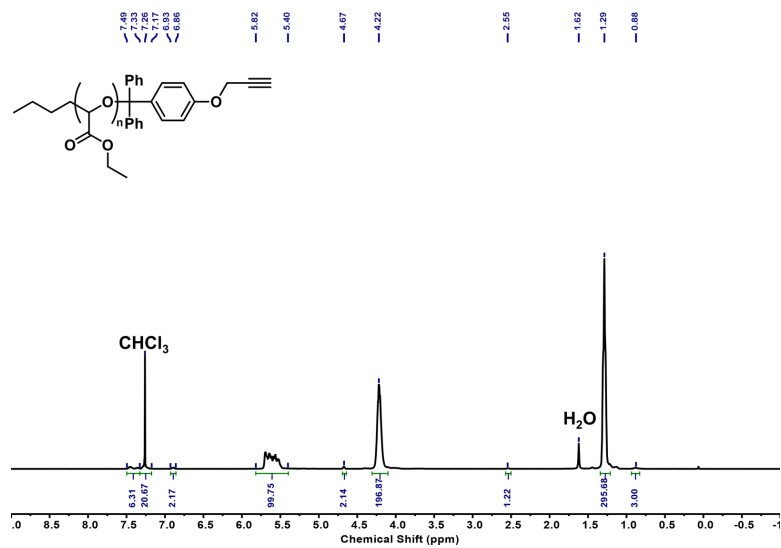


Figure A4.5. ¹H NMR spectrum of PEtG-2 (CDCl₃, 400 MHz).

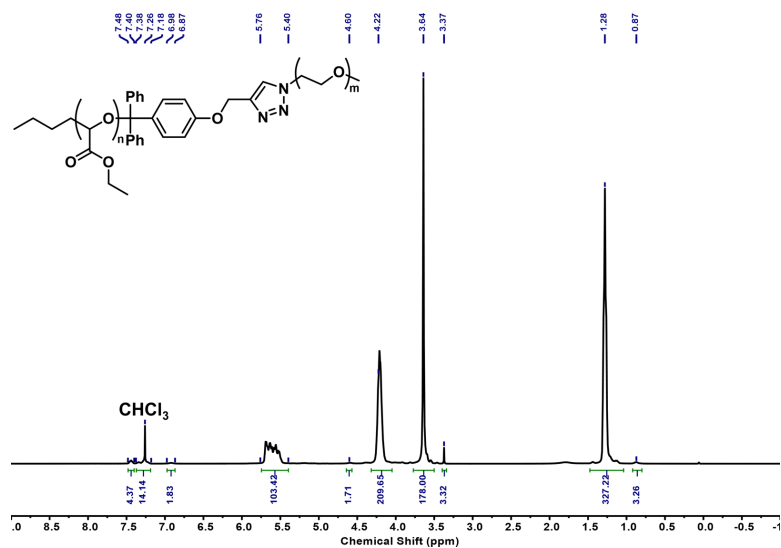


Figure A4.6. ¹H NMR spectrum of PEG-PEtG (CDCl₃, 400 MHz).

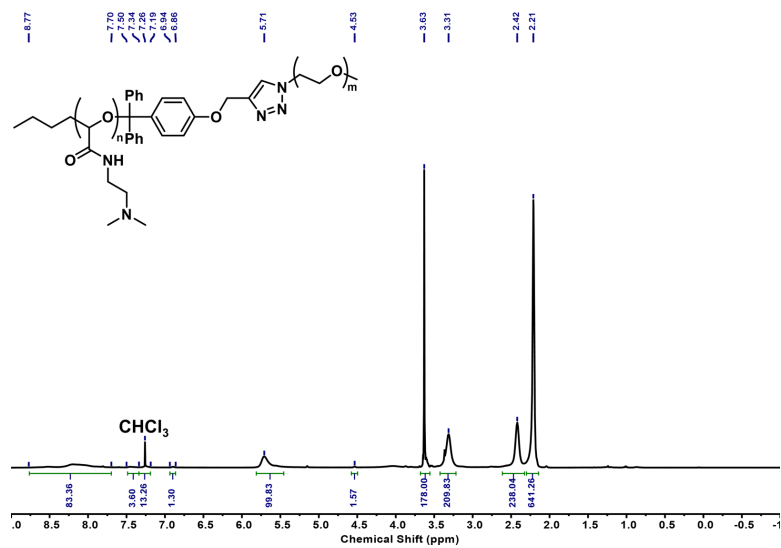


Figure A4.7. ^1H NMR spectrum of PEG-PGAm(DMAE) (CDCl_3 , 400 MHz).

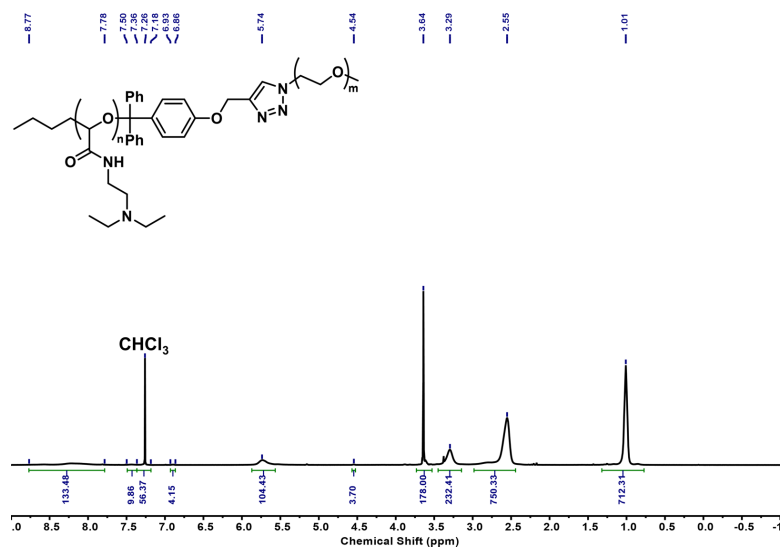
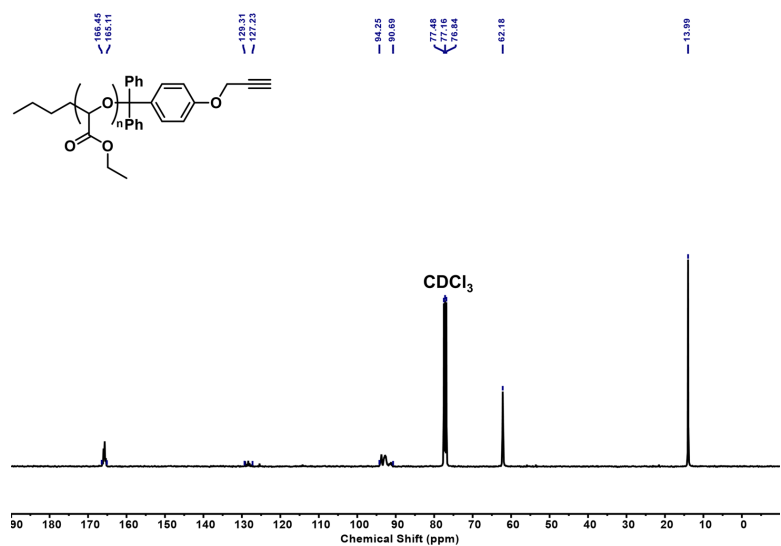
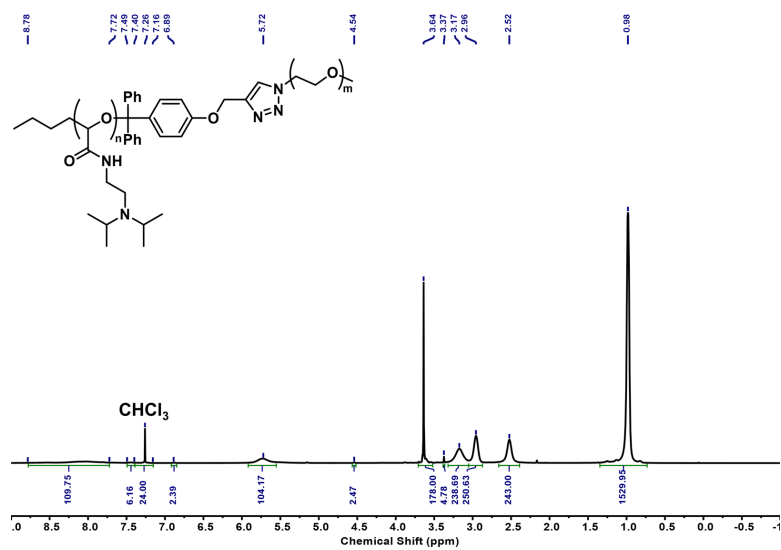


Figure A4.8. ^1H NMR spectrum of PEG-PGAm(DEAE) (CDCl_3 , 400 MHz).



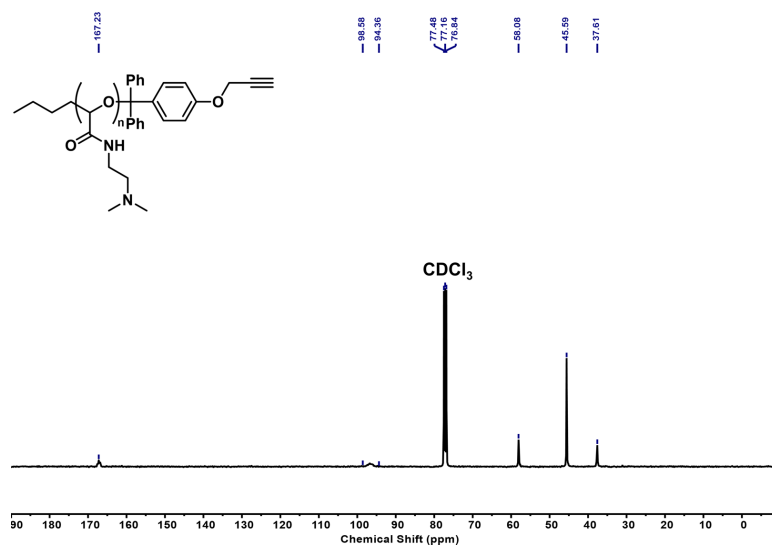


Figure A4.11. ^{13}C NMR spectrum of PGAm(DMAE) (CDCl_3 , 100 MHz).

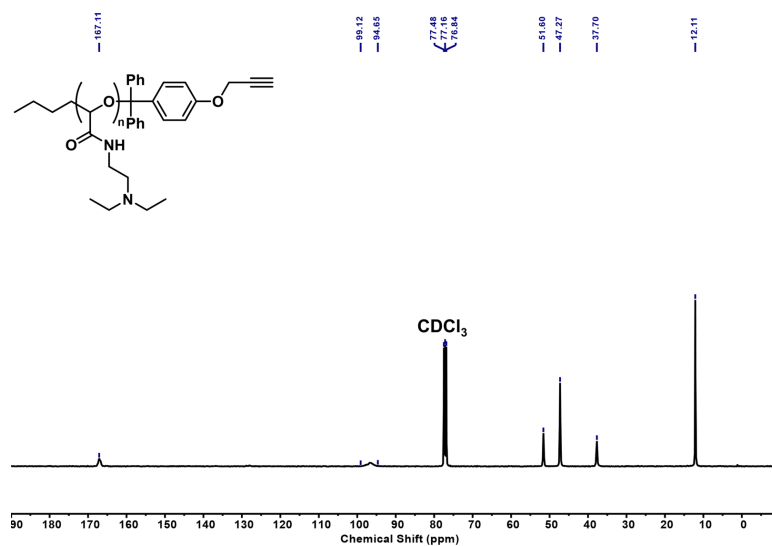


Figure A4.12. ^{13}C NMR spectrum of PGAm(DEAE) (CDCl_3 , 100 MHz).

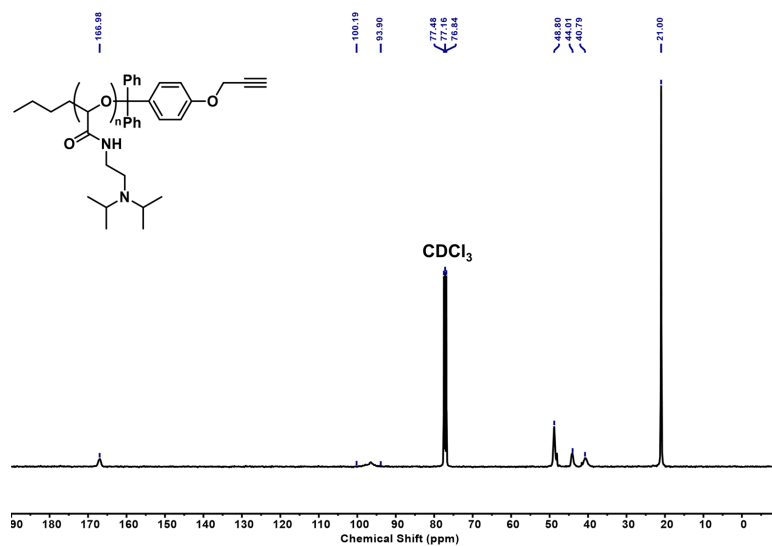


Figure A4.13. ¹³C NMR spectrum of PGAm(DPAE) (CDCl₃, 100 MHz).

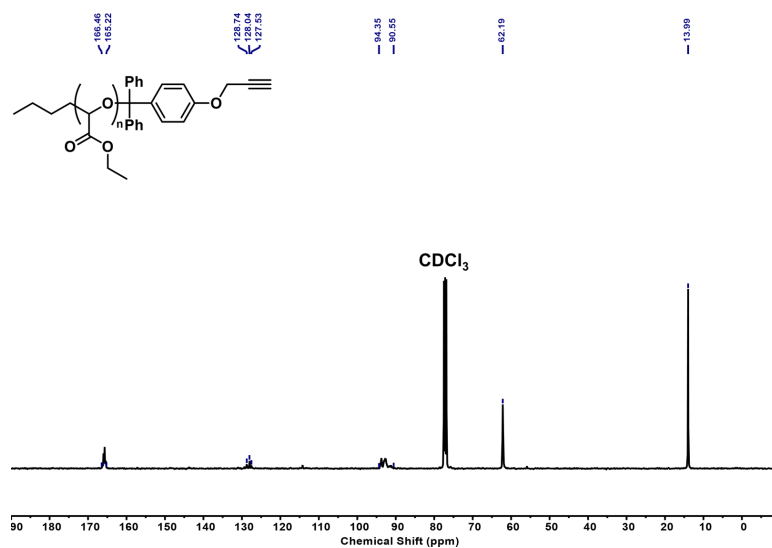


Figure A4.14. ¹³C NMR spectrum of PEtG-2 (CDCl₃, 100 MHz).

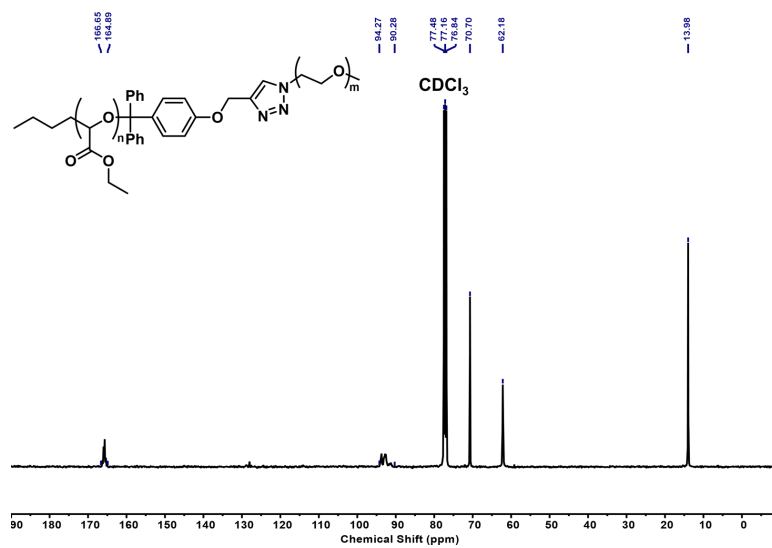


Figure A4.15. ¹³C NMR spectrum of PEG-PEtG (CDCl₃, 100 MHz).

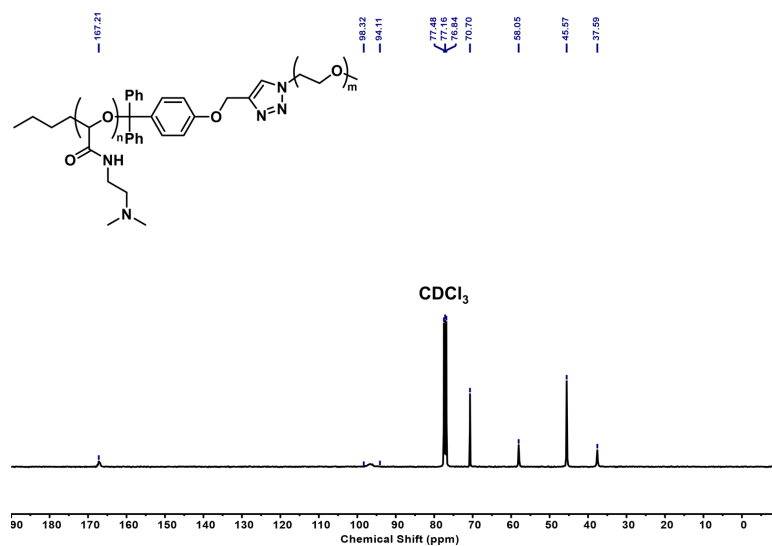


Figure A4.16. ¹³C NMR spectrum of PEG-PGAm(DMAE) (CDCl₃, 100 MHz).

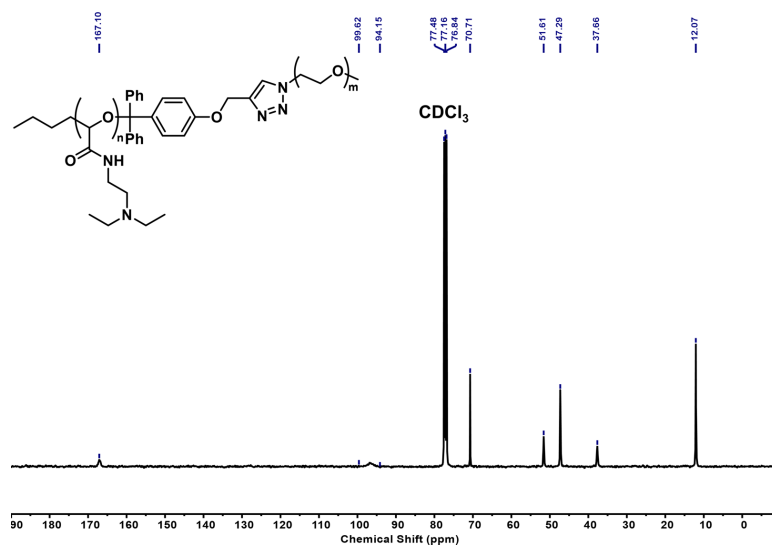


Figure A4.17. ¹³C NMR spectrum of PEG-PGAm(DEAE) (CDCl₃, 100 MHz).

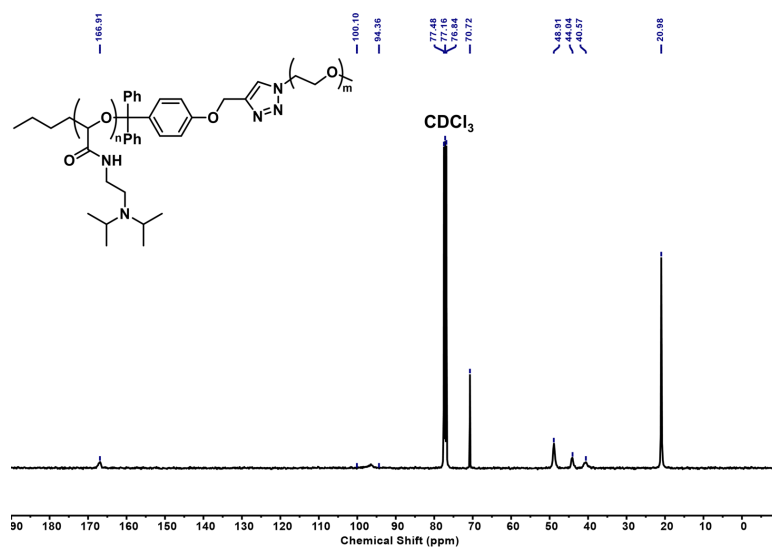


Figure A4.18. ¹³C NMR spectrum of PEG-PGAm(DPAE) (CDCl₃, 100 MHz).

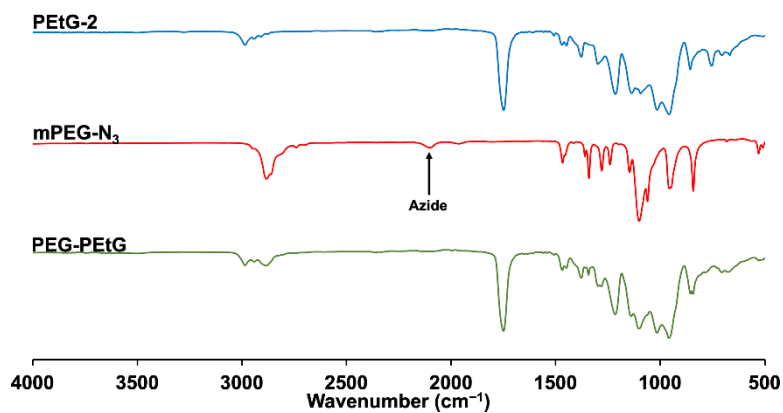


Figure A4.19. Overlay of FT-IR spectra of **PEtG-2**, **mPEG-N₃**, and **PEG-PEtG**. The azide stretch peak at $\sim 2100\text{ cm}^{-1}$ disappears in the final copolymer, indicating that no free **mPEG-N₃** impurity is present.

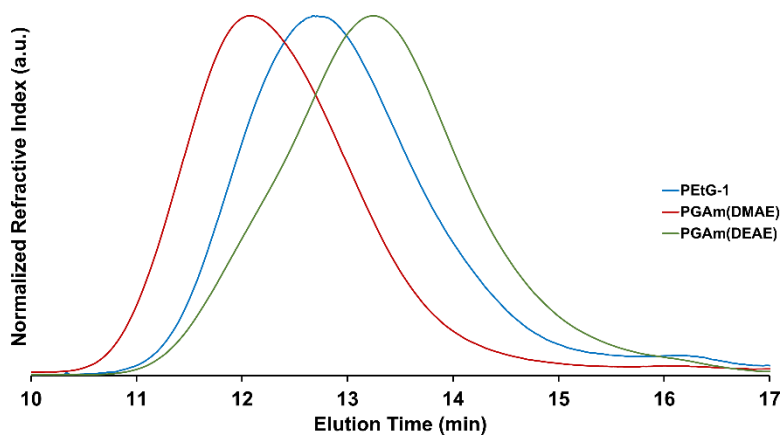


Figure A4.20. Overlay of chromatograms of the homopolymers **PEtG-1**, **PGAm(DMAE)**, and **PGAm(DEAE)**. **PGAm(DPAE)** was not soluble in the DMF eluent and thus could not be run on the column.

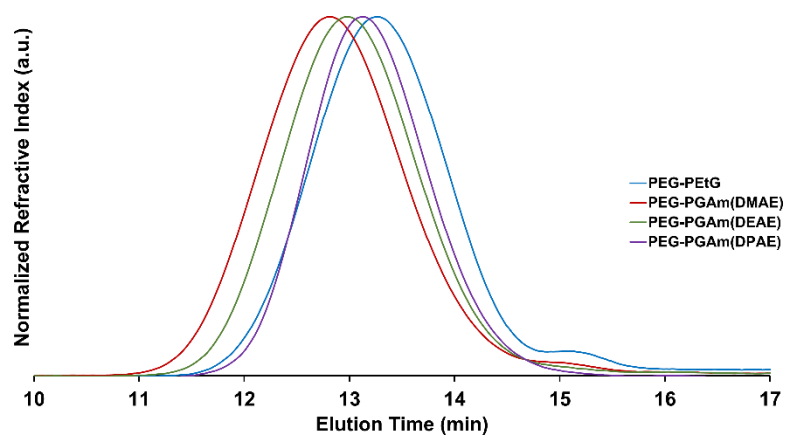


Figure A4.21. Overlay of the chromatograms of the block copolymers PEG-PEtG, PEG-PGAm(DMAE), PEG-PGAm(DEAE), and PEG-PGAm(DPAE).

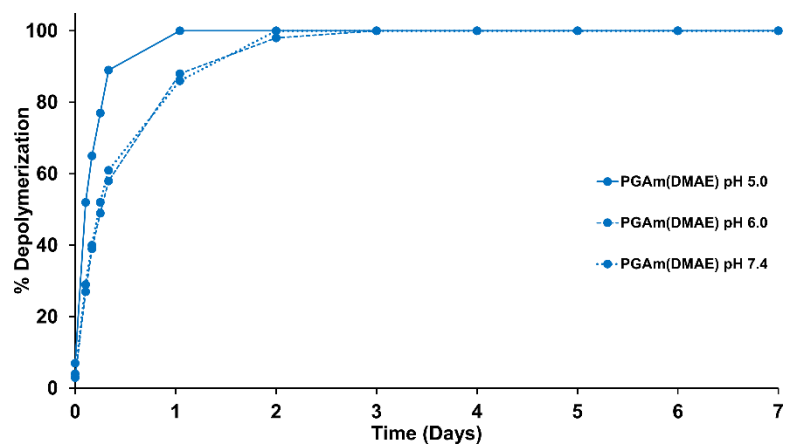


Figure A4.22. Depolymerization over time for PGAm(DMAE) at different pH levels, as measured by ^1H NMR spectroscopy. Deuterated phosphate buffer (0.2 M; pH 7.4) or deuterated citrate buffer (0.2 M; pH 5.0, 6.0) was used as the solvent.

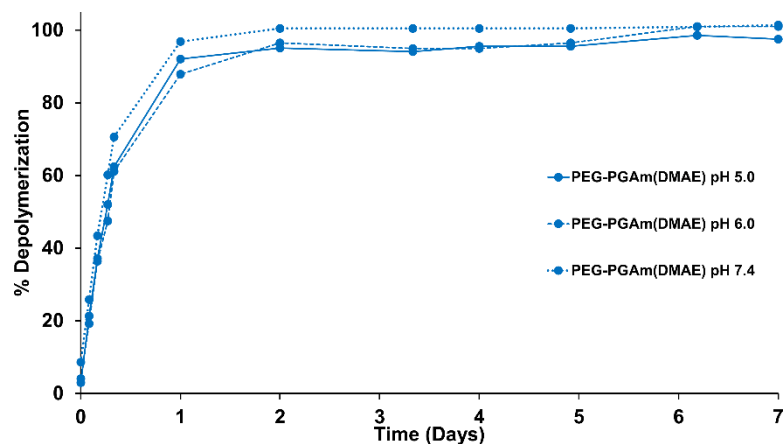


Figure A4.23. Depolymerization over time for **PEG-PGAm(DMAE)** at different pH levels, as measured by ^1H NMR spectroscopy. Deuterated phosphate buffer (0.2 M; pH 7.4, 8.0) or deuterated citrate buffer (0.2 M; pH 5.0, 6.0) was used as the solvent.

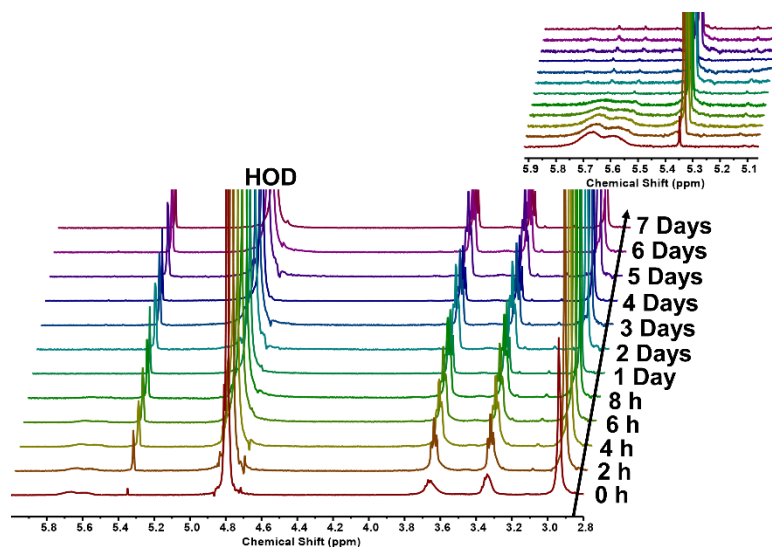


Figure A4.24. Depolymerization of **PGAm(DMAE)** over time in deuterated citrate buffer (0.2 M; pH 5.0) monitored by ^1H NMR spectroscopy (400 Hz). The peaks from the citrate buffer salts have been cropped out of the spectrum.

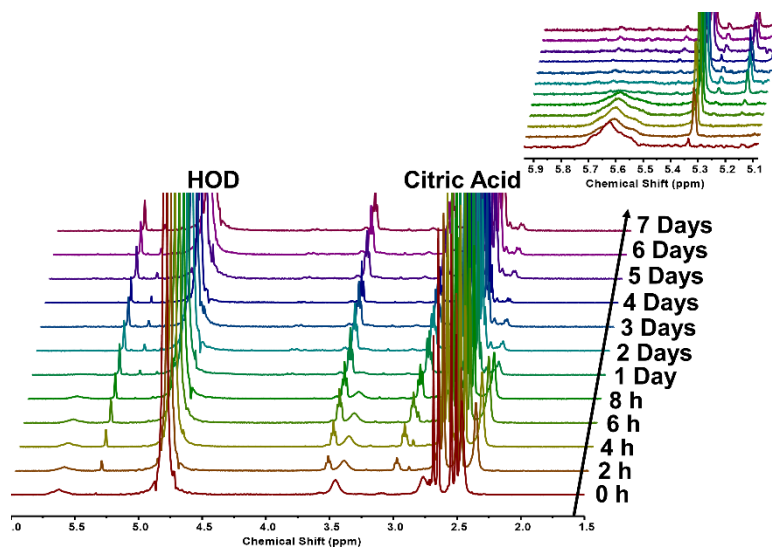


Figure A4.25. Depolymerization of **PGAm(DMAE)** over time in deuterated citrate buffer (0.2 M; pH 6.0) monitored by ^1H NMR spectroscopy (400 Hz).

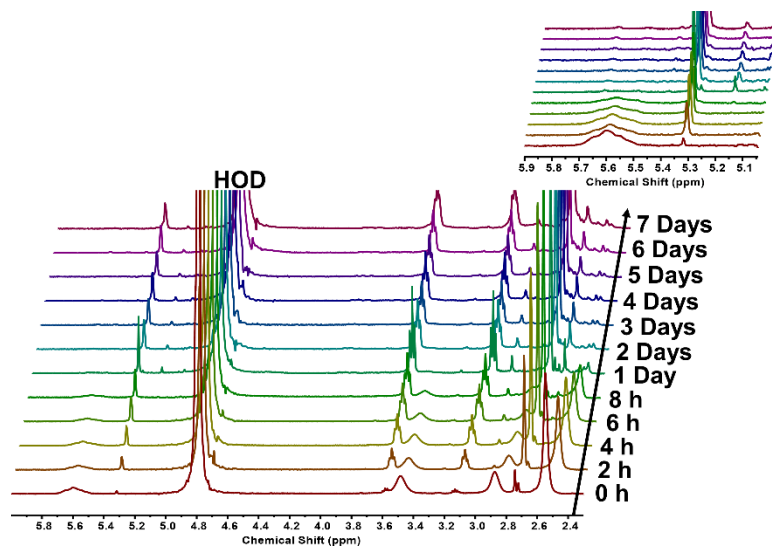


Figure A4.26. Depolymerization of **PGAm(DMAE)** over time in deuterated phosphate buffer (0.2 M; pH 7.4) monitored by ^1H NMR spectroscopy (400 Hz).

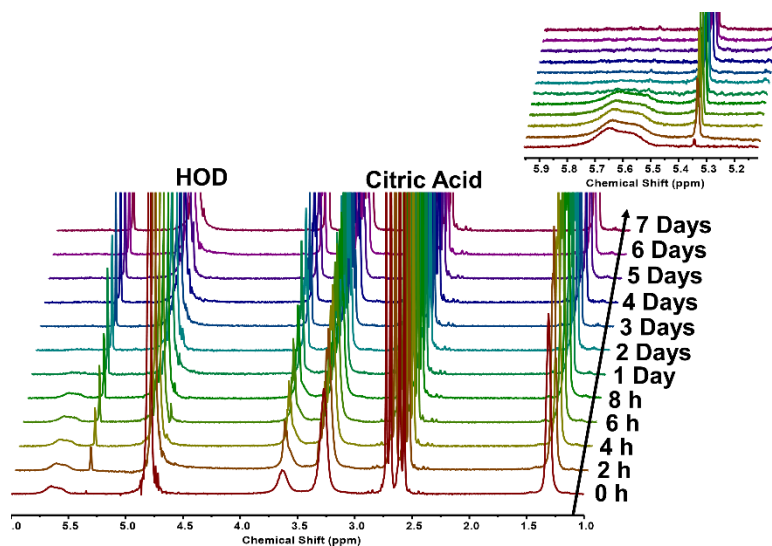


Figure A4.27. Depolymerization of PGAm(DEAE) over time in deuterated citrate buffer (0.2 M; pH 5.0) monitored by ^1H NMR spectroscopy (400 Hz).

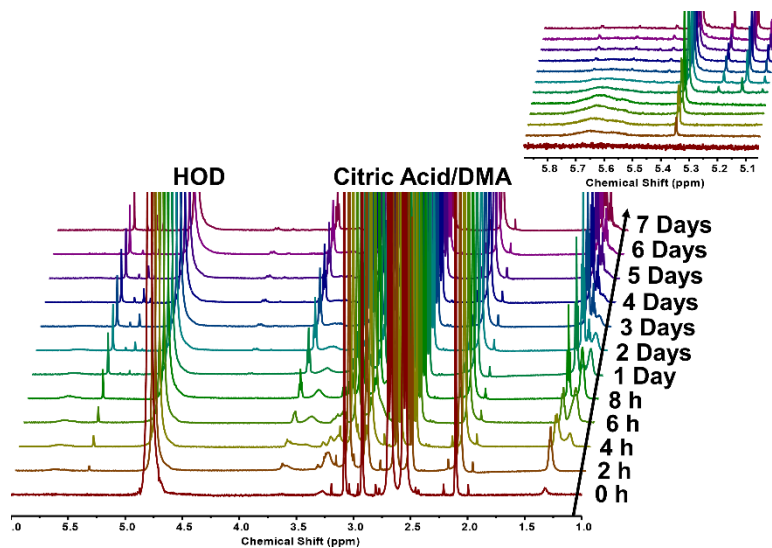


Figure A4.28. Depolymerization of PGAm(DEAE) over time in deuterated citrate buffer (0.2 M; pH 6.0) monitored by ^1H NMR spectroscopy (600 Hz). DMA was added as an internal standard.

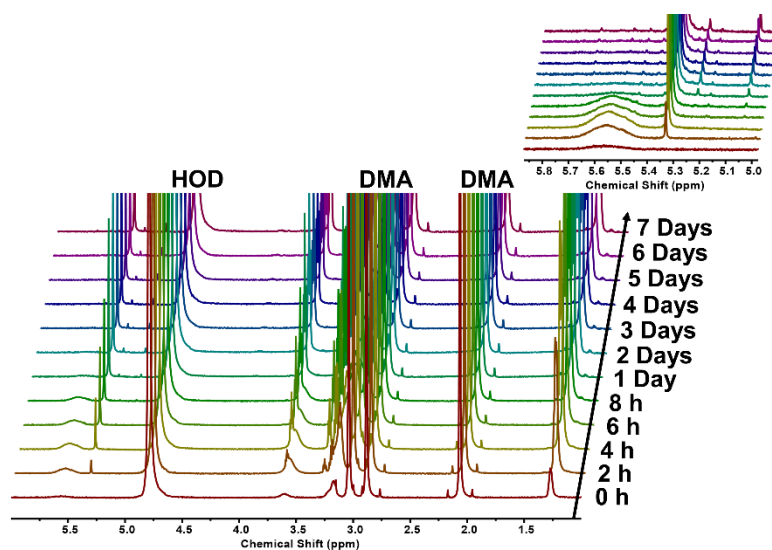


Figure A4.29. Depolymerization of **PGAm(DEAE)** over time in deuterated phosphate buffer (0.2 M; pH 7.4) monitored by ^1H NMR spectroscopy (600 Hz). DMA was added as an internal standard.

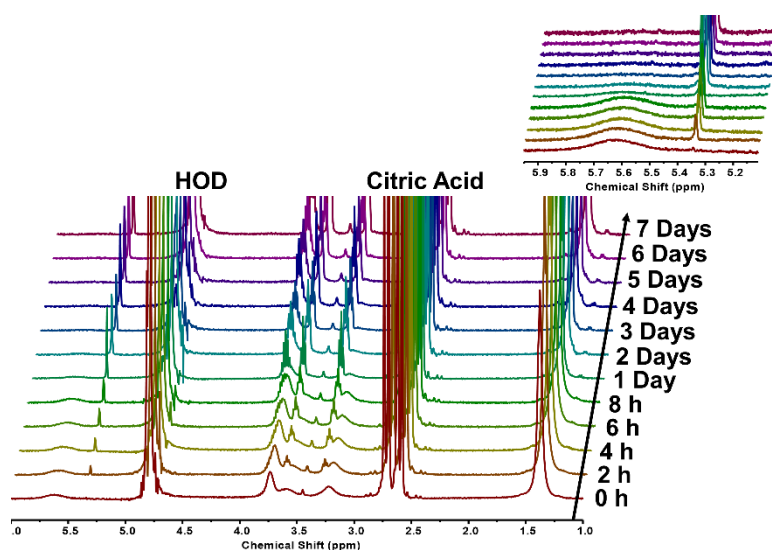


Figure A4.30. Depolymerization of **PGAm(DPAE)** over time in deuterated citrate buffer (0.2 M; pH 5.0) monitored by ^1H NMR spectroscopy (400 Hz).

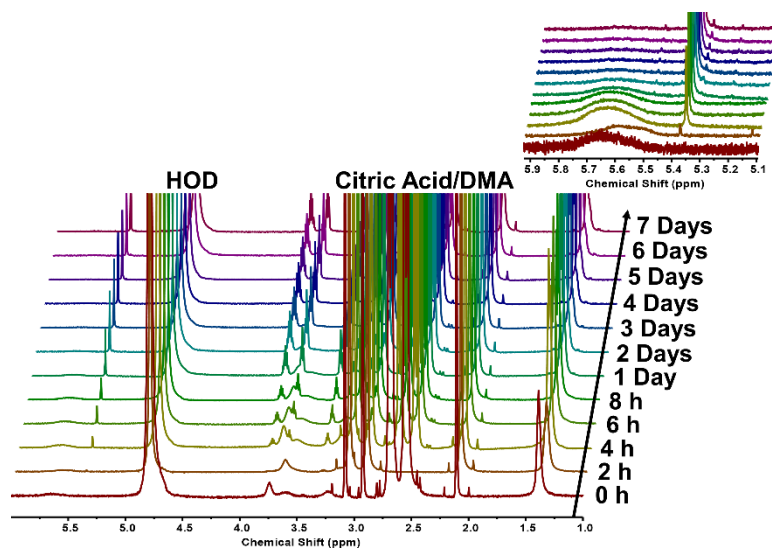


Figure A4.31. Depolymerization of **PGAm(DPAE)** over time in deuterated citrate buffer (0.2 M; pH 6.0) monitored by ^1H NMR spectroscopy (600 Hz). DMA was added as an internal standard.

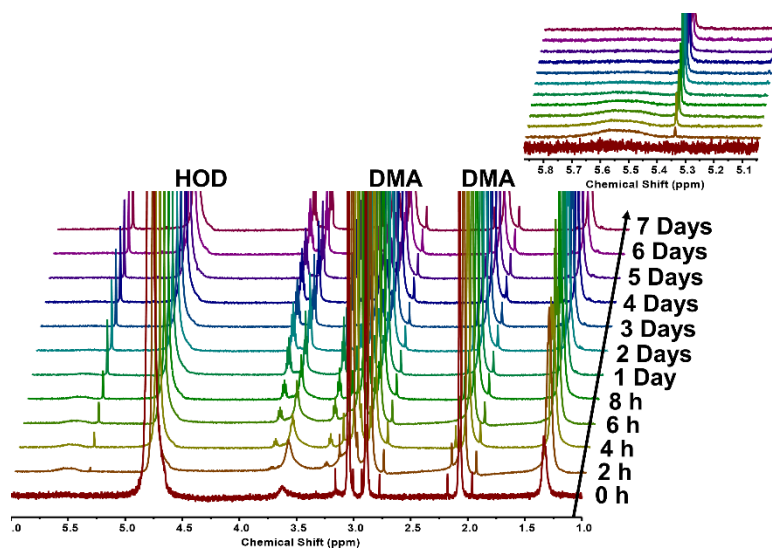


Figure A4.32. Depolymerization of **PGAm(DPAE)** over time in deuterated phosphate buffer (0.2 M; pH 7.4) monitored by ^1H NMR spectroscopy (600 Hz). DMA was added as an internal standard.

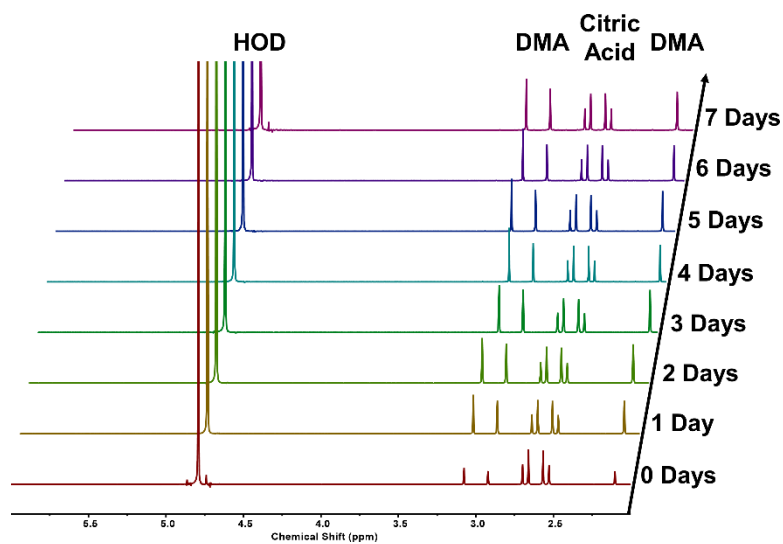


Figure A4.33. Depolymerization of **PETG-1** over time in deuterated citrate buffer (0.2 M; pH 5.0) monitored by ^1H NMR spectroscopy (400 Hz). DMA was added as an internal standard.

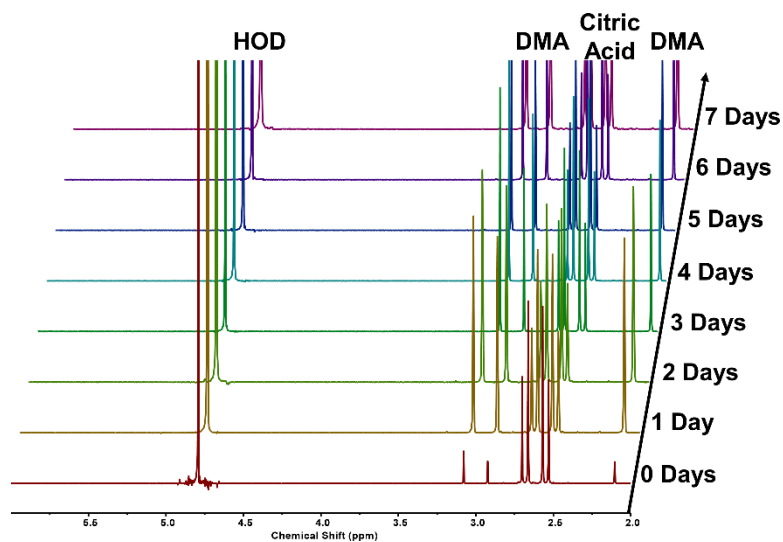


Figure A4.34. Depolymerization of **PETG-1** over time in deuterated citrate buffer (0.2 M; pH 5.0) monitored by ^1H NMR spectroscopy (400 Hz). DMA was added as an internal standard.

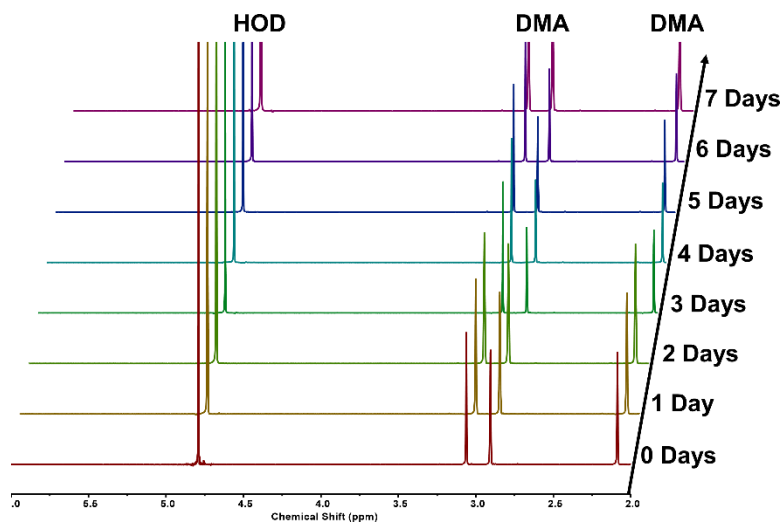


Figure A4.35. Depolymerization of **PETG-1** over time in deuterated phosphate buffer (0.2 M; pH 7.4) monitored by ^1H NMR spectroscopy (400 Hz). DMA was added as an internal standard.

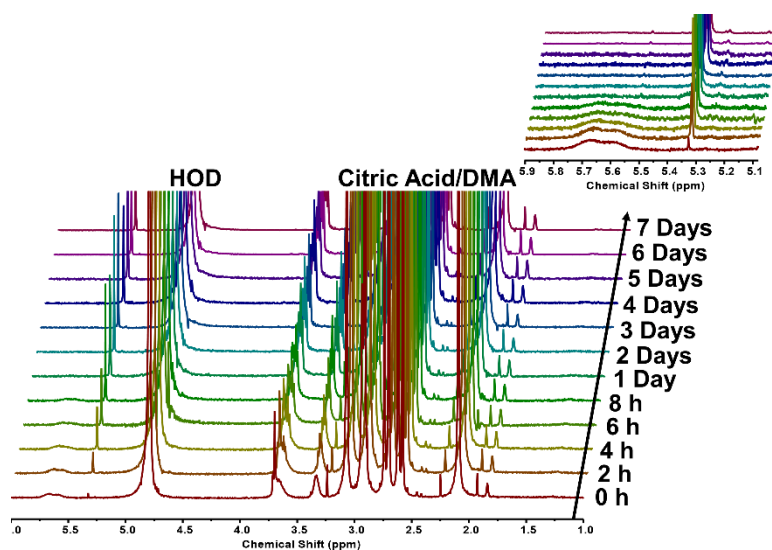


Figure A4.36. Depolymerization of **PEG-PGAm(DMAE)** over time in deuterated citrate buffer (0.2 M; pH 5.0) monitored by ^1H NMR spectroscopy (400 Hz). DMA was added as an internal standard.

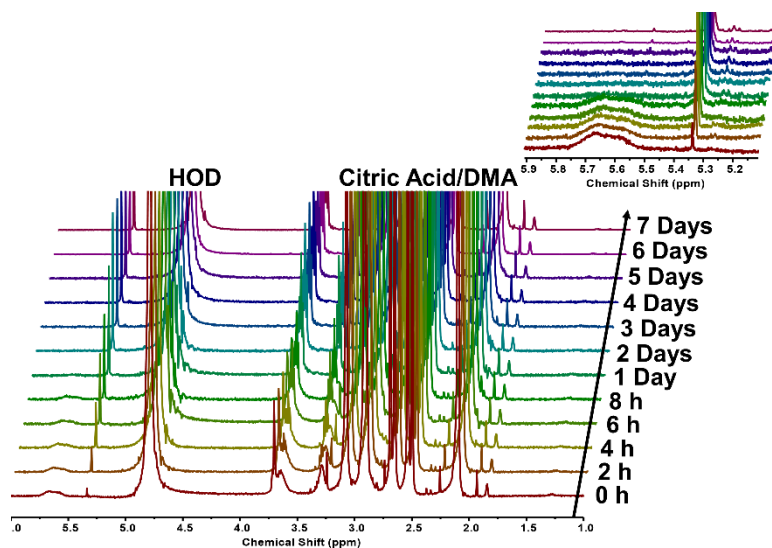


Figure A4.37. Depolymerization of PEG-PGAm(DMAE) over time in deuterated citrate buffer (0.2 M; pH 6.0) monitored by ^1H NMR spectroscopy (400 Hz). DMA was added as an internal standard.

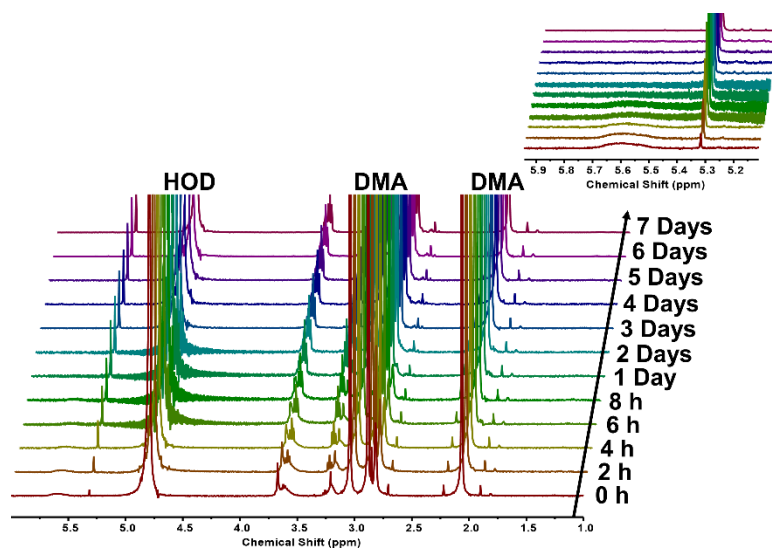


Figure A4.38. Depolymerization of PEG-PGAm(DMAE) over time in deuterated phosphate buffer (0.2 M; pH 7.4) monitored by ^1H NMR spectroscopy (400 Hz). DMA was added as an internal standard.

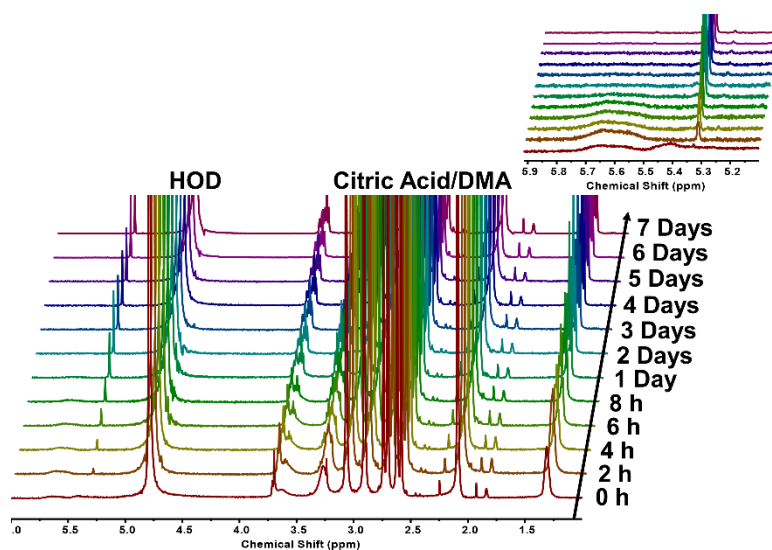


Figure A4.39. Depolymerization of **PEG-PGAm(DEAE)** over time in deuterated citrate buffer (0.2 M; pH 5.0) monitored by ^1H NMR spectroscopy (400 Hz). DMA was added as an internal standard.

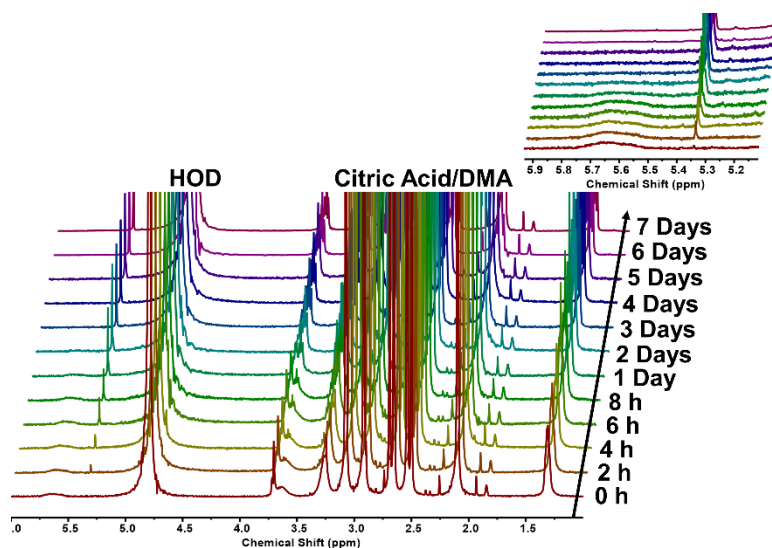


Figure A4.40. Depolymerization of **PEG-PGAm(DEAE)** over time in deuterated citrate buffer (0.2 M; pH 6.0) monitored by ^1H NMR spectroscopy (400 Hz). DMA was added as an internal standard.

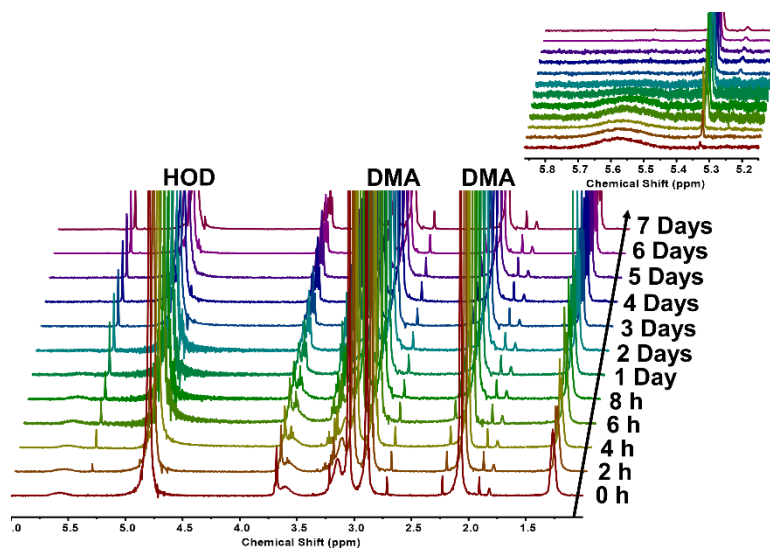


Figure A4.41. Depolymerization of **PEG-PGAm(DEAE)** over time in deuterated phosphate buffer (0.2 M; pH 7.4) monitored by ^1H NMR spectroscopy (400 Hz). DMA was added as an internal standard.

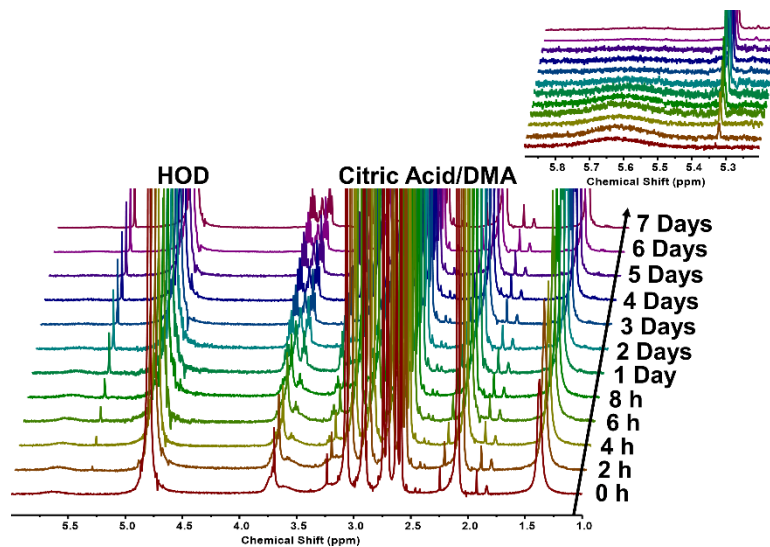


Figure A4.42. Depolymerization of **PEG-PGAm(DPAE)** over time in deuterated citrate buffer (0.2 M; pH 5.0) monitored by ^1H NMR spectroscopy (400 Hz). DMA was added as an internal standard.

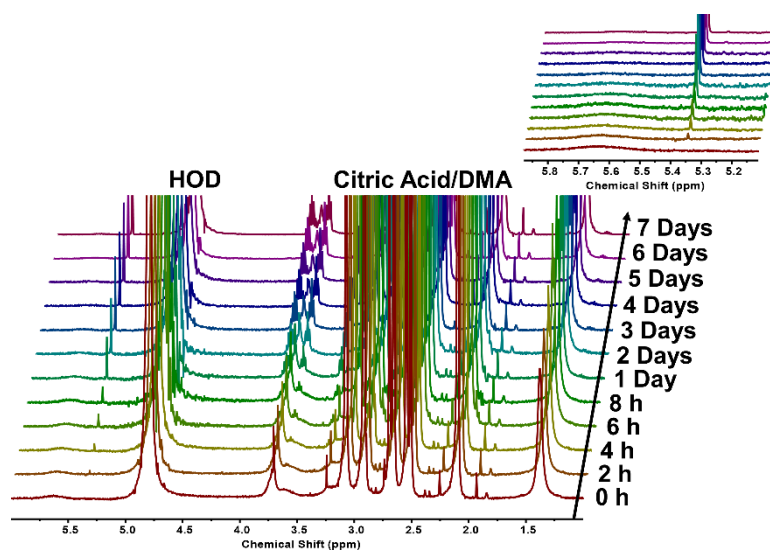


Figure A4.43. Depolymerization of **PEG-PGAm(DPAE)** over time in deuterated citrate buffer (0.2 M; pH 6.0) monitored by ^1H NMR spectroscopy (400 Hz). DMA was added as an internal standard.

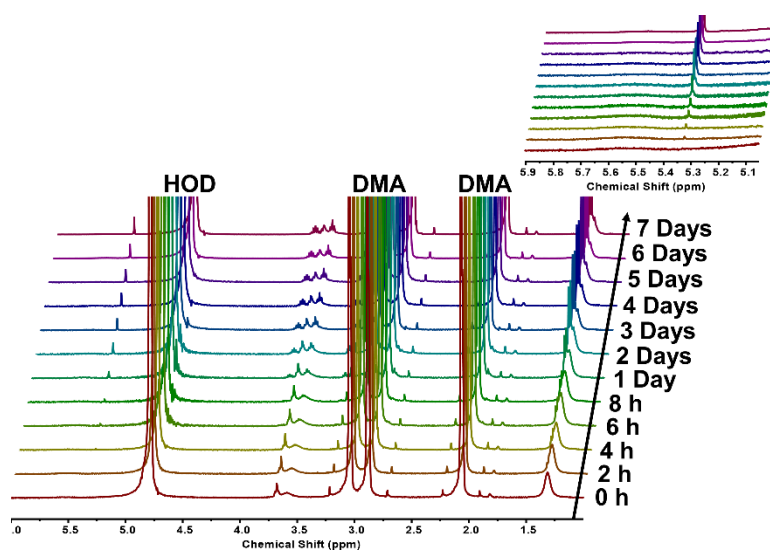


Figure A4.44. Depolymerization of **PEG-PGAm(DPAE)** over time in deuterated phosphate buffer (0.2 M; pH 7.4) monitored by ^1H NMR spectroscopy (400 Hz). DMA was added as an internal standard.

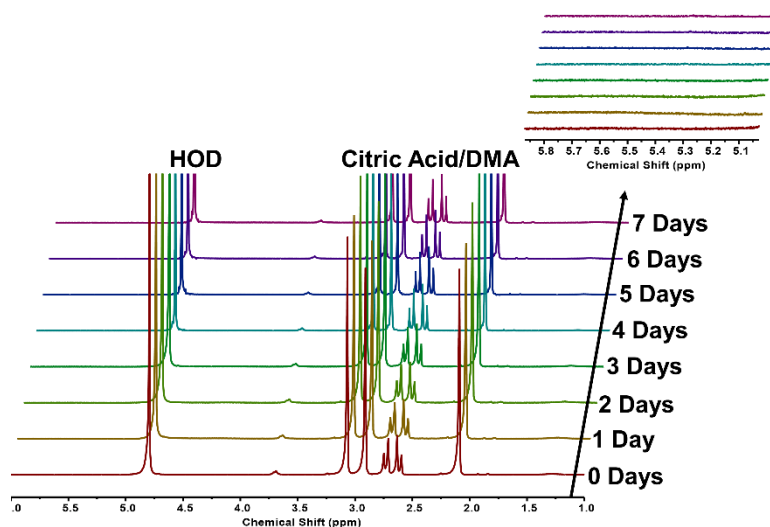


Figure A4.45. Depolymerization of **PEG-PEtG** over time in deuterated citrate buffer (0.2 M; pH 5.0) monitored by ^1H NMR spectroscopy (400 Hz). DMA was added as an internal standard.

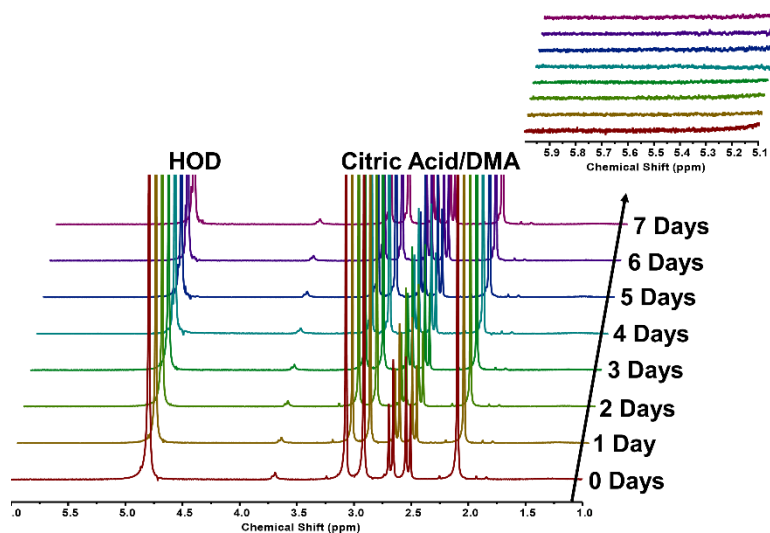


Figure A4.46. Depolymerization of **PEG-PEtG** over time in deuterated citrate buffer (0.2 M; pH 6.0) monitored by ^1H NMR spectroscopy (400 Hz). DMA was added as an internal standard.

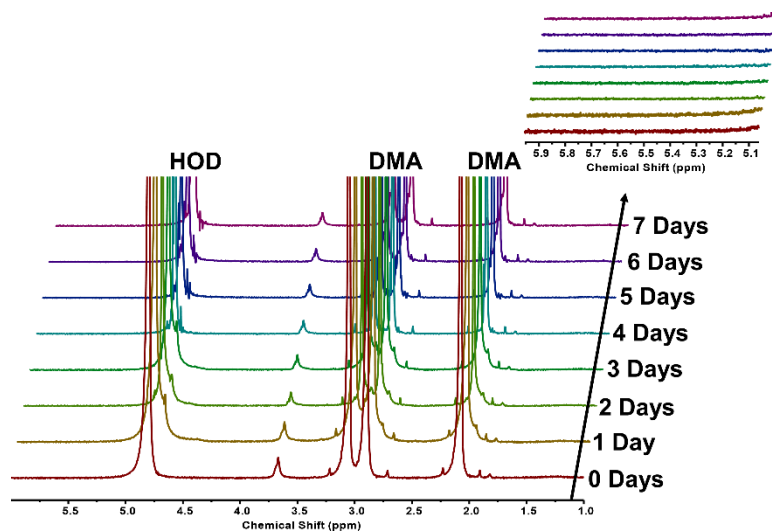


Figure A4.47. Depolymerization of **PEG-PEtG** over time in deuterated phosphate buffer (0.2 M; pH 7.4) monitored by ^1H NMR spectroscopy (400 Hz). DMA was added as an internal standard.

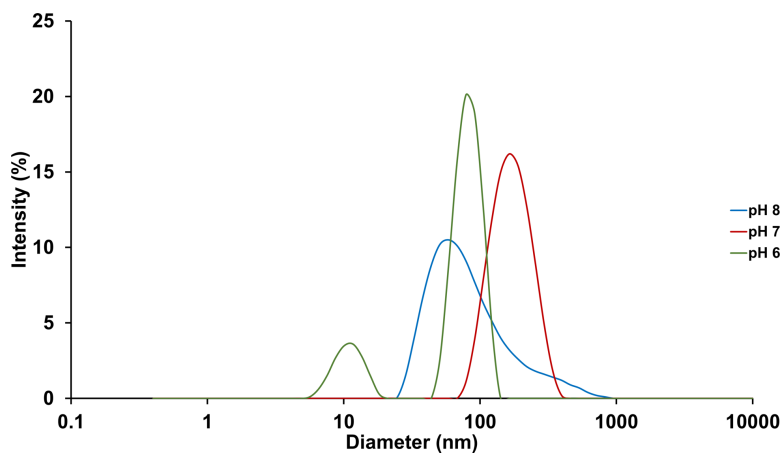


Figure A4.48. Intensity distributions for **PEG-PGAm(DPAE)** assemblies at different pH levels (at 25 °C).

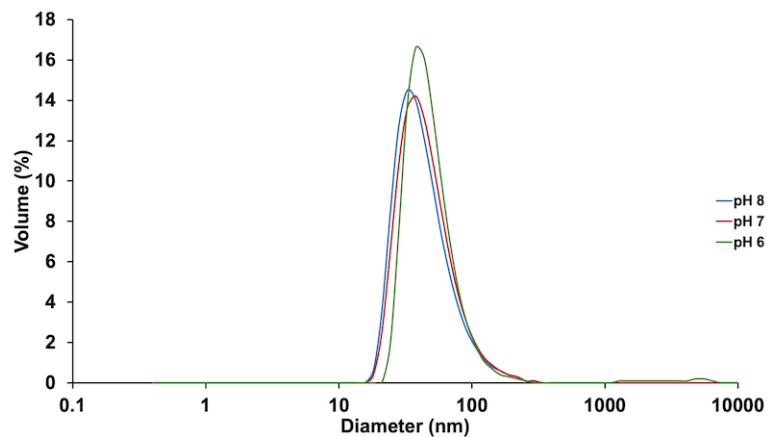


Figure A4.49. Volume distributions of **PEG-PEtG** assemblies at different pH levels (25 °C).

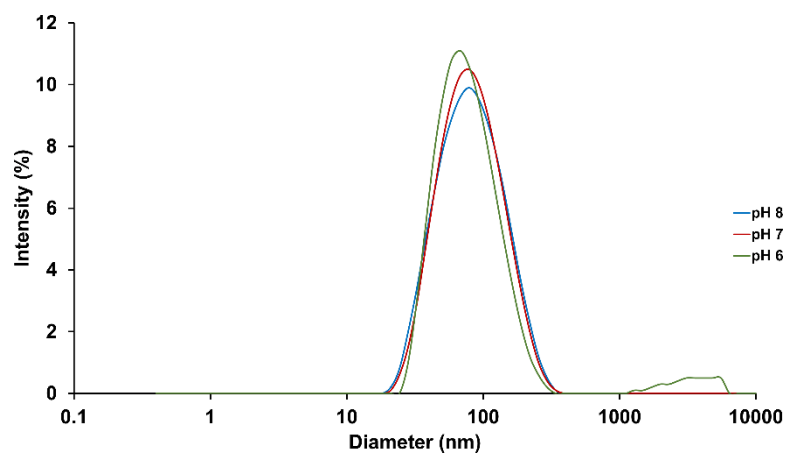


Figure A4.50. Intensity distributions for **PEG-PEtG** assemblies at different pH levels (at 25 °C).

Appendix 5

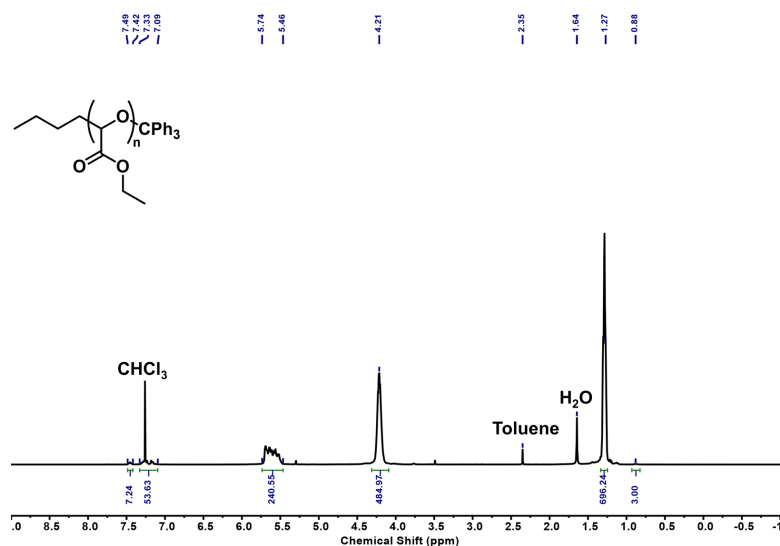
5 Supplemental Data for Chapter 6 Including ^1H and ^{13}C NMR Spectra, Size-Exclusion Chromatograms, Depolymerization Studies, Complexation Studies, and Cytotoxicity Assays

Figure A5.1. ^1H NMR spectrum of PEtG-Trit (CDCl_3 , 400 MHz).

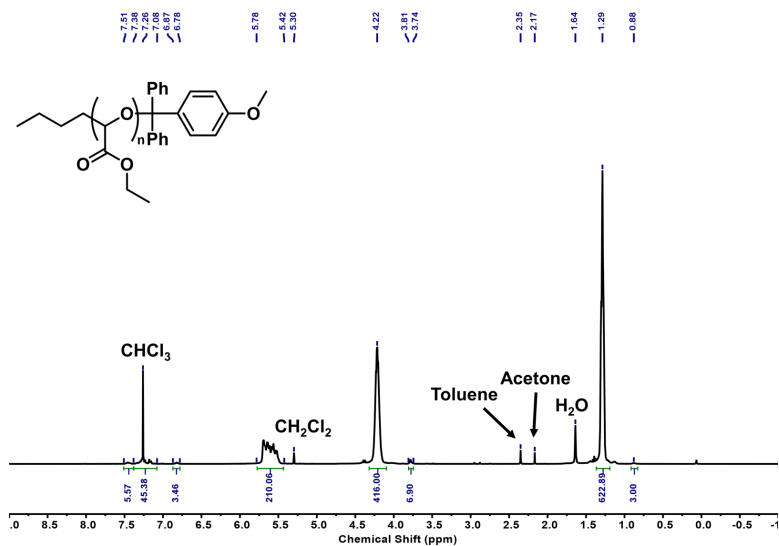


Figure A5.2. ¹H NMR spectrum of PEtG-MMT (CDCl₃, 400 MHz).

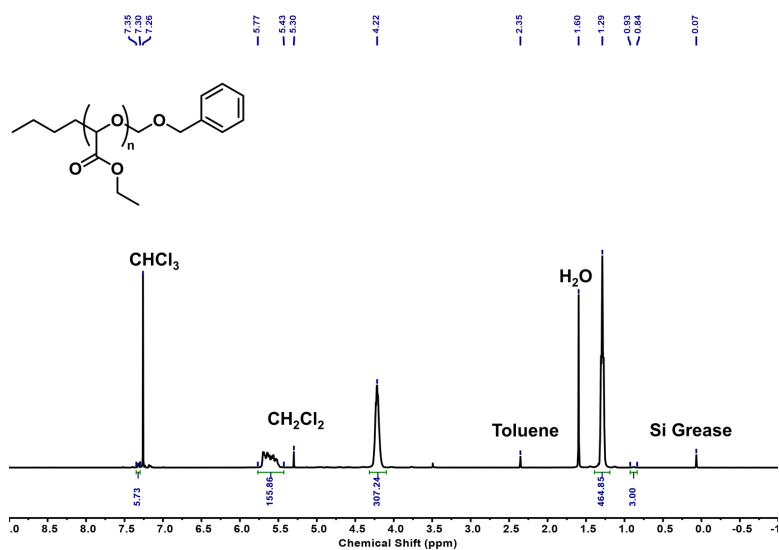


Figure A5.3. ¹H NMR spectrum of PEtG-BOM (CDCl₃, 400 MHz).

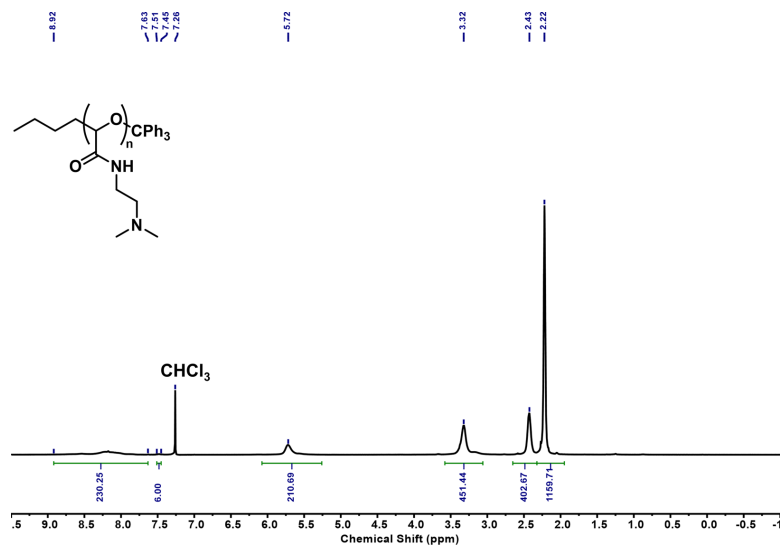


Figure A5.4. 1H NMR spectrum of PGAm-DMAE-Trit (CDCl₃, 400 MHz).

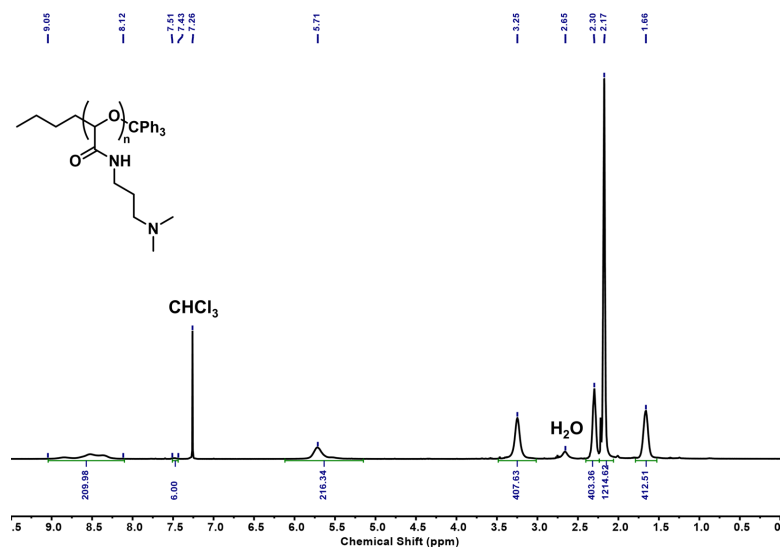


Figure A5.5. 1H NMR spectrum of PGAm-DMAPr-Trit (CDCl₃, 400 MHz).

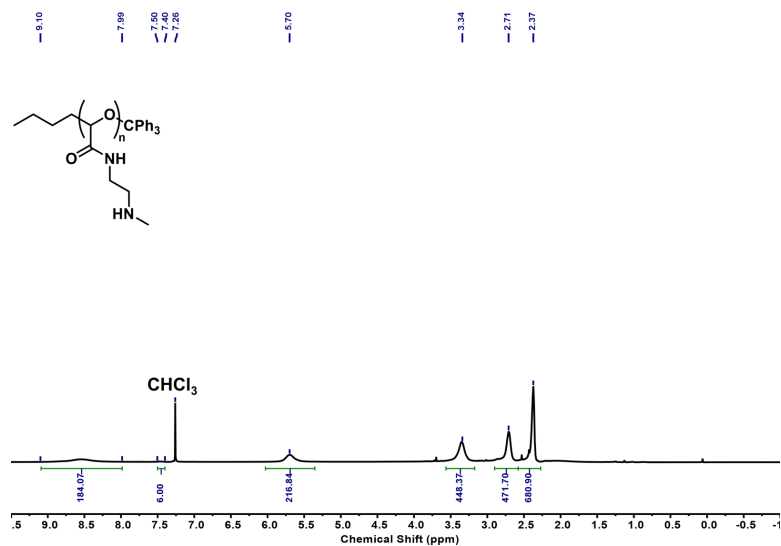


Figure A5.6. ^1H NMR spectrum of PGAm-MAE-Trit (CDCl₃, 400 MHz).

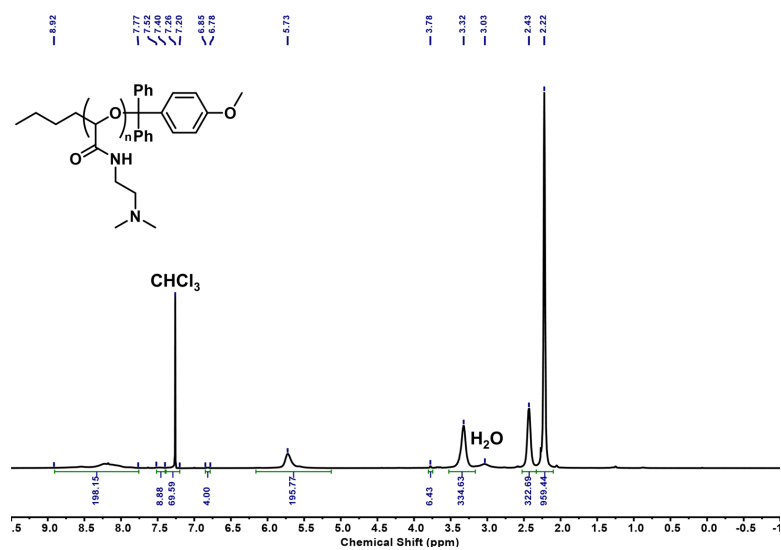


Figure A5.7. ^1H NMR spectrum of PGAm-DMAE-MMT (CDCl₃, 400 MHz). End group analysis reveals that a large portion of the polymer initiated with residual water and therefore has a 4-monomethoxytrityl end-cap at both ends.

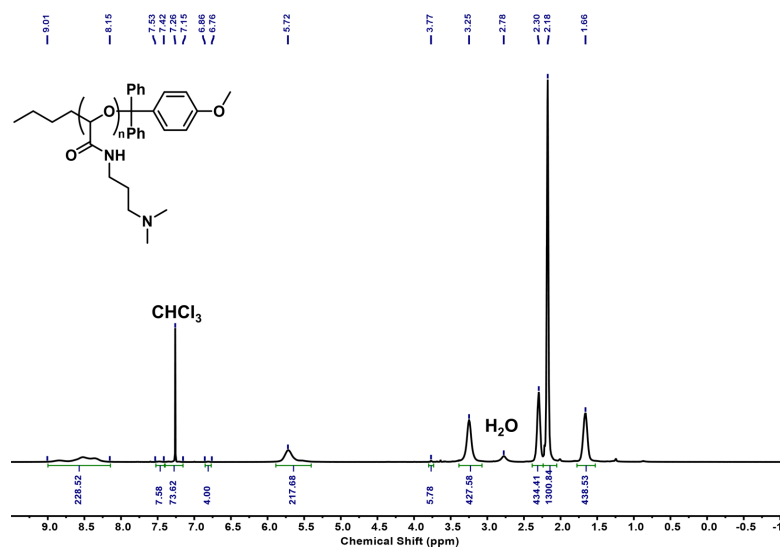


Figure A5.8. ¹H NMR spectrum of PGAm-DMAPr-MMT (CDCl₃, 400 MHz). End group analysis reveals that a large portion of the polymer initiated with residual water and therefore has a 4-monomethoxytrityl end-cap at both ends.

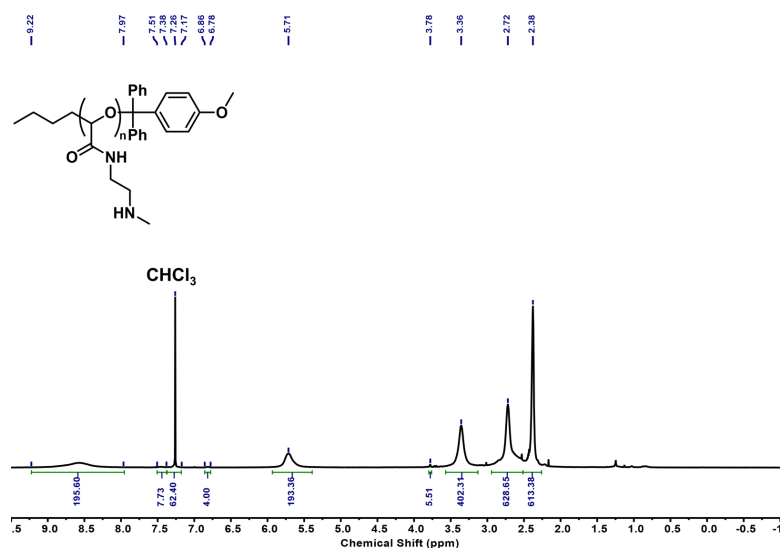


Figure A5.9. ¹H NMR spectrum of PGAm-MAE-MMT (CDCl₃, 400 MHz). The peak at 2.72 ppm has a higher than expected integration due to an overlapping H₂O peak. End group analysis reveals that a large portion of the polymer initiated with residual water and therefore has a 4-monomethoxytrityl end-cap at both ends.

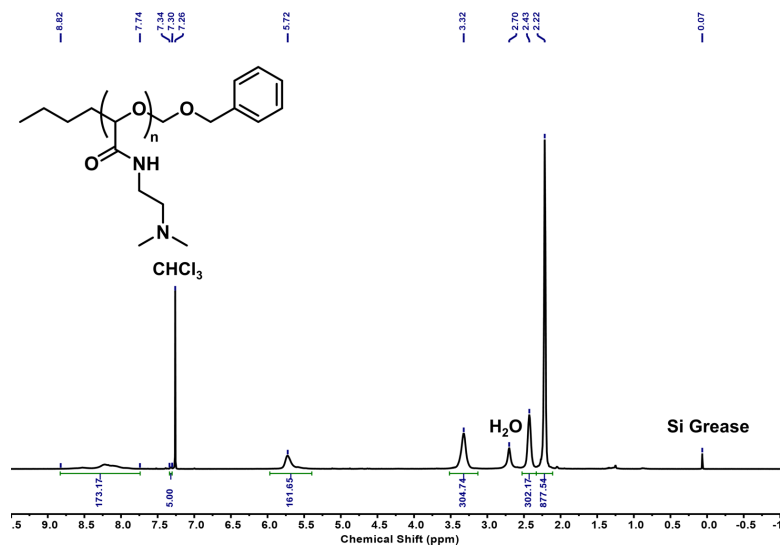


Figure A5.10. ¹H NMR spectrum of PGAm-DMAE-BOM (CDCl₃, 400 MHz).

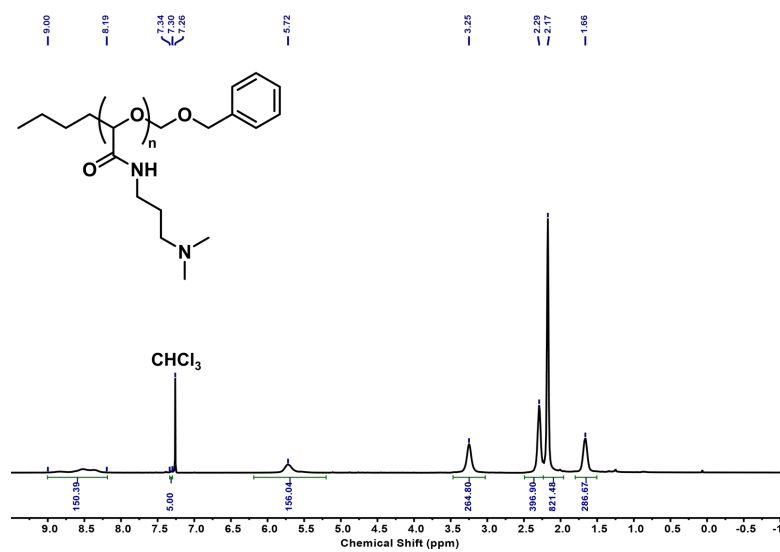


Figure A5.11. ¹H NMR spectrum of PGAm-DMAPr-BOM (CDCl₃, 400 MHz).

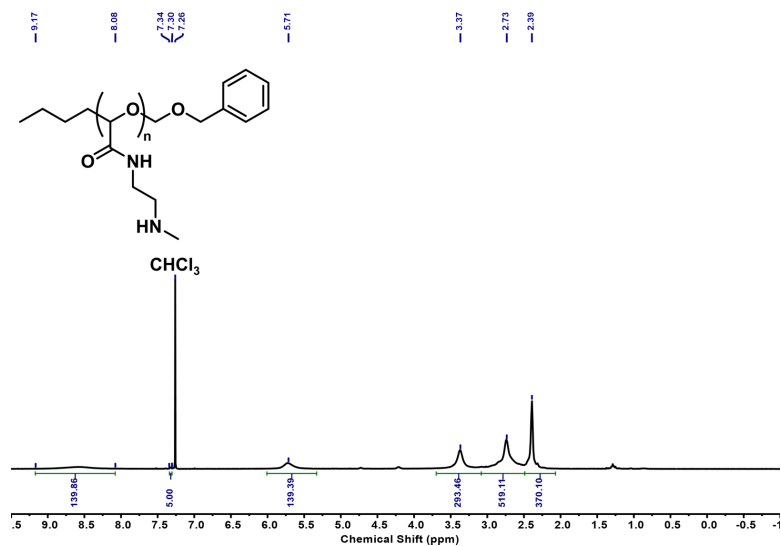


Figure A5.12. ^1H NMR spectrum of **PGAm-MAE-BOM** (CDCl₃, 400 MHz). The peak at 2.73 ppm has a higher than expected integration due to an overlapping H₂O peak.

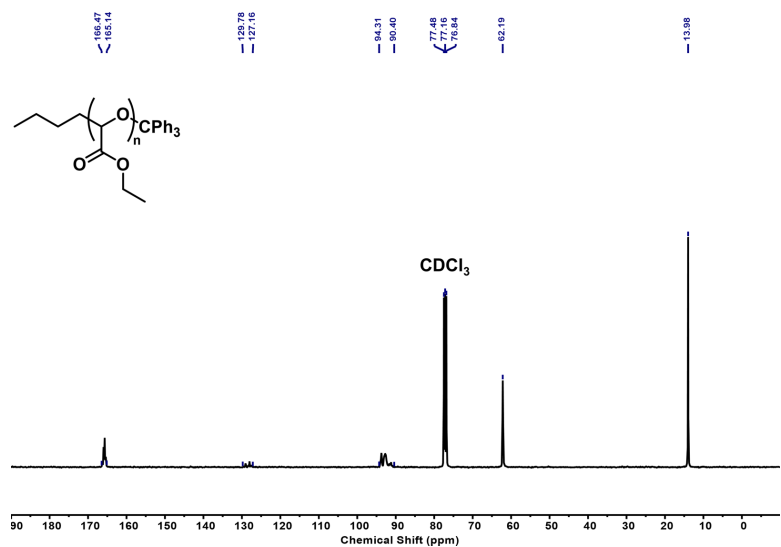


Figure A5.13. ^{13}C NMR spectrum of **PETg-Trit** (CDCl₃, 100 MHz).

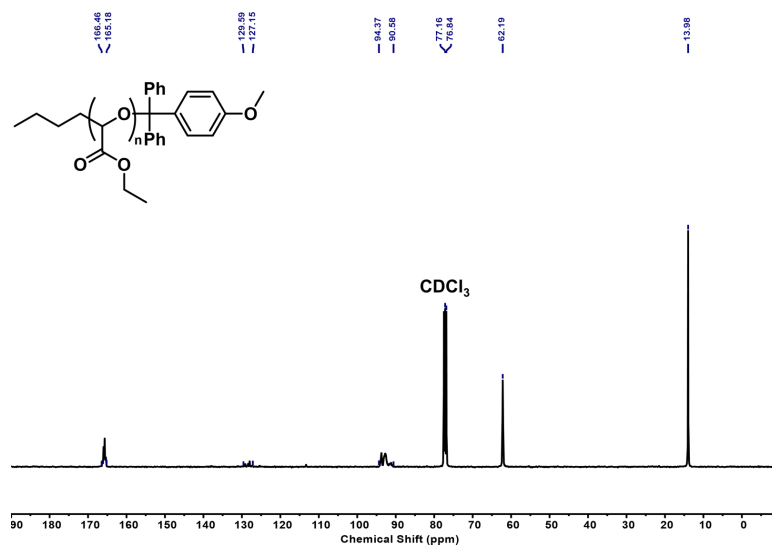


Figure A5.14. ¹³C NMR spectrum of PETG-MMT (CDCl₃, 100 MHz).

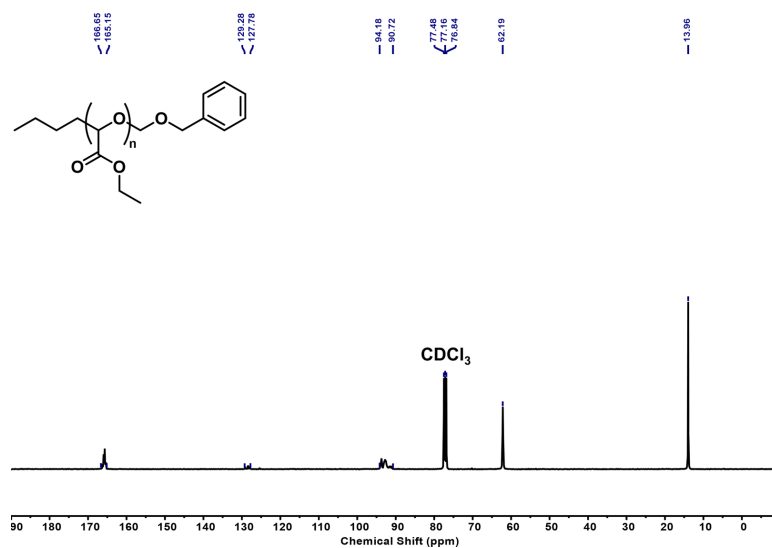


Figure A5.15. ¹³C NMR spectrum of PETG-BOM (CDCl₃, 100 MHz).

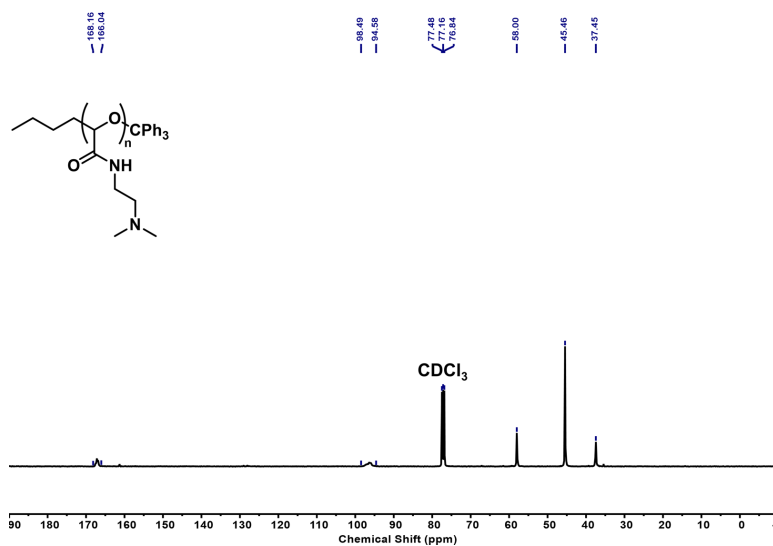


Figure A5.16. ¹³C NMR spectrum of PGAm-DMAE-Trit (CDCl₃, 100 MHz).

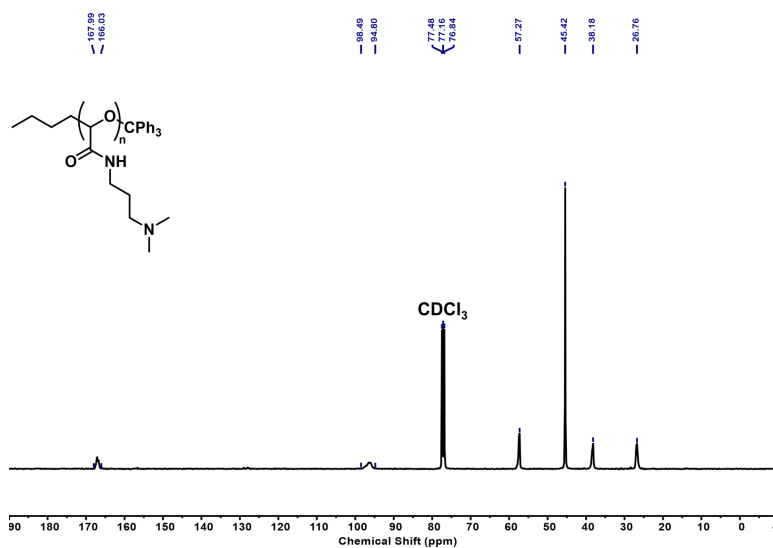


Figure A5.17. ¹³C NMR spectrum of PGAm-DMAPr-Trit (CDCl₃, 100 MHz).

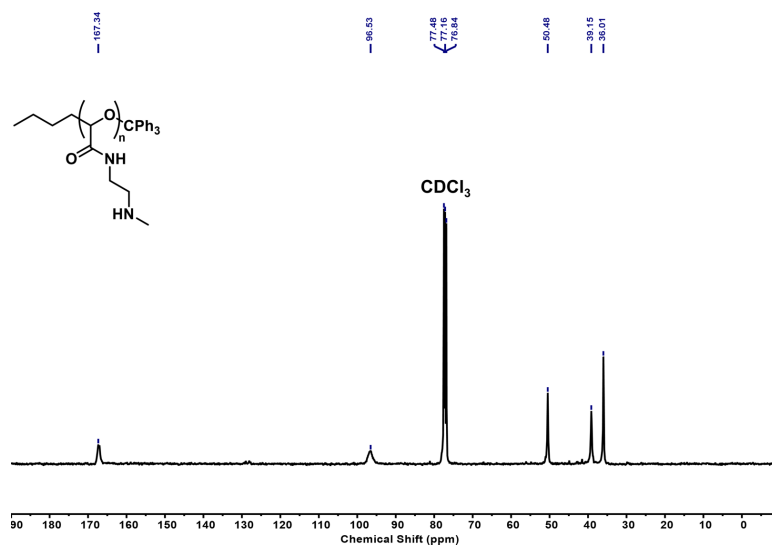


Figure A5.18. ^{13}C NMR spectrum of PGAm-MAE-Trit (CDCl₃, 100 MHz).

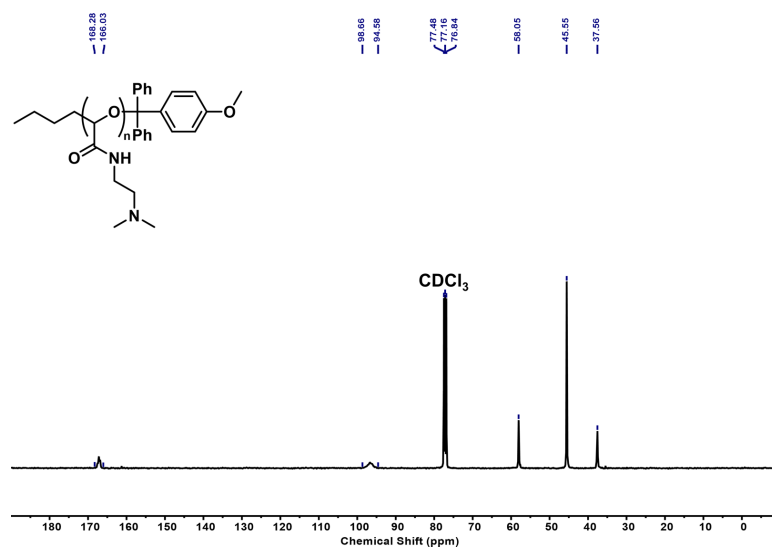


Figure A5.19. ^{13}C NMR spectrum of PGAm-DMAE-MMT (CDCl₃, 100 MHz).

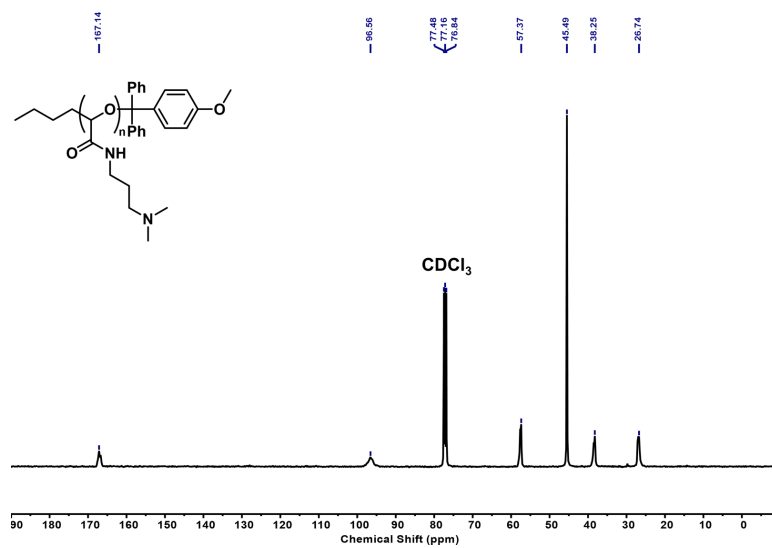


Figure A5.20. ^{13}C NMR spectrum of PGAm-DMAE-MMT (CDCl₃, 100 MHz).

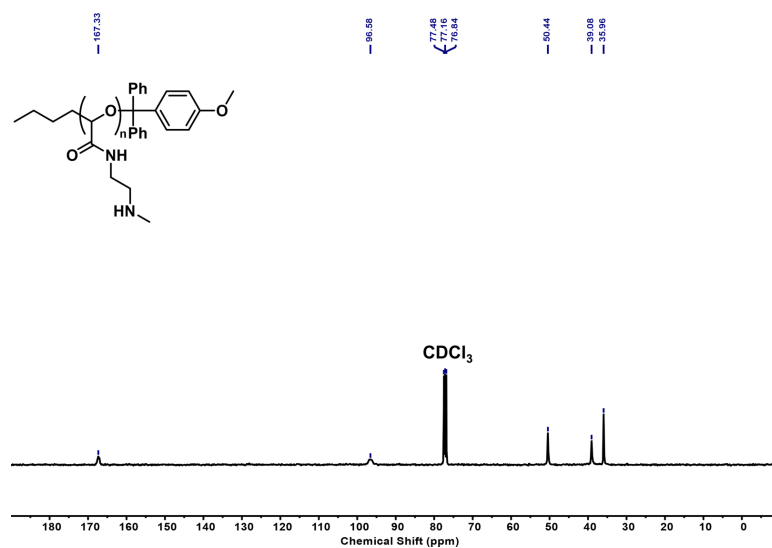


Figure A5.21. ^{13}C NMR spectrum of PGAm-MAE-MMT (CDCl₃, 100 MHz).

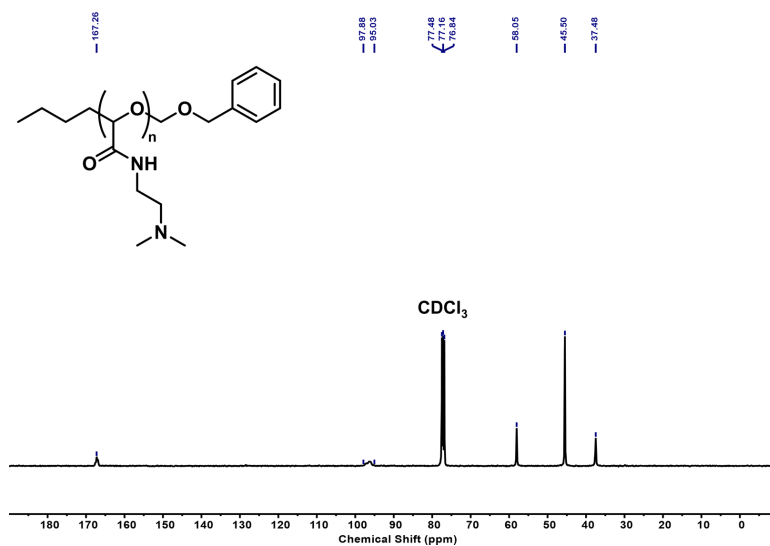


Figure A5.22. ^{13}C NMR spectrum of PGAm-DMAE-BOM (CDCl_3 , 100 MHz).

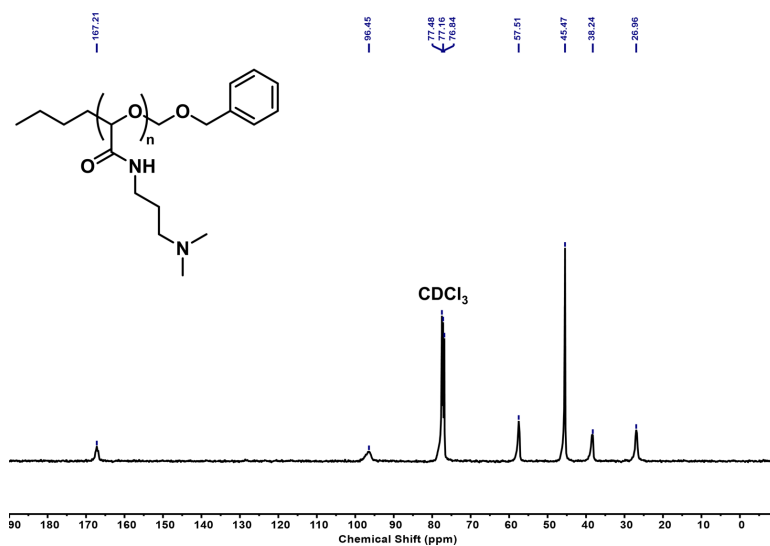


Figure A5.23. ^{13}C NMR spectrum of PGAm-DMAPr-BOM (CDCl_3 , 100 MHz).

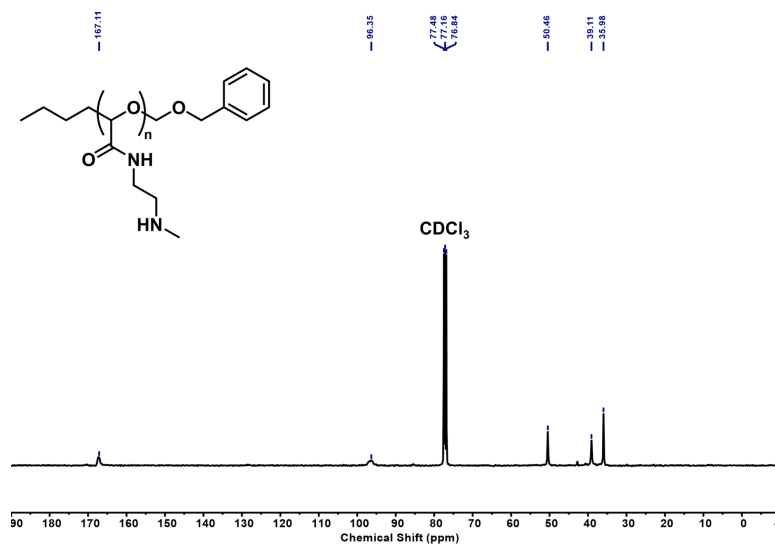


Figure A5.24. ^{13}C NMR spectrum of PGAm-MAE-BOM (CDCl₃, 100 MHz).

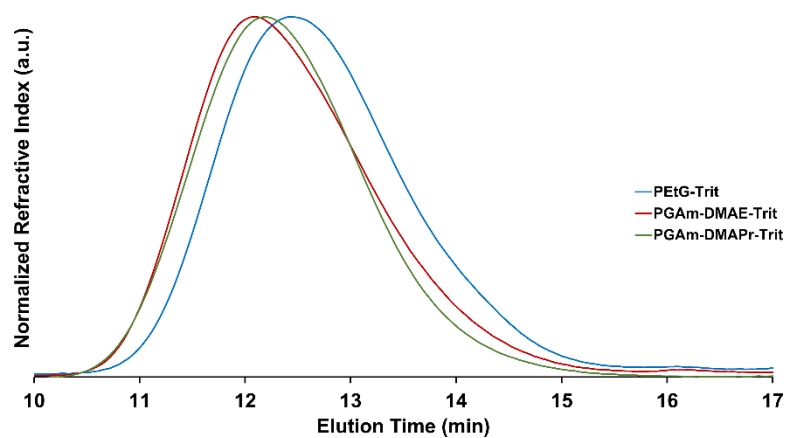


Figure A5.25. Size-exclusion chromatograms of trityl end-capped polymers in DMF. PGAm-MAE-Trit did not elute under these conditions.

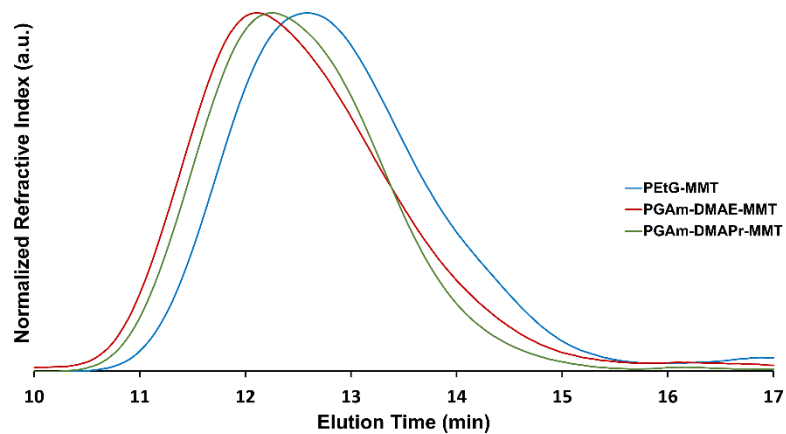


Figure A5.26. Size-exclusion chromatograms of 4-monomethoxytrityl end-capped polymers in DMF. **PGAm-MAE-MMT** did not elute under these conditions.

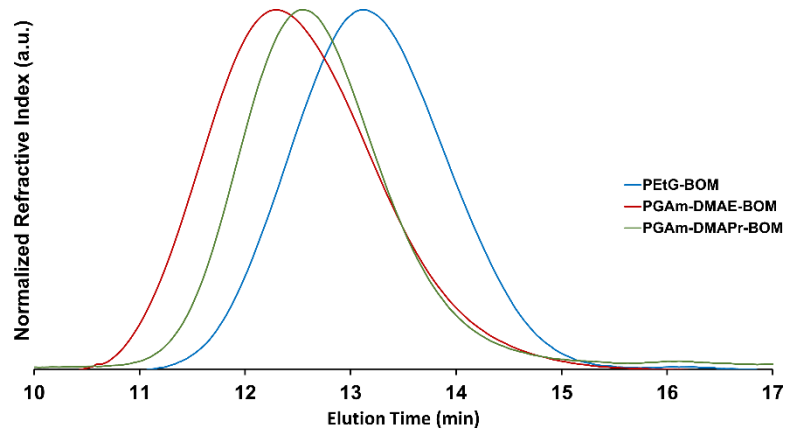


Figure A5.27. Size-exclusion chromatograms of benzyloxymethyl end-capped polymers in DMF. **PGAm-MAE-BOM** did not elute under these conditions.

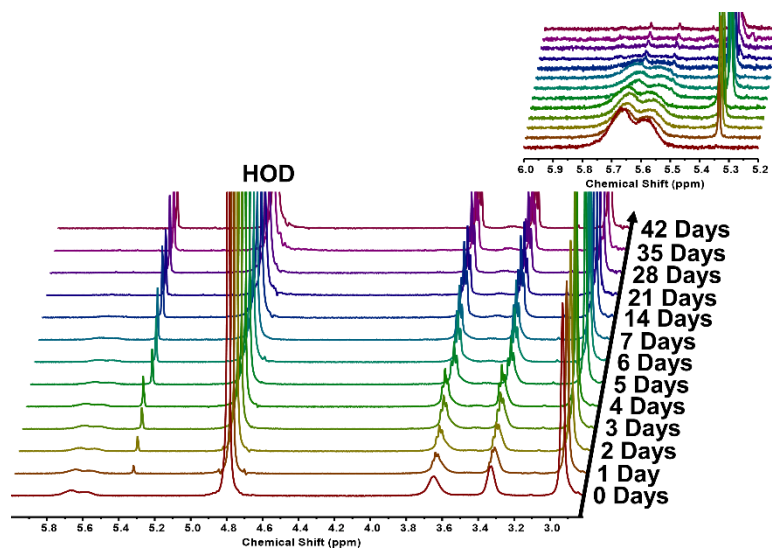


Figure A5.28. Depolymerization of PGAm-DMAE-Trit in citrate buffered D₂O (0.2 M, pH = 5.0) monitored by ¹H NMR spectroscopy (400 MHz). The peaks from the citrate buffer have been cropped off.

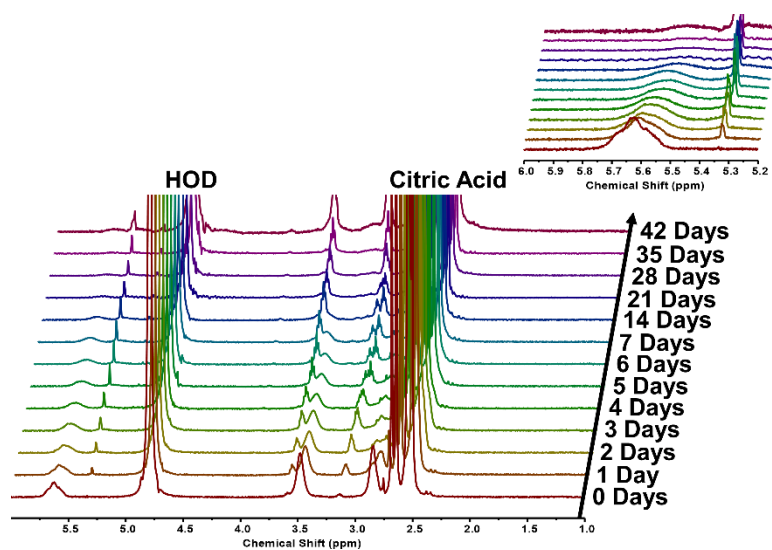


Figure A5.29. Depolymerization of PGAm-DMAE-Trit in citrate buffered D₂O (0.2 M, pH = 6.0) monitored by ¹H NMR spectroscopy (400 MHz).

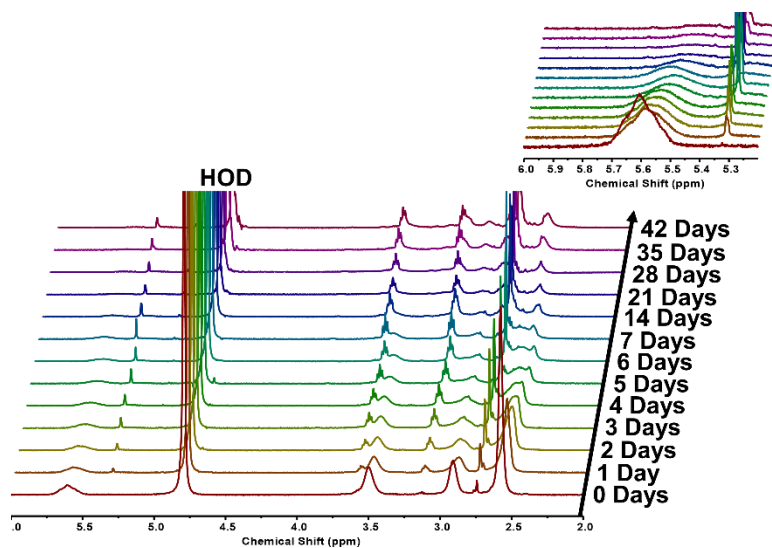


Figure A5.30. Depolymerization of **PGAm-DMAE-Trit** in phosphate buffered D_2O (0.2 M, pH = 7.4) monitored by 1H NMR spectroscopy (400 MHz).

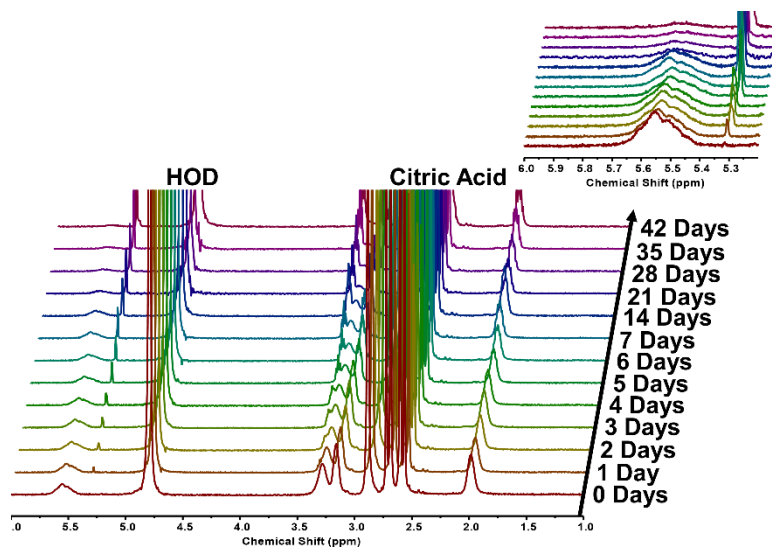


Figure A5.31. Depolymerization of **PGAm-DMAPr-Trit** in citrate buffered D_2O (0.2 M, pH = 5.0) monitored by 1H NMR spectroscopy (400 MHz).

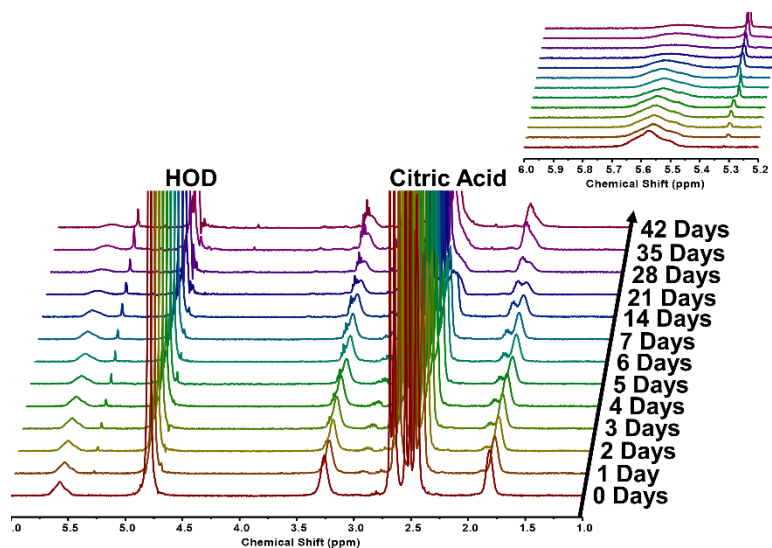


Figure A5.32. Depolymerization of PGAm-DMAPr-Trit in citrate buffered D₂O (0.2 M, pH = 6.0) monitored by ¹H NMR spectroscopy (400 MHz).

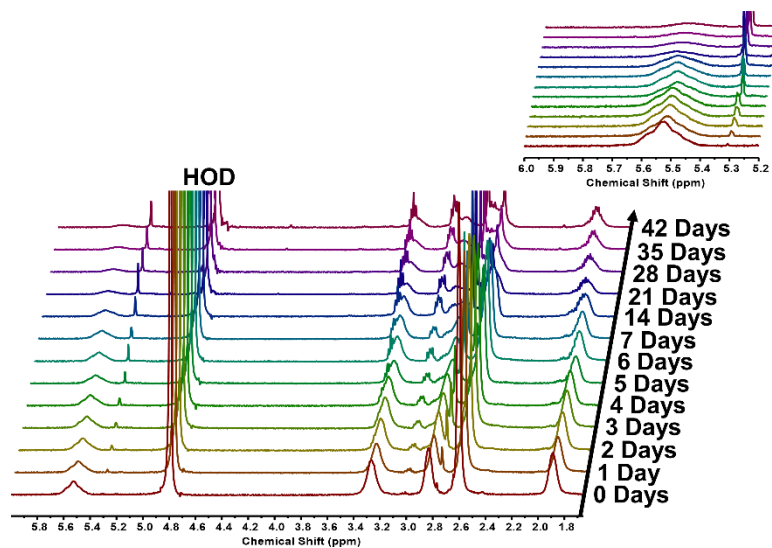


Figure A5.33. Depolymerization of PGAm-DMAPr-Trit in phosphate buffered D₂O (0.2 M, pH = 7.4) monitored by ¹H NMR spectroscopy (400 MHz).

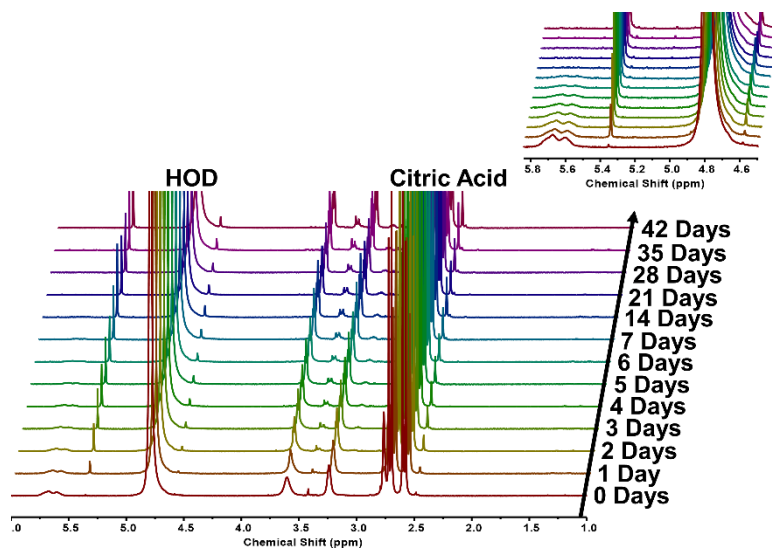


Figure A5.34. Depolymerization of PGAm-MAE-Trit in citrate buffered D_2O (0.2 M, pH = 5.0) monitored by ^1H NMR spectroscopy (600 MHz).

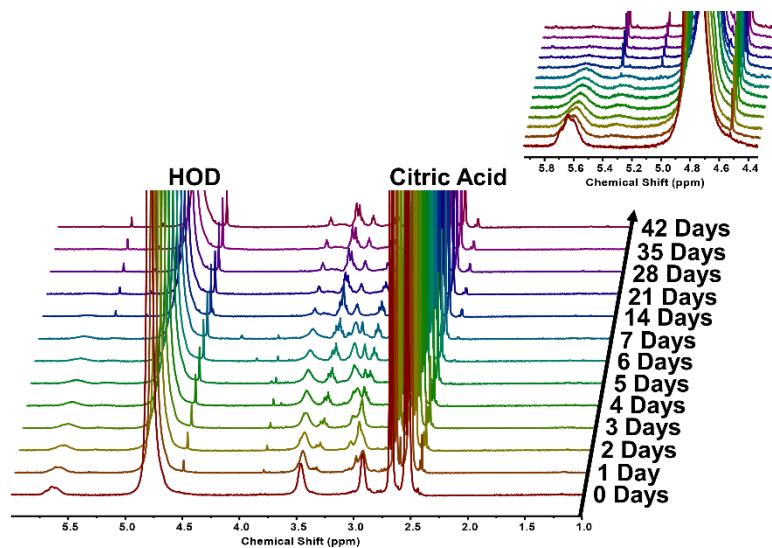


Figure A5.35. Depolymerization of PGAm-MAE-Trit in citrate buffered D_2O (0.2 M, pH = 6.0) monitored by ^1H NMR spectroscopy (600 MHz).

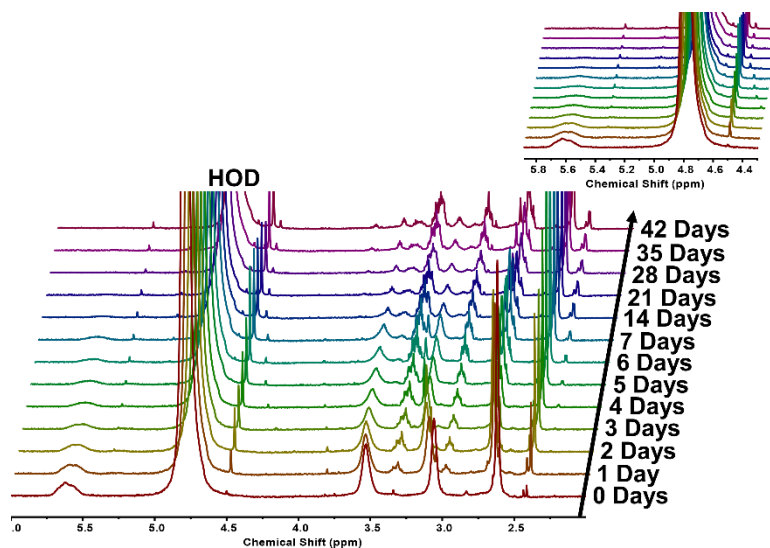


Figure A5.36. Depolymerization of **PGAm-MAE-Trit** in phosphate buffered D_2O (0.2 M, $pH = 7.4$) monitored by 1H NMR spectroscopy (600 MHz).

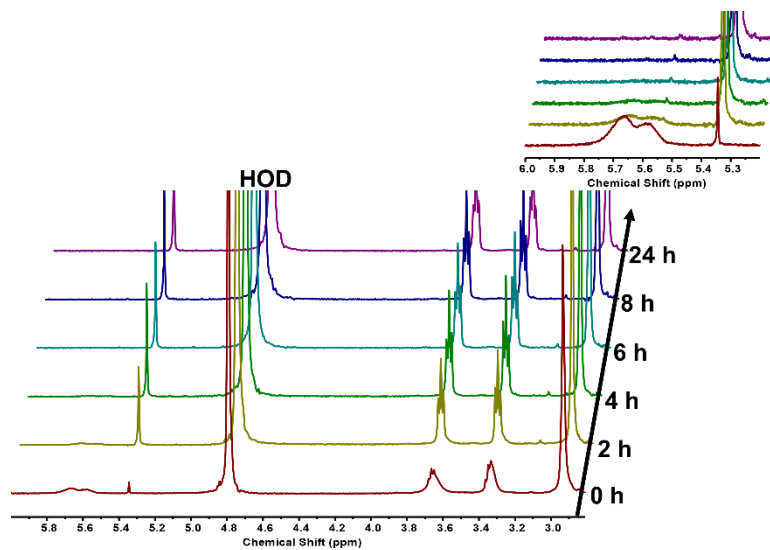


Figure A5.37. Depolymerization of **PGAm-DMAE-MMT** in citrate buffered D_2O (0.2 M, $pH = 5.0$) monitored by 1H NMR spectroscopy (400 MHz). The peaks from the citrate buffer have been cropped off.

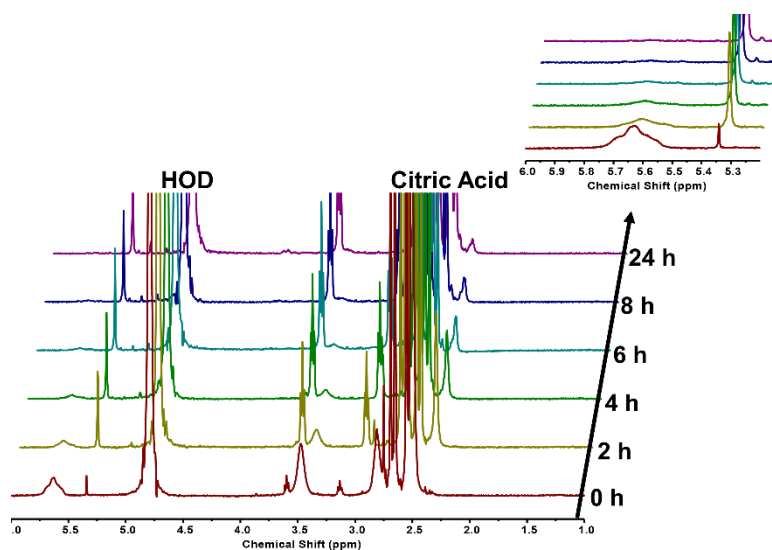


Figure A5.38. Depolymerization of **PGAm-DMAE-MMT** in citrate buffered D₂O (0.2 M, pH = 6.0) monitored by ¹H NMR spectroscopy (400 MHz).

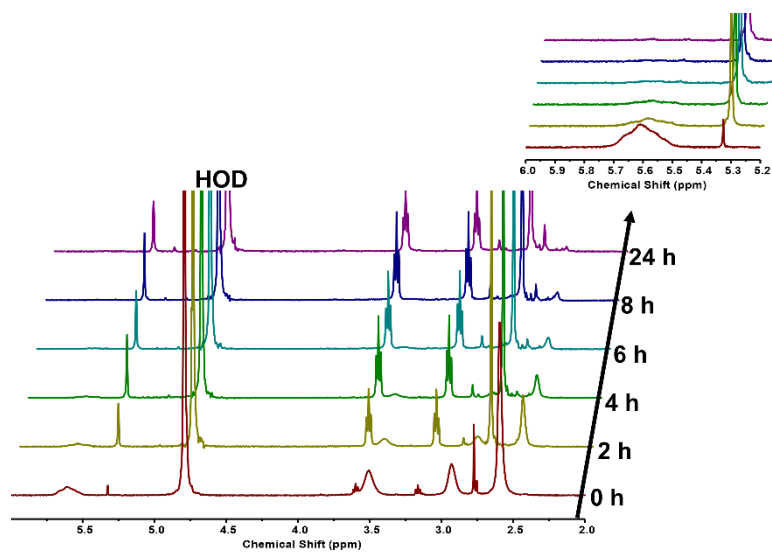


Figure A5.39. Depolymerization of **PGAm-DMAE-MMT** in phosphate buffered D₂O (0.2 M, pH = 7.4) monitored by ¹H NMR spectroscopy (400 MHz).

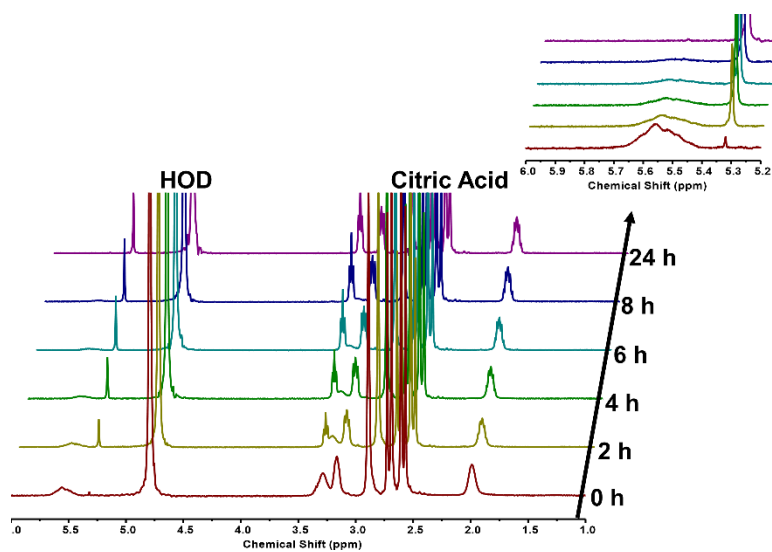


Figure A5.40. Depolymerization of PGAm-DMAPr-MMT in citrate buffered D_2O (0.2 M, pH = 5.0) monitored by ^1H NMR spectroscopy (400 MHz).

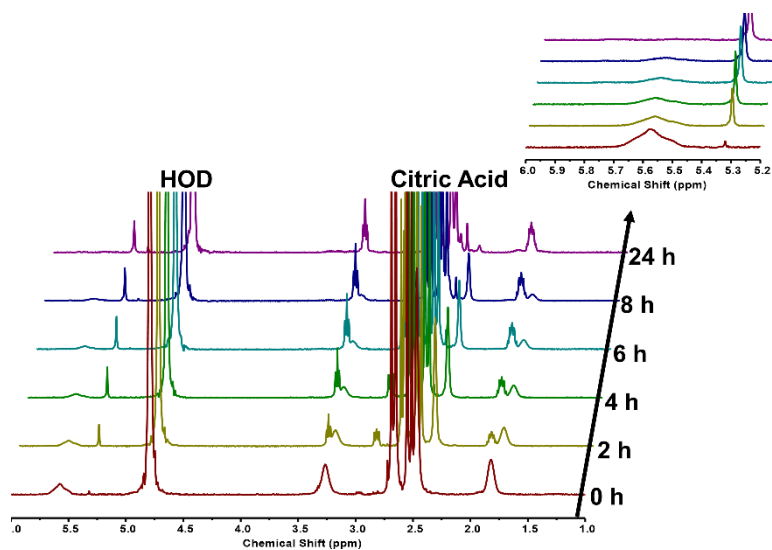


Figure A5.41. Depolymerization of PGAm-DMAPr-MMT in citrate buffered D_2O (0.2 M, pH = 6.0) monitored by ^1H NMR spectroscopy (400 MHz).

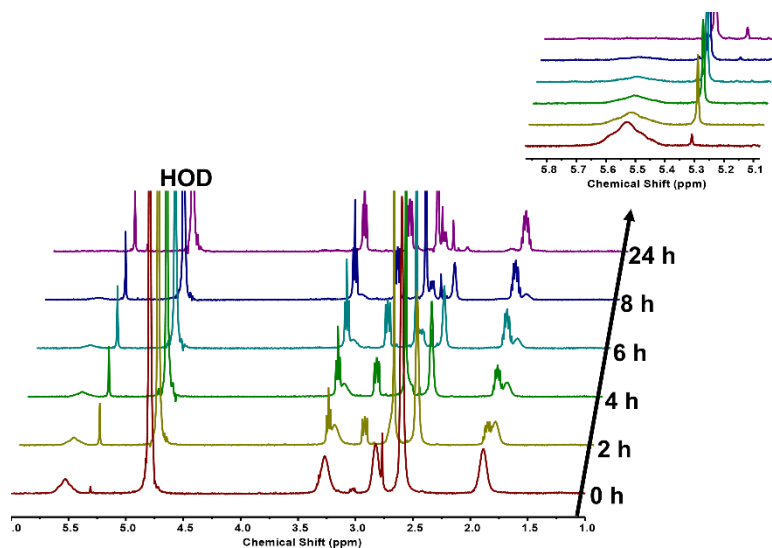


Figure A5.42. Depolymerization of PGAm-DMAPr-MMT in phosphate buffered D₂O (0.2 M, pH = 7.4) monitored by ¹H NMR spectroscopy (400 MHz).

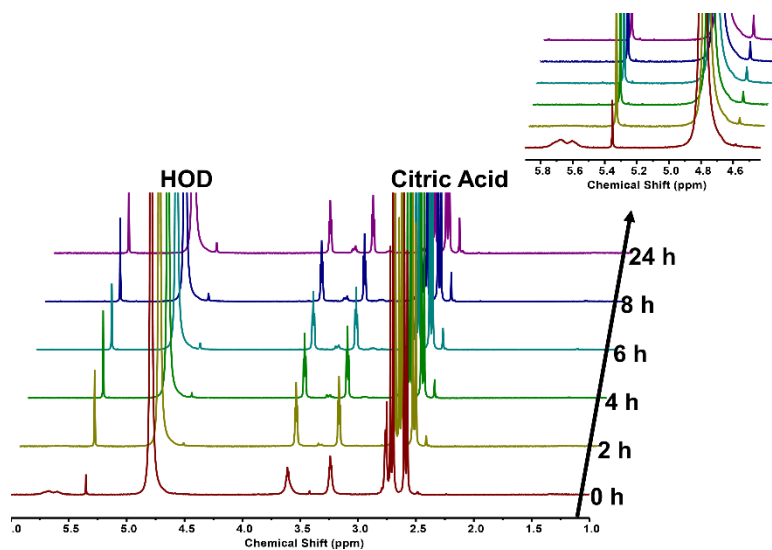


Figure A5.43. Depolymerization of PGAm-MAE-MMT in citrate buffered D₂O (0.2 M, pH = 5.0) monitored by ¹H NMR spectroscopy (600 MHz).

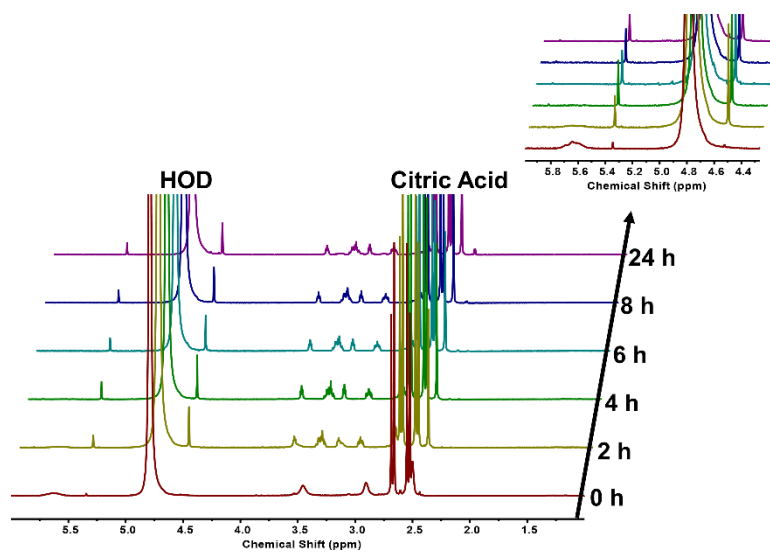


Figure A5.44. Depolymerization of PGAm-MAE-MMT in citrate buffered D₂O (0.2 M, pH = 6.0) monitored by ¹H NMR spectroscopy (600 MHz).

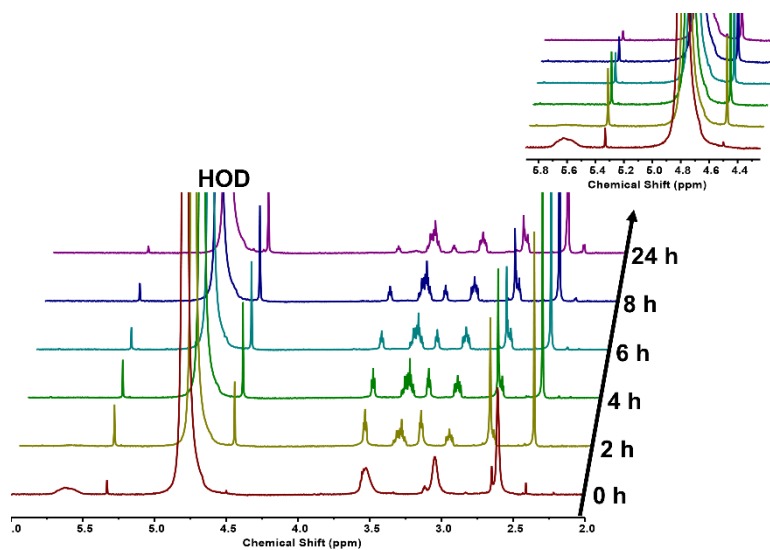


Figure A5.45. Depolymerization of PGAm-MAE-MMT in phosphate buffered D₂O (0.2 M, pH = 7.4) monitored by ¹H NMR spectroscopy (600 MHz).

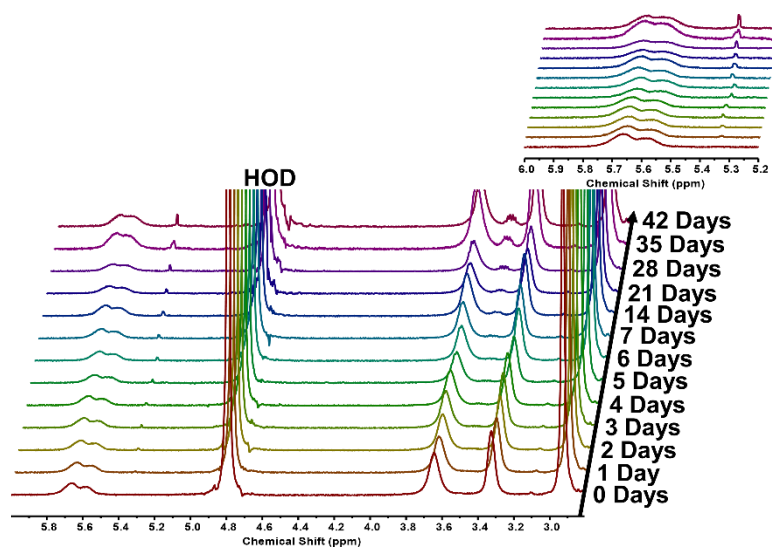


Figure A5.46. Depolymerization of PGAm-DMAE-BOM in citrate buffered D₂O (0.2 M, pH = 5.0) monitored by ¹H NMR spectroscopy (400 MHz). The peaks from the citrate buffer have been cropped off.

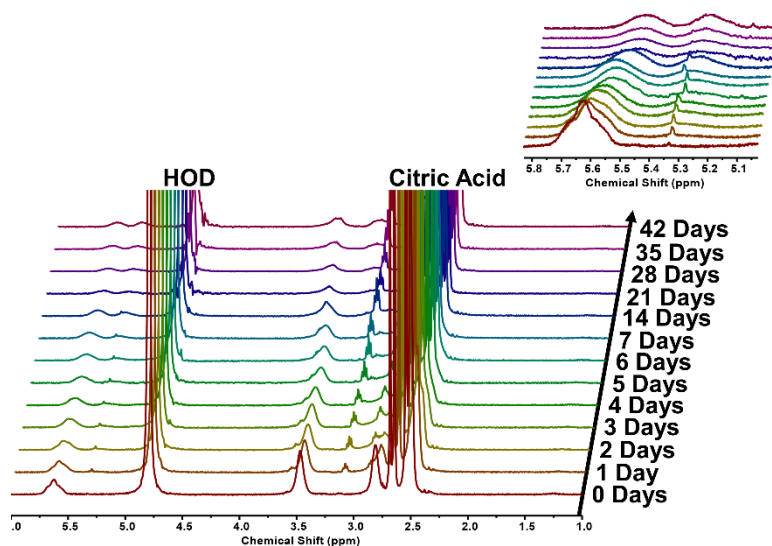


Figure A5.47. Depolymerization of PGAm-DMAE-BOM in citrate buffered D₂O (0.2 M, pH = 6.0) monitored by ¹H NMR spectroscopy (400 MHz).

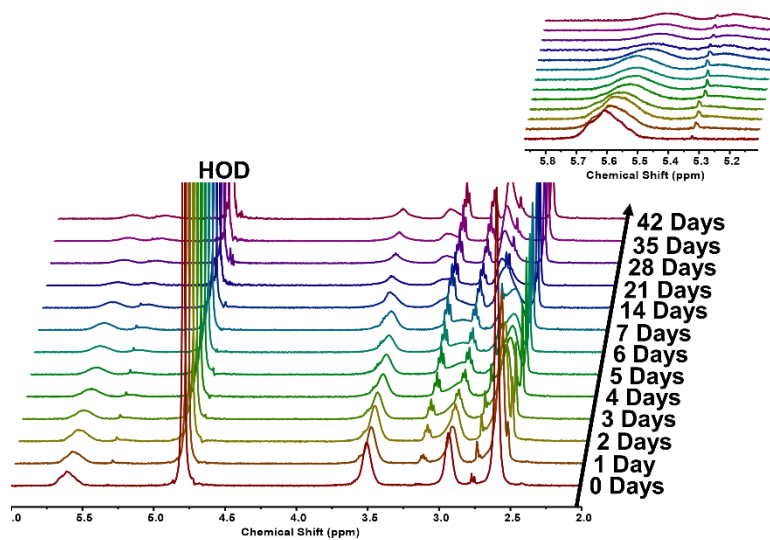


Figure A5.48. Depolymerization of **PGAm-DMAE-BOM** in phosphate buffered D₂O (0.2 M, pH = 7.4) monitored by ¹H NMR spectroscopy (400 MHz).

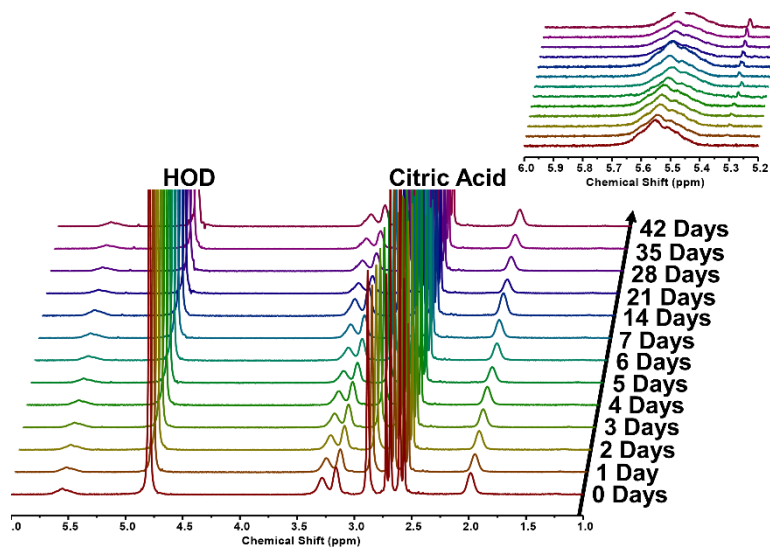


Figure A5.49. Depolymerization of **PGAm-DMAPr-BOM** in citrate buffered D₂O (0.2 M, pH = 5.0) monitored by ¹H NMR spectroscopy (400 MHz).

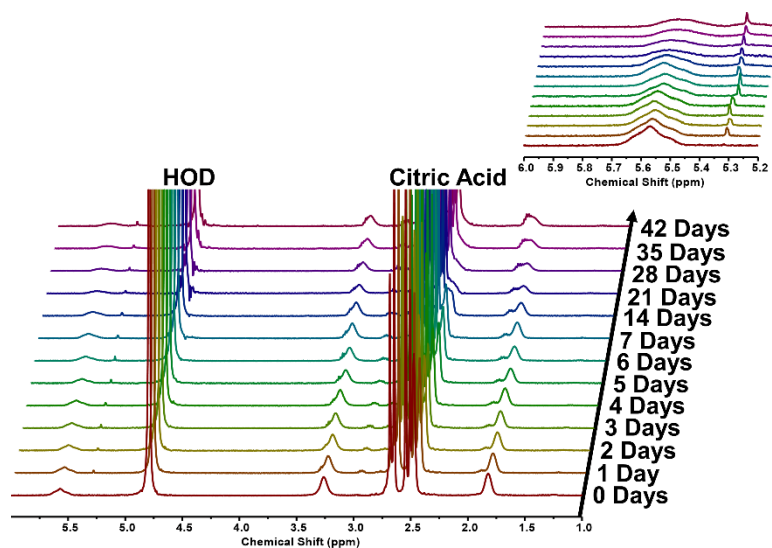


Figure A5.50. Depolymerization of PGAm-DMAPr-BOM in citrate buffered D_2O (0.2 M, pH = 6.0) monitored by ^1H NMR spectroscopy (400 MHz).

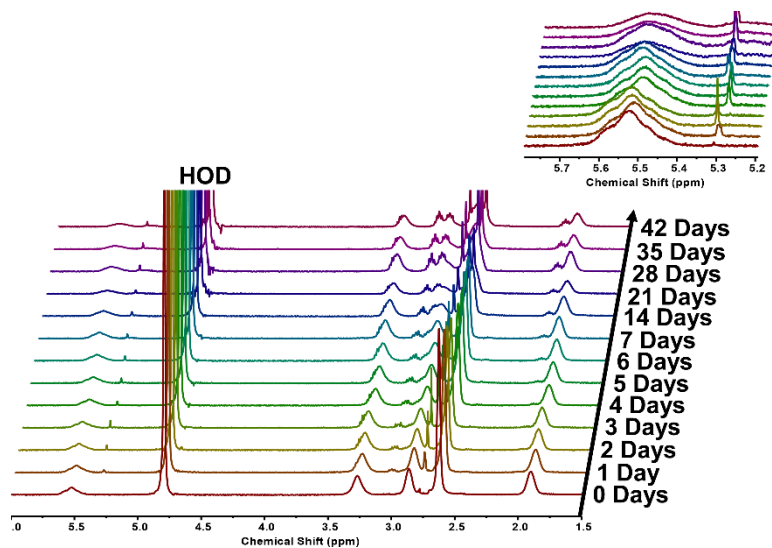


Figure A5.51. Depolymerization of PGAm-DMAPr-BOM in phosphate buffered D_2O (0.2 M, pH = 7.4) monitored by ^1H NMR spectroscopy (400 MHz).

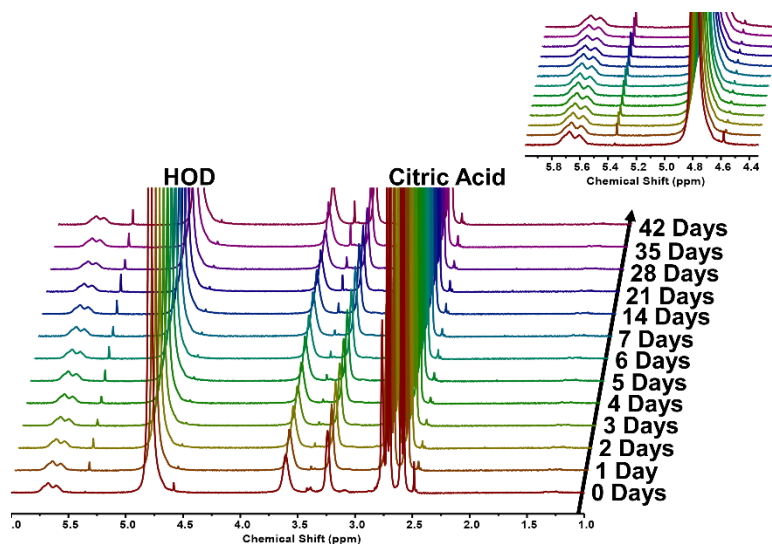


Figure A5.52. Depolymerization of PGAm-MAE-BOM in citrate buffered D_2O (0.2 M, pH = 5.0) monitored by ^1H NMR spectroscopy (600 MHz).

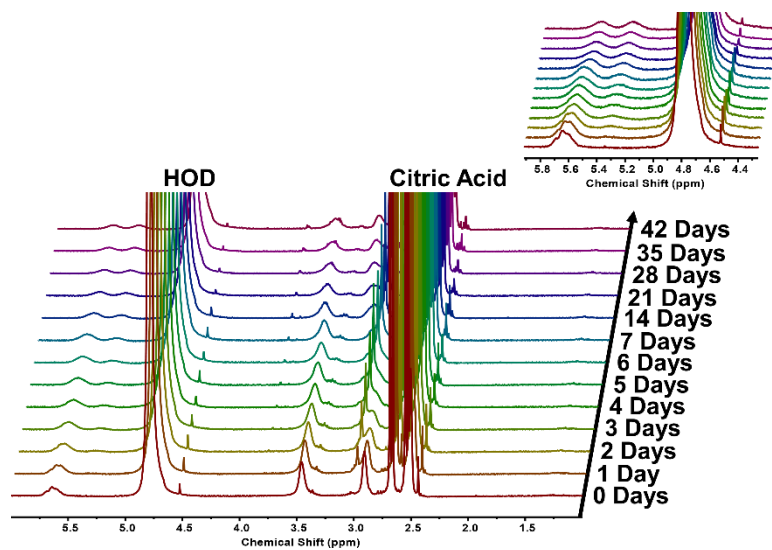


Figure A5.53. Depolymerization of PGAm-MAE-BOM in citrate buffered D_2O (0.2 M, pH = 6.0) monitored by ^1H NMR spectroscopy (600 MHz).

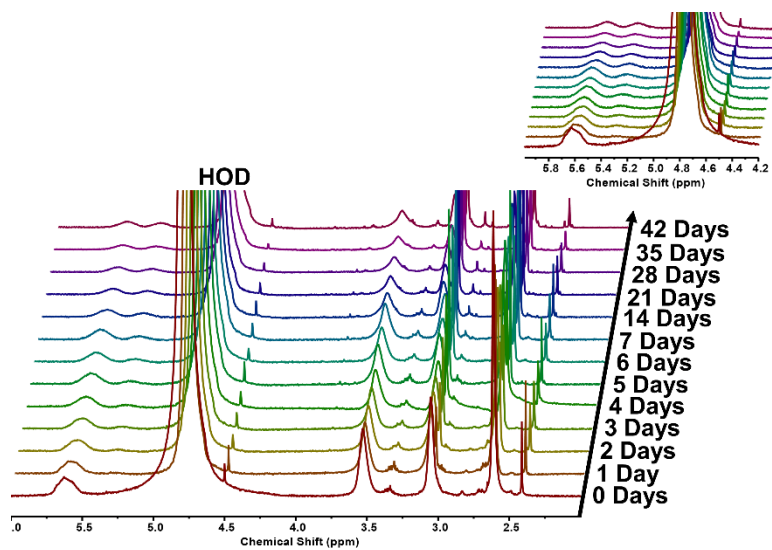


Figure A5.54. Depolymerization of **PGAm-MAE-BOM** in phosphate buffered D_2O (0.2 M, pH = 7.4) monitored by ^1H NMR spectroscopy (600 MHz).

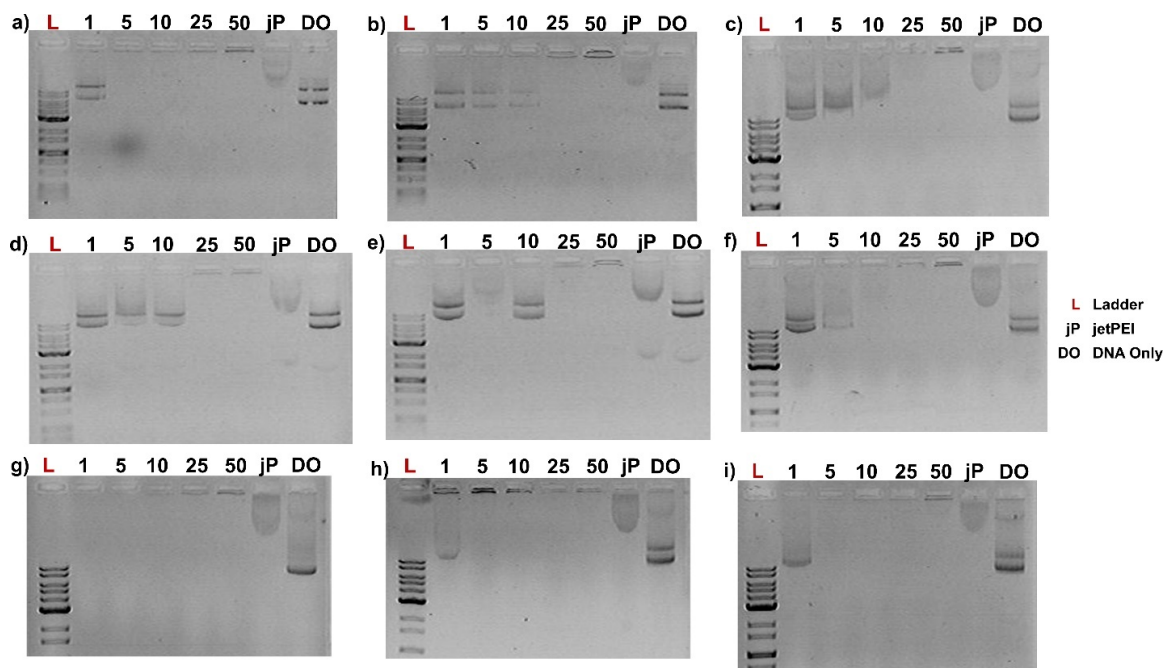


Figure A5.55. Gel electrophoresis of polyplexes at different N/P ratios (1, 5, 10, 25, 50) along with a commercial transfection agent (jetPEI; N/P = 5) and free pDNA. Polyplexes were prepared in purified water and gel electrophoresis was run after a 15 min incubation time: a) PGAm-DMAE-Trit, b) PGAm-DMAE-MMT, c) PGAm-DMAE-BOM, d) PGAm-DMAPr-Trit, e) PGAm-DMAPr-MMT, f) PGAm-DMAPr-BOM, g) PGAm-MAE-Trit, h) PGAm-MAE-MMT, i) PGAm-MAE-BOM. Images are shown in negative contrast.

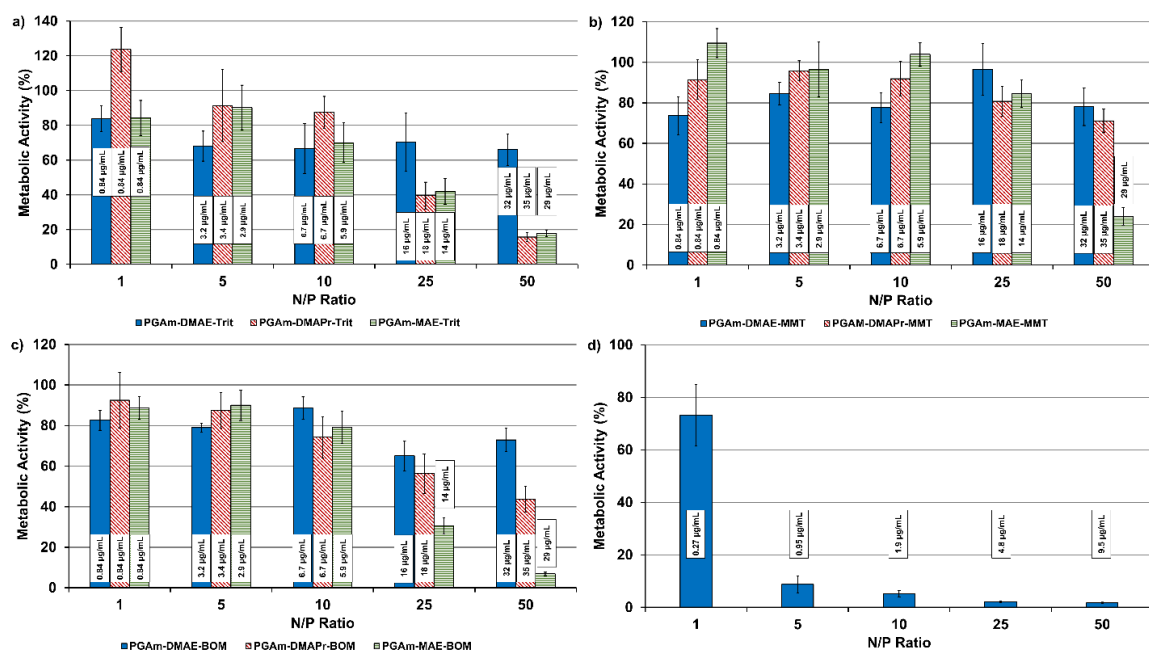


Figure A5.56. MTT assays of HEK 293T cells treated with varying N/P ratios of pDNA-PGAm polyplexes for 48 h (pDNA concentration = 1.5 µg/mL): a) Polyplexes composed of PGAm with a trityl end-cap, b) Polyplexes composed of PGAm with a MMT end-cap, c) Polyplexes composed of PGAm with a BOM end-cap, d) Polyplexes composed of jetPEI. The final concentration of the polycation is given for each column. Error bars represent the standard deviation of the replicate (n = 6) measurements.

Curriculum Vitae for Quinton E. A. Sirianni

Education

- 09/2016–Present.
Ph.D. in Organic Chemistry, The University of Western Ontario, London, Ontario, Canada.
Thesis topic: The Synthesis and Application of Polyglyoxylamides.
Research supervisor: Prof. Elizabeth R. Gillies.
- 09/2010–04/2014.
B.Sc. in Chemical Biology, Thompson Rivers University, Kamloops, British Columbia, Canada.

Research Experience

- 2016–Present.
Graduate Research Assistant, The University of Western Ontario, London, Ontario, Canada.
Research topic: The Synthesis and Application of Polyglyoxylamides.
Research supervisor: Prof. Elizabeth R. Gillies.
- 2013–2014.
Undergraduate Research Assistant, Thompson Rivers University, Kamloops, British Columbia, Canada.
Research topic: The Synthesis of a Biphenyl Containing Different Tertiary Amide Directed Metalation Groups at the 4 and 4' Positions.
Research supervisor: Prof. J. Norman Reed.

Work Experience

- 2018–2021.
Undergraduate Student Mentor, The University of Western Ontario, London, Ontario, Canada.
 - Chemistry 4491 student Erika Remigio (2020–2021 academic year)
 - Chemistry 4491 student Ivana Perkucin (2019–2020 academic year)
 - Chemistry second year volunteer Tegan Wilder (2019 fall term)
 - Chemistry summer volunteer Amna Muhammad (2019 summer).
 - Chemistry 4491 student Ashleigh Aliberti (2018–2019 academic year).
- 2017–2020.
Teaching Assistant, The University of Western Ontario, London, Ontario, Canada.
 - Laboratory instructor for Chemistry 2272 (Analytical) (2019–2020)
 - Tutor for students in Chemistry 2223 (Organic) (2019)
 - Laboratory instructor for Chemistry 2223 (Organic) (2017–2018)

Publications

- Sirianni, Q. E. A.; Wang, T.D.; Borecki, A.; Ronald, J.A.; Gillies, E. R. Depolymerizing Polyplexes for DNA Transfection. *In Preparation*.
- Sirianni, Q. E. A.; Such, G. K.; Gillies, E.R. pH-Responsive Polyglyoxylamides with a pH-Mediated Solubility and Depolymerization Switch. *Submitted*.
- Rabiee Kenaree, A.; Sirianni, Q. E. A.; Classen, K.; Gillies, E. R. Thermoresponsive Self-Immolative Polyglyoxylamides. *Biomacromolecules* **2020**, *21*, 3817–3825. (Co-first author with ARK)
- Sirianni, Q. E. A.; Gillies, E. R. The Architectural Evolution of Self-Immolative Polymers. *Polymer* **2020**, *202*, 122638.
- Ree, L. H. S.; Sirianni, Q. E. A.; Gillies, E. R.; Kelland, M. A. Systematic Study of Polyglyoxylamides as Powerful, High-Cloud-Point Kinetic Hydrate Inhibitors. *Energy & Fuels* **2019**, *33*, 2067–2075.

- Sirianni, Q. E. A.; Rabiee Kenaree, A.; Gillies, E. R. Polyglyoxylamides: Tuning Structure and Properties of Self-Immolative Polymers. *Macromolecules* **2019**, *52*, 262–270.

Conference Presentations

Presenter is underlined

- Sirianni, Q. E. A.; Gillies, E. R. Smart Nanoassemblies from Self-Immolative Cationic Polyglyoxylamides. 104th Canadian Chemistry Conference and Exhibition, **2021**, Oral presentation
- Sirianni, Q. E. A.; Rabiee Kenaree, A.; Gillies, E. R. Polyglyoxylamides: Tuning the Properties of Self-Immolative Polymers for Biomedical Applications. 35th Annual Meeting of the Canadian Biomaterials Society, Québec City, Québec, Canada **2019**, Oral presentation.
- Sirianni, Q. E. A.; Rabiee Kenaree, A.; Gillies, E. R. Polyglyoxylamides: Self-Immolative Polymers with Potential Biomedical Applications. 101st Annual Meeting of the Canadian Society for Chemistry, Edmonton, Alberta, Canada, **2018**, Oral presentation.
- Sirianni, Q. E. A.; Rabiee Kenaree, A.; Gillies, E. R. Polyglyoxylamides: Amide Analogues of Polyglyoxylates. 8th Annual Nano Ontario Conference, Toronto, Ontario, Canada, **2017**, Poster presentation.
- Sirianni, Q. E. A.; Gambles, M. T.; MacDonald, J. P.; Gillies, E. R. Polyglyoxylamides: A Novel Class of Stimuli-Responsive Polymers. 100th Annual Meeting of the Canadian Society for Chemistry, Toronto, Ontario, Canada, **2017**. Poster presentation.

Awards and Honours

- 2020.
Queen Elizabeth II Graduate Scholarship, The University of Western Ontario, London Ontario, Canada.

- 2019.
Queen Elizabeth II Graduate Scholarship, The University of Western Ontario, London Ontario, Canada.
- 2019.
Canadian Biomaterials Society Travel Award, Annual Meeting of the Canadian Biomaterials Society, Québec City, Québec, Canada.
- 2018.
Queen Elizabeth II Graduate Scholarship, The University of Western Ontario, London Ontario, Canada.
- 2017.
NSERC Canada Graduate Scholarship – Master’s Program, The University of Western Ontario, London Ontario, Canada.
- 2017.
Ontario Graduate Scholarship (Declined), The University of Western Ontario, London Ontario, Canada.
- 2016.
Ontario Graduate Scholarship, The University of Western Ontario, London Ontario, Canada.
- 2011–2013.
Dean’s Honour Role, Thompson Rivers University, Kamloops, British Columbia, Canada.
- 2010.
President’s Entrance Scholarship, Thompson Rivers University, Kamloops, British Columbia, Canada.

Courses Taken

- 01/2019–04/2019.
Introduction to Nanobiotechnology.
Instructor: Prof. Jin Zhang.
Grade: A (88%).
- 03/2018–04/2018.
Advanced Nucleic Acid Chemistry.
Instructor: Prof. Robert Hudson.
Grade: A (88%).
- 03/2018–04/2018.
Advanced Polymer Chemistry II.
Instructor: Prof. Joe Gilroy.
Grade: A (89%).
- 09/2017–10/2017.
Advanced Chemical Communications.
Instructor: Prof. Elizabeth Gillies.
Grade: A (94%).
- 01/2017–02/2017.
Advanced Polymer Chemistry I.
Instructor: Prof. Joe Gilroy.
Grade: A (92%).
- 11/2016–12/2016.
Advanced NMR Spectroscopy I.
Instructor: Prof. Kim Baines.
Grade: A (92%).
- 11/2016–12/2016.
Advanced Medicinal Chemistry.

Instructor: Prof. Len Luyt.

Grade: A (87%).